Faculté des géosciences et de l'environnement
Institut de Géologie et Paléontologie

Late Cretaceous to Eocene geology of the South Central American forearc area (southern Costa Rica and western Panama): Initiation and evolution of an intra-oceanic convergent margin

Thèse de doctorat

présentée à la

Faculté des géosciences et de l'environnement
de l'Université de Lausanne

par

David M. Buchs

DEA en sciences de la Terre de l'Université de Lausanne

Jury

Prof. Lukas Baumgartner (Président du colloque)
Prof. Peter-Olivier Baumgartner (Directeur de thèse)
Prof. Richard Arculus (Expert)
Prof. Gérard Stampfli (Expert)
Prof. Othmar Müntener (Expert)

LAUSANNE
2008

UNIL | Faculté des géosciences
et de l'environnement

Imprimatur

Vu le rapport présenté par le jury d'examen composé de

Président du colloque	: M. le Professeur Lukas Baumgartner
Directeur de thèse	: M. le Professeur Peter-Olivier Baumgartner
Expert externe	: M. le Professeur Richard Arculus
Expert interne	: M. le Professeur Gérard Stampfli
Expert interne	: M. le Professeur Othmar Müntener

le Conseil de Faculté autorise l'impression de la thèse de

Monsieur David Buchs

Titulaire d'un Diplôme d'études approfondies en sciences de la Terre de l'Université de Lausanne

intitulée

Late Cretaceous to Eocene geology of the South Central American forearc area (southern Costa Rica and western Panama): initiation and evolution of an intra-oceanic convergent margin

Lausanne, le 12 septembre 2008

Le Doyen de la Faculté des géosciences et de l'environnement

Professeur Lukas Baumgartner

Acknowledgments

Lausanne, 13th September 2008

Index

Abstract

The southern Central American volcanic front lies on the SW edge of the Caribbean Plate, inboard of the subducting Cocos and Nazca Plates. It is one of the most studied intra-oceanic convergent margins around the world, which is generally interpreted to have developed in the late Cretaceous along an oceanic plateau (the Caribbean Large Igneous Province or CLIP) and to be currently undergoing a regime of subduction erosion. In the last decades a particular effort has been made to understand subduction-related processes on the basis of geophysical and geochemical studies.

In southern Costa Rica and western Panama accretionary complexes and structures at the base of the volcanic front have been exposed in response to subduction of aseismic ridges and transforms. On-land exposures are located as close as to 15 km from the trench and provide a unique opportunity to better understand some of the processes occurring along the subduction zone. We provide new constraints on the origins of these exposures by integrating a comprehensive field work, new geochemical, sedimentary and paleontological data, as well as structural observations based on remote imaging. A new Campanian to Eocene tectonostratigraphy is defined for the forearc area located between the Osa Peninsula (Costa Rica) and the Azuero Peninsula (Panama). Our results show that the outer margin is composed of a complicated arrangement of igneous complexes and overlapping sedimentary sequences that essentially comprise an arc basement, primitive island-arc rocks, accreted seamount fragments and accretionary mélanges.

Evidences are provided for the development of the southern Central American arc on the top an oceanic plateau. The subduction initiation along the SW edge of the Caribbean Plate occurred in the Campanian and led to formation of primitive island-arc rocks characterized by unusual geochemical affinities broadly intermediate between plateau and arc affinities. The arc was mature in the Maastrichtian and was forming a predominantly continuous landbridge between the North and South Americas. This allowed migration of terrestrial fauna between the Americas and may have contributed to the Cretaceous-Tertiary crisis by limiting trans-equatorial oceanic currents between the Pacific and the Atlantic.

Several units composed of accreted seamount fragments are defined. The nature of the units and their structural arrangement provide new constraints on the modes of accretion of seamounts/oceanic islands and on the evolution of the margin since subduction initiation. Between the late Cretaceous and the middle Eocene, the margin recorded several local episodes of seamount accretion alternating with tectonic erosion. In the middle Eocene a regional tectonic event may have triggered strong coupling between the overriding and subducting plates, leading to higher rates of seamount accretion. During this period the situation along the margin was very similar to the present and characterized by subducting seamounts and absence of sediment accretion. The geological record shows that it is not possible to ascribe an overall erosive or accretionary nature to the margin in the past and, by analogy, today, because (1) accretionary and erosive processes exhibit significant lateral and temporal variations and (2) it is impossible to estimate the exact amount of material tectonically eroded from the margin since subduction initiation.

In southern Costa Rica, accreted seamount fragments point toward a plume-ridge interaction in the Pacific in the late Cretaceous/Paleocene. This occurrence of accreted seamount fragments and morphology of the Pacific Ocean floor is indicative of the formation of the Cocos-Nazca spreading system at least ~40 Ma prior to the age proposed in current tectonic models.

In Panama, we identified a remarkably-well preserved early Eocene oceanic island that accreted in the middle Eocene. The accretion probably occurred at very shallow depth by detachment of the island in the trench and led to an exceptional preservation of the volcanic structures. Exposures of both deep and superficial parts of the volcanic edifice have been studied, from the submarine-shield to subaerial-postshield stages. The stratigraphy allowed us to distinguish lavas produced during the submarine and subaerial stages. The lava compositions likely define a progressive diminution of source melting and a decrease in the temperature of erupted melts in the latest stages of volcanic activity. We interpret these changes to primarily reflect the progressive migration of the oceanic island out of the melting region or hotspot.

Résumé

L'arc volcanique du sud de l'Amérique Centrale se situe sur la marge SW de la Plaque Caraïbe, au-dessus des plaques subduites de Cocos et Nazca. Il s'agit de l'un des arcs intra-océaniques les plus étudiés au monde, qui est généralement considéré comme s'étant développé à la fin du Crétacé le long d'un plateau océanique (le Plateau Caraïbe ou CLIP) et se trouvant actuellement dans un régime de subduction érosive. Au cours des dernières décennies, des efforts particuliers ont été faits pour comprendre les processus liés à la subduction sur la base d'études géophysiques et géochimiques.

Au sud du Costa Rica et à l'ouest du Panama, des complexes d'accrétions et structures à la base de l'arc volcanique ont été exposés grâce à la subduction de rides asismiques et de failles transformantes. Des affleurements, situés jusqu'à seulement 15 km de la fosse, offrent une possibilité unique de mieux comprendre quelques uns des processus ayant lieu le long de la zone de subduction. Nous présentons de nouvelles contraintes sur l'origine de ces affleurements en alliant une étude de terrain poussée, de nouvelles données géochimiques, sédimentaires et paléontologiques, ainsi que des observations structurales effectuées en télédétection. Une nouvelle stratigraphie tectonique entre le Campanien et l'Eocène est définie pour la région d'avant-arc située entre la Péninsule d'Osa (Costa Rica) et la Péninsule d'Azuero (Panama). Nos résultats montrent que la partie externe de la marge est composée d'un arrangement complexe de roches ignées et de séquences sédimentaires de recouvrement qui comprennent principalement le socle de l'arc, des roches d'arc primitif, des fragments de monts sous-marins accrétés et des mélanges d'accrétion.

Des preuves sont données pour le développement de l'arc volcanique du sud de l'Amérique Centrale sur un plateau océanique. Le début de la subduction le long de la marge SW de la Plaque Caraïbe a eu lieu au Campanien et a généré des roches d'arc primitif caractérisées par des affinités géochimiques particulières, globalement intermédiaires entre des affinités de plateau et d'arc insulaire. L'arc était mature au Maastrichtien et formait un isthme essentiellement continu entre l'Amérique du Nord et l'Amérique du Sud. Ceci a permis la migration de faunes terrestres entre les Amériques et pourrait avoir contribué à la crise fin Crétacé - Tertiaire en réduisant les courants océaniques sub-équatoriaux entre le Pacifique et l'Atlantique.

Plusieurs unités composées de fragments de monts sous-marins accrétés sont définies. La nature et l'arrangement structural de ces unités définissent de nouvelles contraintes sur les modes d'accrétion des monts sous-marins/îles océaniques et sur l'évolution de la marge depuis la formation de la zone de subduction. Entre la fin du Crétacé et l'Eocène moyen, la marge a enregistré plusieurs épisodes ponctuels d'accrétion de monts sous-marins alternant avec de la subduction érosive. A l'Eocène moyen, un événement tectonique régional pourrait avoir causé un fort couplage entre les plaques supérieure et inférieure, menant à des taux plus important d'accrétion de monts sous-marins. Durant cette période, la situation le long de la marge était très semblable à la situation actuelle et caractérisée par la présence de monts sous-marins subductants et l'absence d'accrétion de sédiments. L'enregistrement géologique montre qu'il n'est pas possible d'attribuer une nature érosive ou accrétionnaire à la marge dans le passé ou -par analogie- aujourd'hui, parce que (1) les processus d'accrétion et érosifs varient fortement spatialement et temporellement et (2) il est impossible d'évaluer la quantité exacte de matériel tectoniquement enlevé à la marge depuis le début de la subduction.

Au sud du Costa Rica, certains fragments de monts sous-marins accrétés sont représentatifs d'une interaction entre une ride et un point chaud dans le Pacifique au Crétacé terminal/Paléocène. L'existence de ces fragments de monts sous-marins et la morphologie du fond de l'Océan Pacifique indiquent que la formation de la ride de Cocos-Nazca s'est formée au moins ~40 Ma avant l'âge proposé par les modèles tectoniques actuels.

Au Panama, nous avons identifié une île océanique d'âge début Eocène qui a été accrétée à l'Eocène moyen. L'accrétion a eu lieu à très faible profondeur par détachement de l'île dans la fosse, et a mené à une exceptionnelle préservation des structures volcaniques. Des affleurement comprenant aussi bien des parties basses et hautes de l'édifice volcanique on été étudiées, depuis la phase sous-marine bouclier jusqu'à la phase subaérienne post-bouclier. La stratigraphie nous a permis de différencier les laves de la phase sous-marine de celles de la phase subaérienne. La composition des laves indique une diminution progressive de l'intensité de la fusion partielle de la source et une diminution de la température des laves produites durant les derniers stades de l'activité volcanique. Nous interprétons ces changements comme étant liés à l'éloignement progressif de l'île océanique de la zone de fusion ou point chaud.

Chapter 1: Introduction

1.1. Geological setting

1.1.1. The Caribbean Plate

The Caribbean Plate is composed of normal and overthickened oceanic crust surrounded by transforms and subduction zones (Figure 1.1). The crust was drilled by DSDP leg 15 and ODP leg 165 and a basaltic basement was reached at 5 sites in the Caribbean Sea. Based on the results of these drillings [*Donnelly*, 1973; *Donnelly et al.*, 1973; *Bence et al.*, 1975; *Sigurdsson et al., 1997*; *Sinton et al.*, 1998, 2000; *Kerr et al.*, 2002] and early seismic refraction studies [*Edgar et al.*, 1971], it was proposed that a late Cretaceous oceanic plateau covers most of the Caribbean Plate. Some contributions assigned an exotic Pacific origin to the plateau, with a subsequent westward migration of South America relative to the Caribbean Plate [e.g. *Burke et al.*, 1988; *Pindell et al.*, 2005, 2006], whereas some authors prefer an *in situ*, inter-American formation for the Caribbean Plateau [e.g. *Meschede and Frisch*, 1998; *James*, 2006]. Igneous complexes with similar plateau-like geochemical signatures and ages (Turonian, ~90 Ma) have been interpreted to represent portions of the Caribbean Plateau obducted onto adjacent margins during the emplacement at its present location [e.g. *Donnelly et al.*, 1990; *Kerr et al.*, 1996; *Sinton et al.*, 1998]. Similarly, many igneous complexes exposed along southern Central America (Figure 1.2) are believed to be part of the Caribbean Plateau [e.g. *Sinton et al.*, 1997].

The circum-Caribbean plateau-like complexes and bulk of the Caribbean Plate have been widely interpreted to be originally part of a single oceanic plateau and grouped under generalizing terms "CLIP" (Caribbean Large Igneous Province) or "CCOP" (Caribbean-Colombian Oceanic Plateau). However, several observations question the potential existence of the CLIP: (1) seismic studies from Venezuelan to Colombian basins have shown that overthickened areas in the Caribbean Plate are separated by normal oceanic crust [*Mauffret and Leroy*, 1997; *Diebold et al.*, 1999] (Figure 1.1), (2) $^{40}Ar/^{39}Ar$ ages from plateau-like basalts in the Circum Caribbean range from 139 to 55 Ma [*Lapierre et al.*, 2000; *Révillon et al.*, 2000; *Mauffret et al.*, 2001; *Hoernle et al.*, 2002; *Hoernle et al.*, 2004; *Escuder-Viruete et al.*, 2007], which is much longer than the duration of formation of other plateaus [e.g. *Storey et al.*, 2007; *Bryan and Ernst*, 2008], even though this could be possibly explained by the thermochemical plume model [*Lin and Keken*, 2005], (3) some igneous complexes exposed along northern South America, generally considered to be part of the CLIP, have been considered to have a distinct origin than the CLIP by some authors [*Kerr and Tarney*, 2005], (4) geochemistry of the CLIP show a large variability [e.g. *Kerr et al.*, 2002], which is not observed in other oceanic plateaus, (5) many circum-Caribbean igneous complexes lack high MgO (picritic) lavas, which are considered by some authors to be an intrinsic characteristic of Large Igneous Provinces (LIPs) [e.g. *Kerr*, 2003; *Campbell*, 2007], (6) if the hypothesis of *in situ* formation of the Caribbean Plateau relative to South America turns out to be correct [e.g. *Meschede and Frisch*, 1998; *James*, 2006], the igneous complexes exposed along Colombia and Ecuador would not represent obducted/accreted portions of the CLIP, and (7) apart of the principle of parsimony, there is no argument definitely ruling out the existence of several plateaus generated by different volcanic systems on the Caribbean Plate.

To explain the wide range of ages of the plateau-like igneous complexes in the Caribbean *Hoernle et al.* [2004] propose that the CLIP may represent a long-term accumulation and

amalgamation of the products of intraplate volcanism through the subduction process. However this model requires large-scale subduction backsteps and the abandon of intra-oceanic volcanic arcs during amalgamation of large intraplate volcanic structures. Such abandoned volcanic arcs have not been observed so far in the Caribbean, which probably indicates that the wide age range of the igneous complexes is not related to large-scale amalgamation.

Testing the existence of the CLIP is well beyond the scope of this study but we will show that, in southern Central America, "CLIP" or "CCOP" terms have been inappropriately used for some igneous complexes with plateau affinities. New constraints on the initiation of the subduction in this area and later tectonic development of the margin further question the validity of systematic association of circum-Caribbean plateau-like igneous complexes with the CLIP.
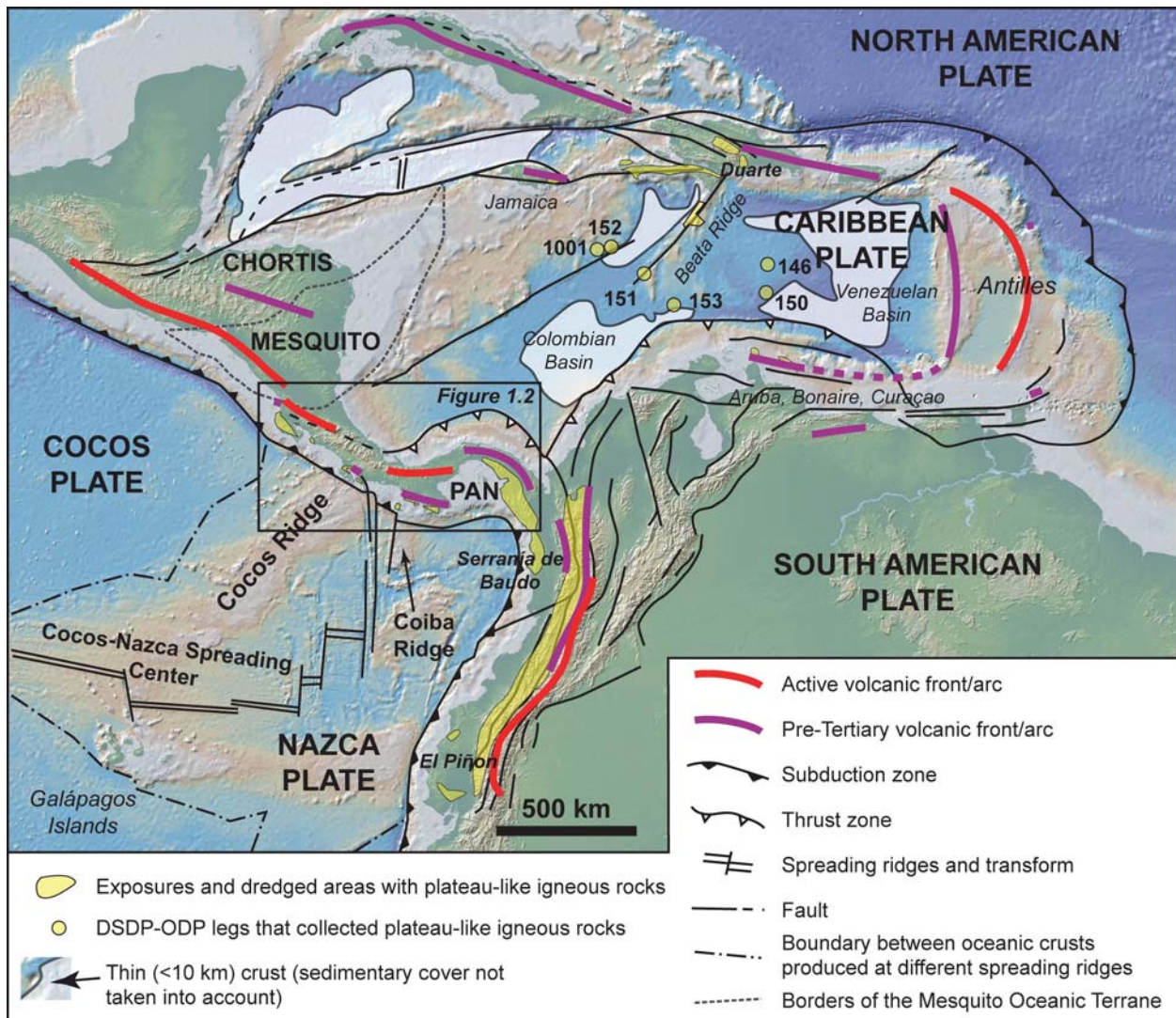
Figure 1.1: *Tectonic setting of the Panama Microplate (PAN). Colored background map from GeoMapApp [2007]. Lineaments and plate limits modified after Meschede and Barckhausen [2001] and Pindell et al. [2005, 2006]. Areas of thin "normal" oceanic crust after Mauffret and Leroy [1997].*

1.1.2. Circum-Caribbean volcanic arcs

The Caribbean Plate is bracketed at both eastern and western sides by active volcanic arcs (Figure 1.1). In the east, the Lesser Antilles Volcanic Arc is related to subduction of the North American Plate toward the west [e.g. *MacDonald et al.*, 2004]. In the west, subduction of the

Cocos and Nazca plates toward the east controls the formation of the Central American Volcanic Front/Arc [e.g. *Carr et al.*, 2007]. Abandoned arcs in the circum-Caribbean are found along the Cayman Trough, Hispaniola, Cuba and Puerto Rico in the north, and along the South Caribbean Foldbelt in the south (see *Kerr et al.* [2003] for a comprehensive review of the circum-Caribbean arcs). These abandoned arcs are made of a wide range of high- to low-Fe suites and date back to Jurassic(?) and Lower Cretaceous [*Kerr et al.*, 2003]. Some of them are thus anterior to the formation of the bulk of the CLIP ~90 Ma.
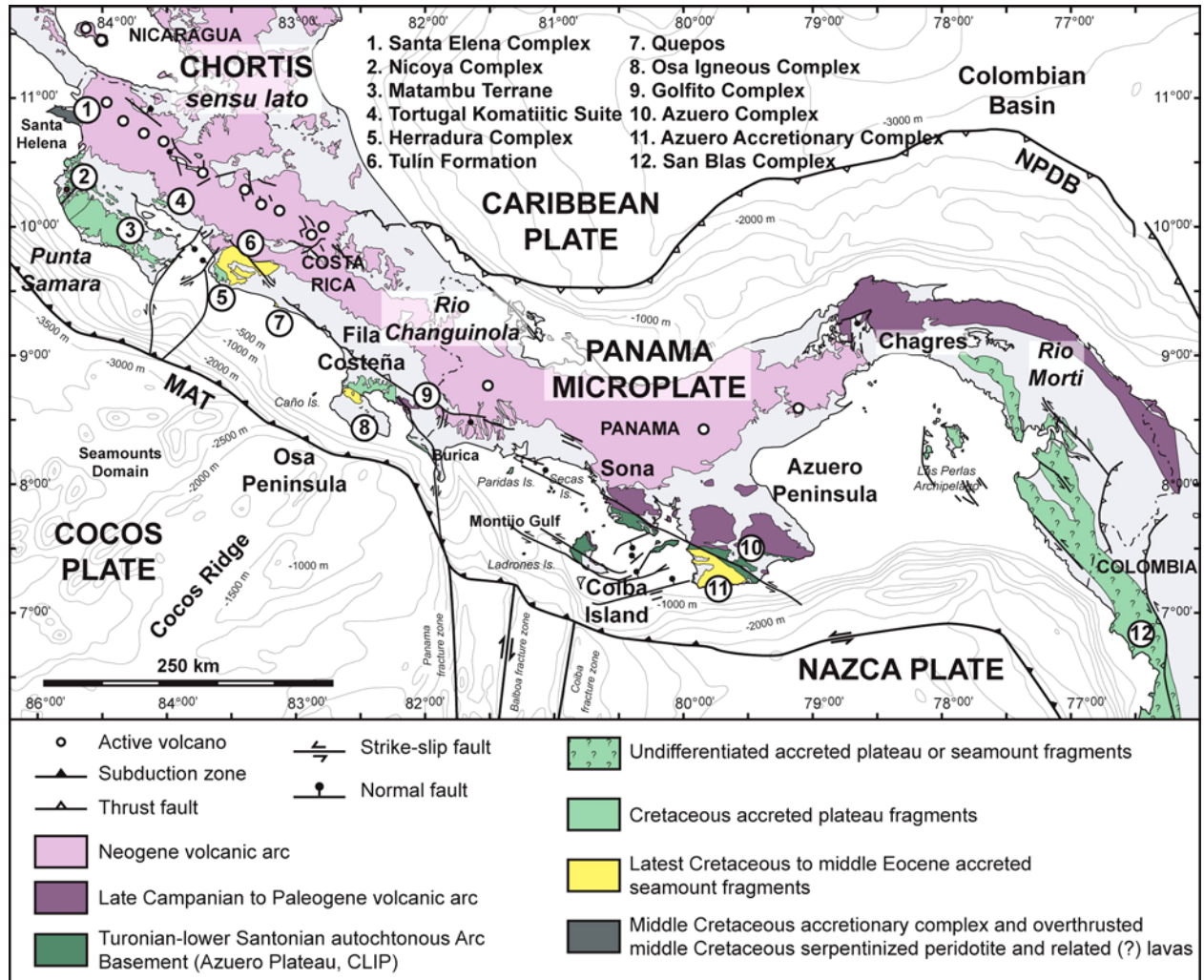
***Figure 1.2:** Simplified geological map of Southern Central America based on national geological maps of the area and results from this study. Bathymetry based on Smith and Sandwell [1997]. Quaternary faults from USGS open-file reports [Cowan et al., 1998; Montero et al., 1998; Paris et al., 2000]. Numbers indicate igneous complexes exposed along the forearc, NPDB=North Panama Deformed Belt, MAT=Mid American Trench. Autochtonous and accreted oceanic complexes are defined on the basis of our new results and stratigraphic data from previous contributions [Bandy and Casey, 1973; Baumgartner et al., 1984, 2008; Di Marco, 1994; Arias, 2003; Flores, 2003; Bandini et al., 2008].*

Locally, late Cretaceous supra-subduction igneous rocks in the circum Caribbean have been tectonically and/or petrologically linked to the CLIP: (1) In Aruba and Bonaire arc-related igneous rocks point toward a Santonian-Campanian collision between the CLIP and an intra-oceanic volcanic arc (represented by the Bonaire Washikemba Formation and Aruba batholith), which may have triggered a subduction reversal along the Great Antillan Arc [*White et al.*, 1998;

Thompson et al., 2004], (2) some late Cretaceous igneous rocks in Jamaica are similar to the arc successions of Bonaire [*Hastie*, 2007, written communication 2008] and may thus record a similar tectonic history, (3) the subducting CLIP may have participated to formation of latest Cretaceous high-Mg andesites in Puerto Rico [*Jolly et al.*, 2007] and (4) late Cretaceous arc-related igneous rocks in western Ecuador may represent an intra-oceanic arc emplaced on the SE edge of the CLIP and subsequently accreted onto the NW South American margin [*Allibon et al.*, 2005, in press; *Vallejo et al.*, 2006; *Vallejo*, 2007] or autochtonous igneous rocks contaminated by subducted/accreted enriched material [*Chiarada and Fontboté*, 2001, 2002]. Due to poor exposures and/or preservation of pristine structures the link between some late Cretaceous volcanic arcs and the CLIP is essentially based on time constraints and geochemistry. Detailed stratigraphic studies are still needed to confirm these interpretations.

1.1.3. Geological overview of the southern Central American forearc

1.1.3.1. Tectonic setting

The South Central American Arc lies on the Panama Microplate (also described as Chorotega and Choco blocks), which is a SW extension of the Caribbean Plate bounded by thrust zones and transforms (Figure 1.1). Thrusted boundaries have formed since the collision of the southern Central America Arc with the continental South American plate in the late Miocene (12.8-9.5 Ma) [*Coates et al.*, 2004]. In earlier history of the South Central American Arc, most authors consider that the Panama Microplate was located further west (relative to South America) in the Pacific [e.g. *Mann et al.*, 2007].

The South Central American Arc is situated at the junction of five plates and tectonic block: the Caribbean Plate, South American Plate, Cocos Plate, Nazca Plate and Chortis Block (Figure 1.1). The Chortis Block is in contact with the Panama Microplate along a late Cretaceous suture zone made of an assemblage of pre-Campanian oceanic terranes called Mesquito Composite Oceanic Terrane. This suture is distinct from northern Chortis Block (Chortis Block s.str.) that is composed of several terranes with strictly continental records [*Flores et al.*, 2007; *Baumgartner et al.*, 2008]. Northern extension of the Panama Microplate is delimited by the North Panama Deformed Belt in the east [*Adamek et al.*, 1988; *Silver et al.*, 1990] and a diffuse thrust belt in the Cordillera Central of Costa Rica [*Marshall et al.*, 2000; *Denyer and Alvarado*, 2007]. The eastern edge of the Panama Microplate is suturing with the South American Plate along the Atrato Valley [*Taboada et al.*, 2000; *Trenkamp et al.*, 2002]. Compression along the SE border of the Panama Microplate controls the formation of the South Panama Deformed Belt in the forearc area [*Mann and Kolarsky*, 1995]. Bending of the South Central American Arc occurred since the Miocene in response to a compressional event [*Mann and Corrigan*, 1990; *Coates et al.*, 2004]. Deformation of the arc was controlled by a NW tectonic escape of the central Panama between NW-SE striking left-lateral faults located in Azuero area and in Eastern Panama [*Mann and Corrigan*, 1990]. CASA GPS network indicates that motions vectors between the Caribbean Plate and the Panama Microplate are decoupled and, conjointly with seismicity, that bending of the isthmus is currently inactive [*Kellog and Vega*, 1995; *Trenkamp et al.*, 2002]. The Caribbean Plate converges toward the Panama Microplate at a rate of ~3-4 mm/a [*Trenkamp et al.*, 2002], which may result in a compression along the North Panama Deformed Belt. Convergence of the Panama Microplate toward the South American Plate in the east is of ~7 mm/a, which is ~4 mm/a faster than the migration of the western Caribbean Plate toward the same direction [*Trenkamp et al.*, 2002].

The Cocos and Nazca plates subduct under the Panama Microplate. Due to the initial breakup of the Farallon Plate ~23 Ma and subsequent spreading and ridge jumps [*Barckhausen et al.*, 2001; *Werner et al.*, 2003; *Lonsdale*, 2005], the morphology and age of these plates show large along-axis variations [*von Huene et al.*, 1995, 2000]. From the north of Costa Rica toward the north, the Cocos Plate is composed of a strongly-dipping smooth crust derived from the East Pacific Rise. Between north of Costa Rica and western Panama, the Cocos Plate is made of a younger moderately-dipping crust, partially covered by seamounts, and formed at Cocos-Nazca Spreading Center. Close to the border between Costa Rica and Panama, intra-oceanic transforms delimit the southern extension of the Cocos Plate and may have displaced initially contiguous Cocos and Coiba aseismic ridges. These ridges are composed of drown oceanic islands produced above the Galapagos Hotspot and Cocos-Nazca Spreading Center [e.g. *Werner et al.*, 1999]. Further toward the south is found the younger Nazca Plate which resembles the southern extension of the Cocos Plate and formed at the Cocos-Nazca Spreading Center.

The morphology of the subducting oceanic plates along the Central American Isthmus has a strong influence on tectonics of the overriding plate and supra-subduction magmatic processes. Collision of the Cocos ridge with the volcanic arc 8-1 Ma (most probably 2 Ma) ago in southern Costa Rica [*McMillan et al.*, 2004 and references therein] resulted in a strong uplift and shortening throughout the isthmus, associated with a local cessation of volcanism [e.g. *Kolarsky et al.*, 1995a]. Along-strike migrations toward the south of intra-oceanic transforms [*MacMillan et al.*, 2004] controlled the formation of the Fila Costeña Thrust Belt [*Morell et al.*, 2008] and, possibly, triggered uplift of some portions of the outer forearc area between southern Costa Rica and western Panama. Subduction of relatively buoyant plates irregularly covered by topographic highs causes the forearc area to be variously uplifted and exposed along the margin [*Fisher et al.*, 1998; *Gardner et al.*, 2001; *Sak et al.*, 2004], to distances as close as to ~20 km from the trench. Such exposures provide a unique opportunity to study deep sections of the outer margin, which is composed of a complicated arrangement of arc-related rocks, accreted material and overlap sequences.

1.1.3.2. Plateau-like igneous complexes and arc basement

Exposures of accretionary complexes and igneous complexes made of early Cretaceous to Miocene seamounts, plateaus and sediments are exposed along Costa Rican-Panamean outer margin (see *Denyer et al.* [2006] for a general review from northern Costa Rica to western Panama). Early to late Cretaceous basaltic complexes with plateau-like geochemical affinities are found all along the margin from northern Costa Rica to western Panama (Figure 1.2). Although they have been considered for a long time to pertain to a same basement complex called "Nicoya Complex" (from the Nicoya Peninsula, northern Costa Rica) [*Dengo*, 1962], recent contributions indicated that important tectonostratigraphic differences exist from one exposure to another. Thus, the use of the term "Nicoya Complex" apart of the Nicoya Peninsula is inadequate [e.g. *Denyer et al.*, 2006]. Following *Flores* [2003] we use that term for the northernmost exposures of the Nicoya Peninsula (Figure 1.2).

In the forearc of eastern Panama, *Bandy and Casey* [1973] described "basement rocks" composed of interbedded basalts and late Cretaceous radiolarian cherts. In the same area, plateau-like basalts have been sampled and analyzed by *Lissinna* [2005], indicating a possible continuation of the plateau-like volcanic rocks toward the Colombian margin. These rocks, herein described as the "San Blas Complex" (following the terminology of *Coates et al.*, [2004]),

may be a lateral equivalent of the 73-78 Ma (^{40}Ar/^{39}Ar) igneous complexes found in the Serranía de Baudó (western Colombia, see also *Kerr et al.* [1997]) and of some of the plateau-like igneous complexes of western Panama and Costa Rica.

Plateau-like igneous complexes exposed along the uplifted outer margin of Costa Rica and Panama range in age from 76 to 139 Ma (^{40}Ar/^{39}Ar) [*Hoernle et al.*, 2002, 2004]. They have been widely considered to be part of the CLIP on the basis of a similar geochemistry and, partly, ages. However, we note that little attempt has been made to use sedimentary and structural observations to further constrain this interpretation. New stratigraphic constraints from northern Costa Rica [*Bandini et al.*, 2008] illustrate the exotic nature of the Nicoya Complex that represent an oceanic plateau initially formed in the Pacific realm before being partly accreted onto the margin. Similarly, plateau-like igneous complexes exposed along the forearc of southern Central America may be part of accretionary complexes and genetically unrelated to the CLIP, even though they have similar ages and geochemistry.

Extension beneath the isthmus of the igneous complexes exposed in the outer margin of southern Central America and their extension toward the Caribbean is poorly constrained. Seismic and tomographic profiles across the volcanic front in northern Costa Rica shown that the arc basement is constituted by an overthickened oceanic crust, distinct from the Nicaraguan basement, potentially representing the western extension of the Caribbean Plate and "Caribbean Plateau" beneath the volcanic front [*Bowland and Rosencrantz*, 1988; *Bowland*, 1993; *Sallarès et al.*, 1999; *Walther et al.*, 2000; *Sallarès et al.*, 2001; *Auger et al.*, 2007; *Flueh and von Huene*, 2007; *MacKenzie et al.*, 2008]. This interpretation is consistent with geochemical results, which preclude a continental origin for the arc basement [*Feigenson et al.*, 2004], though an on-going continentalization of an oceanic basement has been suggested by some authors [e.g. *Vogel et al.*, 2004]. Geochemistry of recent adakitic magmatism observed in Panama [e.g. *Goss and Kay*, 2006] may further support the presence of an oceanic plateau under the arc as suggested by *Rausch and Wörner* [2007]. Since the introduction of a "Caribbean sill event" model by *Burke et al.* [1978], the idea of a South Central American Arc developing on the edge of a Caribbean Plateau is largely accepted and used in many models and interpretations (e.g. *Deering et al.*, 2007; *Wörner et al.*, in press; *Geldmacher et al.*, submitted). However, clear evidence validating this hypothesis has not been provided yet in southern Central America.

1.1.3.3. Subduction-related processes along the margin

The Costa Rican Margin is one of the most studied convergent margins around the world. Geophysical studies, drilling and dredging off Central America during the last two decades significantly improved our knowledge of the area and subduction processes, which are among the keys to the understanding of earthquake genesis. It has been postulated that no accretion is occurring at present along the margin and that the current regime of subduction is erosive [*Ranero and von Huene*, 2000; *Vannucchi et al.*, 2001, 2004].

On the other hand, the on-land geology of Costa Rica documents a history of accretionary events that spans the last 100 Ma. It is well-documented that oceanic plateaus, seamounts and trench-fill sediments accreted since the Aptian-Cenomanian in northernmost Costa Rica [Santa Elena, *Baumgartner and Denyer*, 2006] and since the late Campanian in the Nicoya Peninsula [*Schmidt-Effing*, 1979; *Denyer and Baumgartner*, 2006; *Bandini et al.*, in press]. Towards central and southern Costa Rica accretionary events have been dated as middle to late Eocene [Quepos, *Baumgartner et al.*, 1984; *Denyer et al.*, 2006] and range from late Cretaceous to middle

Miocene in the Osa area [*Di Marco et al.*, 1995; *this study*]. In western Panama accretionary processes may have initiated in late Cretaceous and continued at least until middle Eocene [*this study*]. Hence, the southern Central America provides a good opportunity to study unusual rock exposures that are susceptible to provide important constraints on accretionary processes, and to make some comparison with on-going processes along the subduction zone.

1.2. Objectives and Method

1.2.1. Objectives

This study was primarily designed to better understand the geology of uplifted portions of the outer margin between the southern Costa Rica (Osa Peninsula) and western Panama (Azuero Peninsula), over an area of ~450 km along-strike (Figure 1.3). Particular efforts were made to:

a) identify the arc basement (Chapter 2)

b) provide reliable constraints on the age of subduction initiation along the SW edge of the Caribbean Plate (Chapter 2)

c) recognize accreted fragments of seamount and define their origins and mode of emplacement along the margin (Chapters 3-5)

d) better constrain the evolution of the southern Central American margin between the late Cretaceous and Eocene (~50 Ma-long history) (summarized in Chapter 7).

1.2.2. Analytical techniques

This study was carried out on the basis of a multidisciplinary approach, combining (1) extensive field work (~6 months duration), (2) comprehensive rock sampling (>350 samples, complementing previous sampling by *Buchs and Stucki* [2001] and *Buchs* [2003] in southern Costa Rica, thin sections and location data will be deposited at the Geologic Library, Lausanne University), a geochemical study of the igneous rocks (Appendix), remote tectonic analyses and biochronologic dating of the formations. Biochronologic datings were integrally performed by C. Baumgartner-Mora, P.O. Baumgartner, A.N. Bandini, S.-J. Jackett and M.-O. Diserens at the Institute of Geology and Paleontology (University of Lausanne, Switzerland). This study partly benefited from the earlier works in the Osa Peninsula and Golfito area by *Buchs and Stucki* [2001] and *Buchs* [2003].

1.2.2.1. Field work

The area of study extends over forest reserves, national parks, poorly exploited woods and, in a minor proportion, grazing and cultivated lands. Most of the area is thus covered by vigorous tropical vegetation. Although some rocks are exposed along road cuts, fresh rocks are readily weathered and best outcrops are located along rivers and shorelines at low tide. Due to a poorly-developed road/track system the sites of study are generally distant of modern facilities. It is a challenging situation to carry out a geological survey. Over six months of field work have been required to gather observations and samples used in this study.

Along the shores and rivers, stratigraphic sequences are discontinuously exposed. Apart of the tropical environment, this is due to a very active tectonics in the area. GIS-supported

satellite imagery allowed us to identify fault patterns. On the field the faults were often recognized by the presence of landslides. Faulted zones are also frequently characterized by gaps of exposure due to a very efficient weathering in deformed rocks.

In order to define the tectonostratigraphy of the studied area we made local observations that were progressively integrated in a broader geological scheme with the help of geochemistry. Our mapping was based on on-site observations as well as boulder occurrences in the river beds. This technique allowed us to map some of the most remote areas at the scale of drainage basins and to *literally* track tectonostratigraphic contacts. Although boulders in the river beds were used to track lithologic contacts, virtually all the samples were collected in place.

1.2.2.2. Geochemical analyses

Igneous samples were chosen for their relative freshness on the basis of microscope observations of glasses and minerals. Samples were cut, crushed and reduced into powder at the Institute of Mineralogy and Geochemistry, University of Lausanne. Rock powders were prepared with a tungsten carbide mill. Replicate analyses of some depleted samples prepared with an agate mill shown that, apart of Ta, the use of the tungsten carbide mill did induced contamination (Ta was not used in geochemical interpretations). 6.000 g. of Li-tetraborate was added to 1.200 g. of rock powder and fused in a Pt crucible to obtain lithium tetraborate glass beads. Whole-rock major element abundances were determined on the lithium tetraborate glass beads using a Philips PW2400 XRF spectrometer at the Institute of Mineralogy and Geochemistry, University of Lausanne. Major and minor element contents were recalculated on an anhydrous base for interpretations. Trace element contents were determined using a LA-ICP-MS instrument equipped with a 193 nm ArF excimer laser (Lambda Physik, Germany) interfaced to an ELAN 6100 DRC quadrupole ICP-MS (Perkin Elmer, Canada) at the Institute of Mineralogy and Geochemistry, University of Lausanne. Operating conditions of the laser included a 170 mJ output energy, 10 Hz repetition rate and 120 μm ablation pit size. Helium was used as a cell gas. Dwell time per isotope ranged from 10 to 20 ms, peak hopping mode was employed. An SRM 612 glass from NIST was used as an external standard. 3 ablations per tetraborate glass bead were made to obtain the trace element contents. Results are presented in Appendix C.

Major element compositions of clinopyroxenes, plagioclases and melt inclusions contained in the studied volcanic rocks were determined by wavelength-dispersive analysis on a CAMECA SX50 and a JEOL JXA-8200 electron microprobe at the Institute of Mineralogy and Geochemistry, University of Lausanne. Control measurements performed on both instruments show consistent results. The microprobes were operated at 15 kV with beam 20 nA currents for the clinopyroxenes. 15 kV and 7 nA were used for plagioclases and melt inclusions. Counting times were 10 s for alkalis and silicon and 15-20 s for other elements. Data were reduced with the PAP program. Trace element abundances were further determined using the LA-ICP-MS instrument at the Institute of Mineralogy and Geochemistry, University of Lausanne. Operating conditions of the LA-ICP-MS were largely similar to those used for the tetraborate glass beads. The pit size was set at 80 μm. The repetition rate and other parameters did not change. Results are presented in the Appendix.

Due to lack of time, isotopic analyses of basaltic rocks initially planned to be performed in this study were restricted to six "pilot samples" from the Osa Igneous Complex. The analyses were performed on whole rock powders prepared in an agate mill at the Universiy of Lausanne. Powders were leached and both leachates and residues analyzed at the Department of

Mineralogy (University of Geneva) to obtain U-Pb, Rb-Sr, and Sm-Nd isotope compositions. Leaching procedure was similar as in *Chiaradia and Fontboté* [2003]. Differences of isotopic composition between leachates and residue rock fractions allowed us to identify samples that potentially suffered from alteration processes. As a result, Pb and Sr isotope compositions were not taken into account for interpretations.
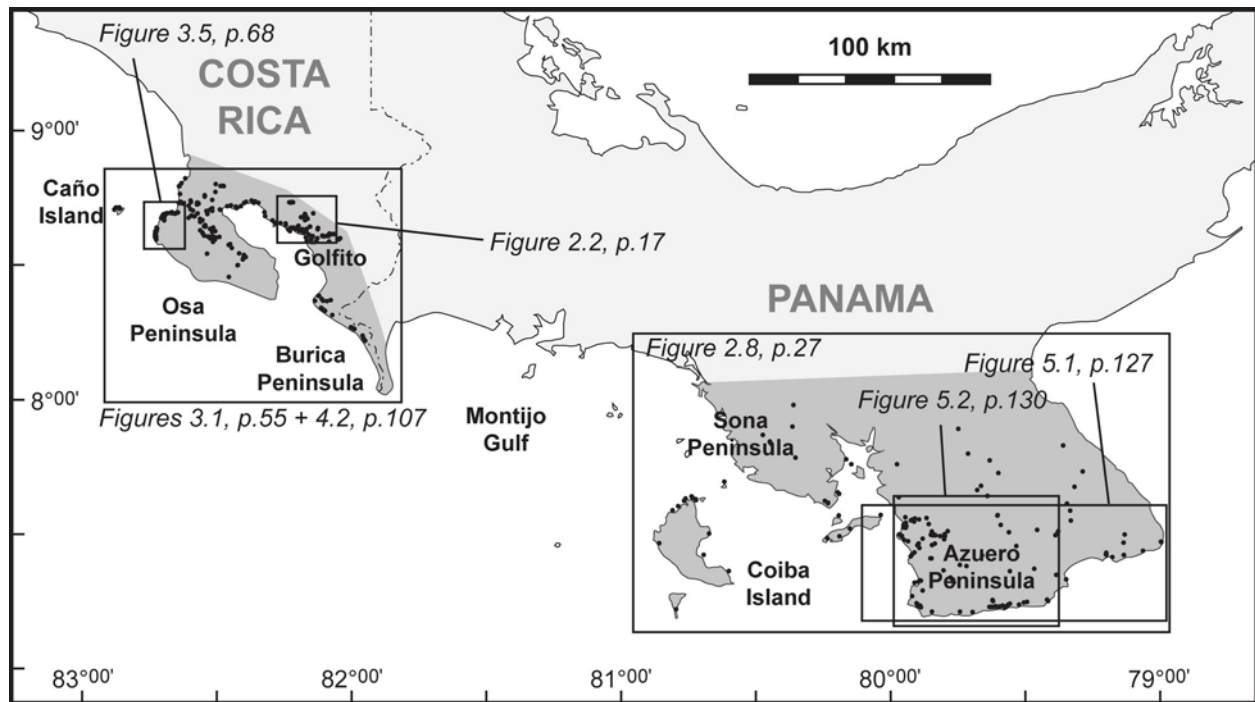
Figure 1.3: *localisation of maps shown in following chapters. Dark grey fields represent the area of study. Black circles are samples used during this study, partly recovered by Buchs and Stucki [2001] and Buchs [2003] in the Osa Peninsula and Golfito area.*

Chapter 2: Late Cretaceous Arc Development along the SW Caribbean Plate: Insights from the Golfito Complex (Costa Rica) and Azuero Complex (Panama)

This chapter is based on a manuscript submitted for a publication in G3 (Geochemistry, Geophysics, and Geosystems) that should be ultimately part of a G3 thematic publication on the geology of Central America. Chapter 2.7.3 will be further developed and submitted as an independent manuscript to Geology.

2.1. Introduction

Volcanic arcs are complicated geological systems that evolve through time in response to many parameters chiefly depending on the nature of the subducting plate and regional tectonic/geodynamic regime [e.g. *Pearce and Peate*, 1995]. Although each volcanic arc is characterized by a unique history, a similar scheme of evolution is observed. The earliest stage of evolution of an arc is associated with subduction initiation and is notably characterized by "primitive" supra-subduction magmas. Next stages of the evolution are characterized by a quick replacement of the primitive arc by a more mature, durable supra-subduction system. Finally, ultimate stages of the arc evolution occur when the arc accretes along a convergent margin or subducts. Proto-arc rocks produced during the first stage are generally difficult to study because they often become rapidly buried under younger deposits of the mature arc. Although some contributions detailed the nature of such proto-arc lavas [e.g. *Stern and Bloomer*, 1992] there is still a strong need for stratigraphic and geochemical studies dedicated to the understanding of infant arc systems.

Southern Central America comprises some of the most studied volcanic arc/front and related subduction zone in the world. Significant efforts have been made to explore the subduction factory through geophysical and geochemical studies [e.g. *Ranero and von Huene*, 2000; *Hoernle et al.*, 2008], whereas constraints arising from the geological record of the early history of the area has remained relatively poorly exploited. We present here new geological and geochemical results that provide a new insight into the origins of the southern Central American Arc. New constraints are given for the initiation of the subduction, the nature of the arc basement and paleogeography of the late Cretaceous inter-American area.

2.2. Previous constraints on the South Central American arc initiation

Although Tertiary arc volcanism in southern Central America has been studied for a long time [e.g. *de Boer et al.*, 1995], the initiation of the arc has been poorly constrained, because older arc products are buried under younger volcanism (Costa Rica) or are located in remote and hardly-accessible areas (eastern Panama) (Figure 1.2). In northern Costa Rica (Nicoya Peninsula), early petrographic studies on the sediments have shown that Albian to Paleogene detrital deposits contain arc-derived grains [*Lundberg*, 1982, 1991; *Rivier*, 1983; *Baumgartner et al.*, 1984; *Astorga*, 1987; *Calvo and Bolz*, 1994]. Pebbles of igneous rocks from detrital deposits of Punta Samara (Nicoya Peninsula) were interpreted to represent a record of primitive arc

magmatism in southern Central America [*Patino et al.*, 2004]. However, in all the previous contributions, the age of the sediments was poorly constrained. New comprehensive tectonostratigraphy of the Nicoya Peninsula shows that the earliest record of arc-derived material is Coniacian [*Flores*, 2003; *Bandini et al.*, 2008]. This material is however unrelated to the latest Cretaceoous to Tertiary volcanic arc of southern Central America and was probably produced by an intra-oceanic volcanic arc in the Pacific realm [*Baumgartner et al.*, 2008]. Igneous pebbles from Punta Samara analyzed by *Patino et al.* [2004] (undefined age) are sedimentarilly associated with boulders of Paleocene shallow-water limestones [*Flores*, 2003] and, thus, may be post-Cretaceous and unrelated to the earliest history of the South Central American Arc. In southern Costa Rica, upper Campanian arc-derived tuffaceous sediments are exposed in the back-arc area [*Mende*, 2001] close to contemporaneous differentiated volcanic rocks [*Fisher and Pessagno*, 1965]. In the forearc area, the oldest reported occurrence of arc-derived sediments is Paleocene [*Di Marco*, 1994]. In Panama, new ^{40}Ar/^{39}Ar ages of arc-related igneous rocks [*Lissinna et al.*, 2002, 2006; *Lissinna*, 2005; *Wörner et al.*, 2005, 2006, in press] are in good accordance with previous stratigraphic and geochemical contributions [*Del Giudice and Recchi*, 1969; *Maury et al.*, 1995] and indicate that the arc is as old as the Maastrichtian (66 Ma). On the basis of ages and geochemical constraints from central and western Panama *Wörner et al.* [in press] propose that the "early" 66 Ma arc rocks were emplaced on top of the CLIP and indicate a large spectrum of mantle compositions at the onset of arc magmatism. In contrast we show in this paper that the onset of arc magmatism occurred at least 7 Ma prior to 66 Ma, in the late Campanian (~75-73 Ma). We further provide the first stratigraphic observations and geochemical data from southern Costa Rica and western Panama showing that proto-arc intrusives and lavas emplaced into and on top of a late Cretaceous oceanic plateau and that the earliest supra-subduction magmas were probably produced by little input of slab-derived fluid into the still-hot lithospheric mantle associated to the oceanic plateau.

2.3. Geologic review of the Golfito and Azuero complexes

2.3.1. The Golfito Complex

The Golfito Complex is located in southern Costa Rica between the Tertiary Fila Costeña Thrust Belt [*Morell et al.*, 2008] and the late Cretaceous-Eocene Osa-Burica Accretionary Igneous Complex (Chapter 3) (Figures 1.2, 2.2).

The Golfito Complex is composed of a sequence of late Cretaceous to Tertiary volcanic rocks, hemipelagic sediments and volcano-sedimentary deposits [*Dengo*, 1962; *Schmidt-Effing*, 1979; *Obando*, 1986; *Di Marco*, 1994; *Di Marco et al.*, 1995]. The stratigraphy has been subdivided by *Di Marco et al.* [1995] into three tectonostratigraphic units: (1) an Igneous Basement, composed of pre-late Campanian lava flows, (2) the Golfito Formation, a volcano-sedimentary sequence made of interlayered lava flows and late Campanian to middle Maastrichtian sediments, and (3) the Achiote Formation, a middle Maastrichtian to Paleocene volcaniclastic-tuffitic sequence, containing material related to acidic volcanism. Although recent tectonics affected the pristine arrangement of these tectonostratigraphic units, they are considered to form a continuous sequence from the late Cretaceous to the Paleocene [*Di Marco*, 1994; *Di Marco et al.*, 1995]. Some of the sediments of the Golfito Formation were deposited synchronously to the emplacement of the basaltic lava flows, as indicated by the occurrences of

hemipelagic limestone xenoliths within the lavas and dykes crosscutting hemipelagic sediments [*Obando*, 1986; *Di Marco*, 1994].

The lavas include basalt, basaltic andesite, basaltic trachyandesite and trachyandesite [*Di Marco*, 1994; *Hauff et al.*, 2000], which are globally badly preserved and suffered from low-T alteration [*Di Marco*, 1994]. Geochemical affinities similar to the CLIP are suggested by trace elements and radiogenic isotopes [*Hauff et al.*, 2000].

Paleomagnetic data from the Golfito Complex indicate it formed at ~5°N [*Frisch et al.*, 1992; *Di Marco et al.*, 1995]. The complex is thus located now under similar latitude or ~4° degrees further north than at the time of its formation. This is unlike other plateau-like igneous complexes of Costa Rica, such as the Nicoya and Burica complexes, which formed in the southern hemisphere between ~6°S and ~17°S respectively [*Di Marco et al.*, 1995].

Several interpretations for the origin of the Golfito Complex have been proposed. On the basis of geochemical results, the complex was interpreted to represent an uplifted piece of a Caribbean oceanic plateau basement [*Hauff et al.*, 2000], an accreted plateau segment [*Denyer et al.*, 2006] or an accreted paleo-Galapagos hotspot track [*Hoernle and Hauff*, 2007]. *Di Marco et al.* [1995] proposed that the complex could represent a marginal piece of the Caribbean oceanic plateau transported northward by strike slip along the rim of the Caribbean Plate.

2.3.2. The Azuero Complex

The Azuero Complex is defined herein as the ensemble of exposures and terranes delimited by the Sona Peninsula, Azuero Peninsula and Coiba Island (Figure 1.2).

Attempt of comprehensive stratigraphy associated with a mapping at 1:250'000 scale of the Azuero Complex was originally made for mining purposes by *Del Giudice and Recchi* [1969]. These authors proposed a regional stratigraphy based on a correlation of paleontologic dates and rock facies which has been re-used and adapted in more recent contributions. Following these contributions, the Azuero Complex can be subdivided into two lithostratigraphic groups: (1) an Igneous Basement made of ultramafic-mafic to silicic igneous rocks, associated with minor volumes of sediments and metamorphic rocks, and (2) shallow-water limestone and volcano-sedimentary sequences stratigraphically overlying the Igneous Basement.

2.3.2.1. Igneous basement

Ultramafic-mafic igneous rocks from the basement occur predominantly in SW Azuero, south Sona and Coiba Island. They are composed of basalt, picrite, gabbro, agglomerate, diabase and minor occurrences of sediments [*Del Giudice and Recchi*, 1969; *Kolarsky et al.*, 1995b; *Lissinna*, 2005; *Hoernle and Hauff*, 2007]. Along the Rio Torio (Azuero), lava flows are interbedded with hemipelagic limestones containing Campanian-Maastrichtian (84-66 Ma) pelagic foraminiferans [*Del Giudice and Recchi*, 1969; *Tournon et al.*, 1989]. At Torio Beach, interbedded radiolarites within massive and pillowed lavas flows have a Coniacian age (89-85 Ma) [*Kolarsky et al.*, 1995b; ranges of radiolarian ages revised in *Buchs et al.*, submitted]. $^{40}Ar/^{39}Ar$ ages of the ultramafic-mafic igneous basement range from 115 to 21 Ma and, thus, comprise paleontological ages [*Hoernle et al.*, 2004; *Lissinna*, 2005; *Hoernle and Hauff*, 2007; *Hoernle*, written communication, 2008]. A $^{40}Ar/^{39}Ar$ age of ~115 has been obtained for a pillow basalt near Playa Venado (Azuero) [*Lissinna*, 2005; *Hoernle*, written communication, 2008], which complements previous K/Ar date of ~98 Ma [*Bourgois et al.*, 1982]. Ultramafic-mafic

suites of the basement have plateau-like and OIB-like geochemistry and have been interpreted to belong to the CLIP and accreted pieces of the paleo-Galapagos hotspot track, respectively [*Hoernle et al.*, 2002, 2004; *Lissinna*, 2005; *Hoernle and Hauff*, 2007; *Wörner et al.*, in press]. Structural relationships between these two types of igneous rocks and their distribution in the Azuero Complex have not been characterized yet. Paleomagnetic data from the Rio Güerra (Azuero) obtained in late Cretaceous hemipelagic limestones on the top of mafic igneous rocks indicate that these sediments formed at ~2°N, in similar paleolatitudes than the Golfito Complex [*Di Marco et al.*, 1995] and SW Caribbean Plate (Colombian Basin) [*Acton et al.*, 2000].

Intermediate to differentiated lavas and related intrusives are exposed mostly in the central and northern Azuero Complex [*Del Giudice and Recchi*, 1969; *Metti and Recchi*, 1972; *Kolarsky et al.*, 1995b; *Lissinna*, 2005; *Wörner et al.*, in press]. These igneous rocks have typical arc-related geochemical signatures and represent an extinct volcanic arc [*Lissinna*, 2005; *Wörner et al.*, in press]. The intermediate to differentiated igneous rocks are locally stratigraphically associated with volcanic sediments and tuffites [*Del Giudice and Recchi*, 1969]. A K/Ar age of 69±10 Ma was obtained for a quarz-diorite from La Pitalosa (Azuero) [*Del Giudice and Recchi*, 1969]. In the same area, hemipelagic limestones similar to the late Cretaceous limestones from the Rio Torio are observed, with a variable detrital and tuffitic component [*Del Giudice and Recchi*, 1969]. $^{40}Ar/^{39}Ar$ ages of the igneous arc rocks range from ~ 66 to 40 Ma [*Lissinna*, 2005; *Wörner et al.*, in press]. An age trend is observed throughout the Azuero Complex and western Panamean Isthmus, with youngest $^{40}Ar/^{39}Ar$ ages in the north and oldest ages in the south (schematically illustrated on Figure 1.2). On the basis of these ages, it has been proposed that a progressive shift of the volcanic front toward the Caribbean Plate occurred during the Tertiary, possibly as a response to subduction erosion and/or slab flattening [*Lissinna et al.*, 2002].

Metatuff, metabasalt and metabasite pertaining to the Igneous Basement were found along the Rio Torio (Azuero) and Rio San Rafael (Sona) [*Del Giudice and Recchi*, 1969; *Tournon et al.*, 1989]. The metamorphic rocks reached amphibolite facies and were partly retromorphosed to greenschist facies in Azuero. They followed an anticlockwise P-T path prograde from low T/low P to medium T/high P in Sona and low to medium T/low P in Azuero [*Tournon et al.*, 1989]. In both sites the metamorphic rocks are cut by younger unmetamorphosed dolerites and are unconformably overlain by late Cretaceous limestones in the Rio Torio [*Del Giudice and Recchi*, 1969; *Tournon et al.*, 1989]. According to *Del Giudice and Recchi* [1969], the age of the limestones represents a maximal age of formation for the metamorphic rocks. *Tournon et al.* [1989] reported major and minor element compositions for some amphibolites. However, immobile trace element compositions are still required to better characterize affinities and origins of the protoliths.

2.3.2.2. Overlap sequences

Sediments unconformably resting on the Igneous Basement (overlap sequences) are composed of the lower Eocene to lower Miocene Tonosi Formation (south Azuero Complex) and by the Neogene Macaracas Formation (north Azuero Complex) [*Recchi and Miranda*, 1977; *Kolarsky et al.*, 1995b; *Krawinkel et al.*, 1999].

The Tonosi Formation is roughly composed of a ~2000m thick turbiditic sequence with minor occurrences of shallow-water carbonate and detrital deposits [*Kolarsky et al.*, 1995b]. Transgressive lower to middle Eocene conglomerate, sandstone and shallow-water limestone constitute the base of the sequence, which rests on the top of the Igneous Basement both onland

and offshore, between the Coiba Island and Azuero Peninsula. The Tonosi Formation was subdivided into two major lithologic units [*Kolarsky et al.*, 1995b]. The age of the lower unit is early Eocene to early Oligocene (~55 to 30 Ma) and was deposited in shallow-water, paralic environments [*Kolarsky et al.*, 1995b; *Krawinkel et al.*, 1999]. The upper unit has a late Oligocene to early Miocene age (~30 to 15 Ma) and was deposited in a deeper forearc environment [*Kolarsky et al.*, 1995b; *Krawinkel et al.*, 1999]. Facies and compositional changes between the two units are observed and result from variations of the forearc environment in response to tectonics [*Krawinkel et al.*, 1999].

The Macaras Formation crops out in northern Azuero and is composed of tuffite, arenite and recifal limestones deposited in neritic and terrestrial environments [*Geological Map of Panama*, 1991; *Krawinkel et al.*, 1999].

2.4. Results

This chapter presents our most important results on the Golfito and Azuero complexes. A revised tectonostratigraphy is provided for the two complexes on the basis of new stratigraphic observations and age constraints. Basic structural arrangements, sediments and volcanic rocks are described. New geochemical data are presented for the igneous rocks.

2.4.1. Golfito Complex

2.4.1.1. Tectonostratigraphy

Lithological associations recognized during this study concord with previous stratigraphic observations in the area. The Golfito Complex is composed of (1) an igneous basement, (2) the Golfito Formation and (3) the Achiote Formation [*Obando*, 1986; *Di Marco*, 1994; *Di Marco et al.*, 1995] (Figure 2.1).

A new sedimentary facies was recognized in the SE area of the complex [*Alvarado G.*, 2002, oral communication, Campaña Geológica Escuela Centroamericana] and is defined here as the Monita lithostratigraphic unit (Figure 2.1). This unit is made of siliceous, tuffaceous laminated mudstones (mostly distal turbidites) with frequent interbeds of carbonate mass flows that range from dm-thick calciturbidites to m-thick cobbly carbonate debris flows. The carbonate clasts of the latter formed in a shallow carbonate bank environment. Biomicrites contain fragments of red algae, benthic foraminifera, echinoderms, mollusk shells and bryozoans. Locally, rodoliths are found in large quantities and form rodolithic debris flows interlayered with the other sediments. Biogenic grains found in the mudstones are sponge spicules, pelagic Foraminifera and echinoderms. They contain a tuffaceous component which is made of fine ash. Small-sized (<5 cm) rounded clasts of volcanic sediments and tuffites are observed. Veins of chalcedony possibly resulting from the dissolution of siliceous sponge spicules in the mudstones are frequently found in the calcareous lithologies. This lithostratigraphic unit shares the tuffaceous lithologes with the Achiote Formation and possibly rests with a transitional contact on the latter. Sedimentary structures indicate a deeper marine slope environment beneath shallow carbonate banks. Fossil associations found in the Monita lithostratigraphic unit differ from those of the Fila de Cal Formation [e.g. *Yuan*, 1984, 1991]. Limestone clasts show packstones with *Lithothamnium*, incrusting Foraminifera, few planktonic Globigerinacea and the following larger benthic Foraminifera: *Helicolepidina nortori, Lepidocyclina* sp., *Pseudophragmina* sp.,

Helicostegina sp., squizont forms of *Nummulites* sp. *Sphaerogypsina* sp., *Asterocyclina* sp., *Asterocyclina asterisca*, *Eofabiania* sp., *Fabiania* sp. and *Dictyoconus* sp. This assemblage is characteristic of a late Eocene age.
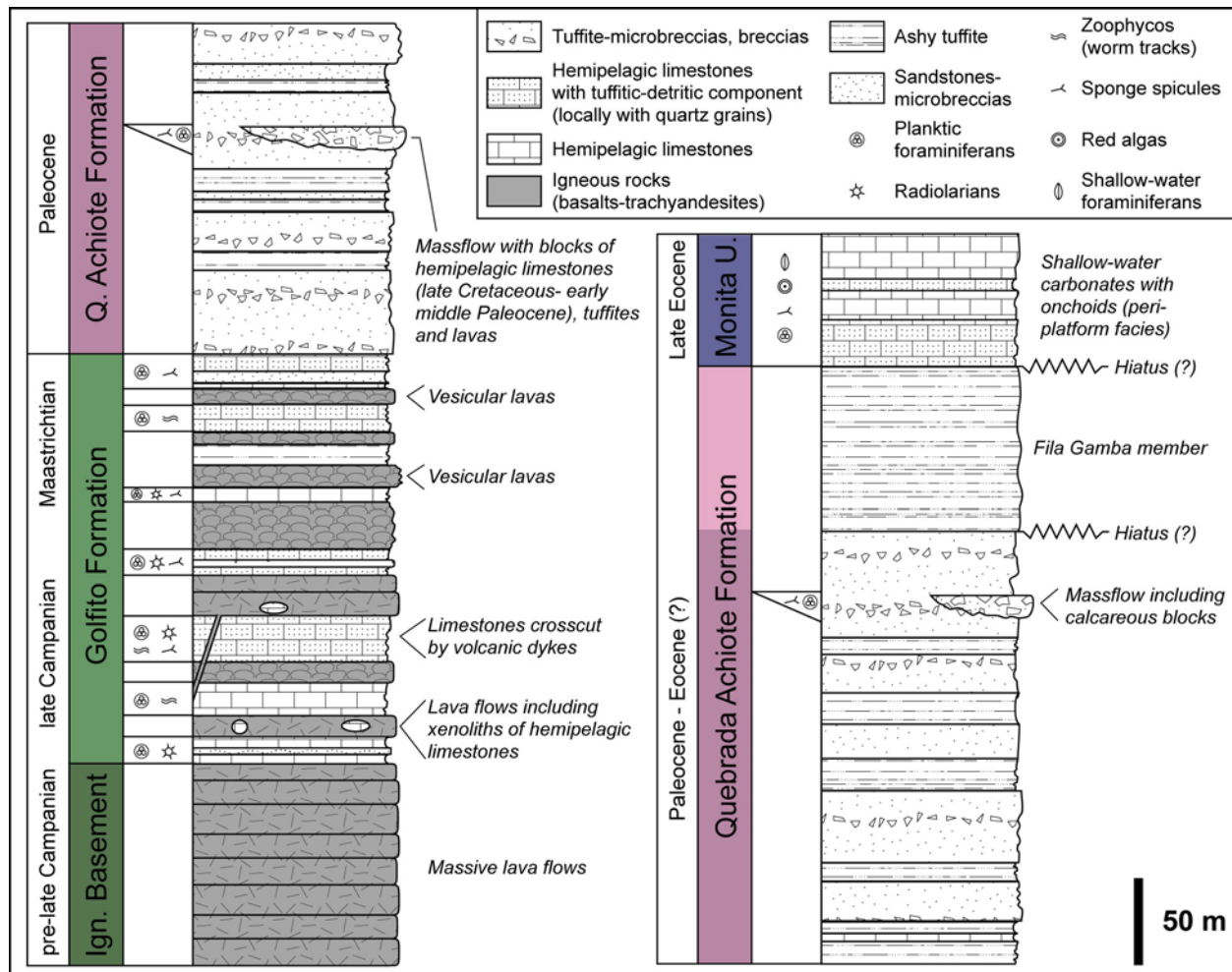
Figure 2.1: *Synthetic tectonostratigraphy of the Golfito Complex (modified after Di Marco, [1994]). Monita U.=Monita lithostratigraphic unit.*

2.4.1.2. Structural arrangement

Spatial arrangement of the tectonostratigraphic units is controlled by a complicated fault system [*Mende and Astorga*, 2007] that defines fault-bounded blocks (Figure 2.2). Contact of the Golfito Complex with accreted fragments of plateau and seamounts of the Osa Igneous Complex (Chapter 3) occurs along a recent subvertical fault that likely reactivated an older thrust zone and erased original structural relationships. Contact of the Golfito Complex with accreted fragments of plateau of the Burica Peninsula (Chapter 3) is buried under younger tuffaceous and alluvial deposits. Orientation of the rivers, topographic highs and scarps are linked to the fault system [*Mende and Astorga*, 2007].

During our mapping, we recognized that the fault-bounded blocks have been variously uplifted and tilted, exposing both superficial and deep parts of the stratigraphic sequence. Occurrence of folds or related structures (e.g. fold cleavage) has not been observed, indicating that the complex chiefly behaved brittely during the deformation. This is similar to occurrence of

fault-bounded blocks in the Osa Peninsula that have been related to the subduction of the Cocos Ridge [*Sak et al.*, 2004]. Hence, the structural patterns of the Golfito Complex seem to be controlled by the recent entrance of the Cocos Ridge into the subduction zone.

The intensity of uplift of the Golfito Complex is not well constrained. However, we note that in many places younger deposits have been eroded and deeper parts of the stratigraphic sequence (such as the Igneous Basement) are exposed. Degree of erosion is higher in blocks located along major faults. This indicates that the complex is likely composed of a deep portion of the inner forearc.
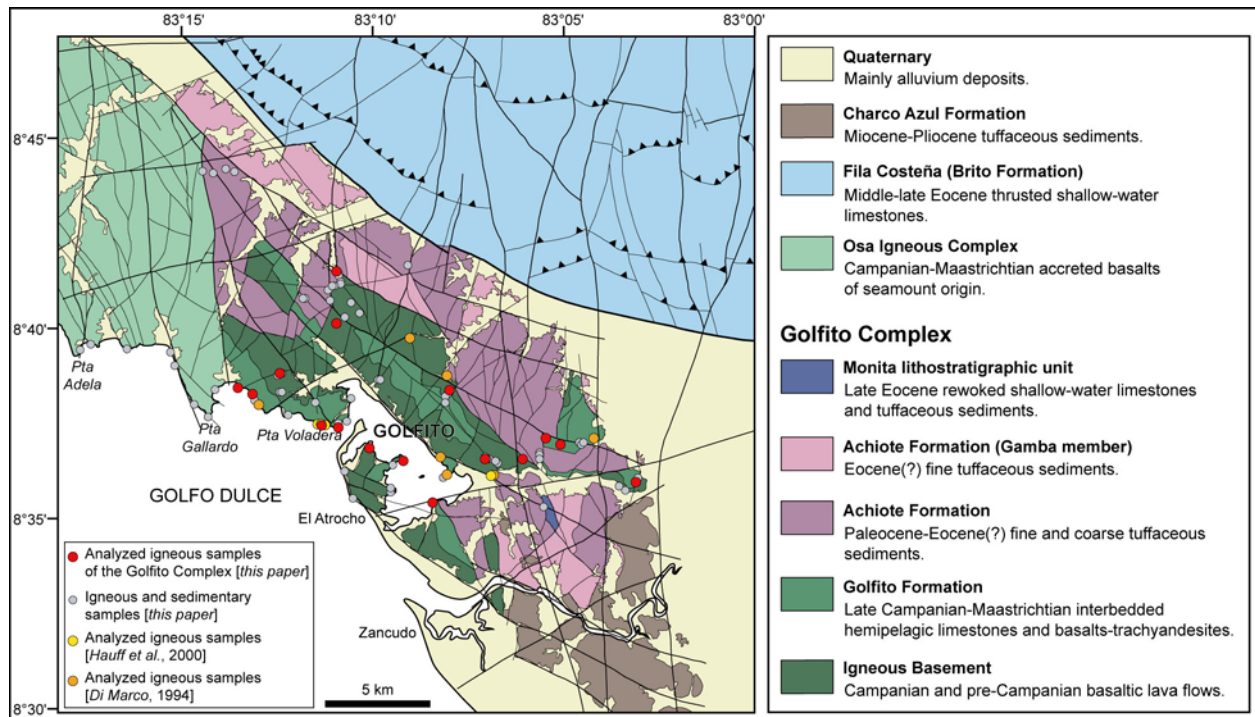
Figure 2.2: *Geological map of the Golfito Complex. Faults based on Mende and Astorga [2007]. Geology modified after Di Marco [1994] and Mende and Astorga [2007].*

2.4.1.3. Sedimentary rocks

The oldest rocks found in the Golfito Complex are composed of mafic-intermediate igneous massive lava flows and associated autobreccias of the Igneous Basement (Figure 2.1). Although an absolute age has not been defined for these rocks, the Igneous Basement is stratigraphically underlying the late Cretaceous Golfito Formation and, thus, is sub-contemporaneous or anterior to this formation. A stratigraphic continuity between the Igneous Basement and the Golfito Formation is also supported by geochemical results (see Chapter 2.4.1.3).

The oldest sediments of the Golfito Complex are composed of grey to reddish hemipelagic limestones of the Golfito Formation (Figure 2.1). These sediments occur mostly as plurimetric beds interlayered in massive and pillowed lava flows. In some cases, they are found as xenoliths within massive lava flows (chilled margins are observed) or are crosscut by mafic dykes [*Obando*, 1986; *Di Marco*, 1994; *this study*] (Photo 2.1). Ages of deposition of the sediments and lavas are thus well defined by pelagic foraminiferan associations found in the hemipelagic limestones. The ages range from the late Campanian to the Maastrichtian (75-66

Ma) [*Di Marco*, 1994]. Pelagic foraminiferans are commonly broken in the sediments, indicating a partial reworking by bottom sea currents. Zoophycos ichnofossils are frequent in the micritic sediments [*Di Marco*, 1994].

Pluricentimetric angular fragments of mafic rocks are locally embedded within the hemipelagic limestones of the Golfito Formation. The fragments share similar petrographic characteristics with the igneous rocks of the Igneous Basement and Golfito Formation, indicating that some of the lava flows pertaining to these units were partly reworked during the late Cretaceous. The record of mafic detrital input is also represented by numerous plagioclase and clinopyroxene fragments observed in the hemipelagic limestones.

In the Golfito Formation, an intermediate-siliceous detrital input is also recognized. In some hemipelagic limestones, scarce quartz fragments are notably observed. Toward the top of the formation, a greenish-bluish tuffaceous component made of fine ash volumetrically increases and becomes particularly important in the Maastrichtian (Figure 2.1). In regard to the presence of fine tuffites, it is clear that the Golfito Formation deposited in the vicinity of a subaerial explosive volcanism. This is in good agreement with observation of sponge spicules in the hemipelagic limestones, which attests a near-shelf environment of deposition for these sediments. Interestingly, we observed that the tuffaceous component increases while thickness and frequency of occurrence of the lava flows diminish. The size of the tuffaceous clasts increases toward the top of the sequence and becomes particularly large in the Achiote Formation (see below). Hence, vanishing of the submarine mafic-intermediate volcanism of the Golfito Formation was accompanied by a progressive development of a more acidic subaerial volcanism in the vicinity.

The Paleocene-Eocene Achiote Formation [*Di Marco*, 1994] is characterized by tuffaceous and detrital deposits in absence of lava flows (Figure 2.1). The tuffaceous component is composed of fine ashes, large (>1 cm) pumice fragments and euhedral acicular plagioclases of possible fallout origin (Photo 2.2). The detrital component is made of fragments of intermediate to silicic volcanic clasts (andesites-dacites), zoned plagioclases, greenish clinopyroxenes, brownish amphiboles, rounded quartz with corrosion embayments, echinoderms and reworked sediments. Petrographic observations are thus consistent with further development of a subaerial intermediate-acidic volcanism in the vicinity of the Golfito Complex after the Maastrichtian. The age of the Achiote Formation is given by blocks of reworked Paleocene hemipelagic limestones embedded in the detrital deposits [*Di Marco*, 1994], as well as by ages of under- and overlying formations.

The stratigraphic development of the Golfito Complex ends with the deposition of the late Eocene Monita tectonostratigraphic unit. The lithologic and petrographic characteristics of this unit (Chapter 2.4.1.1) indicate that the intermediate-acidic volcanism in the vicinity of the Golfito Complex was still active in the late Eocene.

2.4.1.4. *Volcanic rocks*

Volcanic rocks ranging from basalts to trachyandesites occur as thick (~10 m) massive to thin pillowed lava flows. Mineral assemblage of the lavas is composed of subhedral plagioclase, euhedral clinopyroxene and Fe-Ti oxides. Pristine or altered olivines have not been observed. The thicker lava flows have a coarse intersertal to subophitic fabric. Although these igneous rocks are clearly effusive, their coarse mineralogy makes them very similar to microgabbros. The thin lava flows have globally a similar mineralogy and fabric than thick flows, with finer mineral

sizes. Some pillow lavas have a porphyric texture with clinopyroxene phenocrysts. Small-sized spherical vesicles (<3 mm) filled with calcite, zeolites and/or chlorite are observed in the thin lavas of the upper part of the Golfito Formation.

Replacement of pristine minerals by secondary phases during low-T alteration processes is observed throughout the complex. This type of alteration occurs in a much lower intensity in contiguous igneous complexes (i.e. the Osa Igneous Complex and the Burica Complex, Chapter 3). Interstitial glasses found in the lavas of the Golfito Complex are ubiquitously replaced by secondary phases such as chlorite or palagonite. All the plagioclases are argilitized and many clinopyroxenes are chloritized. In few samples, euhedral secondary quartz minerals are found in interstitial glass and in close proximity to granophyres (Photo 2.3).

2.4.1.5. Whole rock geochemistry

Due to the low-T alteration that affected the igneous rocks of the Golfito Complex, mobile elements (i.e. Cs, Rb, Ba, U, Pb, Sr, Na, K) were used with precautions. Samples bearing secondary quartz minerals and granophyres appeared to have an anomalously high silica content interpreted to reflect silica enrichments in the lavas by fluid flows or an assimilation of silica-rich melts or rocks by the basaltic magma. The extra silica content was likely drained from surrounding siliceous limestones into the lava flows. Hence, samples of igneous rocks with secondary quartz minerals were used only for comparisons of immobile trace elements. Geochemical data from previous contributions [e.g. *Hauff et al.*, 2000] are in good agreement with our results (Figures 2.3, 2.4a).

The lavas of the Golfito Complex have a larger range of SiO_2 content than other plateau-like igneous complexes in southern Central America, ranging from 50.6 to 58.1 wt% SiO_2. On a TAS diagram (Figure 2.3a), they show a restricted subalkaline trend, ranging from basalt to trachyandesite fields. This trend indicates that despite high alteration, some mobile elements (like Na and K) have not been extensively remobilized at a scale larger than a sample.

K_2O-SiO_2 and FeO^*/MgO-SiO_2 variations are consistent with a low K - medium Fe differentiation trend for the Golfito Complex (Figure 2.3b, c). MgO content ranges from 4.9 to 9.6 wt%. For decreasing MgO, FeO^* increases to reach a maximum at 4.5 wt% MgO, and then decreases in the most evolved lavas. For decreasing Mg# (Mg# = 100 x mol [MgO] / (mol [MgO] + mol [FeO^*])), TiO_2, Na_2O and K_2O increases (Figure 2.3e, Appendix) and CaO and Al_2O_3 decreases (Figure 2.3f, g). Previous observations indicate that the differentiation trend of the Golfito Complex is different than the trend of typical oceanic plateaus (such as the Nicoya Complex).

REE compositions of the Golfito Complex show plateau-like affinities broadly similar to the Nicoya Complex (Figure 2.4a). However subtle variations in the LREE content are observed. On a PM-normalized multielement diagram (Figure 2.5a), similar variations are present in the most incompatible immobile elements (i.e. Th and Nb). Rb, Ba, Pb and Sr contents show large variations between the lavas, indicating a possible remobilization of these mobile elements during the alteration or an influence of the source composition. Ti content is globally low and forms a negative anomaly on the multielement patterns. Similarly, a low Eu content is observed for some samples.

Variations of the most incompatible immobile elements in the Golfito Complex are best illustrated on a $(Nb/La)_{PMn}$-$(La/Sm)_{PMn}$ diagram (Figure 2.3h). On such a diagram, the Golfito
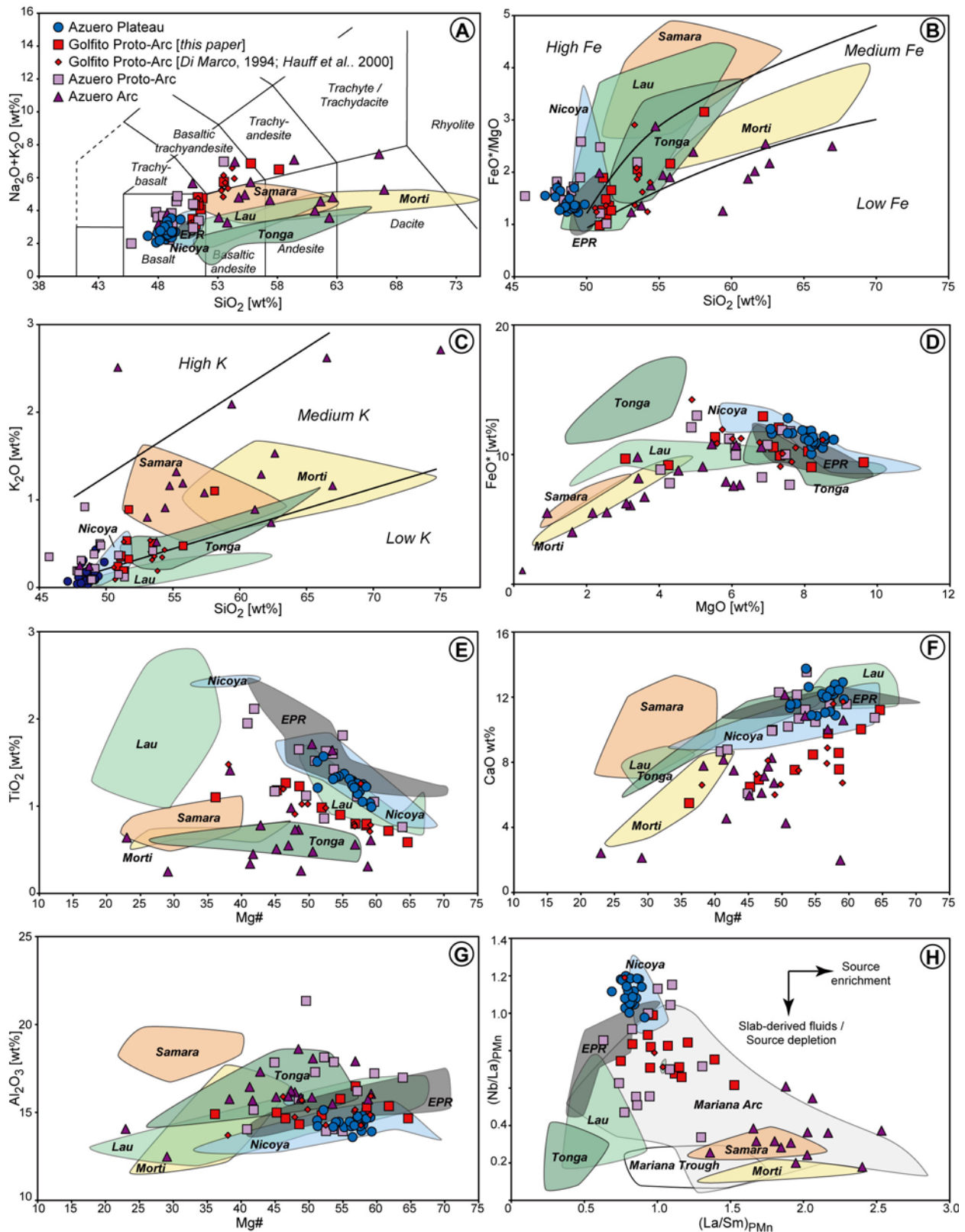
Figure 2.3: *Geochemistry of the igneous rocks of the Golfito and Azuero complexes, with comparison to "Samara Arc" [Patino et al., 2004], "Morti Arc" [Maury et al., 1995], East Pacific Rise MORBs (EPR) [Su and Langmuir, 2003], Nicoya Complex (oceanic plateau) [Hauff et al., 2000], Tonga Arc [Turner and Hawkesworth, 1997], Lau Basin [Turner and Hawkesworth, 1997], Mariana Arc and Trough [GEOROC online database]. A) TAS diagram after Le Maitre et al. [1989]. B) FeO*-SiO$_2$ diagram after Arculus [2003]. C) K$_2$O-SiO$_2$ diagram after Le Maitre et al. [1989]. E-F) Mg# = 100 x mol [MgO] / (mol [MgO] + mol [FeO*]). H) Primitive mantle after McDonough and Sun [1995]. Analyses were plotted on an anhydrous basis for figures A-G.*
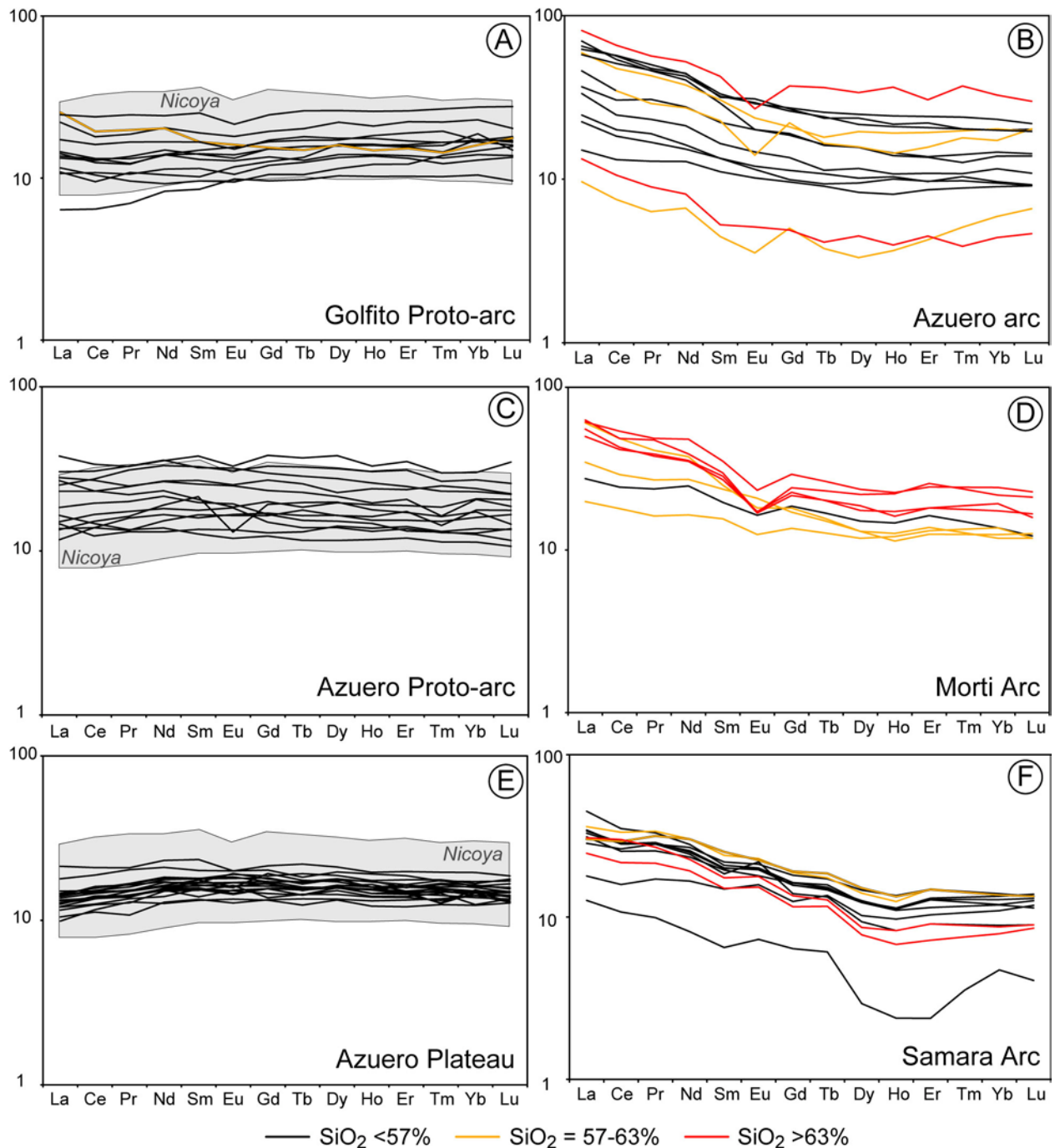
Figure 2.4: *Chondrite-normalized REE diagrams. Chondrite after McDonough and Sun [1995]. Samara Arc after Patino et al. [2004], Morti Arc after Mauri et al. [1995] and Nicoya Complex after Hauff et al. [2000].*

Complex form a trend bracketed at both ends by the fields of plateau-like igneous rocks (Nicoya Complex and Azuero Plateau) and early Tertiary arc-related igneous rocks from the Azuero Peninsula. Similar observation is made on MgO/FeO^*-SiO_2, FeO^*-MgO and TiO_2-$Mg\#$ diagrams, with a Golfito trend located between the trends of the plateaus suites and Azuero Arc (Figure 2.2).

The degree of differentiation of the lavas, as indicated by MgO and SiO2 contents or Mg#, correlates with the stratigraphic position of the samples. The most differentiated lavas are found in the upper Golfito Formation that contains the latest stage of volcanism and, conversely,

the less differentiated rocks are found in the Igneous Basement that forms the oldest part of the Golfito Complex. Clear temporal correlation has not been found in the trace element contents.
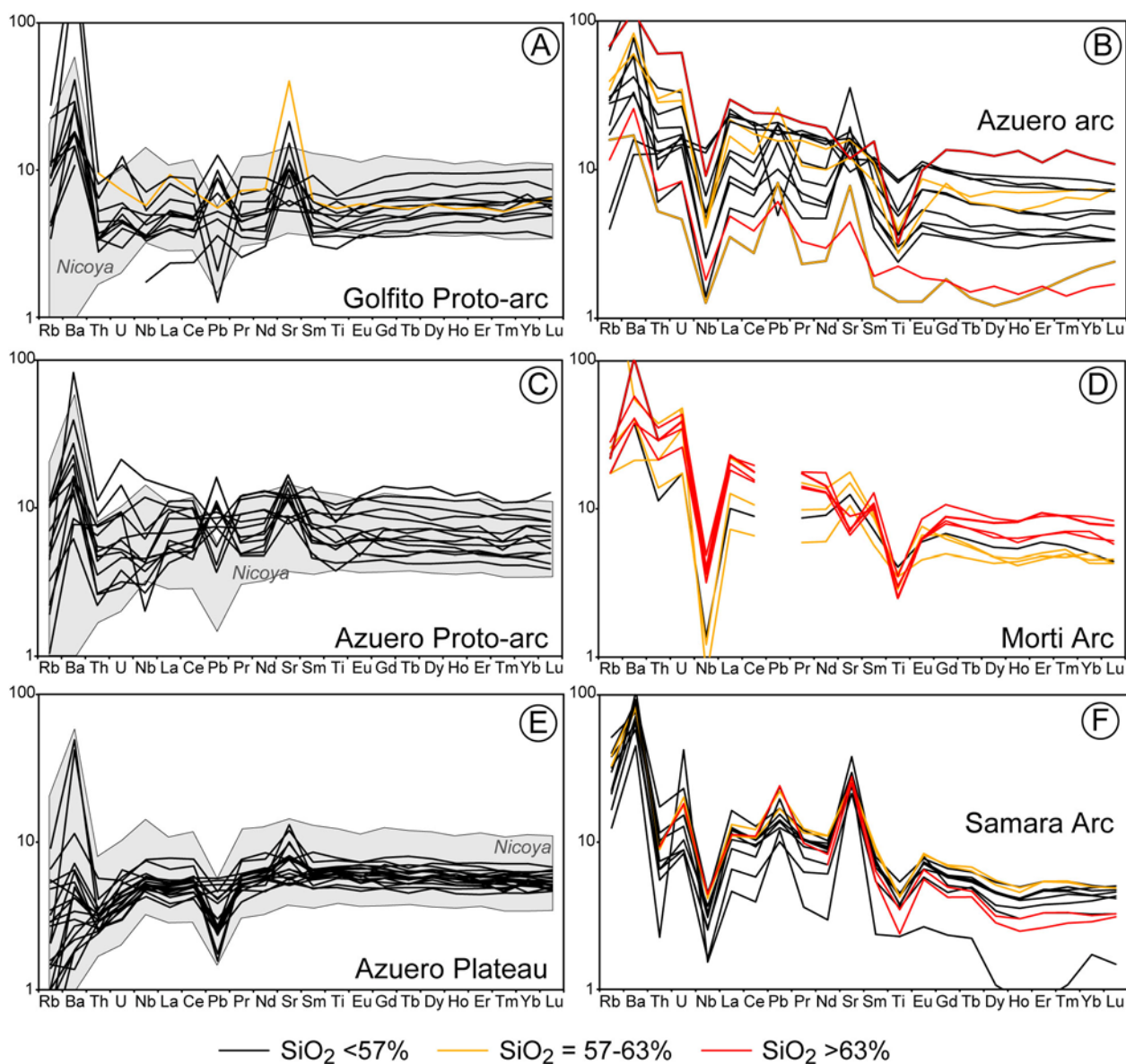
Figure 2.5: *Primitive mantle-normalized REE diagrams. Primitive mantle after McDonough and Sun [1995]. Samara Arc after Patino et al. [2004], Morti Arc after Maury et al. [1995] and Nicoya Complex after Hauff et al. [2000].*

2.4.1.6. Clinopyroxene geochemistry

In order to better constrain the affinities of the altered igneous rocks of the Golfito Complex, three samples were chosen among the analyzed igneous rocks for clinopyroxene analyses. Following samples were selected for their well-preserved clinopyroxenes and position in the stratigraphic sequence: (1) a coarse basalt from the Igneous Basement (sample DB02-042), (2) a basalt from the upper part of the Igneous Basement (sample DB02-101), and (3) a fine-grained porphyric trachyandesite from the upper part of the Golfito Formation (sample DB02-175) (Photos 2.4-2.6). Analyzed clinopyroxenes are part of the matrix (samples DB02-042 and
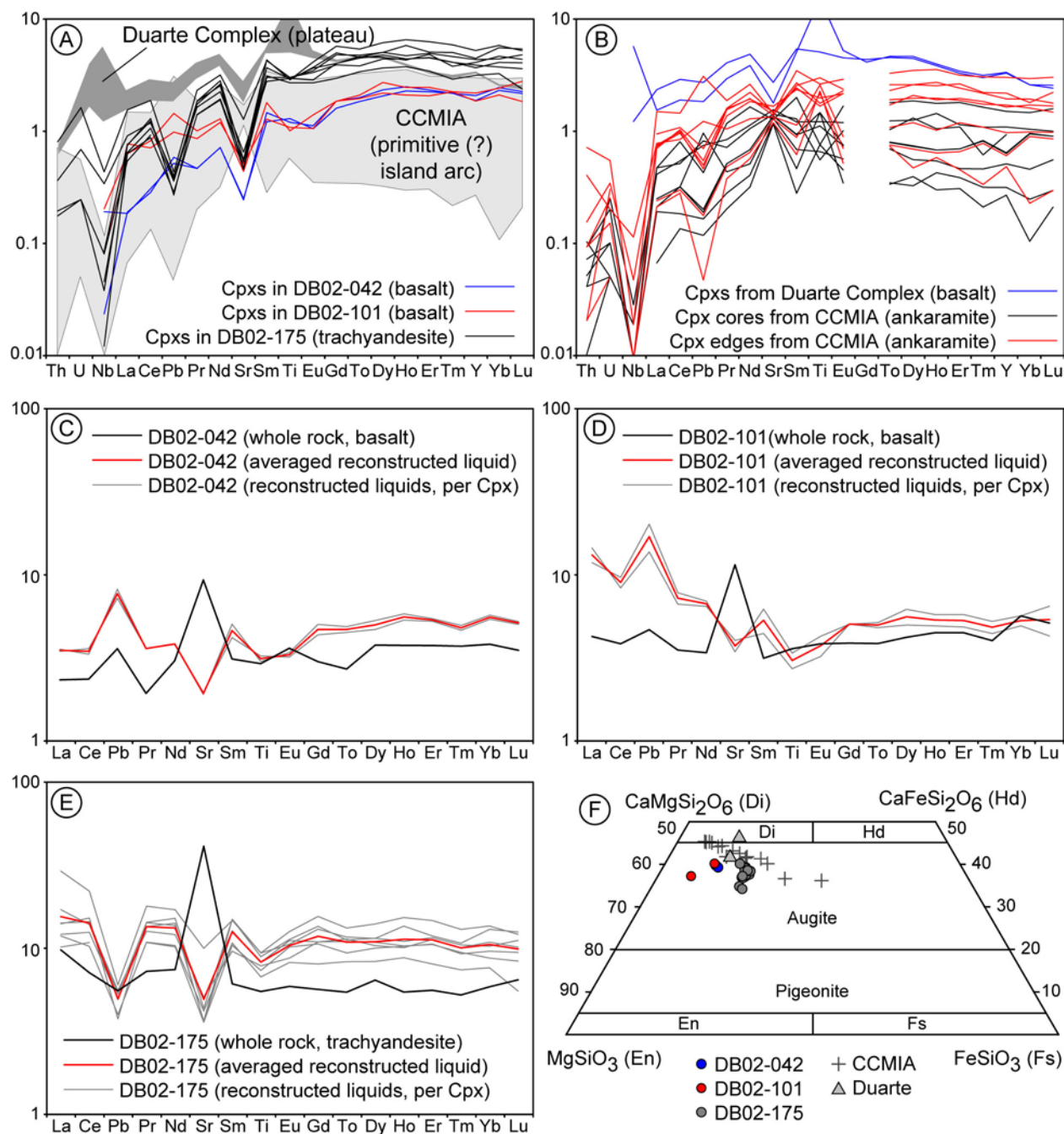
Figure 2.6: A-B-F) *Primitive mantle-normalized multielement diagram of clinopyroxenes from the Golfito Complex, with comparison to clinopyroxenes from the CCMIA (Cala-Cayo-Macuchi Island Arcs, Ecuadorian intra-oceanic arcs possibly formed on top of an oceanic plateau) [Allibon et al., in press] and the Duarte Complex (oceanic plateau) [Mamberti, 2001]. **C-E)** Primitive mantle-normalized multielement diagram of reconstructed liquids in equilibrium with analyzed clinopyroxenes and respective whole rock content. **F)** Di-Hd-En-Fs classification diagram for the clinopyroxenes from the Golfito Complex, Duarte Complex and CCM Island Arcs (Di=Diopside, Hd=Hendenbergite, En=Enstatite and Fs=Ferrosilite). **A-E)** Primitive mantle normalisation values after McDonough and Sun [1995]. **C-D)** Partition coefficient from Kelemen et al. [2003].*

DB02-101) or phenocrysts (sample DB02-175). Absence of resorbtion texture or reaction rim is argument for a crystallization of the clinopyroxenes in equilibrium with the original melt of the lava flows (i.e. the clinopyroxenes are not inherited). Analyzed clinopyroxenes of the Golfito Complex have been compared with clinopyroxenes of a ~86 Ma oceanic plateau in Hispaniola

(Duarte Complex, *Mamberti* [2001]) and clinopyroxenes from the latest cretaceous Ecuadorian arcs, possibly formed on the top of a plateau in the Pacific (Cala-Cayo-Macuchi or CCM Island Arcs, *Allibon et al.* [in press]).

Clinopyroxenes from the Golfito Complex have a low range of composition, plotting in the Augite field in a Di-Hd-En-Fs diagram (Figure 2.6f). Trend observed in this diagram is believed to be controlled by fractional crystalization in the Golfito suites. Clinopyroxenes with lowest MgO content are found in the sample DB02-175, with Mg#=71-75, which is the most evolved analyzed lava. Clinopyroxenes in the samples DB02-042 and DB02-101 have Mg#=82-83 and Mg#=83-90, respectively. Major element contents of the Golfito clinopyroxenes are similar to clinopyroxene compositions of the Duarte Complex and CCM Island Arcs, with a slightly lower content in CaO (Figure 2.6f).

Trace element contents of the clinopyroxenes of the Golfito Complex show a characteristic depletion in the most incompatible elements on a PM-normalized multielement diagram (Figure 2.6a). The clinopyroxenes have very consistent signatures within hosting samples, but distinct patterns are observed among different rocks. Concordantly to the evolved character of hosting rock, clinopyroxenes in the trachyandesite DB02-175 have the highest content in incompatible elements. These observations strengthened the hypothesis that the clinopyroxenes are not inherited. Samples DB02-042 and DB02-175 are strongly depleted in Th, U, Nb and LREE, whereas sample DB02-101 is moderately depleted in the same elements. Nb, which is a highly incompatible element in clinopyroxenes, forms a systematic negative anomaly on the PM-normalized multielement patterns. Sole exception to this observation comes from a sample of the Duarte oceanic plateau which contains anomalously high Nb and Ti possibly due to inclusions of Nb-Ti rich oxides in the analyzed mineral. In the Golfito complex and CCM Island Arcs, clinopyroxenes have both positive and negative Pb anomalies, whereas clinopyroxenes from the Duarte Complex have a systematic negative Pb anomaly. Sr, Ti and Eu contents are low in all the clinopyroxenes of the Golfito Complex.

Chemistry of the clinopyroxenes of the Golfito Complex was used to reconstruct original liquids in equilibrium with these minerals. In order to better constrain our modelization, various datasets of mineral-liquid partition coefficients were tested [*Larsen*, 1979; *Hart and Dunn*, 1993, *Gaetani et al.*, 2003; *Kelemen et al.*, 2003]. No significant differences in our results were observed by using distinct Kd sets. Coefficients from *Kelemen et al.* [2003] (mostly based on early results by *Hart and Dunn* [1993]) were finally chosen for their consistency and exhaustiveness within the spectrum of elements used in our modelization. Reconstructed liquids in equilibrium with analyzed clinopyroxenes were compared with whole rock analyses in PM-normalized multielement diagrams (Figure 2.6c, d, e).

Patterns of reconstructed liquids and whole rock are in broad agreement for samples DB02-042 and DB02-175 (Figure 2.6c, e), whereas, for sample DB02-101, reconstructed liquids have a spoon-shaped pattern distinct from the plateau-like pattern of the whole rock (Figure 2.6d). All the reconstructed liquids have higher calculated element contents than respective whole rock. For all the samples, Sr, Ti and Eu negative anomalies are present in the reconstructed liquids and absent in the whole rock signatures. Globally high contents in calculated elements and Sr, Ti and Eu negative anomalies are attributed to coheval crystallization of plagioclase and Fe-Ti oxides with the clinopyroxenes. In samples DB02-042 and DB02-101, positive Pb anomalies are observed in both reconstructed liquid and whole rock patterns, while in sample DB02-175 negative Pb anomalies are observed in both reconstructed liquid and whole rock signatures. Similar anomalies are also observed in measured compositions of
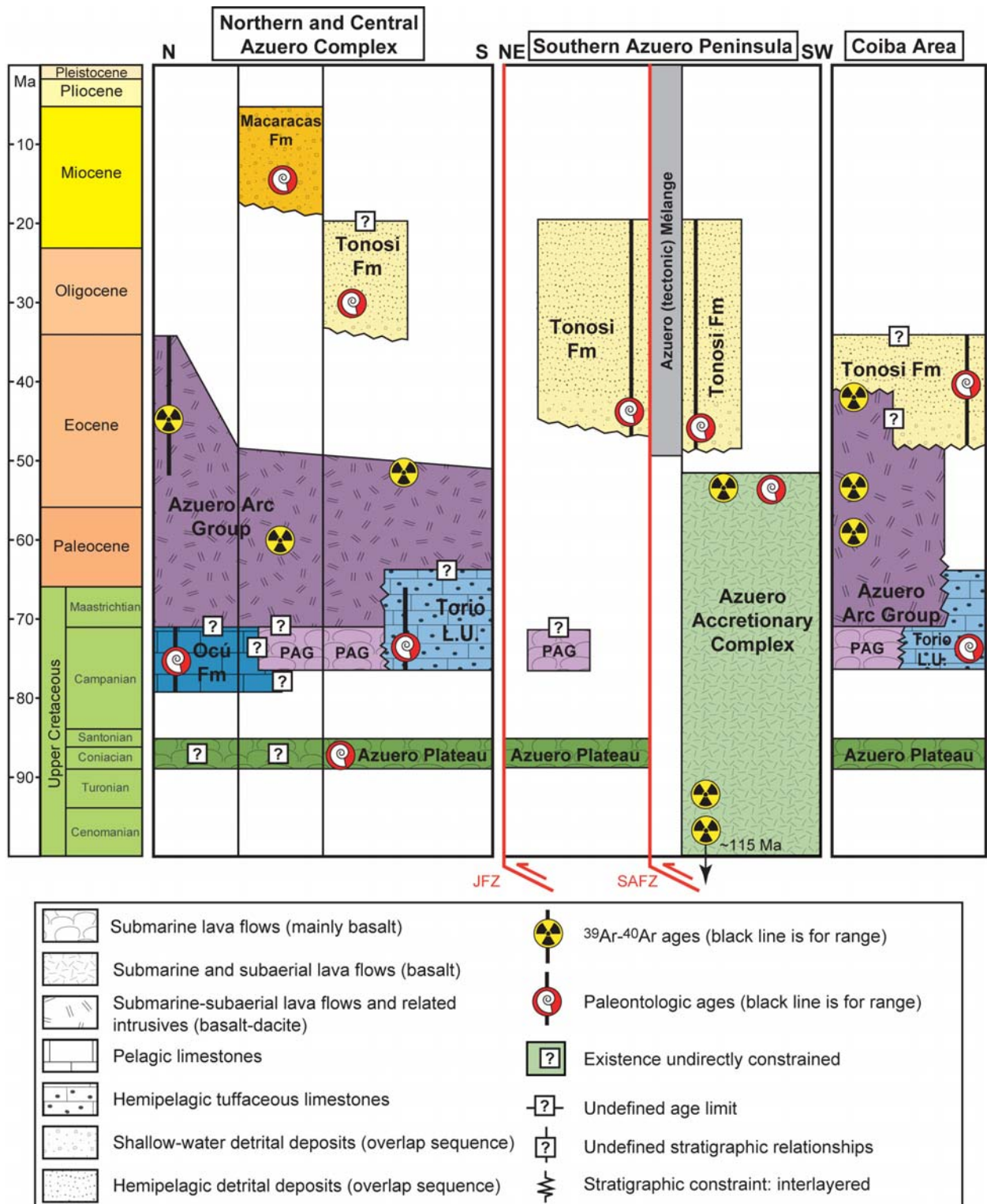
Figure 2.7: *Attempt of a synthetic tectonostratigraphic chart for the Azuero Complex. Gaps may be either depositional or observational. Ages includes paleontologic data (Kolarsky et al., 1995b; this study) and ⁴⁰Ar/³⁹Ar data (poor-quality radiometric ages in disagreement with stratigraphic constraints were discarded) [Hoernle et al., 2002, 2004; Lissinna, 2005; Hoernle and Hauff, 2007]. JFZ=Joaquín Fault Zone. SAFZ=Sona-Azuero Fault Zone. PAG=Proto-Arc Group. Torio L.U.=Torio Lithostratigraphic Unit.*

clinopyroxenes (Figure 2.6a). It is important to note here that, due to higher compatibility of Pb in plagioclases and sulfides, coeval plagioclase and sulfides crystallization during the

clinopyroxene growth cannot account for positive Pb anomalies in the reconstructed liquids. It is actually expected that contemporaneous plagioclase and Fe-Ti oxide crystallization would tend to lower the Pb content in the liquid. Hence, in reconstructed liquids obtained from unaltered clinopyroxenes, positive Pb anomalies relates to source composition.

2.4.2. Azuero Complex

2.4.2.1. Tectonostratigraphy

Synthesis of our new data and results from previous contributions defines a new tectonostratigraphy for the Azuero Complex, which includes: (1) the Azuero Plateau, (2) the Azuero Proto-Arc Group, (3) the Ocú formation and Torio lithostratigraphic unit, (4) the Azuero Arc Group, (6) the Azuero Accretionary Complex, (7) the Azuero Mélange, (8) the Tonosi Formation and (9) the Macaracas Formation (F). New units are briefly defined below.

The Azuero Plateau is exposed over a broad area in the Azuero Peninsula, Sona Peninsula and on Coiba Island (Figure 2.8). It is essentially composed of massive and pillowed lava flows with plateau-like affinities (see Chapter 2.4.2.6.). Small volumes (<<1% of the unit) of red siliceous pelagic sediments intercalated with the lavas are observed and contain radiolarians in rare places. Biogenic ages from interlayered radiolarites are Coniacian-early Santonian (89-85 Ma) [*Kolarsky et al.*, 1995b, ranges of radiolarian ages revised in *Buchs et al.*, submitted]. $^{40}Ar/^{39}Ar$ ages from the basalts [*Lissinna*, 2005] indicate a pre-Campanian, presumably late Turonian to Santonian age of formation for the unit, that is in broad agreement with sedimentary ages. Stratigraphic relationships indicate that the Azuero Plateau underlies other units of the Azuero Complex and likely represent the arc basement (Figure 2.7).

The Azuero Proto-Arc Group is composed of massive and pillowed lava flows as well as dykes crosscutting late Cretaceous to early Tertiary formations. Similarly to the Azuero Igneous Complex, this group is exposed over a large area (Figure 2.8). Near-arc geochemical affinities and porphyric textures are distinctive parameters of this group. The bulk of the age of formation is inferred to be late Cretaceous on the basis of stratigraphic relationships with other dated units.

The Ocú formation and Torio lithostratigraphic unit, initially regrouped as the "Ocú Formation" by *Del Giudice and Recchi* [1969] are composed of pelagic and hemipelagic calcareous sediments of late Cretaceous age. The pelagic Ocú Formation *sensu stricto* is exposed in the northern Azuero Complex, whereas the hemipelagic Torio lithostratigraphic unit crops out in the southern area (Figure 2.8). The Torio lithostratigraphic unit differs from the Ocú Formation by greenish-dark grey colors, tuffaceous and detrital components, flazer beddings and interlayered proto-arc- and/or arc-related igneous rocks. The Ocú Formation is composed of grey micritic limestones empty of significant detrital and tuffaceous components.

The Azuero Arc Group is composed of an arc-related sequence made of volcanic rocks and associated tuffites and volcanic clastics lacking of fossil. As defined by stratigraphic relationships with the Torio lithostratigraphic unit [*Del Giudice and Recchi*, 1969; *Kolarsky et al.*, 1995b; *this study*] and $^{40}Ar/^{39}Ar$ ages of the volcanic rocks [*Lissinna*, 2005; *Wörner et al.*, in press], the age of formation of the group ranges from the late Cretaceous to the Eocene (~66 to 40 Ma).

The Azuero Accretionary Complex is a middle Eocene accretionary complex made up of Cretaceous to middle Eocene accreted seamounts. This complex composes the SW edge of the Azuero Peninsula and an area near Playa Venado (Figure 2.8). Complete description and

interpretation of this accretionary complex is beyond our scope here and is developed in Chapter 5. Geochemical data, $^{40}Ar/^{39}Ar$ dates and observations of exposures along the shores have been already provided by *Hoernle et al.* [2002, 2004], *Lissinna* [2005] and *Hoernle and Hauff* [2007].

The Azuero Mélange is a tectonic mélange that forms a ~1 km thick belt at the interface between the Azuero Plateau and Azuero Accretionary Complex (Figure 2.8). It is composed of highly deformed rocks initially pertaining to adjacent formations and fragments of seamounts.
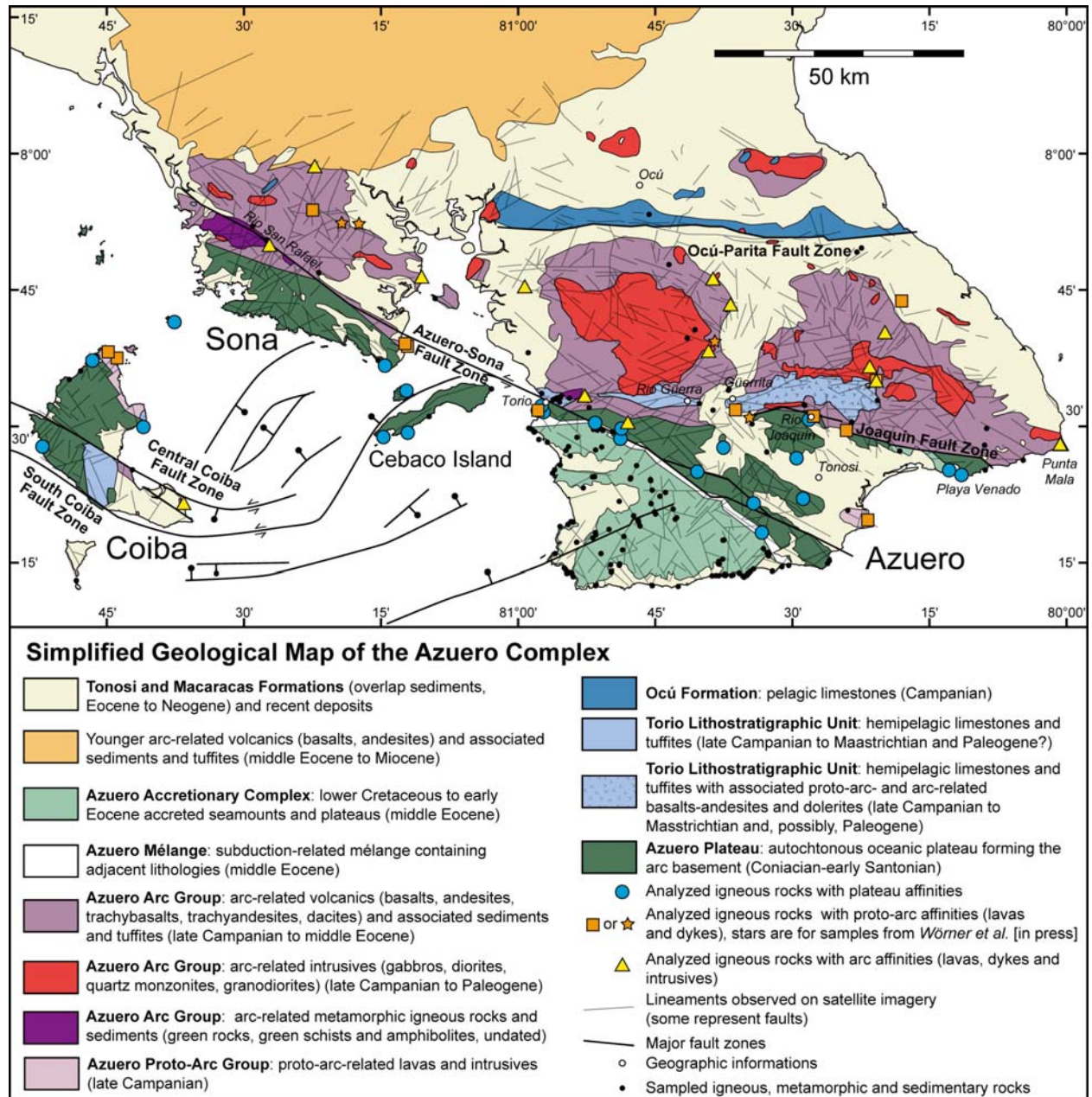
Figure 2.8: Simplified geological map of the Azuero Complex. Modified after the Panama Geologic Map (Mapa Geológico República de Panamá), 1:250,000 [DGRM, 1991]. Offshore faults after Kolarsky et al. [1995b].

2.4.2.2. Structural arrangement

The Azuero Complex has a broadly similar tectonic pattern observed in southern Costa Rica, with recent faults delimiting variously uplifted blocks (Figure 2.8). In the large area comprised by the Azuero Complex, faults of major importance have been recognized. The South Coiba, Central Coiba and Sona-Azuero fault zones [*Kolarsky et al.*, 1995b] have a NW-SE strike, whereas the Ocú-Parita Fault Zone [*Kolarsky et al.*, 1995b] and the Joaquín Fault Zone [*this study*] have a broad W-E orientation (Figure 2.8). A left-lateral strike-slip motion has been recognized along the NW-SE fault zones [*Kolarsky et al.*, 1995b]. Although field constraints are poor, it seems that all the major fault systems are mostly subvertical and associated with a strong deformation of the rocks. Landscape morphology, landslides and hydrothermal springs tends to indicate that the major fault zones are currently active.

The major fault systems are often flanking lithologic boundaries (Figure 2.8). This may be due to (i) strong differences in uplift and erosion between both sides of the faulted zones or (ii) conduction of the deformation and development of faulted zones along older lithologic boundaries. Along the Joaquín Fault Zone, the Azuero Arc Group lies directly in contact with the Azuero Plateau (Figure 2.8). Since the Azuero Igneous Complex is the basement of the arc, it appears that the area located on the SW side of the fault was uplifted relatively to NW side. The Azuero Mélange mostly follows the orientation of the Sona-Azuero Fault Zone (Figure 2.8). The mélange is a boundary between the Azuero Plateau and the Azuero Accretionary Complex. Thus, it seems that in this case, the faulted zone was produced by a conduction of the deformation along the lithologically-weakened mélange zone. These two examples indicate that both difference in uplifts and conduction of the deformation along older lithologic boundaries control the development of major fault zones in the Azuero Complex. Exposures of metamorphic rocks along some major fault systems (Figure 2.8) indicate that the degree of uplift have been significant in some areas of the Azuero Complex.

Arrangement of the faults (or lineament geometry) was studied using spatial distribution tools. Preliminary results (not illustrated) tend to indicate that differences in the orientation of the lineaments exist among distinct mapped units (Figure 2.8). However, due to poor exposure conditions in the igneous formations there is currently a lack of observations of fault plane, which are required to better constrain the lineament analysis. Forthcoming studies should try to collect more structural observations on the field so as to better constrain the tectonic development of the area.

2.4.2.3. Sedimentary rocks

Sediments found in the Azuero Plateau are exclusively composed of pelagic red cherts interbedded in lava flows. Although these cherts are locally in tectonic contact with the lavas, preserved stratigraphic contacts are locally observed, indicating that the sediments were deposited at the same time of emplacement than the lavas. Radiolarian associations found in some cherts yielded a late Cretaceous (possibly Coniacian, ~88 Ma) age [*Kolarsky et al.*, 1995b].

The Ocú Formation is composed of foraminiferan-bearing light grey micritic limestones. Detrital or tuffitic components are absent in this formation, pointing toward a pelagic environment of deposition. A Campanian-Maastrichitan age (~84-66 Ma) has been proposed on the basis of assemblages of pelagic foraminiferans [*Del Giudice and Recchi*, 1969]. Our samples provided a Campanian age (Chapter 2.4.2.4).

The Torio lithostratigraphic unit is composed of dark grey-greenish hemipelagic limestones locally developing flazer beddings. Tuffaceous and detrital components are locally observed. Pelagic foraminiferan associations yielded Campanian-Maastrichitan for the Torio lithostratigraphic unit [*Del Giudice and Recchi*, 1969]. A sample from Coiba Island provided a late Campanian age (Chapter 2.4.2.4). Detrital grains found in the most detrital layers notably include quartz, amphibole, pumice, and zoned feldspar fragments that point toward a source composed of a intermediate-differentiated volcanism. Subaerial volcanism is indicated by greenish interbeds rich in ash. The detrital fraction in the limestones tends to increase toward the top of the formation. Subaerial conditions in the vicinity of the sites of deposition of the Torio lithostratigraphic unit are also indicated by the presence of benthic foraminiferan fragments in the hemipelagic limestones of the Güerra River [*Del Giudice and Recchi*, 1969]. Near Güerrita, Torio and in northern Coiba Island, the Torio lithostratigraphic unit is interbedded with proto-arc- and arc-related lavas and crosscut by proto-arc- and arc-related dykes (Figure 2.8) (Photo 2.7). In NW Coiba Island, a continuous sequence showing interbedded proto-arc lavas and dykes with Campanian calcareous deposits contains an intermediate-differentiated volcanic detrital component.

Sedimentary deposits found in the Azuero Arc Group are composed of well-bedded tuffitic-detrital sediments fed by a proximal subaerial intermediate-acidic volcanism. In some places, the sediments have a calcareous component. The deposits are locally interbedded with arc-related volcanic rocks or crosscut by arc-related volcanic dykes. Biochronologic dating of the sediments was impossible due to the lack of preserved fossil.

Sediments of the Tonosi Formation, which represent an overlap sequence on the top of the Azuero Complex, were collected in many sites (Figure 2.8). The detrital component found in the formation is predominantly composed of basaltic fragments and minor alkali feldspars and amphiboles *Krawinkel et al.* [1999]. In addition to the observations made of *Krawinkel et al.* [1999], monocristalline quartz and multiply zoned plagioclases were encountered in the lower Tonosi Formation. A near-arc location seems thus to be confirmed for the entire Tonosi Formation. New ages based on benthic foraminiferans for the sediments in contact with older igneous units indicate that the Tonosi overlap sequence deposited diachronously over the Azuero Complex, between the middle Eocene (~40 Ma) and the Oligocene (~28 Ma) [*Baumgartner-Mora et al.*, 2008] (see also Chapter 5 for more informations on the Tonosi Formation).

2.4.2.4. Biostratigraphy

Two limestone samples from the Ocú Formation (525844/873241, UTM WGS84) yielded rich and well preserved assemblages of planktonic Foraminifera. The biochronologic age of the samples can be constrained by the co-occurrence of *Globotruncana ventricosa* and *Globotruncanita elevata* to the *G. ventricosa* and to the lower half of the R. calcarata zones. This corresponds to lower to upper Campanian, or much of magnetic zone 33n (approximately 79 to 73 my).

The most abundant planktonic Foraminifera are the serial forms such as *Heterohelix* spp. with uniserial, biserial and triserial forms with inflated globular chambers. In the *Globotruncanidae*, the monokeeled, conical trochospiral forms are dominant, these forms can be associated in general to the *Globotruncanita* genus, we distingued *Globotruncanita stuartiformis* and Globotruncanita elevata. We found also some inflated forms with two well developed and widely spaced keels, we determined these forms as *Globotruncana ventricosa* and G. sp. cf. *G.*

hilli. Additional forms recovered include *Hedbergella holmdelensis* and *Archaeoglobigerina cretacea*.

A Campanian-Maastrichitan age has been proposed by Del Giudice and Recchi, (1969) on the basis of the following species : *Globotruncana lapparenti* (ranging from the upper part of the *Dicarinella asymetrica* Zone to the base of the *Globotruncana aegyptica* Zone, Santonian to lower Maastrichtian), *Globotruncana ventricosa* (ranging form the *G. ventricosa* Zone to the middle of the *Globotruncana gansseri* Zone, lower Campanian to upper Maastrichtian), Rosita contusa (ranging from the upper *G. gansseri* Zone to the *Abadhomphalus mayaroensis* Zone, upper Maastrichtian). Based on the individual ranges of the cited species this list must summarize the observations in at least two samples with distinct stratigraphic positions. The first two cited species correspond to a range similar to the range of our samples, but the presence of *R. contusa* clearly indicates an upper Maastrichtian age. We ignore, if this species was observed in the Ocu area or the Rio Torio area, where we suspect younger ages of the Torio lithostratigraphic unit.

A hemipelagic limestone from NW Coiba Island (415710/844800, UTM WGS84), part of the Torio lithostratigraphic unit, yielded scarce and fragmented planktonic Foraminifera. Although preservation is poor, and entire specimens are rare, the presence of *Radoglobotruncana calcarata* allows to constrain this sample to the *R. calcarata* zone which corresponds to the upper Campanian, upper part of magnetic zone 33n (approximately 75-73 my).

Planktonic Foraminifera are mixed with radiolarians such as *Spumellaria* and conical multisegmented *Nassellaria*. *Planomalinidae* comprise some forms with low trocospire and a smooth wall, with globular chambers which increase in size rapidly in the last whorl. We determined some forms as *Globigerinelloides* cf. *prairiehillensis*. The *Globotruncanidae* are rare but fragments of *Radotruncana calcarata* are present, these are associated to monokeeled flat forms, and double keeled flat forms, such as *Globotruncana linneiana*. Few forms with trapezoidal chambers and slightly convex spiral are also present. Futhermore, we distinguished *Globotruncana* sp. cf. *G. fornicata*, Globotruncanita sp. cf. *G. stuartiformis*, *Globotruncanella* sp., *Globigerinelloides prairiehillensis*, and *Pseudoguembelina* sp.

2.4.2.5. Volcanic rocks

Volcanic rocks of the Azuero Plateau are composed of basalt sheet flows and pillow basalts. Polarity of the lavas is generally normal and reversed pillow lavas are preferentially observed in the vicinity of major fault zones. Textures of the lavas are ophitic to intersertal, with ubiquitous plagioclase, clinopyroxene, opaque minerals and glass, and few olivines in some lava flows. The degree of alteration of the lava is low in comparison to the volcanic rocks of the Golfito Complex. However, the glass and olivine are frequently altered. Little alteration of the clinopyroxene or plagioclase has been seen in our samples. Small clinopyroxene and/or plagioclase phenocrysts are rarely encountered. The unit is characterized by recurrent occurrences of plagioclase phenocrysts in the lava flows. At Punta Madroño (western Playa Venado) a thick lava flow contains plagioclase megacrysts up to 6 cm in length that accumulated at the top of the flow by floatation (Photos 2.9 and 2.10). Similar lava flows have been previously described in Deccan Traps as "Giant Plagioclase Basalts" and interpreted as a product of plagioclase accumulation and magma mingling and mixing in subvolcanic magmatic chambers [*Higgins and Chandrasekharam*, 2007]. In many sites located close to exposures of the Azuero Proto-Arc Group or Azuero Arc Group, proto-arc-related or arc-related dykes crosscuts

the Azuero Igneous Complex. This is a major constraint for the development of the Azuero Complex and southern Central American Arc that demonstrates that the Azuero Plateau stratigraphically underlies earliest arc rocks. Arc-related and proto-arc-related dykes crosscutting the Azuero Plateau are notably observed near Torio (504495/832730, UTM WGS84, at low tide exclusively, Photo 2.8), along the Rio Joaquín, close to the Joaquín Fault Zone (560250/831725, UTM WGS84), along the Rio Quebro (522705/830475, UTM WGS84) and along the road between Tonosi and La Miel, close to the Joaquín Fault Zone (567460/829260, UTM WGS84) (Figure 2.8).

Volcanic rocks of the Azuero Proto-Arc Group are composed of basaltic to basaltic trachyandesitic lava flows and dykes. The dykes are essentially encountered in the Azuero Plateau and Torio lithostratigraphic unit. *Wörner et al.* [in press] report lava samples with similar geochemical affinities from the Chagres Igneous Complex (central Panama, Figure 1.2) and the Azuero Arc Group (Figure 2.8), which are described as "enigmatic CLIP-arc rocks". In details samples meeting geochemical criteria to be part of our "Proto-Arc Group" (see Chapter 2.4.2.8) are classified by *Wörner et al.* [in press] either as "CLIP oceanic basement", "Early Arc" or "CLIP-arc" and include samples PAN-03-004, PAN-05-009, PAN-05-029, PAN-06-204 and PAN-06-205 exclusively. In our opinion other samples classified as "CLIP-arc" by *Wörner et al.* [in press] are more alike maturate supra-subduction igneous rocks and unrelated to our Proto-Arc Group. The texture and mineralogy of the volcanic rocks from the Azuero Proto-Arc Group exhibit a large variability among our samples, with subophitic, intersertal and porphyric textures. These rocks are essentially constituted by clinopyroxene, plagioclase, opaque mineral and glass (no olivine has been observed). Plagioclase, clinopyroxene, orthopyroxene, amphibole and alkali-feldspar are frequently found as phenocrysts in the lavas and dykes. On the field, this may be used as a distinctive feature between the volcanic rocks of the Azuero Plateau and Azuero Proto-Arc Group. The amount of phenocrysts ranges from <1% to ~45%. Mode and degree of alteration are similar to the rocks of the Azuero Plateau.

The Azuero Arc Group is composed of a large variety of volcanic rocks ranging in composition from basalt to dacite. Both submarine and subaerial lava flows have been observed in association to large intrusive complexes and eroded lava domes. Large intrusives are generally associated with high reliefs that control the landscape morphology. In the central Azuero Complex, granodioritic intrusives cover large areas and are distributed along a well-defined NW-SE trend (figure 2.8). Aa flows are frequently observed for andesitic lavas. Well preserved volcanic morphologies tend to indicate that a younger volcanism occurred in the northern part of the Azuero Complex and possibly developed along rifted/faulted zones. Lavas have typical intergranular to porphyric textures. Multiply zoned plagioclase, alkali feldspar, greenish clinopyroxene, amphibole and quartz are typical phenocrysts in the porphyric lavas. Intrusive complexes are both constituted by mafic and acidic igneous rocks. The differentiated intrusives frequently contain large amphiboles and zircons, which may be used for $^{40}Ar/^{39}Ar$ and U-Pb datings.

2.4.2.6. *Metamorphic rocks*

Occurrences of metamorphic rocks are restricted along major fault zones (Figure 2.8). Our samples of green schists and green rocks from the Rio Torio (Azuero) contain numerous preserved fragments of intermediate lavas, pumices and reworked euhedral crystals such as zircons. Some of the samples exhibit a preserved sedimentary-tuffitic texture, whereas some

others underwent a strong deformation leading to schistosity formation. Similar observations were made on the field along the Rio San Rafael (Sona). Although the timing of formation and exhumation of these rocks remains poorly constrained, our observations tends to indicate that they initially belonged to an intermediate-differentiated volcanic environment, presumably the Azuero Arc Group. As a consequence, we propose here to include the metamorphic rocks in the Azuero Arc Group. Observation by *Del Giudice and Recchi* [1969] of late Cretaceous limestones stratigraphically resting on the metamorphics in the Rio Torio has not been confirmed. It seems rather than numerous faulted contacts characterize the lithologic arrangement of this area.

2.4.2.7. Chemistry of the Azuero Plateau

The lavas of the Azuero Plateau have similar compositions than the lavas of the Nicoya Complex. Their range of SiO_2 content is very low, with 47.1 to 49.9 wt% SiO_2 (Figure 2.3a). TAS, K_2O-SiO_2 and FeO*/MgO-SiO_2 variations are consistent with a low K - high Fe (tholeiitic) differentiation trend (Figure 2.3a-c). MgO content shows a remarkable constancy among our samples and ranges from 7.1 to 8.8 wt%. For decreasing MgO, FeO* constantly increases (Figure 2.3d). For decreasing Mg#, TiO_2, Na_2O and K_2O increases (Figure 2.3e, Appendix) and CaO and Al_2O_3 decreases (Figure 2.3f, g).

REE contents of the Azuero Plateau show plateau-like affinities similar to the Nicoya Complex (Figure 2.4e). Global enrichments of REE are very consistent in comparison to the Nicoya or Golfito complexes. A similar consistency is preserved on a normalized multielement diagram (Figure 2.5e). Rb, Ba, Pb and Sr contents show large variations among the samples, which are attributed to low-T alteration. Nonetheless, many samples exhibit a negative Pb anomaly that is inconsistent with alteration effects and relates to source composition.

$(Nb/La)_{PMn}$-$(La/Sm)_{PMn}$ variations are, again, very consistent and similar to the Nicoya Complex (Figure 2.3h). On Figure 2.3h, the Azuero Plateau shares a similar composition with a sample from the Golfito Complex. Most lavas of the Golfito Complex and the Azuero Proto-Arc Group have lower $(Nb/La)_{PMn}$ and higher $(La/Sm)_{PMn}$.

2.4.2.8. Chemistry of the Azuero Proto-Arc Group

Igneous rocks from the Azuero Proto-Arc Group have low to intermediate SiO_2 content, ranging from 45.8 to 53.5 wt% (Figure 2.3a). TAS, K_2O-SiO_2 and FeO*/MgO-SiO_2 variations indicate a low K - high Fe (tholeiitic) differentiation trend distinct from the volcanic rocks from the Golfito Complex (Figure 2.3a-c). MgO content ranges from 4.0 to 8.1 wt%. For decreasing MgO, FeO* constantly increases until ~5 wt% and then decreases (Figure 2.3d). For decreasing Mg#, TiO_2, Na_2O and K_2O increases (Figure 2.3e, Appendix B) and CaO and Al_2O_3 decreases (Figure 2.3f, g). All these trends are distinct from the Golfito trends.

REE content shows plateau-like affinities similar to the Nicoya Complex, Azuero Plateau, Golfito Complex or Azuero Proto-Arc Group (Figure 2.4e). Small differences are however observed with the Nicoya and Azuero plateau lavas. There is a LREE enrichment/depletion and a negative Eu anomaly for some samples that is similar to variations observed in the Golfito Complex. As seen on a PM-normalized multielement diagram, strong similarities exist between the Azuero Proto-Arc Group and the Golfito Complex, which both have global plateau affinities associated with positive Pb anomaly and Ti-Nb negative anomalies in some samples (Figure 2.5c). On a $(Nb/La)_{PMn}$-$(La/Sm)_{PMn}$ diagram, similar variations are

observed for the Azuero Proto-Arc and the Golfito Complex, with a slightly lower $(Nb/La)_{PMn}$ in the Azuero Proto-Arc (Figure 2.3h).

2.4.2.9. Chemistry of the Azuero Arc Group

Volcanic rocks of the Azuero Arc Group have highly variable SiO_2 content, ranging from 48.0 to 75.0 wt% (Figure 2.3a). TAS, K_2O-SiO_2 and $FeO*/MgO$-SiO_2 variations indicate a medium K - low Fe differentiation trend (Figure 2.3a-c). MgO content spans a large range, from 0.2 to 6.8 wt%. For decreasing MgO, $FeO*$ constantly increases until ~5 wt% and then decreases (Figure 2.3d). For decreasing Mg#, TiO_2, Na_2O and K_2O increases (Figure 2.3e, Appendix) and CaO and Al_2O_3 decreases (Figure 2.3f, g). On the major-minor element diagrams (Figure 2.3), evolution trends of the arc-related lavas from the Rio Morti (eastern Panama) are similar to the Azuero Arc Group. Arc-related rocks from Punta Samara (northern Costa Rica) share some similarities with the Azuero Arc Group in terms of SiO_2, TiO_2, $FeO*$, Na_2O and K_2O contents. The "Samara Arc" has on the other hand a globally lower MgO content and much higher CaO and Al_2O_3 contents at the same Mg# (Figure 2.3).

REE content of the Azuero Arc Group is enriched in the most incompatible elements (i.e. LREE) (Figure 2.4e). Most differentiated samples have a negative Eu anomaly likely due to plagioclase fractionation. Similar REE patterns are observed for the Samara and Morti arcs (Figure 2.4d, f). Enrichment in the most incompatible elements is also recognized on a PM-normalized multielement diagram, as well as Nb-Ti negative anomalies and a Pb positive anomaly for most samples (Figure 2.5b). Samara and Morti arcs have similar multielement patterns than the Azuero Arc Group (Figure 2.5d, f).

The Nb negative anomaly associated with the enrichment in the non-conservative incompatible elements (i.e. more mobile in fluids) of the volcanic rocks from the Azuero Arc Group is well illustrated on a $(Nb/La)_{PMn}$-$(La/Sm)_{PMn}$ diagram (Figure 2.3h). On this diagram, the Samara and Morti arcs have similar characteristics than the Azuero Arc Groups. All the arc-related samples are included within the field of the Mariana Arc (i.e. a typical high-Fe medium-K arc suite), which is distinct from the Tonga Arc (i.e. a typical high-Fe low-K arc suite).

2.5. Discussion on the origin of the Golfito Complex

2.5.1. Environmental conditions

The stratigraphy indicates that the Golfito Complex has remained in a volcanic environment from the Campanian (~75 Ma) to present. In the late Cretaceous, a submarine mafic-intermediate volcanism was active and progressively vanished out in the Maastrichtian (~68 Ma). During this period, eruption rates lowered, allowing the deposition of hemipelagic carbonates between the lava flows. Records of subaerial intermediate-acidic volcanism located in the vicinity of the Golfito Complex are first observed in the Maastrichtian and have continued until present. The stratigraphy clearly shows that the mafic-intermediate volcanism of Golfito was partly synchronous to the more acidic volcanism in the late Cretaceous. Similar observations were made in the late Cretaceous limestones of the Rio Changuinola (NW Panama) by *Fisher and Pessagno* [1965].

In the Golfito Complex, a shallowing-upward sequence is recognized, with hemipelagic limestones and distal detrital deposits at the base and proximal detrital deposits and periplatform

carbonates at the top. However, faunal association and sedimentary facies show that the complex has likely remained in the vicinity of a shelf during all his history. The first presence of a subaerial environment close to the Golfito Complex is recorded in the Maastrichtian (~68 Ma).

2.5.2. An atypical magma genesis for the Golfito Complex

Despite igneous rocks from the Golfito Complex have flat chondrite-normalized REE patterns similar to oceanic plateau (Figure 2.4a), major, minor and some trace element contents point toward affinities clearly distinct from typical oceanic plateaus such as the Nicoya Complex *sensu stricto* (northern Costa Rica) (Figure 2.3). We present here geochemical arguments that are in opposition to the commonly-accepted idea that the Golfito Complex is an oceanic plateau and propose a new interpretation.

It is well known that some elements are good discriminative parameters of magma produced in supra-subduction zones [e.g. *Pearce and Peate*, 1995]. Subduction zones are characterized by the presence of hydrated fluids released by the subducting slab that trigger melting of the overlying mantle wedge and lead to the production of arc lavas with characteristic enrichment in Pb and depletions in Nb and Ti, notably. Nb and Ti are useful elements in altered rocks, because they are strongly immobile during the alteration [e.g. *Winchester and Floyd*, 1977].

In the Golfito Complex, Ti content at a given Mg# is significantly lower than oceanic plateau lavas, but is higher than typical medium Fe (Tonga) or high Fe (Azuero) arc lavas (Figure 2.3e). In the Golfito lavas a Nb negative anomaly is variously observed among the samples (Figures 2.3g, 2.4a). For Pb content we note that: (1) some liquids in equilibrium with unaltered clinopyroxenes have positive Pb anomalies that relates to the source composition (Figure 2.6), (2) compositions of the Golfito clinopyroxenes have both positive and negative Pb anomalies and (3) positive Pb anomalies are observed in clinopyroxenes of supra-subduction lavas (CCM Island Arcs), but absent in the Duarte oceanic plateau (Figure 2.6). Hence, the Golfito lavas have both supra-subduction and oceanic intraplate signatures in terms of Pb content. We interpret positive Pb and Nb-Ti negative anomalies present in many (but not all) of the Golfito lavas as an indication of the formation of the Golfito lavas in a supra-subduction zone environment.

We further propose here that the Golfito lavas were produced along an initiating subduction on the margin of an oceanic plateau. As shown on a $(Nb/La)_{PMn}$-$(La/Sm)_{PMn}$ diagram (Figure 2.3h), the supra-subduction signature found in the Golfito igneous rocks is variously expressed among the samples. This may be due to low fluid contents present in the upper plate during the initiation of the subduction. A hybrid character is also recognized for many elements in the Golfito lava, with Golfito compositions defining an array between plateau and intraoceanic arc rocks (Figure 2.3). However, Nb, Ti, CaO and incompatible element (e.g. REE) contents show that the Golfito lavas are distinct from typical intraoceanic IAT and associated back-arc basins (Figure 2.3). PM-normalized multielement patterns indicate rather that the Golfito lavas have plateau-like signature with an overprinted arc-like signature expressed in Nb, Pb and Ti (Figure 2.5), which is expected if the asthenospheric mantle above the initiating subducting slab was associated with a plateau. Immobile radiogenic isotopes data by *Hauff et al.* [2000] (i.e. Sm-Nd system) are consistent with this interpretation.

Clinopyroxenes analyzed in the DB02-101 intersertal basalt are enriched in the most incompatible elements (Figure 2.6a). This causes an unusual spoon-shaped pattern for the

reconstructed liquids in a PM-normalized multielement diagram (Figure 2.6c). Interestingly, in this sample, the reconstructed liquid is different from the whole rock composition. This may be explained by (1) enrichment of the most incompatible elements in clinopyroxenes crystallizing in the latest stages of solidification of the lava or (2) presence of amphiboles in the melt at the time of the onset of the crystallization of the clinopyroxenes in the crust, which has not been preserved during the ascent of the magmas. In the DB02-101 basalt, analyzed clinopyroxenes have relatively high Mg# (83-90). They are part of the matrix and are in contact with interstitial glass. Enrichment of incompatible elements may have occurred in the last-remaining interstitial liquids of the lava (i.e. the glass), whereas relatively high Mg# may have been maintained due to concurrent Fe-oxide crystallization in these liquids. The first hypothesis is thus in agreement with the petrography of the lava. The second hypothesis seems to be in good agreement with the existence of cryptic amphiboles in arc environments [*Davidson et al.*, 2007]. However, as shown by *Davidson et al.* [2007], amphibole fractionation during differentiation of the arc magmas induces a decrease of Dy/Yb with increasing SiO_2. This decrease is not observed in the Golfito volcanic suites (diagram not shown). This may be related to an unstable plumbing system during the early arc history. Hence, spoon-shaped patterns calculated on the basis of the clinopyroxene compositions for some of the Golfito lavas are attributed to late-stage processes in the crystallizing lavas rather than a source and/or deep-magmatic processes.

2.6. Discussion on the origins of the Azuero Complex

2.6. 1. Summary of the stratigraphic development and implications

The formation of the autochtonous tectonostratigraphic units of the Azuero Complex starts in the Coniacian-ealry Santonian (89-85 Ma) with the emplacement of the Azuero Plateau on the top of an unknown basement.

The limestones of the Ocú Formation were deposited on top of the Azuero Plateau in the late Cretaceous (upper Campanian, ~75-73 Ma) beyond significant influence of active volcanism. Calcareous-tuffitic sediments of the Torio lithostratigraphic unit have partly similar ages that may extend to the early Tertiary. From the Campanian to Maastrichitian, this formation is synchronous to the emplacement of submarine lavas with proto-arc affinities. Younger Maastrichtan and early Tertiary limestones of the Torio lithostratigraphic unit deposited synchronously to the emplacement of the intrusives and lavas of the Azuero Arc Group. There are strong similarities in the facies, stratigraphic context and faunal associations between the Torio lithostratigraphic unit and the late Cretaceous limestones of the Rio Changuinola (NW Panama) [*Fisher and Pessagno*, 1965]. The Torio lithostratigraphic unit may thus represent a lateral equivalent of the Changuinola limestones.

Apparent age gap between deposition of Ocú and Torio limestones and formation of the Azuero Plateau (Figure 2.7) may be due to (1) a sampling bias, i.e. early Campanian limestones have not been sampled yet, (2) bottom see currents impeding deposition of sediments on top of the Azuero Plateau during the early Campanian, and/or (3) pre-late Campanian removal of early Campanian deposits on top of the plateau due to tectonics. Oceanic currents in the Caribbean at this time are attested by broken planktonic foraminiferan in the Golfito Formation [*Di Marco*, 1994] and seismic stratigraphy in the western Caribbean [*Bowland and Rosencrantz*, 1988; *Bowland*, 1993].

Dykes of the Azuero Proto-Arc Group crosscut the Azuero Plateau and Torio lithostratigraphic unit in several locations, constraining the emplacement of the Azuero Proto-Arc Group on top of the Azuero Plateau and partly above the Torio lithostratigraphic unit in the late Cretaceous (most probably synchronously to deposition of the Golfito Formation, ~75-70 Ma).

The bulk of the Azuero Arc Group have $^{40}Ar/^{39}Ar$ ages ranging from the Maastrichtian (synchronously to Chagres volcanism, ~66 Ma) to the middle Eocene (~40 Ma) [*Lissinna, 2005; Wörner et al.*, in press]. In this period, the volcanic arc was forming a well-defined front presently delimited by acidic intrusives of the central Azuero Complex (Figure 2.8). In the northern Azuero Complex, late Eocene (~34 Ma) arc-related sequences are found, indicating a migration of the arc away from the trench with time [*Lissinna et al.*, 2002]. The initiation of the migration is constrained by both ages distribution [*Lissinna*, 2005] and accretionary processes (see Chapter 5) to the middle Eocene (~45 Ma) (Figure 2.7). Front of acidic intrusives in northern Azuero possibly illustrate the arc migration and should be dated in the future (Figure 2.8). Although the younger arc is considered herein to be part of the Azuero Arc Group, it is composed of distinct magmatic suites [*Lissinna*, 2005; *Wörner et al.*, in press; *this study*] that should be defined and mapped independently in forthcoming studies.

Ages of emplacement of the Cretaceous to early Eocene (~115 Ma to 55 Ma) allochtonous rocks of the Azuero Accretionary Complex along the Caribbean Plate are constrained by the ages of the accreted rocks, the age of initiation of the subduction along the Caribbean Plate, the age of the sediments of the lower Tonosi Formation that overlap the complex and the age of arc retreat inboard of the accreted material (see Chapter 5). Accretionary events may have occurred between the late Cretaceous (~75 Ma) and the middle Eocene (~45 Ma). Bulk of the accreted material in the SW Azuero Peninsula accreted in the middle Eocene (see Chapter 5). The formation of the Azuero Mélange is associated with subduction processes and the construction of the Azuero Accretionary Complex. It initially developed along a paleo-subduction zone. The Azuero Accretionary Complex was accreted very close to the late Cretaceous arc front (Figure 2.8). Late Cretaceous to early Tertiary arc-related igneous rocks are also found very close to the trench on Coiba Island (Figure 2.8). These observations indicate that tectonic erosion has played an important role along the margin during the arc development. Preserved accretionary prisms along the margin imply that the erosion occurred intermittently with accretion (see also Chapter 3).

Interestingly, migration of the arc front away from the trench in the middle Eocene (~45 Ma) correlates with the final stage of growth of the Azuero Accretionary Complex and ages of the lower Tonosi Formation overlapping in the southern Azuero Complex [*Kolarsky et al.*, 1995b; *Baumgartner-Mora et al.*, 2008]. This may reflect a change in the tectonic setting at this time, associated with flattening of the slab under the Azuero Complex. This is in agreement with stratigraphic observations of a regional erosional discontinuity in the Eocene [e.g. *Weyl*, 1960; *Kolarsky and Mann*, 1995; *Kolarsky et al.*, 1995b].

2.6.2. The Azuero Complex: a record of an arc developing on an oceanic plateau

Basaltic lava flows of the Azuero Plateau have typical plateau signatures, with $(Nb/La)_{PMn} \approx 1.1$ and $(La/Sm)_{PMn} \approx 0.8$ (Figures 2.3h, 2.4e, 2.5e). Although the unit lacks high-MgO lavas commonly associated with oceanic plateaus [e.g. *Kerr*, 2003], major and minor

element trends similar to the Nicoya Complex *sensu stricto* are consistent with an oceanic plateau origin (Figure 2.3). Sedimentary and stratigraphic observations indicate high rates of eruption in a pelagic environment during the late Cretaceous. Therefore, this unit is interpreted to be made of a ~89-85 Ma oceanic plateau underlying the arc-related lavas of the Azuero Complex. Further extension of the plateau under the southern Central American Arc is indirectly constrained by occurrences of primitive island arc lavas with particular magmatic affinities elsewhere along the southern Central American Isthmus (see Chapter 2.7.2).

Volcanic rocks of the Azuero Proto-Arc Group have geochemical affinities very similar to the lavas of the Golfito Complex, with low content in Nb-Ti, high contents in Pb and similar incompatible element patterns than oceanic plateaus (Figure 2.3e, 2.4c, 2.5c). Similarly to the Golfito Complex these characteristics are variously expressed among the samples (Figure 2.3h). However, some differences exists with the Golfito Complex, as higher FeO*, CaO and Al_2O_3 contents in the Azuero Proto-Arc Group (Figure 2.3b, f, g). Due to particular plateau-like affinities combined with typical near-arc signatures (i.e. low Nb-Ti contents and high Pb content) and emplacement of the Azuero Proto-Arc on the top of the Azuero Plateau, we interpret the bulk of the Azuero Proto-Arc group to represent a record of the onset of the arc magmatism along the Azuero Plateau in the late Cretaceous. In details, all igneous samples have not been dated and it is possible that some of the Azuero Proto-Arc igneous rocks formed in the Tertiary, well after the onset of arc magmatism. Actually, we suspect that some portions of pristine mantle source present during the arc initiation may have been preserved in later arc stages, allowing younger formation of magmas with proto-arc signatures. Precise radiometric ages and isotope data are needed for the Proto-Arc igneous rocks to verify this hypothesis.

Igneous rocks of the Azuero Arc Group are characterized by typical arc-related signatures (Figures 2.3, 2.4, 2.5). The group represents a submarine to subaerial arc that developed between the late Cretaceous and the late Eocene (see also *Lissinna* [2005] and *Wörner et al.* [in press]). High incompatible elements content, low Nb-Ti contents and enrichment in slab-derived mobile elements (e.g. K or Pb) are indications that the "Azuero Arc" is issued from a mature supra-subduction magmatic system that followed the emplacement of the older Azuero Proto-Arc Group.

Even though trace element contents of the Azuero Arc Group are similar to the igneous rocks of the Punta Samara [*Patino et al.*, 2004] (Figures 2.4, 2.5), important differences arise in terms of major and minor elements content (Figure 2.3), with notably lower FeO*/MgO, CaO and Al_2O_3 in the "Azuero Arc". Late Cretaceous - early Tertiary Arc-related igneous rocks from the Rio Morti area [*Maury et al.*, 1995] have broadly similar characteristics than the Azuero Arc Group (Figures 2.3, 2.4, 2.5) and may have initially be part of a same arc. The Morti, Samara and Azuero arcs are all enriched in the most incompatible trace elements (Figure 2.3e, 2.4, 2.5). This argues against a primitive island arc or proto-arc origin for these suites. High FeO*/MgO of the Samara Arc seem to be controlled by an unusually low MgO content rather than the low FeO* content typical of IAT suites (e.g. the Tonga Arc, Figure 2.3).

2.7. Onset of the arc magmatism in southern Central America: description and implications

Though being ~400 km distant form each other, the Golfito Complex (southern Costa Rica) and the Azuero Complex (western Panama) define a consistent tectonostratigraphy that

point toward a similar tectonic development of the area: in the late Campanian (~75-73 Ma) subduction initiated along the SW margin of the Caribbean Plate, leading to the development of an arc on top of an oceanic plateau. In this chapter, we describe a model for the arc initiation and discuss some other implications of our results.

2.7.1. Early history of an island arc developing on an oceanic plateau

2.7.1.1. Onset of subduction

In the late Campanian (~75-73 Ma) what will become later the NW edge of the Caribbean Plate was composed of an old (late Jurassic ?) oceanic crust overthickened by a Turonian-ealry Santonian (~89-85 Ma) oceanic plateau (Figure 2.10). This plateau is presently exposed in the Azuero Complex and has been defined here as the Azuero Plateau (Figure 2.9a). It probably extends under the arc toward the Caribbean and may comprise the overthickened Colombian Basin (see Chapter 2.7.2). We propose that initiation of a subduction zone along the Azuero Plateau in the late Campanian (~75-73 Ma) was triggered by an increase of E-W compressive stresses (Figure 2.10). Development of a thrust zone along the oceanic plateau was facilitated by rheologic contrasts in the lithosphere [*Niu et al.,* 2003] and, possibly, by an intra-oceanic transform along the edge of the plateau [e.g. *Toth and Gurnis*, 1998; *Hall et al.*, 2003; *Stern*, 2004].

Although our data do not strictly impede an *in situ* origin for the Caribbean Plate [e.g. *Meschede and Frisch*, 1998], tectonic processes leading to onset of subduction along the Azuero Plateau are best explained by allochtonous models [e.g. *Pindell et al.*, 2005, 2006; *Mann et al.*, 2007]. We propose here that late Campanian E-W compressive stresses developed along the SW edge of the Azuero Plateau (or trailing edge of the "CLIP") in response to (1) progressive incorporation of a partly-overthickened oceanic crust ("CLIP") between the W-migrating Americas in the latest Cretaceous as a response of the opening of the Atlantic Ocean and (2) Campanian collisions of the "CLIP" and, possibly, CCM Island Arcs with South America in Ecuador [*Vallejo et al.*, 2006; *Vallejo*, 2007], resulting in a propagation of subduction along the trailing edge of the "CLIP" (Figure 2.10).

2.7.1.2. Arc initiation

In the late Campanian (~75-73 Ma), only ~10 Ma after the cessation of plateau volcanism, subduction initiated along the Azuero Plateau. Igneous rocks produced by supra-subduction magmatism commenced to emplace within and on top of the plateau (Figure 2.9b). These rocks are exposed today in the Golfito and Azuero complexes and pertain to the Golfito Igneous Basement, the Golfito Formation, and the Azuero Proto-Arc Group (the later being partly found as intrusives within the Azuero Plateau). At the onset of subduction the mantle above the subducting plate was part of the pristine lithosphere associated to the oceanic plateau. Fluids proceeding from subducted sediments and serpentinites of the slab were progressively released into the overlying mantle, causing a melting of the plateau-related mantle. As a consequence, igneous rocks with affinities very similar to oceanic plateaus were produced.

(A) pre-late Campanian (>75 Ma)

oceanic
currents

"Normal" Oceanic Crust

Oceanic Plateau

Pelagic limestones

Oceanic crust

Pelagic sediments

Overthickened lithosphere

(B) late Campanian (75-73 Ma)

Submarine volcanism

Seamount

Proto-arc

Onset of dehydration processes and fluid flow within plateau-related lithosphere

(C) latest Campanian (~71 Ma)

Submarine volcanism

Subaerial volcanism

Arc

Tuffaceous deposits

Lithosphere delamination / Refreshing mantle wegde

(D) Maastrichtan (~70 to 66 Ma)

Continuous landbridge

Latest Cretaceous Oceanic Plateau (Inner Osa Igneous Complex, Costa Rica)

on-going "continentalization"

(E) Eocene (~45 Ma)

Retreating volcanic front in Panama

Seamount

Slab flatening and subduction erosion

Figure 2.9: Model of the arc development in Southern Central America between the late Cretaceous and the Eocene. Full explanations are given in chapter 2.7.1.

Recent cessation of the plateau volcanism at the time of arc initiation was certainly associated with high thermal gradients in the mantle wedge. Hence, only little addition of slab-derived fluids may have been required to drive the sub-plateau mantle under melting conditions so as to produce proto-arc magmas. This may explain why slab-related signatures are variously expressed among proto-arc samples. Insignificant fluid influence during melting resulted in formation of proto-arc igneous rocks almost indistinguishable from typical oceanic plateaus or the "CLIP". This is an important point that provides an explanation for the difficulty in southern Central America to recognize proto-arc igneous rocks on the basis of geochemical data alone.

Field observations show that proto-arc magmas were produced at various distances to the trench, leading to eruption over a broad area (Figure 2.8). Progressive development of superficial magma chambers are recorded by the presence of zoned phenocrysts in the lavas of the Azuero Proto-Arc Group. Low rates of eruption allowed a deposition of hemipelagic limestones between the lava flows, which are observed today in the Golfito Formation and Torio lithostratigraphic unit.
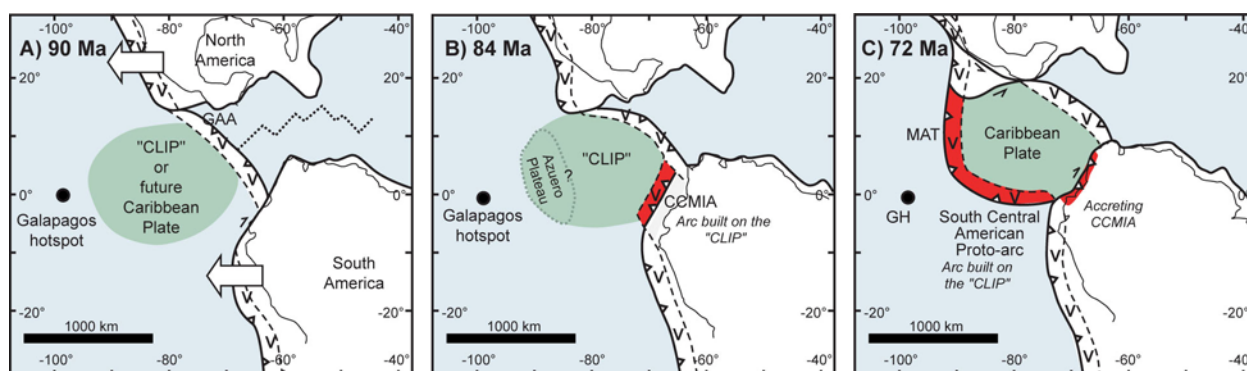
Figure 2.10: *late Cretaceous tectonic reconstruction of inter-American province [modified after Kennan and Pindell, submitted]. Red color: arc initiated along an oceanic plateau.* **A)** *The bulk of the CLIP is emplaced. Due to the opening of the Atlantic, the Americas migrate westward. GAA=Great Antilles Arc [e.g. Pindell et al., 2005].* **B)** *The Azuero Plateau forms in the western part of the future Caribbean Plate. The Cala-Cayo-Macuchi Island Arcs (CCMIA) initiates along the S-SW edge of the CLIP [Vallejo, 2007]. This initiation correlates to collision between the GAA and leading edge of the CLIP at ~85 Ma [White et al., 1999; Thompson et al., 2004].* **C)** *In the late Campanian collision of the CCMIA with South America [Luzieux et al., 2007; Vallejo et al., 2007; Vallejo, 2007] leads to propagation of subduction along the western edge of the CLIP and partial accretion. The South Central American Proto-arc is emplaced on top of the Azuero Plateau, along the trailing edge of the CLIP. In the latest Cretaceous the South Central American Arc may form a landbridge between the Americas, allowing terrestrial migrations.*

2.7.1.3. Arc maturation

In the latest Campanian (~71 Ma) the supra-subduction magma genesis evolved through maturation processes toward more typical arc signatures (Figure 2.9c). Though being currently difficult to fully understand mechanisms controlling early arc maturation on top of the plateau, we propose that initiation of mantle convection led to a refreshment of the wedge by "normal" depleted upper mantle, commonly associated to intra-oceanic volcanic arcs. Refreshment of the wedge may have been facilitated by emplacement of slab-derived mafic melts at the base of the

sub-plateau lithosphere, increasing the mantle density and causing delamination of the lithospheric roots of the plateau. Maturation was probably associated to development of preferential paths of melt migration through the overlying plate, leading to apparition of superficial magma chambers. At this stage, existence of differentiated magmas and developing subaerial volcanism was recorded in the hemipelagic sediments of the Golfito Complex, Azuero Complex and Rio Changuinola area. A well-defined volcanic front progressively developed along the subduction zone that is represented today by a belt of silic intrusives in the Azuero Complex (Figure 2.8). Whether formation of silicic magmas is linked to fractional crystallization and differentiation of mafic melts in magma chambers [e.g. *Ewart and Hawkesworth,* 1987] or melting of supra-subduction mafic intrusives previously emplaced under the volcanic front [e.g. *Tamura and Tatsumi*, 2002; *Leat et al.*, 2003] remains to be constrained. Understanding which process was effective in the early South Central American Arc may be of significant interest for the debate of the role of the oceanic plateaus in the continent formation [e.g. *Ben-Avraham*, 1981; *Niu et al.*, 2003; *Kerr and Mahoney*, 2007].

In the Maastrichtian (~70 to 66 Ma), proto-arc magmatism progressively vanished as the volcanic arc maturated (Figure 2.9d). Subaerial volcanism became widespread, resulting in abundant tuffaceous deposits in both forearc and backarc areas. Continentalization of the plateau associated to supra-subduction magma genesis possibly initiated. Along-strike and temporal shifts between accretion and subduction erosion may have happened and led to the construction of accretionary prisms along the forearc. In the middle Eocene (~45 Ma) abrupt changes in the subduction system (i.e. slab flattening, subduction erosion) caused the arc to retreat in Panama [*Lissinna et al.*, 2002]. This retreat preserved older structures from burial under younger volcanic deposits.

2.7.2. Nature of the arc basement in southern Central America

To date, "CLIP nature" of the arc basement in southern Central America has been constrained by seismic imaging and geochemical studies of recent volcanic rocks only. Although there are many exposures of late Cretaceous volcanic rocks with plateau affinities along the forearc of southern Central America, no evidence of these rocks being part of the basement of the early arc have been provided. Our observations in the Azuero Complex have shown that proto-arc rocks overlay a Coniacian-early Santonian (~89-85 Ma) oceanic plateau. This is the first direct evidence of an oceanic plateau underlying primitive arc-related igneous rocks in South Central America. We have shown that unusual affinities of the Azuero Proto-Arc Group are linked to the emplacement of these volcanic rocks on the top of the Azuero Plateau and the initiation of the subduction in the late Campanian. Hence, igneous rocks with affinities similar to the Azuero Proto-Arc Group may be used to delimit the extension of the plateau under the arc.

Lavas with proto-arc signatures are exposed in the Golfito Complex. These lavas are found in association with late Cretaceous hemipelagic limestones. This is very similar to the tectonostratigraphy of the Azuero Complex and points toward a similar basement for the two complexes. This hypothesis is further strengthened by similar late Cretaceous latitudes of the Golfito Complex, Azuero Complex and western Colombian Basin [*Frisch et al.*, 1992; *Di Marco et al.*, 1995; *Acton et al.*, 2000]. Interestingly, in the Golfito Igneous Basement, a basaltic sample by *Hauff et al.* [2000] has geochemical characteristics very similar to the Azuero Plateau (Figure 2.3h). This sample is located close to an active fault that is associated with the longest and

largest escarpment of the Golfito area. It may thus be part of an exhumed deeper portion of the arc composed of an oceanic plateau.

In the vicinity of the Golfito Complex, volcanic rocks with plateau affinities, part of the Inner Osa Igeous Complex (formerly named "Rincon Block" after *Di Marco*, [1994]), are exposed in the Osa and Burica peninsulas [*Di Marco*, 1994; *Hauff et al.*, 2000; Chapter 3]. Coniacian-Santonian (~87-84 Ma) formation ages of these rocks are defined by radiolarians in associated sediments [*Di Marco*, 1994; *Diserens*, 2002; Chapter 3]. Younger $^{40}Ar/^{39}Ar$ ages of the lava flows [*Hoernle et al.,* 2002] postdate Paleocene ages of forearc sediments deposited on the top of the Osa Igneous Complex [*Di Marco*, 1994; *Di Marco et al.*, 1995]. As a consequence these ages do not represent formation ages of the lavas (see also discussion in Chapter 3.5.3). Although bulk of the igneous rocks of the Inner Osa Igneous Complex have a similar geochemistry and age than the Azuero Plateau, these rocks do not pertain to the arc basement and are accreted, allochtonous fragments of a Pacific oceanic plateau (see also Chapter 3). An allochtonous origin for these rocks is well defined by: (1) distinct facies of the sediments associated to plateau lavas in the Inner Osa Igneous Compelx and Azuero Plateau, (2) distinct geochemistry for some igneous rocks of the Inner Osa Igneous Complex, and (3) the late Cretaceous latitudinal position of the Osa Igneous Complex (Burica Peninsula) that differs from the position of the near-arc formations of the Golfito and Azuero complexes at the same time [*Frisch et al.*, 1992; *Di Marco et al.*, 1995] (see chapters 2.2.3. and 2.2.4.).

In the Nicoya Peninsula (northern Costa Rica), late Cretaceous paleolatitudes are distinct from those of the Golfito and Azuero complexes [*Di Marco et al.*, 1995]. An allochtonous origin (distinct from the "CLIP") has been proposed for some part of the plateau rocks in Nicoya [e.g. *Flores et al.*, 2004; *Bandini et al.*, 2008]. However, some portions of the Nicoya Peninsula were emplaced close to an arc system in the Coniacian [*Flores*, 2003], indicating that an oceanic plateau may form the arc basement in northern Costa Rica. The Herradura Complex (northern Costa Rica) may represent a possible lateral extension of this plateau. More stratigraphic constraints are nonetheless required to associate these complexes to the arc basement and "CLIP".

The Herradura Complex (northern Costa Rica) is composed of Coniacian-Santonian igneous rocks with an oceanic plateau origin [*Hauff et al.*, 1997, 2000]. This complex is exposed in the foreland of a Maastrichtian to early Eocene accreted oceanic island [*Arias*, 2003]. If strike-slip motion did not significantly affect the pristine arrangement of the area, it is required that the late Cretaceous Herradura Complex emplaced along the margin subsequently to the younger Tulín Formation and, thus, is composed of accreted fragments of an oceanic plateau distinct from the arc basement.

In the Rio Chagres area (central Panama, canal area), *Wörner et al.* [2005] described a complicated arrangement of late-Cretaceous to Tertiarty arc-related volcanic rocks. No oceanic basement was observed. However, a more recent contribution reported the presence of volcanic rocks with affinities similar to the proto-arc igneous rocks of the Golfito and Azuero complexes [*Wörner et al.*, in press]. As a consequence it appears that the plateau may extent in eastern Panama and be exposed in the San Blas Complex. Along the Pacific coast of Eastern Panama, volcanic rocks with plateau affinities have actually been observed [*Lissinna*, 2005]. However, these rocks have a probable Campanian-Maastrichtian age [*Bandy and Casey*, 1973] that is very similar to the age of the oldest arc rocks of eastern Panama [*Maury et al.*, 1995; *Wörner et al.*, 2005, 2006, in press]. It is therefore unlikely that the San Blas Complex is part of the arc basement. Similarly to South Costa Rican igneous complexes with plateau affinities (i.e. the

Inner Osa Igneous Complex), the eastern Panamean plateau rocks are exotic with respect to the Caribbean Plate and are part of an accretionary complex [*Coates et al.*, 2004]. Campanian-Maastrichtian igneous rocks with plateau affinities in western Colombia (Serranía de Baudó) [*Kerr et al.*, 1997] may represent a lateral extension of the eastern Panamean accretionary complex. These rocks may thus be unrelated to the "CLIP". Further field work and mapping are needed in this area to better constrain the presence of accretionary complexes.

In the Rio Changuinola area (NW Panama - SE Costa Rica), late Cretaceous sediments similar to the Torio lithostratigraphic unit of the Azuero Complex are exposed [*Fisher and Pessagno*, 1965]. Although some basaltic lava flows seem to be associated with these limestones [*Lissinna*, 2005], geochemistry of these lavas has not been reported. Once again, further work is needed in the area to constrain the affinities of these lavas. If proto-arc rocks are recognized, this may help to link the plateau underlying the primitive island arc to the overthickened oceanic crust observed in the Colombian Basin.

In summary to preceding observations, we propose that a Coniacian-early Santonian (~89-85 Ma) oceanic plateau underlies most of the southern Central American Isthmus. This plateau is exposed in the Azuero Complex and defines the Azuero Plateau (Figures 1.2, 2.8). A typical exposure of this plateau is located along the shores south of Torio and was previously described by *Kolarsky et al.* [1995b, Figure 13]. The plateau may extend toward the Colombian Basin and be part of the oceanic plateau encountered in this area [*Bowland and Rosencrantz*, 1988; *Bowland*, 1993]. It served as a nucleus for subsequent accretions of igneous rocks with both plateau and OIB affinities. Igneous rocks with plateau affinities that are not part of the arc basement and accreted are exposed along the forearc area in: (1) most parts of the Nicoya Peninsula (northern Costa Rica), (2) the Herradura Complex (northern Costa Rica), (3) the Inner Osa Igneous Complex exposed in the Osa and Burica peninsulas (southern Costa Rica), (4) eastern Panama (San Blas Complex by *Coates et al.* [2004]), and (5) western Colombia (Serranía de Baúdo). These igneous rocks are part of accretionary complexes and do strictly not pertain to the "CLIP" in the sense they were initially separated from the overthickened crust forming parts of the Caribbean Plate.

2.7.3. A late Cretaceous migration pathway between the Americas

The South Central American proto-arc rocks are found in the Golfito Complex (southern Costa Rica), Azuero Complex (western Panama) and in the Rio Chagres area (central Panama, *Wörner et al.* [in press]). Occurrences of this rocks points toward a continuous proto-arc between southern Costa Rica and central Panama in the latest Cretaceous. In this section we further discuss the extension of this arc and explore implications in terms of terrestrial vertebrate migration.

In northern Costa Rica (Punta Samara), undated boulders of volcanic rocks embedded in Paleocene sediments have been interpreted to record the erosion of a late Cretaceous Primitive Island Arc [*Patino et al.*, 2004]. However, these volcanic rocks have relatively high incompatible elements content and a FeO* content much lower than typical IAT (Figures 2.3d, 2.4, 2.5). This is not in agreement with a primitive island arc origin. A Coniacian arc-related subaerial volcanism is recorded in the same area, pointing toward the presence of a much older arc in southern Nicaragua [*Flores*, 2003]. Whether volcanic boulders at Punta Samara proceeded from an arc resting on the Mesquito Oceanic Terrane or from an arc emplaced on the margin of the Caribbean Plate remains undefined. Tertiary arc volcanism of northern Costa Rica unfortunately

buried many of the late Cretaceous formations and poor constraints on the arc initiation have been preserved in this area. It is however very likely that a proto-arc developed in central-northern Costa Rica in the late Cretaceous.

Paleocene arc deposits and volcanic rocks are exposed over much of southern Central America, from northern Costa Rica to eastern Panama [e.g. *Schmidt-Effing*, 1979; *Maury et al.*, 1995; *Mende*, 2001]. These deposits recorded the presence of a maturing arc system that followed the onset of subduction along the edge of the Caribbean Plate. Our observations from the Golfito Complex and Azuero Complex indicate that subaerial volcanoes and shallow-water environments were present during the late Cretaceous in the area. Similarly, late Cretaceous shallow-water limestones rest on the arc margin in northern Costa Rica [*Jaccard et al.*, 2001]. Although indications of shallow-water environments have not been reported along the Maastrichtian-Paleocene volcanic arc of eastern Panama [*Maury et al.*, 1995; *Coates et al.*, 2004; *Wörner et al.*, 2005], it is clear from our observations that shallow-water and subaerial environments were very common along the volcanic arc in the late Creaceous-early Tertiary. This is in good accordance with observations on the biota speciation that point toward subaerial environments for Central America in the late Cretaceous-early Tertiary [*Briggs*, 1994].

As indicated by *Briggs* [1994], tectonic reconstructions of the Caribbean and biological constraints from ancient fauna migrations and biota speciation have been at odds for a long time. Many tectonic reconstructions have suggested a formation of the Central American Arc far from South America in the late Cretaceous/early Tertiary. On the other hand, an inter-Americas migration pathway in the late Cretaceous and Paleocene is indicated by the fossil record of terrestrial vertebrates in North and South America [*e.g. Gayet et al.*, 1992; *McCarthy*, 2005, and references therein]. According to *Briggs* [1994], migration of terrestrial fauna in the late Cretaceous through the Antilles or currently-drown Aves arc unlikely occurred because no one has pointed out that these arcs were composed of more than a string of small, isolated islands. Thus, in accordance with the most recent tectonic models (see *Mann et al.*, [2007]) and our results indicating that subaerial volcanism was widespread along the southern Central American Arc in the latest Cretaceous/early Tertiary, we propose that the southern Central American Arc was forming a possible pathway for the migration of the terrestrial vertebrates in that time (Figure 2.10c). This proposition is in accordance with latest Cretaceous ages of "interaction" between intra-oceanic island arcs and the South America [*Luzieux et al.*, 2006; *Vallejo et al.*, 2006; *Vallejo*, 2007].

Current geological data provide poor constraints on the history of the South Central American landbridge during the Tertiary. Nonetheles arc shifting in western Panama in the middle Eocene [*Lissinna et al.*, 2002] indicates that the South Central American Arc has probably a complicated history. Migration paths of terrestrial animals may have been temporarily broken during middle Eocene tectonic events. Such a situation is actually in agreement with mammal migrations occurring through the Antilles at this period [*Iturralde-Vinent and MacPhee*, 1999; *Iturralde-Vinent*, 2006].

Closure of the Panamean Isthmus ~4 Ma [*Coates et al.*, 1992; *Haug and Tiedemann*, 1998] shows that, though many parts of the late Cretaceous arc were above the sea level, some remained under submarine condition for a long time, allowing a communication between the Pacific and Atlantic Oceans through a Panama isthmian strait [*Collins et al.*, 1996]. Connexion between the Pacific and Atlantic Oceans seems to be further supported by $\delta^{18}O$ record of phosphatic fish debris from North Africa that point toward paleo-Pacific westward currents at the Cretaceous-Tertiary boundary. However, the Panamean strait should have remained relatively

narrow so as to allow the migration of the terrestrial vertebrates on rafts. The late Miocene regional unconformity observed in the Darien area, previously interpreted as a record of the collision of the Panama Microplate with the South American Plate [*Coates et al.*, 2004], was more likely induced by a rapid increase in the rates of convergence between the two plates.

2.8. Summary and Conclusions

1. The Golfito Complex comprises (1) a pre-late Campanian igneous basement, (2) a late Campanian to Maastrichtian volcano-sedimentary formation, and (3) younger detrital and peri-platform deposits. The base of the Golfito sequence is composed of a proto-arc that developed on the top of an oceanic plateau between the late Campanian and the Maastrichtian (~75 to 66 Ma). In the Maastrichtian and early Tertiary, proto-arc magmatism vanished in the Golfito area and was progressively buried under younger deposits derived from a nearby maturing, subaerial volcanic arc.

2. The Azuero Complex is composed of (1) an autochtonous basement made of Coniacian-early Santonian (~89-85 Ma) oceanic plateau, (2) a late Campanian (~75-73 Ma) to Maastrichtian (?) proto-arc emplaced on the top of the plateau, (3) a late Cretaceous to Eocene (~70 to 45 Ma) arc that followed the development of the proto-arc, (4) a late Cretaceous to Eocene accretionary complex that is in contact with the oceanic plateau along a tectonic mélange, and (5) a diachronous middle Eocene to Oligocene (~45 to 25 Ma) regional overlap sequence. The stratigraphic development of the Azuero Complex shows that a late Campanian to Maastrichtian (?) proto-arc formed on top of a Turonian-early Santonian (~89-85 Ma) oceanic plateau defined here as the "Azuero Plateau". In the Maastrichtian, the proto-arc was progressively replaced by a more mature, subaerial arc.

3. The Golfito and Azuero complexes contain strong stratigraphic and geochemical constraints indicating that initiation of subduction in southern Central America occurred in the late Campanian (~75-73 Ma) along the late Cretaceous (~89-85 Ma) Azuero Plateau.

4. The onset of subduction along the Azuero Plateau produced unusual supra-subduction igneous rocks that are exposed from southern Costa Rica to western Panama [*this study*] and central Panama [*Wörner et al.*, in press]. These rocks are part of proto-arc sequences defined in this study. Proto-arc igneous rocks are characterized by an unusual geochemistry intermediate between typical oceanic plateaus and intra-oceanic island arcs. Due to high thermal gradients in the sub-plateau lithosphere at the onset of arc magmatism and various influences of slab-derived fluids in the earliest supra-subduction magmas some proto-arc igneous rocks are very similar and sometimes indistinguishable from typical oceanic plateaus.

5. Dikes of proto-arc igneous rocks within the Azuero Plateau and occurrences of proto-arc igneous rocks from southern Costa Rica to central Panama constitute strong indications of an oceanic plateau forming the basement of the South Central American Arc. The Azuero Plateau may extend further toward the Colombian Basin and pertain to the overtickened Caribbean crust. It served as a nucleus for accretion of oceanic plateaus and seamounts of Pacific origins.

6. The initiation of subduction along the SW edge of the Caribbean Plate was followed in the late Cretaceous and early Tertiary by a combination of erosion and accretion that is attested by the closeness of early arc sequences to the trench/paleo-subduction zones and the presence of uplifted accretionary complexes, notably in the SW side of the Azuero Peninsula and southern Costa Rica (see also Chapters 3 and 5).

7. Many igneous complexes with plateau affinities exposed along the outer margin of Costa Rica and Panama are exotic with respect to the Caribbean Plate and, thus, do not pertain to the early arc basement (i.e. the Azuero Plateau). These complexes are not strictly part of the "CLIP" since their origins are distinct from the overthickened Caribbean crust.

8. In the late Cretaceous/early Tertiary, the southern Central American Proto-Arc was likely extending from northern Costa Rica to eastern Panama. Many areas along the southern Central American Arc were characterized by subaerial and shallow-water environments. This may have constituted a pathway between North and South America for terrestrial vertebrates, reconciling the geological observations with the fossil record and speciation processes.

9. In the Azuero Complex, we observed a unique sequence composed of an oceanic plateau at the base and younger arc-related intrusive and extrusive rocks emplaced into- and above the plateau. This provides a unique opportunity to explore into details possible petrologic mechanisms linking the oceanic plateaus to the continents.

Photo 2.1: *Proto-arc basaltic dike intruding late Campanian hemipelagic limestones and proto-arc lavas of the Golfito Formation (shoreline at Golfito, ~406100/936100 UTM WGS84). Note soft behavior of poorly lithified sediments at the contact with the dyke.*
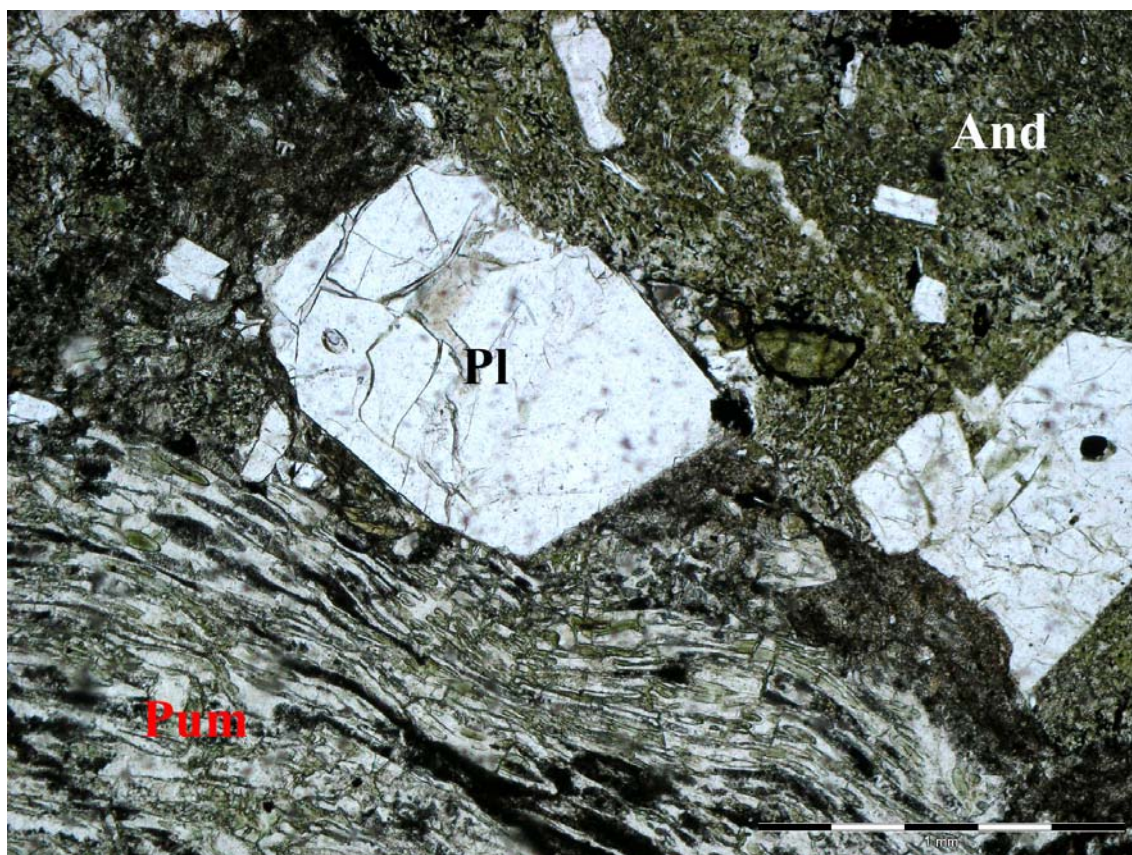
Photo 2.2: *Microphotograph of a coarse tuffite from the Achiote Formation (sample DB02-090). Fragments: Pl=plagioclase, And=andesite, Pum=pumice.*
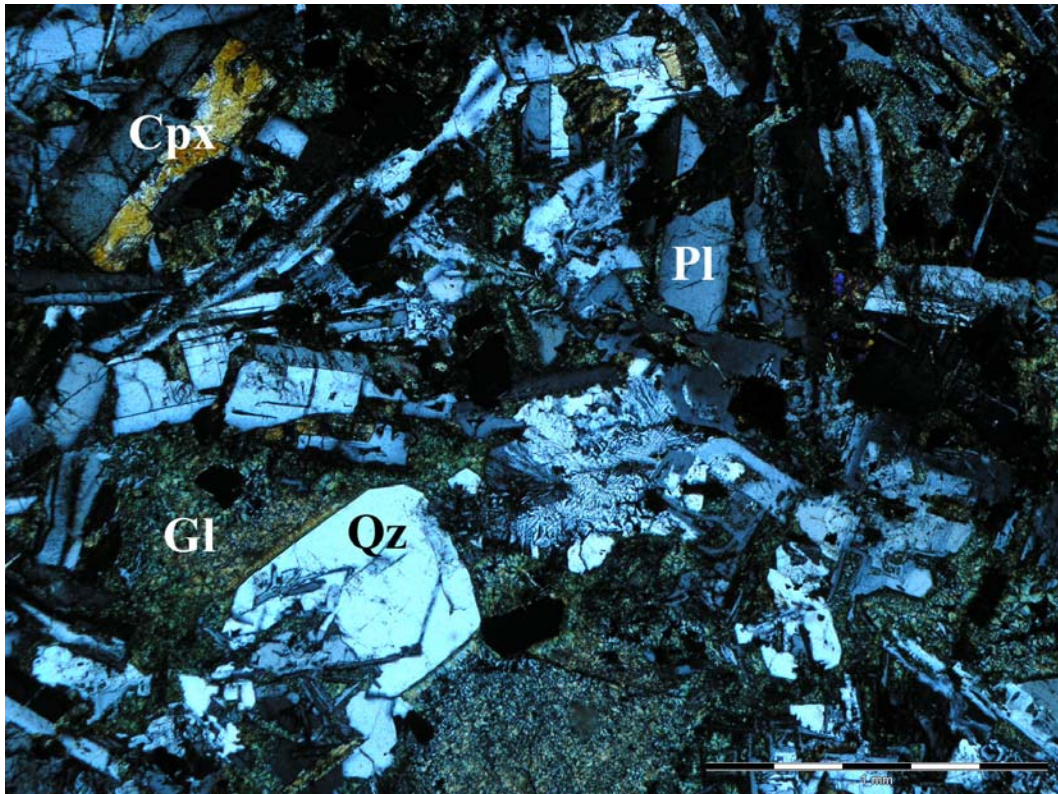
Photo 2.3: *Microphotograph (polarized light) of a coarse basalt with occurrences of secondary quartz in interstitial glass. Gl=glass (altered), Qz=quartz, Pl=plagioclase, Cpx=magnesian clinopyroxene.*
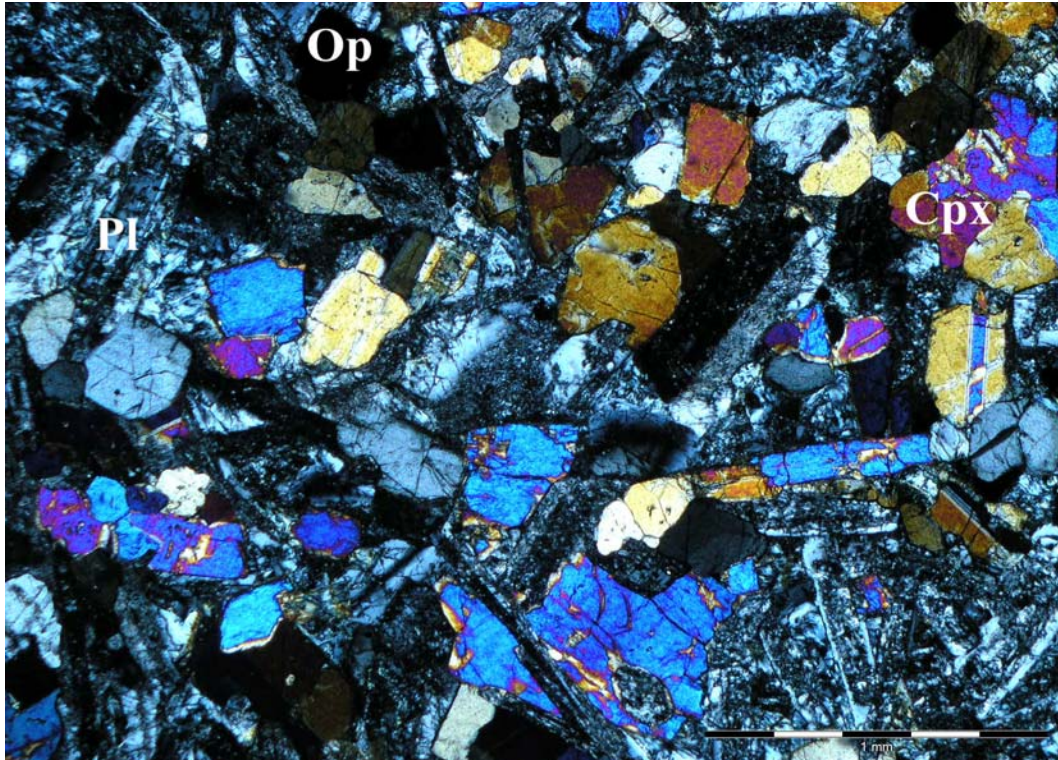
Photo 2.4: *Microphotograph (polarized light) of DB02-042 coarse basalt. Op= opaque minerals (Fe-Ti oxides and sulfides).*
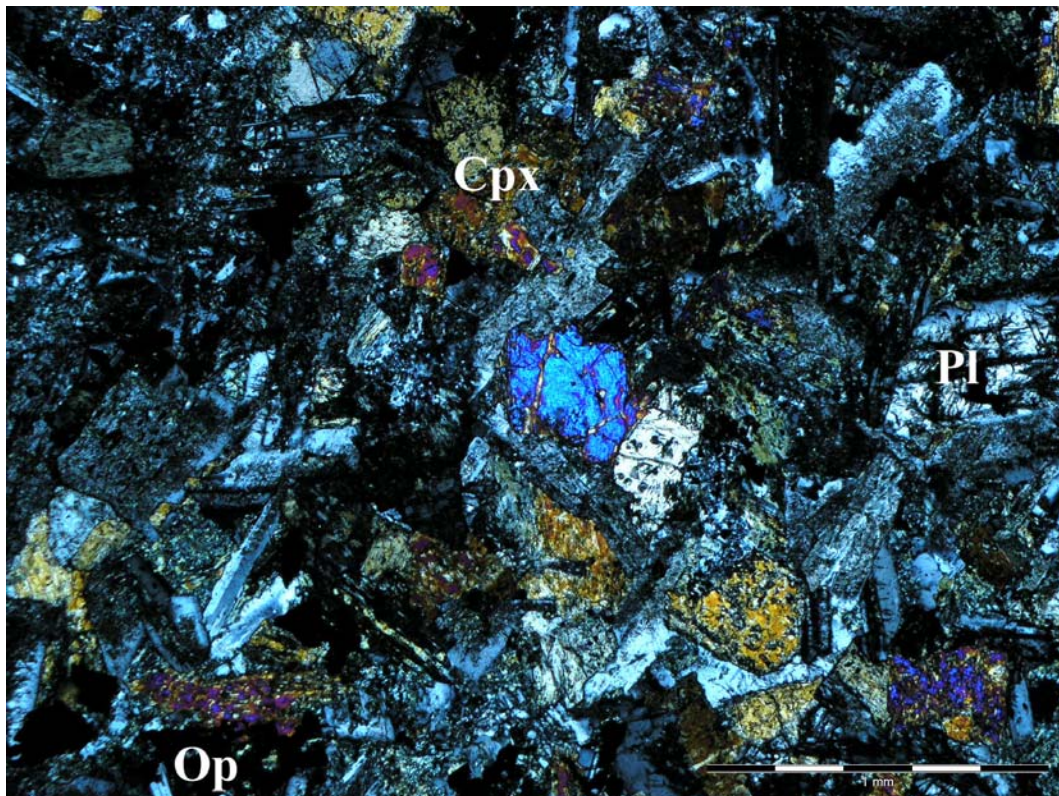
Photo 2.5: *Microphotograph (polarized light) of DB02-101 coarse basalt. Note cpx at the center is better preserved than global state of the whole rock.*
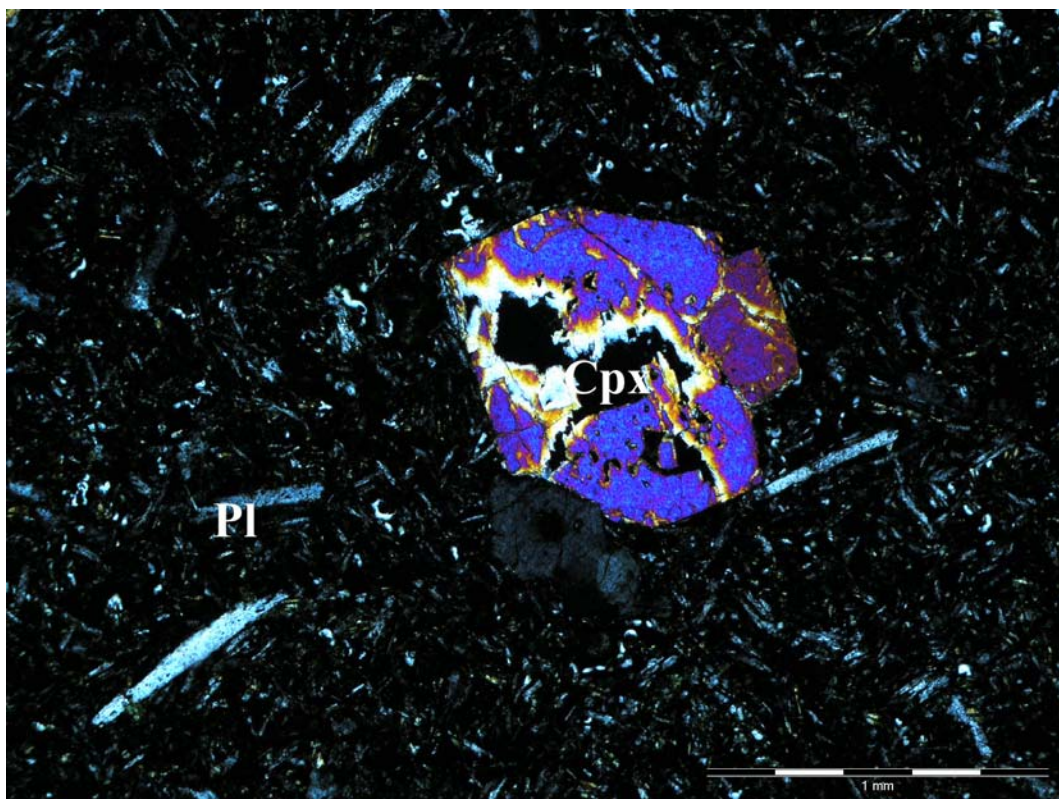
Photo 2.6: *Microphotograph (polarized light) of DB02-175 porphyric basalt.*

Photo 2.7: *Proto-arc basaltic dike intruding a late Campanian hemipelagic limestone of the Torio lithostratigraphic unit (northern Coiba Island, 415710/844800, UTM WGS84). These limestones grades upward to tuffaceous sediments. Similarly to the Golfito Formation, these sediments were unlithified at the time of intrusion.*

Photo 2.8: *Details of the chilled margin of a proto-arc basaltic sill intruding the Azuero Plateau along Torio shoreline (504495/832730, UTM WGS84). Plagioclase phenocrysts accumulated at the top of the sill by flotation. The sill is fed by a dike emplaced along a paleo-fault.*

Photo 2.9: *Giant plagioclase basalt in the Azuero Plateau (Punta Madroño, Playa Venado, southern Azuero, 587640/820775, UTM WGS84).*

Photo 2.10: *Giant plagioclase basaltic flow in the Azuero Plateau (Punta Madroño, Playa Venado, southern Azuero, 587640/820775, UTM WGS84). White dots are giant plagioclases.*

Chapter 3: Late Cretaceous to Miocene Seamount Accretion and Mélange Formation in the Osa and Burica Peninsulas (Southern Costa Rica): Episodic Growth of a Convergent Margin

This chapter is based on a manuscript in review that has been submitted to "Geology of the area between North and South America, with focus on the origin of the Caribbean Plate", Geological Society of London special publication, in preparation, edited by K.H. James, M.A. Lorente and J. Pindell. Some of the following results were used in a Comment to Vannucchi et al. [2006].

3.1. Introduction

The Osa and Burica peninsulas lies in southern Costa Rica, on the southwestern edge of the Caribbean Plate, along the convergent margin between Central America and the subducting Cocos Plate (Figures 1.1, 1.2). The peninsulas lie directly above the submarine Cocos ridge, an aseismic volcanic ridge which rises ~2000 m above the adjacent sea floor and constitutes a significant topographic high entering the subduction zone [*Walther*, 2003]. The subducting ridge formed above the Galapagos hotspot 13.0-14.5 Ma ago [*Werner et al.*, 1999] and is currently moving northeastward at a rate of ~90 mm/y [*Trenkamp et al.*, 2002]. It is believed to have started colliding with the Caribbean plate 8-1 Ma (most probably ~2 Ma) ago [*MacMillan et al.*, 2004, and references therein], causing forearc shortening, large-scale block tilting and local cessation of volcanism [*Kolarsky et al.*, 1995a; *Fisher et al.*, 1998, 2004; *Abratis and Wörner*, 2001; *Gräfe et al.*,, 2002; *Morell et al.*, 2008]. The Osa and Burica peninsulas were uplifted and emerged in response to the Cocos Ridge subduction, with an estimated average long-term rate of uplift of 1-2 mm/y [*Corrigan et al.*, 1990; *Collins et al.*, 1995; *Mann and Kolarsky*, 1995]. Their morphology is controlled by active faults, interpreted to intimately relate to the morphology and roughness of the subducting plate, that define large tilted, variously uplifted blocks [*Sak and Fisher*, 2004; *Vannucchi et al.*, 2006] (Figure 3.1b).

In southern Central America, subduction initiation occurred in the Campanian along a Coniacian-early Santonian oceanic plateau (Chapter 2, see also discussion of ages in Chapter 3.4.4.1). This plateau is exposed on the Azuero Peninsula (western Panama) and represents the first clear occurrence of arc basement in southern Central America. The Azuero Plateau may represent the SW edge of a larger oceanic plateau that extends eastward into the Caribbean, generally defined as the Caribbean Large Igneous Province (CLIP) or Caribbean-Colombian Oceanic Plateau (CCOP) [e.g. *Kerr et al.*, 2003; *Hoernle et al.*, 2004] (Figure 1.1). Due to the location of the South Central American Arc in the western Caribbean and on the basis of similar geochemistry and ages of the igneous rocks, many igneous complexes exposed along the forearc of Central America have been associated to the CLIP [e.g. *Sinton et al.*, 1997]. However these data cannot rule out the possibility that the igneous complexes were initially distinct volcanic edifices that became subsequently amalgamated along the margin by accretionary processes. Tectonostratigraphic constraints are thus needed to better understand the origins of these igneous complexes.

The purpose of this study is to present new geological, geochemical and palaeontological data on both the inner (isthmus side) and outer southwestern Osa Peninsula and Burica Peninsula

in order to characterize the age, tectonostratigraphy and internal arrangement of the exposed rocks. The area of study lies only 15 km from the Middle American Trench and, thus, represents one of the outermost sections of the Costa Rican margin. It provides onland access to rocks and structures that usually lie deep under the sea, close to the subduction zone. Indeed, rock exposures in the Osa Peninsula are generally expected to be collected/observed during drilling and dredging only. Their significance in terms of accretionary processes and tectonic erosion is developed here on the basis of: (1) 6 months of field survey over the entire area, (2) petrological characteristics of 455 samples, (3) geochemical analyses of the igneous rocks and (4) a micropalaeontological survey. We further show that igneous complexes exposed on the Osa and Burica peninsulas are exotic with respect to the Caribbean Plate and, as a consequence, are not part of the CLIP.

3.2. Geologic setting of the Osa and Burica peninsulas

In the literature the Osa Peninsula has been divided into two main units based on dominant lithology: (1) the Osa Igneous Complex (originally defined as the "Rincon Block" by *Di Marco* [1994]) and (2) the Osa Mélange (originally defined as the "Osa Caño Accretionary Complex" by *Di Marco* [1994] (Figure 3.1). We first propose here that the Osa Igneous Complex is not limited to the Osa Peninsula and extends toward the SE in the Burica Peninsula. In the Burica Peninsula, the complex comprises a late Cretaceous igneous complex called "Burica Complex" or "Burica Terrane" by previous authors [e.g. *Obando*, 1989; *Di Marco*, 1994; *Hauff et al.*, 2000]. Whereas the Osa Igneous Complex is present in both the Osa and Burica peninsulas, exposures of the Osa Mélange are restricted in the outer part of the Osa Peninsula. Most of the area is unconformably overlain by Paleocene to Pleistocene sediments called herein "overlap sequences", in opposition to underlying rocks forming the "basement" (Figure 3.1).

The basement rocks of the Osa Peninsula were seen for a long time to be part of the "Nicoya Complex", an accreted oceanic plateau cropping out in the NW Nicoya Peninsula [*Denyer and Baumgartner*, 2006]. However, strong incompatibilities between the Nicoya Complex and the Osa area exist in terms of age, lithology, and tectonostratigraphy of igneous and sedimentary rocks, as well as geochemistry [e.g. *Denyer et al.*, 2006]. In this chapter we focus on the geology of the NW Osa Mélange and Osa Igneous Complex. A colored geological map of the area is given by *Buchs and Baumgartner* [2007]. Figure 3.1 is an updated grayscale version of this map.

3.2.1. The Osa Igneous Complex

The Osa Igneous Complex is limited on the trenchward, SW side by the Osa Mélange and on the landward, NE side by the late Cretaceous to early Tertiary Golfito Complex. The latter is broadly composed of: (1) a proto-arc that developed on the top of the CLIP in the Campanian to Maastrichtian, and (2) younger overlapping sediments (Figures 2.1, 3.1). The lateral extension of the Osa Igneous Complex toward the NW is not known. Toward the SE it extends in the Burica Peninsula and, possibly, in the Montijo Gulf (western Panama, Figure 1.2).

The Igneous Complex is composed by basalts, microgabbros, dolerites and minor gabbros, with rare (<1%) intercalations of radiolarian cherts, black shales, and pelagic limestones [*Dengo*, 1962; *Tournon*, 1984; *Obando*, 1986; *Berrangé and Thorpe*, 1988; *Di Marco*, 1994; *Di*
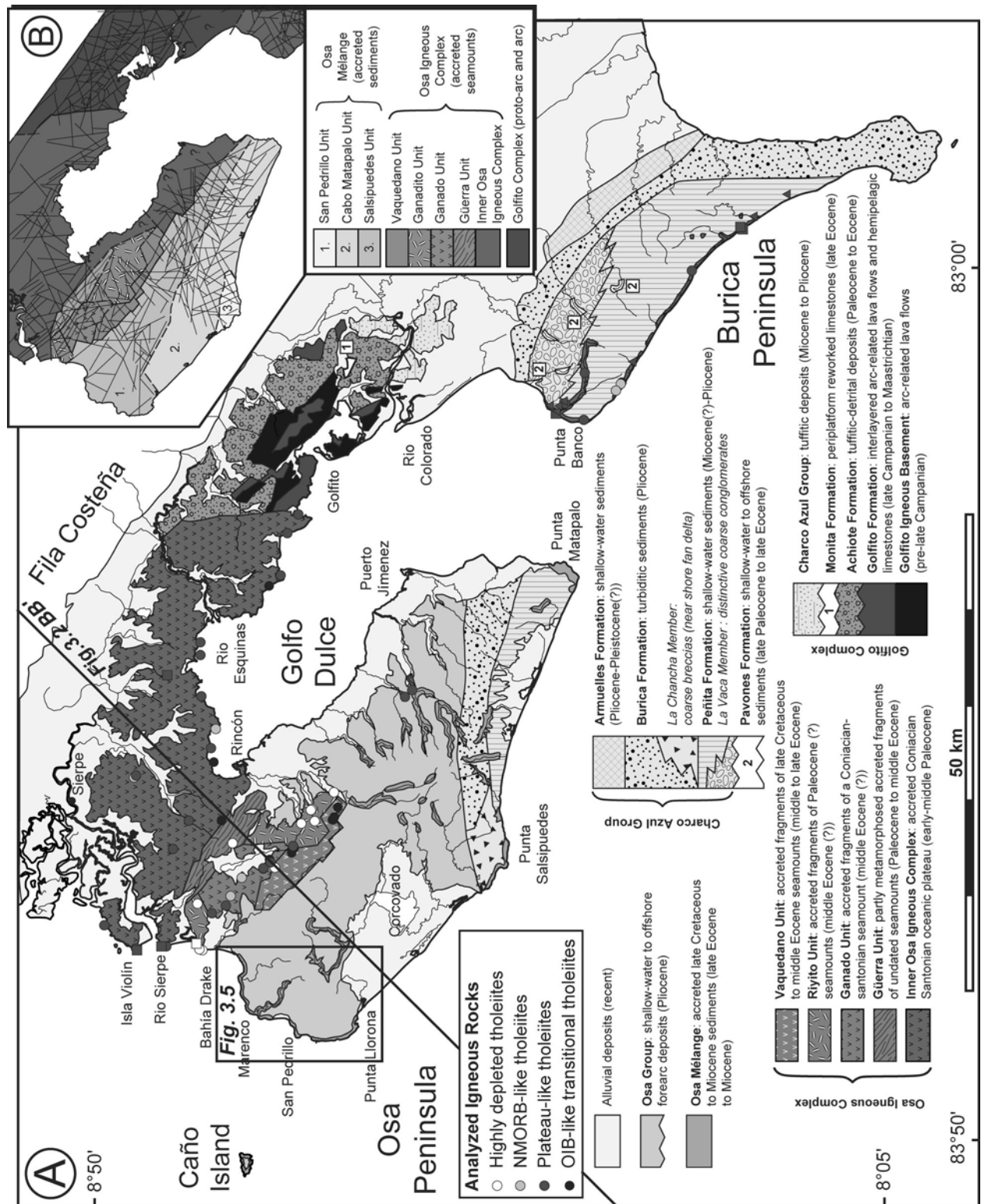
Figure 3.1: A) *Geological map of the Golfo Dulce area modified after Buchs and Baumgartner [2007] and references therein. Analyzed igneous rocks: circles = samples from this study, squares = samples from Hauff et al. [2000], triangles = samples from Di Marco [1994], partly re-analyzed in this study.* **B)** *Geological map of the Golfo Dulce area illustrating basement rocks (i.e. underlying recent alluvial deposits, as well as overlap sediments of the Charco Azul and Osa Groups). Lineaments are based on satellite imagery (pixel size of 28.5 m) and DEM (3 arc seconds). Lineaments in the Golfito area are from Mende and Astorga [2007].*

Marco et al., 1995; *Buchs*, 2003]. Radiolarian and foraminiferal assemblages from these sediments provide ages ranging from Campanian to Eocene [*Di Marco*, 1994]. K-Ar ages of the basalts range from late Cretaceous to Eocene [Berrangé *et al.*, 1989]. ^{40}Ar/^{39}Ar datings range from 54.5 ± 1.5 to 62.1 ± 0.6 Ma [*Hauff et al.*, 2000; *Hoernle et al.*, 2002]. Basalt geochemistry indicates compositions ranging across NMORB-like, plateau-like and OIB-like affinities [*Berrangé and Thorpe*, 1988; *Di Marco*, 1994; *Meschede and Frisch*, 1994; *Hauff et al.*, 2000]. Origins proposed until now for the Complex are: (1) a back-arc basin [*Berrangé and Thorpe*, 1988], (2) a volcanic arc in the Osa Peninsula and an accreted Pacific seamount in the Burica Peninsula [*Obando*, 1986; *Di Marco*, 1994], (3) an uplifted western Caribbean Plateau [*Meschede et al.*, 1999; *Denyer et al.*, 2006], (4) an accreted aseismic ridge [*Hauff et al.*, 2000; *Hoernle et al.*, 2002, 2004; *Denyer et al.*, 2006; *Vannucchi et al.*, 2006], and (5) accreted seamounts [*Buchs*, 2003]. This wide range of interpretation may be due to highly heterogeneous geochemical affinities and the lack good stratigraphic markers in the igneous rocks.

3.2.2. The Osa Mélange

The Osa Mélange was recognized and differentiated from the Nicoya Complex by *Baumgartner* [1986] and *Baumgartner et al.* [1989], who postulated the presence of an Eocene accretionary prism cropping out on the outer Osa Peninsula and Caño Island. *Di Marco* [1994] and *Di Marco et al.* [1995] subdivided the Mélange into three tectonostratigraphic units, from NE to SW: (1) the San Pedrillo Unit, (2) the Cabo Matapalo Unit and (3) the Punta Salsipuedes Unit (Figure 3.1).

The San Pedrillo Unit consists of a deformed matrix of detrital and siliceous sediments enclosing variable amounts of blocks of igneous rocks, pelagic sediments and resedimented shallow-water carbonates [*Di Marco et al.*, 1995]. The siliceous fraction of the matrix was dated as middle Eocene on the basis of radiolarian assemblages [*Azéma et al.*, 1983]. The igneous blocks have been interpreted as remnants of accreted seamounts by most authors [e.g. *Di Marco et al.*, 1995; *Vannucchi et al.*, 2006], but geochemical affinities of the lava blocks are not determined.

The Cabo Matapalo Unit comprises a detrital matrix containing blocks of late middle Eocene to middle Miocene pelagic limestones. Decimetric blocks of basalts occur within the pelagic limestones [*Di Marco et al.*, 1995].

The Salsipuedes Unit contains "large bodies" of limestones in a fine-grained greywacke matrix [*Di Marco et al.*, 1995]. The ages of the limestones are poorly constrained; a single, Paleocene age was determined by *Azéma et al.* [1983]. Interbedded dark shales and greywackes within the limestones [*Di Marco et al.*, 1995] indicate that this unit is not a mélange *sensu stricto*, but more likely a dismembered sequence.

Various origins and genetic mechanisms have been proposed for the Osa Mélange. *Di Marco et al.* [1995] suggest that the San Pedrillo Unit represents accreted Eocene trench-fill sediments associated with variable amounts of blocks of igneous and sedimentary rocks originally on the subducting plate. These authors see the external part of the Osa Peninsula (the Cabo Matapalo and Salsipuedes units) made by offscraped lenses of Eocene to Miocene pelagic limestones and distal detrital sediments. *Meschede et al.* [1999] postulate that the Osa Mélange is a product of underplated material generated by the tectonic erosion of an outer arc wedge structure at the interface between the descending and overriding plates. *Vannucchi et al.* [2006, 2007] interpret the Osa Mélange as a tectonically disrupted accreted package of oceanic

lithologies that are exotic to the overriding Caribbean Plate. In this interpretation, the mélange suffered pervasive metamorphism and exhibit a "ghost stratigraphy suggesting dismemberment of a classic sequence of oceanic crust". That interpretation is discussed by *Buchs and Baumgartner* [2007].

3.2.3. The overlap sequences

The overlap sequences rest unconformably upon the basement rocks of the Osa Igneous Complex and Osa Mélange. They are composed of: (1) the late Paleocene to late Eocene Pavones Formation, (2) the early Pliocene to early Pleistocene (or younger) Charco Azul Group, and (3) the late Miocene to Pleistocene Osa Group (Figure 3.1).

The late Paleocene to late Eocene Pavones Formation is the oldest overlap sequence in the area [*Obando*, 1986; *Di Marco*, 1994; *Di Marco et al.*, 1995] (Figure 3.1a). This formation crops out in the Burica Peninsula and deposited on the top of previously deformed igneous rocks of the Osa Igneous Complex [*Obando*, 1986; *Di Marco*, 1994] (Figure 3.1a). The Pavones Formation comprises an association of periplatform, reworked shallow-water limestones and siliceous pelagic limestones [*Obando*, 1986; *Di Marco*, 1994]. Although *Di Marco* [1994] considered this formation to be devoid of arc/continent-derived material and to have deposited on the slope of an intra-oceanic seamount, a re-examination of Paleogene samples collected by *Di Marco* [1994] in the Rio La Vaca [*Di Marco et al.*, 1995, p. 13, Figure 7] revealed they contain quartz, zoned plagioclase and green amphibole grains, similarly to earlier observations by *Obando* [1986]. Hence, we propose that the occurrence of these grains constrains the depositional environment of the Pavones Formation close to an arc, presumably a forearc slope. In the middle Eocene, the formation is characterized in the Quebrada Piedra Azul by the unusual occurrence of thick boulders beds reworking fragments of a carbonate platform [*Di Marco et al.*, 1995].

The Charco Azul Group was comprehensively studied by *Corrigan et al.* [1990], *Coates et al.* [1992] and *Collins et al.* [1995]. information It has been subdivided into: (1) the early Pliocene Peñita Formation that uncomformably sits upon the Pavones Formation and basement rocks, (2) the late Pliocene Burica Formation, conformably resting on the Peñita Formation, and (3) the early Pleistocene or younger Armuelles Formation, conformably resting on the Burica Formation (Figure 3.1a). The Peñita Formation is composed of as much of 1200 m of clayed, blue-green siltstone and litharenite consistently rich in benthic and planktic foraminifers, deposited in a forearc slope environment [*Coates et al.*, 1992]. The basal formation is coarse with locally channeled conglomerates, some of which form a distinctive suite defined as La Vaca Member by *Coates et al.* [1992] (Figure 3.1a). These coarse deposits defined a detrital paralic and fan-delta depositional environment at the base of the Charco Azul Group. The Burica Formation consists of about 2800 m of mostly fine-grained, volcaniclastic turbidite deposits with local megabreccias formed by large-scale intraformational slumps [*Coates et al.*, 1992]. The La Chancha Member is a distinctive coarse facies interpreted to represent canyon fill within the trench slope on which the Burica turbidites were deposited [*Coates et al.*, 1992] (Figure 3.1a). Finally, the Armuelles Formation consists of ~370 m of channelled pebbly conglomerate and unconsolidated greenish-blue litharenite and siltstone in the lower part, and predominant grey-blue, clayed siltstone and fine litharenites in the upper part [*Coates et al.*, 1992].

The Osa Group rests on an erosional unconformity cut into the basement rocks in the northern and central Osa Peninsula. This surface is covered by a veneer of paleosoils and

continental deposits hosting the gold deposits of Osa [*Berrangé and Thorpe*, 1988]. Late Miocene to Pliocene sediments hosting the placer gold deposits give way upwards to thick turbidite fan deposits representing a deepening sequence, similarly to the Charco Azul Group. Indeed, *Coates et al.* [1992] note that the Osa Group may actually represent a lateral extension of the Charco Azul Group in northern Osa Peninsula.

In summary to this chapter we can state that the overlap sequences exposed in the Osa and Burica peninsulas are indications of at least two major tectonic events that occurred prior to the deposition of the sediments. The first one preceded unconformable hemipelagic, forearc deposits of the basal Pavones Formation (late Paleocene) [*Di Marco et al.,* 1995]. The second one preceded the unconformable, near-shore deposits of the lower Peñita Formation (early Pliocene) [*Coates et al.,* 1992]. The Charco Azul Group defines a transgressive-regressive cycle between the early Pliocene and the Pleistocene [*Coates et al.*, 1992; *Collins et al.,* 1995]. In the middle Eocene, thick beds bearing shallow-water limestone boulders are observed in the Pavones Formation [*Di Marco et al.,* 1995], which may also represent a record of a third tectonic event. The nature of the overlap sequences provides constraints on the tectonic evolution of the margin. Their significance is discussed below, along with the accretionary record of the Osa Igneous Complex and Osa Mélange.

3.3. Mélanges: nature and origins

In this study, a special emphasis is made on the description and interpretation of the Osa Mélange. Mélanges are generally considered to be very complicated rock bodies and, illustratively, are frequently described as "chaotic rock bodies". We present below a succinct, non exhaustive review on the mélanges, their origins and commonly associated problems. We defined also a nomenclature for our descriptions of the Osa Mélange.

3.3.1. Mélange definition

A recognized definition of a mélange was introduced by *Raymond* [1984] as: "a body of rock mappable at a scale of 1:24 000 or smaller and characterized both by the lack internal continuity of contacts and strata and by the inclusion of fragments and blocks of all sizes, both exotic and native, embedded in a matrix of finer-grained material". The occurrence of fragments and blocks of all size is characteristic of the fractal nature of a mélange (i.e. a repetition of the same block-in-matrix texture at various scales, or "scale independence" by *Medley* [1994]).

The use of the term "mélange" following *Raymond* [1984] requires an *a priori* knowledge of the origin of the described rock body, because it is necessary to make a distinction between exotic and native blocks. When exotic blocks are not found in a rock body without internal stratal continuity, *Raymond* [1984] proposes the use of the term "dismembered unit". However, identification of genetic characteristics may be regarded as a problem in a classification of block-in-matrix rocks because it is sometime difficult to make a distinction between exotic and native blocks. Indeed, *Raymond* [1984] mentions and discusses this issue. Maybe for this reason the use of the term "mélange" in the literature is widely used independently of the definition proposed by *Raymond* [1984] with a broader, simpler meaning of "block-in-matrix rock". This use tends to be confusing because the term "mélange" has thus been attributed to rock bodies having very distinctive fabrics, compositions, origins and geological meanings.

The confusion arising from the use of the term "mélange" led *Medley* [1994, 2001] to propose the term "bimrock" for rock bodies that contain competent blocks of varied lithologies, embedded in sheared matrices of weaker rock. *Medley* [1994, 2001] introduces this term in a geological engineering purpose and defines the bimrock as "a mixture of rocks, composed of geotechnically significant blocks with a bonded matrix of finer texture". "Geotechnically significant blocks" means that there is mechanical contrast between blocks and matrix. Accordingly, Medley's definition is founded on geometric and mechanical parameters. This approach successfully avoids possible confusions related to genetic considerations. On the other hand, it emphasises deformation that may play a role in the formation of the block-in-matrix rocks by introducing a mechanical contrast between the blocks and the matrix as a fundamental parameter. However, some block-in-matrix rocks (such as the Osa Mélange) may locally lack a significant mechanical contrast between the blocks and the matrix.

In view of mélange definitions by *Raymond* [1984] and *Medley* [1994, 2001], it clearly appears that a precise characterization of block-in-matrix rocks is not straightforward and, in absolute, may actually be impossible. Along with complicated fabrics observed in block-in-matrix rocks this likely explains the significant variations in the meaning attributed to the term *mélange* in literature. In this chapter, we adopt the geologic terminology introduced by *Raymond* [1984] and use the terms "mélange" and "dismembered unit" in the sense presented in the beginning of this chapter. The terms "block" or "fragment" are used for geometric bodies regardless of their origins. "Grain" (size=125µm-2mm), "granule" (size=2-4mm), "pebble" (size=4-64mm), "cobble" (size=64-256mm) and "boulder" (size>256mm) are blocks/fragments of sedimentary origin. We arbitrarily use herein the sedimentary term "large boulder" as a rock fragment larger than 10m.

3.3.2 Recognizing the origin of a Mélange

A mélange may be produced by (1) purely sedimentary processes, (2) purely tectonic processes, or (3) combined sedimentary and tectonic processes [*Raymond*, 1984]. Typical examples of mélanges produced by sedimentary processes are olistostromes or debris flow deposits which are commonly produced by erosion or gravitational reworking of older rocks and/or unlithified sediments along steep slopes [e.g. *Hampton and Lee*, 1996]. Tectonic mélanges are often produced at subduction zones along the interface between subducting and overriding plates. They are frequently composed of metamorphosed igneous/sedimentary fragments embedded in a shally and/or serpentinitic matrix. Literature contains a wide diversity of names for these mélanges, such as flow mélange [*Cloos*, 1984], mélange belt [*Doubleday et al.*, 1994 a, b], serpentinite mélange [*Chang et al.*, 2000] or suture zone ophiolitic mélange [e.g. *Dupuis et al.*, 2005]. Finally, mélange produced by both sedimentary and tectonic processes ("polygenetic mélanges" after *Raymond* [1984]) are generally a result of sedimentary mélange overprinted by tectonic deformation. Wildflysches are certainly the most illustrative example of a polygenetic mélange. They are produced in orogenic zones by deformation of olistostromic sediments deposited at the front of nappes [e.g. *Alonso et al.*, 2006].

Preceding examples highlight the fact that mélanges are produced by a large spectrum of geological processes encountered along convergent margins. General criteria allowing to distinguish between several origins are given by *Raymond and Terranova* [1984]: (1) the nature of contacts (depositional or structural), (2) the relationships to surrounding units, including paleogeographic considerations, (3) the nature of the matrix, (4) the internal structure

of the rock body, (5) the presence or absence of features indicative of soft sediment deformation, and (6) the presence or absence of deformation and metamorphism within inclusions. In addition to these criteria a particular effort was made in our study to characterize the nature and ages of the blocks and matrix. This allowed us to make a precise comparison of the mélange with surrounding units.

3.3.3 Field work in the Osa Mélange

Due to high complexity generally associated to mélanges, a particularly-detailed field work was made in the San Pedrillo Unit (inner Osa Mélange). Geological correlations and observations were made at scales ranging from a thin section to the entire unit (i.e. several km). We carried out detailed mapping at 1:5000 scale of the NW edge of the Osa Peninsula and Caño Island (Figures 3.4, 3.5). Comprehensive maps are presented in *Buchs and Stucki* [2001]. Lithologies of variously deformed rocks were characterized on the basis of a systematic sampling over the entire area (Figure 3.5). Although our study was restricted in the NW part of the Osa Peninsula, it provides constraints applicable to the entire San Pedrillo Unit.

3.4. Results

3.4.1. The Osa Igneous Complex

A new tectonostratigraphy is proposed for the Osa Igneous Complex that is based on: (1) newly-recognized differences in geochemistry of the igneous rocks (Chapter 4), (2) mapping of distinctive igneous and sedimentary rock formations, and (3) previous and new paleontologic dates from the sediments associated to the igneous rocks (Figure 3.9).

A comprehensive geochemical study of the Osa Igneous Complex is well beyond the scope of this Chapter and is presented in Chapter 4. However, we choose here to use $(La/Sm)_{CIn}$ and $(Sm/Yb)_{CIn}$ ratios based on the geochemical study exposed in Chapter 4 as representative parameters of the geochemical variations encountered in the Osa Igneous Complex. In tholeiitic and alkaline rocks of Costa Rica these ratios generally show a good correlation with Sm-Nd and Lu-Hf isotopic compositions [e.g. *Hauff et al.*, 1997, Chapter 4]. Hence, they are considered here to represent useful discriminative parameters in terms of source composition and origins. In the text, these ratios are expressed as "highly depleted" when $(La/Sm)_{CIn}$=0.3-0.4 and $(Sm/Yb)_{CIn}$=0.7-0.9, "NMORB-like" when $(La/Sm)_{CIn}$=0.5-0.6 and $(Sm/Yb)_{CIn}$=0.8-1.1, "plateau-like" when $(La/Sm)_{CIn}$=0.7-1.0 and $(Sm/Yb)_{CIn}$=0.8-1.3, and "OIB-like" when $(La/Sm)_{CIn}$=0.9-3.7 and $(Sm/Yb)_{CIn}$=1.4-4.9. Plateau-like igneous rocks describe herein are distinct from E MORB in terms of Nb and major element contents and resemble typical oceanic plateaus (Chapter 4).

The Osa Igneous Complex is subdivided into: (1) the Inner Osa Igneous Complex, and an Outer Osa Igneous Complex composed of (2) the Güerra Unit, (3) the Ganado Unit, (4) the Riyito Unit and (5) the Vaquedano Unit (Figures 3.1, 3.2). All these units are bounded by recent (active?) fault zones and are broadly oriented NW-SE, parallel to the Mid American Trench (Figure 3.1b).

3.4.1.1. The Inner Osa Igneous Complex

The Inner Osa Igneous Complex is exposed in the isthmus side of the Osa Peninsula and in the Burica Peninsula. In the NE it is in contact with the arc-related Golfito Complex. In the northern Osa Peninsula it is in contact with the Güerra Unit, whereas in the southern Osa Peninsula it is bordered by the Osa Mélange (Figures 3.1, 3.2B-B'). NW extension of the boundaries of the inner Osa Igneous Complex is poorly or not expressed on reflection profile P 1600 (NW Osa, Figure 3.2A-A'). However on-land exposures in close vicinity (~15-30 km) tend to indicate that the Inner and Outer Osa Igneous complexes as well as San Pedrillo Unit (inner Osa Mélange) are still present in this part of the margin.
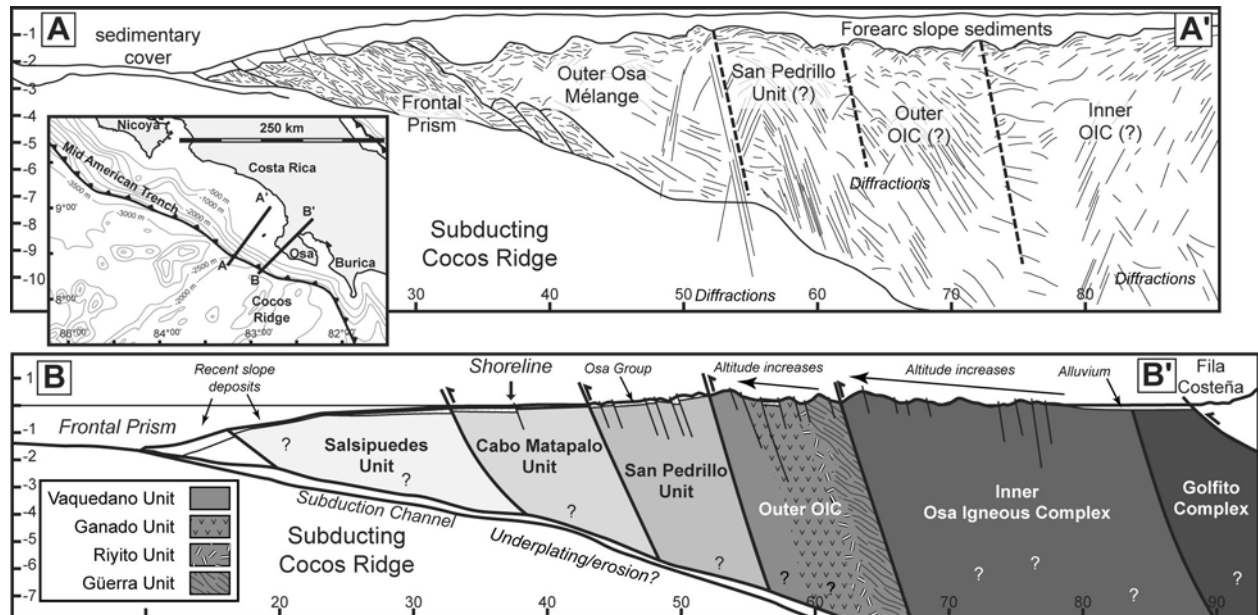
Figure 3.2: *Comparison of seismic and on-land interpretations for the NW Osa Mélange and Osa Igneous Complex. **A-A')** Depth converted interpretation of multichannel reflection profile P 1600 from the upper plate basement (modified after Kolarsky et al. [1995a], full references and data in Kolarsky et al. [1995a], vertical exaggeration: 2x). The profile is only ~15 and ~30 km distant from the San Pedrillo Unit exposed on Caño Island and other units exposed on the Osa Peninsula, respectively. Dashed lines represent possible extensions of unit boundaries projected from cross-section B-B'. **B-B')** SW-NE cross-section through the Osa Peninsula and forearc slope (vertical exaggeration: 2x). Topography is from GeoMapApp (online georeferred database). Note particular changes in topography correlating with suture zones between the Inner Osa Igneous Complex, Outer Osa Igneous Complex and San Pedrillo Unit (Inner Osa Mélange).*

The inner Osa Igneous Complex is composed over 99% of basaltic, massive-columnar lava flows and pillow lavas that constitutes a thick rock pile, several km in thickness (Figure 3). The lavas consist of sub-ophitic, intersertal and intergranular basalts and coarse basalts and microgabbros with plagioclase, clinopyroxene, oxides, interstitial glass, minor amounts of sulfides and occasionally altered olivine. Three occurrences of intrusive rocks have been observed in the Inner Osa Igneous Complex, which consist of a sill located along the shore close to Rincón (Golfo Dulce), dolerites exposed at Punta Banco (Burica Peninsula) and a gabbro in the Quebrada Sábalo (inner, isthmic side of Osa). The sill is characterized by an atypical microlitic texture with K-feldspar and acicular brown amphibole. The gabbro has a very peculiar poikilitic texture with plagioclase phenocrysts. Occasionally, lenses and layers, 1-3 m thick, of

red cherts and black shales are observed between the lava flows. These sediments constitute a very minor amount of the Inner Osa Igneous Complex. Along the shore of the Golfo Dulce (Punta Esperanza, 539.9/291.3, Costa Rican coordinates), a 20 m thick intercalation of arenite, microbreccia and breccia, named "Esperanza Formation" by *Mende* [2001], crops out within the volcanic sequence. The sediments contain basaltic material similar to the lavas of the Inner Osa Igneous Complex. To date, this deposit constitutes a unique occurrence of detrital material in the Inner Osa Igneous Complex.

Lava flows and sediments dip predominantly to NE. Orientation of the pillow lavas indicates that the series are both in normal and overturned position. Occurrences of overturned pillow lavas are found over the entire unit but are much less frequent than series in normal position. A low-T submarine alteration in the zeolite facies is expressed in the lavas by a low to moderate alteration of the glass and silicate minerals. All samples collected in the Inner Osa Igneous Complex are devoid of greenschist metamorphism. Strong deformation is locally observed and associated to intensive veining of the rocks. Veins are generally filled with calcite and zeolite. Small-scale structures potentially indicating folding of the rocks (e.g. oblique cleavages in the sediments) have not been observed. Deformation seems to have predominantly occurred in a brittle mode and resulted in the formation of fault-bounded lenses of relatively undeformed rocks. The lenses are well seen along the shore of the Burica Peninsula and are observed at scales ranging from several meters to possibly several hundreds of meter. In the Inner Osa Igneous Complex the presence of both overturned pillow lavas and lenses of rock bodies is indicative of a tectonic dismemberment of a very large unit or of an imbrication of several "smaller" rock bodies.

Age of formation of the basalts is defined by radiolarians associations found in intercalated cherts to the Coniacian-Santonian (~89-84 Ma) [*Di Marco*, 1994; *Diserens*, 2002; *this study*] (see also Chapter 3.4.4.1 for more details). Two tholeiitic (low-K) basalts yield whole rock $^{40}Ar/^{39}Ar$ Ar total fusion isochron ages of 64.2 ± 1.1 and 54.5 ± 1.5 Ma [*Hoernle et al.*, 2002]. K-Ar ages on similar igneous rocks range from 78.0 ± 2 to 44.8 ± 8 Ma [*Berrangé et al.*, 1989]. Discrepancy between biochronological and radiometric ages is discussed in Chapter 3.5.3.

Geochemistry of the igneous rocks is principally tholeiitic with plateau-like affinities showing consistency with an oceanic, intra-plate origin (Figures 3.1a, 3.3). However, igneous rocks with distinct oceanic, intraplate affinities are locally observed, such as NMORB-like and OIB-like tholeiitic lava flows (Figures 3.1a, 3.3a). Dolerites from Punta Banco (Burica) have NMORB-like tholeiitic, intraplate affinities and the sill close to Rincón is a basaltic trachyandesite with OIB-like, intraplate oceanic affinities. Local variations of the geochemical affinities point toward distinct origins for the igneous rocks that compose the Inner Osa Igneous Complex (Chapter 4).

3.4.1.2. The Güerra Unit

The Güerra Unit is in contact with the Inner Osa Igneous Complex along its landward edge, and with the Riyito and Ganado units along its seaward edge (Figure 3.1). On a SW-NE crossection the transition from the Inner Osa Igneous Complex to the Güerra Unit is marked by changes in the topography (Figure 3.2B-B'). In the NE side of the contact, the altitude progressively increases toward the contact and then suddenly drops further seaward. This morphology is likely controlled by the presence of a major, possibly-active tectonic contact between the Güerra Unit and the Inner Osa Igneous Complex that may be controlled by

overthrusting of the Inner Osa Igneous Complex toward the SW. The contact may control the morphology of Osa shoreline along the Golfo Dulce, indicating that it partly postdates recent deposition of the Osa Group and may be associated to an active fault (Figure 3.1).
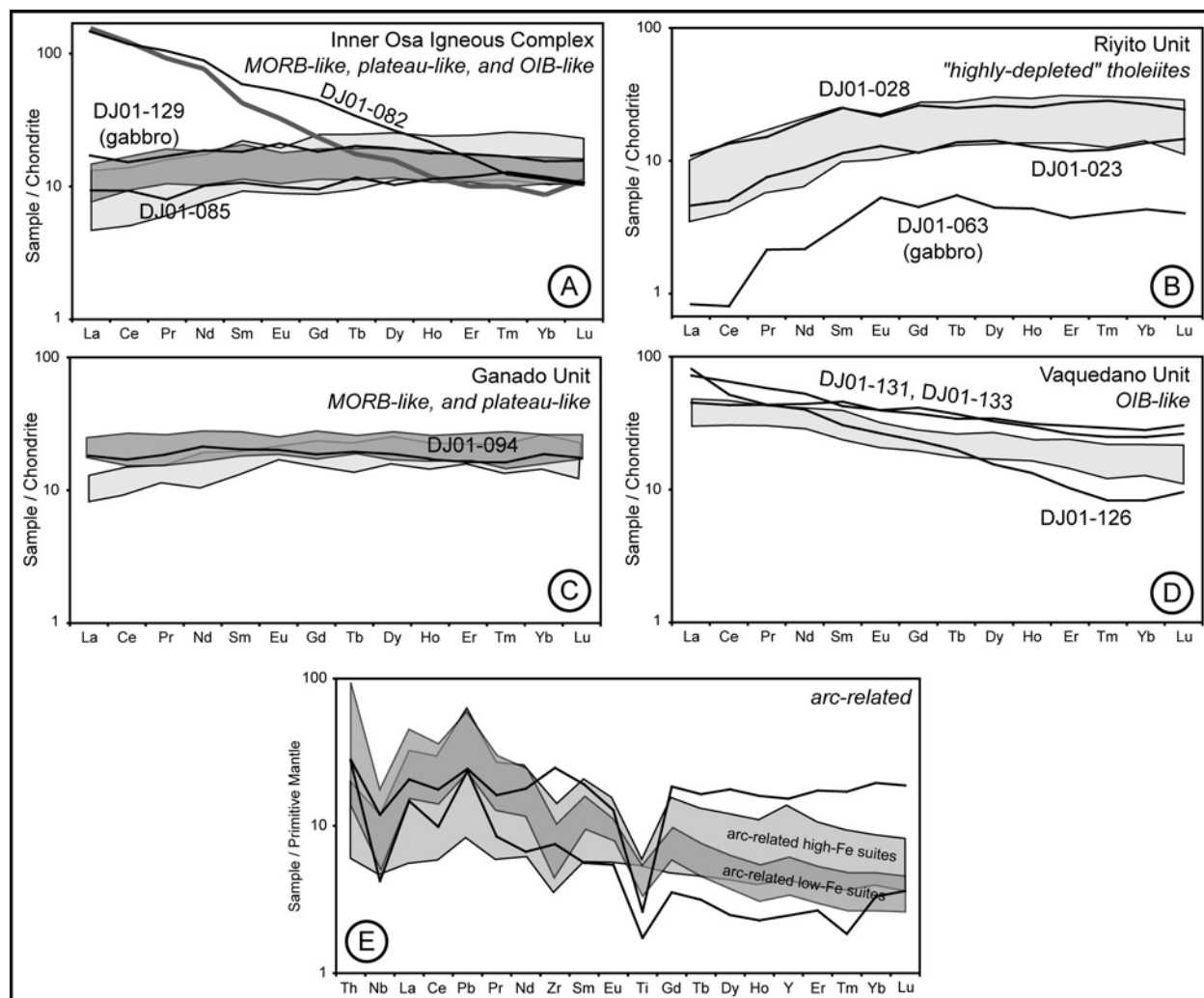
Figure 3.3: A-D) *REE diagrams for the basalts and gabbros of the Osa Igneous Complex (grey areas, organised per unit) and basaltic olistoliths of the San Pedrillo Unit (black lines with sample references). Samples from the San Pedrillo Unit were individually associated with most similar unit of the Osa Igneous Complex. Normalisation values are from McDonough & Sun [1995]. "Highly-depleted", "NMORB-like", "plateau-like" and "OIB-like" denominations are defined in Chapter 3.4.1.* ***E)*** *Multielement diagram of two dacitic olistoliths from the San Pedrillo Unit. Normalisation values are from Mac Donough and Sun [1995]. For comparison, 11-17 Ma high-Fe (tholeiitic) basalts-andesites and 8-12 Ma low-Fe (calc-alkalic) basalts-dacites from Costa Rican forearc volcanics are plotted (grey areas, Abratis, [1998]). Note that the dacitic olistoliths and igneous rocks from the Osa Igneous Complex have dissimilar affinities in terms of REE, notably.*

In contrast to the Inner Osa Igneous Complex, the Güerra Unit is characterized by stronger deformation and prehnite-pumpellyite to greenschist metamorphic facies. This metamorphism is unique in the area of study. The unit is broadly composed of metamorphosed/altered igneous rocks, marble, recrystallized micritic limestones and metamorphosed volcaniclastic sediments. These lithologies constitute a complicated arrangement of variously-deformed lenses extending at scales over 100 m that is interpreted to be a result of a

tectonic imbrication of several large rock bodies. The less deformed lenses exhibit little deformed volcano-sedimentary textures, whereas the most deformed lenses are characterized by pervasive ductile deformation and associated schistosity that erased most pristine textures. There is a good correlation between the intensity of the metamorphism and the degree of deformation (i.e. most deformed rocks exhibit highest metamorphic grades). Strike of the rock lenses is NW-SE with a NE moderate/subvertical dip. Similar orientation is marked by the schistosity in the most deformed rocks and by preserved volcano-sedimentary beddings in the less deformed rocks. This orientation is parallel to the contact of the Güerra Unit with the Inner Osa Igneous Complex.

As a consequence to locally strong deformation, many protoliths of the Güerra Unit were difficult to identify. However it is clear that the unit is composed of a wide range of rocks and contains a larger proportion of sediments than the Inner Osa Igneous Complex. In the less deformed areas we notably recognized preserved textures of vesicular pillow lavas interbedded with reddish, recrystallized limestones. These lavas consist of transitional basalts with OIB-like, intraplate affinities. However, due to sediment recrystallisation it was not possible to observe preserved fossils in our samples. In other places, spilitized porphyric pillow lavas were found. These lavas have tholeiitic affinities associated to highly-depleted incompatible element content. These two examples of "preserved" volcano-sedimentary sequences are very similar in terms of sedimentary facies and geochemistry to some sequences of the Vaquedano and Riyito units (see below). Hence, by analogy with other units forming the Outer Osa Igneous Complex and probable role of the unit in the construction of the Osa Igneous Complex (Chapter 3.4.1.5), the formation age of the rocks composing the Güerra Unit is probably late Cretaceous-Eocene.

3.4.1.3. The Ganado Unit

The Ganado Unit is exposed in the SW side of the Güerra Unit and is in contact with other units of the Outer Osa Igneous Complex and the Osa Mélange (Figure 3.1).

This unit consists of pillowed and massive basaltic/basaltic-andesitic flows locally intruded by aphyric basaltic dykes, dolerites and gabbros. Intrusive rocks form a minor portion of the sequence (<10%) and are preferentially observed close to the Osa Mélange. Most common textures of the lavas are sub-ophitic, intersertal and intergranular with plagioclases, clinopyroxenes, oxides, interstitial glass and minor amounts of olivines and sulfides. Intrusive rocks have doleritic and ophitic textures with plagioclases, clinopyroxenes, oxides and co-magmatic amphiboles in some samples. In the volcanic rocks a low-T submarine alteration in the zeolite facies is frequently observed. A stronger alteration is also observed in the intrusive rocks and volcanic rocks at the contact. This alteration is notably characterized by extensive argilitization of the plagioclases and epidote formation. It certainly occurred in response to hydrothermal circulation triggered by the emplacement of the intrusive rocks prior to emplacement of the unit along the margin. In some gabbros, curvilinear clivages are observed. This attests that the gabbros were deformed by the time of their cooling, rapidly after their emplacement. A ~2 m thick layer of red radiolarian chert, interbedded with micro-gabbro lava flows, was the sole occurrence of sediments encountered in the stratigraphic sequence. Radiolarians provided a Coniacian-Santonian (~89-84 Ma) age (see also Chapter 3.4.4.1 for more details).

The lava flows dip preferentially NE and are found both in inverse and normal positions. The volcanic rocks underwent a similar deformation to the Inner Osa Igneous Complex. These observations and occurrences of intrusive bodies (i.e. deep crustal exposures) at the contact with surrounding units indicate that the igneous rocks forming the Ganado Unit underwent a significant tectonic dismemberment. The unit may have formed through imbrication of distinct volcanic sequences or dismemberment of a single, very large rock body.

Two geochemically distinct groups of igneous rocks are found in the Ganado Unit. The first group is composed of tholeiitic basaltic lava flows and aphyric dykes. It is characterized by plateau-like affinities consistent with an oceanic, intraplate origin (Figure 3.3c). Although this group appears to be similar to the plateau-like lavas of the Inner Osa Igneous Complex, discriminative geochemical differences exist between the two, notably in terms of Nb content (Chapter 4). One exception to this observation comes from a lava flow associated to the Campanian radiolarian chert. Although this lava has plateau-like affinities, it consists of a transitional tholeiite with Nb content similar to the tholeiites from the Inner Osa Igneous Complex. It is interpreted here to represent a record of a late stage of volcanism of the Ganado plateau-like "series". The second geochemical group of the Ganado Unit is mainly expressed in the dolerites and gabbros emplaced into the plateau-like group, as well as in a few massive lava flows. This group is composed of NMORB-like tholeiites with oceanic intraplate affinities similar to the NMORB-like tholeiites of the Inner Osa Igneous Complex (Figure 3.3c).

3.4.1.4. The Riyito Unit

The Riyito Unit is a composite (non-contiguous) unit exposed at both the NW and SE edges of the Ganado Unit. It is in contact with the Güerra Unit in the NE and the Vaquedano Unit and Osa Mélange in the SW (Figure 3.1).

The unit is composed of volcano-sedimentary sequences including small, well-formed pillow lavas, sheet flows and minor occurrences of sediments and hyaloclastites. The lavas are basaltic in composition and locally vesicular. They ubiquitously contain plagioclase phenocrysts embedded in a subophitic-intersertal-microlitic matrix made of plagioclases, clinopyroxenes, oxides, matrix glass and minor amount of sulfides. The porphyric nature of these lavas has been used on the field to constrain the extension of the unit. Vesiculated hyaloclastites are locally observed between pillow lavas, possibly indicating eruption under shallower conditions for some parts of the volcanic rocks. Alteration of the igneous rocks is low to moderate and consistent to low-T oceanic alteration. The sediments represent less than 3% of the total volume of the sequence and are predominantly exposed along the Rio Riyito (central Osa). The sediments are broadly composed of turbiditic beds reworking basaltic igneous rock fragments. Plagioclase-phyric dykes intruding lava flows are present in the lower part of the Rio Riyito. In the Punta Ganadito (western Osa) crustacean microcoprolites have been encountered in a deep ocean sequence [*Buchs et al.*, in press].

The lava flows dip NE with pillow lavas in both normal and overturned positions. Exposures of the the Riyito Unit are clearly non-contiguous and separated by the Ganado Unit. Hence, similarly to the Inner Osa Igneous Complex, the Riyito Unit shows indications of dismemberment that possibly resulted from an imbrication of distinct rock bodies.

Hauff et al. [2000] provided a $^{40}Ar/^{39}Ar$ age of 62.1 ± 0.6 Ma (Paleocene, total fusion on whole rock matrix) for a basaltic sample of the Punta Ganadito. Fossils allowing a precise dating of the interlayered sediments have not been encountered.

Volcanic rocks are all tholeiitic and exhibit very consistent geochemistry. They are characterized by an unusual high depletion in the most incompatible elements that is consistent with an oceanic intraplate origin (Figure 3.3b).

3.4.1.5. The Vaquedano Unit

The Vaquedano Unit is exposed along the Osa Mélange and is in contact with the Ganado and Riyito units (Figure 3.1).

This unit is composed of a complicated imbrication of volcano-sedimentary sequences exhibiting distinct lava morphologies, geochemistry, ages and sedimentary associations. It broadly consists of vesiculated, small-shaped pillow basalts and lava flows, reddish pelagic limestones, detrital sediments and hyaloclastites. Lavas form the majority of the sequences (>85%) and consist of ophitic, subophitic, intersertal and spherulitic basalts with plagioclase, titanoaugite, olivine pseudomorphs, oxides, glassy matrix and minor amount of sulfides. A few pillow breccias and hyaloclastites are locally interbedded with the lavas. The pelagic limestones locally occur as deformed xenoliths embedded in massive lava flows, indicating an incorporation of unlithified sediments into the lavas by the time of their emplacement. Most commonly, the limestones form interbeds within the pillowed and massive lava flows. Occasional sponge spicules possibly indicate that some of the limestones formed in nutriment-rich oceanic currents. A sample of late Cretaceous micritic limestone contained two badly-preserved fragments of red alga. In the Osa Igneous Complex, this is the sole occurrence of material originating from a shallow-water environment. Detrital basaltic sediments that consist of <50 m thick turbidites and pebbly-cobbly breccias are locally intercalated with volcanic rocks.

Ages of the volcano-sedimentary sequences are well constrained by fossil assemblages found in the pelagic limestones. These sediments contain late Cretaceous *Inoceramus* fragments and Campanian to middle Eocene Foraminifera [*Di Marco*, 1994; *Buchs*, 2003; *Baumgartner-Mora*, Oral Communication, 2006]. This is the largest range of ages observed for the sequences of the Osa Igneous Complex, which spans ~40 Ma. The igneous rocks yielded K-Ar ages of 55.3 ± 6 to 40.8 ± 4 Ma that are broadly similar to biochronologic ages [*Berrangé et al.*, 1989].

In both lava flows and sediments the layers predominantly dip NE, with both normal and reverse positions of pillow lavas. Although the lavas are ubiquitously reddish as a response to an early low-T, oceanic oxidization/alteration, no trace of higher temperature alteration of metamorphism has been encountered. The unit is composite and made of large (100 m length/width and bigger) rock bodies identified on the basis of distinct volcano-sedimentary associations, ages and geochemistry. Similarly to the Inner Osa Igneous Complex, the Güerra Unit and possibly the Riyito Unit, the Vaquedano Unit resulted from an imbrication of several rock bodies.

Volcanic rocks are composed of transitional to alkalic basalts with OIB-like affinities (Figure 3.3d). Although these rocks share intraplate oceanic affinities they are characterized by a wide range of immobile incompatible element contents throughout the unit. This is incompatible with a common origin of the volcanic rocks. However, good consistency of the geochemistry is observed in samples collected close to each others, at scales <250 m, which is in agreement with an imbrication of large rock bodies forming the Vaquedano Unit.
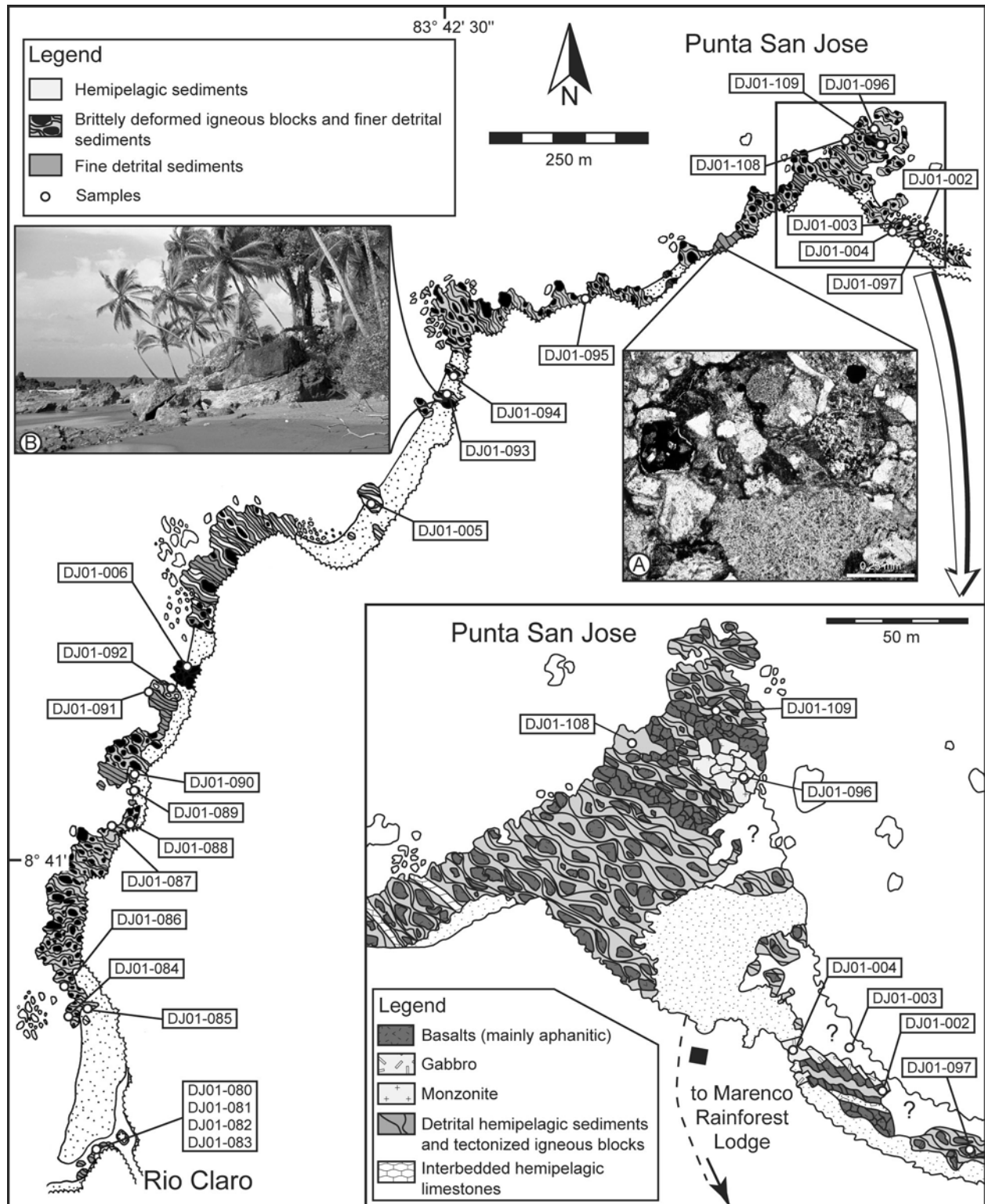
Figure 3.4: *Detail geological map of the Rio Claro area.* ***A)*** *Basalt olistolith embedded within a cataclasite matrix.* ***B)*** *Microphotograph of a volcanic microbreccia principally made of basaltic grains.* ***A-B)*** *highlight the large variability in the clast size observed in the San Pedrillo Unit. Costal exposures of NW Osa and Caño Island have been integrally mapped in a similar way [Buchs and Stucki, 2001].*

3.4.2. The NW Osa Mélange (San Pedrillo Unit)

3.4.2.1. Sedimentary fabric

Despite the existence of a highly pervasive deformation, the San Pedrillo Unit exhibits a relatively well-defined lithological arrangement [*Buchs and Stucki*, 2001; *Buchs and Baumgartner*, 2003]. Compositional variations of the formations and recurrence of a finite number of lithologies are observed, providing the opportunity to map the mélange at 1:5000 and larger scales (Figures 3.4, 3.5). In general, the NW Osa Mélange is characterized by alternations of (1) areas dominated by igneous blocks embedded within a deformed sedimentary matrix and (2) areas composed by deformed sedimentary layers lacking a significant amount of large (>1m) blocks and predominantly made by fine-grained (<5cm) detrital or hemipelagic sediments (Figures 3.4, 3.6a). Alternations of lithologies trend NW-SE, with a strong variation of the dip (Figure 3.6b). Sedimentary structures, such as layering, size grading and laminations are frequently observed throughout the unit and are oriented parallel to the lithological alternations. The lithological arrangement and systematic orientation of layered sediments is interpreted to be a result of an imbrication of distinct rock bodies characterized by a lenticular shape (Figure 7b).

A detrital (sedimentary) fraction is ubiquitously observed in the San Pedrillo Unit. It is indicated by the presence of clasts ranging from grains to large boulders, embedded within sedimentary deposits (Figure 5, see also paragraph 4.2.3.). Intense tectonic brecciation of large igneous blocks may lead locally to a possible confusion of the San Pedrillo Unit with a tectonic mélange *sensu stricto* [e.g. *Meschede et al.*, 1999]. However, we observed that (1) the large blocks are systematically found within debris flow layers and are rarely embedded within cataclased rocks and (2) geochemical compositions of the igneous blocks located close to each other and embedded within the same sedimentary deposits preclude a provenance from a unique volcanic series (see below). Thus, the igneous blocks of the San Pedrillo Unit are olistoliths pertaining to the detrital component of the mélange rather than
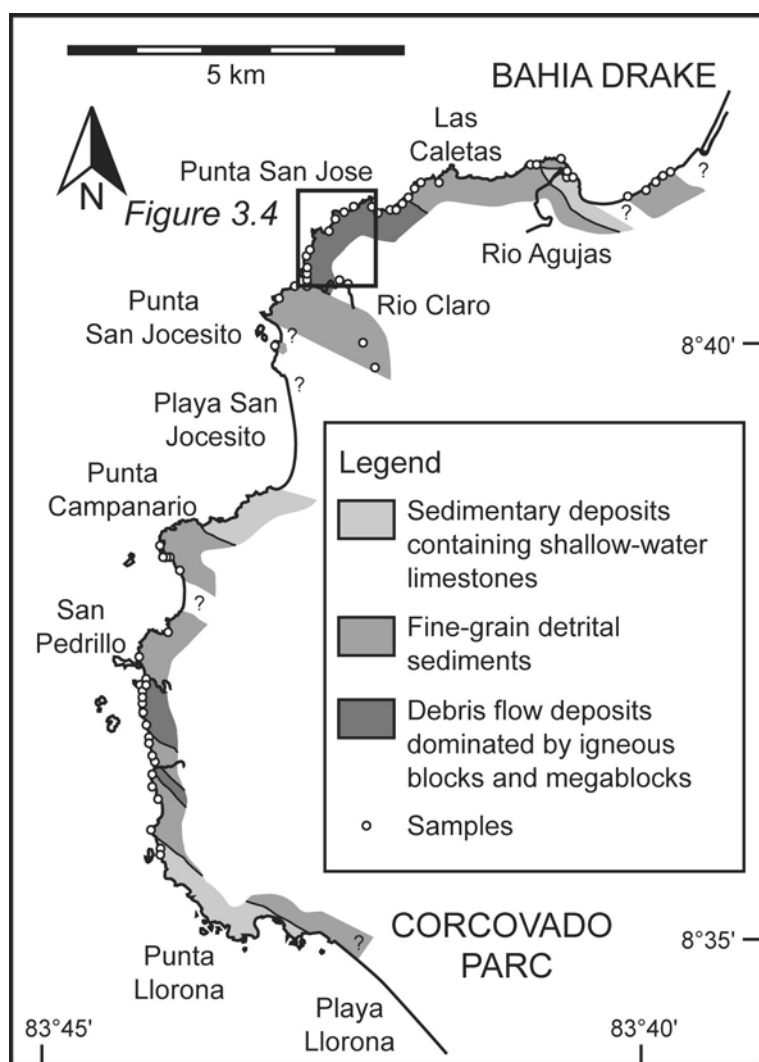
Figure 3.5: *Simplified geological map of the NW San Pedrillo Unit illustrating recurrent lithologic associations.*

preserved portions of tectonically-dismembered igneous sequences. A direct consequence of this observation is that there is a sedimentary fabric throughout the entire San Pedrillo Unit that predates a younger tectonic overprint.
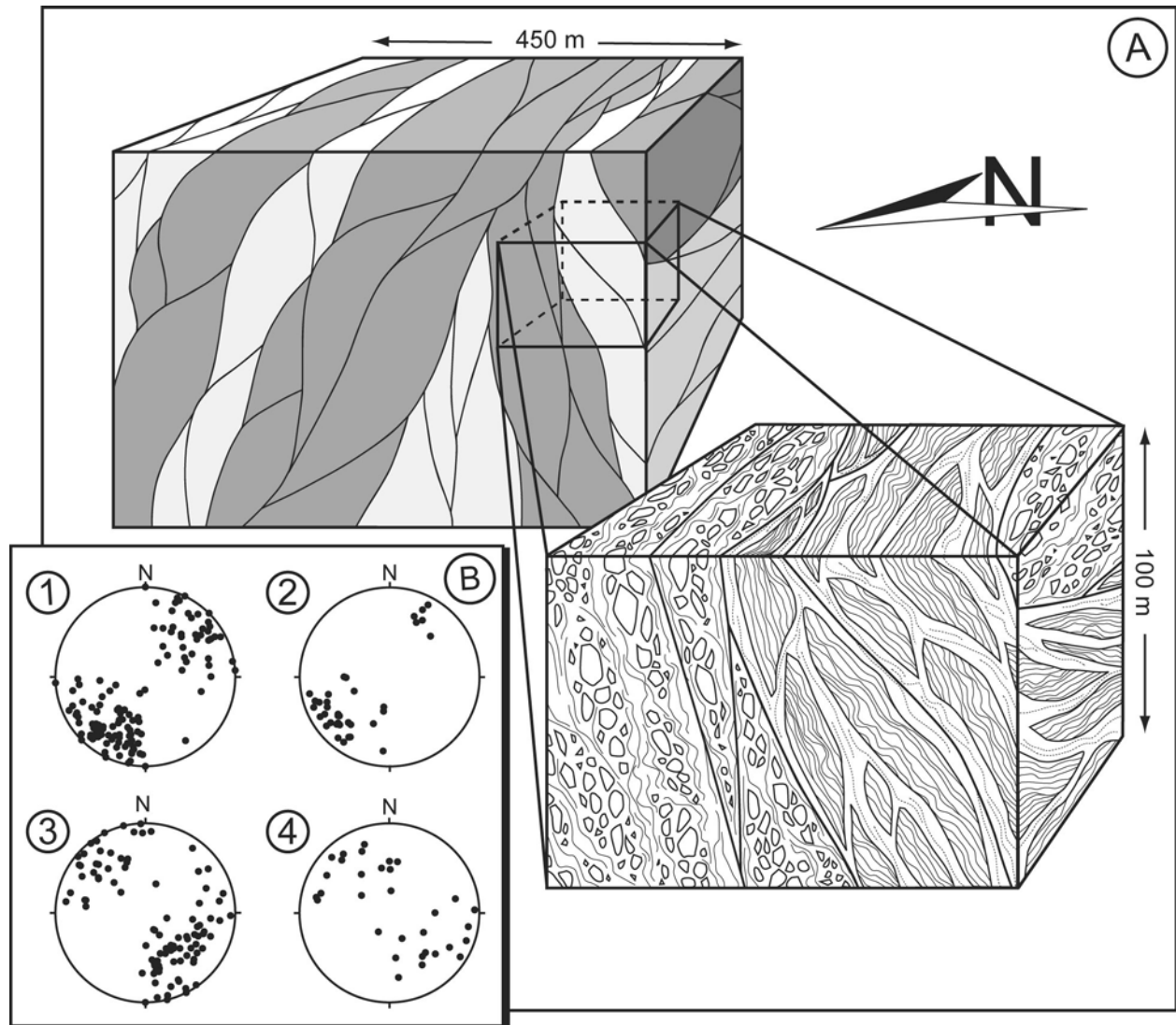
Figure 3.6: *A) Structural model of the NW Osa Mélange illustrating the block-in-matrix texture and disrupted sedimentary layers at a small scale. At a larger scale, the chaotic arrangement of the mélange is replaced by lithologically-coherent lenses.* ***B)*** *Orientations of principal shear planes observed in the mélange. (1) and (2) are shear planes mainly parallel to the orientation of the trench, that crop out on the Osa Peninsula, respectively on the Caño Island. (3) and (4) represent shear planes predominantly perpendicular to the orientation of the trench, that are exposed on the Osa Peninsula, respectively on the Caño Island. The two families of shear planes show a large variability in their orientation that is consistent with a lenticular arrangement of the lithologies in the San Pedrillo Unit.*

3.4.2.2. Tectonic Fabric

Pervasive tectonic overprint in the San Pedrillo Unit may be divided into (1) active subvertical faulting and (2) earlier deformation. The former has been attributed to uplift and block tilting controlled by the morphology of the subducting Cocos Ridge [*Sak et al.*, 2004].

This implies that adjacent coastal exposures may actually represent different structural levels of the Osa Mélange.

Earlier deformation occurred in a low-grade metamorphic environment, below the field stability of greenschists. In a few cases, igneous olistoliths embedded in the sedimentary, low-grade metamorphic matrix show a higher metamorphic facies with the presence of epidote, prehnite and pumpellyite. These facies are likely inherited from their environment of formation prior to their incorporation to the San Pedrillo Unit. Although some deformed rocks are green due to chlorite formation, metamorphism observed in our samples from the Osa Mélange has not exceeded a prehnite-pumpellyite facies. This is an important dissimilarity of the Osa Mélange with other mélanges that commonly contain greenschist, amphibolite or blueschist grade blocks.

Tectonic deformation and related phases that occurred prior to the final exhumation of the San Pedrillo Unit are comprehensively described by *Vannuchi et al.* [2006]. Their results are summarized and discussed conjointly with our observations in Chapter 3.6.3.

3.4.2.3. Lithologies

A large variability in terms of lithologic composition is observed in the San Pedrillo Unit. During our 1:5000 mapping, a detailed characterization of the lithologies was performed (Figure 3.4). However, the extent of the lithological variations is such that it is fundamentally not possible to constitute a complete report of all the rocks. Hence, we describe here only the most representative associations of lithologies.

The San Pedrillo Unit may be roughly divided into 3 types of lithologies: (1) sedimentary deposits containing shallow-water limestones (~20% volume of the San Pedrillo Unit), (2) debris flow deposits dominated by igneous olistoliths (~25% volume of the San Pedrillo Unit) and (3) fine-grain detrital sediments (~55% volume of the San Pedrillo Unit).

The sedimentary deposits containing shallow-water limestones

Shallow-water limestones occur mainly as pebbles and boulders embedded in a dark, tuffitic matrix. They form matrix-supported breccias that are encountered on Caño Island and between Playa San Josecito and Punta Llorona (Figure 6). This lithology appears as sedimentary layers that have an apparent thickness of 2 to 30 m and were probably emplaced by debris flow events. The matrix is composed by altered ashy tuffites that were intensively deformed during tectonic processes. The limestone clasts are frequently recrystallized and fragmented. Sometimes they comprise over 50% of calcite veins. The matrix was injected within and between the clasts, indicating that the tuffites behaved softly and were poorly compacted during the beginning of the tectonic history within the mélange.

Limestone beds, 0.5 to 3m thick, are encountered in the areas of Agujitas, Marenco and Caño (Figure 3.5). These deposits represent an accumulation of largely dominant carbonate grains without a significant amount of tuffitic matrix. They are interpreted as calci-turbidites interbedded with tuffitic greywackes, volcarenites and microbreccias that notably contain fragments of mafic to differentiated volcanic sources. During tectonic deformation the beds underwent fracturing, brittle boudinage and injection of under- and overlying muddy sediments, creating networks of sedimentary dykes. These limestones allowed us to date the deposition of the sediments forming the mélange (see below).

The shallow-water limestone olitsoliths and turbidites contain carbonate grains and pebbles formed in a platform and/or peri-platform environment. They include mainly red algae, larger Foraminifera, echinoderms and sponge spicules. An associated detrital fraction consists of fragments of pyroxene, zoned plagioclase, quartz, basalts and intermediate to acidic lavas. Detrital quartz and fragments of dacites occasionally occur as nuclei of red algal oncoliths. The Larger Foraminifera indicate a late Eocene age (see below). Thus, the depositional age of these shallow-water derived calcareous debris flows and calci-turbidites is late Eocene or younger.

Similarities of composition, faunal assemblages and age of the shallow-water carbonates of the San Pedrillo Unit likely indicate a common origin. In the NW Osa Mélange they are associated through primarily-sedimentary processes with products of a differentiated volcanism that is represented by ashy tuffites, quartz fragments, and silica-rich igneous blocks. The geochemical compositions of the silica-rich igneous blocks indicate an arc-related affinity (see below). Thus, it is clear that the carbonates must have formed in the vicinity of a volcanic arc.

The debris flow deposits dominated by igneous olistoliths

Debris flow deposits with large amounts of igneous boulders and large boulders are concentrated in the Marenco and San Pedrillo areas (Figures 3.4b, 3.5). The olistoliths locally exceed a size of 50m, indicating that the thickness of the debris flow deposits is similar to this size or superior. The olistoliths consist of basalts (~70%), differentiated igneous rocks (~25%), gabbros and hydrothermally-altered gabbros (~2%), radiolarites (~1%), limestones (~1%) and detrital sediments (~1%). They are embedded within a matrix of detrital sediments composed of grains, granules and pebbles of minerals and rocks. The matrix exhibits a composition analogous to the igneous blocks, indicating a similar provenance of the detrital material. The provenance of the igneous olistoliths is shown by their geochemical composition (see below), which points toward two main sources: (1) a highly heterogeneous basaltic source of oceanic intraplate origin and (2) an arc-related igneous source.

The olistoliths and the matrix are deformed and crosscut by a dense network of zeolite, calcite and quartz veins. An intensive brittle deformation affected the igneous blocks, resulting in strong tectonic brecciation. As a consequence, it may locally be particularly hard to make a distinction between the matrix and the blocks. This may explain the confusion of the Osa Mélange with a tectonically dismembered igneous sequence by some authors. However, in some places an association of well-rounded igneous and calcareous pebbles is observed in sedimentary layers, clearly indicating a primary sedimentary origin of the igneous blocks (see below). The sedimentary origin of the igneous blocks is further strengthened by the large variability of geochemical affinities observed within the igneous rocks that is clearly incompatible with disruption of a unique magmatic suite or magmatic suites proceeding from a similar tectonic setting.

Radiolarites and pelagic limestones occur as isolated blocks or in sedimentary association with igneous olistoliths. Within the igneous olistoliths radiolarites are in stratigraphic contact with lava flows. Pelagic limestones are interbedded within reddish pillow lava sequences. The radiolarians encountered in isolated blocks of sediments or in association with lava flows are Campanian-Maastrichtian in age. Radiolarian assemblages are dissimilar to those of the radiolarian cherts of the Osa Igneous Complex (see Chapter 3.4.4.1 for details). The pelagic limestones provided ages ranging from the Campanian to the middle Eocene, similar to the ages of the calcareous sediments found in the Outer Osa Igneous Complex (Vaquedano Unit). Faunal

compositions of the pelagic limestones of the San Pedrillo Unit are similar to those of the Vaquedano Unit.

The fine-grain detrital sediments

Fine-grain detrital sediments form the predominant lithology in the San Pedrillo Unit (~55% of the mapped volume) (Figure 3.5). They range from mudstone, greywacke, siltite, arenite to microbreccia. The detrital fraction is composed of mineral and lithic fragments (Figure 3.4a). A matrix component predominantly of siliceous-calcareous-tuffitic oozes is observed in some samples (up to 95% of the mode). The mineral fragments consist of clinopyroxenes (~50%), plagioclases (~40%), opaque minerals (~10%) and quartz (<1%). Lithoclasts are predominantly fragments of basalts (~95%) and, to a lesser extent, differentiated igneous rocks (~5%) and limestones grains (<1%). When observed, the siliceous-calcareous matrix of the detrital sediments contains a few recrystallized radiolarians and planktonic Foraminifera, which are not sufficiently preserved to allow age determination.

The occurrence of (1) pelagic faunas and (2) quartz fragments and tuffites within the fine-grain detrital sediments constrains their environment of deposition to a hemipelagic setting. The lithologies in this group range over a wide compositional field that is fully described by a mixing between two end-members: (1) siliceous-calcareous hemipelagic oozes (e.g. mudstones, biomicrites and radiolarian cherts) and (2) a detrital component (forming e.g. litharenites and arkosic arenites).

At Punta Campanario, <2m thick debris flow layers are intercalated with the fine-grained detrital sediments. Wihtin the debris flow deposits, shallow-water limestone pebbles occur in association with basaltic, andesitic and dacitic pebbles that are both angular and well rounded [*Buchs and Baumgartner*, 2007, p. 4, Figure 2a]. The association of mafic, intermediate and differentiated igneous material with grains of shallow-water limestones is in agreement with observations made in other, previously described lithologies of the mélange. In addition, the presence of well-rounded elements of basalts and dacites indicates that this material was transported in a river system or was abraded along a shoreline. As a consequence, the sources of the detrital material encountered in the San Pedrillo Unit were at least partially emerged at the time of their erosion. Large foraminiferans encountered in the grains of shallow-water limestones provided late Eocene ages, similar to the age of the rest of the shallow-water limestones in the San Pedrillo Unit (see below). Late Eocene is thus a limit age of formation of the fine-grained detrital sediments (i.e. they are late Eocene or younger).

A minor fraction (<2%) of lenses of radiolarian cherts, intercalated within the fine-grained detrital sediments, is present in the San Pedrillo Unit. These sediments contain <10% of plagioclase, clinopyroxene and glass fragments. Radiolarians are early Eocene in age, apparently in disagreement with the ages of the calcareous grains. Occurrence of these sediments and significance of their age are discussed below.

3.4.2.4. Geochemistry of the igneous olistoliths

Pervasive dense networks of hydrothermal veins within the San Pedrillo Unit indicate that hydrothermal fluids circulated throughout the mélange. The fluids may have altered some of the igneous rocks. However, we observed that, in some cases, the cores of the biggest igneous

olistoliths remained surprisingly well-preserved (Figure 3.4b). We sampled those cores and relatively unaltered igneous blocks to perform geochemical analyses [*Buchs and Stucki*, 2001].

Four groups of igneous rocks have been recognized within the Osa Mélange on the basis of immobile trace element contents. We subdivided them into intermediate-differentiated igneous rocks and basaltic igneous rocks.

The intermediate-differentiated rocks are represented by blocks and megablocks of dacites, rhyodacites, monzonites and granophyres. Three samples of dacites and monzonite were selected in this group of blocks for their apparent freshness. Their incompatible element patterns are highly variable, indicating both enrichment and depletion in the LREE and highly incompatible elements (Figure 3.3e). We note a systematic $(Nb/La)_{nCI} < 0.6$ and $(Ce/Pb)_{nPM} < 1$ (Figure 3.3e). Since La and Nb are known to be immobile during alteration processes (e.g. Verma, 1992), the La/Nb ratio is believed to represent a primary feature consistent with an arc-related origin of the samples. A positive Pb anomaly is also observed, which may be due to sediment-derived fluids within the accretionary prism or represent a primary feature. In the light of the high incompatible element contents in the samples, the Pb positive anomaly could hardly be related to secondary processes because it would require a strong alteration that has not been observed in the analyzed rocks. Accordingly, these rocks have both primary La/Nb and Ce/Pb consistent with a near-arc origin. Indeed, their composition is similar to Miocene high-Fe (tholeiitic) and low-Fe ("calc-alkalic") suites of the Costa Rican forearc (Figure 3.3e) [*Abratis*, 1998].

The olistoliths of basaltic rocks span a large domain in terms of geochemical composition (Figure 3.3a-d). Groups showing similar affinities on the basis of their immobile element composition were recognized, which point toward oceanic intraplate origins of the basaltic olistoliths. Three groups of volcanic rocks were recognized with characteristic REE contents: (1) tholeiitic plateau-like basalts with $(La/Sm)_{CIn}{\approx}1.0$ and $(Sm/Yb)_{CIn}{\approx}1.0$, (2) highly depleted tholeiitic basalts and gabbros with $(La/Sm)_{CIn}=0.2\text{-}0.4$ and $(Sm/Yb)_{CIn}{\approx}0.9$ and (3) OIB-like alkali-transitional basalts with $(La/Sm)_{CIn}=1.0\text{-}2.6$ and $(Sm/Yb)_{CIn}=1.6\text{-}4.6$. Igneous samples from the San Pedrillo Unit are compared in terms of REE content to the igneous rocks of the Osa Igneous Complex on Figure 3.3. Strong geochemical similarities exist between these two groups of rocks. It seems actually that most of the igneous olistoliths present in the San Pedrillo Unit have an equivalent in the Osa Igneous Complex. Similarities are detailed below, conjointly with sedimentary associations.

3.4.2.5. *Similarities between the basaltic olistoliths and the Osa Igneous Complex*

Igneous olistoliths occur in debris flow deposits throughout the San Pedrillo Unit. Some of them comprise a sedimentary cover and interlayered sediments. Hence, both geochemistry and sedimentary associations may be used to point out possible origins for the olistoliths. We make here a detailed description for a representative selection of these olistoliths, with emphasis on the similarities between these rocks and sequences observed in the Osa Igneous Complex.

Basalt DJ01-085, with plateau-like affinities and OIB-like alkali basalt DJ01-082 were both collected in an olistostromic deposit at the Rio Claro (Figure 3.4). An atypical microlitic texture with K-feldspar and acicular brown amphibole is recognized in the alkali basalt that is similar to the texture of the sill exposed close to Rincón in the Inner Osa Igneous Complex (Chapter 3.4.1.1.). The two samples of the San Pedrillo Unit from the Rio Claro debris flow

deposit show strong geochemical similarities with igneous rocks of the Inner Osa Igneous Complex (Figure 3.3a).

Plateau-like gabbro DJ01-129 from San Pedrillo area has a very distinctive poikilitic texture and REE content similar to the poikilitic gabbro sampled in the Inner Osa Igneous Complex (Chpater 3.4.1.1., Figure 3.3a).

Basalt DJ01-094 from Marenco area has geochemical affinities similar to plateau-like igneous rocks of the Ganado Unit (Figure 3.3c). These rocks are also characterized by a lower Nb/Y ratio than plateau-like igneous rocks from the Inner Osa Igneous Complex, pointing toward distinct origins (Chapter 4).

Highly depleted tholeiitic lavas DJ01-023 and DJ01-097 were sampled in olistotromic deposits close to Marenco (Figure 3.4). They are characterized by plagioclase-phyric textures and REE contents highly similar to the lava flows from the Riyito Unit (Figure 3.3b). The sample DJ01-023 was embedded in a sedimentary layer conjointly with a cobble of sediment containing *Palaxius osaensis* coprolites. This coprolite species has been first identified in sediments of the Riyito Unit (Chapter 6) and, thus, may be considered as a highly-specific marker of this unit.

Reddish alkali/transitional basalts DJ01-131 and DJ01-133 were sampled in olistostromic deposits close to the San Pedrillo ranger station. These samples have similar geochemical affinities to igneous rocks of the Vaquedano Unit (Figure 3.3d). They are associated to late Cretaceous to Eocene pelagic sediments similar to the limestones of the Vaquedano Unit.

3.4.3. Contact between the Osa Igneous Complex and the Osa Mélange

The Osa Mélange is in contact with the Osa Igneous Complex along a NW-SE fault zone that extents through the Osa Peninsula (Figure 3.1). In NW Osa, the Mélange is directly in contact with the Vaquedano Unit, whereas in the SE Osa the Mélange it borders the Inner Osa Igneous Complex. The nature of the contact is similar in both NW and SE Osa. This contact probably extends further toward the NW and is illustrated on a seismic line ~35km off the Osa Peninsula by the presence of diffractions [*Kolarsky et al.*, 1995b] (Figure 3). Similarly to the fault zone at the Güerra Unit-Inner Osa Igneous Complex interface, the topography is indicative of a major, possibly-active tectonic contact between the Osa Igneous Complex and the Osa Mélange (Figure 3.2B-B'). In the Outer Osa Igneous Complex, the altitude broadly increases toward the contact where it reaches a high and then strongly lowers toward the Osa Mélange. This may be caused by a thrust of the Osa Igneous Complex upon the Osa Mélange along an inverse fault.

Deformation of the rocks from the Osa Igneous Complex progressively increases toward the fault zone and marks a transition to the Osa Mélange. The deformation is characterized by the appearance of a pervasive intense brecciation of the igneous rocks associated to a complicated vein network. In an area of <300m from the Mélange, the igneous sequences were brittely deformed and reduced to a tectonic mélange with "preserved" igneous blocks embedded within cataclased igneous rocks. In the Vaquedano Unit higher volumes of sediments are intercalated with igneous rocks and preferentially accommodated the deformation, leading to a better preservation of the igneous rocks.

The edge of the San Pedrillo Unit in contact with the Osa Igneous Complex is globally similar in terms of geology and structure to the rest of the San Pedrillo Unit. Tectonic

incorporation of brecciated blocks of the Osa Igneous Complex in a ~100 m thick layer may occur at the transition between the two complexes. However, the small thickness of this layer indicates that no significant tectonic incorporation of the Osa Igneous Complex into the Osa Mélange has occurred.

3.4.4. Biostratigraphy

New paleontologic ages used during the recognition and interpretation of the units forming the Osa Igneous Complex and San Pedrillo Unit (inner Osa Mélange) are documented in this chapter. Radiolarian ages from the Osa Igneous Complex given by *Diserens* [2002] are newly evaluated using updated fossil ranges. Radiolarian ages from the Azuero Plateau (Azuero Complex, western Panama, Chapter 2) given by *Kolarsky et al.* [1995b] are reappraised following the same method so as to provide reliable comparisons of biochronologic ages for some Costa Rican-Panamean igneous complexes predominantly composed of plateau-like igneous rocks.

3.4.4.1. Radiolaria in the Osa Igneous Complex and San Pedrillo Unit

The radiolarian biostratigraphy (Figure 3.7) for the late Cretaceous is based on work by *Riedel and Sanfilippo* [1974], *Dumitrica* [1975], *Foreman* [1975, 1977], *Pessagno* [1976], *Taketani* [1982], *Sanfilippo and Riedel* [1985], *Schaaf* [1985], *Thurow* [1988], *O'Dogherty* [1994], *Hollis and Kimura* [2001], *Vishnevskaya* [2001, 2007], while *Foreman* [1973], *Sanfilippo and Riedel* [1973], *Nishimura* [1987, 1992], *Sanfilippo and Nigrini* [1998] were used in dating the Paleogene samples. For more details on the technique used to date samples see *Bandini et al.* [2006, 2008].

Azuero Complex, western Panama

Sample JC-86-A7 (Torio shore, *Kolarsky et al.* [1995b]): occurrence of *Crucella plana* and *Alievium praegallowayi* gives a Turonian-early Santonian age. This fauna was illustrated in *Kolarsky et al.* [1995b] and is used herein for comparison with the radiolarian assemblages from the Osa Igneous Complex illustrated in this study (see discussion below).

Inner Osa Igneous Complex

Sample GDM 9116 (Punta Banco, Burica Peninsula, *Diserens* [1994]): The occurrence of *Theocampe urna* and *Praeconocaryomma universa* gives an early Turonian-early Maastrichtian age. Sample FBJ 90174 (Punta Esquinas, eastern coast of Golfo Dulce, *Diserens* [1994]): occurrence of *Lithatractus pusillus*, *Acanthocircus yaoi* and *Crucella cachensis* gives a Coniacian-Santonian age.

Ganado Unit

Sample DB02-199 (~505.6/297.3 Costa Rican coordinates, this study): occurrence of *Archaespongoprunum bipartitum*, *Eostichomitra* sp. and *Theocampe salillum* gives a Coniacian-Santonian age.
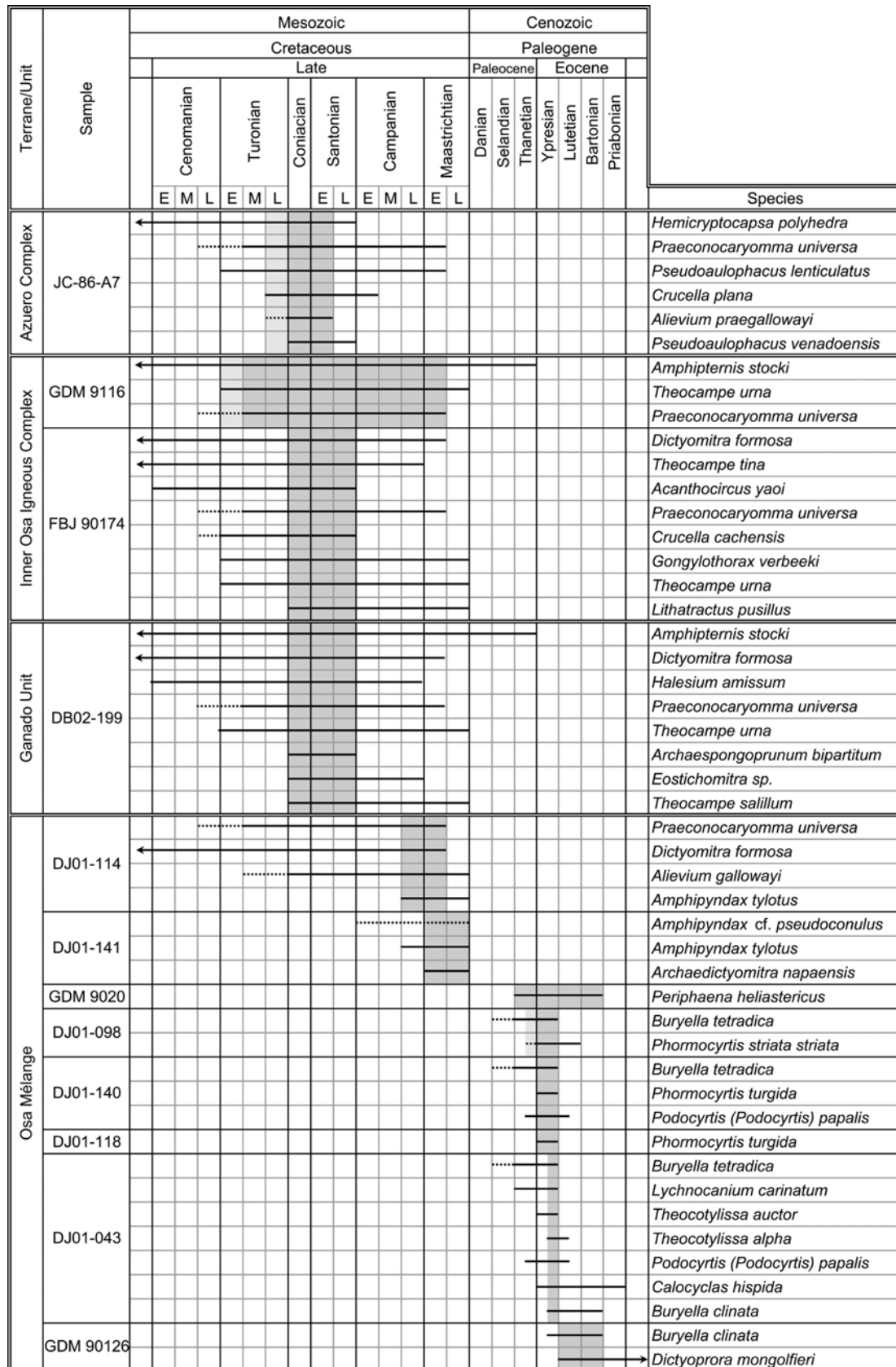
Figure 3.7: *Ranges and occurrences of Cretaceous and Paleogene radiolarian species from samples of the Azuero Complex (Azuero plateau, data from Kolarsky et al. [1995b]), the Osa Igneous Complex (inner Osa Igneous Complex and Ganado Unit, data from Diserens [2002] and this study) and the San Pedrillo Unit (inner Osa Mélange, data from Diserens [2002] and this study). Ages of sample formation are given by grey fields (details in Chapter 3.4.4.1).*

San Pedrillo Unit (inner Osa Mélange)

Sample DJ01-114 (this study): occurrence of *Lithatractus pusillus*, *Acanthocircus yaoi* and *Crucella cachensis* gives a late Campanian-early Maastrichtian age. Sample DJ01-141 (this study): occurrence of *Archaedictyomitra napaensis* gives a Maastrichtian age.

Sample GDM 9020 (*Diserens* [2002]): occurrence of *Periphaena heliasteriscus* gives a Thanetian-Bartonian age. Sample DJ01 (this study): occurrence of *Phormocyrtis striata striata* and *Buryella tetradica* gives a late Thanetian-Ypresian age. Sample DJ01-140 (this study): occurrence of *Phormocyrtis turgida* and *Buryella tetradica* gives an Ypresian age. Sample DJ01-118 (this study): occurrence of *Phormocyrtis turgida* gives an Ypresian age. Sample DJ01-043 (this study): occurrence of *Theocotylissa alpha*, *T. auctor*, *Buryella clinata*, *B. tetradicta* and *Lychnocanium carinatum*, gives a late Ypresian age. Sample GDM 90126 (*Diserens* [2002]): occurrence of *Dictyoprora mongolfieri* and *Buryella clinata* gives a Lutetian-Bartonian age.

Discussion

Radiolarian cherts of similar ages (Coniacian-Santonian) have been found in the Azuero Plateau [*Kolarsky et al.*, 1995b], the Inner Osa Igneous Complex [*Di Marco*, 1994; *this study*] and the Ganado Unit [*this study*]. All these units are predominantly composed of igneous rocks with plateau affinities (see also Chapter 4). Despite poor radiolarian preservation and weak abundance in the studied sediments, samples proceeding from these units yielded different faunal assemblage. The fauna of sample JC-86-A7 (Azuero Plateau, Azuero Complex, W Panama) is characterised by the association of *Hemicryptocapsa polyhedra*, *Praeconocaryomma universa*, *Pseudoaulophacus lenticulatus*, *P. venadoensis*, *Crucella plana* and *Alievium praegallowayi* [Kolarsky et al. 1995b]. The assemblage of sample FBJ 90174 (Inner Osa Igneous Complex) is characterised by the association of *Dictyomitra formosa*, *Theocampe tina*, *T. urna*, *Acanthocircus yaoi*, *Praeconocaryomma universa*, *Crucella cachensis*, *Gongylothorax verbeeki* and *Lithatractus pusillus*. The assemblage of sample DB02-199 is characterised by the association of *Amphipternis stocki*, *Dictyomitra formosa*, *Halesium amissum*, *Praeconocaryomma universa*, *Theocampe urna*, *T. salillum*, *Archaespongoprunum bipartitum* and *Eostichomitra* sp. These three assemblages coming from three different units share only two commonly illustrated species in the published Late Cretaceous radiolarian faunas (*Dictyomitra formosa*, *Praeconocaryomma universa*). Some precautions are required in the interpretation of faunal assemblages since preservation and methodology may differ between samples and workers, respectively. However, we note that in samples of similar ages, associated on the field to similar igneous rocks, faunal assemblages possibly point toward distinct palaeoenvironments. This observation is in good agreement with occurrences of partly distinct sedimentary facies among the units.

Radiolaria occur in a variety of lithologies in the Osa Mélange. Ribbon-bedded red cherts associated with basalts in seamount-derived blocks (samples DJ01-114 and DJ01-141) contain Campanian-Maastrichtian radiolarian assemblages. Samples DJ01-141 occurs on the field in association with large blocks of basalt containing interbeds of pelagic limestones of similar ages.

The San Pedrillo Unit contains an important amount of pelitic hemipelagic to pelagic lithologies that range from originally ribbon-bedded muddy chert to siliceous and tuffaceous mudstones that partly form the mélange matrix. Radiolaria and sponge spicules are locally abundant in all these lithologies. Faunal assemblages indicate in general a late Paleocene-middle

Eocene age, in broad agreement with middle Eocene ages from *Azéma et al.* [1983]. However, the better preserved samples (DJ01-140 and DJ01-043) restrict the age to the early Eocene.

3.4.4.2. Larger benthic Foraminifera in the San Pedrillo Unit

Larger benthic foraminifera occur together with other shallow-water benthic bioclasts in limestone clasts-olistoliths and calciturbidites of the San Pedrillo Unit in the NW Osa Peninsula and Caño Island. The well-lithified samples only allowed determination in thin sections that were studied in light microscopy and cathodoluminescence. Although there are some compositional variations from one outcrop to another, faunal assemblages are similar and, in general, have a late Eocene age derived from the larger foraminifera [see also *Azéma et al.*, 1983]. On the NE and SE coasts of Caño island, redeposited shallow-water material occurs in isolated blocks of calcarenites and calcirudites showing clasts of lime packstone, grainstone and bindstone and grains of basalt, chert, and feldspar [*Mora et al.*, 1989]. The limestone clasts contain the following bioclasts: articulate coraline algae (dominant), larger foraminifera, smaller planktonic and benthic foraminifera, crinoids, siliceous sponge spicules, bryozoans and green algae. The clasts show stylolitized contacts and several phases of fracturing and vein infill by opal-quartz and then calcite. Although the larger foraminifera found at the studied localities are recrystallized, partly silicified and fractured, we could identify the following assemblage [*Mora et al.*, 1989]: *Amphistegina grimsdalei*, *Amphistegina lopeztrigoi*, *Amphistegina parvula*, *Asterocyclina* sp., *Discocyclina* sp., *Eoconuloides* sp., *Eofabiania cushmani*, *Eofabiania* sp., *Fabiania cubensis*, *Lepidocyclina* sp., *Linderina* sp*., Nummulites floridensis*, *Pararotalia* sp., *Sphaerogypsina globulus*. This indicates a late Eocene age with reworking of some middle Eocene forms.

At Punta Campanario (Figure 3.5) limestone clasts occur in a variety of debris flow breccias with a tuffitic mudstone to greywacke matrix. Lithoclasts are calcarenites to calcirudites with volcanic content. Samples DB02-024/026 contain well-preserved, but abraded and sometimes broken Larger Foraminifera that are clearly size sorted (in general forms of less than 4mm size). The assemblages include *Operculinoides* sp*.,* small globulose and small flat forms of *Nummulites* sp. such as: *Nummulites dia, Nummulites* cf. *macquiaveri*, *Orthophragmina* sp*.,* neolepidine *Lepidocyclina* sp., such as *Lepidocyclina chaperi, Lepidocyclina* cf. *antillea, Lepidocyclina canellei, Lepidocyclina pustulosa, Sphaerogypsina globules*, *Amphistegina* sp., *Discocyclina* sp*., Pseudophragmina* sp. Most of these forms indicate middle to late Eocene age; some are restricted to late Eocene.

One sample yielded Late Cretaceous shallow water bioclasts. A spiculite from Agujitas (sample DJ01-019) contains poorly preserved *Pseudorbitoides sp.*, *Sulcoperculina sp.*, *Omphalocyclus sp.*, this material is reworked from a probable Late Cretaceous carbonate bank.

3.4.4.3. Planktonic Foraminifera in the San Pedrillo Unit

Planktonic foraminifera occur in pelagic limestones mostly associated with basaltic olistoliths. Rocks were studied in polished thin sections by light- and cathodoluminescence microscopy. No isolated forms could be obtained, which leaves the specific determinations with some uncertainty. The ages range from Campanian-Maastrichtian for a majority of blocks to middle Eocene. Similar ages and sedimentary facies are observed in the pelagic limestones of the Vaquedano Unit [*Di Marco*, 1994; *Buchs*, 2003; *this study*].

3.5. The Osa Igneous Complex: discussion and interpretation

3.5.1. A well-organized highly-composite complex

The Osa Igneous Complex is made up of an imbrication of several rock bodies that is recognized on the basis of a converging line of observations: (1) pillow lavas are frequently found in overturned position, (2) a strong deformation is locally observed that is very likely related to thrust zones, (3) small-scaled (<100m) tectonic lenses clearly occur in some units, (4) biochronologic dating provides late Cretaceous to middle Eocene ages of formation for the igneous rocks, and (5) geochemistry points toward a large diversity of intraplate, oceanic origins for the igneous rocks (Figure 3.3, Chapter 4).

Although geochemical and age characteristics are strongly heterogeneous at a scale of the complex (i.e. tens of km), detailed characterization of the volcano-sedimentary sequences allowed us to recognize five units that define composite rock belts with similar trench-parallel strikes (Figures 3.1b). This arrangement and the presence of various intra-oceanic volcanic rocks are typical of accretionary complexes, or accretionary belts [e.g. *Dickinson,* 2008]. This suggests that the Osa Igneous Complex is an accretionary complex made up of several pieces of accreted igneous sequences initially pertaining to seamounts, plateaus and/or the "normal" oceanic seafloor (see discussions below).

3.5.2. Size and arrangement of accreted rock bodies

Due to a lack of extended exposures and limited occurrences of stratigraphic markers, size of imbricated rock bodies and imbrication mechanisms are poorly constrained. However, with the exception of the Ganado Unit we note that large igneous intrusive rocks lack in the Osa Igneous Complex. This indicates that the imbricated rock bodies represent superficial sequences of volcanic edifices, probably originally restricted in the few uppermost km or hundred of meters of the crust. Dolerites and gabbroic rocks of the Ganado Unit are devoid of significant crystal accumulations and were possibly originally located in superficial levels of one or several volcanic edifice(s). As a consequence, we propose an estimate of less than 4 km for the maximal thickness of the imbricated, dismembered rock bodies forming the Osa Igneous Complex. In the Vaquenano Unit and Güerra Unit, distinct geochemical affinities, volcano-sedimentary sequences and biochronologic ages are encountered at scales ~500 m. In these cases it appears clearly that the thickness of the accreted sequences may be as low as ~250 m. These units exhibit the highest amount of accreted sediments (~20%) among the Osa Igneous Complex, potentially indicating that subducting seamounts accrete preferentially by scrapping off thin layers of "strong" igneous rocks along "weak" sedimentary layers when there is interlayered sediment in the volcanic sequences. In the seamounts where the amount of interlayered sediments is too low to scrap off thin rock bodies, several km-thick piles of igneous rocks may detach and accrete to the overriding plate, as notably imaged in Japan when the coupling between the overriding and subducting plate is sufficiently high [*Park et al.,* 1999]. Several km (2-3 km) thick piles of rock are thus believed to compose most of the Ganado Unit, Riyito Unit and Inner Osa Igneous Complex. In the light of these considerations the Inner Osa Igneous Complex is probably made up of numerous accreted pieces of seamounts, though it is predominantly composed of very similar Campanian plateau-like igneous rocks.

Contrary to amalgamated terranes of Northern America [e.g. *Coney,* 1989], indication of large strike-slip motion has not been observed the Osa Peninsula. Large fault zones associated to

left-lateral strike-slip motion were recognized in western Panama [*Kolarsky and Mann,* 1995], but no precise quantification of possible displacement was provided. The geology of western Panama does not exhibit evidence of large strike-slip displacements (Chapter 2). Hence, it seems that the Osa Igneous Complex provides opportunity to recognize accretion-related structures that normally tend to be quickly lost through disaggregation by later tectonics. Relatively good preservation of the rocks bodies and frequent occurrences of overturned pillow lavas may be related to an emplacement of the rocks bodies by duplexing or fault propagation folding at large scale. However, detailed structural observations are still required to better constrain this hypothesis.

Three major sutures bound the Inner and Outer Osa Igneous Complexes and mark the contact with the island arc (Golfito Complex) and the Osa Mélange (Figure 3.2B-B'). These sutures correlate to the landscape morphology (i.e. occurrence of incised valleys and slope variations over broad areas) and are interpreted here as ancient tectonic contacts used by recent and/or active faults. Interestingly, along-strike extension of the sutures is not clearly seen on nearby seismic profile P 1600 [*Kolarsky et al.,* 1995a] (Figure 3.2A-A'). Closeness of on-land sutures and units (~15-30 km) make us believe that allochtonous and accreted igneous rocks forming the outer forearc and the San Pedrillo Unit are still present at site of profile P 1600. Hence, they are probably not recognized by offshore seismic imaging due small velocity and structural contrasts between the units. Location of possibly-active tectonic contacts along the edge of the units indicates that the compressive regime associated to the incoming of the Cocos Ridge [e.g. *Kolarsky et al.,* 1995a; *Morell et al.,* 2008] or, more generally, topographic irregularities on the top of the oceanic floor, develop faulting preferentially along weaknesses in the crust, such as ancient sutures. The landscape morphology associated to the tectonic contacts is representative of an overthrust of landward units onto seaward units. This may be a result of a reactivation of ancient inverse fault zones, such as paleo-décollements at the base of the innermost units. Although formation of fault-bounded blocks is likely triggered by the topography of the subducting plate [e.g. *Sak et al.,* 2004; *Vannucchi et al.,* 2006], this mechanism alone cannot account for the existence of large inverse fault zone and we suggest here that it may be combined with a compressive stress in the outermost forearc area and pre-existence of weak crustal boundaries along the margin. Recognition of fault-bounded blocks appears thus to be a very useful tool in terms of geological mapping, because faulting tend to develop along geological boundaries.

3.5.3. Argon loss induced by tectonics?

In the Inner Osa Igneous Complex ages of lava formation are given by sediments and $^{40}Ar/^{39}Ar$ dates. Coniacian-Santonian (~89-84 Ma) siliceous pelagic sediments are interbedded with the lavas in several places. Two basalts from the Burica Peninsula and Isla Violín gave dissimilar $^{40}Ar/^{39}Ar$ ages of 54.5 ± 1.5 Ma (late Paleocene-early Eocene) and 64.2 ± 1.1 Ma (early Paleocene), respectively (total fusion on whole rock matrix) [*Hoernle et al.,* 2002].

It may be considered that occurrence of basalts formed at different times is not a big issue in a composite complex, but it is troubling that (1) there is no overlap between the radiometric and biochrononologic ages and (2) the radiometric method provides the youngest ages. Furthermore, the 54.5 ± 1.5 Ma (late Paleocene-early Eocene) intra-oceanic basalt sampled in the Burica Peninsula is stratigraphically covered by the ~56-59 Ma (late Paleocene) arc-derived sediments of the Pavones Formation. Older ages of the overlap sediments indicate that the

$^{40}Ar/^{39}Ar$ age does not represent an age of formation. As a consequence, the basalt certainly experienced Ar loss after its formation. This loss may be related to syn- or post-accretion tectonics and deformation. Hence, it appears clearly in this case that the age of formation of the lava is more efficiently defined by the biochronologic dates.

Figure 3.8 illustrates a comparison between radiometric ages of the igneous rocks and ages of corresponding units based on paleontological data. Although there is a large variability in the biochronologic ages due to heterogeneity of the unit and/or poor age accuracy of the fossil assemblages, it appears clearly that many samples from the Inner Osa Igneous Complex and Golfito Complex (considered here solely for the Ar-loss issue) have lower radiometric than biochronologic ages. This is very likely due to Ar loss after the formation of the igneous rocks. Moreover, we note on Figure 3.8 that mean ages are globally shifted to the left of a line of similar biochronologic and radiometric ages. This indicates that there is a tendency of Ar loss among dated samples. In the view of the geological heterogeneity and tendency of Ar loss in the dated samples, it appears that good agreement between $^{40}Ar/^{39}Ar$ ages and the range of K/Ar ages as pointed out by *Hoernle and Hauff* [2007] is most likely a result of randomness rather than a convergence of radiometric ages obtained by different methods.
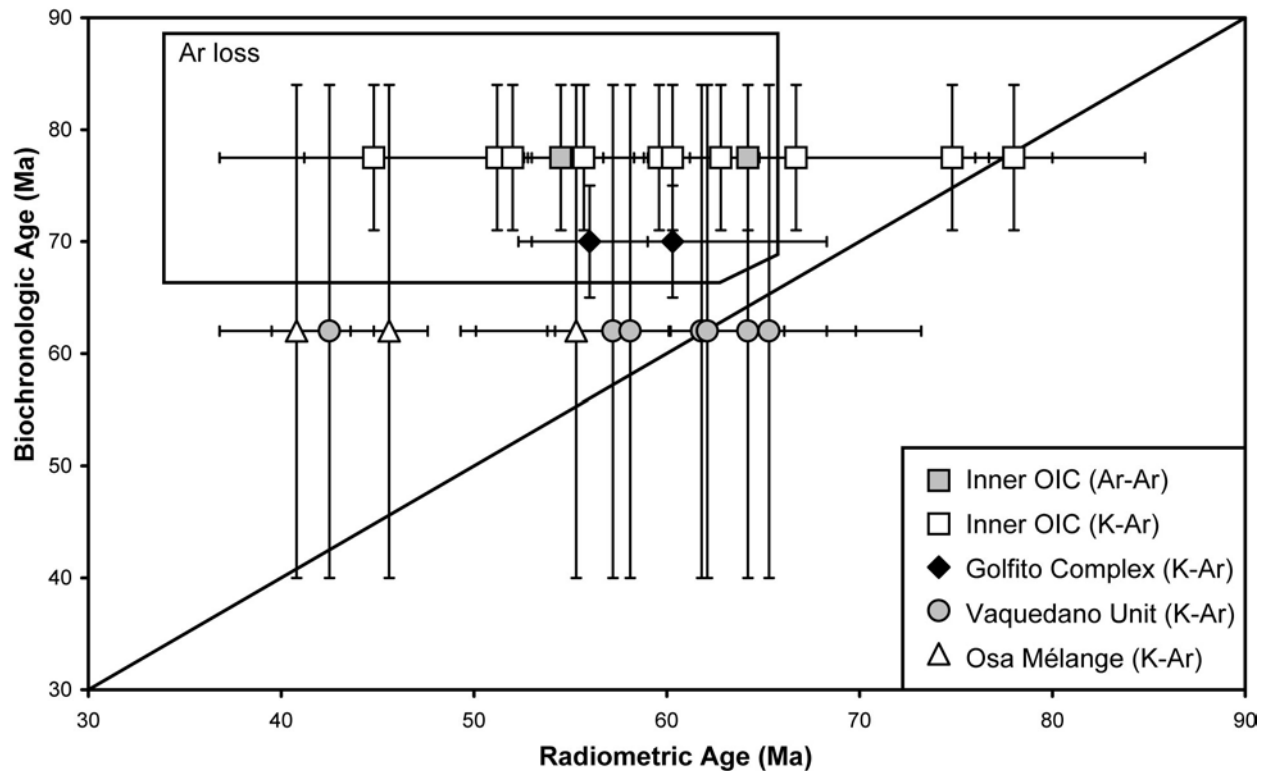
Figure 3.8: *Radiometric vs. biochronologic ages for some igneous samples of the Osa Igneous Complex and Osa Mélange, with error bars. Biochronologic ages are inferred from the tectonostratigraphy as defined in this study. Whole rock K/Ar ages are from Berrangé et al. [1989] and whole rock $^{40}Ar/^{39}Ar$ total fusion isochron ages from Hauff et al. [2000] and Hoernle et al. [2002]. Large variability in the biochronologic ages is due to large range of formation ages for some units and/or poor age accuracy of fossil assemblages. Some samples have inconsistent biochronologic and radiometric ages within the incertitude range that is attributed to Ar loss.*

Interestingly, lowest radiometric ages point toward a ~45 Ma (middle Eocene) age (Figure 3.8). This age corresponds broadly to the age of accretion of the Outer Osa Igneous

Complex (see below), potentially indicating that massive Ar loss from the igneous rocks may occur in response to increased tectonics along the margin such as that induced by seamount accretion.

In the light of preceding remarks, it appears that $^{40}Ar/^{39}Ar$ or K/Ar ages have to be interpreted with a lot of precaution in the case of the Osa Igneous Complex. Hence, we chose here to consider radiometric dates to represent minimal ages of formation only. Biochronologic and radiometric discrepancies pointed out in this study further raises an important interrogation about the interpretation of ages determined by $^{40}Ar/^{39}Ar$ dating for other (low-K) basaltic samples reported for south Central America [e.g. *Sinton et al.*, 1997; *Hauff et al.*, 2000; *Hoernle et al.*, 2002, 2004]. These ages should thus be used with a lot of precaution and in adequation with stratigraphic data.

3.5.4. Origin and Significance of the Units

The units forming the Osa Igneous Complex consist of mostly unmetamorphosed accreted fragments of igneous rocks that range from a few hundred of meters to several km in size. In this section, we make a summary of the units and discuss their probable origin and implication in terms of accretionary processes.

One of the most intriguing features of the Osa Igneous Complex is the low occurrence of intercalated arc-derived or continental sediments. Such detrital deposits are very commonly observed in other accretionary complexes [e.g. *Isozaki et al.*, 1990; *Dickinson*, 2008]. Furthermore, with the exception of the Güerra Unit, the Osa Igneous Complex have apparently not suffered metamorphism (greenschist facies and higher). However, metamorphism is very commonly observed in accreted rocks [e.g. *Maruyama and Liou*, 1989; *Isozaki et al.*, 1990; *Dickinson*, 2008]. Accretionary complexes predominantly composed of poorly metamorphosed igneous rocks are scarce and examples from the Alexander Island in Antarctica [*Doubleday et al.*, 1994a, b] and Northern California Coast Ranges [*Shervais et al.*, 2005] show that greenschists may locally represent a significant portion of the accreted material. Indeed, to our knowledge, oceanic terranes of the Solomon Islands [e.g. *Petterson et al.*, 1997, 1999] are the sole occurrence of an accretionary complex similar to the Osa Igneous Complex, i.e. essentially composed of oceanic sequences devoid of significant metamorphism and trench-fill sediments. Below, we point out other similarities between these two complexes.

3.5.4.1. The Inner Osa Igneous Complex

The Inner Osa Igneous Complex is predominantly composed of Coniacian-Santonian (~89-84 Ma) tholeiitic basalts with plateau-like, oceanic intraplate affinities. Minor NMORB-like and OIB-like igneous rocks occur as sills, small intrusions and, possibly, interlayered lava flows. The volcano-sedimentary sequences are almost devoid of detrital material and, hence, indicative of submarine volcanism. Rare thin interbeds of siliceous pelagic sediments point toward high effusive rates for the lavas. Absence of carbonate banks indicate that they probably emplaced under the CCD. Detrital sediments of the Esperanza Formation are interpreted to be a product of submarine erosion of the plateau-like lavas prior to the accretion. Consistency of rocks forming the Inner Osa Igneous Complex tends to indicate that they initially belonged to a unique volcanic edifice.

In comparison, the Azuero Plateau (Azuero Complex, W Panama) is made up of tholeiitic, plateau-like basalts and minor intercalations of siliceous pelagic sediments. It represents a Coniacian-early Santonian (~89-85 Ma) oceanic plateau that forms the arc basement (Chapter 2). On this basis, it may be consider that the Inner Osa Igneous Complex and Azuero Plateau are highly similar and have a same origin. This interpretation has to be discarded for 4 reasons: (1) dissimilarities exist in terms of sedimentary facies and, eventually, faunal assemblages between the two units, (2) the Inner Osa Igneous Complex contain NMORB-like and OIB-like igneous rocks not observed yet in the Azuero Plateau, (3) lavas from both units have dissimilar ranges of Mg# (Chapter 4) and, (4) proto-arc igneous rocks crosscut the Azuero Plateau, but have not been observed in the Osa Igneous Complex. Absence of proto-arc dykes in the Inner Osa Igneous Complex which are frequently seen in the Azuero Plateau is a key point that indicates an allochtonous origin for the Inner Osa Igneous Complex, and a location far from the subduction zone at the time of arc initiation (late Campanian). Hence, we propose that sequences of the Inner Osa Igneous Complex were initially part of a Pacific oceanic plateau distinct from the CLIP that accreted along the margin to the South Central American Arc and CLIP-related basement.

It is important to note here that despite existence of striking similarities of geochemistry and age between the Azuero Plateau and Inner Osa Igneous Complex, the former is strictly part of the CLIP whereas the later is allochtonous and unrelated to the CLIP. Hence, it appears that systematic association of Central American exposures of oceanic plateau with the CLIP on the basis of geochemistry and radiometric dating only [e.g. *Sinton et al.*, 1998] is inappropriate. Our results suggest that possible genetic link of plateau-like igneous complexes with the CLIP should be more carefully constrained with the help of tectono-stratigraphy and field observations.

The Malaita accretionary prism (Solomon Islands), known to have formed by accretion of the subducting Ontong-Java Plateau [*Petterson et al.*, 1999; *Mann and Taira*, 2004, *Phinney et al.*, 2004; *Taira et al.*, 2004], share many similarities with the Inner Osa Igneous Complex: (1) accreted rocks are in a very-low metamorphic facies [e.g. *Petterson et al.*, 1997], (2) occurrences of trench-fill deposits lack [e.g. *Petterson et al.*, 1997], (3) sequences of the Malaita Volcanic Group (Malaita Island) predominantly contain igneous rocks with plateau affinities and minor interbeds of siliceous sediments [*Petterson et al.*, 1997], (4) sequences partly overturned during accretion and development of fault-propagating folds [*Petterson et al.*, 1997; *Phinney et al.*, 2004], and (5) the Makira Terrane (Makira Island) contain igneous rocks having NMORB signatures interbedded with plateau igneous rocks [*Petterson et al.*, 1999]. These similarities are another argument for an accreted oceanic plateau origin for the Inner Osa Igneous Complex. Thick (900-1770 m) pelagic limestones observed on the top of the Malaita Volcanic Group [e.g. *Petterson et al.*, 1995] have no apparent equivalent in the Inner Osa Igneous Complex. We interpret this dissimilarity as a consequence of (1) distinct travel times of the two oceanic plateaus on the oceanic floor before their accretion (i.e. < 25 Ma for the Inner Osa Igneous Complex (see Chapter 3.5.5) and ~94-105 Ma for the Ontong-Java Plateau [e.g. *Petterson et al.*, 1999, and references therein]), which resulted in few occurrences and preservation of calcareous sedimentary covers in the Inner Osa Igneous Complex, and/or (2) summital areas of the Inner Osa Igneous oceanic plateau below the CCD, pointing toward a lower crustal thickness for the Inner Osa Igneous plateau or distinct paleo-oceanographic conditions.

3.5.4.2. The Güerra Unit

The Güerra Unit is characterized by the highest metamorphic grade and deformation observed in the Osa Igneous Complex and Osa Mélange. It marks the contact between the Inner and Outer Osa Igneous Complexes and is composed of various rock bodies that include rock sequences similar to the Riyito and Vaquedano units in terms of igneous geochemistry and sediment facies. It is exposed along the Outer Osa Igneous Complex but is apparently lacking along the contact between the Outer Osa Igneous Complex and the San Pedrillo Unit (Figure 3.1b). This geometrical arrangement and compositional similarities with some units of the Outer Osa Igneous Complex indicate that the Güerra Unit formed after the formation of the Inner Osa Igneous Complex and prior to the emplacement of the Outer Osa Igneous Complex. Along-strike disappearance of the unit may be an artefact due to poor exposures in southern and northern Osa or linked to tectonic erosion at some places along the margin, prior to the accretion of the San Pedrillo Unit. Compositional heterogeneity of the Güerra Unit indicates it was likely triggered by low rates of accretion and several seamount subductions before the emplacement of the Vaquedano, Ganado and Riyito Units. In this interpretation, the Güerra Unit remained close to the décollement zone for a relatively long time, potentially recording some of the processes that occur at the interface between the overriding and subduction plates. As suggested in the case of sediment underplating [*Moore*, 1989], a long duration of residence close to the décollement may result in a strong deformation of accreted material, similar to that of the Güerra Unit. Deformation and/or fluid flows through the unit may have been a source of metamorphic catalysis, in a similar way than formation of metabasalts in the Franciscan complex [e.g. *Nelson*, 1995].

3.5.4.3. The Ganado Unit

The Ganado Unit is composed of Coniacian-Santonian plateau-like and NMORB-like tholeiites emplaced in an oceanic intraplate setting. The plateau-like lavas have lower Nb/Y ratios than similar rocks of the Inner Osa Igneous Complex, indicating that these two units have dissimilar origins (Chapter 4). The Ganado Unit may represent a large fragment of accreted seamount that originally developed in submarine conditions on the Pacific Plate. The occurrence of large intrusive rocks in the unit likely indicates that the seamount underwent a severe dismemberment in the vicinity of the trench as a response to slab flexuration [e.g. *Kobayashi et al.*, 1987] and/or during the accretion due to coupling between the overriding and subducting plates. Dismemberment of the seamount in the trench environment may have caused a removal of pelagic sediments initially capping the edifice, presently lacking in the unit.

3.5.4.4. The Riyito Unit

The Riyito Unit is mostly composed by Paleocene or older (?) highly-depleted tholeiites. It represents an assemblage of various seamount fragments. Peculiar geochemical affinities indicate that these seamounts were generated very close to a mid-ocean ridge (Chapter 4). Although the top of the seamounts may have reach relatively shallow water to allow the formation of highly-vesiculated hyaloclastite, all accreted lavas and detrital material issued from the erosion of the seamounts were emplaced in submarine conditions. Similarly to the Ganado Unit, pelagic sediments deposited on the top of the seamounts before their incoming into the subduction zone may have been removed close to the trench by gravitational collapsing.

3.5.4.5. The Vaquedano Unit

The Vaquedano Unit is principally made up of Campanian to Eocene alkali-transitional basalts with OIB-like signatures. These igneous rocks are an example of what has been commonly considered as "Oceanic Island Basalts" emplaced in oceanic intraplate settings. Geochemical and ages variations indicates the unit is composed of an imbricate of relatively thin (<250 m) volcano-sedimentary sequences with distinct origins. The unit is devoid of shallow-water limestones, indicating that the accreted rock bodies initially formed in submarine environments.

Interbeds of pelagic limestones are frequently found within the lavas of the Vaquedano Unit. Alkaline igneous rocks and frequent sedimentary intercalations are indicative of low eruption rates, generally associated to the latest stage of eruption of oceanic intraplate volcanoes [e.g. *Clague and Dalrymple*, 1987]. Thus, the Vaquedano Unit is likely composed of superficial layers of seamounts. Accretion by "peeling" of relatively-thin, superficial rock bodies was certainly facilitated by the existence of weak layers (i.e. interlayered sediments) in the subducting volcanoes.

Important differences exist between the Vaquedano Unit and the Riyito Unit, Ganado Unit and Inner Osa Igneous Complex: (1) sizes of accreted seamount fragments are much lower in the Vaquedano Unit, (2) detachment of rock bodies was easier in the Vaquedano Unit due to the occurrence of weak layers in the superficial parts of the subducting seamounts, (3) the Vaquedano Unit has more heterogeneous geochemical affinities, and (4) ages of the accreted material spans a longer period of time (~40 Ma). These differences show that the construction of the Vaquedano Unit was characterized by an accumulation of superficial layers proceeding from distinct seamounts. External position of the Vaquedano Unit (i.e. in contact with the Osa Mélange) may be attributed to an emplacement during the latest stage of growth of the Osa Igneous Complex. These observations tend to indicate that the Vaquedano Unit has a particular significance in terms of accretionary processes. We propose that this unit marks a transition between two subduction regimes: (1) a regime characterized by strong coupling between overriding and underlying plates and an accretion of thick/large rock bodies proceeding from subducting seamounts (i.e. Ganado and Riyito units), and (2) a regime characterized by a lower coupling and/or an absence of large seamount subduction leading to little accretion or tectonic erosion. Similarities in the size of accreted rock bodies and composition between the Vaquedano and Güerra Units arise very likely from the transitional character of these two units in terms of subduction regime. We suggest that the Güerra Unit marks a transition from little seamount accretion to seamount accretion and the Vaquedano Unit from seamount accretion to little seamount accretion (see also below). The Vaquedano Unit has remained mostly undeformed and poorly metamorphosed in comparison to the Güerra Unit. This may be due to a rapid emplacement of the Osa Mélange on the edge of the Vaquedano Unit and to a shorter time of residence of the Vaquedano Unit in the vicinity of the décollement relatively to the Güerra Unit.

3.5.5. Construction of the Osa Igneous Complex

Our model for the construction of the Osa Igneous Complex is principally constrained by the tectonostratigraphy of the area (Figure 3.9), under the assumption that the complex did not suffered from post-accretion reorganisation due to along-strike displacements. There are several regional, stratigraphic and structural aspects that have been taken into account to constrain the model: (1) accretion may have occurred since the late Campanian only (~73-70 Ma), i.e. after the

initiation of the subduction in southern Central America (Chapter 2), (2) the oldest possible age of accretion of a volcano-sedimentary sequence is defined by the youngest age of formation of the sequence, (3) units in external (seaward) position accreted after units in internal (landward) position, (4) overlap sequences (i.e. arc-derived sediments unconformably resting on accreted rocks) define a minimal age of accretion of underlying accreted rocks, (5) tectonic erosion may possibly occur between periods of accretion, and (6) deformed, metamorphosed volcano-sedimentary sequences remained longer in the vicinity of the décollement than undeformed, unmetamorphosed volcano-sedimentary sequences. Growth of the margin by successive stacks of rock bodies is well documented in the Osa area by a chiefly progressive diminution of the ages toward the trench (Figure 10).
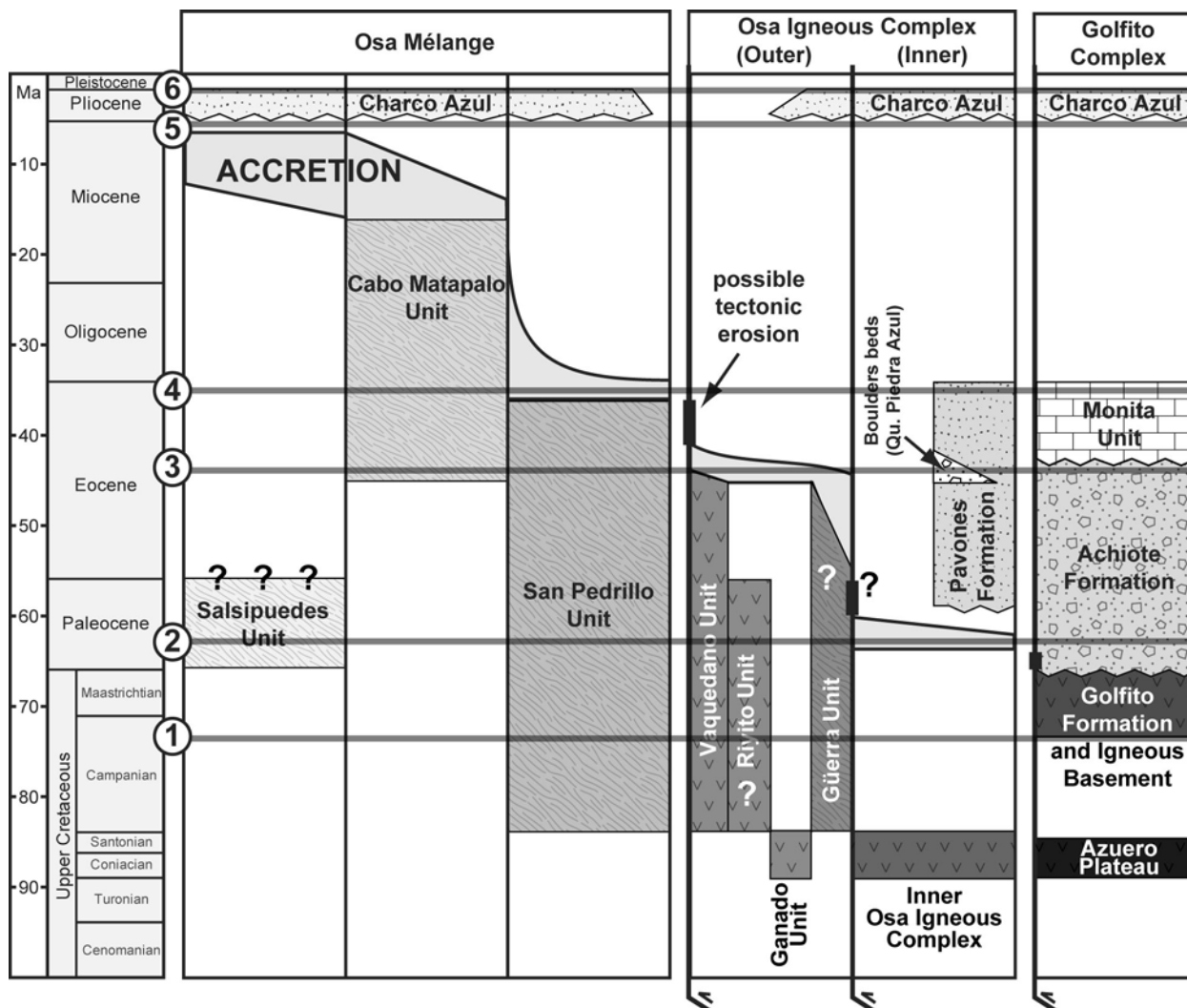
Figure 3.9: *Tectonostratigraphy of the Osa and Burica Peninsulas [partly based on data from Berrangé and Thorpe, 1988; Coates et al., 1992; Di Marco et al., 1995]. Horizontal lines represent major tectonic events along the south Costa Rican margin: (1) subduction initiation (Chapter 2), (2) accretion of the Inner Osa Igneous Complex, (3) accretion of the Ganado and Riyito Units, (4) possible seamount subduction leading to formation of the San Pedrillo Unit, (5) subsidence of the margin (unidentified origin, tectonic erosion?), and (6) possible incoming of the Cocos Ridge. Grey areas represent age ranges of possible accretion for corresponding units. Note that ages of the accreted units roughly define a development of the margin toward the trench through time. Dark bars represent age ranges of possible tectonic erosion. Succinct definition of the formations and units is provided on Figure 3.1.*

Construction of the Osa Igneous Complex may be resumed as follows. Subsequently to subduction initiation along the southwestern Caribbean Plate in the late Campanian (event 1 on Figure 3.9), portions of arc basement and proto-arc were removed from the margin by subduction erosion. This resulted to a progressive migration of the trench toward the Caribbean. Due to that erosion the Golfito Complex was located close to the trench by the early Paleocene and sediments proceeding from the arc were entirely subducted (Figure 3.10a). In the early-middle Paleocene the Inner Osa Igneous Complex formed by partial accretion of a subducting oceanic plateau (Figure 3.10b, event 2 on Figure 3.9). Subsequently to the emplacement of the Inner Osa Igneous Complex, possible tectonic erosion and/or entire subduction of the oceanic plateau caused the outer margin to subside, allowing deposition of arc-derived hemipelagic sediments of the late Paleocene Pavones Formation (Figure 3.10b). From the late Paleocene to the early Eocene, the subduction regime was characterized by low rates of superficial accretion of small seamounts that led to the formation of the Güerra Unit and a continuous deposition of the Pavones Formation on the forearc slope (Figure 3.10c). In the middle Eocene, a group of late Cretaceous-Paleocene seamounts entered the subduction zone and accreted, resulting in the formation of the Ganado and Riyito units (Figure 3.10d, event 3 on Figure 3.9). The seamount accretion squeezed the previously-formed Güerra Unit between the Inner Osa Igneous Complex and newly-accreted Ganado and Riyito units, preserving it from subsequent tectonic erosion. This event may have been recorded in the Pavones Formation by deposition of the limestone boulders found in the Quebrada Piedra Azul [*Di Marco et al.*, 1995] (Figure 3.9). The area comprising the Golfito Complex was possibly uplifted, partly eroded and subsided, leading to subsequent deposition of peri-platform deposits of the Monita Unit (Figure 3.9, Chapter 2). After this event, subduction regime was again characterized by low rates of accretion with possible tectonic erosion that led to the construction of the Vaquedano Unit and removal of some portions of the margin (Figure 11e).

In summary to this chapter, we observe that the construction of the Osa Igneous Complex occurred by multiple events of high-rate accretion which alternated with low-rate accretion and/or tectonic erosion. Although this is broadly similar to other well-studied convergent margins [e.g. North America: *Byrne and Fisher*, 1987; *Dickinson*, 2008; Japan: *Isozaki et al.*, 1990] the Osa Igneous Complex is characterized by pulses of high-rate accretion, or episodic accretionary events, that are associated with the emplacement of fragments of oceanic plateau and seamounts. Such events may be facilitated by incoming of large topographic highs into the subduction zone and, possibly, regional tectonic changes in the middle Eocene that resulted in a stronger coupling between the overriding and subducting plates (Chapter 7). Arc-derived sediments are lacking in the Osa Igneous Complex. This indicates that the sedimentary supply in the trench remained low or that the convergence rate between the overriding and subducting plates was sufficiently high to allow entire subduction of the trench-fill deposits (see discussion on the San Pedrillo Unit below). Whether these characteristics are symptomatic of an erosive or accretionary margin, they are discussed below along with constraints from the Osa Mélange.

A early Paleocene (~ 65 Ma)

proto-arc

Incoming oceanic plateau (will form the Inner Osa Igneous Complex)

Tectonic erosion

Caribbean Plate

B middle Paleocene (~ 60 Ma)

Inner Osa Igneous Complex

mature subaerial arc

oceanic currents?

Caribbean Plate

end of high-rate accretion regime

trailing edge of the subducting plateau

C late Paleocene to early Eocene (~58 to 48 Ma)

Inner Osa Igneous Complex

Pavones Formation

Caribbean Plate

low-rate accretion regime

Güerra Unit

D middle Eocene (~45 Ma)

Ganado Unit   Güerra Unit   Inner Osa Igneous Complex

Riyito Unit

Caribbean Plate

high-rate accretion regime

E middle Eocene (~38 Ma)

Ganado Unit (C)   Güerra Unit (D)   Inner Osa Igneous Complex (E)

Riyito Unit (B)

Caribbean Plate

Vaquedano Unit (A)

low-rate accretion regime, tectonic erosion

F late Eocene (~34 Ma)

Osa Igneous Complex

arc-derived sediments

mass wasting

A B C D E

Caribbean Plate

sediment Underplating

forearc uplift in response to seamount subduction

catastrophic, high sediment input

G Oligocene (~28 Ma)

Osa Igneous Complex

San Pedrillo Unit

A B C D E

Caribbean Plate

San Pedrillo Unit is accreted

high sediment input (?)

Figure 3.10 (previous page): Model of accretionary processes in the Osa transect of the mid-American Trench (middle Campanian to Oligocene, not to scale). A) Margin just after the subduction initiation, undergoing overall tectonic erosion. B) Accretion by large-scale duplexing of pieces of a Coniacian-Santonian oceanic plateau; initiation of the construction of the Osa Igneous Complex. C) Period of low-rate accretion; formation of the metamorphic, highly composite Güerra Unit. D) Various fragments of large seamounts accrete and squeeze the Güerra Unit onto the Inner Osa Igneous Complex; Ganado and Riyito Units are emplaced. E) Period of low-rate accretion and intermittent tectonic erosion; formation of the highly composite Vaquedano Unit. F) a seamount subduction causes a strong uplift of the forearc, leading to the gravitational collapse of the paleo-Osa Igneous Complex and large production of sediments. Large volumes of sediment proceeding form the forearc quickly deposit into the trench and lead to the formation of the San Pedrillo Unit. G) Possible growth of the San Pedrillo Unit by successive accretion of sediments derived from the forearc and arc areas.

3.6. Construction of the Osa Mélange

3.6.1. The San Pedrillo Unit: an unusual polygenetic mélange

The San Pedrillo Unit is made up of a complicated arrangement of lenticular, dismembered sequences composed of variously-clastic sediments (Figure 3.6). Although the sediments may contain blocks very similar to portions of the Osa Igneous Complex, some components such as shallow-water limestones, differentiated igneous rocks, ash deposits or finer hemipelagic sediments are clearly lacking in the Osa Igneous Complex and mostly proceeded from a volcanic arc. In a thin, ~100 m thick layer along the Osa Igneous Complex, the San Pedrillo Unit tectonically incorporated some material of the igneous complex. Extension of this tectonic incorporation is however very limited in comparison to the size of the San Pedrillo Unit. Hence, in regard to ubiquitous occurrence of sediments forming the San Pedrillo Unit and poor tectonic incorporation of the Osa Igneous Complex at the contact with the mélange, it is clear that the Osa Mélange was not simply produced by tectonic, or basal erosion of the Osa Igneous Complex as suggested by *Meschede et al.* [1999].

Vannucchi et al., [2006, 2007] proposed that the rocks forming the San Pedrillo Unit are dominated by basalt, chert, and shallow-water limestone resulting from accretion of seamounts. In this interpretation, the Osa Mélange is a dismembered unit characterized by a pervasive metamorphism (partly in greenschist facies) that formed by accretion at depth of a "classic sequence of oceanic crust". According to the same interpretation the material forming the San Pedrillo Unit consists of uppermost crustal sequences initially part of a "seamount system" that accreted to form the Osa Igneous Complex [*Vannucchi et al.*, 2006, p. 16, Figure 14]. This interpretation is inconsistent with our results for several reasons: (1) Lithologies forming the San Pedrillo Unit were studied into details in the field during more than two months [*Buchs and Stucki,* 2001] (Figure 3.4) and further constrained by microscope observation of 134 samples. During our mapping we observed that the bulk of the San Pedrillo Unit is composed of detrital sediment that incorporates various amounts of clasts ranging from grains to large boulders. This is atypical in classic sequences of Pacific oceanic crust. Furthermore, rocks forming the San Pedrillo Unit are not dominated by basalt, chert and shallow-water limestones but by fine-grain detrital sediments and olistostromic deposits (Figure 3.5). (2) A significant portion of the material forming the San Pedrillo Unit proceeded from a volcanic arc. Arc-related and seamount-related olistoliths sedimentarily embedded in the same debris flow deposits are observed

throughout the San Pedrillo Unit, indicating that the mélange is not a product of the dismemberment/erosion of the Osa Igneous Complex only. (3) The Osa Igneous Complex is not a "seamount system" accreted at the same time of the San Pedrillo Unit but is a composite accretionary complex that developed between the early-middle Paleocene and middle Eocene. For this reason accretion of the bulk of the Osa Igneous Complex cannot have triggered the formation of the San Pedrillo Unit. (4) Although some deformed rocks are green due the presence secondary chlorite, we have not observed metamorphosed rocks in the greenschist facies. Hence, it seems that the San Pedrillo Unit remained at relatively shallow depth during its formation.

We propose here that the occurrence of highly deformed sedimentary deposits throughout the San Pedrillo Unit is representative of a polygenetic mélange, with a block-in-matrix texture primarily controlled by clastic sedimentation and subsequently deformed during accretion. Numerous subduction mélanges around the world are characterized by hard metamorphic blocks embedded in a weaker metamorphosed matrix generally made up of shales or serpentinite, e.g. in the: Franciscan Complex [e.g. *Dickinson*, 2008, and references therein], Kodiak Convergent Margin [e.g. *Byrne and Fisher*, 1987], Japanese convergent margin (e.g. *Isosaki et al.*, 1990), Alexander Island of Antartica [*Doubleday et al.*, 1994a, 1994b], Lichi Mélange of Taiwan [e.g. *Chang et al.*, 2000], and Burma-Java Subduction Complex [e.g. *Pal et al.*, 2003]. Unlike these mélanges, the San Pedrillo Unit is predominantly composed of unmetamorphosed hard blocks embedded in an unmetamorphosed hard matrix. This specificity of the San Pedrillo Unit with respect to other mélanges worldwide is further discussed in the following sections.

3.6.2. The sedimentary record in the San Pedrillo Unit

3.6.2.1. Origins of the sediments

We have previously shown that the San Pedrillo Unit is composed of three main types of lithologies, which composes the bulk of the inner Osa Mélange: (1) sedimentary deposits containing shallow-water limestones, (2) debris flow deposits dominated by igneous olistoliths, and (3) fine-grain detrital sediments (Figure 3.5). All these lithologies are characterized by a detritic, clastic component that range from grains to large boulders embedded within a finer sedimentary matrix. On the basis of composition of the matrix and clasts, three main, distinct sources are recognized for the material composing the San Pedrillo Unit: (1) a palaeo-Osa Igneous Complex, (2) a subaerial volcanic arc and (3) pelagic-hemipelagic sediments.

Striking similarities exist between the basaltic olistoliths embedded in the sedimentary matrix of the San Pedrillo Unit and the volcano-sedimentary sequences of the Osa Igneous Complex (Chapter 3.4.2.5). These similarities are well-defined in terms of geochemistry, ages (late Cretaceous to middle Eocene), faunal assemblages encountered in the sediments associated to the lava flows and facies of the sediments. Although the Osa Igneous Complex is a composite unit made up of a wide range of late Cretaceous to middle Eocene igneous and sedimentary rocks, some of these rocks have very unusual geochemical affinities or contain very particular fossils such as Crustacean microcoprolites. Indeed, similarities between the San Pedrillo basaltic olistoliths and the Osa Igneous Complex are very specific in some cases. Hence, the bulk of the basaltic olistoliths encountered in the San Pedrillo Unit were very likely originally part of the palaeo-Osa Igneous Complex. The sedimentary mode of emplacement of the olistoliths is well constrained by the sedimentary fabric recognized throughout the San Pedrillo Unit and points toward mass wasting along the margin by the time of formation of the Osa Mélange. Parts of the

finer detrital material of the San Pedrillo Unit (e.g. unidentifiable rock fragments and crystals) may also be sedimentarily related to the palaeo-Osa Igneous Complex.

A subaerial volcanic arc is believed to have provided significant parts of the material forming the San Pedrillo Unit (Chapter 3.4.2.). Arc-derived material consists of fragments (grains to large boulders) of differentiated volcanic rocks and reworked and interlayered late Eocene shallow-water limestones, as well as dark ashy tuffites in the mélange matrix. The association of dark ashy tuffites with fragments of shallow-water limestones form one of the three principal lithologic associations recognized in the San Pedrillo Unit, described here as the "sedimentary deposits containing shallow-water limestones" (Figure 3.5). This recurrent rock association further constrain the origin of the shallow-water limestones to an arc environment. The differentiated and basaltic olistoliths are locally associated within the same debris flow deposits, indicating that these rocks proceeded from a similar paleo-environment. This is another argument pointing toward a paleo-Osa Igneous Complex for the bulk of the basaltic olistoliths.

The pelagic-hemipelagic sediments consist of undated siliceous-calcareous hemipelagic oozes intercalated with fine-grained detrital sediments and deformed lenses of early Eocene radiolarian cherts. We relate the hemipelagic oozes to background sedimentation commonly observed in near-trench environments [e.g. *Carter,* 1979]. The detritic fraction variously expressed in these sediments has a composition pointing toward a predominant basaltic source and a minor differentiated source that may represent an erosion of the palaeo-Osa Igneous Complex and a subaerial volcanic arc, respectively. The early Eocene radiolarian cherts are devoid of arc-derived material and, thus, may have originated in a pelagic environment, presumably on the slope of a seamount or on the ocean floor. Scarce igneous olistoliths associated to Campanian-Maastrichtian radiolarites (not found yet in the Osa Igneous Complex), may have been tectonically incorporated from subducting seamounts into the San Pedrillo Unit in a process similar to that proposed by *Okamura* [1991] for some mélanges in the Mino Terrane (Japan).

3.6.2.2. Emplacement of the sediments into the trench

The sedimentary record preserved in the San Pedrillo Unit is a highly valuable source of information, allowing a better understanding of the southern Costa Rican margin at the time of the mélange formation (Figure 3.11).

Sediments of the San Pedrillo Unit are indicative of a significant detrital input variously expressed among the lithologies, which culminates in the debris flow deposits and the sedimentary deposits containing shallow-water limestones. Occurrence of large boulders of igneous rocks derived from both the paleo-Osa Igneous Complex and a subaerial volcanic arc were embedded conjointly in thick debris flow layers prior to accretion of the mélange. Hence, the San Pedrillo Unit was partly produced by removal of large portions of the forearc area through mass wasting. At the time of deposition of the sediments, the palaeo-Osa Igneous Complex was presumably undergoing a strong uplift that led to disaggregation of unstable slopes by gravity. The material was gravitationally driven to the trench, partly incorporating arc-derived sediments transiting through by-passes, and ultimately formed thick pile of sediments close to the subduction zone. The carbonate material was displaced or reworked either grain by grain or as limestone clasts and gravitationally transported together with ashy tuffites toward the trench. Grain by grain displacement/reworking, possibly triggered by storm events or earthquakes, resulted in calci-turbidites relatively poor in ashy material owing to hydrodynamic winnowing.

Limestone clast reworking occurred together with the mobilization of abundant arc-derived volcanic material, possibly triggered by earthquakes and/or slope instabilities and resulted in debris flows with a variable amount of carbonates.

Fine-grain detrital sediments and hemipelagic siliceous limestones deposited on the forearc slope and in the vicinity of the trench during periods of lower detrital input. In this view, the hemipelagic limestones represent the background sedimentation in the forearc environment that was sporadically affected by catastrophic events leading to deposition of significant amounts of detrital material [e.g. *Underwood and Bachman*, 1982]. Hence, the sedimentary fabric of the San Pedrillo Unit, characterized by layers of various clast size (i.e. grains to large boulders) (Figure 3.4, 3.5), may be regarded as a consequence of variations in degree of clastic input in the trench environment.
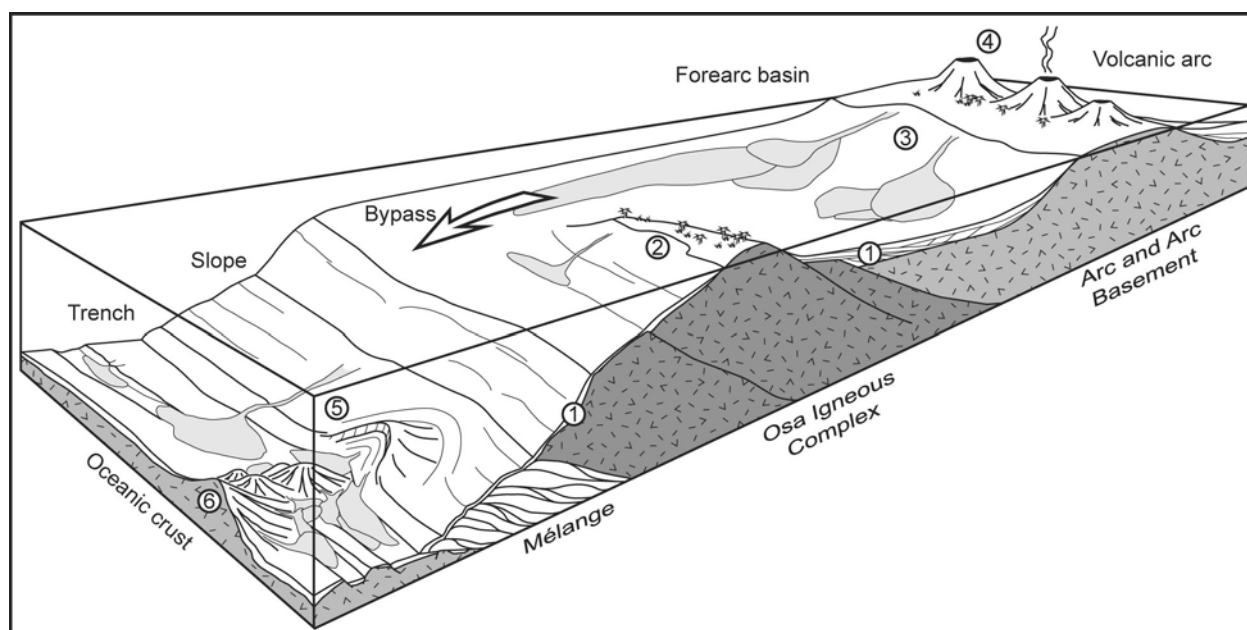
Figure 3.11: *Palinspastic reconstruction of the south Costa Rican margin in the late Eocene, based on the sedimentary record observed in the San Pedrillo Unit. The forearc area undergoes an important uplift possibly in response to seamount subduction. Large amount of sediments are deposited in the trench and quickly accreted to form the San Pedrillo Unit. The sediments are composed of volcanic fragments of the arc (1), late Eocene shallow-water carbonates originally deposited/produced along the arc (2), late Cretaceous-middle Eocene clasts (grains to large boulders) of the paleo-Osa Igneous Complex (3), and early-middle Eocene hemipelagic and tuffaceous sediments of the forearc slope-basin (4). Minor reworking of previously accreted portions of the San Pedrillo Unit is possible (5). Minor volumes of sediments and basalt derived from collapsing seamounts may have been deposited into the trench or may be tectonically incorporated into the mélange during the subduction of the seamounts (6), but remain very limited in comparison to the volume of detrital material coming from the upper plate.*

The age of deposition of the sediments of the San Pedrillo Unit in the trench is constrained to the late Eocene by the limestone beds containing shallow-water fauna. This age is in agreement with the age of the youngest rocks of the Cabo Matapalo Unit (middle Miocene), which were accreted subsequently to the San Pedrillo Unit. This age is also in relatively good agreement with the stratigraphy of the forearc area inboard of the Osa Peninsula that contains

>1000 m-thick arc-derived turbidites deposited during the Oligocene-early Miocene [*Henningsen*, 1963]. Occurrence of these deposits points toward high rates of clastic sediment production close to the arc at this time, which has remained preserved from erosion.

3.6.3. Deformation

Vannucchi et al., [2006] provided a detailed structural analysis of the San Pedrillo Unit and outlined four tectonic phases that occurred prior to the exhumation. According to their results and our observations, the tectonic record indicates that the clastic sediments were unlithified at the beginning of subduction. During the first stages of underthrusting, the sediments progressively lost their fluid content and deformation changed from an underthrust regime to underplating and shortening within the upper plate wedge. After the constitution of the San Pedrillo Unit and prior to its uplift, new tectonic events occurred, possibly in response to repeated collisions of seamounts with the margin.

Shear planes presumably related to the SP-D$_3$ and SP-D$_4$ phases [*Vannucchi et al.*, 2006], which correspond to an underplating regime, are defined by the precipitation of calcite, zeolites and quartz minerals. They crosscut the stratification and trend NE-SW with steep dips and, in conjunction with the orientations of stratification, they delimit lenses of consistent sedimentary facies (Figure 3.6). Calcite, zeolites and quartz veins are ubiquitously encountered within the San Pedrillo Unit. This indicates that pervasive fluid circulation took place during the first stages of the tectonic history of the mélange (SP-D$_1$), as previously suggested by *Vannucchi et al.*, [2006]. The density of the veins locally increases and may exceed 50% in the formations. It is thought to be associated with hydrofracturation. Preferential fluid drainage is indicated by high density of vein networks and occurred within areas dominated by igneous and calcareous olistoliths. These observations likely indicate that fluids associated to poorly lithified sediments play a predominant role during accretion of the San Pedrillo Unit.

3.6.4. Accretion of the San Pedrillo Unit

3.6.4.1. An accretion primarily triggered by catastrophic sediment supply

The presence of debris flow deposits containing large boulders of igneous rocks in the San Pedrillo Unit has to be considered as a record of highly catastrophic events that affected the trench environment in the late Eocene. We propose that a rapid increase of the sediment supply in the trench triggered the formation of the San Pedrillo Unit (Figure 3.10f, g).

Cloos and Shreve [1988] first proposed the existence of an inlet, or "subduction channel", at the interface between the subducting and overriding plates. In their model, the geometry of the inlet is temporally linked to the tectonic environment and tends to accommodate the subducting plate morphology, the sedimentary supply and the fluid content of the subducting sediments. A rapid increase of the sediment supply may fill topographic depressions and dramatically increase the sediment pile in the vicinity of the subduction zone. With sufficiently low rates of convergence and/or sufficient sediment supply, trench deposits may outgrow the subducting capacity of the subduction channel and ultimately lead to growth of an accretionary prism [e.g. *Moore*, 1989; *Le Pichon et al.*, 1993; *Lallemand et al.*, 1994]. Recent geological evidence from Italy show that subduction channel at shallow depth may be exposed in uplifted ancient convergent margins [*Vannucchi et al.*, 2008].

It is generally considered that the convergence between the Farallon and Caribbean Plate was not strongly oblique in the Eocene [*Meschede and Barckhausen*, 2001; *Pindell et al.*, 2005]. The rate of convergence may thus have been similar or faster to present day (~10 mm/y, *DeMets* [2001]) and, so, sediments in the trench were driven quickly (most probably in less than 500 ky) into the subduction zone. This is corroborated by the presence of low sediment induration in the San Pedrillo Unit at the onset of deformation [*Vannucchi et al.*, 2006]. In this context, deposition of large volumes of sediments over a short period of time in the trench provided an excess of material in the subduction zone, which over-filled the subduction channel. The excess sediments accumulated at shallow level, progressively lost fluid content and accreted to form the San Pedrillo Unit. Whereas this kind of process is generally associated to frontal accretion of the sediment [e.g. *Le Pichon et al.*, 1993; *Lallemand et al.*, 1994], structures in the San Pedrillo Unit indicate that the sediments accreted by underplating [*Vannucchi et al.*, 2006].

The structural fabric of the NW Osa Mélange indicates massive sediment fluid loss at the beginning of underthrusting, provoking changes in the regime of deformation [*Vannucchi et al.*, 2006]. Along erosive margins, fluid contents within subducting sediments play an important role in the control of subduction erosion. Fluids released from the subducting plate may increase hydrofracturing of the upper plate and trigger the removal and subduction of lenses of several kilometres in width and length [*Ranero and Von Huene*, 2000]. High fluid content of subducting sediments tends to prevent accretion and enhance subduction [e.g. *Cloos and Shreve*, 1988; *Moore*, 1989; *Seno*, 2007, 2008]. Thus rapid fluid expulsion likely occurred during underthrusting of the San Pedrillo Unit. Large amount of clastic sediments and low argileous component in the unit likely enhanced the ability of the subducted material to quickly dewater. Fluid expulsion caused a migration of the décollement toward the subducting plate and, consequently, accretion of subducting material. Due to strongly disturbed internal arrangement of the San Pedrillo Unit, it is unclear if this process repeatedly occurred or not to form the unit. For a similar reason it is not possible to know if significant portions of accreted material were removed between possible multiple events of accretion. Nonetheless, the presence of the San Pedrillo Unit indicates overall net accretion in southern Costa Rica during the late Eocene continuing until at least the middle Miocene with the subsequent emplacements of the Cabo Matapalo and Salsipuedes units.

3.6.4.2. *The San Pedrillo Unit: a record of a margin collapse in response to seamount subduction*

Large volumes of sediment deposited in the trench and produced by mass wasting along the Costa Rican margin during the late Eocene indicate that significant changes in the subduction dynamics took place in the area at that time. This event was likely caused by seamount subduction along the palaeo-Osa Igneous Complex.

Seamount subduction is a common process along many active margins. It has been notably observed along the Nankai Trough [*Park et al.*, 1999; *Kodaira et al.*, 2000], the New Hebrides Trench [*Collot and Fisher*, 1989], the New Zealand margin [Collot *et al.*, 2001] and the Mid American Trench [*Von Huene et al.*, 1995]. Subduction of a seamount is accompanied by a zone of tectonic deformation in the upper plate and a re-entrant in the margin on the steep slope behind the subducting seamount [*Von Huene et al.*, 1995]. This process creates a zone of slope failure that migrates upward and generates the deposition of reworked sediments in the trench area [*Dominguez et al.*, 2000; *Hühnerbach et al.*, 2005]. The amount of material disrupted in the

margin by seamount subduction is about four to five times the volume of the subducting seamount, of which about three quarters seems to be recycled downslope, backfilling the scar [*Hühnerbach et al.*, 2005]. The volume of reworked material of the margin may be even larger, depending on the brittleness of the margin [e.g. *Collot et al.*, 2001]. For example, along the Hikurangi margin (New Zealand), *Collot et al.* [2001] reported the presence of (1) a giant debris avalanche constituted by up to 2 km thick blocky deposits covering an area of ~3400 km^2 and (2) a 65-170 m thick debris flow covering an area of ~8000 km^2 that extends over 100 km from the trench fill. According to these authors, the deposits were generated in response to oblique seamount subduction that removed several thousands km^3 of material from the margin and created an indentation of the slope 65 km landward from the trench. Such present-day observations indicate that a seamount subduction may generate large volumes of clastic material redepositing into the trench and forming deposits similar to the sediments of the San Pedrillo Unit. Therefore, we propose that sediments of the San Pedrillo Unit were triggered by the subduction of a seamount (or several seamounts) during the late Eocene. The presence of subducting seamounts along the Central American margin during this period is in good accordance with the presence of accreted seamounts in the Azuero Peninsula (western Panama) (Chapter 5).

Subducting seamount along the paleo-Osa Igneous Complex in the late Eocene may have possibly enhanced the ability of the San Pedrillo Unit to accrete by underplating at shallow-level, rather than in the greenschist metamorphic facies or by frontal off-scrapping. Sandbox experiments have shown that subducting seamounts may trigger temporary migration of the décollement upward [*Dominguez et al.*, 2000], thus temporarily and locally increasing the thickness of the subduction channel. Such mechanism may allow partial subduction of sediments in the wake of downing seamounts and underplating at shallow level [*Bangs et al.*, 2006] (Figure 3.10f). If this mechanism triggered the accretion of the San Pedrillo Unit it may indicate that the unit formed very rapidly, possibly through a unique event of accretion.

The bulk of the reworked material in the San Pedrillo Unit proceeded from the partial collapsing of the upper plate. It remains possible, however, that some igneous and sedimentary blocks were tectonically incorporated into the mélange matrix directly from disaggregating subducting seamounts. If a similar process is involved in the genesis of some mélanges [e.g. *Okamura*, 1991], this was nonetheless an insignificant process in the formation of the San Pedrillo Unit because (1) the fabric is primarily controlled by sedimentary processes and (2) the bulk of the basaltic blocks and associated pelagic sediments proceeded from an older accretionary prism (the paleo-Osa Igneous Complex). Early Eocene radiolarian cherts sporadically encountered in the mélange as deformed lenses may represent a record of partial tectonic incorporation of subducting seamounts into the San Pedrillo Unit as well as minor proportion of basaltic olistoliths associated to Campanian-Maastrichtian radiolarites.

3.6.5. Accretion of the Cabo Matapalo and Salsipuedes units

The Cabo Matapalo and Punta Salsipuedes units constitute the outermost extension of the Osa Mélange, presumably emplaced onto the San Pedrillo Unit by accretion processes [*Di Marco*, 1994; *Di Marco et al.*, 1995] (Figure 3.1). Review and interpretation of these units is not the aim of this study, but their presence indicates that accretionary processes may have continued until the Miocene, prior to the exhumation of the Osa basement and subsequent deposition of the Charco Azul Group (Figure 3.9).

According to *Di Marco* [1994], the Cabo Matapalo Unit may have formed similarly to the San Pedrillo Unit, whereas the Salsipuedes Unit may represent sediments detached from the subducting plate that accreted onto the Cabo Matapalo Unit. Further stratigraphic, structural and geochemical data are nonetheless required to better constrain these interpretations.

3.7. The southern Central American margin: erosive or accretionary?

3.7.1. Erosive and accretionary margins

Since early work by *von Huene and Lallemand* [1990], it is widely recognized that convergent margin may be subdivided into two classes, one dominated by accretion and net growth of accretionary prisms and the second by tectonic erosion, absence of accreted material and trench retreat [e.g. *von Huene and Scholl*, 1991; *Clift and Vannucchi*, 2004]. Each type composes approximatively half of the convergent margins observed at the present time around the world. Distinction between these two types of margins has been initially based on long-term forearc subsidence and associated landward retreat of the trench [*von Huene and Lallemand*, 1990]. New contributions have shown that erosive or nonaccretionary margins are notably characterized by higher forearc slope angle, higher rate of orthogonal convergence between the descending and overriding plates, and lower rate of sediment delivery into the trench than accretionary margins [*Clift and Vannucchi*, 2004]. The higher forearc slope angle in accretionary margins has been attributed to material removal at the base of the overriding plate, causing subsidence and normal faulting of the forearc taper [e.g. *Ranero and von Huene*, 2000]. Lower rate of trench sediment supply and higher rate of orthogonal convergence between the plates is intrisically related to the ability of the subduction zone to accommodate and subduct the sedimentary input (see discussion in Chapter 3.6.4.1). Basal erosion of the overriding plate has been attributed to hydrofracturation induced by percolating slab-related fluids [e.g. *Le Pichon et al.*, 1993; *von Huene et al.*, 2004] or abrasion/tunnelling by subducting seamounts and ridges [e.g. *Clift and Vannucchi*, 2004, *Kukowski and Oncken*, 2006]. It is important to note here that distinction between erosive and accretionary margins *at long terms* has been principally based on the recognition on seismic profiles of the occurrence or non-occurrence of an accretionary prism composed of sedimentary material [e.g. *von Huene and Scholl*, 1991, p. 282, Figure 3; *Clift and Vannucchi*, 2004, p. 2, Figure 1].

The Central American margin is generally considered to be currently nonaccretionary [e.g. *Ranero and von Huene*, 2000; *Meschede*, 2003; *Ranero et al.*, 2007]. In northern Costa Rica, recent active subduction erosion has been demonstrated on the basis of geophysical studies and drillings that shown that the outer forearc underwent a recent, rapid subsidence associated to normal faulting [*Vannucchi et al.*, 2001, 2003]. On the other hand, late Cretaceous-Tertiary accretionary complexes are commonly observed along the margin (for a review see *Denyer et al.* [2006]). This apparent contradiction between present-day observations and the geological record is commonly attributed to a hypothetical recent change of the subduction regime from accretion to erosion [e.g. *Vannucchi et al.*, 2006]. We show below that mechanisms presently observed along the margin are on the contrary in good agreement with the geological record and are actually extremely difficult to interpret in terms of subduction accretion/erosion over long periods of time.

3.7.2. Hidden accretionary complexes along intra-oceanic subduction systems

We have shown that exposed forearc in southern Costa Rica recorded several events of accretion indicating than the margin developed seaward through episodic growth. The Osa Igneous Complex recorded two events of significant growth by seamount accretion that occurred in the Maastrichtian/early Paleocene with the emplacement of the Inner Osa Igneous Complex and, probably, in the middle Eocene with the emplacement of the Ganado and Riyito units (Figures 3.9, 3.10). The San Pedrillo Unit was emplaced onto the Osa Igneous Complex in the late Eocene subsequently to rapid, large sedimentary supply into the trench possibly in response to seamount subduction. To our knowledge, development of convergent margins over long periods of time (late Cretaceous to middle Eocene) by accretion of mostly igneous rocks has not been observed yet out of the southern Central American margin. Whether this is due to observation bias or to a specificity of the Costa Rican margin is difficult to assess. It is possible that the unusual nature of the Costa Rican margin (i.e. an arc built on an oceanic plateau, Chapter 2) has led to unusual accretionary processes between the late Cretaceous and middle Eocene. Alternatively, igneous accretionary complexes may be very common along intra-oceanic convergent margins and only poorly exposed.

While sediment accretion along convergent margins is easily demonstrated by seismic imaging of accreted sediments, seamount accretion as recorded in the Osa Igneous Complex may be hardly recognized in intra-oceanic subduction systems, because density and velocity contrasts between basaltic terranes and arc-related igneous rocks inboard of accretionary complexes may be very low and reflectors poorly expressed in the igneous rocks. Density and velocity contrasts may be particularly low along the Costa Rican margin because the arc basement is composed of an oceanic plateau highly similar to accreted volcanic rocks (Chapter 2). In fact, seismic profiles in the Nicoya Peninsula [e.g. *Sallarès et al.*, 1999, 2001] failed to image the composite, partly accretionary nature of the area, which has recently been well documented by on-land, tectonostratigraphic reconstructions [e.g. *Flores*, 2003; *Bandini et al.*, 2008]. Magnetic signatures of upper plate structures investigated between Nicoya and Osa peninsulas point toward a composition of the margin wedge similar to the igneous complex found onshore on the Nicoya Peninsula [*Barckhausen et al.*, 1998]. However, accreted material exposed in southern Costa Rica on the Osa Peninsula has not been recognized on seismic profiles in close proximity [*Kolarsky et al.*, 1995a; *Ranero and von Huene*, 2000] (Figure 3.2), although these profiles very likely comprise accreted igneous rocks and mélanges containing igneous olitholiths similar to those expose in the Osa Peninsula.

Observations from Costa Rica show that, along intra-oceanic convergent margins, igneous accretionary complexes may have remained hidden in numerous cases and their occurrence widely underestimated. This raises an important interrogation about the validity of the consensual model of erosive margin [e.g. *von Huene and Scholl,* 1991; *Clift and Vannucchi,* 2004], because unidentified (seamount) accretion may have occurred along many intra-oceanic convergent margins devoid of accreted sediments. Hence, some intra-oceanic subduction systems presently regarded as erosive may actually be accretionary over long periods of time, even if accreted sediment lacks and local and/or temporary erosion presently occurs.

3.7.3. Accretion vs erosion: the case of the southern Central American margin

Development of the Osa Igneous Complex in cross-section view (Figures 3.2, 3.10) shows that the southern Costa Rican margin experienced at least two events of episodic growth

(i.e. emplacements of the Inner Osa Igneous Complex and Riyito-Ganado Units) separated by periods of tectonic erosion or low-rate accretion (i.e. erosion of the arc basement and formation of the Güerra and Vaquedano Units). On map views of southern Central America (Figure 1.2) and southern Costa Rica (Figure 3.1b) it appears that igneous accretionary complexes characterised by distinct geochemical affinities [e.g. *Hauff et al.*, 2000; *this study*] are randomly distributed along the forearc. They have a fairly limited along-strike extension at the scale of the entire margin that is related to "small size" of accreted seamount fragments. Old events of tectonic erosion are well illustrated on a map view by arc-related and arc basement rocks occurring close to the present-day trench on Coiba Island or to the Osa Igneous Complex in southern Costa Rica (Chapter 2, this study). They may also be marked by limited along-strike extension of the Güerra and Vaquedano units in Osa. Hence, without implying any sediment accretion, it seems that the southern Central American margin experienced variations in accretion/erosion rates in both time (i.e. seaward-landward variations seen on cross-section view) and space (i.e. along-strike variations seen on map view).

Exposed igneous complexes along the forearc of Costa Rica and Panama contain a subduction record spanning from the Maastrichitian to the Eocene. Over this ~25 Ma-long period, the subduction regime has been globally characterized by no sediment accretion, seamount subduction, as well as subduction erosion. This is a situation very similar to the present-day margin. However, it is clear that in some parts of the old margin, seamount accretion led to the construction of several km thick accretionary complexes (Figure 3.1). Therefore, understanding the erosive/accretionary nature of the margin between the Maastrichtian and Eocene is only achievable by estimating the amount of material added to- and removed from the margin over the period of interest. This seems however to be extremely difficult to carry out in the case of the southern Central American margin for four main reasons: (1) occurrences of on-land arc basement and accretionary complexes are scarce comparatively to margin length, (2) current geophysical techniques cannot make a clear, precise distinction between composite, igneous accretionary complexes and the arc basement, (3) precise estimation of the total amount of eroded material is not possible because the shape of the margin prior to erosive events is unknown, and (4) the eroded material subducted into the mantle (?) cannot be observed with current geophysical techniques, impeding estimation of the exact volume of this material.

Since the late Eocene, evolution of the margin is poorly constrained by the geological record. Sole on-land occurrence of late Eocene and younger accretionary complex comes from the Osa Peninsula where the Osa Mélange indicates an overall growth of the margin by sediment accretion. Other areas close to the trench have been imaged trough seismic profile and apparently lack large, sedimentary accretionary wedges and are composed by basaltic rocks [e.g. *Ranero and von Huene*, 2000]. Accreted fragments of seamounts may actually compose most of the younger part of the margin. Hence, difficulties similar to older south Central American accretionary complexes exist in quantifying net accretion or erosion along the margin since the Eocene.

In conclusion to preceding observations, it seems that even if the present-day margin apparently lacks active accretionary prisms composed of sediments, seamount accretion and tectonic erosion may coexist and/or quickly alternate through time. This is in very good accordance with older geological record present in exposed accretionary complexes along southern Central America. Due to possible local growths of the margin by seamount accretion and difficulties in estimating volumes of eroded material, it is not clear if seamount subduction is associated to net growth or erosion of the margin over long periods of time. As a consequence,

there is currently no way to unequivocally define the southern Central American margin as erosive or accretionary.

3.8. Summary and conclusions

The Osa and Burica Peninsulas are parts of the outer forearc of southern Central America that were recently uplifted in response to the subduction of the Cocos Ridge. Rocks exposed in these peninsulas may be of significant interest for understanding key processes of convergent margins such as tectonic accretion, tectonic erosion and seismogenesis along the subduction zone. The basement rocks of the Osa and Burica Peninsula were studied through a multidisciplinary approach combining a geological survey, sedimentology, palaeontology, geochemistry, structural observations and remote tectonic analyses.

The basement is broadly composed of (1) the Osa Igneous Complex that extends from the inner Osa Peninsula to the Burica Peninsula and, possibly, further into the Montijo Gulf (western Panama) and NW off Osa, and (2) the Osa Mélange that is exposed in the seaward side of the Osa Peninsula and Caño Island (Figures 3.1, 3.2). The Osa Igneous Complex is an accretionary complex made up of late Cretaceous to middle Eocene fragments of oceanic plateau and seamounts. The Inner Osa Igneous Complex is composed of fragments of a Coniacian-Santonian oceanic plateau that accreted in the early-middle Paleocene and was followed by emplacement of the Outer Osa Igneous Complex. The Outer Osa Igneous Complex is composed of Coniacian-Santonian to middle Eocene seamount fragments that accreted during (1) a period of low rate accretion / tectonic erosion between the middle-late Paleocene and the middle Eocene (Güerra Unit), (2) a period of net growth in the middle Eocene (Ganado and Riyito Units) and (3) another period of low rate accretion / tectonic erosion in the middle-late Eocene, prior to the emplacement of the Osa Mélange.

The Osa Mélange is an accretionary complex composed of (1) the San Pedrillo Unit, (2) the Cabo Matapalo Unit and (3) the Punta Salsipuedes Unit (Figures 3.1, 3.2). The San Pedrillo Unit is a polygenetic mélange predominantly made up of deformed fine-grain detrital sediments and olistostromic deposits including late Cretaceous to late Eocene material. This material was sedimentarily removed from the forearc area in the late Eocene and is essentially composed of rocks that proceeded from the palaeo-south Central American volcanic arc and the palaeo-Osa Igneous Complex. Landslide formation along the margin was presumably triggered by seamount subduction. Underplating at shallow level of the San Pedrillo Unit resulted from a combination of high, catastrophic sediment supply into the trench and quick dewatering of the subducted sediments, possibly driven to depth on the trailing edge of subducting seamounts. The Cabo Matapalo Unit may have formed in a similar way during the Miocene, whereas the Punta Salsipuedes Unit was formed by off-scrapping and frontal accretion of pelagic sediments in the Miocene [*Di Marco et al.*, 1995]. Further work is required to better constrain the origins of these two units.

Our detailed study of the southern Costa Rican margin shows that faulting induced by the subducting Cocos Ridge is not solely controlled by the topography of the descending plate [e.g. *Sak et al.*, 2004], but equally by compression and possible reactivation of ancient suture zones between the units, leading to the formation of recent and/or active backthrusts. Faulting associated to the trusts may greatly participate to the control of the morphology of the area but is not clearly seen on offshore seismic profiles. Sutures zones were initially located along palaeo-

décollements and, thus, are considered to represent fossil subduction zones. In Osa they provide an interesting on-land opportunity to study some remote processes of convergent margins such as fluid flows along the décollement or, possibly, through the outer crystalline forearc [*Ranero et al.*, 2008].

The Osa Igneous Complex was accreted onto the south western margin of the Caribbean Plate which is composed of an arc built on an oceanic plateau (Chapter 2). Hence, the Osa Igneous Complex is exotic with respect to the Caribbean Plate and should no longer be considered as being part of the CLIP. No clear genetic link exists between the oceanic plateau forming the arc basement and the igneous rocks exposed in the Osa Igneous Complex. It is unclear if these lavas were emplaced above a same hotspot or not. This raises an interrogation about the belonging to the CLIP of accreted igneous complexes of northern South America.

Similarly to other well-studied convergent margins in the world, the southern Costa Rican margin shows that accretionary prisms developed by episodic growth. In the case of the Osa Igneous Complex, we identified pulses of accretion of large fragments of oceanic plateau and seamounts presumably related to episodic incoming of oceanic plateau and large seamounts and/or tectonic changes at a regional scale, separated by periods of low-rate accretion and tectonic erosion. The accretion of the San Pedrillo Unit was triggered by a catastrophic event along the margin, presumably a seamount subduction.

Geological record of the south Central American forearc between the late Cretaceous to middle Eocene is similar and consistent with current situation along the margin. In the early stage of the margin evolution, it is notably clear that no significant amount of sediment accretion occurred and that several seamounts were driven into the subduction zone. In the Osa Igneous Complex, northern Costa Rica and western Panama, growth of the margin is attested by the presence of accreted seamount fragments that certainly extend offshore and have not been recognized on seismic profiles. As a consequence, it is clear that net growth of the margin at long terms is not restricted to sediment accretion but may result from the presence of incoming seamounts along the margin. In absence of precise information concerning the amount of material removed from the margin by tectonic erosion, this indicates that the present-days margin may be accretionary rather than erosive. In presence of seamount subduction, it seems actually that there is currently no way to make a clear estimate of the nature of the south Central American margin over a representative period of time.

Chapter 4: Geochemistry of the Osa Igneous Complex and the late Cretaceous/Paleocene Farallon Plate Break-up

This chapter has been designed to ultimately constitute a paper illustrating the geochemical diversity of the Osa Igneous Complex and its implication on the evolution of the Cocos and Nazca plates.

4.1. Introduction

Tectonic reconstructions are fundamentally based on integrating a wide range of information such as magnetic anomalies of the ocean floor, paleolatitudes indicated by magnetic data and geology, and identification of suture zones that represent ancient, possibly now-missing, oceanic basins or plate limits. Understanding the tectonic development of an area is also intrinsically related to the geometry and velocities of the plates [e.g. *Ferrari et al.*, 2008]. The continents or continental blocks are a keystone for the development of accurate reconstructions, because they represent relatively undeformable, buoyant tectonic features easily preserved through time. Oceanic plates, on the other hand, generally have a much more complicated geometrical evolution and tend to be removed from the geological record by subduction, hence impeding precise reconstruction for ancient times. We show here that accretionary complexes containing accreted seamount fragments may, in some cases, constitute a useful tool to characterize the evolution of oceanic plates that can no longer be reconstructed on the basis of preserved portions of the ocean floor.

The southern Costa Rican margin is located in the SW edge of the Caribbean Plate and Large Caribbean Igneous Province (CLIP), just inboard of the subducting Cocos Plate and Cocos Ridge (Figure 1.1). The Cocos Ridge represents a ~17 Ma to recent drowned seamount chain produced above the Galapagos Hotspot, in the vicinity of the Cocos-Nazca spreading system [*Werner et al.*, 1999, 2003; *Werner and Hoernle*, 2003]. Due to recent incoming 8-1 (most probably ~2) Ma ago of the Cocos Ridge into the subduction zone [*MacMillan et al.*, 2004 and references therein] the forearc in southern Costa Rica has been intensively uplifted [e.g. *Kolarsky et al.*, 1995a, *Sak et al.*, 2004], leading to exposure of an accretionary complex in Osa and Burica peninsulas (Figure 1.2). The accretionary complex of southern Costa Rica is composed of a complicated imbricate of late Cretaceous to middle Eocene seamount fragments (Chapter 3) that have been interpreted on the basis of geochemistry and radiometric dates to represent parts of a paleo-Galapagos Hotspot track, or an old aseismic ridge possibly produced above the Galapagos Hotspot [*Hauff et al.*, 1997, 2000; *Hoernle et al.*, 2002; *Hoernle and Hauf*, 2007]. Rock exposures of southern Costa Rica provide thus a unique opportunity to study the evolution of hotspot volcanism through time [*Hoernle et al.*, 2002]. We present in this chapter new geochemical data and a refined interpretation concerning possible origins of the igneous rocks composing the south Costa Rican accretionary complex, with a special focus on the tectonic evolution of the Cocos and Nazca plates. Our interpretations are further constrained by an updated tectonostratigraphy based on detailed field work in the area (Chapter 3).

4.2. Tectonic and geologic settings of the southern Costa Rican margin and Osa Igneous Complex

4.1.1. Tectonic setting

In western Pacific off Central America, the Cocos and Nazca plates are produced at the Cocos-Nazca spreading system that propagates westward and join the East Pacific Rise at a triple junction made of active mid-oceanic ridges (Figure 4.1). The Cocos and Nazca plates subduct under the North American Plate in the north, South American Plate in the south and Panama Microplate in between. Distinct NE and SE absolute plate motions between the Cocos and Nazca plates [*De Mets*, 1991, 1992; *Trenkamp et al.*, 2002] are probably linked to sustainability of the Cocos-Nazca spreading system.
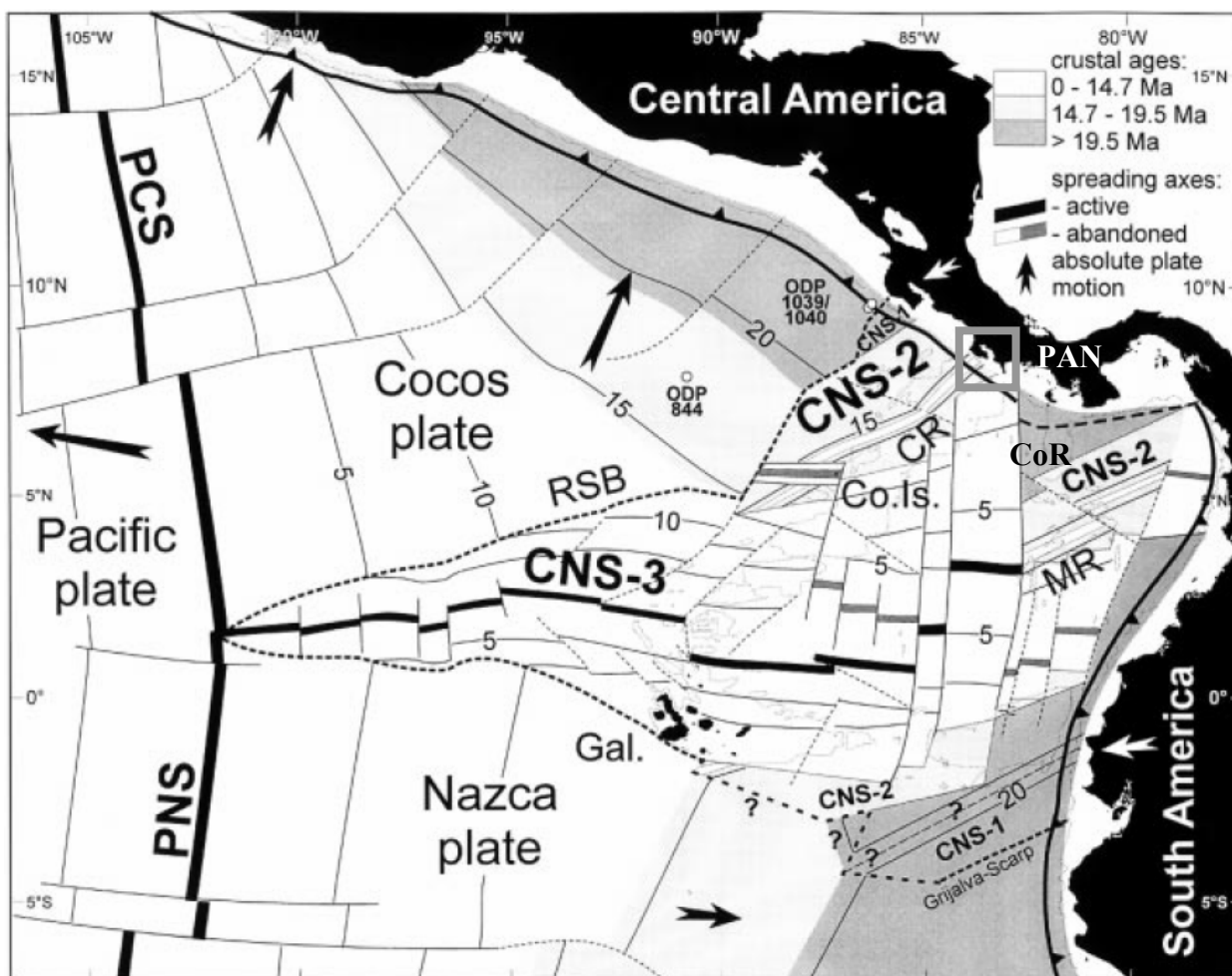
Figure 4.1: *Tectonic map of the Cocos and northern Nazca plates [from Meschede et al., 1999]. CNS-1, CNS-2=precursors 1 and 2 of the Cocos-Nazca spreading system. CNS-3=present Cocos-Nazca spreading system. CR=Cocos Ridge, CoR=Coiba Ridge, MR=Malpelo Ridge, PCS=Pacific-Cocos spreading system, PNS=Pacific-Nazca spreading system, Gal.=Galapagos Islands/Hotspot, RSB="rough smooth boundary", PAN=Panama Microplate. The Osa Igneous Complex is included within the grey square.*

Off Central America, the morphology and age of the Cocos and Nazca plates exhibit large along-axis variations [e,g, *von Huene et al.*, 1995, 2000]. From northern Costa Rica toward the north, the Cocos Plate is composed of a strongly-dipping smooth crust derived from the East

Pacific Rise. Between northern Costa Rica and western Panama, the Cocos Plate is made of a younger, moderately-dipping crust partially covered by seamounts that formed at the Cocos-Nazca spreading system. Differences in morphology between these two areas define a limit commonly referred to as the "rough smooth boundary" [*Hey*, 1977]. Close to the border between Costa Rica and Panama, intra-oceanic transforms delimit the southern extension of the Cocos Plate and may have displaced initially contiguous Cocos and Coiba aseismic ridges. Along with the Malpelo Ridge, these ridges are composed of drowned oceanic islands that recorded a long interplay history between the Galapagos Hotspot and Cocos-Nazca spreading system [e.g. *Werner et al.*, 1999; *Harpp et al.*, 2005]. Further toward the south is found the younger Nazca Plate which resembles the southern extension of the Cocos Plate and formed at the Cocos-Nazca spreading system.

The morphology of the subducting oceanic plates along the Central American Isthmus has a strong influence on tectonics of the overriding plate and supra-subduction magmatism. Collision of the Cocos ridge with the volcanic arc around 2 Ma ago in southern Costa Rica [*McMillan et al.*, 2004] resulted in a strong uplift and shortening throughout the isthmus, associated with a local cessation of volcanism [e.g. *Kolarsky et al.*, 1995a]. Along-strike migrations toward the south of intra-oceanic transforms [*MacMillan et al.*, 2004] controlled the formation of the Fila Costeña Thrust Belt [*Morell et al.*, 2008] and, possibly, triggered the uplift of some portions of the outer forearc area between southern Costa Rica and western Panama. Subduction of relatively buoyant plates irregularly covered by topographic highs causes the forearc area to be variously uplifted and exposed along the margin [*Fisher et al.*, 1998; *Gardner et al.*, 2001; *Sak et al.*, 2004], to distances as close as to ~20 km from the trench. Such exposures provide a unique opportunity to study deep sequences of the outer margin, which is composed of a complicated arrangement of arc-related rocks, accreted material and overlap sequences.

The Cocos and Nazca plates are believed to be a product of the break-up of the Farallon Plate in the Miocene (~23 Ma) and subsequent ridge jumps [e.g. *Barckhausen et al.*, 2001; *Werner et al.*, 2003; *Lonsdale*, 2005]. The age of initiation of the Cocos-Nazca spreading system has been based on the occurrence of a portion of ocean floor off Nicoya (northern Costa Rica), which represents the oldest preserved portion of oceanic crust produced at the Cocos-Nazca spreading system (CNS-1 on Figure 4.1). This portion of oceanic crust is not necessarily indicative of the age of initiation of this spreading system. Along the eastern Pacific, most of the pre-Miocene ocean floor has subducted and, as a consequence, it is possible that the initiation of the Cocos-Nazca spreading system occurred well before the Miocene, but was not documented by reconstructions based on preserved portions of the ocean floor.

4.1.2. Geologic review of the Osa Igneous Complex

The Osa Igneous Complex is a composite accretionary complex located in the forearc of southern Costa Rica, in the Osa and Burica peninsulas (Figures 1.2, 3.1). A complete geological survey and geological interpretation of the complex is provided in Chapter 3. We provide below a summary of this study.

The Osa Igneous Complex is made up of a complicated arrangement of Coniacian-Santonian to middle Eocene fragments of an oceanic plateau and seamounts that accumulated along the SW Caribbean Plate between the early-middle Paleocene and late Eocene. The complex is comprised between the Campanian-Eocene Golfito Complex that is part of the southern Central American arc (Chapter 1) and the NE Osa Mélange (San Pedrillo Unit), a late

Eocene accretionary complex predominantly made up of underplated olistostromic trench deposits (Chapter 3) (Figure 3.2). The Osa Igneous Complex recorded two events of high-rate accretion separated by periods of low-rate accretion or tectonic erosion, indicating that the South Costa Rican margin grew through episodic growth since the initiation of the subduction in the late Campanian (~75-73 Ma) (Chapters 2, 3).

4.1.2.1. The Inner Osa Igneous Complex

The Osa Igneous Complex can be broadly divided into (1) the Inner Osa Igneous Complex and (2) the Outer Osa Igneous Complex (Figures 3.1, 3.2). The Inner Osa Igneous Complex was emplaced during the early-middle Paleocene along the arc. It is mainly composed of several-km thick imbricates of unmetamorphosed, well-preserved pillowed and massive basaltic lava flows and sills, with few local occurrences of gabbroic rocks as well as minor occurrences of pelagic sediments. The complex comprises large (probably several km thick) fragments of a Coniacian-Santonian oceanic plateau that formed in the Pacific and subsequently accreted along the Caribbean Plate (and CLIP).

4.1.2.2. The Outer Osa Igneous Complex

The Outer Osa Igneous Complex is composed of four tectonostratigraphic units: (1) the Güerra Unit, (2) the Ganado Unit, (3) the Riyito Unit, and (4) the Vaquedano Unit (Figures 3.1, 3.2). The Güerra Unit is found on the edge of the Inner Osa Igneous Complex. It is composed of late Cretaceous-middle Eocene (?) igneous and sedimentary rocks intensively altered or metamorphosed in the greenschist facies. This unit is characterized by the higher metamorphic grade of the Osa Igneous Complex and exhibit a strong, pervasive deformation. It is made up of a wide range of lenticular rock bodies that appear to be similar to the rocks encountered in the other units of the Outer Osa Igneous Complex. The Güerra Unit was likely formed by repeated accretion of summital pieces of subducting seamounts between the emplacement of the Inner Osa Igneous Complex (early-middle Paleocene) and the accretion of the Ganado and Riyito units (probably middle Eocene).

The Ganado Unit is essentially composed of massive and pillowed basaltic lava flows similar to the Inner Osa Igneous Complex. However, the Ganado Unit is characterized by a higher content of intrusive rocks that comprise aphyric dykes, dolerites and gabbros. One occurrence of radiolarian chert associated to a lava flow provided a Coniacian-Santonian age for this unit. The Ganado Unit has been interpreted to represent a large accreted fragment of seamount emplaced along the margin probably in the middle Eocene, which suffered form partial dismemberment by collapsing on the forebulge and/or by faulting during the accretion and subsequent uplift.

The Riyito Unit is a composite unit made up of relatively-undeformed and unmetamorphosed pillowed and massive basaltic lava flows characterized by an atypical plagioclase-phyric texture. Minor occurrences of hyaloclastites, intrusive rocks and basaltic sediments are locally observed. Tectonostratigraphic constraints and one ^{40}Ar/^{39}Ar age [*Hauff et al.*, 2000] indicates a Paleocene age of probable formation for the volcanic rocks. However Ar-loss in accreted rocks from southern Costa Rica (Chapter 3) may result in an erroneous age of formation for this unit. In absence of biochronologic dates for the Riyito Unit, we let here the age of formation opened between the late Cretaceous and Paleocene. The Riyito Unit is composed of

several seamount fragments that probably accreted contemporaneously or sub-contemporaneously with the Ganado Unit in the middle Eocene.

The Vaquedano Unit formed between the emplacement of the Ganado and Riyito units (midde Eocene) and first accretionary events of the Osa Mélange (late Eocene). Similarly to the Güerra Unit, it formed by repeated accretion of summital pieces of subducting seamounts. It is composed of lenticular rock bodies made up of a wide range of volcano-sedimentary sequences. The sequences predominantly comprise reddish, vesicular pillow basalts and massive basaltic lava flows with interbedded hyaloclastites and latest Cretaceous-middle Eocene pelagic limestones. Locally detrital sediments are observed. One sample yielded red algae fragments indicating that some of the subducted seamounts partly developed in subaerial environment.

4.1.2.3. The Osa Igneous Complex: an unusual accretionary complex

The Osa Igneous Complex is an accretionary complex mostly composed of basaltic igneous rocks initially emplaced in submarine conditions. Arc/continent-derived clastic material commonly observed in other circum-Pacific accretionary complexes [e.g. *Isozaki et al.*, 1990; *Dickinson et al.*, 2008] lack, which may be attributed to entire subduction of arc-derived sediments deposited into the trench or low-rate sediment production at the time of formation of the complex (Chapter 3).

Overturned pillow lavas and intrusive rocks are locally exposed, indicating that recent and accretionary tectonics probably led to a disruption of the accreted seamount fragments. However, apart of the Güerra Unit, the complex remained relatively well-preserved in terms of alteration and metamorphism (i.e. below the greenschist facies). Accreted igneous rocks in other circum Pacific accretionary complex frequently exhibit higher metamorphic grades [e.g. *Isozaki et al.*, 1990; *Dickinson*, 2008]. That points toward a shallow depth of accretion for the Osa Igneous Complex.

Preceding observations indicate that the Osa Igneous Complex represents a very unusual occurrence of accretionary complex. It constitutes a unique opportunity to study relatively well-preserved accreted volcano-sedimentary sequences that may potentially provide useful informations on the tectonic evolution of plates subducted under the south Costa Rican margin between the early-middle Paleocene and late Eocene.

4.3. Results

Location of samples and geochemical results are presented in the Appendix. The geochemistry is based on our own samples (n=57) as well samples from *Di Marco* [1994] (n=7, 2 samples re-analyzed) and samples from *Hauff et al.* [2000] (n=10). Comparison of our results with results from *Hauff et al.* [2000] shows no important interlab analytical bias in terms of major, minor and trace element compositions. For convenience the igneous rocks are named here "highly-depleted" when $(La/Sm)_{CIn}$=0.3-0.4 and $(Sm/Yb)_{CIn}$=0.7-0.9, "NMORB-like" when $(La/Sm)_{CIn}$=0.5-0.6 and $(Sm/Yb)_{CIn}$=0.8-1.1, "plateau-like" when $(La/Sm)_{CIn}$=0.7-1.0 and $(Sm/Yb)_{CIn}$=0.8-1.3, and "OIB-like" when $(La/Sm)_{CIn}$=0.9-3.7 and $(Sm/Yb)_{CIn}$=1.4-4.9.

4.3.1. Volcanic textures

The Osa Igneous Complex can be chiefly subdivided into tholeiitic and transitional/alkalic igneous rocks that are characterized by distinct textures. In some cases, these textures may be used on the field to map the extension of the units or accreted sequences.

4.3.1.1. Tholeiites

The tholeiitic lavas commonly consist of sub-ophitic and intersertal basalts and micro-gabbros with plagioclase, clinopyroxene, opaque minerals (Fe-Ti oxides and sulfides), interstitial glass and, occasionally, altered olivine. Ophitic and intergranular textures are observed in a much lesser extent. Pillow lavas commonly exhibit a spherulitic texture. Igneous rocks from the Riyito Unit are characterized by ubiquitous plagioclase-phyric texture and occurrence of vesicles in some samples.

Intrusive tholeiites locally occur and are characterized by doleritic, sub-ophitic and ophitic textures, with mineral assemblages predominantly composed of plagioclase, pyroxenes and oxides (olivine has not been observed). Some of the tholeiitic intrusive rocks of the Ganado Unit contain magmatic amphiboles.

4.3.1.2. Transitional/alkalic lavas and sills

The transitional/alkalic lava flows have commonly ophitic and sub-ophitic textures with clinopyroxene (frequently Ti-augite), plagioclase, opaque minerals, vesicles (filled by chlorite, calcite and/or zeolites), and, in some cases, badly preserved olivines. Feldspathoids have not been observed, indicating that this group of rocks is probably more transitional than "truly alkalic". Pillow lavas frequently have a spherulitic or microlitic texture with $Ol \pm Cpx \pm Pl$ phenocrysts.

One occurrence of alkalic sill was encountered in the Inner Osa Igneous Complex, which is characterized by an intergranular texture composed of plagioclase, K-feldspar, acicular brown amphibole and opaque minerals.

4.3.2. Alteration

Apart of the Güerra Unit, a limited alteration is observed in our samples. Best preserved igneous rocks are generally coarse lava flows. Olivine has been almost systematically replaced by chlorite or calcite. Glass has been ubiquitously replaced by secondary phases such as palagonite. Microlitic groundmass has been frequently altered and replaced by argilous phases. Pyroxene has been generally well preserved and exhibit minor alteration by secondary chlorite. Alteration of plagioclase is various, though globally slightly higher than for the pyroxene, and dominated by argilitization. These observations show that the bulk of the igneous rocks composing the Osa Igneous Complex suffered from a low-T, oceanic alteration and unlikely exceed a zeolite metamorphic facies. Due to this alteration, mobile elements such as Sr, Pb, U, Ba, Rb or Cs have not been used in this study.

The tholeiitic intrusive rocks found in the Ganado Unit exhibit a slightly higher alteration. Plagioclase has been frequently sericitized and pyroxenes replaced by chlorite. Epidote is a common phase in these rocks and magmatic amphiboles frequently exhibit a rim

composed of secondary, alteration-related amphibole. These features may indicate higher alteration than for the rest of the well-preserved igneous rocks, likely in the prehnite-pumpellyite metamorphic facies. On the field epidote concentrates around the intrusive rocks. This indicates that the higher alteration observed in the Ganado Unit is probably related to hydrothermal circulations induced by emplacement of subvolcanic intrusive rocks in the seamount before the accretion.

The Güerra Unit exhibits the highest metamorphic grade and alteration in the Osa Igneous Complex with frequent occurrences of epidote and mineral assemblages typical of the greenschist metamorphism. The alteration and greenschist metamorphism have been interpreted as a consequence of high deformation and fluid flow in the vicinity of the paleo-décollement (Chapter 3). Apart of one spilitized basalt (DB02-207) and one relatively well preserved basalt (DB02-191), the igneous rocks of this unit have not been analyzed in this study.
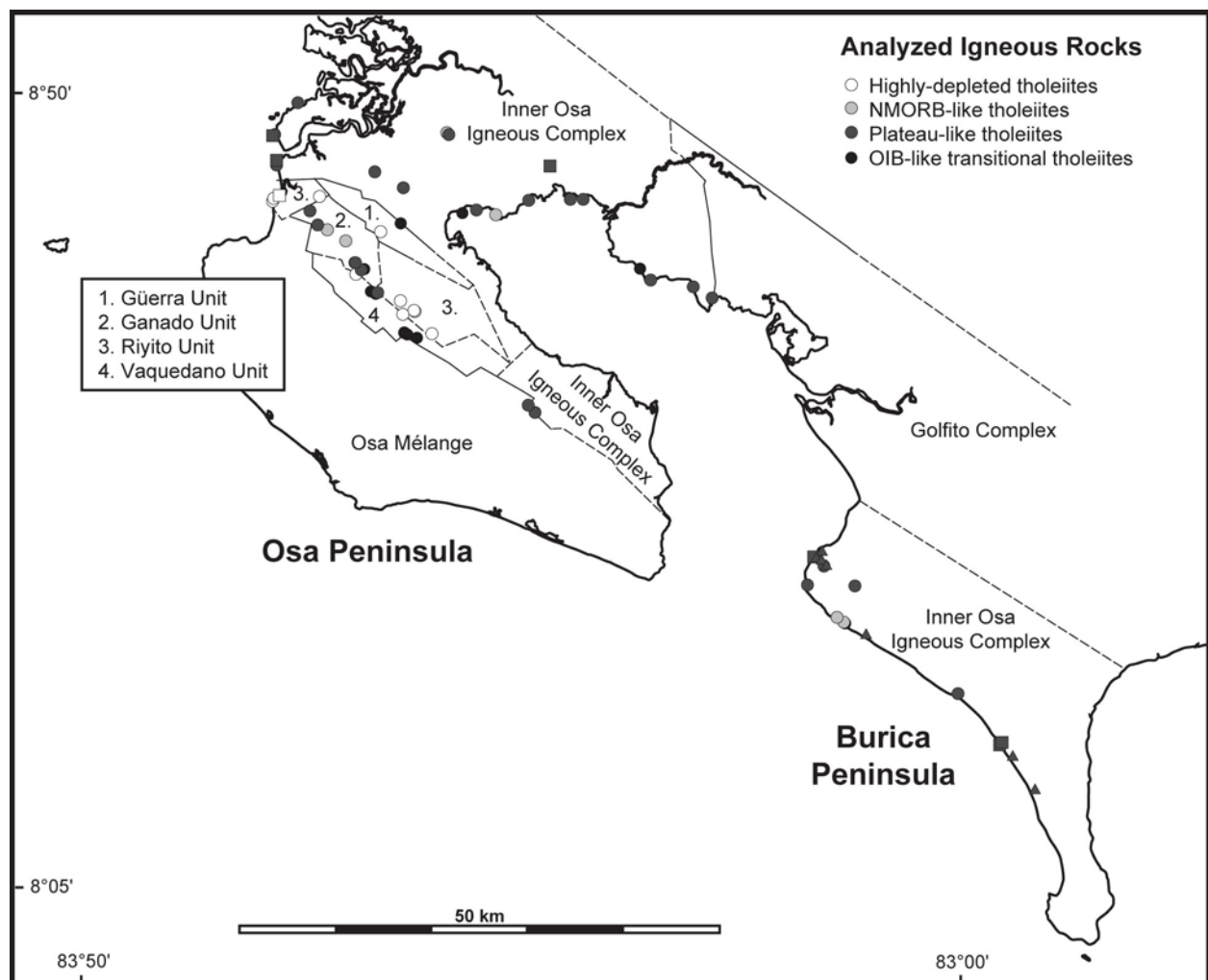
Figure 4.2: *Localisation of the analyzed samples and units forming the Osa Igneous Complex. Circles=samples from this study, triangles=re-analyzed samples from Di Marco [1994], samples from Hauff et al. [2000].*
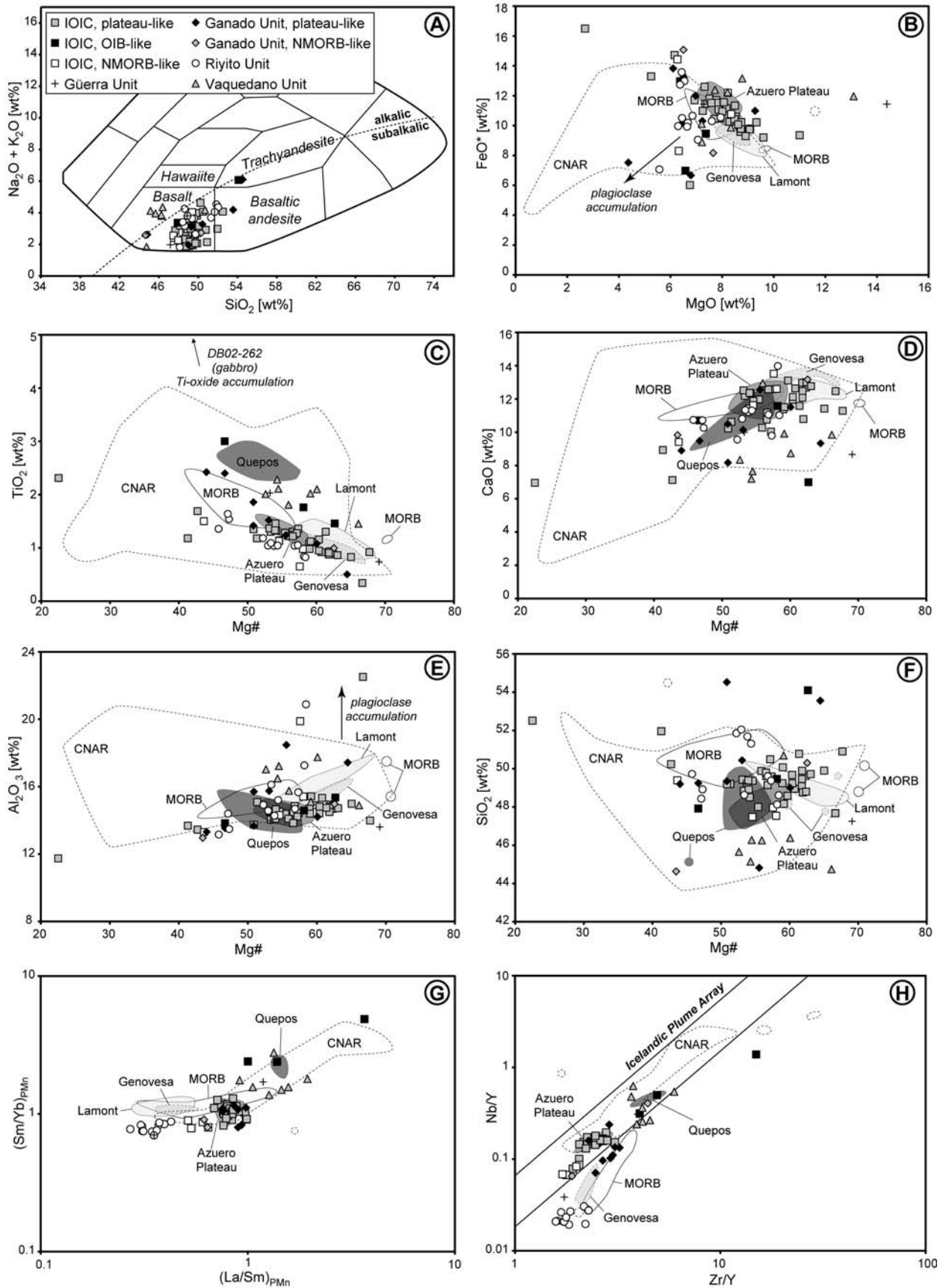
Figure 4.3 (previous page): Geochemistry of the igneous rocks from the Osa Igneous Complex and selected rocks for comparison. MORB=East Pacific Rise MORBs, averaged per segment [Su and Langmuir, 2003], Genovesa=Genovesa Submarine Ridge, Galapagos Hotspot [Harpp et al., 2003], Lamont=MOK off-axis seamount along the East Pacific Rise [Allan et al., 1989], Quepos accreted seamount, Costa Rica [Hauff et al., 2000], CNAR=aseismic ridges on Cocos and Nazca plates [Harpp et al., 2005], Azuero Plateau=oceanic plateau forming the arc basement in southern Central America [Chapter 2], PM=Primitive Mantle [McDonough and Sun, 1995]. A) TAS classification after Cox et al. [1979], alkalic-subalkalic subdivision after Irvine and Baragar [1971]. Sample symbology following the terminology defined in Figure 4.2. H) Nb/Y-Zr/Y diagram and Icelandic Plume Array after Fitton et al. [1997].

4.3.3. Major and trace elements

Spatial arrangement of recurrent compositions of igneous rocks was used in Chapter 3 to constrain the extension of the units forming the Osa Igneous Complex. Indeed, repartition of igneous rock species in the Osa Igneous Complex defines well-organized patterns (Figure 4.2). Recurrence of similar rock species in a unit was interpreted as a result of accretionary processes, with seamount fragments accreted at the same time and proceeding from the same or similar volcanic edifices. The composition of the igneous rocks encountered in these units is described below (full results are given in Appendix - Tables 2 and 3).

4.3.3.1. Inner Osa Igneous Complex

The igneous rocks forming the inner Osa Igneous Complex can be broadly divided into plateau-like, NMORB-like and OIB-like groups. The plateau-like group constitutes the major part of the unit and is composed of basaltic and basaltic-andesitic tholeiitic lavas and intrusive rocks. These rocks have the larger range of SiO_2 and MgO contents in the Osa Igneous Complex, with SiO_2=47.67-52.51 wt% and MgO=9.60-2.69 wt% (Figure 4.3a, b). In Figure 4.3b a sample from *Hauff et al.* [2000] with relatively high MgO (11.01 wt%) and Ni (249 ppm) contents, as well as Mg#=68 may represent a relatively unfractionated parental magma. On the same figure, sample with relatively low MgO (6.75 wt%) and FeO* (6.01 wt%) is a gabbro with cumulative plagioclase (sample DB02-227). FeO*-MgO variations (Figure 4.3b) show that the plateau-like tholeiites overlap the field of the Azuero Plateau (arc basement, Chapter 2), but define a larger array with, notably, a higher MgO content. This tendency is also observed on TiO_2-Mg#, CaO-Mg#, Al_2O_3-Mg# and SiO_2-Mg# diagrams (Figures 4.3c-f). Trace elements contents are highly similar to the Azuero Plateau with high Ti and Nb contents and broadly flat multielement patterns (Figures 4.3g, h and 4.4a). On a Nb/Y-Zr/Y diagram (after *Fitton et al.* [1997]), the plateau-like tholeiites are comprised in the Icelandic Plume Array (Figure 4.3h).

The NMORB-like group is composed of basaltic tholeiitic lavas and intrusive rocks. Apart of one sample that shows evidence for plagioclase accumulation (Figure 4.3e), tendencies are similar to the plateau-like rocks in terms of major element content and TiO2 (Figures 4.3a-f) and, hence, distinct than typical NMORB suites. Trace element contents are broadly depleted in the most incompatible elements (i.e. Th, Nb and LREE) (Figures 4.3g, h and 4.4b). However, a Nb positive anomaly is still observed on multielementary diagrams and, as opposed to "true" NMORBs, the samples plot in the Mantle Plume Array in the Nb/Y-Zr/Y diagram (Figures 4.3h and 4.4b).

The OIB-like group is basaltic to trachyandesitic in composition (Figure 4.3a). Basaltic samples are lava flows with tholeiitic affinities, whereas the trachyandesitic sample represents an alkalic sill with, notably, K-feldspar and acicular amphibole. The OIB-like igneous rocks have a higher Ti content than plateau-like or NMORB-like tholeiites at a given Mg# (Figure 4.3c). They have a similar Al2O3 content, but variously differ from the plateau-like and OIB-like tholeiites in terms of other major element compositions (Figures 4.3a-f).

4.3.3.2. Ganado Unit

Igneous Rocks of the Ganado Unit have been divided into plateau-like and NMORB-like rocks that occur in similar proportions throughout the unit. Plateau-like igneous rocks range from basaltic to trachyandesitic compositions (Figure 4.3a), with MgO=7.24-4.37 wt% and FeO*=6.67-13.83 wt% (Figure 4.3b). Globally, these rocks show similar tholeiitic affinities and compositions in terms of major element and TiO_2 contents than plateau-like tholeiites of the Inner Osa Igneous Complex (Figure 4.3a-f). A trachyandesitic sample with plagioclase-phyric texture (sample DB05-162) likely suffered from plagioclase accumulation, as notably attested by high Al_2O_3 content (Figure 4.3e). A low-Si sample (DB02-198b, SiO_2=44.82 wt%) with high Al_2O_3 content (18.48 wt%) has a transitional affinity (Figures 4.3a, e, f). This sample has been dated by radiolarian assemblages to the Coniacian-Santonian and interpreted to represent a last stage of volcanism in the Ganado Unit (Chapter 3). Trace element contents of the plateau-like igneous rocks are similar in terms of REE compositions to the plateau-like rocks of the Inner Osa Igneous Complex (Figure 4.3g). However, most plateau-like rocks of the Ganado Unit have a low Nb content, making them fall under the Icelandic Plume Array (but slightly above the MORB array) on a Nb/Y-Zr/Y diagram (Figures 4.3h, 4.4c). Exceptions to this observation come from the transitional basalt DB02-198b and a lava flow (DB05-149) located close to the contact between the Ganado and Vaquedano units.

NMORB-like igneous rocks are composed by two amphibole-bearing gabbros (DB02-262 and DB05-158) intruding the plateau-like lavas of the Ganado Unit. The NMORB-like gabbros have major contents consistent with the plateau-like rocks, with cumulative Ti-oxide in the sample DB02-262, and cumulative plagioclase in the sample DB05-158 (Figures 4.3a-f, 4.4c). Immobile trace compositions are similar to NMORB-like tholeiites of the Inner Osa Igneous Complex (Figures 4.3g, h, 4.4c).

4.3.3.3. Riyito Unit

Igneous lavas and intrusive rocks forming the Riyito Unit have tholeiitic affinities with SiO_2=48.13-52.05 wt%, MgO=7.94-5.57 wt% and FeO*=7.07-13.58 wt% (Figure 4.3a, b). FeO* content at a given MgO is slightly lower than in other tholeiitic rocks of the Osa Igneous Complex (Figure 4.3b). TiO_2 content at a given Mg# is globally lower than in rocks plotted on the Figure 4.3c. On a CaO-Mg# diagram, the Riyito tholeiites have lower CaO content at a given Mg# than MORBs form the East Pacific Rise (Figure 4.3d). Plagioclase accumulation may have occurred in some samples and led to higher Al_2O_3 at a given Mg# (Figure 4.3e). Rocks not affected by Plagioclase accumulation have a lower Al_2O_3 content than MORBs at a given Mg#. On a SiO_2-Mg# diagram the Riyito igneous rocks have generally lower SiO_2 content at a given Mg# than MORBs (Fgure 4.3f). Four samples collected in a restricted area (Punta Ganadito, NW Osa) have a higher SiO_2 content.
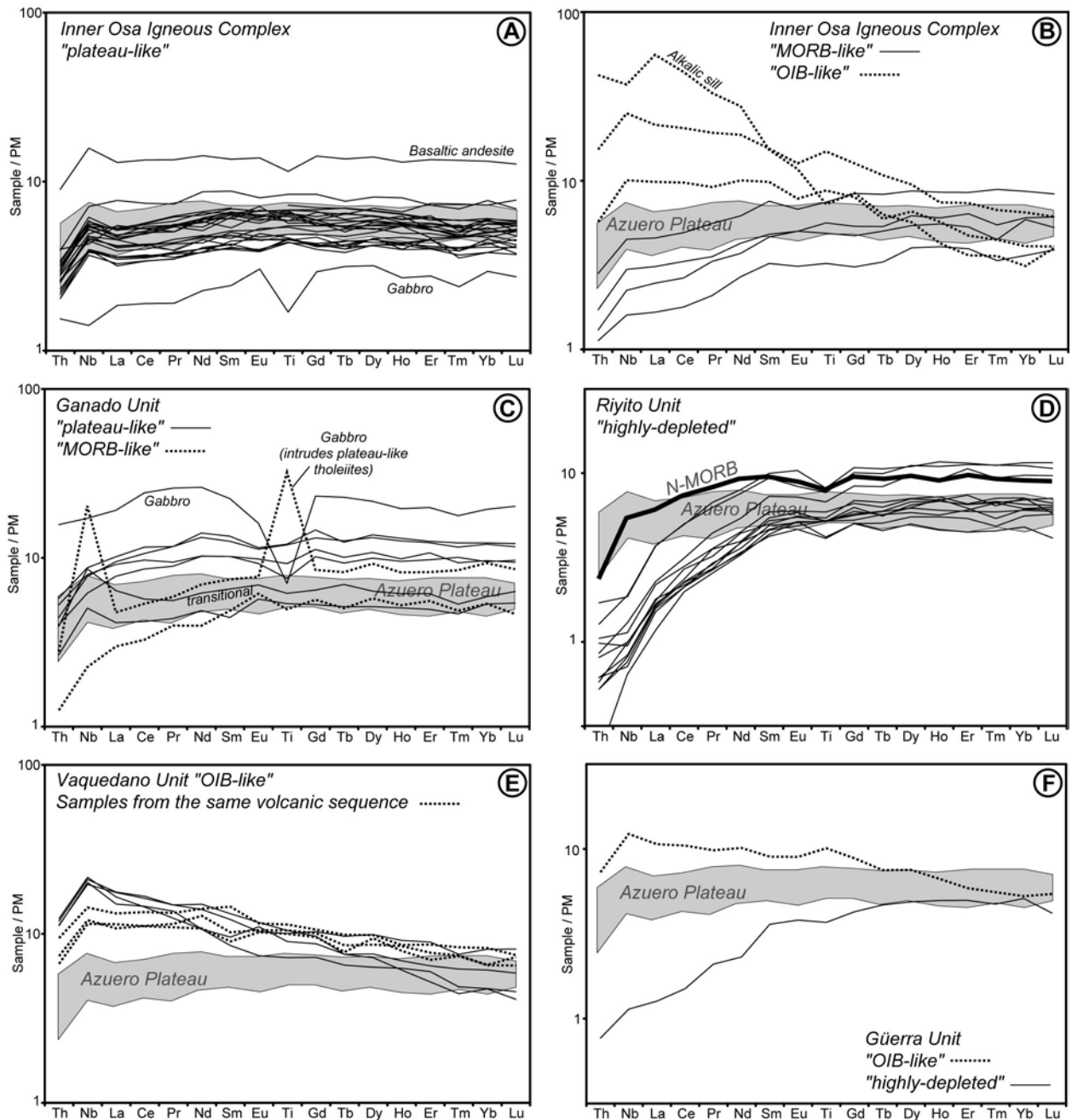
Figure 4.4: *PM-normalized multielement diagram of the igneous rocks of the Osa Igneous Complex. Azuero Plateau=oceanic plateau forming the arc basement in southern Central America [Chapter 2], PM=Primitive Mantle [McDonough and Sun, 1995], N-MORB after Hofmann [1988].*

Immobile element compositions show that the Riyito tholeiites are extremely depleted in the most incompatible elements (i.e. Th, Nb, LREE) (Figures 4.3g, h, 4.4d). These rocks are indeed more depleted than MORBs and constitute an end-member on a Nb/Y-ZrY diagram (Figure 4.3h). Very low Nb and Ti contents are assessed by negative anomalies in multielement patterns (Figure 4.4d). Preliminary Pb, Nd and Sr isotopic results are in agreement with former results by *Hauff et al.* [2000] and indicate that these rocks have a source similar to the East Pacifc Rise MORBs (not shown).

4.3.3.4. Vaquedano Unit

Basaltic Lava flows from the Vaquedano Unit have alkalic/transitional affinities with SiO_2=44.74-50.69 wt%, MgO=13.10-7.21 wt% and FeO*=8.89-13.16 wt% (Figures 4.3a, b). Due to the highly composite nature of the unit and a possible provenance of the samples from very distinct seamounts, FeO*-MgO variations lack of systematic (Figures 4.3b). Transitional/Alkalic affinities are further illustrated by higher TiO_2, lower CaO, higher Al_2O_3 and lower SiO_2 contents at a given Mg# than the bulk of the Osa Igneous Complex composed of tholeiitic rocks (Figures 4.3c-f). Immobile trace element contents show a progressive enrichment in the most incompatible elements (i.e. Nb and LREE), broadly similar to signatures of the Quepos terrane that represents an accreted oceanic island in Costa Rica (Figures 4.3g, h, 4.4e). Trace element patterns are consistent with "typical" OIB affinities with a positive Nb anomaly (Figure 4.4e). Most of the samples plot in the Icelandic Plume Array in a Nb/Y-Zr/Y diagram (Figure 4.3h). Three samples coming from a restricted area of the unit plot under the Iceland Plume Array on the same diagram. These samples have a very consistent chemistry in terms of major and trace elements (Figure 4.4e), indicating they may pertain to a same volcanic sequence.

4.3.3.5. Güerra Unit

Two analyzed basalts from the Güerra Unit have distinct affinities. One resembles the highly-depleted tholeiites forming the Riyito Unit. The other one is similar to the transitional/alkalic lavas from the Vaquedano Unit. The similarities between these rocks are well observed in terms of trace element contents, as notably illustrated on $(Sm/Yb)_{PMn}$-$(La/Sm)_{PMn}$, Nb/Y-Zr/Y and multielement diagrams (Figures 4.3g, h, 4.4f).

4.3.4. Sr-Nd-Pb Isotope Ratios

Sr-Nd-Pb isotope ratios have been determined for six samples from the Inner Osa Igneous Complex and Riyito Unit (Appendix - Table 6). Isotope ratios were measured for both leachate and rock residue fractions, which allowed us to recognize samples that suffered from alteration
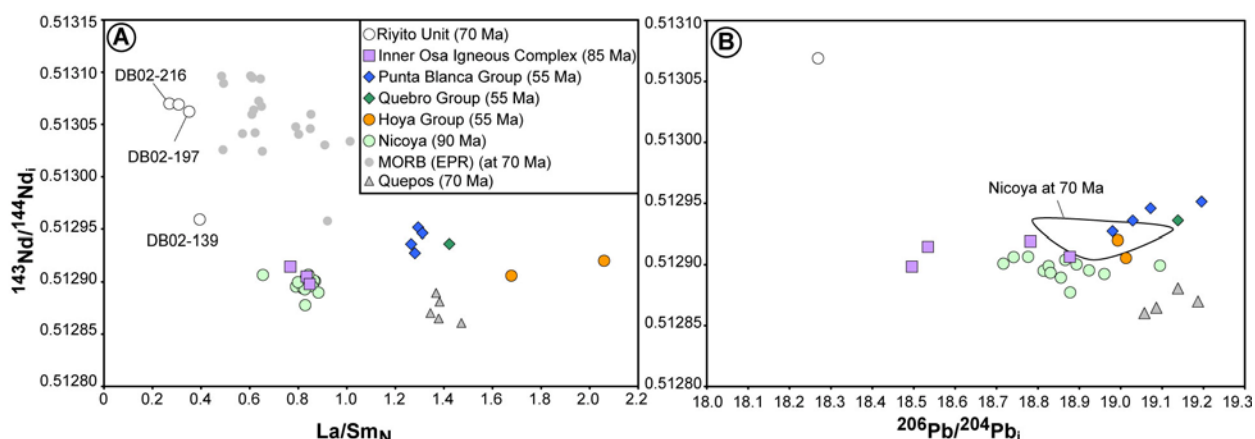
Figure 4.5: *Labelled samples are from this study. Punta Blanca and Quebro Groups are defined in Chapter 4, isotope data are from Lissinna [2005] and Hoernle et al. [2002]. Nicoya complex and Quepos oceanic island are from Hauff et al. [2000]. MORB are from Su and Langmuir [2003].* **(A)** *Note overall correlation between ratios of incompatible immobile elements and Nd isotope ratios and similitude of plateau-like rocks (Inner Osa Igneous Complex and Nicoya Complex).*

and should not be taken into consideration for geochemical interpretation. For this reason, Sr and Pb isotope have not been used here. Similarly, three samples have shown important Nd isotope variation between leachate and rock residue fraction, impeding their use. Forthcoming studies should concentrate on isotope analyses on mineral separates.

Radiogenic isotope data from *Hauff et al.* [2000], *Hoernle et al.* [2002] and *Lissinna* [2005] have been used to compare the units defined in our study. It is important to note that all these data were obtained following a similar procedure in the same laboratory (Geomar, Kiel). Due to the fact that leaching performed by *Hauff et al.* [2000] shown effects of Rb alteration, the Sr isotope ratios have not been used here.

In terms of radiogenic initial Nd composition two of our samples from the Riyito Unit have similar compositions to a sample by *Hauff et al.* [2000] from the same unit (Figure 4.5). In a $^{143}Nd/^{144}Nd$-La/Sm$_N$ diagram these samples are located in the continuation of an array defined by the East Pacific Rise at 70 Ma. Radiogenic Nd content is thus similar to MORB, although the Riyito Unit is globally more depleted in terms of highly incompatible element contents than the MORB (see also Figure 4.4d). A depleted character is also seen in Riyito samples from *Hauff et al.* [2000] in terms of radiogenic initial Pb compositions (e.g. Figure 4.5b). DB02-139 from the same unit has minor initial radiogenic Nd but is still more depleted in the most incompatible elements and slightly enriched in radiogenic Nd than samples from other Costa Rican and Panamean oceanic igneous complexes (Figure 4.5a).

The Inner Osa Igneous Complex is characterized by incompatible element contents and radiogenic initial Nd similar to the Nicoya Complex (Figure 4.5). However we note differences in terms of radiogenic initial Pb compositions between these two complexes, with partly more enriched compositions for the Nicoya basalts and gabbros (e.g. Figure 4.5b).

4.3.5. Melt inclusions in plagioclase phenocrysts from the Riyito Unit

The Riyito Unit is characterized by occurrence of plagioclase-phyric and -ultra-phyric lavas and intrusive rocks. The plagioclase phenocrysts are locally as large as 1.5 cm in length but generally are only a couple of mm in length. Melt inclusions are frequent in the plagioclase phenocrysts and range from <10 μm to ~300 μm in length. In order to better constrain the highly-depleted nature of the Riyito lavas, microprobe and LA-ICP-MS analyses were carried out on both the plagioclases and related inclusions. Sample DB02-216 was chosen for its good preservation and occurrence of particularly large melt inclusions. This sample is characterized by a subopthitic texture with plagioclase + clinopyroxene + olivine (altered) + spinels + Fe oxides and sulfides. Analytical results are given in Appendix - Tables 7 and 8.

4.3.5.1. Plagioclase and inclusion textures

Size of the melt inclusions define a bimodal repartition with numerous small-scale (<10 μm) inclusions and rare large-scale inclusions (>100 μm). Spatial arrangement of the inclusions defines zonations indicating that they were incorporated into plagioclases at specific periods during the growth of the phenocrysts (Figure 4.6a). Larger inclusions show partial recrystallization with formation of olivine, pyroxene, Ti-oxide and, in some inclusions, feldspar.

The plagioclase phenocrysts are euhedral with typical twins and cleavages. Birefringence highlights complex zonations within the minerals, with a global trend of higher birefringences toward the mineral borders. Cracks within the crystals generally propagate from the borders

toward the cores and frequently disappear along strong birefringence constrasts. Hence, birefringence constrasts are probably located along mechanical constrasts within the mineral. Lower birefringences in the plagioclases correlate with presence of small melt inclusions and form rims around the large inclusions.

4.3.5.2. Geochemistry of the inclusions and hosting minerals

Zonations of the plagioclase phenocrysts are well illustrated by qualitative compositional maps obtained by microprobe scanning (Figures 5.6b-e). It can be observed on Figure 4.6 that the chemical zoning correlates with birefringence variations. Sodic rims (~50-75 %An) with compositions similar to matrix plagioclases are observed around the plagioclase phenocrysts, reflecting the latest stages of growth of the minerals in the host lava. On Figures 4.6b and c it can be seen that the plagioclase phenocryst underwent partial resorbtion prior to formation of the high Na outer rim. Inner parts of the phenocrysts are more calcic, with anorthitic composition (~80-90 %An). Complex zonations are observed in the innermost parts of the minerals. These observations point toward a xenocryst origin for some plagioclase phenocrysts.

Melt inclusions are bordered by low anorthitic rims (~55-80 %An) that formed during post-entrapment crystallization (i.e. growth of the host mineral toward the inclusion, subsequently to melt entrapment) (Figure 4.6). It is important to note here that post-entrapment crystallization processes likely affected initial composition of the trapped melt similarly to plagioclase fractionation in a magma chamber. Possibilities of re-homogenization of the inclusions by re-heating were discarded due to the presence of cracks along the inclusions, which may have caused inappropriate escape of the melts. Interestingly, some of these cracks developed prior to the formation of post-entrapment rims around the inclusion as illustrated on Figure 4.7a. This may indicate that the trapped melt remained liquid until crack formation in the innermost mineral. As a consequence of a prolonged stay at high T some elements may have possibly experimented diffusion between the host mineral and the inclusion prior to melt quenching. Figures 4.7b and c show a typical microprobe profile through a large inclusion and host mineral. Microprobe profiles illustrate well the differences in composition between the recrystallized melts and plagioclases and were used to determine Ca content for La-ICP-MS analyses. On Figure 4.7 we note that the inclusion rim is composed of much lower-An plagioclase than the host mineral. This is in good accordance with post-entrapment growth of the hosting mineral. From the rim toward the plagioclase core, anorthitic component progressively, linearly increases and do not show evidence of element diffusion that would be demonstrated by a progressive mixing of plagioclase and melt contents at the interface as indicated by Fick's first law of diffusion ($J=-D(dc/dx)$, J=diffusive flow, c=concentration, x=distance along diffusion path, D=diffusivity). Diffusion of trivalent or divalent incompatible elements such as REE is even less effective in anorthite than monovalent cations [*Cherniak*, 2003] and, hence, did not occur in analyzed samples.

Figure 4.8 shows a selection of trace element compositions obtained by LA-ICP-MS of melt inclusions and host plagioclases. Pit size was set at the maximum size for each inclusion, allowing an "ablation averaging" of the recrystallized trapped melts. When several ablations

Figure 4.6 (next page): (A) *Plane-polarized microphotograph of DB02-216 basalt with plagioclase phenocryst (Pl1) and melt inclusions. **(B-E)** Qualitative compositional maps obtained by microprobe scanning. Circles are LA-ICP-MS ablation pits, line is microprobe profile shown on Figure 4.7.*
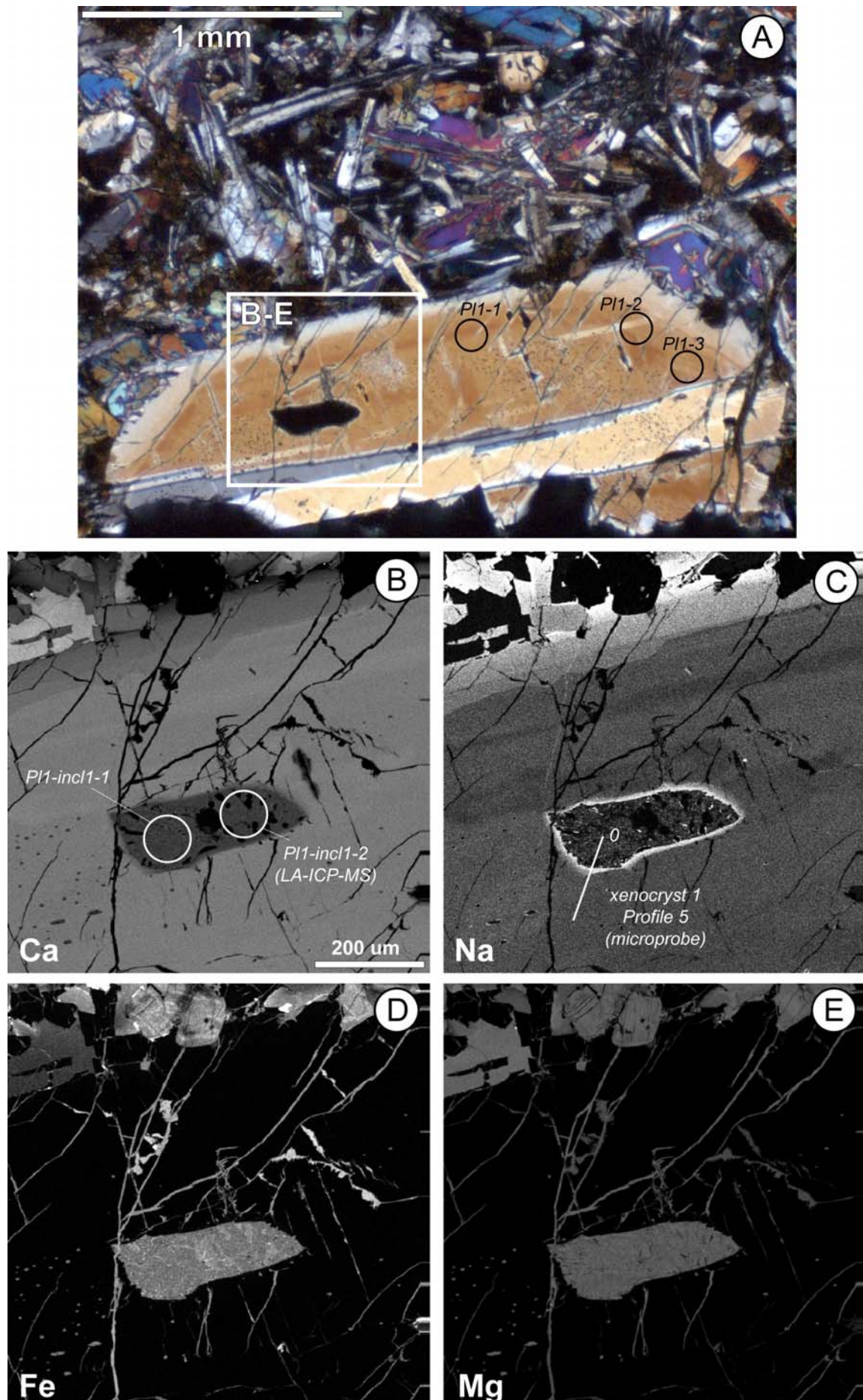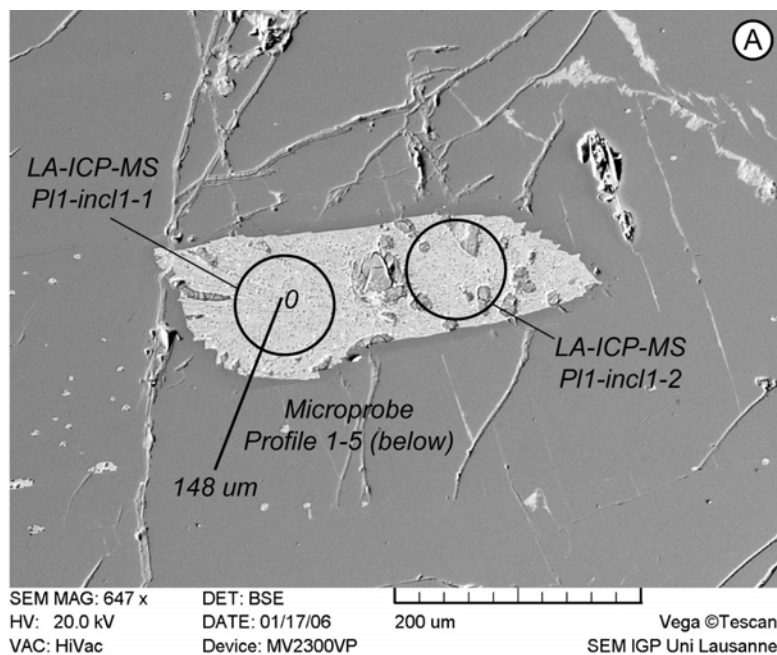
Figure 4.7: (A) Back scattered electron image of inclusion 1 in plagioclase 1 (Figure 4.6) with location of LA-ICP-MS ablation pits and microprobe profile 1-5. Note post-entrapment minerals inside the inclusion (dark grey minerals are altered olivine) and vanishing of some cracks along post-entrapment inclusion rim.
(B-C) Microprobe profile 1-5.
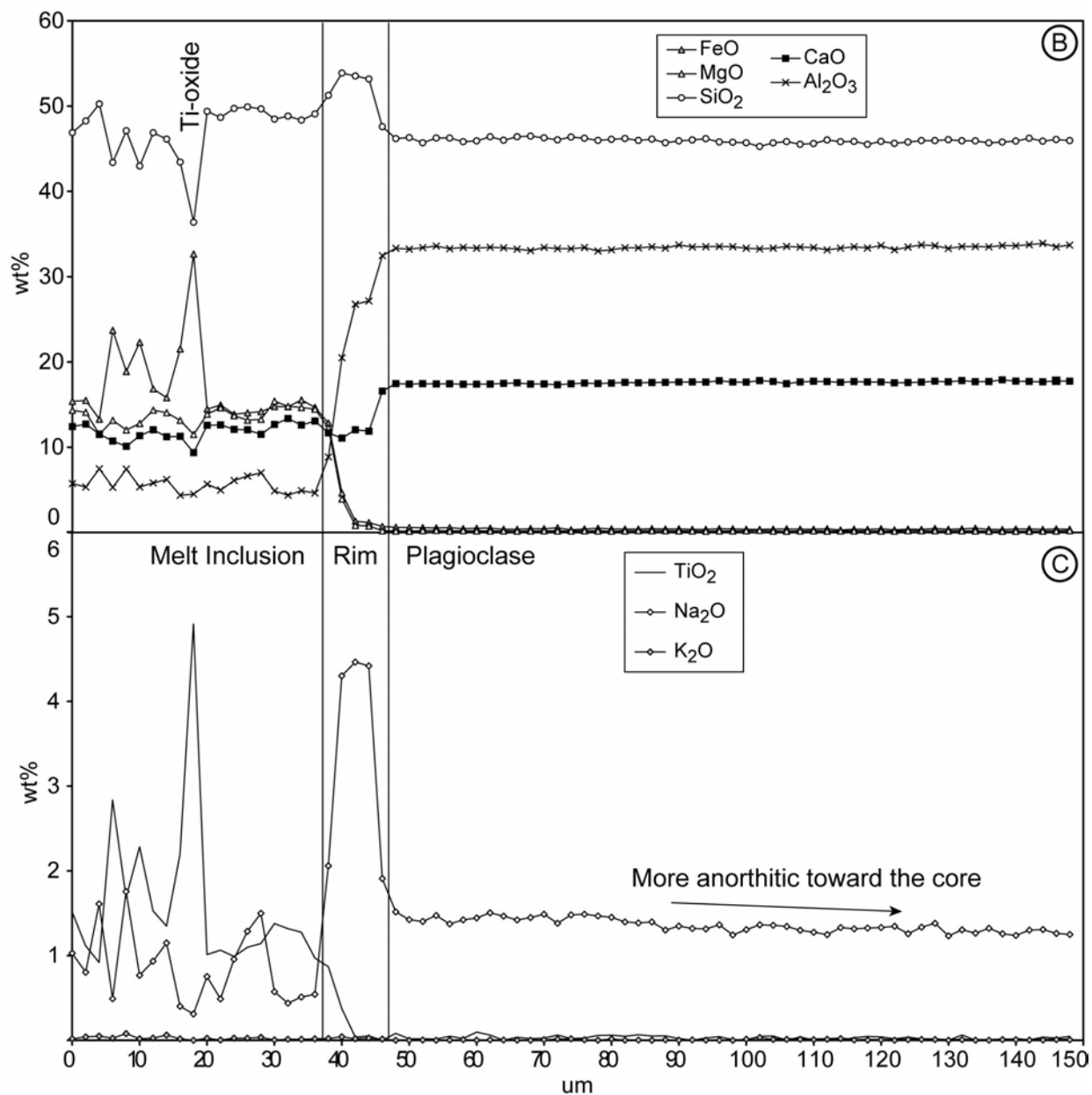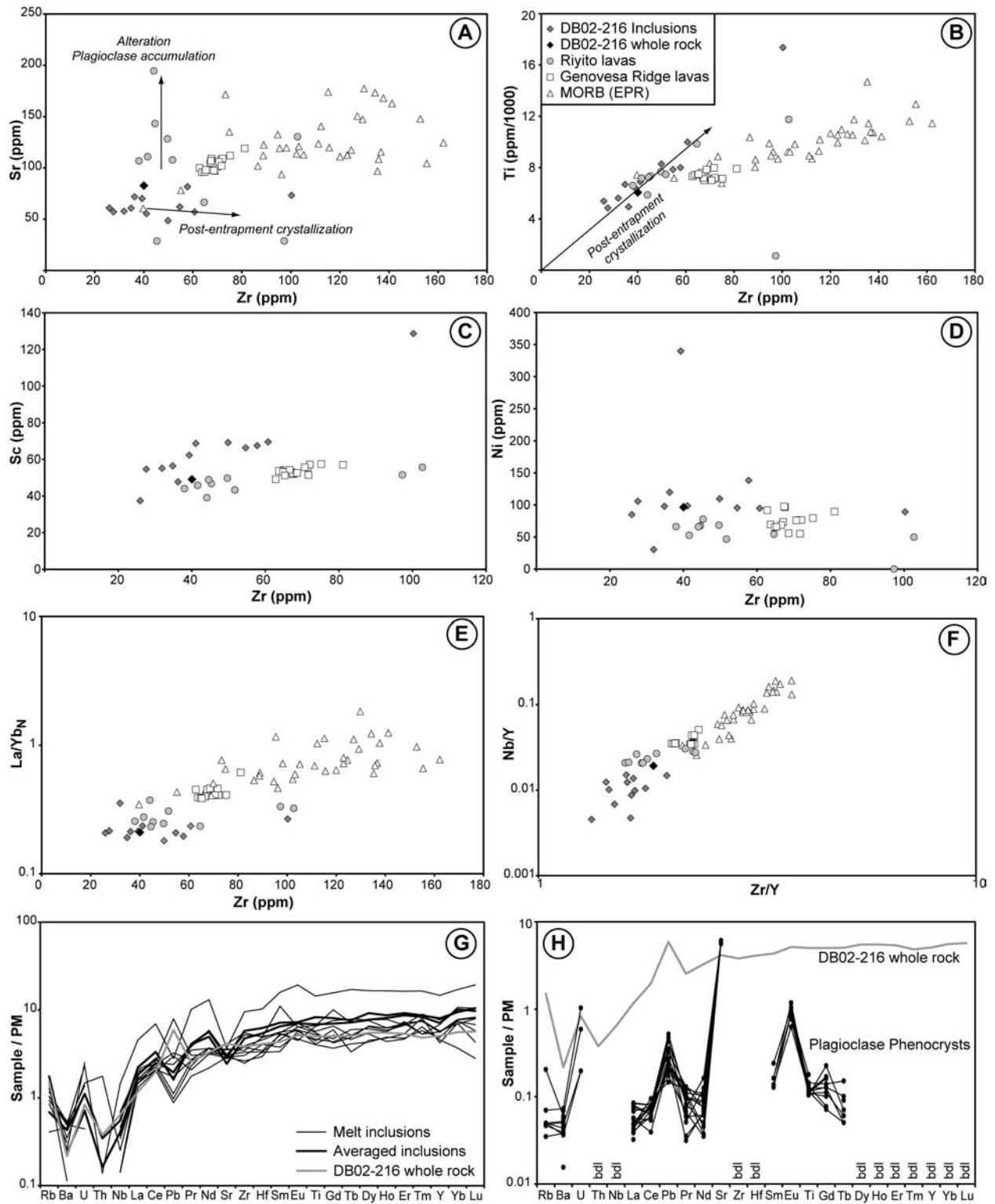
Figure 4.8: *(A-D) Binary plots of selected trace elements illustrating post-entrapment crystallization effects on the composition of melt inclusions. (A) Low Sr in trapped melt is related to removal by crystallizing host mineral. (C) Sc content illustrates lesser degree of differentiation in trapped melt than erupted lavas. (E) La/Sm$_N$-Zr diagram illustrating consistency of REE ratios between melt inclusions and host lava and non-influence of post-entrapment crystallization. (F) Weird depleted character of melt inclusions in terms of Nb/Y-Zr/Y in the MORB-Genovesa-Riyito Unit array. (G-H) PM-normalized multielement diagram of melt inclusions and host plagioclases. MORB data from Su and Langmuir [2003], Genovesa Ridge data from Harpp et al. [2003], PM after McDonough and Sun [1995].*

were available for a same inclusion, they were averaged to provide more reliable data. Melt inclusions show very similar compositions to hosting whole rock with, notably, a strong depletion in the most incompatible element contents (Figure 4.8g). Due to post-entrapment crystallization of host plagioclase the trapped melts exhibit a negative Sr anomaly. U, Pb and Eu contents were too low in the host plagioclase (Figure 4.8h) to allow depletion of these elements in the melt inclusions. Effect of post-entrapment crystallization is also shown on Figures 4.8 b-d by coeval increase of trace elements not incorporated into plagioclase (i.e. Ti, Zr, Sc and Ni). In the melt inclusions La/Yb_N remains constant with increasing Zr. Sc-Zr array of melt inclusions does not enclose composition of host whole rock and have globally higher Sc content attributed to lesser degrees of pyroxene fractionation than in the host lava (Figure 4.8c).

On a Nb/Y-Zr/Y diagram (after *Fitton et al.* [1997]) trapped melts are dissimilar to host rock and constitute a depleted end-member in the MORB-Riyito Unit array (Figure 4.8f). Behavior of this pair of incompatible element ratios cannot be explained by post-entrapment crystallization processes as shown by extremely low contents of Nb, Zr and Y in host plagioclases (Figure 4.8h). Considering the fact that La/YbN is very consistent between melt inclusions and host rock (Figure 4.8e) Nb/Y dissimilarities appears to be particularly surprising because $D_{Nb} \approx D_{La}$ and $D_Y \approx D_{Yb}$ in basaltic melts.

In conclusion to this chapter we observe that melt inclusions within plagioclase phenocrysts are broadly consistent with geochemical affinities of the Riyito Unit and do not point toward distinctive sources in terms of incompatible elements. Sole exception to this observation arises from the Nb/Y-Zr/Y ratio that is apparently at odd with REE contents. The plagioclase phenocrysts likely represent minerals crystallized in a magma chamber at depth that accumulated at the roof of the chamber. They remained in the chamber for some time and experimented various magmatic supplies and chamber replenishment before being driven by ascending melts toward the surface. Composition of the melt inclusions points toward more primitive melts in the chamber and pyroxene removal from the melt during ascent of the magmas.

4.4. Geochemical constraints on the origins of the Osa Igneous Complex

4.4.1. An assemblage of diverse volcanic sequences

The igneous rocks forming the Osa Igneous Complex exhibit a wide range of geochemical affinities that are well illustrated in terms of immobile incompatible element contents (e.g. Figures 4.3g, 4.4). This geochemical variability is similar to the range of incompatible elements defined by igneous rocks dredged on the aseismic ridges of the Cocos and Nazca plates [e.g. *Harpp et al.*, 2005] (CNAR on Figures 4.3g, h). However, in terms of major element contents, samples from the Osa Igneous Complex have a more consistent chemistry than samples from the aseismic ridges (Figures 4.3b-f).

At small scales, the geochemical consistency between the igneous rocks of the Osa Igneous Complex increases, as demonstrated by some samples collected close form each other in the Riyito or Vaquedano units. However, geochemical consistency within each unit of the Osa Igneous Complex is lower than for igneous complexes composed of a unique volcanic series such as the Quepos terrane, an accreted oceanic island in Costa Rica [*Hauff et al.*, 2000], and the

Azuero Plateau, an oceanic plateau forming the south Central American arc basement (Chapter 2) (Figures 4.3b-f).

Good geochemical consistency of the igneous rocks at low scale progressively lowering at larger scales is interpreted to be a result of the composite nature of the Osa Igneous Complex that formed through multiple events of accretion. Relatively consistent geochemistry within each unit and large chemical variations between the units at the scale of the entire complex is probably due to the mode of growth of the margin by episodic accretion and sampling of various groups of volcanoes through time (Chapter 3). In this view, igneous rocks having a very consistent geochemistry are likely composed of fragments of several volcanoes accreted at the same time, initially produced in a similar tectonic environment, through similar petrogenetic processes. Hence, the geochemistry of these units may be considered as a good indicator of the nature and origins of the accreted oceanic fragments despite an overall composite nature of the complex.

4.4.1. The Vaquedano and Güerra units

Whereas bulk of the Osa Igneous Complex is composed of plateau-like, NMORB-like and highly-depleted tholeiites, the Güerra and Vaquedano Units are predominantly made up of transitional/alkalic OIB-like lavas. In oceanic islands alkalic/transitional lavas are generally found in the latest stage of development of volcanoes (i.e. postshield stage), associated with a drastic diminution of eruption rates [e.g. *Clague and Dalrymple*, 1987]. Occurrence of the alkalic/transitional lavas of the Güerra and Vaquedano units conjointly with frequent interbeds of pelagic limestones points toward a seamount summit origin for the rocks forming these units.

The occurrence of summital pieces of seamounts in the Güerra and Vaquedano units has been interpreted to reflect periods of low coupling between the overriding and subducting plates, allowing accretion of the most superficial layers of the seamount by "peeling" only (Chapter 3). In this model, it is expected to observe a large diversity of seamounts, formed at distinct paleo-environments and times. This is attested by formation ages of the lavas that extend from the late Cretaceous to the middle Eocene in the Vaquedano Unit (Chapter 3). Geochemistry further strengthens this model by large chemical diversity of the lavas in terms of major and immobile trace element contents (Figures 4.3b, g, h).

4.4.2. The Inner Osa Igneous Complex

The Inner Osa Igneous Complex is mainly composed of plateau-like igneous rocks with affinities highly similar to the Azuero Plateau (Figures 4.3, 4.4a). Due to a geochemistry typical of oceanic plateaus it has been associated in recent contributions to pertain to the CLIP along with the Nicoya Complex (northern Costa Rica) [e.g. *Percy et al.*, 2006]. However, though an oceanic plateau origin is very probable, stratigraphy points toward an allochtonous, Pacific origin for both the Inner Osa Igneous Complex (Chapter 3) and the Nicoya Complex [e.g. *Bandini et al.*, 2008]. Distinct origins for the Azuero Plateau, Nicoya Complex and Inner Osa Igneous Compelx are further in agreement with: (1) lead isotope compositions that differ between the Inner Osa Igneous Complex and the Nicoya Complex (Figure 4.5b), (2) broader spectrum of major element contents for the Inner Osa Igneous Complex relatively to the Azuero Plateau (Figures 4.3b-f), and (3) igneous rocks with OIB-like and NMORB-like affinities in the Inner Osa Igneous Complex (Figures 4.3g, h, 4.4b) that are not observed in other plateau-like

igneous complexes in South Central America [e.g. *Hauff et al.*, 2000; *Hoernle and Hauff*, 2007]. As a consequence to preceding observations we propose here that the Inner Osa Igneous Complex represent an accreted oceanic plateau, initially distinct from the CLIP (Azuero Plateau) and the Nicoya Complex.

NMORB-like igneous rocks in the Osa Igneous Complex have major and trace element contents distinct from typical MORBs from the East Pacific Rise, but partly similar to some intraplate rocks from aseismic ridges on the Cocos and Nazca plates (Figure 4.3b-h). Accreted material of the Ontong-Java Plateau share several stratigraphic, structural and geochemical similarities with the Inner Osa Igneous Complex (Chapter 3). Interestingly, interlayered lavas with both plateau and NMORB signatures have been observed in the Makita Terrane (Solomon Islands), which is considered to pertain to accreted basal sequences of the subducting Ontong-Java Plateau [*Petterson et al.*, 1999]. Hence, due to contextual and geochemical similarities of NMORB-like igneous rocks from the Osa and Ontong-Java accreted plateaus it is possible that these rocks represent an intrinsic characteristic of oceanic plateaus not identified yet. Further work in the Osa Igneous Complex should be done to explore this eventuality.

4.4.3. The Ganado Unit

The Ganado Unit is composed of plateau-like tholeiitic lavas intruded by NMORB-like tholeiitic gabbros and dolerites (Figure 4.4c). Most of the plateau-like tholeiites differs from similar rocks of the Inner Osa Igneous Complex by a lower Nb content (Figure 4.3g). Similarly to the Inner Osa Igneous Complex, NMORB-like tholeiites have distinct major and immobile trace element contents than "true" MORB (Figures 4.3b-h), indicating they were likely generated in an intraplate setting. This suggests that the bulk of the Ganado Unit is a large fragment of seamount with predominant plateau-like affinities.

4.4.4. The Riyito Unit

Igneous rocks of the Riyito Unit are composed of tholeiites with unusually low incompatible element contents. These rocks are more depleted in terms of incompatible trace elements than typical N-MORB or depleted MORBs from the East Pacific Rise, although they have similar radiogenic Nd isotope ratios (Figures 4.3h, 4.4d, 4.5a). Similar occurrences of highly depleted tholeiites are restricted to small off-axis seamounts (e.g. the Lamont Seamount Chain along the East Pacific Rise, *Allan et al.* [1989]) or at sites of plume-ridge interaction (e.g. the Genovesa Submarine Ridge and Island, close to the Galapagos Hotspot, *Harpp et al.,* [2002, 2005]). These two occurrences of depleted tholeiites represent an endmember in the MORB compositional array (Figures 4.3b-h). Interestingly, the lavas from the Genovesa Island and Submarine Ridge exhibit similar plagioclase-phyric textures than the Riyito Unit [*Cullen et al.*, 1989; *Barr et al.*, 2004]. These occurrences of highly depleted tholeiites have been interpreted as a product of anomalously high thermal gradient in the depleted upper mantle very close to a ridge, allowing large melting of the MORB source and genesis of anomalously depleted tholeiites [*Allan et al.*, 1989; *Harpp et al.*, 2002, 2005].

Despite an overall similarity between off-axis seamounts, plume-ridge interaction seamounts and the Riyito tholeiites, we note some differences between the accreted rocks in southern Costa Rica and contemporaneous highly-depleted lavas in eastern Pacific. First, occurrences of depleted tholeiites from the East Pacific Rise or Galapagos Hotspot area do no

exhibit as much as depletion in the most incompatible elements as the lavas forming the Riyito Unit (Figures 4.3g, h). Second, whereas the Lamont seamounts and Genovesa Submarine Ridge are clearly in the MORB array in terms of major element and TiO_2 contents, the lavas from the Riyito Unit are not, with lower TiO_2, CaO, Al_2O_3 and SiO_2 at a given Mg# (Figures 4.3b-g, plagioclase accumulation cannot account for these tendencies). A Nb negative anomaly in a multielement diagram is also characteristic of the Riyito tholeiites (Figure 4.4d). That and anomalously low Ti content may indicate specific involvement of a Nb-Ti phase (presumably an oxide) at some stage of the petrogenesis of these particular rocks. Differences between the Riyito and contemporaneous east Pacific lavas are attributed to larger extent of melting of the source (presumably the upper depleted mantle) for the Riyito Unit.

Similarly to the Lamont seamounts or Genovesa Submarine Ridge, we propose that the Riyito tholeiites formed very close to- or at a mid-oceanic ridge. Alternative genetic models may be proposed for these rocks, such as melting of a depleted source in the ascending column of a plume [e.g. *Huang et al.*, 2005]. However, it is clear that intensive melting of a refractory NMORB-like source requires high thermal gradient and/or low lithospheric thickness. In fact, to our knowledge, highly-depleted tholeiites have been exclusively found close to spreading systems, which are obviously characterized by low lithospheric thickness. It seems thus that melting induced by adiabatic decompression is required to produce these particular igneous rocks.

Whether the Riyito tholeiites were initially part of off-axis seamounts or an aseismic ridge produced at a site of plume-ridge interaction may appear more difficult to determine. We note however that: (1) sizes of accreted volcanic edifices were probably higher than typical off-axis seamounts, as shown by occurrences of highly-vesiculated hyaloclastite indicative of relatively shallow-water eruptions, (2) to our knowledge, plagioclase-phyric highly-depleted tholeiites have only been reported from the sites of plume-ridge interaction [*Cullen et al.,*1989; *Hansen and Grönvold*, 2000; *Barr et al.*, 2004], (3) the Osa Igneous Complex and other accretionary complexes of southern Central America contain many indications of oceanic intraplate volcanism that took place between the late Cretaceous and the middle Eocene in the eastern Pacific, attesting the existence of one ore several hotspots in this area during this period [*Hoernle et al.*, 2002], and (4) the lavas forming the Ganado Unit (accreted simultaneously with the Riyito Unit) are composed of both plateau-like and NMORB-like intraplate lavas, indicating that a depleted component is recurrent in accreted fragments of intraplate volcanoes of southern Costa Rica. Hence, there is a convergent line of observations that points toward an origin at a site of plume-ridge interaction for the late Cretaceous/Paleocene tholeiites composing the Riyito Unit.

4.5. Tracking the origins of accreted seamounts of southern Central America

4.5.1. The paleo-Galapagos Hotspot: a potential candidate for the genesis of the accreted material of southern Central America

When a seamount or an oceanic island forms at an oceanic volcanic center it moves along with the lithosphere, becomes part of a seamount chain and is ultimately driven into a subduction zone where it may partly accrete or subduct into the mantle. The journey of the seamount/oceanic island in the ocean is evidently controlled by plate kinematics of the ocean

floor and, when this floor has not been subducted, it is generally possible to determine the origin of the seamount by following the seamount chain.

Late Cretaceous-Eocene accreted seamount and oceanic island fragments exposed along the southern Central American margin indicates that one or several center(s) of intraplate volcanism were located east of the East Pacific Rise during the late Cretaceous-early Tertiary, allowing several incomings of seamount into the subduction zone. However, the ocean floor produced east of the East Pacific Rise in this period has already subducted and is no longer available to constrain the origins of the accreted igneous rocks. On the basis of similar isotopic compositions between the accreted igneous rocks, the CLIP, and the igneous rocks from the Galapagos Archipelago and aseismic ridges of the Cocos and Nazca plates, it has been proposed that the accreted igneous rocks and the CLIP initially formed above a "paleo-Galapagos Hotspot" [*Hauff et al.*, 1997, 2000; *Hoernle et al.*, 2002, 2004; *Hauff and Hoernle*, 2007]. However, compositional space of the Galapagos Hotspot is very large and requires involvement of at least four distinct mantle components in terms of isotope contents [e.g. *Geldmacher et al.*, 2003]. In this context it is very difficult to define a chemical component specific to the Galapagos Hotspot that may have persisted through time and may be unequivocally used to recognize old, Galapagos-derived igneous rocks. Hence, geochemistry alone cannot firmly demonstrate the existence of a genetic link between the Galapagos Hotspot and older accreted seamounts in southern Central America.

Paleomagnetic data may be a useful tool to estimate paleo-latitudes for sites of formation of accreted seamounts. However, the method lacks precision for rocks formed in subequatorial latitudes and, thus, appears to have a rather limited potential for characterizing the origins of fragments of accreted seamounts in southern Central America.

Unit or terrane	Age of formation	Age of acccretion	Travel time
Tulin [1]	Maastrichtian (71-66 Ma)	middle Eocene (49-37 Ma)	17-34 Ma
Quepos [2, 3]	early Paleocene (~64 Ma)	late Paleocene-early Eocene (59-47 Ma)	5-17 Ma
Inner OIC [4, 5]	Coniacian-Santonian (89-84 Ma)	early-middle Paleocene (66-59 Ma)	18-30 Ma
Ganado [4]	Coniacian-Santonian (89-84 Ma)	Eocene (56-37 Ma)	28-52 Ma
Riyito [4]	Late Cretaceous/Paleocene (84-62 Ma)	Eocene (56-37 Ma)	8-47 Ma
Hoya Oceanic Island [4, 6, 7, 8]	early Eocene (52-53 Ma)	middle Eocene (45-40 Ma)	7-13 Ma

Figure 4.9: *Travel times of large accreted fragments of seamount and oceanic island exposed in southern Central America. Ages are constrained by fossil assemblages and ^{40}Ar-^{39}Ar dating: 1) Arias [2003], 2) Baumgartner et al. [1984], 3) Hauff et al. [2000], 4) this study, 5) Di Marco et al. [1995], 6) Hoernle et al. [2002], 7) Hoernle and Hauff [2007], 8) Baumgartner-Mora et al. [2008]. The unit and terranes are located on Figure 1.2.*

Travel times of accreted plateau and seamount/oceanic island fragments between their site of genesis and place of accretion may provide some constraints on the provenance of the accreted material. We summarize the travel time of plateau and large seamount/oceanic island fragments exposed along the southern Central American margin on Figure 4.9. The travel time has been calculated as the age difference between the oldest igneous rocks of a unit/terrane and the overlap sequence on the top of the accreted seamount fragments, *i.e.* arc-derived sediments discordantly deposited on the top of the accreted material, which provides a minimal age of accretion. A similar approach was made for the accreted seamounts in the western Pacific and showed that travel times for these seamounts vary from ~15 Ma to ~165 Ma [*Xenophontos and Osawa*, 2004]. We observe from Figure 4.9 that, even if there is a large incertitude for some units/terranes, the range of travel times is globally low in comparison to the ~150 Ma range observed in accreted seamounts of the western Pacific. This observation is indeed not surprising

considering the fact that the East Pacific Rise has remained probably close (<2500 km) to the southern Central American subduction zone in the late Cretaceous-Tertiary, impeding long time of residence of the seamounts on the ocean floor. We also observe from Figure 4.9 that the travel times of the accreted material are globally similar to the travel time of seamounts off Costa Rica, produced at the Galapagos Hotspot ~17 Ma ago [*Werner et al.*, 2003]. Hence, travel times defined by the tectonostratigraphy of the southern Central American margin are in broad agreement with the existence of a single intraplate eruptive center in the eastern Pacific since the late Cretaceous, which may be the paleo-Galapagos Hotspot. Sole exception to that is the unusually long travel time of the material of the Inner Osa Igneous Complex. This unit may thus have formed in a distinct eruptive center. It is nonetheless clear that refinement of the formation ages of the accreted igneous rocks and age of deposition of the overlap sequences is required to better constrain the origins of the accreted seamount fragments.

4.5.2. Initiation of the Cocos-Nazca spreading system

The Riyito Unit is made up of Late Cretaceous/Paleocene accreted fragments of seamount composed of tholeiites with highly-depleted immobile incompatible elements. These rocks are very unusual in the ocean and have only been encountered in the closest proximity to spreading systems. The geochemistry and tectonostratigraphy of the Outer Osa Igneous Complex indicates that the rocks forming the Riyito Unit were likely produced at a site of plume-ridge interaction. This suggests that the rocks forming the Riyito Unit were generated above the palaeo-Galapagos Hotstpot in the late Cretaceous/early Tertiary, in the direct vicinity of or at a spreading system.
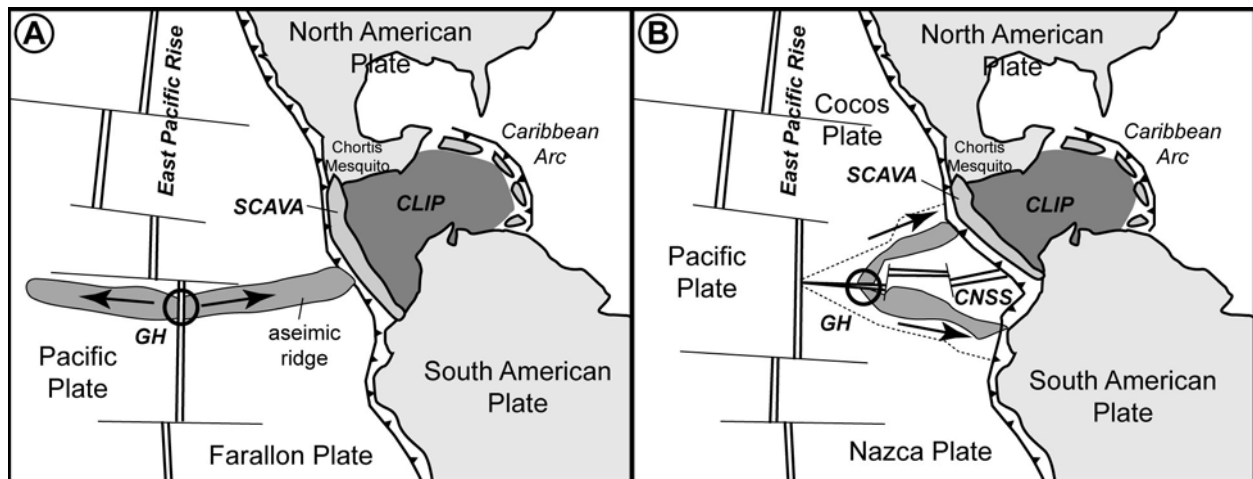
Figure 4.10: Schematic palynspastic reconstruction of the western Caribbean and eastern Pacific showing possible alternatives for plume-ridge interaction in the Paleocene. SCAVA=southern Central American volcanic arc, GH=paleo-Galapagos Hotspot, CNSS=paleo-Cocos-Nazca spreading system. A) The paleo-Galapagos hotspot is located on the East Pacific Rise; an aseismic ridge is driven toward the middle Pacific. B) The paleo-Galapagos hotspot is located on a paleo-Cocos-Nazca spreading system; aseismic ridges only occur on the eastern side of the East Pacific Rise and are not driven toward the middle Pacific.

In the late Cretaceous/early Tertiary, the Galapagos Hotspot may have possibly interfered with two mid-ocean ridges: (1) the East Pacific Rise, or (2) a paleo-Cocos-Nazca spreading system, which produced an ocean floor that has subducted or has not been recognized to date.

Due to the highly depleted nature of the Riyito tholeiites, it appears clearly that the plume-ridge interaction should have generated seamounts at both sides of the spreading system, as notably observed for the Galapagos Hotspot and the Cocos-Nazca spreading system today (Figure 4.1). If a seamount track produced east of the East Pacific Rise in the late Cretaceous/early Tertiary may have subducted, this is not the case for a seamount track initially located west of the East Pacific Rise, which should be observed today somewhere between the East Pacific Rise and the middle Pacific on late Cretaceous/early Tertiary ocean floor (Figure 4.10a). However, bathymetry of the ocean floor in the middle Pacific is clearly devoid of such a paleo-Galapagos Hotspot track [e.g. *Smith and Sandwell*, 1997], indicating that the existence of a spreading system east of the East Pacific Rise is necessary to explain the occurrence of the Riyito tholeiites in southern Costa Rica. As a consequence, we propose that the igneous rocks found in the Riyito Unit recorded an early, Late Cretaceous/Paleocene plume-ridge interaction between the paleo-Galapagos Hotspot and a paleo-Cocos-Nazca spreading system, subsequent to the break-up of the Farallon Plate (Figure 4.10b). Formation of this spreading system in the Late Cretaceous/Paleocene may have been triggered by a re-entrant of the subduction zone between the Americas and/or related to the thermal effect of the paleo-Galapagos Hotspot.

4.6. Conclusions

The Osa Igneous Complex is an assemblage of several fragments of oceanic plateau and seamounts that were presumably produced at the Galapagos Hotspot between the late Cretaceous and middle Eocene. Multiple events of accretion in southern Costa Rica between the early Paleocene and the Eocene led to preservation of various types of igneous rocks that span a large domain in terms of composition and resemble the array defined by the present-day aseismic ridges found on the Cocos and plates.

The Inner Osa Igneous Complex comprises a Coniacian-Santonian accreted oceanic plateau. This oceanic plateau is distinct from the autochtonous Azuero Plateau (western Panama), which represents a Coniacian-early Santonian autochtnous plateau part of the CLIP (Chapter 2). The Inner Osa Igneous Complex differs from the Azuero Plateau by: (1) larger range of major element contents, (2) occurrences of NMORB-like and OIB-like igneous rocks, and (3) stratigraphy (Chapters 2, 3). Similarly, stratigraphy, age and radiogenic isotope ratios clearly indicate that the Nicoya Complex (northern Costa Rica) is an accreted oceanic plateau dissimilar to the Inner Osa Igneous Complex. As a consequence, the Nicoya and Inner Osa Igneous complexes are composed of late Cretaceous oceanic plateaus distinct from the CLIP.

The Outer Osa Igneous Complex is composed of several fragments of accreted seamounts characterized by a large range of compositions that notably comprise plateau-like tholeiites intruded by NMORB-like tholeiites, diverse OIB-like transitional/alkaline lava flows and highly-depleted, plagioclase-phyric igneous rocks. Occurrence of highly-depleted igneous rocks in the Riyito Unit points toward the existence of a plume-ridge interaction in the eastern Pacific during the Late Cretaceous/Paleocene. Absence of aseismic ridge derived from the East Pacific Rise in the middle Pacific today implies the existence of a paleo-Cocos-Nazca spreading center as old as the late Cretaceous/early Tertiary that allowed genesis of the rocks forming the Riyito Unit.

Chapter 5: The late Cretaceous-Eocene Azuero Accretionary Complex (western Panama): Development and Accretion of an Oceanic Island

This chapter has been designed for a paper illustrating the exceptional preservation of an oceanic island in the Azuero Accretionary Complex, with possible implications on the development of oceanic islands and seamount accretion.

5.1. Introduction

In modern oceans numerous seamounts and oceanic islands produced by intraplate volcanism are observed [e.g. *Hillier*, 2007]. These volcanic edifices are distributed over extended areas and constitute anomalously-high topographic heterogeneities on the top of the ocean floor. They have been recognized for a long time to be an important disturbing factor along convergent margins: (1) incoming of seamounts (or ridges) in the subduction zone has a strong impact on the morphology of the forearc slope and trigger mass-wasting [e.g. *Dominguez et al.*, 1998, 2000; *Collot et al.*, 2001; *Huehnerbach et al.*, 2005; *Soh and Tokuyama*, 2002], (2) subducting seamounts cause a basal removal of large portions of the overriding plate by erosive tunneling [e.g. *Ranero and von Huene*, 2000; *Bangs et al.*, 2006; *Kopp et al.*, 2006], which is linked to mass balance of accreted and eroded materials, (3) the seamounts act as large asperities at the interface of the subducting and overriding plates, resulting in a specific seismogeneity [*Cloos*, 1992; *Scholz and Small*, 1997; *Honkura et al.*, 1999; *Kodaira et al.*, 2000; *Abercrombie et al.*, 2001; *Husen et al.*, 2002; *Bilek et al.*, 2003; *Park et al.*, 2004; *Bangs et al.*, 2006], (4) collision of a seamount chain with a volcanic arc may lead to temporary cessation of the arc volcanism [e.g. *Kolarsky et al.*, 1995a], and (5) subducting seamounts play a role in supra-subduction magma genesis, as indicated by seamount-derived signatures in some arc magmas [*Feigenson et al.*, 2004; *Hoernle et al.*, 2008].

Although subducting seamounts have been observed by geophysical imaging [*Barckhausen et al.*, 1998; *Park et al.*, 1999; *Franco and Abbott*, 1999; *Kodaira et al.*, 2000; *Husen et al.*, 2002], mechanisms controlling their ultimate fate -to sink into the mantle or to accrete to the overriding plate- are still poorly understood and have been principally explored through geophysical modeling [e.g. *Cloos et al.*, 1993; *Baba et al.*, 2001]. However, exhumed fragments of accreted seamounts have been observed among many fossil subduction zones in exposed accretionary complexes and may provide important constraints on accretionary processes [e.g. *Cawood*, 1982; *Barnes and Korsch*, 1991, *Okamura*, 1991; *Pillevuit et al.*, 1997; *Timpa et al.*, 2005; *Ueda et al.*, 2000, 2005; *Volkova and Budanov*, 1999; *Bagheri and Stampfli*, 2008].

Despite ubiquitous presence of intraplate volcanoes on the Pacific Ocean floor, access to their internal structure is generally difficult and our understanding of their evolution has been essentially build up on indirect or rather punctual observations. In the Hawaiian chain a generic model of volcanic evolution has been fundamentally developed on the basis of a comparative study between volcanoes at different stages of evolution [e.g. *Clague and Dalrymple*, 1987; *Langenheim and Clague*, 1987]. Drilling, dredging and bathymetric imaging provide important informations on the volcanic structure, but observations are restricted to the uppermost layers of

the volcano, drill cuttings or core samples [e.g. *Moore*, 1965; *Clague et al.*, 1994; *Tarduno et al.*, 2002; *Garcia et al.*, 2007]. Due to poor velocities contrast in the interior of the volcanoes and/or poor seismic resolution, deep sequences of oceanic islands have not been imaged precisely through seismic imaging [e.g. *Weigel and Grevemeyer*, 1999; *Walther*, 2003; *Evangelidis et al.*, 2004; *Sallares et al.*, 2005]. Though many seamounts have been partly accreted and exposed in accretionary complex, they tend to loose their pristine internal arrangement during accretionary processes and generally suffer from metamorphism. Due to low subsidence, intraplate volcanoes produced on slow-motion plates relative to the mantle frame (e.g. the Canarian volcanoes) tends to be strongly eroded down to deep structures, impeding precise characterization of their entire development [e.g. *Carracedo et al.*, 1998; *Carracedo*, 1999]

We present here the first occurrence of an exceptionally well-preserved oceanic island exposed in an accretionary complex. The oceanic island has not been altered by metamorphism and remained remarkably underformed during the accretion. It has been encountered in the late Cretaceous-Eocene Azuero Accretionary Complex (western Panama) and has been recognized on the basis of a comprehensive geological field work, a new tectonostratigraphy of the area (Chapter 2) and geochemical analyses of the igneous rocks. We propose a model of development for the oceanic island and discuss its mode of emplacement along the margin.

5.2. Geologic setting of the Azuero Accretionary Complex

The Azuero Accretionary Complex is located in the Azuero Peninsula, along the southern Central American forearc (Figures 1.2, 2.8, 5.1). It is exposed on the seaward side of the late Cretaceous-middle Eocene southern Central American arc and arc basement, a Coniacian oceanic plateau named "Azuero Plateau" (Chapter 2). On the western side of the peninsula, the Azuero Accretionary Complex is separated from the Azuero Plateau by a mélange that generally follows the orientation of the Azuero-Sona Fault Zone and is defined here as the "Azuero Mélange" (Figure 5.1). On the eastern side of the peninsula the Azuero Accretionary Complex is in contact with the ancient volcanic arc and Azuero Plateau along the Joaquín Fault Zone and other minor faults. We define here the western Azuero Accretionary Complex as the "Hoya Unit" and the eastern Azuero Accretionary Complex as the "Venado Unit" (Figure 5.1). Eocene-Miocene overlap sequences partly composed of arc-derived material are observed throughout the Azuero Peninsula, generally in topographic lows, and have been defined in southern Azuero as the Tonosi Formation [*Kolarsky et al.*, 1995b].

5.2.1. Geologic review of the Azuero Accretionary Complex

Accreted igneous rocks have been first recognized in the Azuero Peninsula on the basis of observations along some parts of the shoreline and road cuts, further interpreted on the basis of geochemistry and radiometric dating [*Hoernle et al.*, 2002; *Lissinna*, 2005; *Hoernle and Hauff*, 2007]. Samples used in these studies were collected both *in situ* and as boulders in the river beds. According to these works, igneous rocks are predominantly composed of igneous rocks ranging from tholeiitic to alkalic basaltic pillows, sheet flows, sills and dikes and grabbroic intrusives. Alkali basalts were often erupted under shallow-water to subaerial conditions and deep water eruptive conditions have been inferred for tholeiitic pillow basalt sequences. Matrix step-heating, plagioclase step-heating and matrix total fusion ^{40}Ar/^{39}Ar analyses yielded 66-21 Ma formation ages for the basalts of the Hoya Unit [*Hoernle et al.*, 2002]. Venado Unit has not

been dated. On the basis of the geochemistry and ages of the igneous rocks the Azuero Accretionary Complex has been interpreted to represent a highly-composite assemblage of several fragments of oceanic islands and seamounts formed at the Galapagos Hotspot and subsequently accreted to the southern Central American margin [*Hoernle et al.*, 2002; *Hoernle and Hauff*, 2007].

5.2.2. Geologic review of the Tonosi Formation

The Tonosi Formation is composed of two major lithologic units, the lower and upper Tonosi formations [*Krawinkel et al.*, 1999]. The age of the lower unit is middle Eocene to early Oligocene (~40 to 30 Ma) and was deposited in shallow-water, paralic environments [*Kolarsky et al.*, 1995b; *Krawinkel et al.*, 1999]. The upper unit has a late Oligocene to early Miocene age (~30 to 15 Ma) and was deposited in a deeper forearc environment [*Kolarsky et al.*, 1995b; *Krawinkel et al.*, 1999]. Facies and compositional changes between the two units have been interpreted to result from variations of the forearc environment in response to tectonics [*Krawinkel et al.*, 1999].
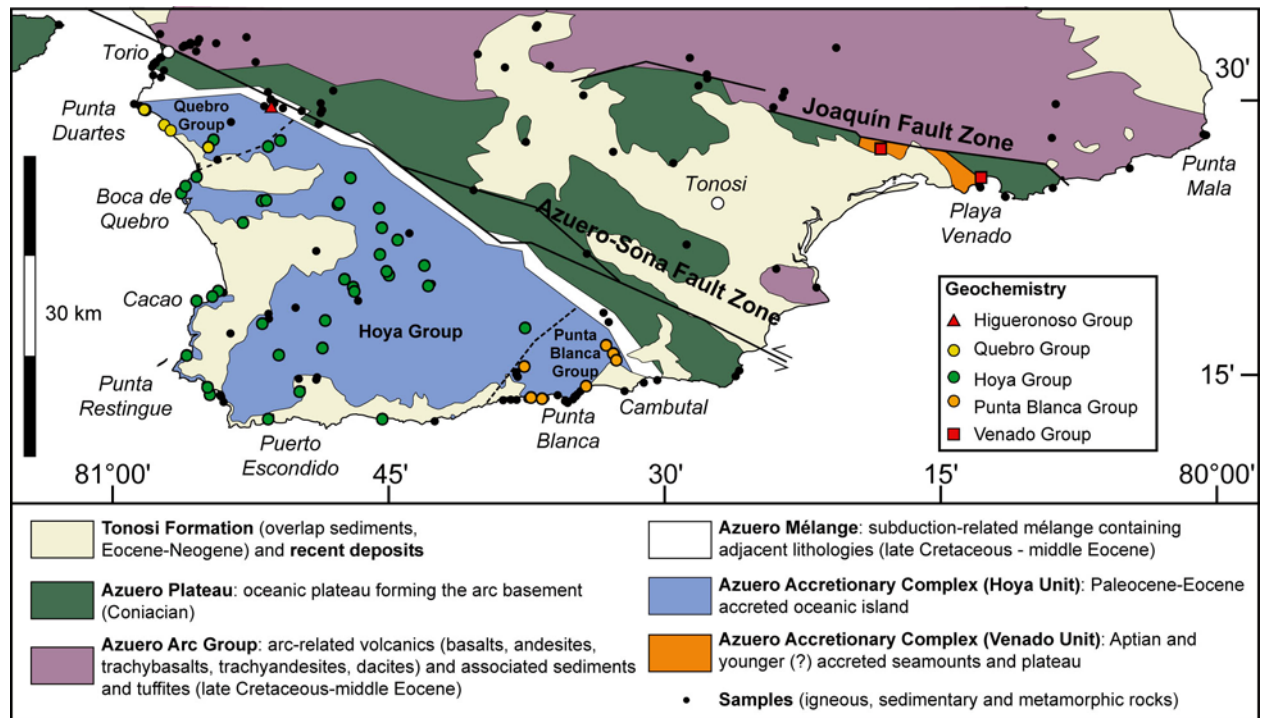
Figure 5.1: Simplified geologic map of southern Azuero (based on Chapter 2), with analyzed igneous rocks and geochemical groups.

Sediments unconformably resting upon the Azuero Accretionary Complex have been principally studied along coastal exposures in southwestern Azuero, between Cambutal and Punta Blanca [*Kolarsky et al.*, 1995b; *Krawinkel et al.*, 1999] (Figure 5.1). These sediments are composed of middle Eocene to lower Miocene thick turbiditic sequences with minor occurrences of shallow-water carbonate and proximal deposits at the base. Close to Punta Blanca shallow-water limestones have been interpreted to rest unconformably upon the igneous basement (i.e. the Azuero Accretionary Complex) [*Kolarsky et al.*, 1995b; *Krawinkel et al.*, 1999]. These limestones have been correlated to similar exposures in the area both on-land and off-shore between the Sona and Azuero Peninsulas (Figure 1.2), indicating they were emplaced during a

regional transgressive event that affected the margin in the middle Eocene [*Kolarsky et al.*, 1995b; *Krawinkel et al.*, 1999].

5.3. Results

We present here new geological and geochemical data from the Azuero Accretionary Complex and overlap sequences, which are interpreted along with new results from an on-going paleontological study in the area [*Baumgartner-Mora et al.*, 2008]. The Hoya Unit has been subdivided into three groups based on specific geochemical affinities and spatial arrangement: (1) the Quebro Group, in the NW Hoya Unit, (2) the Hoya Group, in the central Hoya Unit, and (3) the Punta Blanca Group, in the SE Hoya Unit (Figure 5.1). Geochemical analyses are given in the Appendix.

5.3.1. Dominant lithologies and field relationships

5.3.1.1. Venado Unit

The Venado Unit is composed of massive and pillowed lava flows occurring in similar proportions. Minor occurrences of recrystallized limestones or hydrothermal carbonates have been found between some pillows. The igneous rocks located close to the Joaquín Fault Zone suffered from deformation but the sequence has remained relatively well-organized with pillow lavas in normal position that variously dip 0-60° (no preferential trend). In this area, the lavas are intruded by dolerites and dykes.

5.3.1.2. Hoya Unit - Quebro Group

The Hoya Unit is composed of relatively undeformed and nonmetamorphic rocks. The general arrangement of the rocks differs strongly from other accretionary complexes along the southern Central American Margin such as the Osa Igneous Complex (southern Costa Rica) (Chapters 3, 4) or the Venado Unit. Indeed, rocks in the Hoya Unit appear to be much more organized in the field than other accreted igneous complexes in Costa Rica and Panama. The layers typically dip <45%. Overturned sequences have not been encountered.

The Quebro Group is predominantly composed of basalt sheet flows with frequent columnar cooling joints. Agglomerates (autoclastic breccia) are locally encountered at the base of the flows. The lava flows frequently contain vesicles <5mm in size. Locally picritic flows are interlayered with the basaltic lavas. Mingling textures have been observed in some sub-*in situ* boulders (Photo 5.1). The sheet flows are intercalated with hemipelagic sediments and vesiculated hyaloclastites that may locally form up to 5% of the sequence (Photo 5.2). Pillow lavas have not been found in the Quebro Group.

The interlayered sediments are composed of grey to white calcareous-siliceous deposits that are extensively bioturbated. Evidences for loading of the sediments by overlying lava flows and incorporation of poorly-lithified sediments into the lavas have been found (Photo 5.3). The sediments possibly contain a small proportion of ashfall deposits recognized under the microscope by occurrences of small acicular feldspars. Hyaloclasts are frequent in the sediments. Planktonic microfossils (foraminifera and radiolaria) are observed. Shallow-water fauna are

absent, which points toward deposition of the interlayered sediments out of the influence of shallow-water environments.

5.3.1.3. Hoya Unit - Hoya Group

The Hoya Group contains a large range of distinct lithologies. Absence of good stratigraphic markers, important lateral variation of the sequences and recent tectonics impede precise correlations between the different types of lithology. However, recurrent rock associations and rock types are spatially organized and identifiable on the field. These lithologies are represented on Figure 5.2.

In the northern Hoya Group the sequences are similar to the formations found in the Quebro Group. In the northern central area significant amount of clastic sediments occur. These sediments are composed of grain-supported basaltic breccia devoid of sediment clast. The clasts typically range in size between a few mm to ~1 m and size grading defines layers in the deposits (Photo 5.4). The clasts are represented by fragments of massive basaltic flows with both low and high vesiculation, some basalts exhibiting vesicles up to 3 cm in length. Breccia are locally intercalated with pillow lavas or submarine sheet flows, indicating that the clastic sediments deposited in submarine conditions. The clastic material is occasionally crosscut by basaltic dykes 30 cm to 2 m in thickness. Some dikes are dissected by faults whereas neighbour dykes crosscut the faults, which is evidence for synvolcanic tectonics (Photo 5.5). Chemistry of the dykes indicates they pertain to the OIB-like Hoya volcanic suite (see below).

In the central area of the Hoya Unit, around the highest peaks and along the coast between Puerto Escondido and Cacao, sequences are predominantly composed of basalt sheet flows with frequent columnar cooling joints. The lavas exhibit large vesicles filled up with calcite, with length up to 3 cm. Picritic lavas are occasionally observed as interbeds between the basaltic flows. Autoclastic breccias are sporadically found at the base of the flows. In several places, shallow-water limestones are interbedded with the sheet flows and associated to basaltic breccias and conglomerates. The limestones and very-well rounded basaltic pebbles are indicative of coastal environments (Photo 5.6). Hence, sheet flows with large vesicles located close to the shallow-water limestones may have been emplaced under subaerial conditions. The limestones are predominantly composed of onchoids, echinoderm fragments and benthic foraminiferans. They contain in lesser extent basalt and coral fragments. Foraminiferan assemblages indicate a Paleocene-early Eocene age of deposition for the limestones [*Baumgartner-Mora et al.*, 2008]. At Puerto Escondido a sequence exhibits (from bottom to top): (1) sheet flows, (2) shallow-water limestones bearing well-rounded basalt pebbles, (3) near-shore shallow-water limestones grading to more detrital, turbiditic sequences. This sequence may represent a transgressive event on the top of subaerial lava flows.

Submarine lavas recognized by an association of basaltic sheet flows and pillows are exposed around the subaerial deposits on a map view (Figure 5.2). The sheet flows frequently exhibit cooling joints and large vesicles. They are locally interlayered with picritic lavas. Several sequences exhibit a clear transition from pillowed lavas to clastic deposits and/or shallow-water limestones. This marks a transition from submarine to subaerial lavas and clearly indicates that the submarine lavas are stratigraphically underlying the subaerial deposits. The submarine lavas have been encountered in association with hemipelagic limestones in southern Azuero. The hemipelagic limestones consist of biomicrites containing planktonic foraminiferans, sponge

spicules, and in a lesser extent echinoderm, bryozoan and coral fragments. Dating of these sediments has still to be carried out.

In the most central part of the Hoya Unit, large volumes of intrusive rocks have been observed. They consist of large gabbroic bodies and dyke swarms that constitute a dense, complicated network. Locally the dykes constitute >80% of the exposed rocks (Photo 5.7). Intruded rocks are devoid of pillow lavas but locally consist of breccia. This likely indicates that the intrusives were emplaced in both submarine and subaerial formations. The large amount of intrusives in the area is generally accompanied by an alteration characterized by epidote formation in the intruded rocks. Formations comprising large volumes of intrusives are much more resistant than rocks from other areas of the Azuero Peninsula, which has led to the formation of high reliefs, up to 1500 m high only ~15 km from the coast.
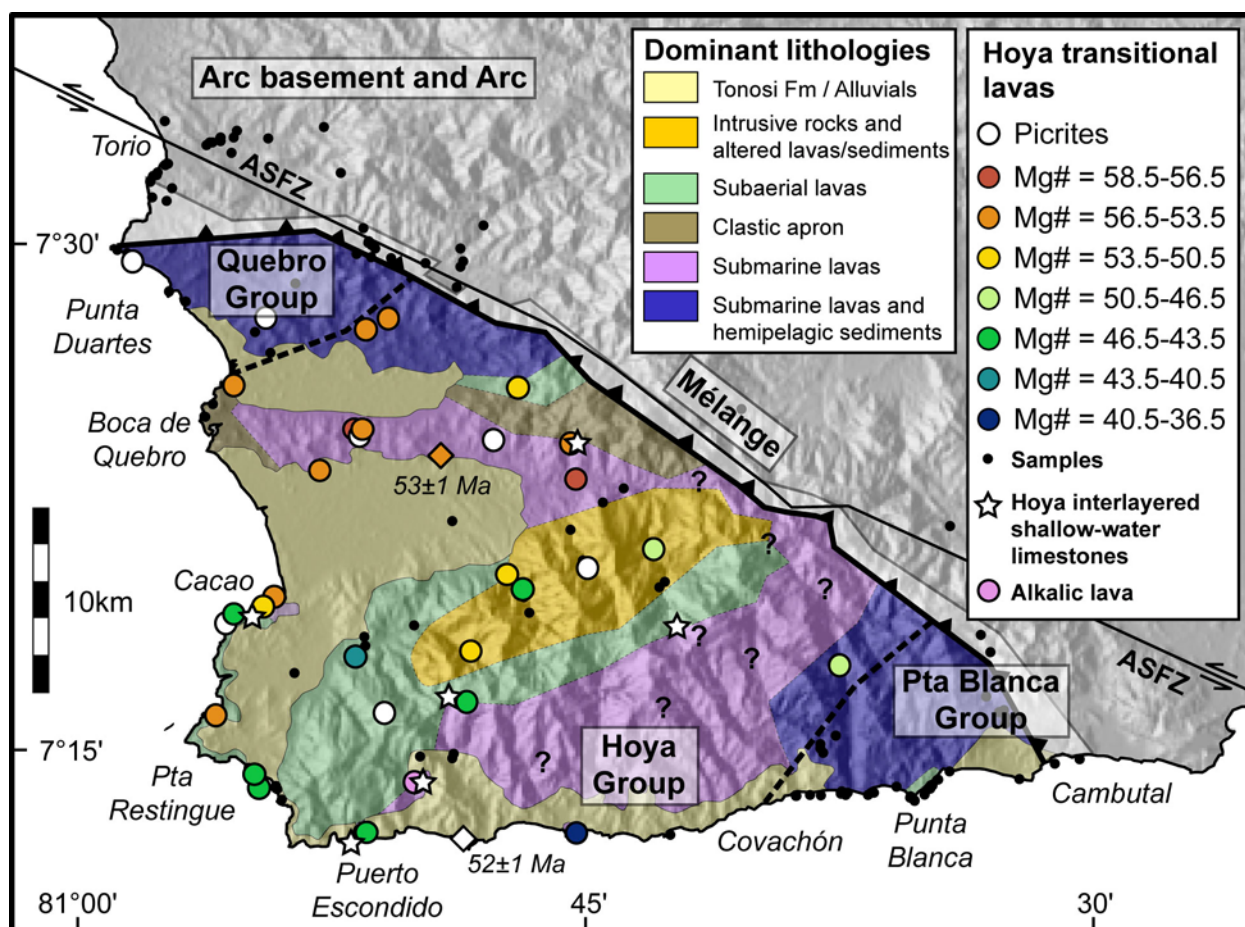
Figure 5.2: *Lithologic arrangement of the Hoya Unit. Mg# of the transitional lava flows, picrite and interlayered shallow-water limestones from the Hoya Group are illustrated for comparison. Diamonds are for samples by Hoernle et al. [2002]. $^{40}Ar/^{39}Ar$ ages defined by consistent plateau are shown [Hoernle et al., 2002]. ASFZ=Azuero-Sona Fault Zone.*

5.3.1.4. Hoya Unit - Punta Blanca Group

The Hoya Unit is predominantly composed of pillowed and massive basalts with minor association of interbedded hemipelagic limestones. Most of the lavas contain small vesicles. The amount of pillows is larger than in submarine sequences of the Hoya Group (Photo 5.8). The limestones are generally composed of white-pink biomicrites bearing planktonic foraminiferans

and reworked biogenic fragments of shallow-water origins. Fossil assemblages are indicative of a middle Eocene age [*Baumgartner-Mora*, written communication, 2006].

At Punta Blanca (literally the "White Point" in Spanish), a particular sequence has been recognized that is composed of interbedded basalt sheet flows, pillow basalts and shallow-water limestones (Photo 5.9). Bomb agglutinates are locally observed with infill of shallow-water calcareous sediments, which is argument for partly subaerial volcanism in a shoaling environment. The limestones are predominantly composed of onchoids and locally exhibit coral in living position on the top of the lava flows. Though faulting may have duplicated some parts of the sequence, the limestones are clearly sedimentarily interbedded between lava flows and do not pertain to the Tonosi Formation as suggested by previous workers [*Kolarsky et al.*, 1995b; *Krawinkel et al.*, 1999; *Hoernle and Hauff*, 2007]. In this area the Tonosi Formation crops out on the beach located east of Punta Blanca and in bordering hills. This formation is characterized by shallow-water limestones that contain large bivalve shells and benthic foraminiferans. The Tonosi limestones have thus a very distinct facies than limestones occurring within the basaltic sequence at Punta Blanca.

Whereas the western and central parts of the Punta Blanca Group are structurally and lithologically consistent, we note that lithologic arrangement of the group in the vicinity of the Azuero Mélange becomes more complicated with, notably, an increase in the diversity of the rock sequences. This may indicate that the eastern side of the Punta Blanca Group is composed of several rocks bodies, possibly amalgamated through tectonic processes.

5.3.1.4. Azuero Mélange

The Azuero Mélange is a tectonic mélange at the interface between the Hoya Unit and the Azuero Plateau. The mélange is made up of deformed, variously altered rock bodies. Some of the rocks are similar to the plateau, whereas some consist of reddish pillow lava, picrite, pelagic siliceous-calcareous sediment and basaltic detrital sediment. The rocks distinct than the plateau sequences have OIB-like affinities (see below). Some of the sediments bear well-preserved planktonic foraminiferan and radiolarian assemblages that remain to be dated.

Along the shoreline between Torio and Punta Duartes a transition from relatively underformed plateau lavas and associated radiolarian cherts to OIB-like igneous rocks has been observed (see also *Kolarsky et al.*, [1995b]). The transition is marked by an occurrence of highly-deformed rocks similar in composition to the Azuero Plateau. This represents a coastal exposure of the Azuero Mélange.

5.3.1.5. Tonosi Formation

The Tonosi Formation rests unconformably on the Hoya Unit and is composed of overlap sequences deposited on the top of the Hoya Unit after emplacement at its present location. Previous workers have associated the transgression of the Tonosi sediments upon the Hoya Unit with a presence of shallow-water limestones or conglomerates grading upward to turbiditic deposits [*Kolarsky et al.*, 1995; *Krawinkel et al.*, 1999] (Photo 5.11). Our observations indicate that the basal Tonosi Formation resting on the Hoya Unit may be locally composed of hemipelagic detrital sediments, as well.

The hemipelagic lower Tonosi Formation is well-seen along costal exposures between Covachón and Punta Restingue and rests at several sites upon the Hoya Group. Other easily-

accessible occurrences are found at Cacao and Punta Duartes. These sediments are made of grey, 10-50 cm-thick beds of frequently turbiditic, micritic-siliceous limestones including various amounts of clastic material. Locally the sequence is folded (Photo 5.10). The detrital fraction is composed of arc-derived, shallow-water limestones and biogenic grains and, probably, Hoya-derived material embedded in a calcareous-siliceous matrix. At the base of the Tonosi Formation, close to the contact with the igneous basement, arc-derived grains have been ubiquitously recognized and consist of: (1) quartz, (2) zoned plagioclase, (3) amphibole and (4) lithic fragments. However, the bulk of the detrital fraction is composed of fragmented basalts and shallow-water limestones that probably proceeded from the Hoya Unit. In some places (e.g. Punta Restingue or Covachón) massflow deposits rework plurimetric clasts of limestones and Tonosi sediments, some of which show evidence for poor lithification at the time of deposition (Photo 5.12). Between Covachón and Puerto Escondido, paralic deposits containing well-rounded pebbles are observed, indicating a possible shallowing upward of the sequence (Photo 5.13). Biogenic fraction of the hemipelagic lower Tonosi Formation consists mostly of planktonic foraminiferans and organic mater. Shallow-water biogenic grains form a minor amount in these sediments. The foraminiferans point toward Eocene ages of deposition [*Baumgartner-Mora*, written communication, 2006].

The shallow-water deposits locally found at the base of the lower Tonosi Formation will be more comprehensively described in a forthcoming study. Our preliminary results are nonetheless in good agreement with previous works and point toward a middle Eocene to Oligocene ages of deposition, which are broadly similar to ages of the hemipelagic lower Tonosi Formation [*Baumgartner-Mora et al.*, 2008].

5.3.2. Igneous rocks

5.3.1.1. Venado Unit

Basalts and intrusive rocks from the Venado Unit have sub-ophitic, intersertal, and intergranular textures. They are composed of olivine, clinopyroxene, plagioclase, opaque minerals and interstitial glass. Minor amount of vesicles with infill by chlorite are common. Plagioclase phenocrysts a few are locally observed.

The degree of preservation of the rocks is relatively good, with replacement of olivine by secondary minerals, and minor chloritzation of clinopyroxene and argilitization of feldspars. The glass has been altered to palagonite. Igneous rocks in contact with intrusives have suffered from higher degrees of alteration notably attested by the presence of epidote.

5.3.1.2. Azuero Mélange

Igneous rocks from the Azuero Mélange have been generally significantly altered. Epidote is commonly found in the rocks and deformation is important. However, the rocks have remained under the greenschist metamorphic facies.

We analyzed one sample from this unit. It is characterized by a trachytic texture and is predominantly composed of feldspars, clinopyroxene and opaque minerals. The degree of preservation of this sample was lower than samples from other units.

5.3.1.2. Hoya Unit

The igneous rocks from the Hoya Unit are very-well preserved. The degree of alteration is low as notably indicated by some picritic lavas containing fresh olivines. Pyroxene and feldspar are well preserved and only glass alteration has occurred. The degree of alteration becomes however much stronger in the vicinity of intrusive rocks. In this case epidote is ubiquitously observed and accompanied by alteration of olivine, pyroxene chloritization and feldspar sericitization and argilitization.

Three types of rocks have been observed in this unit: (1) picrites, (2) transitional igneous rocks, and (3) alkalic igneous rocks. The picrites are characterized by significant amount of olivine phenocrysts that are enclosed in a glassy or microlitic matrix (Photo 5.16). Melt and spinel inclusions are frequent in the olivine. Other phenocrysts and mineral clusters are composed of clinopyroxene, plagioclase and opaque minerals. Some clinopyroxenes have oscillatory zonation and/or are partly resorbed, which is evidence for magma mixing. Vesicles are locally observed.

The transitional lavas have sub-ophitic, intersertal and fluidal textures (Photo 5.14). They are composed of olivine, clinopyroxene, plagioclase, opaque mineral and, in some cases, interstitial glass. A porphyric or glomeroporphiric texture is frequently observed with phenocrysts or clusters of olivine ± clinopyroxene ± plagioclase. Some clinopyroxenes have an oscillatory zonation. The Punta Blanca Group exhibits a distinctive glomeroporphyritic texture. The Quebro Group contains coarser lavas with frequent mineral zoning (Photo 5.15).

The transitional intrusive rocks have been found in the Hoya Group exclusively. They comprise dikes, dolerites, gabbros and one aplite. Dykes are composed of porphyric microlitic or fluidal porphyric lavas with olivine ± clinopyroxene ± plagioclase phenocrysts. The gabbros have intergranular textures with clinopyroxene, plagioclase and opaque minerals. Some clinopyroxenes have an oscillatory zonation. The aplite (DB07-130) was found as a sub-*in situ* boulder in a river bed within the intruded Hoya area and contains feldspars, quartz and amphibole.

Three samples of alkalic igneous rocks have been encountered in the Hoya Group and analyzed. One is a sheet flow (DB07-021) interlayered with shallow-water limestones. It has a fluidal texture, with plagioclase, K-feldspar, brownish clinopyroxene, olivine, opaque minerals and leucite. Another one is a well-rounded pebble (DB06-007) found in shallow-water calcareous sediments resting on the top of transitional lavas at Puerto Escondido. It has a porphyric texture with olivine, feldspars and brown clinopyroxene phenocrysts. The third one is a foid-monzogabbro (DB07-027) found as a boulder in a river bed. The boulder clearly proceeded from the intruded area in the Hoya area. It is composed of zoned plagioclase, K-feldspar, brown clinopyroxene, olivine and nepheline.

5.3.3. Geochemistry

5.3.3.1. Venado Unit

Analyzed samples from the Venado Unit are composed of transitional basalts and dolerite with MgO = 5.56-7.44 (Figures 5.3a, b). Recognition of a trend on major element diagrams is hard in reason of limited number of analyzed samples. However, we can observe on Figures 5a-f that the major element contents are chiefly similar to other accreted oceanic islands, such as the
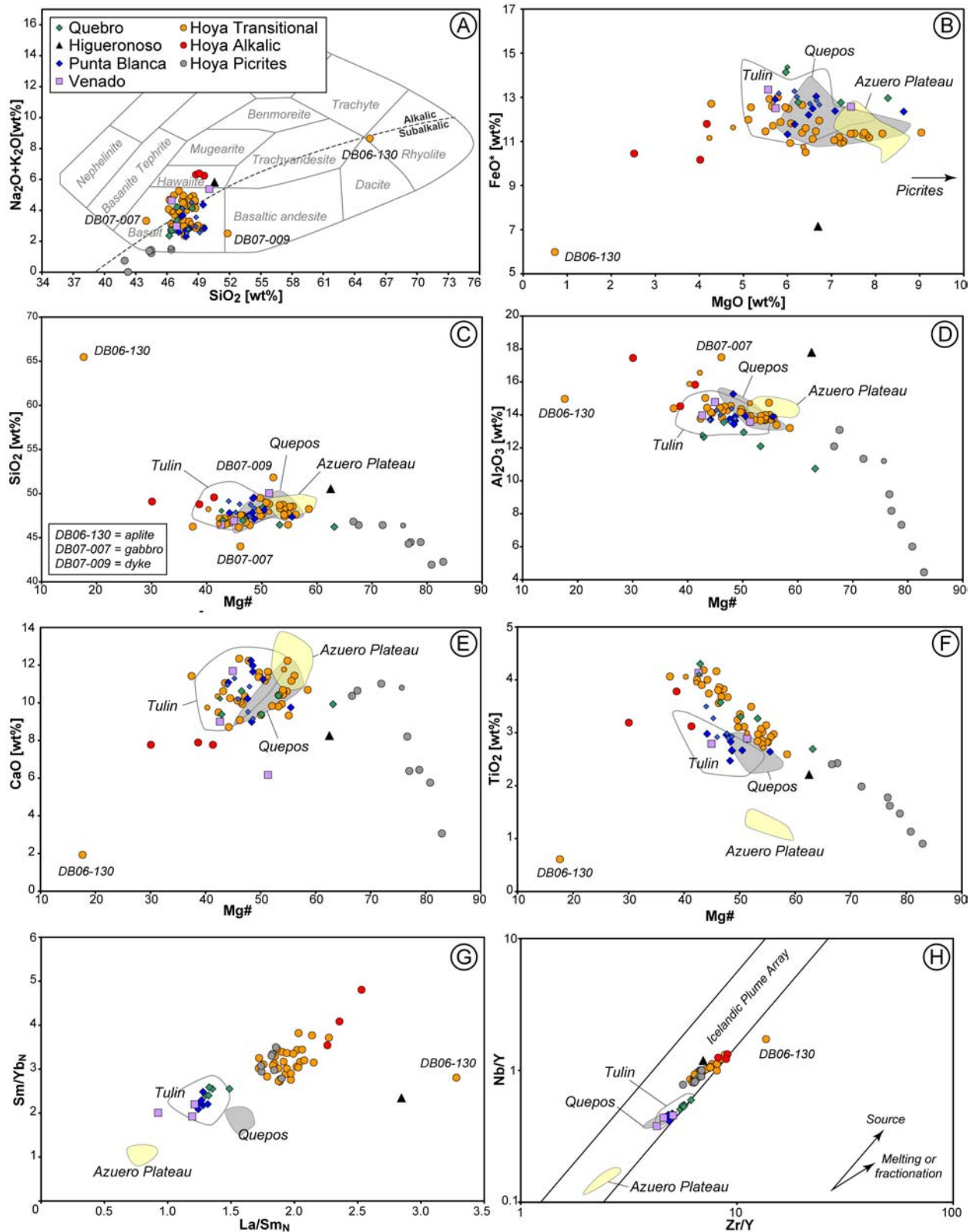
Figure 5.3: *Geochemistry of the igneous rocks from the Azuero Accretionary Complex. Small symbols are analyses from Hoernle et al. [2002]. Quepos = Accreted Oceanic Terrane (central Costa Rica) [Hauff et al., 2000]. Tulin = Tulin Formation, an accreted oceanic island in northern Costa Rica [Arias, 2003]. Azuero = Azuero Plateau (Chapter 2). **A)** TAS classification after Cox et al. [1979]. Alkalic-subalkalic subdivision after Irvine and Baragar [1971]. **G)** Primitive mantle normalized ratios, normalizing values after MacDonough and Sun (1995). **H)** Nb-Y/Zr-Y diagram and Icelandic Plume Array after Fitton et al. [1997].*
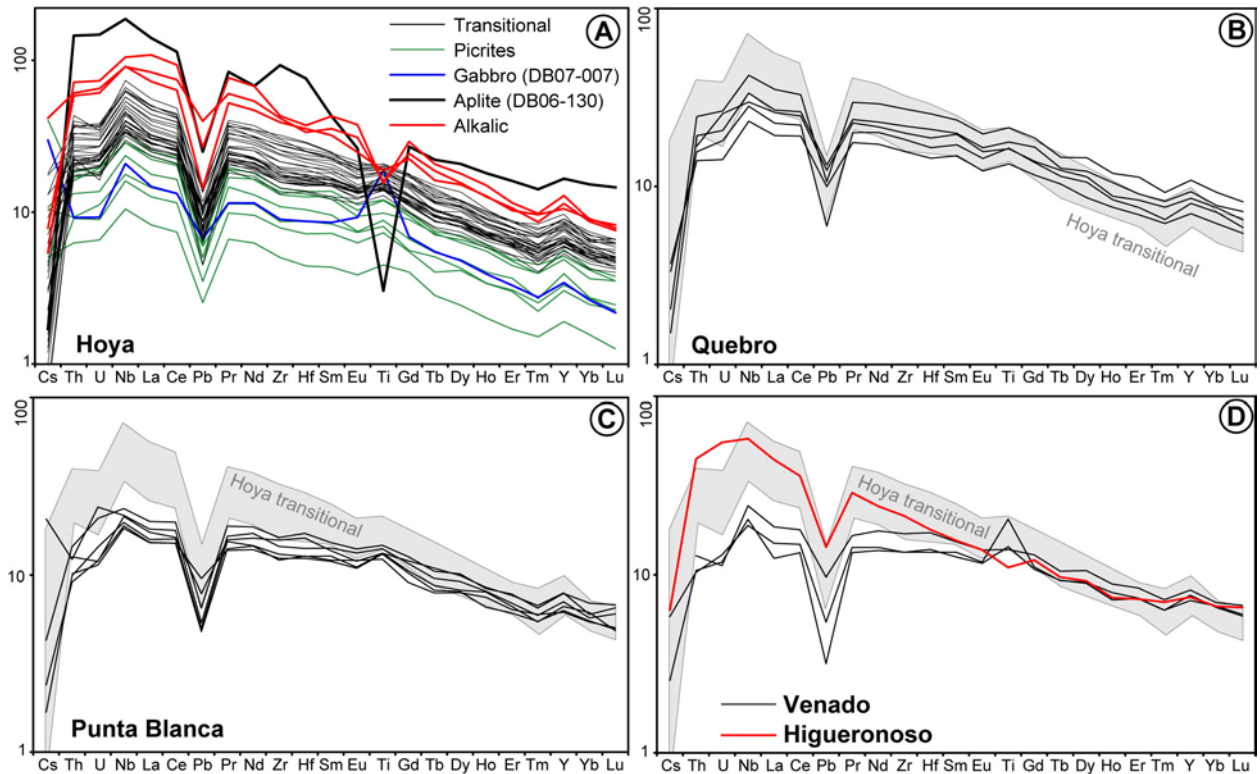
Figure 5.4: *Normalized multielement diagrams for the igneous rocks from the Azuero Accretionary Complex. Normalized on primitive mantle, normalizing values after MacDonough and Sun [1995]. **A)** Hoya Group. **B)** Quebro Group. **C)** Punta Blanca Group. **D)** Venado Unit and Higueronoso Group (Azuero Mélange).*

Tulín Formation (northern Costa Rica) [*Arias*, 2003] and the Quepos Accreted Oceanic Terrane (central Costa Rica) [*Hauff et al.*, 2000].

The Venado Unit is characterized by specific incompatible element contents illustrated on $(Sm/Yb)_N$-$(La/Sm)_N$ and Nb/Y-Zr/Y diagrams, which are broadly similar to the Punta Blanca Group (Figures 5.3g, h). The incompatible element contents are similar to typical oceanic intraplate basalts ("OIB") with a progressive enrichment from HREE to LREE contents and positive Nb and Ti and negative Pb anomalies on a primitive mantle-normalized multielement diagram (Figure 5.4d).

5.3.3.2. Azuero Mélange

One alkaline sample from the Azuero Mélange was analyzed and defines here the "Higueronoso Group". This sample has MgO = 6.69 wt% and, apart a low FeO* content, show strong similarities in terms of major and trace element with alkaline igneous rocks from the Hoya Group (Figures 5.3a-f, 5.4d). The incompatible element content is characterized by a strong enrichment in LREE relative to HREE and high $(La/Sm)_N$ (Figures 5.3g, 5.4d).

On a Nb/Y-Zr/Y diagram, the sample plots close to the Hoya alkaline igneous rocks in the Icelandic Plume Array (Figure 5.3h). Similarly to the Hoya alkaline rocks it is characterized by a moderate positive Nb and negative Pb and Ti anomalies on a normalized multielement diagram (Figure 5.4d).

5.3.3.3. Hoya Unit - Quebro Group

The Quebro Group consists of a consistent suite of transitional basalts. The term transitional is used here for a suite that (1) crosses over the alkalic-subalkalic subdivision after *Irvine and Baragar* [1971] in the TAS diagram (Figure 5.3a), (2) contains both nepheline-normative and hypersthene-normative samples in the CIPW norm and (3) is composed of samples devoid of feldspathoid.

The Quebro suite has MgO = 5.96-12.42 wt%. With lowering MgO, FeO* slightly increases from 12.76 to 14.14 wt% (Figure 5.3b). While Mg# lowers, SiO_2 slightly increases, Al_2O_3 and TiO_2 increases and CaO remains fairly constant (Figures 5.3c-f). On $(Sm/Yb)_N$-$(La/Sm)_N$ and Nb/Y-Zr/Y diagrams the group is similar to the Tulín Formation, Quepos terrane and Punta Blanca Group (Figures 5.3g, h). Apart of U, Th and Cs, the Quebro suite exhibit a progressive increase in the most incompatible elements on a normalized multielement diagram (Figure 5.4b), which is similar to typical OIBs. On the same diagram positive Nb and Ti and negative Pb anomalies are observed. Incompatible element patterns are less enriched in the most incompatible elements than the Hoya Group. They are similar to the Punta Blanca Group, but show higher general enrichment that is also indicated by higher TiO_2 at a given Mg# (Figures 5.3f, 5.4b).

5.3.3.4. Hoya Unit - Hoya Group

The Hoya Group is composed of picrites, transitional igneous rocks and alkali basalts and foid-monzogabbro. On a TAS diagram, the alkalic igneous rocks plot in the field of the hawaiites, whereas the transitional lavas essentially plot in the field of the basalts, with an aplite sample having a rhyolitic composition (Figure 5.3a). The picrites plot partly in the basalt field and out of the basalt field, toward lower Na_2O+K_2O and SiO_2 contents.

In terms of major element compositions the transitional igneous rocks are in the same array than the picrites (e.g. Figures 5.3b-f). These two groups of rocks share similar incompatible element ratios (e.g. Figures 5.3g, h) and are interlayered on the field. As a consequence they are considered here to represent a unique magmatic suite. The transitional igneous rocks have MgO = 0.72-9.04 wt%. From 9.04 to ~7 wt% MgO the FeO* content progressively diminishes, then increases until ~5 wt% MgO, then newly diminishes for lower MgO contents (Figure 5.3b). MgO-FeO* correlation is better for MgO > ~7 wt% than for lower MgO values. Picrites have a high MgO = 12.54-34.36 wt% that positively correlates with FeO* = 10.65-12.69 wt% (Appendix). With lowering Mg#: (1) SiO_2 increases in the picrites, lowers in the transitional basaltic rocks and newly increases in the most differentiated sample (Figure 5.3c), (2) Al_2O_3 strongly increases in the picrite, then moderately increases in the transitional basaltic rocks and aplite (Figure 5.3d), (3) CaO strongly increases in the picrites and slightly decreases in the less magnesian rocks, the aplite being strongly depleted (Figure 5.3e), and (4) TiO_2 progressively increases from the picritic to basaltic samples, the aplite being highly depleted (Figure 5.3f). On Figures 5.3a, c, d two samples show distinctive compositions. First one is a plagioclase-cumulative gabbro from the intruded Hoya area. Second one is a dyke from the same area.

As illustrated on $(Sm/Yb)_N$-$(La/Sm)_N$ and Nb/Y-Zr/Y diagrams (Figures 5.3g, h) and by normalized multielement patterns (Figure 5.4a) incompatible element contents of the picrites and transitional igneous rocks are similar. The aplite sample has higher $(La/Sm)_N$ than the transitional basalts and picrites and is endmember in the Hoya array defined on the Nb/Y-Zr/Y

diagram. Picrites have globally lower $(Sm/Yb)_N$, $(La/Sm)_N$ and Nb/Y-Zr/Y and have lower incompatible element contents than the basaltic samples (Figures 5.3g, h, 5.4a). On a normalized multielement diagram the Hoya transitional suite have OIB-like patterns with positive Nb and Ti and negative Pb anomalies (Figure 5.4a). The gabbro shows evidence for Ti-oxide and plagioclase accumulation (i.e. particularly high Ti-Nb contents and Eu positive anomaly). The aplite has the higher incompatible element contents. It exhibits negative Nb, Eu and Ti anomalies due to Fe-Ti oxides and plagioclase fractionation.

Alkalic igneous rocks from the Hoya Group have low MgO = 2.52-4.17 wt%. At a given Mg# these rocks have higher SiO_2 and Al_2O_3 and lower CaO and TiO_2 contents than the transitional igneous rocks and picrites. $(Sm/Yb)_N$ and $(La/Sm)_N$ are slightly higher for the alkalic rocks than for the transitional suite, but still within a similar range of composition (Figure 5.3g). On a Nb/Y-Zr/Y diagram the alkalic rocks are within the array defines by the transitional suite, in the most enriched terms (Figure 5.3h). On a normalized multielement diagram the alkalic rocks exhibit similar patterns than the transitional suite, with higher incompatible element contents and a Ti negative anomaly.

5.3.3.5. *Hoya Unit - Punta Blanca Group*

The Punta Blanc Group is composed of a transitional suite that plots in the basalt field on a TAS diagram (Figure 5.3a). The igneous rocks have MgO = 5.72-8.64 wt%. FeO content at a given MgO is slightly higher than the Hoya transitional suite or Quebro Group. With decreasing Mg# SiO_2, Al_2O_3 and CaO remains chiefly constant, TiO_2 increases. The Punta Blanca transitional suite differs from the Quebro and Hoya transitional suites by lower TiO_2 content at a given Mg#. Incompatible element contents of the Punta Blanca transitional suite are very similar to the Quebro transitional suite (Figures 5.3g, h, 5.4c). The Punta Blanca group has however lower incompatible element contents at a given Mg# (Figures 5.3f, 5.4c).

5.4. Origin of the Azuero Mélange

The Azuero Mélange is composed of deformed rock bodies that proceeded from the Azuero Plateau (arc basement) and oceanic rocks comprising OIB-like lavas and associated sediments. Hence, we propose that the Azuero Mélange originally formed by accretion of several seamount fragments. Deformation associated to subduction processes and/or strike-slip motion along the Sona-Azuero Fault Zone resulted in tectonic incorporation of lenses of the Azuero Plateau into the mélange. Strong deformation of the plateau close to the mélange is well illustrated along coastal exposures close to Punta Duartes. In this view, the Azuero Mélange may be considered to have formed in the vicinity of the décollement zone and represents a fossil subduction zone.

The nature and mode of deformation of the accreted material found in the Azuero Mélange is very similar to the Vaquedano Unit in the Osa Igneous Complex (southern Costa Rica), which is believed to have been emplaced along the margin in a relatively short period of low-rate accretion (Chapter 3). In absence of ages for the accreted sediments, accretion age of the exotic material of the Azuero Mélange may appear difficult to estimate because, in absolute, possible accretion ages are bounded by the Campanian age of subduction initiation along the southern Central American margin (Chapter 2) and the middle Eocene age of accretion of the

Hoya Unit (see below). However, we note that the late Cretaceous-middle Eocene volcanic front is located very close to the Azuero Mélange (Figure 5.1). This shows clearly that removal of the edge of the Azuero Plateau by subduction processes (i.e. tectonic erosion) occurred after/during the migration of the volcanic front in the middle Eocene and prior to the emplacement of the Hoya Unit in the middle Eocene. As a consequence, it is necessary that the exotic material of the Azuero Mélange accreted in the middle Eocene, shortly before the emplacement of the Hoya Unit. Hence, similarly to the Vaquedano Unit, accretion of the exotic material found in the Azuero Mélange occurred during a relatively short period of time in the middle Eocene.

5.5. Origins of the Azuero Accretionary Complex

5.5.1. Venado Unit

The Venado Unit is composed of transitional lavas and intrusives rocks devoid of large amount of sediments. The geochemistry of the igneous rocks shows OIB-like affinities and points toward an intraplate oceanic origin. Plateau-related igneous rocks crosscutting or intercalated within the Venado Unit have not been observed. Pelagic sedimentary layers have not been found. That points toward an exotic origin for the Venado Unit and we proposed it is composed of one or several accreted fragments of seamount/oceanic island that lost their summital sedimentary layers before the accretion. Ages of formation and accretion of the basalts forming this unit remain to be determined.

5.5.2. Hoya Unit

The Hoya Unit is mostly composed of submarine and subaerial lava flows with OIB-like affinities and characterized by a consistent stratigraphic arrangement. Three groups of igneous rocks have been recognized on the basis of immobile incompatible element contents showing a good spatial arrangement (Figure 5.1). The rocks are globally very well-preserved and have not exceeded a zeolite metamorphic facies. These observations suggest that the Hoya Unit is composed of intraplate oceanic volcanoes accreted along the Azuero Plateau at shallow levels.

The age of formation of the volcanoes has been constrained by $^{40}Ar/^{39}Ar$ between ~66 and ~21 Ma [*Hoernle et al.*, 2002]. However, these ages are locally in disagreement with shallow-water and hemipelagic sediments interlayered in the volcanic sequences that provided Paleocene-early Eocene (66-49 Ma) biochronologic ages [*Baumgartner-Mora et al.*, 2008]. It may be argued that the Hoya Unit is a highly heterogeneous accretionary complex. Our results are at odd with this interpretation. After revising $^{40}Ar/^{39}Ar$ step heating ages by *Hoernle et al.* [2002] it appeared that most of them do not exhibit an unequivocal plateau age and are rather difficult to interpret. Only two samples collected *in situ* by *Hoernle et al.* [2002] have good plateau ages at 53±1 and 53±1 Ma (G46 and AZ-103-2, respectively). These samples pertain to the Hoya Group and are in good agreement with the biochronologic dates from the surrounding sediments. Hence, an early Eocene age of formation is proposed for the accreted oceanic island forming the Hoya Unit. The age of accretion is defined by the age of the overlap sequences deposited on the top of the accreted material. In the case of the Hoya Unit the age of accretion is therefore defined by the Lower Tonosi Formation to the middle Eocene [*Kolarsky et al.*, 1995b; *Baumgartner-Mora et al.*, 2008].

The igneous rocks from the Quebro and Hoya groups are locally interlayered on the field, clearly indicating that they are part of a same accreted oceanic island named here the "Hoya Oceanic Island". This is further strengthened by similar radiogenic isotope ratios between these groups (Figure 4.5). On the other hand, interlayering between the Hoya and Punta Blanca groups has not been observed. Furthermore, the Lower Tonosi Formation resting on the top of the Hoya Oceanic Island is composed of hemipelagic limestones, whereas the same formation resting upon the Punta Blanca Group is composed of shallow-water limestones. This points toward a distinct accretionary history for the two areas and, thus, likely indicates origins at distinct islands. In this view the Hoya Unit formed in the middle Eocene by accretions of two volcanic edifices, the Hoya Oceanic Island and the Punta Blanca Oceanic Island. Geochemical similarities between the Hoya and Punta Blanca groups point toward an origin at a same hotspot, presumably the paleo-Galapagos Hotspot [*Hoernle et al.*, 2002, Figure 4.5].

5.6. The Hoya Oceanic Island

The Hoya Oceanic Island is exposed in an area of >800 km^2 and composed of unmetamorphosed rocks. Highest peaks of the area reach an altitude of 1500 m, which implies that the island has been strongly dissected, providing an access to some of its deeper parts. Indeed, this unusual on-land occurrence of an accreted oceanic island provides an exceptional opportunity to corroborate and better constrain models generally proposed for the development of intraplate oceanic islands [e.g. *Clague and Dalrymple*, 1987].

5.6.1. Stratigraphy of an oceanic island

The rocks forming the Hoya Oceanic Island have been subdivided into five mapable dominant lithologies: (1) submarine lava flows interbedded with minor volumes sediments, (2) submarine lavas devoid of significant amount of interlayered sediments, (3) clastic sediments composed of basalt clasts, (4) subaerial lava flows, and (5) intrusive rocks and altered lavas/sediments (Figure 5.2). The spatial arrangement of these lithologies is well organized and stratigraphic relationships define a transition from the submarine lavas to the clastic sediments and subaerial lavas. We interpret this arrangement as a record of the development of the Hoya Oceanic Island, from submarine-shield to subaerial-shield phases (Figure 5.5). The area dominated by intrusive rocks represents the eruptive center of the Hoya Group. Shoaling of the oceanic island have been recorded by (1) formation of the clastic sediments produced by brecciation of lava flows by gravitational collapse and (2) deposition of shallow-water carbonates and occurrences of well-rounded basaltic pebbles. Shallow-water occurrences are located around the Hoya Group eruptive center (Figure 5.2.), which nicely reflects spatial distribution of coastal lines around the highest point of an oceanic volcano, called here the "Hoya Volcano".

Alkalic lavas from the Hoya Group have been encountered in shallow-water environments. First occurrence is a rounded cobble from coastal sediments interlayered with shallow-water limestones and transitional lava flows at Puerto Escondido (Figure 5.2). Second occurrence is an alkalic lava flow interbedded with shallow-water limestones, ~6 km inland from Puerto Escondido. These occurrences show that (1) the transitional and alkalic series of the Hoya Group coexisted in time and that (2) the alkalic lavas were emplaced in the latest stages of evolution of the oceanic island, under subaerial and/or drowning conditions. The alkalic lavas are
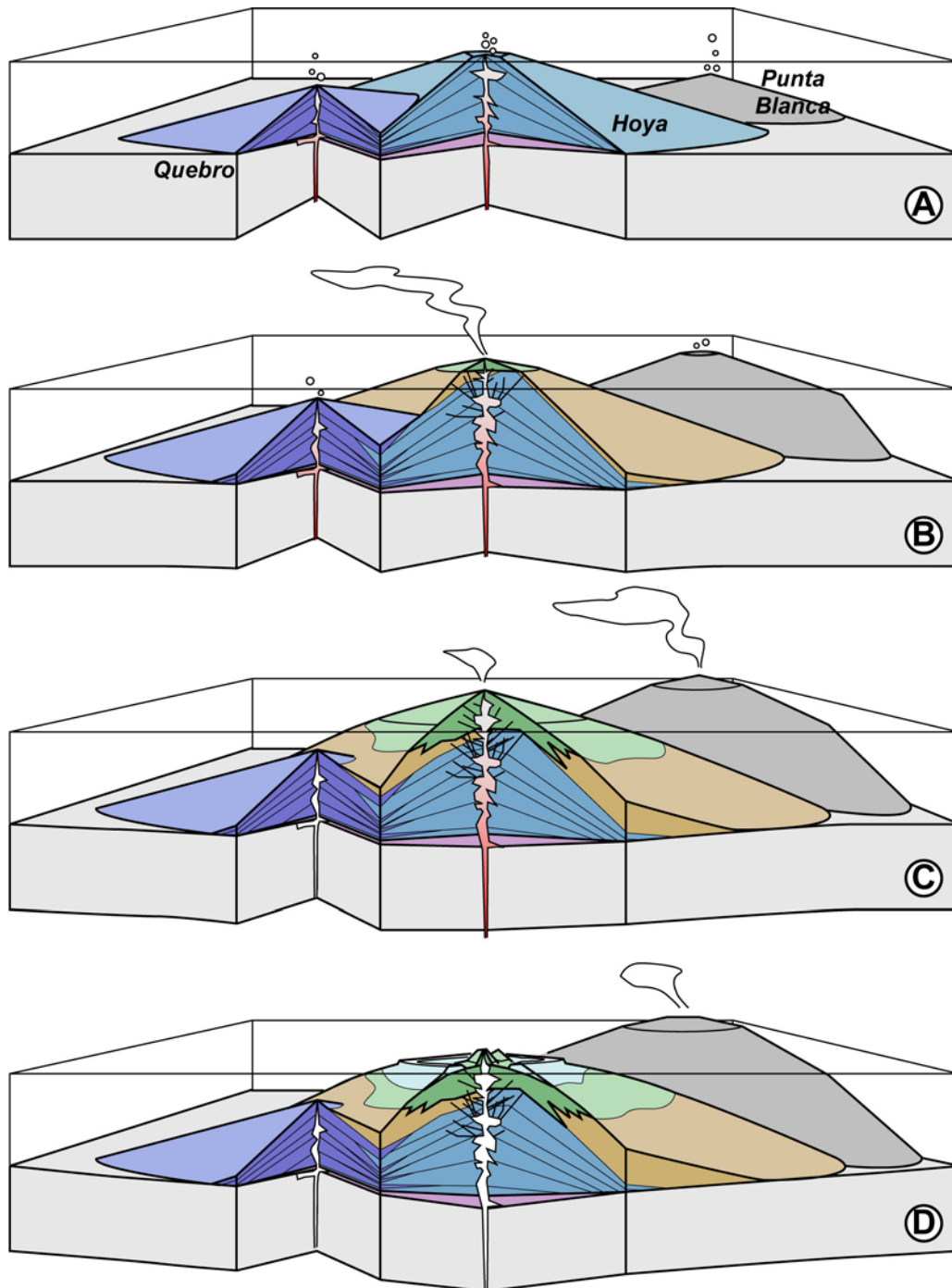
Oceanic island development - Lithologies

Pre-shield stage

Alkalic lavas (not exposed)

Shield stage - submarine

Submarine transitional lavas, predominantly basalt sheet flows (Hoya Group)

Submarine transitionaly lavas and interlayered hemipelagic sediments (Quebro Group)

Shield stage - shoaling and subaerial

Clastic sedimentary apron (Hoya Group)

Predominantly subaerial transitional lavas, minor volumes of shallow-water carbonates (Hoya Group)

Post-shield stage - Atoll

Shallow-water limestones deposited during and after alkalic magmatism

Figure 5.5 (previous page): Development of the Hoya Oceanic Island (partly modified after Clague and Dalrymple [1987] and Garcia et al. [2007]). A) Submarine shield stage, dominated by transitional lavas from the Quebro and Hoya Groups. B) Shoaling of the Hoya Volcano and vanishing of the Quebro Volcano. The shoaling leads to deposition of clastic sediments on the flanks of the Hoya and Quebro volcanoes and ash fall deposits on the Quebro seamount. C) Subaerial development of the Hoya Volcano and vanishing of the magmatism. Transition to the post-shield stage. D) Atoll stage. The Hoya Oceanic Island becomes eroded and subsides, allowing deposition of reefal limestones.

associated here to the post-shield stage of the oceanic island, characterized by the vanishing of the magmatism and progressive erosion and subsidence of the volcano(es) [e.g. *Clague and Dalrymple*, 1987].

The lava flows of the Quebro Group were emplaced in submarine conditions. Frequent intercalation of hemipelagic sediments devoid of shallow-water material within the volcanic sequences indicate that the "Quebro volcano" remained under submarine conditions during its entire development or that subaerial stages have not been preserved. Picrites from the Hoya Group are interlayered with the Quebro lavas indicating that they were produced at the same time. We interpret the Quebro Group as a small submarine volcano initially located close to the Hoya Volcano (Figure 5.5). Eruptions leading to formation of the Quebro Group were less frequent than for the Hoya Group, which led to intercalation of sedimentary layers. This is also illustrated by frequent mineral zoning, larger crystals and mingling textures produced in a less dynamic magmatic system. Ash deposits found in interlayered sediments from the Quebro Group may have been produced at the Hoya Volcano, by hydro-explosion during shoaling of the volcano.

After the post-shield stage, oceanic islands commonly move away from the hotspot and the volcanism vanishes out, the volcanic edifices become progressively eroded and start to subside. This phase is generally associated to growth of an atoll on the top of the ancient volcanoes [e.g. *Clague and Dalrymple*, 1987; *Langenheim and Clague*, 1987] (Figure 5.5d). The atoll development may subsist for a long time under favorable tectonic and eustatic conditions. The island will definitely get drown when the reef growth cannot compensate anymore the subsidence of the volcano and/or sea level rises. In the Hoya Unit thick reefal deposits have not been observed. This may be due to collapse of the atoll (1) in the ocean by large landsliding on the flank of the volcano [e.g. *Moore et al.*, 1995], (2) in the vicinity of the trench in response to slab flexuration [e.g. *Kobayashi et al.*, 1987; *Sano and Kanmera*, 1991], and/or (3) by erosion during uplift of the accreted island. Large limestones blocks (up to several tens of meters in length) observed at Punta Restingue may have initially been emplaced on the top of the volcanic sequences and possibly represent a remnant of the atoll. Large boulders of reefal limestones embedded in the Lower Tonosi Formation at Punta Restingue and Covachón are now embedded in the hemipelagic lower Tonosi Formation, indicating that they have been reworked during or shortly after the accretion of the oceanic island (Figure 5.8).

In the accreted Hoya Oceanic Island the thickness of exposed structures is difficult to estimate. A minimal value is provided by the altitude of the highest mountains that reaches 1.5 km. Today at the Galapagos Hotspot the tallest volcano is ~1700 m above the sea level (volcan Wolf), with a summit distant ~10 km from the ocean. These values are broadly similar with the stratigraphy of the Hoya Oceanic Island (Figure 5.2). Seismic structure of Cocos and Carnegie aseismic ridges, which are composed of drown oceanic islands produced at the Galapagos Hotspot, indicates crustal thickness over ~13 km in their central part [e.g. *Walther et al.*, 2002;
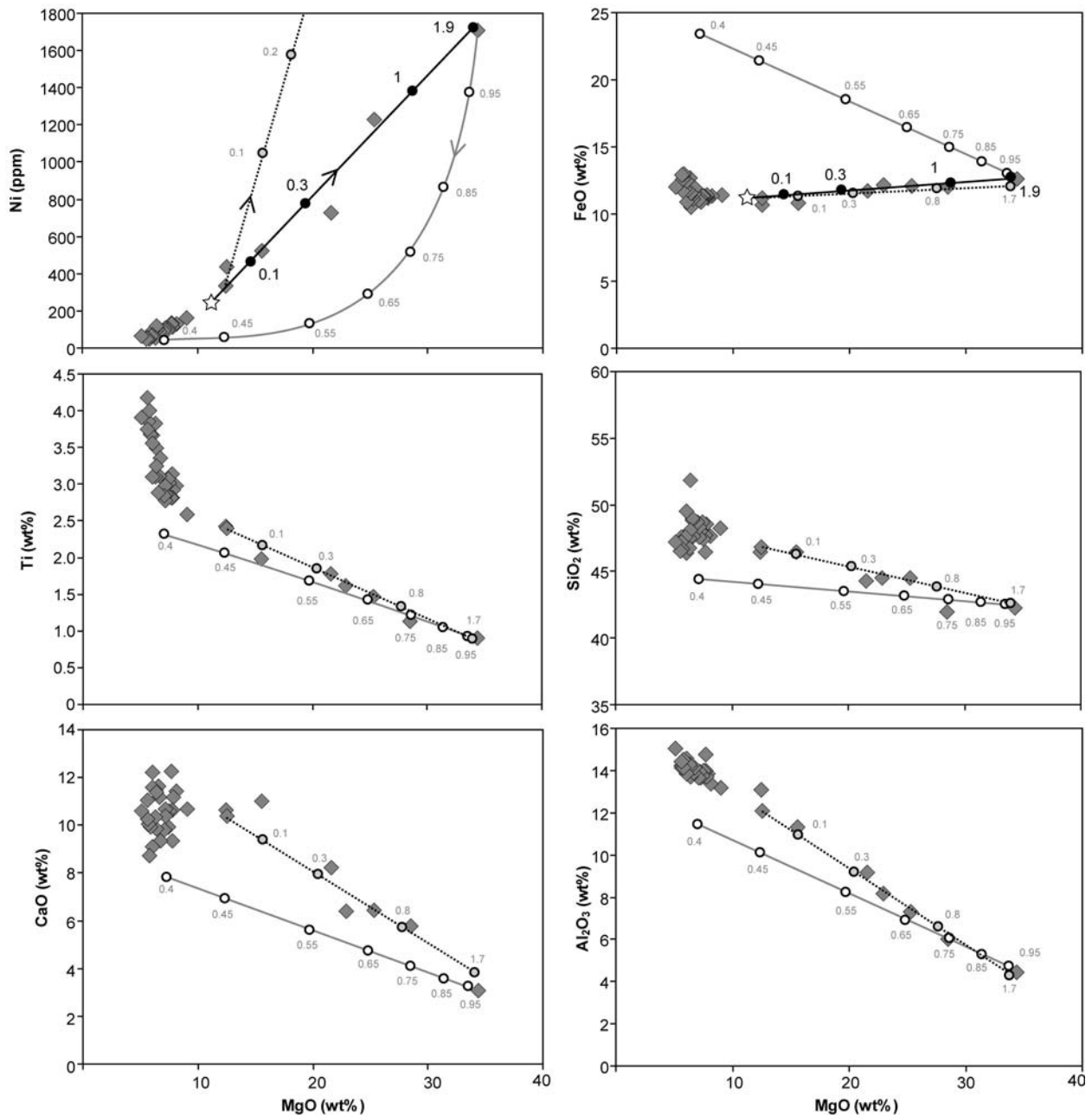
Figure 5.6: *Calculated compositions of picritic liquids obtained by: (1) fractionating olivine from the most magnesian picrite, using a Rayleigh fractionation equation (grey line), (2) accumulating olivine from the less magnesian picrite (dashed line), and (3) accumulating olivine from a theoretical liquid (solid black line for Ni and FeO*, dashed line for TiO₂, SiO₂, CaO and Al₂O₃). Olivine/Melt Fe/Mg KD = 0.3. D^{olivine/liquid} Ni after Kinzler et al. [1990]. Model (3) provides the best estimate in terms of compatible and incompatible element contents.*

Sallares et al., 2005]. This indicates that the thickness of the exposed structures of the Hoya Oceanic Island may exceed by far 1.5 km. Due to truncation of the Hoya Volcanic Island by erosion and occurrence of exposures over a large area, different levels of the edifice are laterally juxtaposed as indicated by our mapping (Figure 5.2). Whether this is a pure effect of lateral variations of the lithologies in a relatively undeformed, strongly truncated oceanic island or an effect of differential block uplifts is difficult to sort out. However, it seems that both processes occurred, resulting in exposure of volcanic sequences originally located several km under the top

of the island. This hypothesis is in agreement with the geochemistry of the transitional lavas (see below).

5.6.2. The Hoya transitional magmatic suite

The Hoya Group is composed of picrites, transitional and alkalic igneous rocks. In this section we interpret the origin of the picrite and further describe the magmatic evolution of the Hoya transitional suite along with stratigraphic constraints.

5.6.2.1. Picritic lavas

The picritic lavas exhibit an olivine porphyric texture. Olivine phenocrysts may exhitbit oscillatory zoning, rounding and resorbtions. This texture tends to indicate that the picrites have been produced by accumulation of olivine in basaltic melts. To test this hypothesis, we performed several calculations simulating addition and removal of olivine from picritic melts defined by our samples. Following models were tested, using $D^{olivine/liquid}$ Ni from *Kinzler et al.* [1990] [$\ln(D_{Ni}^{Ol/Liq}/x_{Fo}^{Ol}) = 0.355 - 1.263 \ln \ln(x_{MgO}^{Liq})$] and $D_{Fe/Mg}^{Ol/Liq} = 0.3$ [*Roeder and Emslie*, 1970]:

1) Olivine removal from the most magnesian picritic sample (DB06-089), using a Rayleigh fractionation model (Figure 5.6).

2) Olivine removal from the most magnesian picritic sample (DB06-089), using an equilibrium fractionation model.

3) Olivine addition from the less magnesian picritic sample (DB07-014) (Figure 5.6).

4) Olivine addition from the most magnesian transitional basalt (DB06-134).

5) Olivine addition from a theoretical liquid intermediate between DB07-014 and DB06-134, with MgO = 10.5 wt%, Ni = 250 ppm and Mg# = 65 (Figure 5.6).

Models (1) and (2) failed in accounting for the major element and Ni contents. Best result was obtained for the model (5). This shows that the picrites are produced by olivine accumulation in liquids with Mg# < 70. Hence it seems that the picrites formed by ponding in superficial layers of the lithosphere, presumably in a magma chamber alimented by non-primitive melts. These melts were generated by fractionation of olivine from a primitive liquid (i.e. with Mg# ~ 70). Picritic lavas occur in both submarine and subaerial layers of the oceanic island (Figure 5.2), indicating that olivine accumulation has been present during a relatively long period of time during the development of the volcano. The transitional basalts likely constitute a liquid line of descent from the theoretical melt with Mg#=65 (Figure 5.3). Interestingly we can observe on Figure 5.3 that Mg# = 65 defines a limit of an apparent compositional gap between Mg# = 65 and 59. It is possible that this gap reflects eruptive dynamics of the Hoya Volcano and should be further investigated in forthcoming studies.

5.6.2.2. Evolution of the magma genesis during the island development

Mg# of the transitional lava flows from the Hoya Group correlate remarkably well with the stratigraphy of the Hoya Unit, providing another support for the presence of an accreted oceanic island in the Azuero Peninsula (Figure 5.2). Flows with high Mg# are preferentially found in the deepest, submarine parts of the edifice. This is evidence for an evolution of the lava
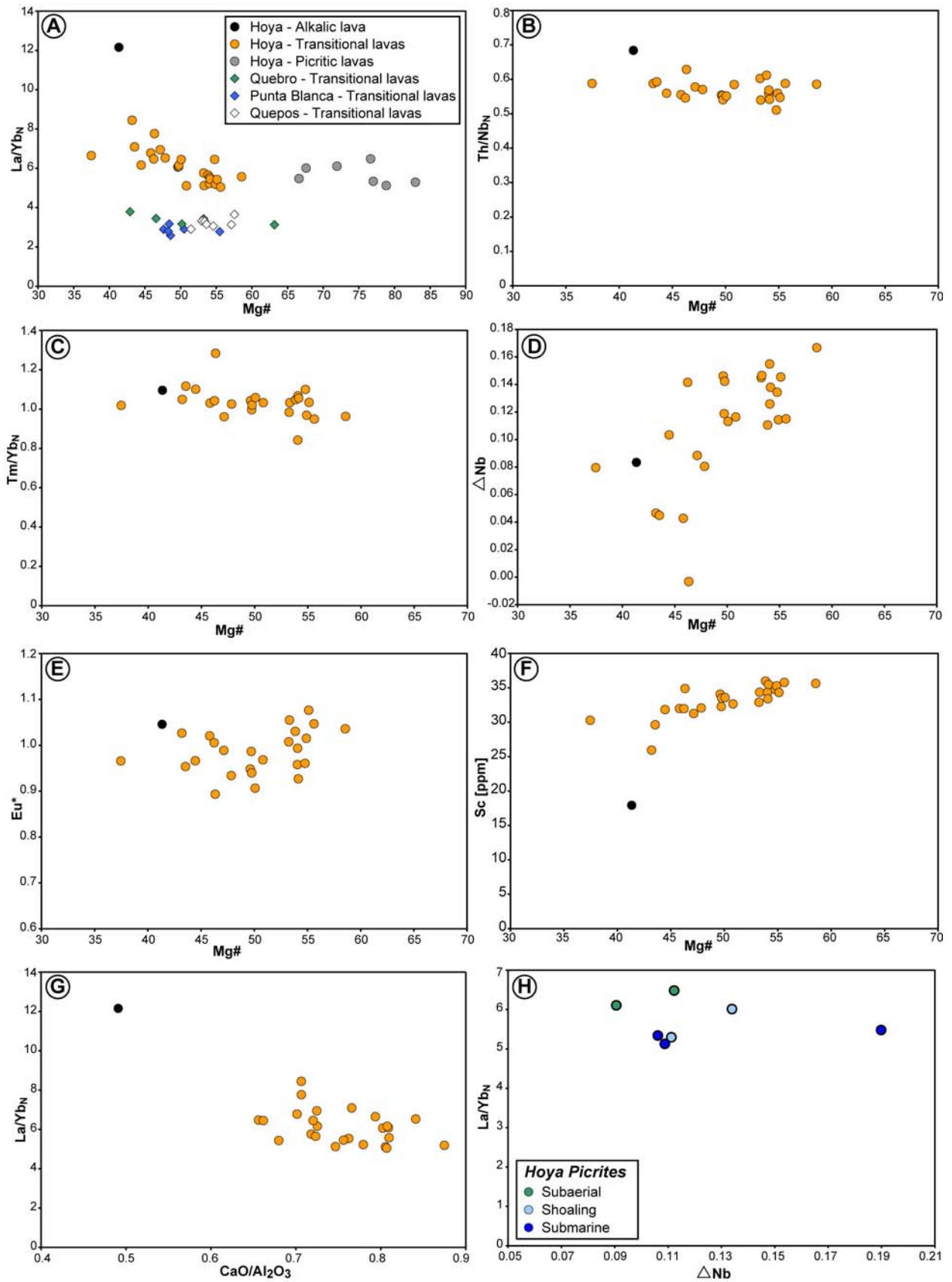
Figure 5.7: *Geochemistry of the lava flows from the Hoya Group (also represented on Figure 5.2). Transitional lavas of Quepos are from Hauff et al. [2000]. Primitive mantle used for normalizing values is from Mac Donough and Sun [1995]. ΔNb = 1.7 + log(Nb/Y) - 1.92 log (Zr/Y) after Fitton et al. [1997].*

chemistry through time, with hottest (less fractionated) magmas erupted during the submarine shield stage of the volcano and coolest (more fractionated) magmas erupted during the final stage of volcanic development.

Typical order of mineral appearance and fractionation in cooling transitional-tholeiitic liquids of ocean islands is: (1) olivine ± spinel, (2) clinopyroxene, (3) plagioclase and (4) Fe-phases such as ilmenite, which is probably due to crystallization at high depth and pressure [e.g. *Villiger et al.*, 2004; 2007]. Recognition of the possible roles of fractionating minerals is important to interpret compositional variations associated to changes of the Mg#. Composition of the Hoya picrites illustrates the predominant role of olivine in the most magnesian liquids. Fractionation of clinopyroxene between Mg# = 59 and 37 is well illustrated by constant decrease of the Sc content (Figure 5.7f), which is in agreement with occurrence of clinopyroxene phenocrysts in the most magnesian basalts. Plagioclase fractionation is more difficult to constrain. On a Eu*-Mg# diagram (Eu* = $Eu_N/[(Sm_N+Gd_N)/2]$) we observe an increase in the Eu negative anomaly from Mg# = 59 to 52, and then a decrease for lower Mg#, which is opposite to expected Eu behavior, normally controlled by plagioclase fractionation (Figures 5.7e, 5.4a). Interestingly, a compositional gap correlates to the inflexion of Eu* at Mg# ≈ 52 or MgO ≈ 7 wt% (Figures 5.3, 5.7). We note that among 11 lava samples with Mg# > 52 one contains plagioclase phenocrysts, whereas among 15 lava samples with Mg# < 52 10 contain plagioclase phenocrysts. It seems thus that the changes observed in terms of Eu* and the compositional gap at Mg# ≈ 52 is controlled by onset of plagioclase crystallization. The increase of Eu content at Mg# ≈ 52 may be due to buffering of Eu by plagioclase, limiting the effect of fractionation by clinopyroxene. Analyses of mineral compositions are nonetheless needed to better understand processes of mineral fractionation and Eu content evolution. In the basaltic lavas SiO_2 diminishes and TiO_2 increases with lowering Mg#, indicating that Fe-phases did not play a significant role in the liquid line of descent at Mg# > 35 (Figure 5.3c).

We observe on Figure 5.7a that the evolution of the transitional basalt flows exhibit an inverse correlation between Mg# and La/Yb_N, indicating that the lavas erupted during the last stages of volcanism were significantly enriched in highly incompatible elements (i.e. LREE or La) relative to the early transitional lavas. We further observe on Figure 5.7a that the Hoya picrites may exhibit a similar tendency that is much less expressed. Correlation between Mg# and La/Yb_N is poor or absent in the transitional series from the Quebro Group, Punta Blanca Group and Quepos accreted oceanic island, indicating the Hoya compositional trend tends to be unusual among oceanic islands. The Mg# - La/Yb_N correlation for the Hoya transitional basalts may be due to (1) clinopyroxene fractionation and progressive depletion of HREE relative to LREE toward the more evolved basalts, and/or (2) evolution of the magma genesis through time, both hypotheses being correlated with a decreasing temperature in the last erupted magmas.

The incompatible element contents of the Hoya transitional basalt flows are characterized by an increase of Tm/Yb_N with lowering Mg#. Since Tm/Yb_N is relatively insensitive to clinopyroxene fractionation (see Figure 2.6 for an illustration of typical composition of clinopyroxenes) the increase in Tm/Yb_N ratio in the younger, most evolved lavas probably reflect variable degrees of melting of a source containing residual garnet. Hence, the tendency defined by the Tm/Yb_N ratio indicates lesser amount of melting in the younger rocks. This may be interpreted as a result of the progressive migration of the oceanic island out of the influence of the melting region or hotspot. Variations of melting should affect as well other incompatible element ratios such as La/Yb_N. Indeed, submarine, older picrites have lower La/Yb_N than subaerial, younger picrites variations (Figure 5.7h). Since the composition of the picrites is not

Lithologies

Alkalic lavas (pre-shield stage)

Transitional lavas (predominantly sheet flows, shield stage)

Transitional lavas and interlayered sediments (shield stage)

Sedimentatry apron (shoaling)

Subaerial transitional and alkalic lavas (shield and post-shield stages)

Shallow-water limestones (atoll stage)

Detrital deposits, products of seamount dismemberment

Hemipelagic-detrital deposits, produced by arc and seamounts erosion (Tonosi Fm)

Figure 5.8 (previous page): *Model of accretion for the Hoya Oceanic Island. **A)** Early Ecoene to middle Eocene: atoll stage of the island, prior to drowning (following Figure 5.5d). **B)** Middle Eocene: partial dismemberment of the drown oceanic island on the forebulge, removal of important portions of the atoll deposits. The volcanic front has migrated landward and the Azuero Mélange formed. **C)** Middle Eocene: accretion of the island by "docking" at very shallow level. Red line represents the developing décollement zone from the subaerial lavas-clastic apron interface (white star). The hemipelagic Tonosi Formation is deposited. **D)** Middle Eocene: incoming of the Quebro seamount in the subduction zone. **E)** Middle Eocene: accretion of the Quebro Group and possibly underplating of other seamounts leads to uplift of the area and deposition of the shallow-water Lower Tonosi Formation.*

controlled by clinopyroxene fractionation but by olivine accumulation alone (see above) these observations confirm lesser extents of source melting in the latest stages of the island evolution. Strong La/Yb$_N$ variations observed for the transitional basalt flows but not for the picrites is likely an effect of clinopyroxene fractionation overprinting the effect of diminishing degree of source melting for the transitional basalts (Figure 5.7a). Isotope and clinopyroxene analyses should be performed to test this interpretation.

ΔNb is a geochemical parameter introduced by *Fitton et al.* [1997] to quantify the deviation of a sample from the bottom line of the Icelandic Plume Array illustrated on Figure 5.3h (ΔNb = 1.7 + log(Nb/Y) - 1.92 log (Zr/Y)). A positive ΔNb value indicates that the sample is within the Icelandic Plume Array. In the transitional basalt flows, we observe that ΔNb lowers and Th/Nb$_N$ increases with lowering Mg# (Figures 5.7b, d). Picrites emplaced under submarine conditions have higher ΔNb than picrites emplaced in subaerial conditions (Figure 5.7h). The pricrites have globally lower ΔNb than the transitional basalts (Figure 5.3h). Similarly to La/Yb$_N$ and Tm/Yb$_N$ vs Mg# trends, all these observations can be explain by lower degree of melting of the source and slightly higher fractionation of Fe-Ti oxides preferentially incorporating Nb in the youngest lavas. Once again, a more precise petrologic study may test this interpretation.

Alkalic igneous rocks of the Hoya Group have very high incompatible element contents and ratios that frequently define endmembers in the Hoya transitional array (Figures 5.3, 5.7). Allkalic igneous rocks from the Hawaii Scientific Drilling Program 2 in the Mauna Kea show similar tendencies [*Huang and Frey*, 2003; *Rhodes and Vollinger*, 2004; *Stolper et al.*, 2004]. In the case of the Mauna Kea it has been shown that migration of the island out of the hotspot led to transition from tholeiitic to alkalic basalts. It is possible that a similar process occurred in the Hoya Oceanic Island and may be tested in forthcoming studies by increasing number of analysed alkalic rocks.

5.6.3. Accretion of the oceanic island

Accreted oceanic islands and seamounts have been recognized along many ancient subduction zones in orogenic belts or active convergent margins [e.g. *Isosaki et al.*, 1990; *Bagheri and Stampfli*, 2008; *Dickinson*, 2008]. Generally the accreted oceanic material suffered from metamorphism in the greenschist and higher facies and underwent a strong deformation. More rarely the accreted material remained relatively unmetamorphosed, but underwent severe dismemberment during the accretion [e.g. *Doubleday et al.*, 1994a, b]. Accreted seamounts in southern Costa Rica remained relatively well-preserved and, therefore, appear to be relatively unusual accreted terranes (Chapters 3, 4). The Hoya Oceanic Island is exceptionally well-

preserved, provides an access to deep parts of volcanic structures and offers a unique possibility to study the stratigraphic and magmatic evolution of an oceanic island. To explain the particularity of the Hoya Oceanic Island an unusual model of accretion seems to be required.

In the literature three general modes of accretion of oceanic igneous sequences have been proposed: (1) tectonic disruption of subducting edifices during the subduction and block/sliver incorporation into accretionary prism or mélanges by offscraping or underplating [e.g. *Maruyama and Liou*, 1989; *Kimura and Mukai*, 1991; *Okamura*, 1991; *Georges*, 1993; *Jones et al.*, 1993; *Ikesawa et al.*, 2005], (2) oceanic crust peeling resulting in repeated incorporation of slices in the accretionary complex by duplexing [e.g. *Cawood*, 1982; *Kimura and Luden*, 1995; *Hashimoto and Kimura*, 1999; *Ikesawa et al.*, 2005], and (3) fragmentation of incoming seamounts in the vicinity of the trench and later incorporation of the fragmented material into accretionary complexes [e.g. *Sano and Kanmera*, 1991]. In southern Costa Rica imbrication of several fragments of seamounts likely occurred by duplexing at shallow level, resulting in relatively poor deformation of the accreted material (Chapter 3). We propose that the Hoya Oceanic Island accreted through a new mode of accretion named herein "docking", i.e. frontal incorporation of the volcanic edifice to the margin (Figure 5.8).

Docking of the Hoya Oceanic Island likely occurred in response to three parameters: (1) slab flattening occurring shortly before the incoming of the oceanic island [*Lissinna et al.*, 2002], (2) the oceanic island encountered a margin devoid of thick piles of accreted sediments and principally composed of an oceanic plateau, and (3) the Hoya Oceanic Island represented a very high topographic heterogeneity on the incoming ocean floor. Combination of these three parameters led to an unusually strong coupling between the incoming oceanic island and the overriding plate that allowed detachment of the island in the trench (Figure 5.8c). The hemipelagic lower Tonosi Formation consists of a typical forearc deposit deposited upon the drown island that recorded this event.

The detachment of the Hoya Oceanic Island from the subducting plate may have occurred in two ways: (1) by décollement formation at the interface between the oceanic crust and the oceanic island, following ancient pelagic sedimentary covers at the base of the intraplate volcanoes [*Lallemand*, oral communication, 2007], or by (2) fault propagation through the oceanic island. Even if sediments at the base of oceanic islands may enhance formation of a basal décollement, it should be reminded that intraplate volcanoes are "anchored" to the lithosphere by intrusive rocks. Hence, first hypothesis would be possible if volcanic edifices behave as a very strong structure in the subduction zone. Seismic results from the Nankai Trough show that subduction at shallow depth tends to develop shear failure in the seaward side of subducting volcanoes in response to high deviatoric stress [*Kodaira et al.*, 2000; *Baba et al.*, 2001] (Figure 5.9). This suggests that, at shallow depths, fault nucleation can develop at relatively high levels within subducting volcanoes. Indeed, our results from southern Costa Rica (Chapter 3) are in good agreement with this model. This highlights the fact that seamounts may not be particularly behaved as a "strong" structure in the subduction zone and suggests that the docking of the Hoya Island most probably occurred by fault propagation within the structure of the volcanoes. Occurrence of clastic sediments in the volcanic structure may have provided the weakness required to nucleate a shear zone in the seaward side of the volcanic edifice (Figure 5.8c, white star).
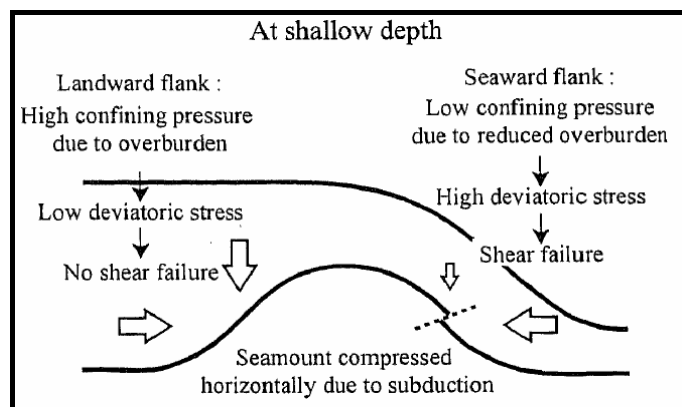
Figure 5.9: *Model of shear development at shallow depth in subducting seamounts (from Baba et al. [2001]).*

At present the center of the accreted oceanic island is located ~50 km from the trench. With a slab angle of ~10°, vertical distance between the summit of the Hoya Unit and the subducting plate is of ~10 km. If the oceanic island was truncated relatively high in its structure during the docking (e.g. 3-4 km deep), it is required that some material accreted under the Hoya Unit. This may indicate that the basement of the accretionary complex is composed of underplated seamounts that amalgamated onto the Azuero Plateau, possibly leading to uplift and exposition of the Hoya Unit (Figure 5.8e). Differential uplifts may have occurred between blocks bounded by ancient fault systems, initially formed on the forebulge and/or during the docking.

The Azuero Mélange recorded the subduction of seamounts prior to the docking of the Hoya Oceanic Island. These seamounts and oceanic island may have been originally part of a same volcanic chain on the ocean floor. The arrangement of the Hoya Unit, apparently forming a re-entrant along the Azuero Plateau (Figures 2.8, 5.1) may be potentially due to erosive tunneling by subducting seamounts prior to incoming of the Hoya Oceanic Island.

5.7. Conclusions

The Azuero Accretionary Complex, previously interpreted as highly heterogeneous accretionary complex [*Hoernle et al.*, 2002; *Hoernle and Hauff*, 2007], is actually composed of a finite number of geologic groups recognized on the basis of tectonostratigraphic and geochemical data. The complex comprises the Venado Unit in eastern Azuero and the Hoya Unit in the southwest, which are essentially composed of unmetamorphosed accreted igneous rocks.

The Venado Unit is made up of fragments of undated seamounts with OIB-like affinities, accreted onto the Azuero Plateau after the onset of subduction along the southern Central American Arc in the Campanian. The Hoya Unit comprises three geologic groups that represent large fragments of accreted oceanic islands predominantly composed of "OIBs": the Quebro, Hoya and Punta Blanca groups. The Quebro and Hoya groups are part of a same early Eocene oceanic island defined here as the Hoya Oceanic Island. This oceanic island was accreted to the margin in the middle Eocene and is separated from the Azuero Plateau by the Azuero Mélange, an oceanic subduction mélange mostly formed in the middle Eocene by seamount subduction, shortly before the incoming of the Hoya Oceanic Island. The Punta Blanca Group is an early Eocene oceanic island accreted to the Hoya Oceanic Island and Azuero Plateau (or Azuero Mélange) in the middle Eocene, shortly after or contemporaneously to the incoming of the Hoya Oceanic Island.

The Hoya Oceanic Island is exposed over an area of >800 km^2, exhibits a very good stratigraphic arrangement and is composed of remarkably well-preserved rock assemblages. It

constitutes an exceptional, potentially unique, occurrence of accreted oceanic island. Our geologic and geochemical results show that several stages of development of the island have been preserved, from the submarine shield until the postshield stages. In the Hoya Group, geochemistry correlates with stratigraphy, providing a remarkable access to the evolution of magma petrogenesis during the growth of the island. On the base of major and trace element compositions we recognized two distinct suites: a transitional series and an alkalic series. We further suggest that the transition between the shield stage and postshield stage was accompanied by a diminution of the degree of source melting and diminution of the temperature of erupted magmas, potentially linking the transitional (shield) suite to the alkalic (postshield) suite. This is interpreted to represent vanishing of the volcanism as the oceanic island moved away from the melting region or hotspot. Isotope and mineral analyses should be performed in the future to better constrain the magmatic evolution of the island, which may serve for comparison with other Pacific oceanic islands and leads to a better understanding of the generation of alkalic melts in oceanic intraplate environments.

The occurrence of the accreted Hoya Oceanic Island indicates that the volcanic edifice accreted through unusual processes of accretion. We propose that the island accreted by "docking", i.e. frontal accretion onto the margin by detachment in the trench. The frontal accretion was possible due to a strong coupling between the oceanic island and the overriding plate as a result of (1) slab flat occurrence along the western Panamean margin in the middle Eocene [*Lissinna et al.*, 2002], (2) collision with a margin composed of an oceanic plateau and (3) unusually high topography formed by the oceanic island on the ocean floor. The detachment likely propagated through the oceanic island from a weak zone at the interface between the subaerial shield stage lava flows and the clastic apron, in the seaward side of the volcanic edifice. Docking was probably followed by seamount underplating that led to emergence of the Hoya Unit.

Photo 5.1: *Mingling texture in the Quebro Group (El Morillo shoreline, ~506450/826300 UTM WGS84).*

Photo 5.2: *Hemipelagic siliceous sediments interlayered between sheet flows of the Quebro Group (El Morillo shoreline, ~506450/826300 UTM WGS84).*

Photo 5.3: *Hemipelagic siliceous sediment below a submarine sheet flow in the Quebro Group (El Morillo shoreline, 506445/826300 UTM WGS84). The sediment was not lithified when the lava emplaced.*

Photo 5.4: *Clastic sedimentary apron of the Hoya Group (near Boca de Quebro, 507515/820020 UTM WGS84). This kind of deposit is indicative of active subaerial volcanism in the vicinity.*

Photo 5.5: *Synvolcanic tectonic activity recorded by dykes in the Hoya sedimentary apron (shoreline near Boca de Quebro, 507945/820710 UTM WGS84). Dike 1 was dissected by a fault, dyke 2 not.*

Photo 5.6: *Layer of near-coastal limestone interbedded in Hoya submarine lava flows (Quebrada Mala, 5273005/818700 UTM WGS84). Note very well rounded vesicular basaltic pebbles.*

Photo 5.7: *Dyke swarm in altered lavas from the Hoya Group (Rio Playita 525200/809300 UTM WGS84).*

Photo 5.8: *Pillow lavas and interpillow hemipelagic limestones in the Punta Blanca Group (Rio Progreso, 541950/802600 UTM WGS84).*

Photo 5.9: *Interlayered shallow-water limestone, bomb agglutinates, reworked basaltic pebbles-cobbles and lava flows (Punta Blanca, ~547200/799900 UTM WGS84). Insert shows a detailed view of the overlying lava flows (in stratigraphic contact). Limestone bed is ~4m thick.*

Photo 5.10: *Hemipelagic basal Tonosi Formation close to Cacao (511700/810125 UTM WGS84).*
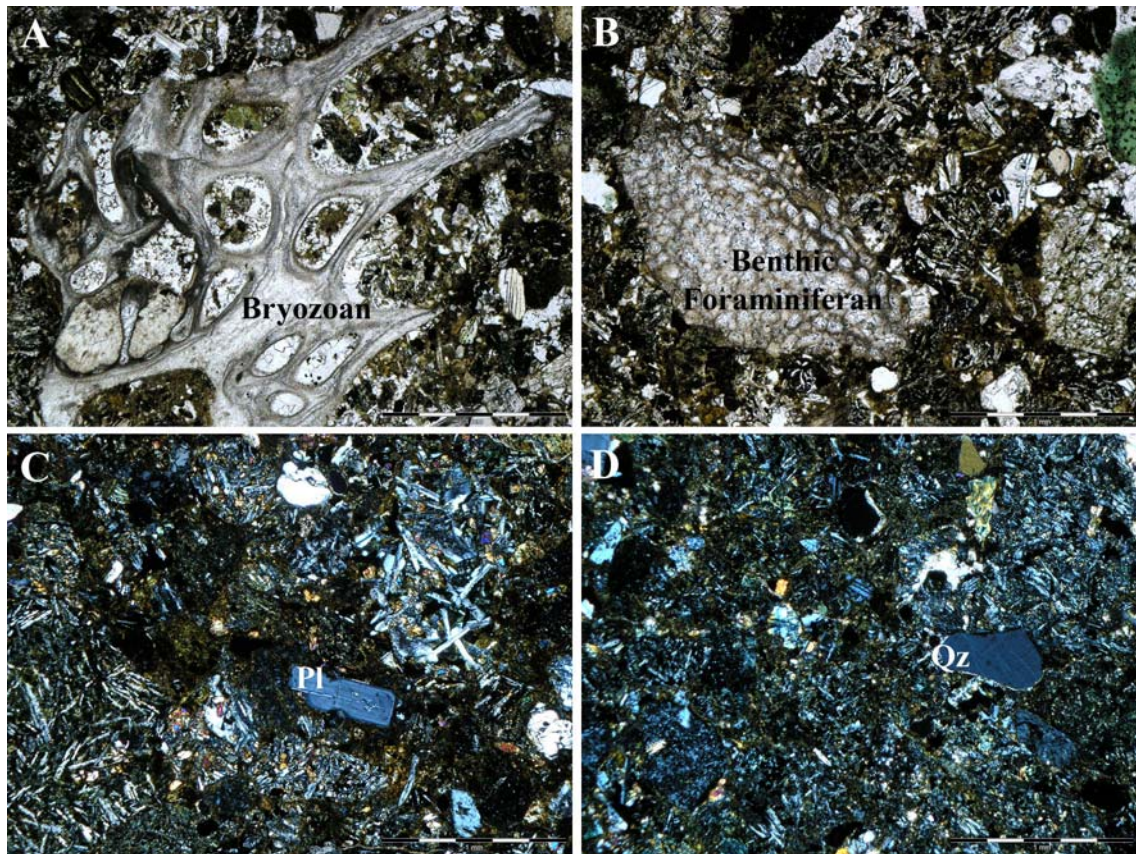
Photo 5.11: *Microphotograph of sample DB06-016 from the lower Tonosi Formation resting upon the Punta Blanca Group. Shallow-water biogenic (A-B), arc-derived grains (C-D), as well as basaltic fragments from the Hoya Unit are observed.*

Photo 5.12: *Mass-flow deposit in the lower Tonosi Formation with fragments of shallow-water limestones, basalts, and poorly-lithified sediments of the Tonosi Formation (Covachón, 540550/799350 UTM WGS84).*

Photo 5.13: *Near-shore deposit in the lower Tonosi Formation between Covachón and Puerto Escondido. Note well-rounded pebbles-cobbles. Pelicans for scale.*
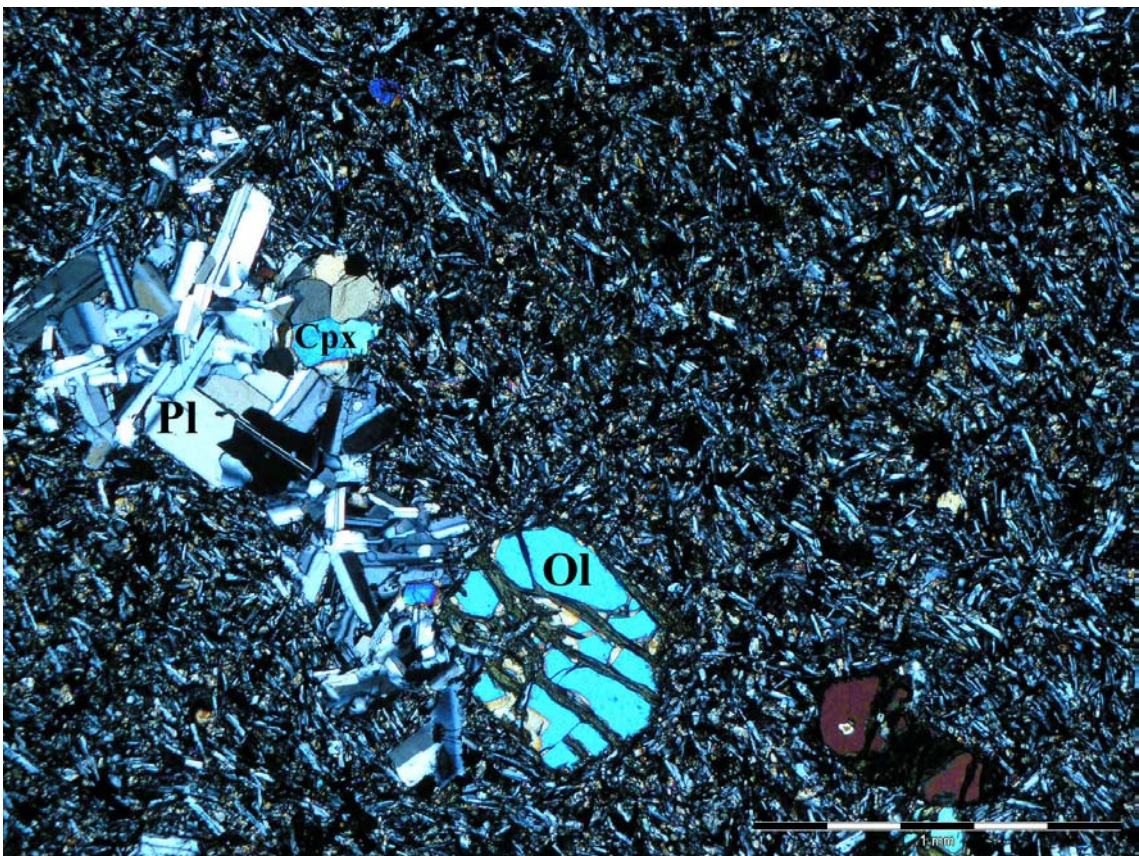
Photo 5.14: *Typical texture of transitional lavas from the Hoya Group (sample DB07-012). Ol=Olivine.*
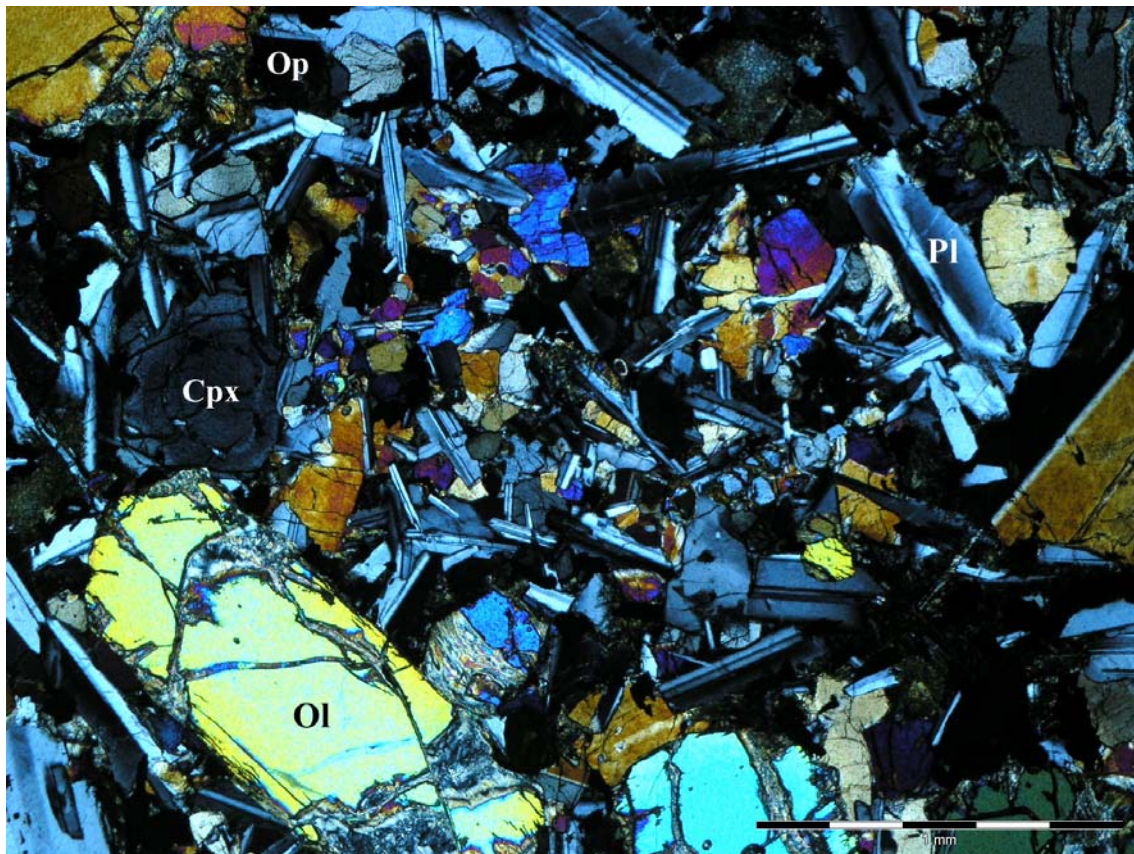
Photo 5.15: *Typical texture of transitional lavas from the Quebro Group (sample DB06-037). Note labeled zoned clinopyroxene.*
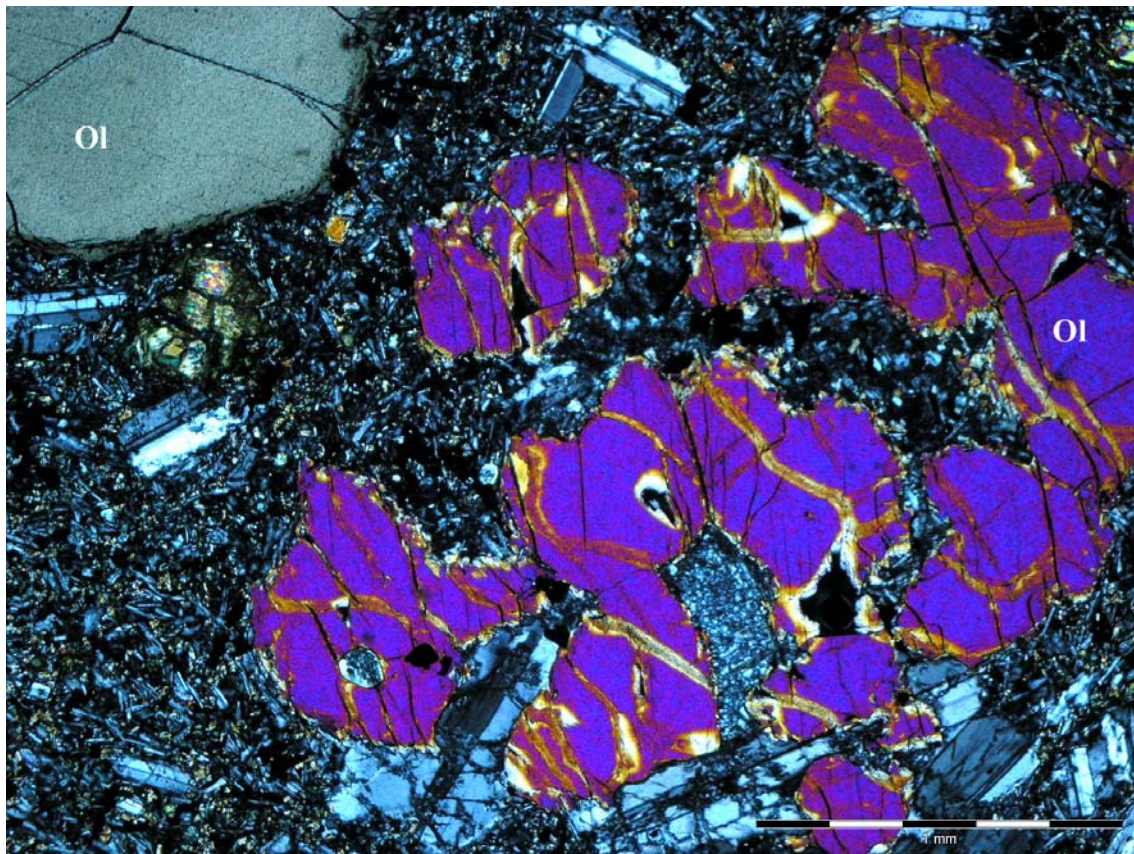
Photo 5.16: *Picrite from the Hoya Group (sample DB06-086). Note resorption and embayment of the olivine phenocryst.*

Chapter 6: Paleocene Thalassinidea Colonization in Deep Sea Environment and the Coprolite *Palaxius osaensis* n. Ichnosp. in Southern Costa Rica

This chapter is based in a paper in press (Revue de Micropaléontologie).

6.1. Introduction

Since the recognition of their internal morphology and potential for classification [*Moore*, 1932], crustacean coprolites have been reported regularly and described in literature. The arrangement and shapes of canals within the crustacean pellets led to the definition of the genus *Palaxius* [*Brönnimann and Norton*, 1960]. These coprolites are believed to have been produced by small burrowing shrimps belonging to the Thalassinidea [*Paréjas*, 1935, 1948].

Some contributions have shown that crustacean larvae were able to migrate easily through oceans and that coprolites may be considered good fossils for stratigraphic correlations [e.g. *Blau et al.*, 1995a]. Nevertheless, the convenience of this tool has been restricted mainly to shallow-water environments, since deposition of crustacean coprolites below 200m seems to be very uncommon.

A new species of crustacean coprolite, *Palaxius osaensis* n. ichnosp., is presented here. It was encountered on the slope of a Paleocene seamount, which formed in the Pacific Ocean and was subsequently accreted to the Central American margin during the Eocene. Due to its atypical environment of deposition, *Palaxius osaensis* n. ichnosp. contributes to the understanding of the palaeo-ecology of the Thalassinidea.
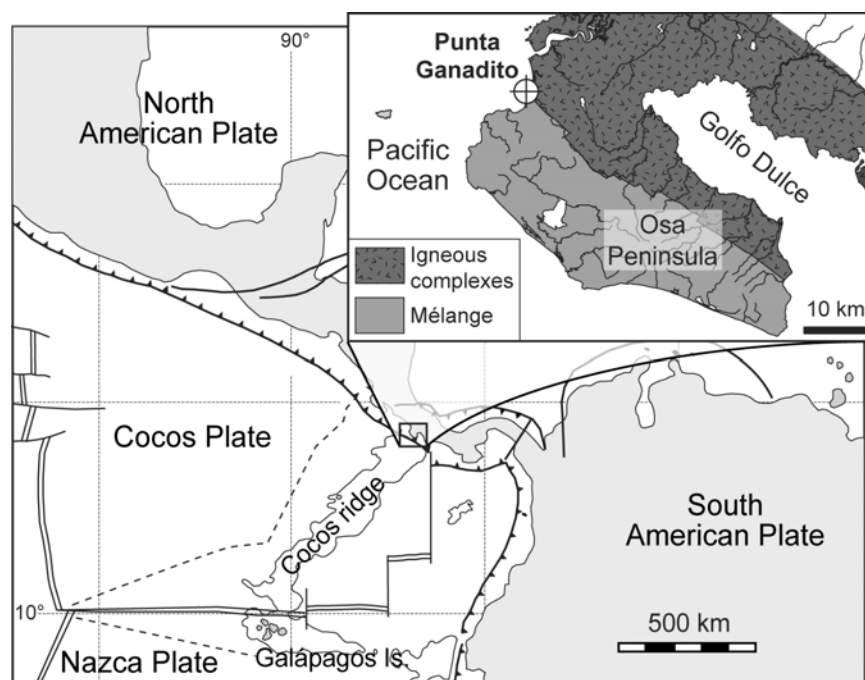
Figure 6.1: General setting and location of coprolites-bearing sediments.

6.2. Origin and composition of the sample

The sample containing the coprolites was found on the NW Osa Peninsula (Costa Rica), at Punta Ganadito (N 8°43'53.2"/W 83°38'57.0", WGS84) (Figure 6.1), along a coastal exposure that is accessible only at low tide. Despite strong tropical weathering that commonly affects the rocks of the area, remarkably fresh material was encountered along the shore and no significant weathering affected the studied sample.

The section where the coprolites were discovered in the Riyito Unit, that is part of an igneous complex made up of accreted slices of oceanic islands and seamounts [*Buchs*, 2003; *Buchs and Baumgartner*, in press]. At Punta Ganadito, the sequence is composed of ~200 m of pillowed lava flows with small, well-shaped, pillows (<50cm in height) that include a minor amount (<1%) of hydrothermally altered siliceous and carbonate sediments. No primary carbonates or shallow-water deposits were encountered at the site, but calcification of siliceous sediments occurs locally. *Hauff et al.* [2000] provided geochemistry and ^{39}Ar-^{40}Ar dates of the lavas that indicate the section was presumably part of a seamount formed in the Pacific Ocean ~62 Ma ago.

Figure 6.2: *Pillow lava outcrop of Punta Ganadito (Costa Rica). The white arrow highlights the occurrence of interpillow sediments containing the coprolites (length of the arrow is ~40 cm).*

The coprolites are present in hydrothermally altered interpillow sediments that occur in small amounts deposited between the tubes of lavas (Figure 6.2). Some of the fossils were fragmented during hydrothermal processes and/or slightly deformed in response to sediment compaction (Figures 6.3a, b). The morphology of the coprolites indicates that they were not transported/reworked over a long distance before being deposited into cavities between the pillow lavas. Thus, they were likely directly emplaced between the lava tubes and/or very close to the cavities. Most of the specimens exhibit a perfect cylindrical shape and contain an internal structure made of longitudinal canals, that is typical for crustacean faecal pellets. Interestingly, the absence of lava vesiculation, shallow-water deposits, detritic sediments, or layers of pelagic sediments in the section indicate that the seamount was in an early stage of development during the deposition of the coprolites. This points toward a deep environment of deposition for the coprolites.

The mineralogical composition of the sample was determined by X-ray diffractometry (XRD) on powder at the Laboratoire de Diffraction (Lausanne University, Switzerland). The analyses revealed that the sample is made entirely of prehnite, which is a mineral commonly related to the hydrothermal alteration of volcanic rocks. The occurrence of a secondary phase as

the principal constituent of the sample indicates that the sediment was altered intensively during hydrothermal process. The composition of the sample is thus consistent with the environment of deposition and indicates that it was totally metamorphosed by circulations of hydrothermal fluids presumably related to volcanic activity. Surprisingly, some pellets remained very well preserved through the hydrothermal activity.
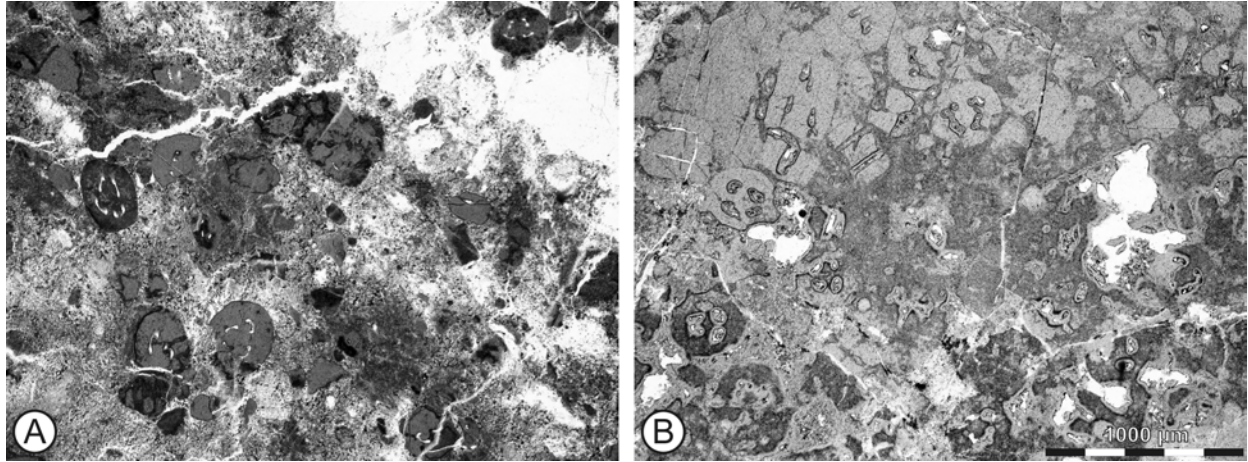
Figure 6.3: Thin-section photographs of the coprolites-bearing sediment. Both light and dark material are made of prehnite.

6.3. Systematic Paleontology

Remarks: In this paper, the systematics of the new coprolite is related to the Favreinidae, a taxonomic term introduced by *Vialov* [1978] for the family of the thalassinid coprolites. This taxonomy was proposed in order to make a clear distinction between the fossils of the coprolite producing animals (Thalassinidea) and their coprolites (Favreinidae) in the systematics. It was notably used by *Schweigert et al.* [1997] and *Senowbari-Daryan et al.* [2003] for the ichnogenus *Palaxius*.

Repository: Holo- and paratypes are stored at the Musée Cantonal de Géologie de Lausanne, Quartier UNIL, Bâtiment Anthropole, 1015 Lausanne, Switzerland. Collection: n° MGL 96121. The stored material includes 1 thin section, sediment chips and two recipients of sediment powder prepared for XRD.

Family FAVREINIDAE Vialov (1978)

Ichnogenus *Palaxius* Brönnimann & Norton (1960)

Type Ichnospecies

Palaxius osaensis n. ichnosp.

Figures 6.3a-b, 6.4a-l, 6.5c

Diagnosis: The ichnogenus *Palaxius* is characterized by longitudinal canals having a crescent outline in cross section [*Brönnimann and Norton*, 1960].

Remarks: The ichnogenus *Palaxius* [*Brönnimann and Norton*, 1960] contains 23 known ichnospecies from the Permian to the Miocene (*Palaxius osaensis* n. ichnosp. included) (see *Senowbari-Daryan et al*. [2003] for a recent review).

Holotype: Thin section DJ-R105 (Figures 6.4a).

Paratypes: Thin section DJ-R105 (Figures 6.5b-l).

Etymology: Named after the Osa Peninsula, where the ichnospecies was found.

Type Locality: Punta Ganadito, Osa Peninsula, Costa Rica   (Figures 6.1, GPS coordinates: N 8°43'53.2"/W 83°38'57.0", WGS84).

Type level: Riyito Unit Paleocene (circa 62 Ma)

Diagnosis: Cylindric coprolite with four longitudinal canals passing through the coprolite. The canals are arranged in two groups of two canals, bilaterally arranged around a symmetry plane. The shape of the canals observed perpendicularly to the symmetry plane is crescent-like for the "dorsal" pair of canals and boomerang-like for the "ventral" pair of canals.

Description: *Palaxius osaensis* n. ichnosp. has near-circular cross-section with diameters ranging from 0.20 to 0.35 mm. It contains two pairs of symmetrical longitudinal canals which are both club-shaped. "Ventral" canals are different from "dorsal" ones, in that they have a boomerang-shape. This feature has not been previously recognized in the thalassinid coprolites. The extremities of the canals observed in a section perpendicular to the symmetry plane of the coprolite are characterized by rounded protuberances. In opposition to the "ventral" canals, the orientation of the "dorsal" canals forms a low angle with the symmetry plane of the coprolite. Outlines of the "ventral" and "dorsal" canals in cross-section have a same length.

Synonym: *Palaxius caucaensis* [*Blau, Moreno and Senff*, 1995, Figure 2b].

Remarks: *Blau et al*. [1995b] defined the ichnospecies *Palaxius caucaensis* on the base of coprolites found in the Campanian-Maastrichtian shallow-water sediments of the Nogales formation (Valle del Cauca, Colombia). *Palaxius caucaensis* [*Blau, Moreno and Senff*, 1995, Figure 2a, c, d, e] exhibits morphological features that are unique among the ichnogenus *Palaxius* and clearly different than *Palaxius osaensis* n. ichnosp. (a differential diagnosis is presented in the next section). However, one specimen presented in *Blau et al*. [1995b] on Figure 2b has morphological parameters (size and canal morphology) highly similar to *Palaxius osaensis* n. ichnosp. [*Blau*, personal communication], indicating these coprolites should pertain to the same ichnospecies. The coprolite presented in *Blau et al*. [1995b] on Figure 2b and *Palaxius osaensis* n. ichnosp. have both a size of ~0.3 mm in diameter, that is smaller than the size of *Palaxius caucaensis* illustrated in *Blau et al*. [1995b] on Figures 2a, c, d and e (~0.5-1.5 mm in diameter). *Blau et al*. [1995b] reasonably attribute the variation in the size of the coprolites to a variation of the size of the producing crustaceans, but did not discuss differences in the morphology between the largest and smallest coprolites. However, we show in the next section that some differences are identifiable. It may be argued that the differences are due to a production of the coprolites at different ontogenetic stages of an unique taxa. Nonetheless, the coprolites found in the Punta Ganadito sequence (and the specimen presented in *Blau et al*. [1995b] on Figure 2b) have a similar size and outline of canals. It appears to be statistically unrealistic that all the coprolites found at the Punta Ganadito were produced exclusively by

juvenile organisms. On the contrary, it is more probable that adult crustaceans participated at least to some extent to their production. Therefore, the coprolite presented in *Blau et al.* [1995b] on Figure 2b may possibly not be produced by the same crustacean species than the largest coprolites of the Nogales formation. We propose thus that the coprolite presented in *Blau et al.* [1995b] on Figure 2b and *Palaxius osaensis* n. ichnosp. pertain to the same ichnospecies, distinct from *Palaxius caucaensis* [*Blau, Moreno and Senff,* 1995, Figures 2a, c, d, e].

Comparisons: Palaxius osaensis n. ichnosp. differs from *Palaxius tetraochetarius* [*Palik,* 1965] by the morphology of the "ventral" canals and the relative size of the "ventral" and "dorsal" canals (i.e. in *Palaxius tetraocharius,* "ventral" canals are smaller than "dorsal" ones and do not have a boomerang-shape) (Figure 6.5). This difference is not due to dissimilarities of preservation between the holotype and paratypes of *Palaxius tetraochetarius* [*Palik,* 1965] and *Palaxius osaensis* n. ichnosp., because a same "ventral" and "dorsal" canal size is equally observed in the smallest and less well preserved coprolites of the Punta Ganadito (Figures 6.4j-l). *Palaxius caucaensis* [*Blau, Moreno and Senff,* 1995, Figures 2a, c, d, e] has canals more intensively curved and located closer to the coprolite edge than *Palaxius osaensis* n. ichnosp. (Figure 6.5). *Palaxius salataensis* [*Brönnimann, Cros and Zaninetti,* 1972] and *Palaxius kumaensis* [*Senowbari-Daryan and Silantiev,* 1991] have both canal orientations and canal curvatures different than *Palaxius osaensis* n. ichnosp (Figure 6.5).

6.4. Origin of the coprolites

The crustacean coprolites of the genus *Palaxius* are commonly interpreted to be the product of some ancestors of the present-day burrowing shrimps of the Thalassinidea. This assumption, initially made by *Paréjas* [1935, 1948] on the basis of a comparison between the morphologies of present day and fossil faecal pellets, has been strengthened recently by the observation of Thalassinoides trace fossils occurring together with *Palaxius* coprolites in the Upper Triassic shallow-water carbonates of Peru [*Senowbari-Daryan and Stanley,* 1986]. *Becker and Chamberlain* [2006] reported a compelling association between anomuran microcoprolites, *Ophiomorpha* burrows and the decapod crustacean *Protocallianassa* in the Late Cretaceous lower shoreface deposits of New Jersey.

Although a correlation of faecal pellets with some taxa was made for recent species [*Moore,* 1932; *Pryor,* 1975], a precise correlation of coprolites with fossil species is fundamentally not achievable because the internal structures of the faecal pellets do not exhibit any morphological distinction among various taxa [*Schweigert et al.,* 1997]. However, the connection of *Palaxius* coprolites to the thalassinid infraorder is consensually accepted and, therefore, the atypical environment of deposition of *Palaxius osaensis* n. ichnosp. in the Osa Peninsula should be considered for any attempt to better constrain the palaeoecology of the Thalassinidea.

Until recently, the palaeoecology of the Thassinidea has been based on the occurrence of coprolites or shrimp fossils. This has been confined principally to soft sea-floor sediments in shallow-waters, but some occurrences have been recorded in deeper environment, such as *Palaxius salataensis* in Liassic hemipelagic limestones of Spain [*Schweigert et al.,* 1997] and *Callianassa clallamensis* in Late Oligocene to Early Miocene bathyal sediments from the state of Washington, USA (East, 2003). Similarly, the present-day global diversity of the Thalassinidea
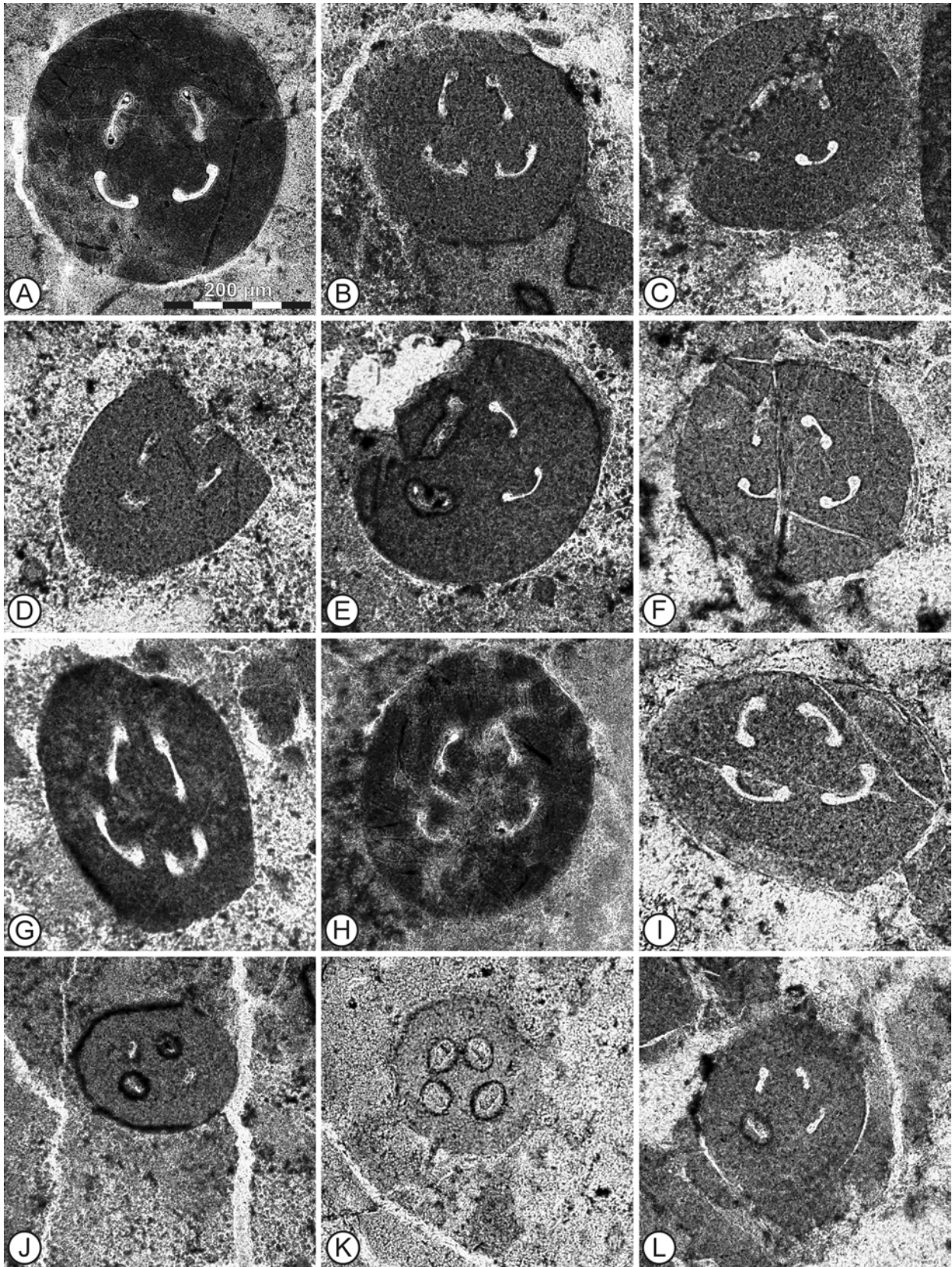
Figure 6.4: Photographs of Palaxius osaensis holotype **(A)** and paratypes **(B-L)**. Scale is for all specimens.
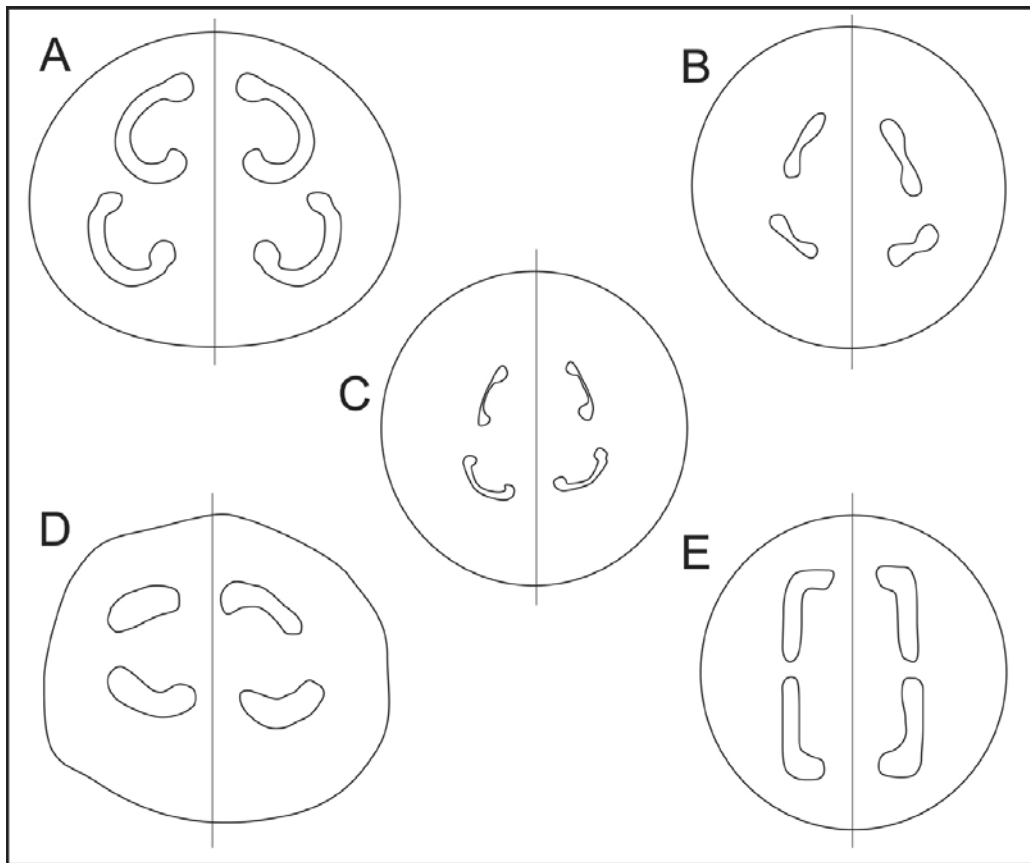
Figure 6.5: Morphology of the four internal canals in the coprolites of the Palaxius genus (transverse sections, normal to symmetry plane). A) Palaxius caucaensis, Blau, Moreno and Senff (1995), redrawn after fig. 4a. B) Palaxius tetraochetarius, Palik (1965), redrawn after plate 1-9, left specimen. C) Palaxius osaensis n. ichnosp. D) Palaxius salataensis, Brönniman, Cros and Zaninetti [1972], redrawn after Figure 2c. E) Palaxius kumaensis, Senowbari-Daryan and Silantiev [1991], redrawn after Figure 4c. Figures are not to scale.

indicates that the majority of species prefer shallow-water rather than bathyal or abyssal environments [*Dworschak*, 2000, 2005]. Nonetheless, some are currently found in deep sites, as illustrated by the Thalassinidae, which is observed until 2000m below sea level, and the Axiidae found even at grater depth (>2000m) [*Dworschak*, 2000].

Apparently there is no contradiction between the deep occurrence of *Palaxius osaensis* n. ichnosp., the fossil record, and the observations of living Thalassinidea. However, we note that in all reported cases the Thalassinidea were intimately associated with soft sediments which constitute a reliable source of nutriments for these organisms. This association is not verified for *Palaxius osaensis* n. ichnosp., given that only very few sediments are associated with the lavas of the Punta Ganadito section. Instead of a food source located in soft sediments, we suggest that hydrothermal activity related to volcanism was sufficient to allow the development of chemosynthetic bacteria, which served to feed the crustacean population. However, no massive sulfide deposits were encountered in the section, thus the hydrothermal activity was certainly too low to allow the development of a large colony, or possibly some Crustacea transited from a distant feeding locality to the site of deposition of the coprolites. In both cases the occurrence of *Palaxius osaensis* n. ichnosp. on the Osa Peninsula points toward a very atypical behavior

among the Thalassinidea, which corresponds to the colonization of a deep seamount slope lacking of significant amount of soft sediment deposits.

In the late Cretaceous Nogales formation (Valle del Cauca, Colombia), a specimen of *Palaxius osaensis* n. ichnosp. was encountered in association with *Palaxius caucaensis* [*Blau, Moreno and Senff*, 1995] [*Blau et al.*, 1995b]. The coprolite of *Palaxius osaensis* n. ichnosp. found in the Nogales formation was deposited at shallow level along a continental margin [*Blau et al.*, 1995b]. In terms of life development, such an environment is strongly different than the environment of deposition of *Palaxius osaensis* n. ichnosp. in the sediments of the Punta Ganadito. Consequently, the occurrences of *Palaxius osaensis* n. ichnospecies deposited at both shallow and deep levels may be interpreted in two ways: 1.- the coprolites were produced by two distinct taxa living in distinct biotopes and producing highly similar faecal pellets or, 2.- the coprolites were produced by a single taxon able to colonize various biotopes at both shallow and deep levels. Interestingly, we observe that the specimens of *Palaxius osaensis* n. ichnosp. encountered in Colombia and Costa Rica were deposited at similar dates (Campanian-Maastrichtian and Paleocene), at sites located close to each other at the scale of the paleo-Pacific Ocean and at similar paleo-latitudes. Such observations would be expected if the coprolites were produced by a single taxon, but further occurrences of *Palaxius osaensis* n. ichnosp. are required in order to provide a definitive answer concerning the faculty of some thalassinid taxa to colonize deep environments in the past.

6.5. Conclusions

A new species of crustacean coprolite, *Palaxius osaensis* n. ichnosp., was discovered on the deep slope of an accreted seamount in Costa Rica. The seamount formed in the Pacific Ocean during the Early Paleocene (~62 Ma) and was colonized by thalassinid shrimps during its first stage of development, presumably in a deep environment.

The location of deposition of the coprolites does not contain any sediment deposits which may have provided a substantial feeding opportunity. The fossiliferous sample suffered intensive hydrothermal alteration that took place in response to the volcanic activity and replaced all the sediment with prehnite. All observations point toward the existence of a chemosynthetic community on the seamount slope during the Early Paleocene, that provided an unusual environment of deposition for the crustacean coprolites.

The occurrence of *Palaxius osaensis* n. ichnosp. in shallow-water sediments of Colombia [*Blau et al.*, 1995b] and the new occurrence in Costa Rica raise some interrogations concerning the ability of some thalassinid taxa to develop at both deep- and shallow-levels biotopes during the late Cretaceous-Paleocene. Further fossil records are required to better constraint the aptitudes of the Thalassinidea to colonize deep-sea environments in the past.

Chapter 7: General Conclusions and Concluding Remarks

7.1. Methodology

The area of study includes a large zone mostly covered by tropical vegetation and lacking occurrence of large outcrops. The studied formations are principally composed of basaltic rocks containing poor stratigraphic markers. To solve difficulties in defining tectonostratigraphy and recognizing the origins of the rocks we adopted a multidisciplinary approach, based on (1) ~6 months of comprehensive field work and sampling, (2) microscope observation of >750 samples, (3) biochronologic dating of the sediments, (4) geochemistry of the igneous rocks, and (5) remote analysis of large structures. A GIS containing all the data was made to better constrain interpretations.

This approach has been performed through three field campaigns. It allowed us to progressively recognize and map different tectonostratigraphic units at large scales. Stratigraphic and structural relationships between the different tectonostratigraphic units have actually been principally constrained on the basis of field work. We observed that geochemical variations of the basalts are frequently coupled with petrographic characteristics of the samples. This helped us to make distinctions on the field between distinct groups of basalt and to efficiently orientate our sampling. The distinctions were further constrained by sedimentary associations, morphology of the igneous rocks and nature of the deformation. This approach resulted in a consistent tectonostratigraphy that appeared to be at odds with some previous interpretations independently based on geochemistry, sedimentology or structural analysis. This demonstrates efficiency of performing comprehensive field work and integrating different data in modern regional studies.

7.2. Arc basement and subduction initiation

The southern Central American arc is consensually regarded as an arc developed on the top of a plateau pertaining the CLIP or CCOP. However, strong evidence for this interpretation has not been provided yet in the literature. During our study along the uplifted southern Costa Rican and western Panamean forearc, we encountered clear field indications illustrating emplacement of late Campanian-Maastrichtian arc-related igneous rocks within and above a Coniacian-early Santonian oceanic plateau defined here as the "Azuero Plateau".

The late Campanian-Maastrichtian arc-related igneous rocks partly compose the basement of the Golfito Complex (southern Costa Rica) and occur in several places as intrusives or lava flows in the Azuero Complex (western Panama). They are locally intercalated with late late Campanian-Maastrichtian hemipelagic limestones of the Golfito Formation and Torio lithostratigraphic unit. The igneous rocks are characterized by an unusual geochemistry, intermediate between the Maastrichtian to middle Eocene Azuero Arc Group and the Azuero Plateau. Incompatible element contents broadly similar to plateau rocks have led many authors to propose a CLIP origin for these rocks. However, our stratigraphic observations and geochemical results clearly indicate that the Campanian arc-related igneous rocks are part of a proto-arc named here "Azuero Proto-Arc", which formed on top of the Azuero Plateau. Hence, occurrence of the Azuero Proto-Arc is evidence for the onset of subduction along the edge of the SW

Caribbean Plate in the late Campanian. Subsequent maturation of the arc in the Maastrichtian led to formation of emerged areas along the margin, potentially allowing migration of terrestrial fauna between the Americas.

Due to arc retreat in western Panama during the middle Eocene [*Lissinna et al.*, 2002], the early development of the southern Central American arc on the top of the Azuero Plateau has remained preserved from burying under younger volcanics. Exposures of the oceanic plateau, proto-arc and arc may allow forthcoming studies to provide new constraints on some poorly-understood subduction-related processes, such as maturation of volcanic arcs and continentalization of the oceanic crust. Metamorphic rocks exposed along the Sona-Azuero Fault Zone may provide an access to deeper processes of the arc development and remain to be studied into details.

7.3. Accreted material

Accreted material exposed along the margin essentially comprises oceanic igneous complexes and a mélange predominantly composed of sediments. Some oceanic igneous complexes are mostly made up of late Cretaceous, plateau-like igneous rocks, which led some authors to propose they are part of the CLIP. Our stratigraphic and geochemical results and published paleomagnetic data indicate that some plateau-like igneous rocks of southern Costa Rica are actually exotic with respect to the Caribbean Plate and, as a consequence, should no longer be considered to be part of the CLIP.

Travel time of the accreted igneous rocks (i.e. the time interval between their genesis and accretion) is in broad agreement with previous geochemical works that suggested a common origin at a paleo-Galapagos Hotspot [e.g. *Hoernle et al.*, 2002]. However, unequivocal evidence for a genetic link between the Azuero Plateau, the accreted igneous rocks in southern Central America, Galapagos Hotspot tracks and volcanic rocks at Galapagos Hotspot has not been provided. This may be investigated in terms of isotope compositions in forthcoming studies, partly on the basis of a comparison between the units defined in our study.

During determination of the extension of the units we observed that the landscape morphology correlates well with main geological boundaries. This is particularly true for major fault zones in the Osa Peninsula that control (or recently controlled) the shape of mountains and shorelines. Recent inverse faulting correlates with fossil subduction zones that were apparently re-used by contemporaneous tectonics. Hence, it seems to us that forthcoming neotectonic models should attempt to take into account the influence of ancient structures on the deformation of the margin.

7.3.1. The Osa Igneous Complex

The Osa Igneous Complex is exposed in the landward side of the Osa Peninsula and in the Burica Peninsula (southern Costa Rica) and may extend to islands of the Montijo Gulf (western Panama). This complex is composed of five units that have essentially remained under the greenschist metamorphic facies. The units are resumed below, from the inner toward outer forearc.

7.3.1.1. The Inner Osa Igneous Complex: late Cretaceous plateau-like seamount rocks

The Inner Osa Igneous Complex is composed of a Campanian-Santonian accreted oceanic plateau that emplaced by shearing off and, possibly, duplexing in the late-middle Paleocene. This accreted plateau is distinct form the CLIP and the allochtonous Azuero Plateau. It is essentially made up of submarine basaltic sequences with very minor association of pelagic siliceous-argilous sediments and gabbroic and doleritic rocks. This assemblage is similar to the volcanic sequences exposed in the Malaita Accretionary Prism that formed by accretion of the subducting Ontong-Java Plateau [e.g. *Petterson et al.*, 1997]. The bulk of the basalts of the Inner Osa Igneous Complex has tholeiitic affinities and a geochemistry similar to the Azuero Plateau. However, our results suggest that the (allochtonous) Inner Osa Igneous Complex differs from the (autochtonous) Azuero Plateau by: (1) major element contents spanning a larger compositional field, (2) occurrence of NMORB-like and OIB-like igneous rocks not recognized yet in the Azuero Plateau, (3) distinct sedimentary facies, and (4) absence of proto-arc dykes.

7.3.1.2. The Güerra Unit: a paleo-subduction zone

The Güerra Unit is composed of undated metamorphosed and altered igneous rocks and sediments that proceeded from subducting seamounts. This unit is interpreted to have formed during a period of low rate accretion between the emplacement of the Inner Osa Igneous Complex and Ganado and Riyito units. Long residence time of the Güerra material in the vicinity of the décollement enhanced metamorphic reactions and triggered a pervasive deformation of the rocks. In this view, the Güerra Unit likely represents a paleo-subduction zone that offers the possibility to study some processes occurring close to the décollement at relatively shallow depth. Metamorphic cooling ages should be provided in the future to better constrain the age of formation of this unit.

7.3.1.3. The Ganado Unit: accreted fragments of a seamount with plateau-like and MORB-like affinities

The Ganado Unit is composed of Coniacian-Santonian accreted submarine lavas and intrusive rocks. The bulk of the lavas is composed of plateau-like tholeiites that differs from the Inner Osa Igneous Complex in terms of Nb content. The bulk of the intrusive rocks have NMORB-like tholeiitic affinities. This unit is interpreted to represent accreted fragments of a seamount partly dismembered during incorporation to the margin. Accretion occurred between emplacement of the Güerra and Vaquedano units, probably during the middle Eocene. The material forming this unit has the largest travel time recognized to date in South Central America that may point toward an origin distinct from the Galapagos Hotspot.

7.3.1.4. The Riyito Unit: insights into the Farallon Plate break-up and deep-sea crustacean colonization on the flank of a seamount

The Riyito Unit is composed of late Cretaceous/Paleocene (?) accreted tholeiites characterized by extremely low contents in the most incompatible elements. This unit formed through several accretions of seamounts, probably sub-contemporaneously to the Ganado Unit. The geochemistry of the igneous rocks is indicative of a genesis at a center of plume-ridge interaction. Conjointly with constraints arising from the morphology of the Pacific Plate, we propose that these rocks recorded an interaction between the paleo-Cocos-Nazca Spreading

System and the paleo-Galapagos Hospot in the late Cretaceous/Paleocene. This implies a break-up of the Farallon Plate at least ~40 Ma prior to ages suggested by current tectonic models.

Sedimentary deposits found between pillow-lavas of a deep-sea volcanic sequence were sampled. These sediments yielded a new species of crustacean microcoprolite that has been described and discussed in terms of crustacean colonization in the deep sea on the flank of a seamount.

7.3.1.5. The Vaquedano Unit: peeling subducting seamounts

The Vaquedano Unit is a highly composite unit made up of accreted slices of late Cetaceous to middle Eocene seamounts. Accreted rocks bodies are characterized by occurrences of OIB-like submarine lavas and associated pelagic-hemipelagic limestones. We interpret this unit as a record of low rate accretion along the southern Costa Rican Margin in the middle Eocene, prior to the formation of the Osa Mélange. The unit formed by repeated superficial peeling of subducting seamounts.

7.3.2. The Osa Mélange

The Osa Mélange is exposed in the outer part of the Osa Peninsula and in Caño Island. It is composed of three tectonostratigraphic units. In our study we have refined model previously proposed by *Buchs and Stucki* [2001] for the origin of the San Pedrillo Unit.

The San Pedrillo Unit composes the most inner part of the Osa Mélange in contact with the Osa Igneous Complex. It is essentially made of sediments that include various proportions of unmetamorphosed igneous and calcareous olistoliths. Basaltic olistoliths are strongly similar to volcano-sedimentary sequences of the Osa Igneous Complex, in terms of both geochemistry and fossil assemblages. These olistoliths are embedded in deformed olistostromic deposit layers that equally contain arc-derived pebbles and large boulders. Hence, we propose that the San Pedrillo Unit formed in response to a gravitational collapse of the margin, leading to reworking of material from the arc and paleo-Osa Igneous Complex. This material deposited into the trench and subsequently accreted at shallow-level by underplating. The margin collapse may have been triggered by a seamount subduction and is biochronologically dated to the late Eocene.

7.3.3. The Azuero Accretionary Complex and Azuero Mélange

7.3.3.1. The Vedano Unit: Aptian OIBs

The Azuero Accretionary Complex is exposed on the Azuero Peninsula and has been subdivided into the Hoya and Venado units. It is principally composed of well-preserved igneous rocks. The Venado Unit is exposed in the southeastern Azuero Peninsula and is in contact with the Azuero Plateau along the Joaquín Fault Zone. It is composed of OIB-like igneous rocks devoid of preserved sediment. We interpret this unit as an accretionary complex. Formation ages are still needed.

7.3.3.2. The Azuero Mélange: a possible Panamean equivalent of the Vaquedano Unit

The Azuero Mélange broadly follows the orientation of the Sona-Azuero Fault Zone on the Azuero Peninsula. Similarly to the Vaquedano Unit in southern Costa Rica this mélange

formed by repeated peeling and accretion of superficial layers of subducting seamounts during the middle Eocene. It was emplaced along the margin shortly before the accretion of the Hoya Unit.

7.3.3.3. The Hoya Unit: exceptionally well-preserved accreted oceanic islands

The Hoya Unit is exposed in the southwestern Azuero Peninsula and is in contact with the Azuero Mélange. The unit comprises three distinct geologic groups defined on the basis of geochemistry and lithology. These groups are essentially composed of early Eocene accreted igneous rocks. Overlap sequences and age of formation of the Azuero Mélange constrain the age of accretion to the middle Eocene.

The Quebro and Hoya groups are composed of a wide range of lithologic facies that include (1) submarine lavas flows and interlayered hemipelagic sediments, (2) clastic sediments reworking basaltic lava flows, (3) shallow-water carbonates interlayered in the lava flows, (4) subaerial lava flows and (5) areas containing large amounts of intrusive rocks. These facies exhibit a good arrangement on the field and are interpreted to represent the internal structure of an accreted oceanic island. This interpretation is strengthened by geochemistry that correlates well with the lithologic arrangement. We further observed changes in composition of erupted magmas during the evolution of the oceanic island. Geochemical changes may be due to temperature lowering in the volcanic system and lesser degrees of source melting as the volcanic island moved away from the melting region or hotspot. Exceptional occurrence of the Hoya Oceanic Island may be further studied in the future in order to better understand the development of intraplate oceanic volcanoes and, possibly, genesis of alkali magmas on the ocean floor.

The Punta Blanca Group is part of another volcanic island accreted onto the Hoya Oceanic Island and Azuero Plateau and Mélange, shortly after or contemporaneously to the emplacement of the Hoya Oceanic Island along the margin. At Punta Blanca, interlayered shallow-water limestones and transitional basalt flows form an unusual oceanic island sequence, distinct to the Tonosi Formation.

7.4. Accretionary processes recorded along the southern Central American margin between the late Cretaceous and Eocene

7.4.1. Dating the accretion

Evolution of the southern Central American Margin between the late Cretaceous and Eocene is intrinsically related to subduction processes. In this study, we recognized and characterized several occurrences of accretionary complex between southern Costa Rica and western Panama. These complexes constitute a geological record of accretionary events that can be dated by: (1) ages of overlap sequences containing arc-derived material deposited upon the accreted sequences, (2) ages of the youngest accreted oceanic rocks within a unit, (3) geometric arrangement of the accreted units in absence of strike-slip motion (i.e. seaward units are accreted subsequently to landward units), (4) cooling ages of metamorphic rocks, and (5) ages of arc-related igneous rocks intruding the accreted material. In our study, ages of accretion have been based on points (1)-(3). Metamorphic rocks of the Osa Igneous and Azuero complexes may provide useful informations on cooling ages and should be studied in forthcoming works.

Accretion ages of Costa Rican and Panamean accretionary complexes are synthesized on Figure 7.1.

7.4.2. Strong coupling induced by unusual margin geometry and regional changes

The igneous accretionary complexes along the Costa Rican margin have globally remained under the greenschist metamorphic facies, indicating accretion at shallow depths. This appears to be relatively unusual in comparison to other accretionary complexes around the world. We propose that accretion at shallow depth may be due to the presence of an unusual arc basement (i.e. an oceanic plateau) along the southern Central American margin that triggered stronger coupling between the overriding plate and subducting volcanic edifices than along other convergent margins.
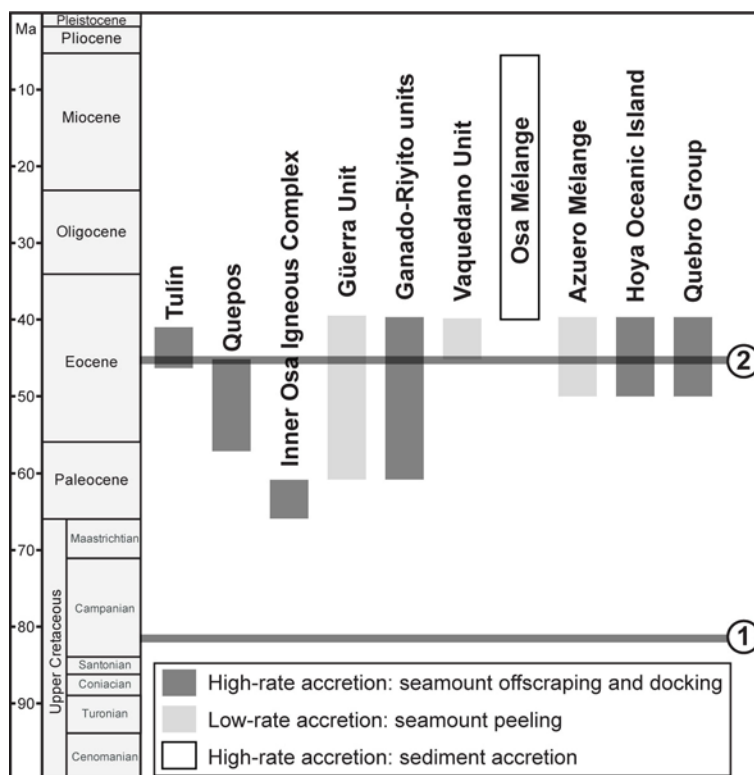
Figure 7.1: Possible accretion ages for accreted material between the Tulín Formation (northern Costa Rica) and the Hoya Unit (western Panama) (based on data from Baumgartner et al. [1984] and Arias [2003] for Tulín and Quepos). 1) Subduction initiation. 2) Arc retreat in western Panama and possible regional tectonic change. Absence of younger accretion ages may be due to an exposure artefact (i.e. younger accreted complexes tend to be located close to the trench and are less easily exposed).

Ranges of possible accretion ages for the southern Central American accretionary complexes define a higher tendency of accretion in the middle Eocene (Figure 7.1). Precaution is required in the interpretation of this tendency because the outer margin is only partly exposed, which may lead to non-representative observations. We note, however, that several important changes occurred at a regional scale along the margin at this time. First, the volcanic front in western Panama (but not in Costa Rica) retreated of about 30 km in response to slab flattening [*Lissinna et al.*, 2002; *this study*]. Second, there is ubiquitous deposition of shallow-water limestones and basal conglomerates resting on igneous basements in the forearc area in the middle-late Eocene, notably represented by the Tonosi Formation in western and eastern Panama and the Fila Costeña in southern and central Costa Rica [e.g. *Yuan*, 1991; *Mann and Kolarsky*, 1995; *Kolarsky et al.*, 1995b; *Baumgartner-Mora et al.*, 2008]. This deposition points toward a global submersion of the margin possibly occurring after a compressional event. Third, accretion in southern Costa Rica radically changed in the middle-late Eocene, from seamount to sediment

accretion. As a consequence it appears that the high tendency of accretion in the middle Eocene may have been triggered by a regional compressive event, which may have resulted in profound and durable changes of the margin development. Exact nature and causes of this event remain to be established.

7.4.3. Subduction accretion versus tectonic erosion: the dilemma

The Costa Rican margin is generally regarded as a typical example of erosive margin, i.e. a margin characterized by a net loss of material along the subduction zone through a representative period of time. This interpretation has been mostly constrained by (1) rapid subsidence of some portions of the margin indicating basal erosion of the overriding plate [*Vannucchi et al.*, 2001] and (2) global absence of on-going sediment accretion [e.g. *Ranero and von Huene*, 2000]. Second argument relates to the geophysical idea that erosive margins are devoid of accreted sediment [*von Huene and Scholl*, 1991; *Clift and Vannucchi*, 2004].

On the other hand, our geologic results show that the southern Central American margin recorded several events of accretion between the late Cretaceous and middle Eocene. During this period of time sediment accretion did not occur but significant amounts of igneous material were added to the margin. In the same time tectonic erosion occurred too, as demonstrated by occurrences of arc-related igneous complexes very close to accreted exotic igneous rocks. In presence of frequent seamount subduction, this appears to be a regional situation very similar to the margin at present. Our results further indicate that: (1) absence of accreted sediments does not impede presence of igneous material added to the margin, and (2) accretion and erosion may occur at the same time along a margin and/or alternate through time.

What is then the volume balance between eroded and accreted material along the margin during the late Cretaceous - middle Eocene and, by analogy, today? To answer this question it is necessary to compare the volumes of material tectonically eroded from- and the amount of exotic material accreted to the margin. This appears to be impossible at present for three reasons: (1) the initial geometry of the margin (directly after subduction initiation) is unknown, (2) it is not possible to distinguish between exotic accreted basalts and the Azuero Plateau with geophysics, and (3) material tectonically eroded from the margin is certainly presently located in the mantle and cannot be quantified directly by geophysical imaging. In conclusion, we suggest that there is currently no unequivocal scientific argument that may allow ascribing an erosive or accretionary nature to the Costa Rican margin.

References

Abbott, D.H., R. Drury, and W.D. Mooney, Continents as lithological icebergs: The importance of buoyant lithospheric roots, *Earth and Planetary Science Letters, 149*, 15-27, 1997.

Abercrombie, R.E., M. Antolik, K. Felzer, and G. Ekstrom, The 1994 Java tsunami earthquake: Slip over a subducting seamount, *Journal of Geophysical Research-Solid Earth, 106*, 6595-6607, 2001.

Abratis, M., Geochemical variations in magmatic rocks from southern Costa Rica as a consequence of Cocos Ridge subduction and uplift of the Cordillera de Talamanca, *PhD tesis, University of Gottingen, Gottingen, Federal Republic of Germany*, 148, 1998.

Abratis, M., and G. Worner, Ridge collision, slab-window formation, and the flux of Pacific asthenosphere into the Caribbean realm, *Geology, 29*, 127-130, 2001.

Acton, G.D., B. Galbrun, J.W. King, R.M. Leckie, H. Sigurdsson, A.L. J., T.J. Bralower, S.N. Carey, W.P. Chaisson, P. Cotillon, A.D. Cunningham, S.L. Hondt, A.W. Droxler, J. Gonzalez, G.H. Haug, K. Kameo, I.L. Lind, V. Louvel, T.W. Lyons, R.W. Murray, M. Mutti, G. Myers, R.B. Pearce, D.G. Pearson, L. Peterson, C., and U. Roehl, Paleolatitude of the Caribbean Plate since the Late Cretaceous, *Proceedings of the Ocean Drilling Program, scientific results, Caribbean Ocean history and the Cretaceous/ Tertiary boundary event; covering Leg 165 of the cruises of the drilling vessel JOIDES Resolution, Miami, Florida, to San Juan Puerto Rico, sites 998-1002, 19 December 1995-17 February 1996, 165*, 149-173, 2000.

Adamek, S., C. Frohlich, and W.D. Pennington, Seismicity of the Caribbean-Nazca Boundary - Constraints on Microplate Tectonics of the Panama Region, *Journal of Geophysical Research-Solid Earth and Planets, 93*, 2053-2075, 1988.

Allibon, J., P. Monjoie, H. Lapierre, E. Jaillard, F. Bussy, and D. Bosch, The rôle of the Cretaceous Caribbean Oceanic Plateau in the genesis of late cretaceous arc magmatism in Ecuador, *Proceedings of the 3rd Swiss Geoscience Meeting, Zürich*, 59-60, 2005.

Allibon, J., P. Monjoie, H. Lapierre, E. Jaillard, F. Bussy, D. Bosch, and F. Senebier, The contribution of the young Cretaceous Caribbean Oceanic Plateau to the genesis of late Cretaceous arc magmatism in the Cordillera Occidental of Ecuador, *Journal of South American Earth Sciences, In Press, Accepted Manuscript*, in press.

Alonso, J.L., A. Marcos, and A. Suarez, Structure and organization of the Porma Melange: Progressive denudation of a submarine nappe toe by gravitational collapse, *American Journal of Science, 306*, 32-65, 2006.

Arculus, R.J., Use and abuse of the terms calcalkaline and calcalkalic, *Journal of Petrology, 44*, 929-935, 2003.

Arias, O., Redefinicion de la Formacion Tulin (Maastrichtiano-Eoceno inferior) del Pacifico Central del Costa Rica, *Revista Geologica de America Central, 28*, 47-68, 2003.

Astorga, A., El Cretácico Superior y el paleógeno de la vertiente pacífica de Nicaragua meridional y Costa Rica septentrional: Origen, evolución y dinámica de las cuencas profundas relacionadas al margen convergente de Centroamérica, Licenciatura thesis, 115 pp., Universidad de Costa Rica, Costa Rica, 1987.

Astorga, A., El puente-istmo de América Central y la evolución de la placa Caribe (con énfasis en el Mesozoico), *Profil, 12*, 1-201, 1997.

Auger, L., G. Abers, E. Syracuse, K. Fischer, W. Strauch, and M. Protti, Crustal Thickness of the Central American Arc, in *MARGINS Workshop to Integrate Subduction Factory and Seismogeneic Zone Studies in Central America*, Heredia, Costa Rica, 2007.

Azéma, J., J. Butterlin, J. Tournon, and P. de Wever, Presencia de material volcano-sedimentario de edad Eoceno medio en la Península de Osa (provincia de Puntarenas, Costa Rica), *10a Conferencia Geologica del Caribe, Cartagena, Colombia [absract]*, 1983.

Baba, T., T. Hori, S. Hirano, P.R. Cummins, J.O. Park, M. Kameyama, and Y. Kaneda, Deformation of a seamount subducting beneath an accretionary prism: Constraints from numerical simulation, *Geophysical Research Letters, 28*, 1827-1830, 2001.

Bagheri, S., and G.M. Stampfli, The Anarak, Jandaq and Posht-e-Badam metamorphic complexes in central Iran: New geological data, relationships and tectonic implications, *Tectonophysics, 451*, 123-155, 2008.

Baksi, A.K., Search for a deep-mantle component in mafic lavas using a Nb-Y-Zr plot, *Canadian Journal of Earth Sciences, 38*, 813-824, 2001.

References

Bandini, A.N., P.O. Baumgartner, and M. Caron, Turonian radiolarians from Karnezeika, Argolis Peninsula, Peloponnesus (Greece), *Eclogae Geologicae Helvetiae, 99*, S1-S20, 2006.

Bandini, A.N., K. Flores, P.O. Baumgartner, S.-J. Jackett, and P. Denyer, Late Cretaceous and Paleogene Radiolaria from the Nicoya Peninsula, Costa Rica: a tectonostratigraphic application, *Stratigraphy, 5*, 3-21, 2008.

Bandy, O.L., and R.E. Casey, Reflector Horizons and Paleobathymetric History, Eastern Panama, *Geological Society of America Bulletin, 84*, 3081-3086, 1973.

Bangs, N.L.B., S.P.S. Gulick, and T.H. Shipley, Seamount subduction erosion in the Nankai Trough and its potential impact on the seismogenic zone, *Geology, 34*, 701-704, 2006.

Barckhausen, U., C.R. Ranero, R. von Huene, S.C. Cande, and H.A. Roeser, Revised tectonic boundaries in the Cocos Plate off Costa Rica: Implications for the segmentation of the convergent margin and for plate tectonic models, *Journal of Geophysical Research-Solid Earth, 106*, 19207-19220, 2001.

Barckhausen, U., H.A. Roeser, and R. von Huene, Magnetic signature of upper plate structures and subducting seamounts at the convergent margin off Costa Rica, *Journal of Geophysical Research, B, Solid Earth and Planets, 103*, 7079-7093, 1998.

Barnes, P.M., and R.J. Korsch, Melange and related structures in Torlesse accretionary wedge, Wairarapa, New Zealand, *New Zealand Journal of Geology and Geophysics, 34*, 517-532, 1991.

Barr, J.A., K.S. Harpp, and D.L. Geist, Plagioclase-Ultraphyric Basalts of the Northern Galapagos and Plume-Ridge Interaction, *Eos Trans. AGU,, 85*, Abstract V43C-05, 2004.

Baumgartner, P.O., El complejo ofiolítico de Nicoya (Costa Rica): Modelos estructurales analizados en función de las edades de los Radiolarios (Calloviense a Santoniense), in *Manual de Geología de Costa Rica*, edited by P. Spechmann, pp. 115-123, Editorial Universidad de Costa Rica, San José Costa Rica, 1984.

Baumgartner, P.O., Discovery of subduction-related melanges on Cano Island and Osa Peninsula (Pacific, Costa Rica, Central America).; Onzieme reunion annuelle des sciences de la terre, *Reunion Annuelle des Sciences de la Terre, 11*, 12, 1986.

Baumgartner, P.O., K. Flores, A.N. Bandini, C. Baumgartner Mora, and D.M. Buchs, Terranes of NW-Costa Rica and the Hess Escarpment: A Pre-Campanian paleo-plate boundary, *18th Caribbean Geological Conference, March 2008, Santo Domingo, Dominican Republic*, 2008.

Baumgartner, P.O., J.A. Obando, C.R. Mora, J.E.T. Channell, and A. Steck, Paleogene accretion and suspect terranes in southern Costa Rica (Osa, Burica, Central America), *Transaction of the 12th Caribbean geological Conference, St croix, U.S., Virgin Islands*, 529 [Abstract], 1989.

Baumgartner-Mora, C., P.O. Baumgartner, D.M. Buchs, A.N. Bandini, and K. Flores, Paleocene to Oligocene Foraminifera from the Azuero Peninsula (Panama): The timing of seamount formation and accretion to the Mid-American Margin, in *18th Caribbean Geological Conference, March 2008, Santo Domingo, Dominican Republic*, 2008.

Becker, M.A., and J.A. Chamberlain Jr., Anomuran Microcoprolites from the Lowermost Navesink Formation (Maastrichtian), Monmouth County, New Jersey, *Ichnos, 13*, 1-9, 2006.

Ben-Avraham, Z., A. Nur, D. Jones, and A. Cox, Continental Accretion - from Oceanic Plateaus to Allochthonous Terranes, *Science, 213*, 47-54, 1981.

Bence, A.E., J.J. Papike, and R.A. Ayuso, Petrology of Submarine Basalts from Central Caribbean - Dsdp Leg 15, *Journal of Geophysical Research, 80*, 4775-4804, 1975.

Berrangé, J.P., D.R. Bradley, and N.J. Snelling, K/ Ar age dating of the ophiolitic Nicoya Complex of the Osa Peninsula, southern Costa Rica, *Journal of South American Earth Sciences, 2*, 49-59, 1989.

Berrangé, J.P., and R.S. Thorpe, The Geology, Geochemistry and Emplacement of the Cretaceous Tertiary Ophiolitic Nicoya Complex of the Osa Peninsula, Southern Costa-Rica, *Tectonophysics, 147*, 193-220, 1988.

Bilek, S.L., S.Y. Schwartz, and H.R. DeShon, Control of seafloor roughness on earthquake rupture behavior, *Geology, 31*, 455-458, 2003.

Blau, J., B. Gruen, and M. Senff, Crustaceen-Koprolithen aus der Trias der westlichen Tethys (Lienzer Dolomiten, Oesterreich; Pragser Dolomiten, Italien) und vom Gondwana-Westrand (oberes Magdalenatal, Kolumbien, Suedamerika), *Palaeontologische Zeitschrift, 67*, 193-214, 1993.

Blau, J., M. Moreno, and M. Senff, Palaxius caucaensis n.sp., a crustacean microcoprolite from the basal Nogales Formation (Campanian to Maastrichtian) of Colombia, *Micropaleontology, 41*, 85-88, 1995.

Bourgois, J., J. Azema, J. Tournon, H. Bellon, B. Calle, E. Parra, J.F. Toussaint, G. Glacon, H. Feinberg, P. Dewever, and I. Origlia, Ages and Structures of the Basic and Ultrabasic Complexes of the Pacific Coast between 3-Degrees-N and 12-Degrees-N (Colombia, Panama and Costa-Rica), *Bulletin De La Societe Geologique De France, 24*, 545-554, 1982.

Bowland, C.L., Depositional History of the Western Colombian Basin, Caribbean Sea, Revealed by Seismic Stratigraphy, *Geological Society of America Bulletin, 105*, 1321-1345, 1993.

Bowland, C.L., and E. Rosencrantz, Upper Crustal Structure of the Western Colombian Basin, Caribbean Sea, *Geological Society of America Bulletin, 100*, 534-546, 1988.

Briggs, J.C., The Genesis of Central-America - Biology Versus Geophysics, *Global Ecology and Biogeography Letters, 4*, 169-172, 1994.

Brönnimann, P., P. Cros, and L. Zaninetti, New Thalassinid Anomuran (Crustacea, Cecapoda) Coprolites from Infraliasic Limestones of the Dolomites, Italy, *Mitt. Ges. Geol. Bergbaustud. Österr., 21*, 921-928, 1972.

Brönnimann, P., and P. Norton, On the classification of fossil fecal pellets and description of new forms from Cuba, Guatemala and Lybia., *Eclogae Geologicae Helvetiae, 53*, 832-842, 1960.

Bryan, S.E., and R.E. Ernst, Revised definition of Large Igneous Provinces (LIPs), *Earth-Science Reviews, 86*, 175-202, 2008.

Buchs, D.M., Etude géologique et géochimique de la région du Golfo Dulce (Costa Rica) : Genèse et évolution d'édifices océaniques accrétés à la marge de la plaque caraïbe, in *unpublished master thesis, Université de Lausanne, Switzerland*, pp. 127, 2003.

Buchs, D.M., and P.O. Baumgartner, The mélange of Osa-Caño (Costa Rica) : an access to the sedimentary processes recorded in an emerged middle Eocene to middle Miocene accretionary prism, *10.Meeting of Swiss Sedimentologists (SWISS SED), [Abstract], Fribourg, Switzerland.*, 2003.

Buchs, D.M., and P.O. Baumgartner, Comment on "From seamount accretion to tectonic erosion: Formation of Osa Mélange and the effects of Cocos Ridge subduction in southern Costa Rica" by P. Vannucchi et al., *Tectonics, 26*, TC3009, doi:10.1029/2006TC002032, 2007.

Buchs, D.M., J. Guex, J. Stucki, and P.O. Baumgartner, Paleocene Thalassinidea colonization in deep-sea environment and the coprolite Palaxius osaensis n. ichnosp. in Southern Costa Rica, *Revue de Micropaléontologie*, in press.

Buchs, D.M., and J. Stucki, Etude géologique, géochimique et structurale du prisme d'accrétion de la péninsule d'Osa, Cosa Rica, in *unpublished diploma thesis, Université de Lausanne, Switzerland*, pp. 103, 2001.

Burke, K., Tectonic Evolution of the Caribbean, *Annual Review of Earth and Planetary Sciences, 16*, 201-230, 1988.

Burke, K., P.J. Fox, and A.M.C. Sengor, Buoyant Ocean-Floor and Evolution of Caribbean, *Transactions-American Geophysical Union, 59*, 405-405, 1978.

Byrne, T., and D. Fisher, Episodic Growth of the Kodiak Convergent Margin, *Nature, 325*, 338-341, 1987.

Calvo, C., and A. Bolz, La Formación Espíritu Santo (Costa Rica): sistema de plataforma carbonatada autóctona del Paleoceno sup.- Eoceno inf., *Revista Geológica de América Central, 13*, 91-95, 1991.

Carr, M.J., I. Saginor, G.E. Alvarado, L.L. Bolge, F.N. Lindsay, K. Milidakis, B.D. Turrin, M.D. Feigenson, and C.C. Swisher, Element fluxes from the volcanic front of Nicaragua and Costa Rica, *Geochemistry Geophysics Geosystems, 8*, 2007.

Carracedo, J.C., Growth, structure, instability and collapse of Canarian volcanoes and comparisons with Hawaiian volcanoes, *Journal of Volcanology and Geothermal Research, 94*, 1-19, 1999.

Carracedo, J.C., S. Day, H. Guillou, E.R. Badiola, J.A. Canas, and F.J.P. Torrado, Hotspot volcanism close to a passive continental margin: The Canary Islands, *Geological Magazine, 135*, 591-604, 1998.

Carter, R.M., Trench-Slope Channels from the New-Zealand Jurassic - Otekura Formation, Sandy Bay, South Otago, *Sedimentology, 26*, 475-496, 1979.

Cawood, P.A., Structural Relations in the Subduction Complex of the Paleozoic New-England Fold Belt, Eastern Australia, *Journal of Geology, 90*, 381-392, 1982.

References

Chang, C.P., J. Angelier, and C.Y. Huang, Origin and evolution of a melange: the active plate boundary and suture zone of the Longitudinal Valley, Taiwan, *Tectonophysics, 325*, 43-62, 2000.

Cherniak, D.J., REE diffusion in feldspar, *Chemical Geology, 193*, 25-41, 2003.

Chiaradia, M., and L. Fontbote, Radiogenic Lead Signatures in Au-Rich Volcanic-Hosted Massive Sulfide Ores and Associated Volcanic Rocks of the Early Tertiary Macuchi Island Arc(Western Cordillera of Ecuador)

10.2113/96.6.1361, *Economic Geology, 96*, 1361-1378, 2001.

Chiaradia, M., and L. Fontbote, Lead isotope systematics of Late Cretaceous Tertiary Andean arc magmas and associated ores between 8 degrees N and 40 degrees S: evidence for latitudinal mantle heterogeneity beneath the Andes, *Terra Nova, 14*, 337-342, 2002.

Chiaradia, M., and L. Fontbote, Separate lead isotope analyses of leachate and residue rock fractions: implications for metal source tracing in ore deposit studies, *Mineralium Deposita, 38*, 185-195, 2003.

Clague, D.A., and G.B. Dalrymple, The Hawaiian-Emperor volcanic chain, in *Volcanism in Hawaii*, edited by R.W. Decker, T.L. Wright and P.H. Stauffer, pp. 5-54, U.S. Government Printing Office, 1987.

Clague, D.A., K.A. Hon, J.L. Anderson, W.W. Chadwick, Jr., and C.G. Fox, Bathymetry of Puna Ridge, Kilauea Volcano, Hawaii, *Miscellaneous Field Studies Map - U*, 1994.

Clift, P., and P. Vannucchi, Controls on tectonic accretion versus erosion in subduction zones: Implications for the origin and recycling of the continental crust, *Reviews of Geophysics, 42*, 2004.

Cloos, M., Flow melanges and the structural evolution of accretionary wedges, in *Melanges: their nature, origin and significance*, vol. 198, *Special Paper - Geological Society of America*, pp. 71-79, 1984.

Cloos, M., Thrust-Type Subduction-Zone Earthquakes and Seamount Asperities - a Physical Model for Seismic Rupture, *Geology, 20*, 601-604, 1992.

Cloos, M., Lithospheric Buoyancy and Collisional Orogenesis - Subduction of Oceanic Plateaus, Continental Margins, Island Arcs, Spreading Ridges, and Seamounts, *Geological Society of America Bulletin, 105*, 715-737, 1993.

Cloos, M., and R.L. Shreve, Subduction-channel model of prism accretion, melange formation, sediment subduction, and subduction erosion at convergent plate margins; Part 1, Background and description, *Pure and Applied Geophysics, 128*, 455-500, 1988.

Coates, A.G., L.S. Collins, M.P. Aubry, and W.A. Berggren, The geology of the Darien, Panama, and the late Miocene-Pliocene collision of the Panama arc with northwestern South America, *Geological Society of America Bulletin, 116*, 1327-1344, 2004.

Coates, A.G., J.B.C. Jackson, L.S. Collins, T.M. Cronin, H.J. Dowsett, L.M. Bybell, P. Jung, and J.A. Obando, Closure of the Isthmus of Panama; the near-shore marine record of Costa Rica and western Panama, *Geological Society of America Bulletin, 104*, 814-828, 1992.

Collins, L.S., A.G. Coates, W.A. Berggren, M.P. Aubry, and J.J. Zhang, The late Miocene Panama isthmian strait, *Geology, 24*, 687-690, 1996.

Collins, L.S., A.G. Coates, J.B.C. Jackson, and J.A. Obando, Timing and rates of emergence of the Limon and Bocas del Torro basins; Caribbean effects of Cocos Ridge subduction?.; Geologic and tectonic development of the Caribbean Plate boundary in southern Central America, *Special Paper - Geological Society of America, 295*, 263-289, 1995.

Collot, J.Y., and M.A. Fisher, Formation of forearc basins by collision between seamounts and accretionary wedges; an example from the New Hebrides subduction zone, *Geology (Boulder), 17*, 930-933, 1989.

Collot, J.Y., K. Lewis, G. Lamarche, and S. Lallemand, The giant Ruatoria debris avalanche on the northern Hikurangi margin, New Zealand; results of oblique seamount subduction, *Journal of Geophysical Research, B, Solid Earth and Planets, 106*, 19,271-19,297, 2001.

Cowan, H., M.N. Machette, K.M. Haller, and R.L. Dart, Map and Database of Quaternary Faults and folds in Costa Rica and Its Offshore Regions. U.S. Department of the Interior U.S. Geological Survey. Open-File report, 98-779. 41 pp. http://greenwood.cr.usgs.gov/pub/open-file-reports/ofr-98-0779/ofr98-779.pdf, 1998.

Cullen, A., E. Vicenzi, and A.R. McBirney, Palgioclase-ultraphyric basalts of the Galapagos archipelago, *Journal of Volcanology and Geothermal Research, 37*, 325-337, 1989.

Davidson, J., S. Turner, H. Handley, C. Macpherson, and A. Dosseto, Amphibole "sponge" in arc crust?, *Geology, 35*, 787-790, 2007.

de Boer, Z.J., M.S. Drummond, M.J. Bordelon, M.J. Defant, H. Bellon, and R.C. Maury, Cenozoic magmatic phases of the Costa Rican island arc (Cordillera de Talamanca).; Geologic and tectonic development of the Caribbean Plate boundary in southern Central America, *Special Paper - Geological Society of America, 295*, 35-55, 1995.

Deering, C.D., T.A. Vogel, L.C. Patino, and G.E. Alvarado, Origin of distinct silicic magma types from the Guachipelin Caldera, NW Costa Rica: Evidence for magma mixing and protracted subvolcanic residence, *Journal of Volcanology and Geothermal Research, 165*, 103-126, 2007.

Del Giudice, D., and G. Recchi, Geología del area del projecto minero de Azuero. Ejectora, Informe Tecnico preparado para el Gobierno de la Republica de Panamá por las Naciones Unidas; Actuando y Participando como Agencia, pp. 48, 1969.

DeMets, C., A new estimate for present-day Cocos-Caribbean Plate motion; implications for slip along the Central American volcanic arc, *Geophysical Research Letters, 28*, 4043-4046, 2001.

DeMets, C., A new estimate for present-day Cocos-Caribbean plate motion; implications for slip along the central American volcanic arc; reply, *Geophysical Research Letters*, 2002.

Dengo, G., *Tectonic-igneous sequence in Costa Rica.; Petrologic studies--A volume in honor of A. F. Buddington*, 133-161 pp., 1962.

Denyer, P., and G.E. Alvarado, Mapa Geológico de Costa Rica 1: 400 000, Librería Francesa S.A., 2007.

Denyer, P., and P.O. Baumgartner, Emplacement of Jurassic-Lower Cretaceous radiolarites of the Nicoya Complex (Costa Rica), *Geologica Acta, 4*, 203-218, 2006.

Denyer, P., P.O. Baumgartner, and E. Gazel, Characterization and tectonic implications of mesozoic-cenozoic ocean assemblages of costa rica and western panama, *Geologica Acta, 4*, 219-235, 2006.

Denyer, P., P.O. Baumgartner, and E. Gazel, Characterization and tectonic implications of Mesozoic-Cenozoic oceanic assemblages of Costa Rica and Western Panama, *Geologica Acta, 4*, 219-235, 2007.

Di Marco, G., Les terrains accrétés du Costa Rica: évolution teconostratigraphique de la marge occidentale de la Plaque Caraïbe, *Mémoires de Géologie (Lausanne), 20*, 1994.

Di Marco, G., P.O. Baumgartner, and J.E.T. Channell, Late Cretaceous-early Tertiary paleomagnetic data and a revised tectonostratigraphic subdivision of Costa Rica and western Panama.; Geologic and tectonic development of the Caribbean Plate boundary in southern Central America, in *Geologic and Tectonic Development of the Caribbean plate boundary in southern Central America*, vol. 295, *Geological Society of America Special Paper*, edited by P. Mann, pp. 1-27, 1995.

Dickinson, W.R., Accretionary Mesozoic-Cenozoic expansion of the Cordilleran continental margin in California and adjacent Oregon, *Geosphere, 4*, 329-353, 2008.

Diebold, J., W. Driscoll Neal, and I. Ew-9501 Science Team, New insights on the formation of the Caribbean basalt province revealed by multichannel seismic images of volcanic structures in the Venezuelan Basin.; Caribbean basins, in *Sedimentary Basins of the World*, vol. 4, edited by P. Mann, pp. 561-589, 1999.

Diebold, J., W. Driscoll Neal, and I. Ew-9501 Science Team, New insights on the formation of the Caribbean basalt province revealed by multichannel seismic images of volcanic structures in the Venezuelan Basin.; Caribbean basins, in *Sedimentary Basins of the World*, vol. 4, edited by P. Mann, pp. 561-589, 1999.

Diserens, M.-O., Upper Cretaceous and Paleogene Radiolarian Biostratigraphy of Southern Costa Rica; Radiolarian faunas from the Rincon Block, Golfito and Burica Terranes, Osa-Cano Accretionary Complex and Herradura Block, unpublished master thesis, 65 pp., 2002.

Dominguez, S., S.E. Lallemand, J. Malavieille, and R. von Huene, Upper plate deformation associated with seamount subduction, *Tectonophysics, 293*, 207-224, 1998.

Dominguez, S., J. Malavieille, and S.E. Lallemand, Deformation of accretionary wedges in response to seamount subduction: Insights from sandbox experiments, *Tectonics, 19*, 182-196, 2000.

Donnelly, T.W., Late Cretaceous Basalts from Caribbean - Possible Flood Basalt Province of Vast Size, *Transactions-American Geophysical Union, 54*, 1004-1004, 1973.

Donnelly, T.W., D. Beets, M.J. Carr, T. Jackson, G. Klaver, J.F. Lewis, R. Maury, H. Schellenkens, A.L. Smith, G. Wadge, and D. Westercamp, History and tectonic setting of Caribbean magmatism., in *The geology of North America*, vol. The Caribbean region, edited by G. Dengo and J.E. Case, pp. 339-374, 1990.

References

Donnelly, T.W., R. Kay, and J.J.W. Rogers, Chemical Petrology of Caribbean Basalts and Dolerites - Leg 15, Deep-Sea Drilling Project, *Transactions-American Geophysical Union, 54*, 1002-1004, 1973.

Doubleday, P.A., P.T. Leat, T. Alabaster, P.A.R. Nell, and T.H. Tranter, Allochthonous Oceanic Basalts within the Mesozoic Accretionary Complex of Alexander Island, Antarctica - Remnants of Proto-Pacific Oceanic-Crust, *Journal of the Geological Society, 151*, 65-78, 1994a.

Doubleday, P.A., and T.H. Tranter, Deformation Mechanism Paths for Oceanic Rocks During Subduction and Accretion - the Mesozoic Fore-Arc of Alexander-Island, Antarctica, *Journal of the Geological Society, 151*, 543-554, 1994b.

Dumitrica, P., Cenomanian Radiolaria at Podul Dimbovitei. Micropaleontological guide to the Mesozoic and Tertiary of the Romanian Carpathians, in *14th European Micropaleontological Colloquium, Romania*, pp. 87-89, Bucharest: Institute of Geology and Geophysics, 1975.

Dupuis, C., R. Hébert, V. Dubois-Côté, C. Guilmette, C.S. Wang, Y.L. Li, and Z.J. Li, The Yarlung Zangbo Suture Zone ophiolitic mélange (southern Tibet): new insights from geochemistry of ultramafic rocks, *Journal of Asian Earth Sciences, 25*, 937-960, 2005.

Dworschak, P.C., Global Diversity in the Thalassinidea (Decapoda), *Journal of Crustacean Biology, 20*, 238-245, 2000.

Dworschak, P.C., Global diversity in the Thalassinidea (Decapoda): an update (1998-2004), *Nauplius, 13*, 57-63, 2005.

Escuder-Viruete, J., A. Perez-Estaun, F. Contreras, M. Joubert, D. Weis, T.D. Ullrich, and P. Spadea, Plume mantle source heterogeneity through time: Insights from the Duarte Complex, Hispaniola, northeastern Caribbean, *Journal of Geophysical Research-Solid Earth, 112*, 2007.

Evangelidis, C.P., T.A. Minshull, and T.J. Henstock, Three-dimensional crustal structure of Ascension Island from active source seismic tomography, *Geophysical Journal International, 159*, 311-325, 2004.

Ewart, A., and C.J. Hawkesworth, The Pleistocene-Recent Tonga-Kermadec Arc Lavas: Interpretation of New Isotopic and Rare Earth Data in Terms of a Depleted Mantle Source Model, *Journal of Petrology, 28*, 495-530, 1987.

Feigenson, M.D., M.J. Carr, S.V. Maharaj, S. Juliano, and L.L. Bolge, Lead isotope composition of central American volcanoes: Influence of the Galapagos plume, *Geochemistry Geophysics Geosystems, 5*, 2004.

Ferrari, O., C. Hochard, and G.M. Stampfli, An alternative plate tectonic model for the Palaeozoic–Early Mesozoic Palaeotethyan evolution of Southeast Asia (Northern Thailand–Burma), *Tectonophysics, 451*, 346-365, 2008.

Fisher, D.M., T.W. Gardner, J.S. Marshall , and P.W. Montero, Kinematics associated with late Cenozoic deformation in central Costa Rica; western boundary of the Panama Microplate, *Geology (Boulder), 22*, 263-266, 1994.

Fisher, D.M., T.W. Gardner, J.S. Marshall, P.B. Sak, and M. Protti, Effect of subducting sea-floor roughness on fore-arc kinematics, Pacific Coast, Costa Rica, *Geology, 26*, 467-470, 1998.

Fisher, S.P., and E.A. Pessagno, Jr., Upper Cretaceous strata of northwestern Panama, *Bulletin of the American Association of Petroleum Geologists, 49*, 433-444, 1965.

Fitton, J.G., A.D. Saunders, M.J. Norry, B.S. Hardarson, and R.N. Taylor, Thermal and chemical structure of the Iceland plume, *Earth and Planetary Science Letters, 153*, 197-208, 1997.

Flores, K., Propuesta tectonoestratigráfica de la región septentrional del golfo de Nicoya, Costa Rica, Licenciatura thesis, 176 pp., University of Costa Rica, Costa Rica, 2003.

Flores, K., P.O. Baumgartner, P. Denyer, A.N. Bandini, and C. Baumgartner-Mora, Pre-Campanian Terranes in Nicoya area (Costa Rica, Middle America), in *2nd Swiss Geoscience Meeting*, pp. 2, Lausanne (Switzerland), 2004.

Flueh, E.R., and R. von Huene, Crustal Structure, in *Central America - Geology, Resources and Hazards*, edited by J. Bundschuh and G.E. Alvarado, pp. 267-276, Taylor and Francis, Oxford, 2007.

Foreman, H.P., Radiolaria from the North Pacific, Deep Sea Drilling Project, Leg 32, *Initial Reports of the Deep Sea Drilling Project, 32*, 579-676, 1975.

Foreman, H.P., Mesozoic Radiolaria from the Atlantic Basin and its borderlands.; Stratigraphic micropaleontology of Atlantic Basin and borderlands, 305-320, 1977.

Foreman, H.P., B.C. Heezen, I.D. MacGregor, G.Z. Forristall, H. Hekel, R. Hesse, R.H. Hoskins, E. Jones, W. John, V. Krasheninnikov, H. Okada, and M.H. Ruef, Radiolaria from DSDP Leg 20.; Initial reports of the Deep Sea Drilling Project, covering Leg 20 of the cruises of the drilling vessel Glomar Challenger; Yokohama, Japan to Suva, Fiji September-November 1971, *Initial Reports of the Deep Sea Drilling Project, 20*, 249-303, 1973.

Franco, H., and D. Abbott, Gravity signatures of terrane accretion, *Lithos, 46*, 5-15, 1999.

Frisch, W., M. Meschede, and M. Sick, Origin of the Central American ophiolites; evidence from paleomagnetic results; with Suppl. Data 92-24, *Geological Society of America Bulletin, 104*, 1301-1314, 1992.

Gaetani, G.A., A.J.R. Kent, T.L. Grove, I.D. Hutcheon, and E.M. Stolper, Mineral/melt partitioning of trace elements during hydrous peridotite partial melting, *Contributions to Mineralogy and Petrology, 145*, 391-405, 2003.

Gans, P.B., I.G. Alvarado, W. Perez, I. MacMillan, and A. Calvert, Neogene evolution of the Costa Rican Arc and development of the Cordillera Central.; Geological Society of America, Cordilleran Section, 99th annual meeting, *Abstracts with Programs - Geological Society of America, 35*, 74, 2003.

Garcia, M.O., E.H. Haskins, E.M. Stolper, and M. Baker, Stratigraphy of the Hawai'i Scientific Drilling Project core (HSDP2): Anatomy of a Hawaiian shield volcano, *Geochemistry Geophysics Geosystems, 8*, 2007.

Gardner, T., J. Marshall, D. Merritts, B. Bee, R. Burgette, E. Burton, J. Cooke, N. Kehrwald, M. Protti, D. Fisher, and P. Sak, Holocene forearc block rotation in response to seamount subduction, southeastern Peninsula de Nicoya, Costa Rica, *Geology, 29*, 151-154, 2001.

Gayet, M., J.C. Rage, T. Sempere, and P.Y. Gagnier, Mode of Interchanges of Continental Vertebrates between North and South-America During the Late Cretaceous and Paleocene, *Bulletin De La Societe Geologique De France, 163*, 781-791, 1992.

Geldmacher, J., B.B. Hanan, J. Blichert-Toft, K. Harpp, K. Hoernle, F. Hauff, R. Werner, and A.C. Kerr, Hafnium isotopic variations in volcanic rocks from the Caribbean Large Igneous Province and Galápagos hot spot tracks, *Geochemistry Geophysics Geosystems, 4*, 1062, doi:10.1029/2002GC000477, 2003.

Geldmacher, J., K. Hoernle, P. van den Bogaard, F. Hauff, and A. Klügel, Age and geochemistry of the Central American forearc basement (DSDP Leg 67 and 84): Insights into Mesozoic arc volcanism and seamount accretion, *Journal of Petrology*, submitted.

George, A.D., Radiolarians in Offscraped Seamount Fragments, Aorangi Range, New-Zealand, *New Zealand Journal of Geology and Geophysics, 36*, 185-199, 1993.

Graefe, K., W. Frisch, I.M. Villa, and M. Meschede, Geodynamic evolution of southern Costa Rica related to low-angle subduction of the Cocos Ridge: constraints from thermochronology, *Tectonophysics, 348*, 187-204, 2002.

Hall, C.E., M. Gurnis, M. Sdrolias, L.L. Lavier, and R.D. Muller, Catastrophic initiation of subduction following forced convergence across fracture zones, *Earth and Planetary Science Letters, 212*, 15-30, 2003.

Hampton, M.A., H.J. Lee, and J. Locat, Submarine landslides, *Reviews of Geophysics, 34*, 33-59, 1996.

Hansen, H., and K. Grönvold, Plagioclase ultraphyric basalts in Iceland: the mush of the rift, *Journal of Volcanology and Geothermal Research, 98*, 1-32, 2000.

Harpp, K.S., V.D. Wanless, R.H. Otto, K. Hoernle, and R. Werner, The Cocos and Carnegie Aseismic Ridges: a Trace Element Record of Long-term Plume-Spreading Center Interaction, *Journal of Petrology, 46*, 109-133, 2005.

Hart, S.R., and K.E. Davis, Nickel Partitioning between Olivine and Silicate Melt, *Earth and Planetary Science Letters, 40*, 203-219, 1978.

Hart, S.R., and T. Dunn, Experimental cpx/melt partitioning of 24 trace elements, *Contributions to Mineralogy and Petrology, 13*, 1-8, 1993.

Hashimoto, Y., and G. Kimura, Underplating process from melange formation to duplexing: Example from the Cretaceous Shimanto Belt, Kii Peninsula, southwest Japan, *Tectonics, 18*, 92-107, 1999.

Hastie, A.R., A.C. Kerr, J.A. Pearce, and S.F. Mitchell, Classification of altered volcanic island arc rocks using immobile trace elements: Development of the Th-Co discrimination diagram, *Journal of Petrology, 48*, 2341-2357, 2007.

References

Hauff, F., K. Hoernle, H.-U. Schmincke, and R. Werner, A Mid Cretaceous origin for the Galápagos hotspot: volcanological, petrological and geochemical evidence from Costa Rican oceanic crustal segments, *Geologische Rundschau, 86*, 141-155, 1997.

Hauff, F., K. Hoernle, P. van den Bogaard, G. Alvarado, and D. Garbe Schoenberg, Age and geochemistry of basaltic complexes in western Costa Rica; contributions to the geotectonic evolution of Central America, *Geochemistry, Geophysics, Geosystems - G 3*, 2000.

Haug, G.H., and R. Tiedemann, Effect of the formation of the Isthmus of Panama on Atlantic Ocean thermohaline circulation, *Nature, 393*, 673-676, 1998.

Henningsen, D., Notes on stratigraphy and paleontology of upper Cretaceous and Tertiary sediments in southern Costa Rica, *American Association of Petroleum Geologists Bulletin, 50*, 562-566, 1963.

Hey, R., Tectonic Evolution of Cocos-Nazca Spreading Center, *Geological Society of America Bulletin, 88*, 1404-1420, 1977.

Higgins, M.D., and D. Chandrasekharam, Nature of Sub-volcanic Magma Chambers, Deccan Province, India: Evidence from Quantitative Textural Analysis of Plagioclase Megacrysts in the Giant Plagioclase Basalts, *Journal of Petrology, 48*, 885-900, 2007.

Hill, R.I., Mantle Plumes and Continental Tectonics, *Lithos, 30*, 193-206, 1993.

Hillier, J.K., Pacific seamount volcanism in space and time, *Geophysical Journal International, 168*, 877-889, 2007.

Hoernle, K., D.L. Abt, K.M. Fischer, H. Nichols, F. Hauff, G.A. Abers, P. van den Bogaard, K. Heydolph, G. Alvarado, M. Protti, and W. Strauch, Arc-parallel flow in the mantle wedge beneath Costa Rica and Nicaragua, *Nature, doi:10.1038/nature06550*, 2008.

Hoernle, K., and F. Hauff, Oceanic Igneous Complexes, in *Central America, geology, resources, hazards*, vol. 1, edited by J. Bundschuh and G. Alvarado, pp. 523-548, 2007.

Hoernle, K., F. Hauff, and P. van den Bogaard, 70 m.y. history (139-69 Ma) for the Caribbean large igneous province, *Geology, 32*, 700, 2004.

Hoernle, K., P. van den Bogaard, R. Werner, B. Lissinna, F. Hauff, G. Alvarado, and D. Garbe-Schonberg, Missing history (16-71 Ma) of the Galpapagos hotspot: Implications for the tectonic and biological evolution of the Americas, *Geology, 30*, 795-798, 2002.

Hofmann, A.W., Chemical Differentiation of the Earth - the Relationship between Mantle, Continental-Crust, and Oceanic-Crust, *Earth and Planetary Science Letters, 90*, 297-314, 1988.

Hollis, C.J., and K. Kimura, A unified radiolarian zonation for the Late Cretaceous and Paleocene of Japan, *Micropaleontology, 47*, 235-255, 2001.

Honkura, Y., Y. Nagaya, and H. Kuroki, Effects of seamounts on an interplate earthquake at the Suruga trough, Japan, *Earth Planets and Space, 51*, 449-454, 1999.

Huang, S., and F.A. Frey, Trace element abundances of Mauna Kea basalt from phase 2 of the Hawaii Scientific Drilling Project: Petrogenetic implications of correlations with major element content and isotopic ratios, *Geochemistry Geophysics Geosystems, 4*, 2003.

Huehnerbach, V., D.G. Masson, G. Bohrmann, J.M. Bull, and W. Weinrebe, Deformation and submarine landsliding caused by seamount subduction beneath the Costa Rica continental margin; new insights from high-resolution sidescan sonar data.; Submarine slope systems; processes and products, *Geological Society Special Publications, 244*, 195-205, 2005.

Husen, S., E. Kissling, and R. Quintero, Tomographic evidence for a subducted seamount beneath the Gulf of Nicoya, Costa Rica: The cause of the 1990 Mw=7.0 Gulf of Nicoya earthquake, *Geophysical Research Letters, 29*, 2002.

Ikesawa, E., G. Kimura, K. Sato, K. Ikehara-Ohmori, Y. Kitamura, A. Yamaguchi, K. Ujiie, and Y. Hashimoto, Tectonic incorporation of the upper part of oceanic crust to overriding plate of a convergent margin: An example from the Cretaceous–early Tertiary Mugi Mélange, the Shimanto Belt, Japan, *Tectonophysics, 401*, 217-230, 2005.

Irvine, T.N., and W.R.A. Bargar, A Guide to the Chemical Classification of the Common Volcanic Rocks, *Canadian Journal of Earth Sciences, 8*, 523-548, 1971.

Isozaki, Y., S. Maruyama, and F. Furuoka, Accreted Oceanic Materials in Japan, *Tectonophysics, 181*, 179-205, 1990.

Jaccard, S., M. Muenster, B.-P. O., C. Baumgartner-Mora, and P. Denyer, Barra Honda (upper Paleocene-lower Eocene) and El Viejo (Campanian-Maastrichtian) carbonate platforms in the Tempisque area (Guanacaste, Costa Rica), *Revista Geologica de America Central, 24*, 9-27, 2001.

James, K.H., Arguments for and against the pacific origin of the caribbean plate: discussion, finding for an inter-american origin, *Geologica Acta, 4*, 279-302, 2006.

Jolly, W.T., J.H. Schellekens, and A.P. Dickin, High-Mg andesites and related lavas from southwest Puerto Rico (Greater Antilles Island Arc): Petrogenetic links with emplacement of the late cretaceous Caribbean mantle plume, *Lithos, 98*, 1-26, 2007.

Jones, G., H. Sano, and E. Valsamijones, Nature and Tectonic Setting of Accreted Basalts from the Mino Terrane, Central Japan, *Journal of the Geological Society, 150*, 1167-1181, 1993.

Kelemen, P.B., G.M. Yogodzinski, and D. W. Scholl, Along-strike Variation in Lavas of the Aleutian Island Arc: Genesis of High Mg# Andesite and Implications for Continental Crust, vol. 138, *Geophysical Monograph Series*, edited by J. Eiler, pp. 223-276, 2004.

Keller, R.A., M.R. Fisk, and W.M. White, Isotopic evidence for Late Cretaceous plume-ridge interaction at the Hawaiian hotspot, *Nature, 405*, 673-676, 2000.

Kellogg, J.N., and V. Vega, Tectonic development of Panama, Costa Rica, and the Colombian Andes: Constraints from Global Positioning System geodetic studies and gravity,, in *Geologic and Tectonic Development of the Caribbean plate boundary in southern Central America*, vol. 295, *Geological Society of America Special Paper*, edited by P. Mann, pp. 75-90, 1995.

Kennan, L., and J. Pindell, Dextral shear, terrane accretion and basin formation in the Northern Andes: explained only by interaction with a Pacific-derived Caribbean Plate, in *Geology of the area between North and South America, with focus on the origin of the Caribbean Plate (in preparation)*, *Geological Society of London (Special Publication)*, edited by K.H. James, M.A. Lorente and J. Pindell, submitted.

Kerr, A.C., Oceanic Plateaus, in *Treatise on Geochemistry*, vol. 3, edited by R.L. Rudnick, H.D. Holland and K.K. Turekian, pp. 537-565, 2003.

Kerr, A.C., La Isla de Gorgona, Colombia: A petrological enigma?, *Lithos, 84*, 77-101, 2005.

Kerr, A.C., and J.J. Mahoney, Oceanic plateaus: Problematic plumes, potential paradigms, *Chemical Geology, 241*, 332-353, 2007.

Kerr, A.C., G.F. Marriner, J. Tarney, A. Nivia, A.D. Saunders, M.F. Thirlwall, and C.W. Sinton, Cretaceous basaltic terranes in western Colombia: Elemental, chronological and Sr-Nd isotopic constraints on petrogenesis, *Journal of Petrology, 38*, 677-702, 1997.

Kerr, A.C., and J. Tarney, Tectonic evolution of the Caribbean and northwestern South America: The case for accretion of two Late Cretaceous oceanic plateaus, *Geology, 33*, 269-272, 2005.

Kerr, A.C., J. Tarney, P.D. Kempton, P. Spadea, A. Nivia, G.F. Marriner, and R.A. Duncan, Pervasive mantle plume head heterogeneity : Evidence from the late Cretaceous Caribbean-Colombian oceanic plateau, *Journal of Geophysical Research, 107*, 2002.

Kerr, A.C., J. Tarney, G.F. Marriner, A. Nivia, G.T. Klaver, and A.D. Saunders, The geochemistry and tectonic setting of late Cretaceous Caribbean and Colombian volcanism, *Journal of South American Earth Sciences, 9*, 111-120, 1996.

Kerr, A.C., J. Tarney, A. Nivia, G.F. Marriner, and A.D. Saunders, The internal structure of oceanic plateaus: inferences from obducted Cretaceous terranes in western Colombia and the Caribbean, *Tectonophysics, 292*, 173-188, 1998.

Kerr, A.C., R.V. White, T.P.M. E., J. Tarney, and A.S. Saunders, No oceanic plateau; no Caribbean Plate? The seminal role of an oceanic plateau in Caribbean Plate evolution.; The circum-Gulf of Mexico and the Caribbean; hydrocarbon habitats, basin formation, and plate tectonics, *AAPG Memoir, 79*, 126-168, 2003.

Kimura, G., and J. Ludden, Peeling Oceanic-Crust in Subduction Zones, *Geology, 23*, 217-220, 1995.

Kimura, G., and A. Mukai, Underplated Units in an Accretionary Complex - Melange of the Shimanto Belt of Eastern Shikoku, Southwest Japan, *Tectonics, 10*, 31-50, 1991.

Kingsley, R.H., and J.G. Schilling, Plume-ridge interaction in the Easter Salas y Gomez seamount chain Easter Microplate system: Pb isotope evidence, *Journal of Geophysical Research-Solid Earth, 103*, 24159-24177, 1998.

References

Kinzler, R.J., T.L. Grove, and S.I. Recca, An Experimental-Study on the Effect of Temperature and Melt Composition on the Partitioning of Nickel between Olivine and Silicate Melt, *Geochimica Et Cosmochimica Acta, 54*, 1255-1265, 1990.

Kobayashi, K., J.P. Cadet, J. Aubouin, J. Boulegue, J. Dubois, R. Vonhuene, L. Jolivet, T. Kanazawa, J. Kasahara, K. Koizumi, S. Lallemand, Y. Nakamura, G. Pautot, K. Suyehiro, S. Tani, H. Tokuyama, and T. Yamazaki, Normal Faulting of the Daiichi-Kashima Seamount in the Japan Trench Revealed by the Kaiko-I Cruise, Leg-3, *Earth and Planetary Science Letters, 83*, 257-266, 1987.

Kodaira, S., N. Takahashi, A. Nakanishi, S. Miura, and Y. Kaneda, Subducted seamount imaged in the rupture zone of the 1946 Nankaido earthquake, *Science, 289*, 104-106, 2000.

Kolarsky, R.A., and P. Mann, Structure and neotectonics of an oblique-subduction margin, southwestern Panama.; Geologic and tectonic development of the Caribbean Plate boundary in southern Central America, in *Geologic and tectonic development of the Caribbean Plate boundary in southern Central America*, vol. 295, *Geological Society of America Special Paper*, edited by P. Mann, pp. 131-157, 1995.

Kolarsky, R.A., P. Mann, S. Monechi, H.D. Meyerhoff, and E.A. Pessagno, Jr., Stratigraphic development of southwestern Panama as determined from integration of marine seismic data and onshore geology.; Geologic and tectonic development of the Caribbean Plate boundary in southern Central America, in *Geologic and tectonic development of the Caribbean Plate boundary in southern Central America*, vol. 295, *Geological Society of America Special Paper*, edited by P. Mann, pp. 159-200, 1995b.

Kolarsky, R.A., P. Mann, and W. Montero, Island arc response to shallow subduction of the Cocos Ridge, Costa Rica.; Geologic and tectonic development of the Caribbean Plate boundary in southern Central America, *Special Paper - Geological Society of America, 295*, 235-262, 1995a.

Kopp, H., E.R. Flueh, C.J. Petersen, W. Weinrebe, and A. Wittwer, The Java margin revisited: Evidence for subduction erosion off Java, *Earth and Planetary Science Letters, 242*, 130-142, 2006.

Krawinkel, H., S. Wozazek, J. Krawinkel, and W. Hellmann, Heavy-mineral analysis and clinopyroxene geochemistry applied to provenance analysis of lithic sandstones from the Azuero-Sona Complex (NW Panama), *Sedimentary Geology, 124*, 149-168, 1999.

Kukowski, N., and O. Oncken, Subduction Erosion - the "Normal" Mode of Fore-Arc Material Transfer along the Chilean Margin?, in *The Andes*, pp. 217-236, 2006.

Lallemand, S.E., P. Schnuerle, and J. Malavieille, Coulomb theory applied to accretionary and nonaccretionary wedges; possible causes for tectonic erosion and/ or frontal accretion, *Journal of Geophysical Research, B, Solid Earth and Planets, 99*, 12,033-12,055, 1994.

Langenheim, V.A.M., and D.A. Clague, The Hawaiian-Emperor volcanic chain; Part II, Stratigraphic framework of volcanic rocks of the Hawaiian Islands, in *Volcanism in Hawaii*, edited by R.W. Decker, T.L. Wright and P.H. Stauffer, pp. 55-84, U.S. Government Printing Office, 1987.

Lapierre, H., D. Bosch, V. Dupuis, M. Polve, R.C. Maury, J. Hernandez, P. Monie, D. Yeghicheyan, E. Jaillard, M. Tardy, B.M. de Lepinay, M. Mamberti, A. Desmet, F. Keller, and F. Senebier, Multiple plume events in the genesis of the peri-Caribbean Cretaceous oceanic plateau province, *Journal of Geophysical Research-Solid Earth, 105*, 8403-8421, 2000.

Larsen, L.M., Distribution of Ree and Other Trace-Elements between Phenocrysts and Peralkaline Undersaturated Magmas, Exemplified by Rocks from the Gardar Igneous Province, South Greenland, *Lithos, 12*, 303-315, 1979.

Le Maitre, R.W., P. Bateman, A. Dudek, J. Keller, J. Lemeyre, M.J. Le Bas, P.A. Sabine, R. Schmid, H. Sorensen, A. Streckeisen, A.R. Wooley, and B. Zanettin, *Igneous Rocks: A Classification and Glossary of Terms*, Blackwell Scientific, Oxford, 1989.

Le Pichon, X., P. Henry, and S.J. Lallemant, Accretion and erosion in subduction zones; the role of fluids, *Annual Review of Earth and Planetary Sciences, 21*, 307-331, 1993.

Leat, R.T., J.L. Smellie, I.L. Millar, and R.D. Larter, Magmatism in the South Sandwich arc, in *Intra-oceanic Subduction Systems: Tectonic and Magmatic Processes*, vol. 219, *Geological Society of London Special Publications*, edited by R.D. Larter and P.T. Leat, pp. 285-313, 2003.

Lin, S.-C., and P.E. van Keken, Dynamics of thermochemical plumes: 1. Plume formation and entrainment of a dense layer, *Geochemistry Geophysics Geosystems, 7*, Q02006, doi:10.1029/2005GC001071, 2006.

Lissinna, B., A profile though the Central American Landbridge in western Panama: 115 Ma Interplay between the Galápagos Hotspot and the Central American Subduction Zone, Unpublished PhD thesis, 102 pp., Christian-Albrechts University, Kiel, 2005.

Lissinna, B., K. Hoernle, F. Hauff, P. van den Bogaard, and S. Sadofsky, The Panamanian island arc and Galápagos hotspot: A case study for the long-term evolution of arc / hotspot interaction, *Geophysical Research Abstracts, 8*, 05106, 2006.

Lissinna, B., K. Hoernle, and P. van den Bogaard, Northern migration of arc volcanism in western Panama: evidence for subduction erosion?, *Eos Transactions, American Geophysical Union, 83*, 1463-1464, 2002.

Lonsdale, P., Creation of the Cocos and Nazca plates by fission of the Farallon plate, *Tectonophysics, 404*, 237-264, 2005.

Lundberg, N., Evolution of the slope landward of the Middle America Trench, Nicoya Peninsula, Costa Rica.; Trench-Forearc geology; sedimentation and tectonics on modern and ancient active plate margins, conference, *Special Publication - Geological Society of London, 10*, 131-147, 1982.

Lundberg, N., Detrital Record of the Early Central-American Magmatic Arc - Petrography of Intraoceanic Fore-Arc Sandstones, Nicoya Peninsula, Costa-Rica, *Geological Society of America Bulletin, 103*, 905-915, 1991.

Luzieux, L.D.A., F. Heller, R. Spikings, C.F. Vallejo, and W. Winkler, Origin and Cretaceous tectonic history of the coastal Ecuadorian forearc between 1 degrees N and 3 degrees S: Paleomagnetic, radiometric and fossil evidence, *Earth and Planetary Science Letters, 249*, 400-414, 2006.

Macdonald, R., C.J. Hawkesworth, and E. Heath, The Lesser Antilles volcanic chain: a study in are magmatism, *Earth-Science Reviews, 49*, 1-76, 2000.

MacKenzie, L., G.A. Abers, K.M. Fischer, E.M. Syracuse, J.M. Protti, V. Gonzalez, and W. Strauch, Crustal structure along the southern Central American volcanic front, *Geochemistry Geophysics Geosystems, 9*, Q08S09, doi:10.1029/2008GC001991, 2008.

MacMillan, I., P.B. Gans, and G. Alvarado, Middle Miocene to present plate tectonic history of the southern Central American volcanic arc.; Continental margins of the Pacific Rim, *Tectonophysics, 392*, 325-348, 2004.

Macpherson, G.J., The Snow Mountain Volcanic Complex - an on-Land Seamount in the Franciscan Terrain, California, *Journal of Geology, 91*, 73-92, 1983.

Mamberti, M., Origin and evolution of two distinct Creaceous oceanic plateaus accreted in Western Ecuador (South America): Petrological, geochemical and isotopic evidence, unpublished PhD thesis, 241 pp., Université Joseph Fourier, Grenoble, 2001.

Mann, P., Overview of the tectonic history of northern Central America.; Geologic and tectonic development of the Caribbean Plate boundary in northern Central America, in *Geologic and tectonic development of the Caribbean Plate boundary in northern Central America*, vol. 428, *Geological Society of America Special Paper*, edited by P. Mann, pp. 1-19, 2007.

Mann, P., and J. Corrigan, Model for Late Neogene Deformation in Panama, *Geology, 18*, 558-562, 1990.

Mann, P., and R.A. Kolarsky, East Panama deformed belt; structure, age, and neotectonic significance.; Geologic and tectonic development of the Caribbean Plate boundary in southern Central America, *Special Paper - Geological Society of America, 295*, 111-130, 1995.

Mann, P., and A. Taira, Global tectonic significance of the Solomon Islands and Ontong Java Plateau convergent zone, *Tectonophysics, 389*, 137-190, 2004.

Marshall, J.S., D.M. Fisher, and T.W. Gardner, Central Costa Rica deformed belt: Kinematics of diffuse faulting across the western Panama block, *Tectonics, 19*, 468-492, 2000.

Marshall, J.S., B.D. Idleman, T.W. Gardner, and D.M. Fisher, Landscape evolution within a retreating volcanic arc, Costa Rica, Central America, *Geology (Boulder), 31*, 419-422, 2003.

Maruyama, S., and J.G. Liou, Possible Depth Limit for Underplating by a Seamount, *Tectonophysics, 160*, 327-337, 1989.

Matsuda, S., and Y. Ogawa, Two-stage model of incorporation of seamount and oceanic blocks into sedimentary melange: Geochemical and biostratigraphic constraints in Jurassic Chichibu accretionary complex, Shikoku, Japan, *The Island Arc, 2*, 7-14, 1993.

Mauffret, A., and S. Leroy, Seismic stratigraphy and structure of the Caribbean igneous province, *Tectonophysics, 283*, 61-104, 1997.

References

Mauffret, A., S. Leroy, J.M. Vila, E. Hallot, B.M. de Lepinay, and R.A. Duncan, Prolonged magmatic and tectonic development of the Caribbean Igneous Province revealed by a diving submersible survey, *Marine Geophysical Researches, 22*, 17-45, 2001.

Maury, R.C., M.J. Defant, H. Bellon, Z.J. de Boer, R.H. Stewart, and J. Cotten, Early Tertiary arc volcanics from eastern Panama.; Geologic and tectonic development of the Caribbean Plate boundary in southern Central America, in *Geological Society of America Special Paper*, vol. 295, edited by P. Mann, pp. 29-34, 1995.

McCarthy, D., Biogeographical and geological evidence for a smaller, completely-enclosed Pacific Basin in the Late Cretaceous, *Journal of Biogeography, 32*, 2161-2177, 2005.

McDonough, W.F., and S.S. Sun, The composition of the Earth.; Chemical evolution of the mantle, *Chemical Geology, 120*, 223-253, 1995.

McMurtry, G.M., P. Watts, G.J. Fryer, J.R. Smith, and F. Imamura, Giant landslides, mega-tsunamis, and paleo-sea level in the Hawaiian Islands, *Marine Geology, 203*, 219-233, 2004.

Medley, E.W., The Engineering Characterization of Melanges and Similar Block-in-Matrix Rocks (Bimrocks), 338 pp., University of California, 1994.

Medley, E.W., Orderly Characterization of Chaotic Franciscan Melanges, *Engineering Geology, 19*, 20-33, 2001.

Mende, A., Sedimente und Architektur der Forearc-und Backarc-Becken von Südost-Costa Rica und Nordwest-Panamá, *Profil, 19*, 1-130, 2001.

Mende, A., and A. Asorga, Incorporating geology and geomorphology in land management decisions in developing countries: A case study in Southern Costa Rica, *Geomorphology, 87*, 68-89, 2007.

Meschede, M., The Costa Rica convergent margin: a textbook example for the process of subduction erosion, *Neues Jahrbuch Fur Geologie Und Palaontologie-Abhandlungen, 230*, 409-428, 2003.

Meschede, M., and U. Barckhausen, The relationship of the Cocos and Carnegie ridges: age constraints from paleogeographic reconstructions, *International Journal of Earth Sciences, 90*, 386-392, 2001.

Meschede, M., and W. Frisch, Geochemical characteristics of basaltic rocks from the Central American ophiolites, *Profil, 7*, 1994.

Meschede, M., P. Zweigel, W. Frisch, and D. Voelker, Melange formation by subduction erosion; the case of the Osa melange in southern Costa Rica, *Terra Nova, 11*, 141-148, 1999.

Metti, A., and G. Recchi, Proyecto Minero Fase III. Geologia de la Peninsula de Sona e Isla de Coiba y reconocimiento geoquimico, Minerales, Ministerio de Comercio e Industrias, Direccion General de Recoursos, 1972.

Montero, W., P. Denyer, R. Barquero, G.E. Alavarado, H. Cowan, M.N. Machette, K.M. Haller, and R.L. Dart, Map and Database of Quaternary Faults and folds in Costa Rica and Its Offshore Regions. U.S. Department of the Interior U.S. Geological Survey, Open-File report, 98-481. 63 pp. http://greenwood.cr.usgs.gov/pub/open-file-reports/ofr-98-0481/, 1998.

Moore, H.B., The Faecal Pellets of the Anomura, *Proc. Roy. Soc. Edinburgh, 52*, 296-308, 1932.

Moore, J.C., Tectonics and hydrogeology of accretionary prisms: Role of the decollement zone, *Journal of Structural Geology, 11*, 1989.

Moore, J.G., Petrology of Deep-Sea Basalt near Hawaii, *American Journal of Science, 263*, 40-&, 1965.

Moore, J.G., W.B. Bryan, M.H. Beeson, and W.R. Normark, Giant Blocks in the South Kona Landslide, Hawaii, *Geology, 23*, 125-128, 1995.

Mora, C., P.O. Baumgartner, and L. Hottinger, Eocene shallow water carbonate facies with larger foraminifera in the Caño Accretionary Complex, Caño Island and Osa Peninsula (Costa Rica, Central America), *12th Caribbean Geolical Conference, St. Croix (USVI), abstract*, 122, 1989.

Morell, K.D., D.M. Fisher, and T.W. Gardner, Inner forearc response to subduction of the Panama Fracture Zone, southern Central America, *Earth and Planetary Science Letters, 265*, 82-95, 2008.

Nelson, B.K., Fluid-Flow in Subduction Zones - Evidence from Nd and Sr-Isotope Variations in Metabasalts of the Franciscan Complex, California, *Contributions to Mineralogy and Petrology, 119*, 247-262, 1995.

Nishimura, A., Paleocene Radiolarian Biostratigraphy in the Northwest Atlantic at Site-384, Leg-43, of the Deep-Sea Drilling Project, *Micropaleontology, 38*, 317-362, 1992.

Nishimura, K., and H. Ishiga, Radiolarian biostratigraphy of the Maizuru Group in Yanahara area, Southwest Japan, *Memoirs of the Faculty of Science (Shimane University), 21*, 169-188, 1987.

Niu, Y.L., M.J. O'Hara, and J.A. Pearce, Initiation of subduction zones as a consequence of lateral compositional buoyancy contrast within the lithosphere: A petrological perspective, *Journal of Petrology, 44*, 851-866, 2003.

O. Dogherty, L., Biochronology and paleontology of Mid-Cretaceous radiolarians from Northern Apennines (Italy) and Betic Cordillera (Spain), in *Memoires de Geologie Lausanne*, vol. 21, pp. 415, 1994.

Obando, J.A., Sedimentología y tectónica del Cretácico y Paleógeno de la region de Golfito, Península de Burica y Península de Osa, Provincia de Puntarenas, Costa Rica, Licenciatura thesis, 211 pp., Escuela Centroamericana de Geología, Universidad de Costa Rica, 1986.

Okamura, Y., Large-scale melange formation due to seamount subduction; an example from the Mesozoic accretionary complex in central Japan, *Journal of Geology, 99*, 661-674, 1991.

Pal, T., P.P. Chakraborty, T.D. Gupta, and C.D. Singh, Geodynamic evolution of the outer-arc-forearc belt in the Andaman Islands, the central part of the Burma-Java subduction complex, *Geological Magazine, 140*, 289-307, 2003.

Palik, P., Remains of crustacean excrement from the lower Cretaceous of Hungary, *Micropaleontology, 11*, 98-104, 1965.

Paréjas, E., L'organisme B de E. Joukowsky et J. Favre, *Compte Rendu des Séances de la Société de Physique et d'Histoire Naturelle de Genève, 52*, 221-224, 1935.

Paréjas, E., Sur quelques coprolithes de Crustacés, *Archives des Sciences, Société de Physique et d'Histoire Naturelle de Genève, 1*, 512-520, 1948.

Paris, G., M.N. Machette, R.L. Dart, and K.M. Haller, Map and Database of Quaternary Faults and Folds in Colombia and its Offshore Regions. 00-0284, U.S. Geological Survey, 60p. http://greenwood.cr.usgs.gov/pub/open-file-reports/ofr-00-0284/, 2000.

Park, J.O., G.F. Moore, T. Tsuru, S. Kodaira, and Y. Kaneda, A subducted oceanic ridge influencing the Nankai megathrust earthquake rupture, *Earth and Planetary Science Letters, 217*, 77-84, 2004.

Park, J.O., T. Tsuru, Y. Kaneda, Y. Kono, S. Kodaira, N. Takahashi, and H. Kinoshita, A subducting seamount beneath the Nankai accretionary prism off Shikoku, southwestern Japan, *Geophysical Research Letters, 26*, 931-934, 1999.

Patino, L.C., G.E. Alvarado-Induni, and T.A. Vogel, Early arc magmatism: geochemical characteristics of volcanic clasts from Punta Sámara, Costa Rica., *Revista Geológica de América Central, 30*, 117-125, 2004.

Patino, L.C., M.J. Carr, and M.D. Feigenson, Local and regional variations in Central American arc lavas controlled by variations in subducted sediment input, *Contrib. Mineral. Petrol., 138*, 283, 2000.

Pearce, J.A., and D.W. Peate, Tectonic Implications of the Composition of Volcanic Arc Magmas, *Annual Review of Earth and Planetary Sciences, 23*, 251-285, 1995.

Pessagno, E.A., Jr., Radiolarian zonation and stratigraphy of the upper Cretaceous portion of the Great Valley Sequence, California Coast Ranges, in *Micropaleontology Special Publication*, vol. 2, pp. 95, 1976.

Petterson, M.G., T. Babbs, C.R. Neal, J.J. Mahoney, A.D. Saunders, R.A. Duncan, D. Tolia, R. Magu, C. Qopoto, H. Mahoa, and D. Natogga, Geological-tectonic framework of Solomon Islands, SW Pacific: crustal accretion and growth within an intra-oceanic setting, *Tectonophysics, 301*, 35-60, 1999.

Petterson, M.G., C.R. Neal, J.J. Mahoney, L.W. Kroenke, A.D. Saunders, T.L. Babbs, R.A. Duncan, D. Tolia, and B. McGrail, Structure and deformation of north and central Malaita, Solomon Islands: tectonic implications for the Ontong Java Plateau Solomon arc collision, and for the fate of oceanic plateaus, *Tectonophysics, 283*, 1-33, 1997.

Phinney, E.J., P. Mann, M.F. Coffin, and T.H. Shipley, Sequence stratigraphy, structural style, and age of deformation of the Malaita accretionary prism (Solomon Arc-Ontong Java Plateau convergent zone), *Tectonophysics, 389*, 221-246, 2004.

Pillevuit, A., J. Marcoux, G. Stampfli, and A. Baud, The Oman exotics: A key to the understanding of the Neotethyan geodynamic evolution, *Geodinamica Acta, 10*, 209-238, 1997.

Pindell, J., L. Kennan, W.V. Maresch, K.P. Stanek, G. Draper, and R. Higgs, Plate kinematics and crustal dynamics of circum-Caribbean arc-continent interactions; tectonic controls on basin development in proto-Caribbean

References

margins.; Caribbean-South American plate interactions, Venezuela, *Special Paper - Geological Society of America, 394*, 7-52, 2005.

Pindell, J., L. Kennan, K.P. Stanek, W.V. Maresch, and G. Draper, Foundations of gulf of mexico and caribbean evolution: eight controversies resolved, *Geologica Acta, 4*, 303-341, 2006.

Presley, T.K., J.M. Sinton, and M. Pringle, Postshield volcanism and catastrophic mass wasting of the Waianae Volcano, Oahu, Hawaii, *Bulletin of Volcanology, 58*, 597-616, 1997.

Pryor, W.A., Biogenic sedimentation and alteration of argillaceous sediments in shallow marine environments, *GSA Bulletin, 86*, 1244-1254, 1975.

Ranero, C.R., I. Grevemeyer, H. Sahling, U. Barckhausen, C. Hensen, K. Wallmann, W. Weinrebe, P. Vannucchi, R. von Huene, and K. McIntosh, Hydrogeological system of erosional convergent margins and its influence on tectonics and interplate seismogenesis, *Geochemistry Geophysics Geosystems, 9*, Q03S04, doi:10.1029/2007GC001679, 2008.

Ranero, C.R., and R. von Huene, Subduction erosion along the Middle America convergent margin, *Nature, 404*, 748-755, 2000.

Ranero, C.R., R. von Huene, W. Weinrebe, and U. Barckhausen, Convergent margin tectonics: A marine perspective, in *Central America - Geology, Resources and Hazards*, edited by J. Bundschuh and G.E. Alvarado, pp. 239-276, Taylor and Francis, Oxford, 2007.

Rausch, S., and G. Wörner, Evolution of adakitic magmas at Volcan Baru (Panama), in *20th Colloquium on Latin American Earth Sciences (Kiel, Germany)*, pp. 294-295, 2007.

Raymond, L.A., Classification of melanges, in *Melanges: their nature, origin and significance*, vol. 198, *Special Paper - Geological Society of America*, edited by A. Raymond Loren, pp. 7-20, 1984.

Raymond, L.A., and T. Terranova, Prologue: The melange problem: a review, in *Melanges: their nature, origin and significance*, vol. 198, *Special Paper - Geological Society of America*, edited by A. Raymond Loren, pp. 1-5, 1984.

Recchi, G., and R. Miranda, Calizas de los Planes-Gauniquito (Tonosi). pp. 27, Dirección General de Recursos Minerales (Panama), 1977.

Revillon, S., E. Hallot, N.T. Arndt, C. Chauvel, and R.A. Duncan, A complex history for the Caribbean plateau: Petrology, geochemistry, and geochronology of the Beata Ridge, south Hispaniola, *Journal of Geology, 108*, 641-661, 2000.

Rhodes, J.M., and M.J. Vollinger, Composition of basaltic lavas sampled by phase-2 of the Hawaii Scientific Drilling Project: Geochemical stratigraphy and magma types, *Geochemistry Geophysics Geosystems, 5*, 2004.

Rivier, F., Síntesis geológica y mapa geológico del área de bajo Tempisque, Guanacaste, Costa Rica, *Informe Semestral del Instituto Geográfico Nacional (Costa Rica), 1*, 7-30, 1983.

Roeder, P.L., and R.F. Emslie, Olivine-Liquid Equilibrium, *Contributions to Mineralogy and Petrology, 29*, 275-&, 1970.

Sak, P.B., D.M. Fisher, and T.W. Gardner, Effects of subducting seafloor roughness on upper plate vertical tectonism; Osa Peninsula, Costa Rica, *Tectonics, 23*, TC1017, doi:10.1029/2002TC001474, 2004.

Sallares, V., J.J. Danobeitia, and E.R. Flueh, Lithospheric structure of the Costa Rican Isthmus: Effects of subduction zone magmatism on an oceanic plateau, *Journal of Geophysical Research-Solid Earth, 106*, 621-643, 2001.

Sallares, V., J.J. Danobeitia, E.R. Flueh, and G. Leandro, Seismic velocity structure across the middle American landbridge in northern Costa Rica, *Journal of Geodynamics, 27*, 327-344, 1999.

Sanfilippo, A., and C. Nigrini, Upper Paleocene-lower Eocene deep-sea radiolarian stratigraphy and the Paleocene/ Eocene series boundary.; Late Paleocene-early Eocene climatic and biotic events in the marine and terrestrial records, in *Late Paleocene-Early Eocene Biotic and Climatic Events in the Marine and Terrestrial Records*, edited by M.-P. Aubry, S.G. Lucas and W.A. Berggren, pp. 244-276, New York: Columbia University Press., 1998.

Sanfilippo, A., and W.R. Riedel, Cenozoic Radiolaria (exclusive of theoperids, artostrobiids and amphipyndacids) from the Gulf of Mexico, DSDP Leg 10, in *Initial Reports of the Deep Sea Drilling Project*, vol. 10, edited by J.L. Worzel, W. Bryant, A.-O.J. Beall, R. Capo, K. Dickinson, H.P. Foreman, L. Robert, B.W. McNeely and L.-A. Smith, pp. 475-611, U.S. Government Printing Office, Washington, D.C., 1973.

Sanfilippo, A., and W.R. Riedel, Cretaceous Radiolaria, in *Plankton Stratigraphy*, edited by H.M. Bolli, J.B. Saunders and K. Perch-Nielsen, pp. 573-630, Cambridge University Press, Cambridge, UK, 1985.

Sano, H., and K. Kanmera, Collapse of ancient oceanic reef complex; what happened during collision of Akiyoshi reef complex? Sequence of collisional collapse and generation of collapse products, *Chishitsugaku Zasshi = Journal of the Geological Society of Japan, 97*, 631-644, 1991.

Saunders, A.D., J. Tarney, A.C. Kerr, and R.W. Kent, The formation and fate of large oceanic igneous provinces, *Lithos, 37*, 81-95, 1996.

Schaaf, A., Un nouveau canevas biochronologique du Crétacé inférieur et moyen: les biozones à radiolaires, *Sciences géologique (Strasbourg) Bulletin, 38*, 227-269, 1985.

Schmidt-Effing, R., Alter und Genese des Nicoya-Komplexes, einer ozeanischen Palaeokruste (Oberjura bis Eozaen) im suedlichen Zentralamerika, *Geologische Rundschau, 68*, 457-494, 1979.

Scholz, C.H., and C. Small, The effect of seamount subduction on seismic coupling, *Geology, 25*, 487-490, 1997.

Schweigert, G., D.B. Seegis, A. Fels, and R.R. Leinfelder, New, internally structured decapod microcoprolites from Germany (Upper Triassic/ lower Miocene), southern Spain (Lower/ Middle Jurassic) and Portugal (Upper Jurassic); taxonomy, palaeoecology and evolutionary implications, *Palaeontologische Zeitschrift, 71*, 51-69, 1997.

Seno, T., Collision vs. subduction: from a viewpoint of slab dehydration, in *The Seismogenic Zone of Subduction Thrust Faults, MARGINS Theoretical and Experimental Earth Science Series*, edited by T.H. Dixon and C. Moore, pp. 601-623, Columbia Univ Press, 2007.

Seno, T., Conditions for a crustal block to be sheared off from the subducted continental lithosphere: What is an essential factor to cause features associated with collision?, *Journal of Geophysical Research, 113*, B04414, 2008.

Senowbari-Daryan, B., E. Kube, and B. Kube, The ichnogenous Palaxius (crustacean corprolite) and description of P. hydranensis n. ichnosp. from the Upper Triassic (Norian part of the "Pantokrator" limestone) of Hydra (Greece), *Paläontologische Zeitschrift, 77*, 115-122, 2003.

Senowbari-Daryan, B., and V.V. Silantiev, New Crustacean Coprolites from the Upper Paleocene of North Caucasus

Translated Title: Neue Crustaceen-Koprolithen aus dem Nord-Kaukasus (O. Paleozaen), *Mitt. Ges. Geol. Bergbaustud. Österr., 37*, 75-82, 1991.

Senowbari-Daryan, B., and G.D. Stanley, Thalassinid anomuran microcoprolites from Upper Triassic carbonate rocks of central Peru, *Lethaia, 19*, 343-354, 1986.

Severinghaus, J., and T. Atwater, Cenozoic geometry and thermal state of the subducting slabs beneath western North America, in *Basin and Range extensional tectonics near the latitude of Las Vegas, Nevada*, vol. 176, *Geological Society of America Memoir*, edited by B.P. Wernicke, pp. 1-22, 1990.

Sigurdsson, H., R.M. Leckie, G.D. Acton, L.J. Abrams, T.J. Bralower, S.N. Carey, W.P. Chaisson, P. Cotillon, A.D. Cunningham, S.L. Hondt, A.W. Droxler, B. Galbrun, J. Gonzalez, G. Haug, K. Kameo, J. King, I.L. Lind, V. Louvel, T.W. Lyons, R.W. Murray, M. Mutti, G. Myers, R.B. Pearce, D.G. Pearson, L.C. Peterson, and U. Roehl, Proceedings of the Ocean Drilling Program; Initial reports; Caribbean ocean history and the Cretaceous/ Tertiary boundary event; covering Leg 165 of the cruises of the Drilling Vessel JOIDES Resolution, Miami, Florida, to San Juan, Puerto Rico, sites 998-1002, 19 December 1995-17 February 1996, *Proceedings of the Ocean Drilling Program, Part A: Initial Reports*, 1997.

Silver, E.A., D.L. Reed, J.E. Tagudin, and D.J. Heil, Implications of the North and South Panama Thrust Belts for the Origin of the Panama Orocline, *Tectonics, 9*, 261-281, 1990.

Sinton, C.W., R.A. Duncan, and P. Denyer, Nicoya Peninsula, Costa Rica: A single suite of Caribbean oceanic plateau magmas, *Journal of Geophysical Research-Solid Earth, 102*, 15507-15520, 1997.

Sinton, C.W., R.A. Duncan, M. Storey, J. Lewis, and J.J. Estrada, An oceanic flood basalt province within the Caribbean plate, *Earth and Planetary Science Letters, 155*, 221-235, 1998.

Sinton, C.W., H. Sigurdsson, R.A. Duncan, R.M. Leckie, G.D. Acton, L.J. Abrams, T. Bralower, J., S.N. Carey, W. Chaisson, P., P. Cotillon, A.D. Cunningham, S.L. Hondt, A.W. Droxler, B. Galbrun, J. Gonzalez, G.H. Haug, K. Kameo, J.W. King, I.L. Lind, V. Louvel, T.W. Lyons, R.W. Murray, M. Mutti, G. Myers, R.B. Pearce, D.G. Pearson, L.C. Peterson, and U. Roehl, Geochronology and petrology of the igneous basement at the lower Nicaraguan Rise, Site 1001.; Proceedings of the Ocean Drilling Program, scientific results,

References

Caribbean Ocean history and the Cretaceous/ Tertiary boundary event; covering Leg 165 of the cruises of the drilling vessel JOIDES Resolution, Miami, Florida, to San Juan Puerto Rico, sites 998-1002, 19 December 1995-17 February 1996, *Proceedings of the Ocean Drilling Program, Scientific Results, 165*, 233-236, 2000.

Sleep, N.H., Ridge-crossing mantle plumes and gaps in tracks, *Geochemistry Geophysics Geosystems, 3*, 2002.

Smith, W.H.F., and D.T. Sandwell, Global sea floor topography from satellite altimetry and ship depth soundings, *Science, 277*, 1956-1962, 1997.

Soh, W., and H. Tokuyama, Rejuvenation of submarine canyon associated with ridge subduction, Tenryu Canyon, off Tokai, central Japan, *Marine Geology, 187*, 203-220, 2002.

Stern, R.J., Subduction initiation: spontaneous and induced, *Earth and Planetary Science Letters, 226*, 275-292, 2004.

Stern, R.J., and S.H. Bloomer, Subduction Zone Infancy - Examples from the Eocene Izu-Bonin-Mariana and Jurassic California Arcs, *Geological Society of America Bulletin, 104*, 1621-1636, 1992.

Stolper, E., S. Sherman, M. Garcia, M. Baker, and C. Seaman, Glass in the submarine section of the HSDP2 drill core, Hilo, Hawaii, *Geochemistry Geophysics Geosystems, 5*, 2004.

Storey, M., A. Duncan Robert, and C. Tegner, Timing and duration of volcanism in the North Atlantic Igneous Province: Implications for geodynamics and links to the Iceland hotspot, *Chemical Geology, 241*, 264-281, 2007.

Su, Y., and C.H. Langmuir, Global MORB chemistry compilation at the segment scale, PhD thesis, Columbia, 2003.

Taira, A., P. Mann, and R. Rahardiawan, Incipient subduction of the Ontong Java Plateau along the North Solomon trench, *Tectonophysics, 389*, 247-266, 2004.

Taketani, Y., Cretaceous radiolarian biostratigraphy of the Urakawa and Obira areas, Hokkaido, *Science Reports of the Tohoku University, 52*, 1-76, 1982.

Tamura, Y., and Y. Tatsumi, Remelting of an andesitic crust as a possible origin for rhyolitic magma in oceanic arcs: An example from the Izu-Bonin arc, *Journal of Petrology, 43*, 1029-1047, 2002.

Tarduno, J.A., R.A. Duncan, and D.W. Scholl, *Proceedings of the Ocean Drilling Program, Initial Reports*, 171 pp., Ocean Drill. Program, College Station, Tex., 2002.

Thompson, P.M.E., P.D. Kempton, R.V. White, A.D. Saunders, A.C. Kerr, J. Tarney, and M.S. Pringle, Elemental, Hf-Nd isotopic and geochronological constraints on an island arc sequence associated with the Cretaceous Caribbean plateau: Bonaire, Dutch Antilles, *Lithos, 74*, 91-116, 2004.

Thurow, J., M. Moullade, H.J. Brumsack, E. Masure, L.J. Taugourdeau, K.W. Dunham, G. Boillot, E.L. Winterer, A.W. Meyer, J. Applegate, M. Baltuck, J.A. Bergen, M.C. Comas, T.A. Davies, C.A. Evans, J. Girardeau, D. Goldberg, J.A. Haggerty, L.F. Jansa, J.A. Johnson, J. Kasahara, J.P. Loreau, E. Luna, J.G. Ogg, M. Sarti, and M.A. Williamson, The Cenomanian/ Turonian boundary event (CTBE) at Hole 641A, ODP Leg 103 (compared with the CTBE interval at Site 398).; Proceedings of the Ocean Drilling Program, Scientific results, Galicia margin; covering Leg 103 of the cruises of the drilling vessel JOIDES Resolution, Ponta Delgada, Azores, to Bremerhaven, Germany, 25 April 1985-19 June 1985, in *Proceedings of the Ocean Drilling Program, Scientific Results*, vol. 103, pp. 587-634, Ocean Drilling Program, College Station, TX, 1988.

Timpa, S., K.M. Gillis, and D. Canil, Accretion-related metamorphism of the Metchosin Igneous Complex, southern Vancouver Island, British Columbia, *Canadian Journal of Earth Sciences, 42*, 1467-1479, 2005.

Toth, J., and M. Gurnis, Dynamics of subduction initiation at preexisting fault zones, *Journal of Geophysical Research-Solid Earth, 103*, 18053-18067, 1998.

Tournon, J., Magmatisme du Mésozoïque à l'actuel en Amérique Centrale: l'exemple du Costa Rica, des ophiolites aux andésites., *Mémoire des sciences de la terre, Université Pierre et Marie Curie, 84*, 335, 1984.

Tournon, J., C. Triboulet, and J. Azéma, Amphibolites from Panama: anticlockwise P-T paths from a Pre-upper Cretaceous metamorphic basement in Isthmian Central America, *Journal of Metamorphic Geology, 7*, 539-546, 1989.

Trenkamp, R., J.N. Kellogg, J.T. Freymueller, and H.P. Mora, Wide plate margin deformation, southern Central America and northwestern South America, CASA GPS observations, *Journal of South American Earth Sciences, 15*, 157-171, 2002.

Turner, S., and C. Hawkesworth, Constraints on flux rates and mantle dynamics beneath island arcs from Tonga-Kermadec lava geochemistry, *Nature, 389*, 568-573, 1997.

Ueda, H., Accretion and exhumation structures formed by deeply subducted seamounts in the Kamuikotan high-pressure/temperature zone, Hokkaido, Japan, *Tectonics, 24*, 2005.

Ueda, H., M. Kawamura, and K. Niida, Accretion and tectonic erosion processes revealed by the mode of occurrence and geochemistry of greenstones in the Cretaceous accretionary complexes of the Idonnappu Zone, southern central Hokkaido, Japan, *Island Arc, 9*, 237-257, 2000.

Underwood, M.B., and S.B. Bachman, Sedimentary facies associations within subduction complexes, *Geological Society, London, Special Publications, 10*, 537-550, 1982.

Vallejo, C., Evolution of the Western Cordillera in the Andes of Ecuador (Late Cretaceous-Paleogene), PhD thesis, 215 pp., Swiss Federal Institute of Technology, Zürich, 2007.

Vallejo, C., R.A. Spikings, L. Luzieux, W. Winkler, D. Chew, and L. Page, The early interaction between the Caribbean plateau and the NW South American Plate, *Terra Nova, 18*, 264-269, 2006.

Vannucchi, P., D.M. Fischer, and T.W. Gardner, Reply to comment by David M. Buchs and Peter O. Baumgartner on ''From seamount accretion to tectonic erosion: Formation of Osa Mélange and the effects of the Cocos Ridge subduction in southern Costa Rica'', *Tectonics, 26*, TC3010, doi:10.1029/2007TC002129, 2007.

Vannucchi, P., D.M. Fisher, S. Bier, and T.W. Gardner, From seamount accretion to tectonic erosion; formation of Osa melange and the effects of Cocos Ridge subduction in southern Costa Rica, *Tectonics, 25*, TC2004, doi:10.1029/2005TC001855, 2006.

Vannucchi, P., S. Galeotti, C.P. D., R.C. R., and R. von Huene, Long-term subduction-erosion along the Guatemalan margin of the Middle America Trench, *Geology (Boulder), 32*, 617-620, 2004.

Vannucchi, P., C.R. Ranero, S. Galeotti, S.M. Straub, D.W. Scholl, and K. McDougall-Ried, Fast rates of subduction erosion along the Costa Rica Pacific margin: Implications for nonsteady rates of crustal recycling at subduction zones, *Journal of Geophysical Research-Solid Earth, 108*, 2003.

Vannucchi, P., F. Remitti, and G. Bettelli, Geological record of fluid flow and seismogenesis along an erosive subducting plate boundary, *Nature, doi:10.1038/nature06486*, 2008.

Vannucchi, P., D.W. Scholl, M. Meschede, and M.R. Kristin, Tectonic erosion and consequent collapse of the Pacific margin of Costa Rica; combined implications from ODP Leg 170, seismic offshore data, and regional geology of the Nicoya Peninsula, *Tectonics, 20*, 649-668, 2001.

Villiger, S., P. Ulmer, and O. Muntener, Equilibrium and fractional crystallization experiments at 0.7 GPa; the effect of pressure on phase relations and liquid compositions of tholeiitic magmas, *Journal of Petrology, 48*, 159-184, 2007.

Villiger, S., P. Ulmer, O. Muntener, and A.B. Thompson, The liquid line of descent of anhydrous, mantle-derived, tholeiitic liquids by fractional and equilibrium crystallization - an experimental study at 1 center dot 0 GPa, *Journal of Petrology, 45*, 2369-2388, 2004.

Vishnevskaya, V.S., Jurassic to Cretaceous radiolarian biostratigraphy of Russia, in *GEOS*, pp. 376, Moscow, 2001.

Vishnevskaya, V.S., New radiolarian species of the family pseudoaulophacidae riedel from the upper cretaceous of the volga region, *Paleontological Journal, 41*, 489-500, 2007.

Vogel, T.A., L.C. Patino, G.E. Alvarado, and P.B. Gans, Silicic ignimbrites within the Costa Rican volcanic front: evidence for the formation of continental crust, *Earth and Planetary Science Letters, 226*, 149-159, 2004.

Volkova, N.I., and V.I. Budanov, Geochemical discrimination of metabasalt rocks of the Fan-Karategin transitional blueschist/greenschist belt, South Tianshan, Tajikistan: seamount volcanism and accretionary tectonics, *Lithos, 47*, 201-216, 1999.

Von Eynatten, H., H. Krawinkel, and J. Winsemann, Plio-Pleistocene outer arc basins in southern Central America (Osa Peninsula, Costa Rica).; Tectonic controls and signatures in sedimentary successions, *Special Publication of the International Association of Sedimentologists, 20*, 399-414, 1993.

von Huene, R., J. Bialas, E. Flueh, B. Cropp, T. Csernok, E. Fabel, J. Hoffmann, K. Emeis, P. Holler, G. Jeschke, M.C. Leandro, I. Perez Fernandez, S.J. Chavarria, H.A. Florez, Z.D. Escobedo, R. Leon, and L.O. Barrios, Morphotectonics of the Pacific convergent margin of Costa Rica.; Geologic and tectonic development of the Caribbean Plate boundary in southern Central America, in *Geologic and Tectonic Development of the Caribbean plate boundary in southern Central America*, vol. 295, *Geological Society of America Special Paper*, edited by P. Mann, pp. 291-307, 1995.

References

von Huene, R., and S. Lallemand, Tectonic Erosion Along the Japan and Peru Convergent Margins, *Geological Society of America Bulletin, 102*, 704-720, 1990.

von Huene, R., C.R. Ranero, and P. Vannucchi, Generic model of subduction erosion, *Geology (Boulder), 32*, 913-916, 2004.

von Huene, R., C.R. Ranero, W. Weinrebe, and K. Hinz, Quaternary convergent margin tectonics of Costa Rica, segmentation of the Cocos Plate, and Central American volcanism, *Tectonics, 19*, 314-334, 2000.

von Huene, R., and D.W. Scholl, Observations at Convergent Margins Concerning Sediment Subduction, Subduction Erosion, and the Growth of Continental-Crust, *Reviews of Geophysics, 29*, 279-316, 1991.

Walther, C.H.E., The crustal structure of the Cocos Ridge off Costa Rica, *Journal of Geophysical Research, B, Solid Earth and Planets, 108*, 2136, doi:10.1029/2001JB000888, 2003.

Walther, C.H.E., E.R. Flueh, C.R. Ranero, R. von Huene, and W. Strauch, Crustal structure across the Pacific margin of Nicaragua: evidence for ophiolitic basement and a shallow mantle sliver, *Geophysical Journal International, 141*, 759-777, 2000.

Weigel, W., and I. Grevemeyer, The Great Meteor seamount: seismic structure of a submerged intraplate volcano, *Journal of Geodynamics, 28*, 27-40, 1999.

Werner, R., K. Hoernle, U. Barckhausen, and F. Hauff, Geodynamic evolution of the Galapagos hot spot system (Central East Pacific) over the past 20 m.y.: Constraints from morphology, geochemistry, and magnetic anomalies, *Geochem. Geophys. Geosyst., 4*, 2003.

Werner, R., K. Hoernle, P. van den Bogaard, C. Ranero, R. von Huene, and D. Korich, Drowned 14-m.y.-old Galapagos Archipelago off the coast of Costa Rica; implications for tectonic and evolutionary models, *Geology, 27*, 499-502, 1999.

Weyl, R., Die Orogene Mittelamerikas (The Middle America orogeny), *Geologische Rundschau, 50*, 605-619, 1960.

White, R.V., J. Tarney, A.C. Kerr, A.D. Saunders, P.D. Kempton, M.S. Pringle, and G.T. Klaver, Modification of an oceanic plateau, Aruba, Dutch Caribbean: Implications for the generation of continental crust, *Lithos, 46*, 43-68, 1999.

Winchester, J.A., and P.A. Floyd, Geochemical Discrimination of Different Magma Series and Their Differentiation Products Using Immobile Elements, *Chemical Geology, 20*, 325-343, 1977.

Wörner, G., R.S. Harmon, G. Hartmann, and K. Simon, Igneous Geology and Geochemistry of the Upper Río Chagres Basin, in *The Río Chagres, Panama: A Multidisciplinary Profile of a Tropical Watershed*, vol. 52, *Water Science and Technology Library*, edited by V.P. Singh and R.S. Harmon, pp. 65-81, 2005.

Wörner, G., R.S. Harmon, and W. Wegner, Geochemical Evolution of igneous rock and changing Magma Sources during the Evolution and Closure of the Central American Landbridge, in *Backbone of the Americas (in preparation)*, *Geological Society of America Memoir*, edited by S. Mahlburg Kay and V. Ramos, in press.

Wörner, G., R.S. Harmon, W. Wegner, and B. Singer, Linking America's Backbone: Geological Development and Basement Rocks of Central Panama, *Geological Society of America Abstracts with Programs, Speciality Meeting, 2*, 60, 2006.

Xenophontos, C., and S. Osozawa, Travel time of accreted igneous assemblages in western Pacific orogenic belts and their associated sedimentary rocks, *Tectonophysics, 393*, 241-261, 2004.

Yuan, P.B., Stratigraphy, sedimentology, and geologic evolution of eastern Terraba Trough, southwestern Costa Rica, 1984.

Yuan, P.B., Comparative sedimentology of shallow-water limestones developed in active tectonic regions; examples from Costa Rica, Central America and eastern Taiwan.; Neotectonics and resources, 43-64, 1991.

Yuan, P.B., and D.R. Lowe, Forearc sedimentation in Terraba Trough, Costa Rica, Central America.; AAPG annual convention with divisions SEPM/ EMD/ DPA; technical program and abstracts, *AAPG Bulletin, 71*, 630, 1987.

Appendix

Table 1. Location of analyzed samples

Sample	Rock name	Locality	Coordinates (WGS84°) Latitude	Longitude	Unit or Group
		Golfito Complex			
DB02-042	Basalt	Quebrada Bolsa	8.690029	-83.181287	Igneous Basement
DB02-057	Basalt	Quebrada Purruja	8.608562	-83.116891	Golfito Formation
DB02-063	Basaltic trachandesite	Quebradas Cacao	8.645755	-83.205878	Igneous Basement
DB02-073	Basalt	Quebrada Bolsa	8.667424	-83.181317	Igneous Basement
DB02-087	Basalt	Quebrada Gambatita	8.608537	-83.100538	Igneous Basement
DB02-101	Basalt	Quebrada Mona	8.638422	-83.132292	Igneous Basement
DB02-138	Basalt	Rio Sorpresa	8.639448	-83.224057	Golfito Formation
DB02-143	Basalt	Playa Gallardo	8.589607	-83.139631	Golfito Formation
DB02-149	Basalt	Punta Mono Congo	8.607709	-83.152324	Golfito Formation
DB02-151	Basaltic trachandesite	Punta El Cabro	8.613154	-83.166853	Igneous Basement
DB02-157	Basalt	Golfito	8.623128	-83.187736	Golfito Formation
DB02-158	Basalt	Punta Larga	8.622214	-83.180468	Golfito Formation
DB02-174	Basalt	Quebrada Km 20	8.617563	-83.090530	Golfito Formation
DB02-175	Trachyandesite	Quebrada Km 20	8.614841	-83.084175	Golfito Formation
DB02-181	Basalt	El Mirador	8.598512	-83.051496	Golfito Formation
		Azuero Complex			
DB05-002	Basalt	South of Torio	7.531524	-80.948197	Azuero Plateau
DB05-047	Basalt	Coralino	7.416265	-80.182557	Azuero Plateau
DB05-072	Basalt	Cebaco	7.485680	-81.241532	Azuero Plateau
DB05-073	Basalt	Cebaco	7.493644	-81.196916	Azuero Plateau
DB05-076	Basalt	Cebaco	7.571038	-81.199308	Azuero Plateau
DB05-080	Basalt	Sona	7.616889	-81.238722	Azuero Plateau
DB06-027	Basalt	Punta Duartes	7.543076	-80.951740	Azuero Plateau
DB06-034	Basalt	Punta Duartes	7.534528	-80.958983	Azuero Plateau
DB06-093	Basalt	Rio Higueronoso	7.511801	-80.853616	Azuero Plateau
DB06-102	Basalt	Rio Quebro	7.482656	-80.807493	Azuero Plateau
DB06-104	Basalt	Rio Quebro	7.501561	-80.805582	Azuero Plateau
DB06-117	Basalt	Coiba	7.626149	-81.774566	Azuero Plateau
DB06-121	Basalt	Coiba	7.468370	-81.866221	Azuero Plateau
DB06-125	Basalt	Coiba	7.504332	-81.681179	Azuero Plateau
DB06-126	Basalt	Isla Canal	7.696763	-81.624358	Azuero Plateau
DB06-136	Basalt	Quebrada Grande	7.372797	-80.472783	Azuero Plateau
DB06-137	Basalt	Quebrada Pava	7.364347	-80.563536	Azuero Plateau
DB06-138	Basalt	Quebrada El Pilón	7.422328	-80.666650	Azuero Plateau
DB06-139	Basalt	Punta Madroño	7.424727	-80.205403	Azuero Plateau
DB06-141	Basalt	Fila near Quebrada Joaquín	7.517556	-80.462051	Azuero Plateau
DB07-043	Basalt	Rio Horcones	7.310511	-80.548368	Azuero Plateau
DB07-044	Basalt	Road near Cerro La Guabita	7.466296	-80.618819	Azuero Plateau
DB07-050	Basalt	Quebrada La Cacica	7.447029	-80.484793	Azuero Plateau
DB05-030	Basalt	Güerra Road	7.535738	-80.597104	Azuero Proto-Arc
DB05-043	Basalt	Road to Punta Tinidero	7.333657	-80.354588	Azuero Proto-Arc
DB05-055	Basalt	Road Tonosi-Las Tablas	7.497902	-80.393865	Azuero Proto-Arc
DB05-057	Basalt	Rio Orio	7.589360	-80.339002	Azuero Proto-Arc
DB05-061	Basalt	Road Tonosi-Las Tablas	7.678150	-80.323162	Azuero Proto-Arc
DB05-062	Basalt	El Carate	7.735392	-80.292702	Azuero Proto-Arc
DB05-069	Basalt	Hicaco	7.652124	-81.197723	Azuero Proto-Arc
DB05-083	Basalt	Hicaco	7.657088	-81.202485	Azuero Proto-Arc
DB05-087	Basalt	Road Sona-Pacora	7.902217	-81.371319	Azuero Proto-Arc
DB06-035	Basalt dyke	Punta Duartes	7.534528	-80.958983	Azuero Proto-Arc
DB06-112	Basalt	Coiba	7.630857	-81.729789	Azuero Proto-Arc
DB06-113	Basaltic trachyandesite dyke	Coiba	7.642072	-81.746082	Azuero Proto-Arc
DB06-120	Basalt	Coiba	7.642027	-81.746082	Azuero Proto-Arc
DB07-015	Dolerite	Rio Varadero	7.315245	-80.828449	Azuero Proto-Arc
DB07-049	Dolerite	Rio Joaquin	7.524104	-80.453885	Azuero Proto-Arc
DB05-024	Trachyandesite	Road Mariato-Atalaya	7.762228	-80.983068	Azuero Arc
DB05-027	Basaltic trachyandesite	Road near S. Jose	7.776394	-80.638234	Azuero Arc
DB05-028	Andesite	Road near San Jose	7.729139	-80.606118	Azuero Arc
DB05-048	Basaltic andesite	Punta Mala	7.472447	-80.000033	Azuero Arc
DB05-050	Gabbro (basaltic andesite)	Punta Mala	7.472649	-80.001383	Azuero Arc
DB05-052	Microgranite	Punta Mala	7.473212	-80.002279	Azuero Arc
DB05-053	Basaltic andesite	Punta Mala	7.473212	-80.002279	Azuero Arc

Table 1. Location of analyzed samples (continued)

Sample	Rock name	Locality	Coordinates (WGS84°) Latitude	Longitude	Unit or Group
		Azuero Complex (continued)			
DB05-056	Granodiorite	Rio Orio	7.589360	-80.339002	Azuero Arc
DB05-058	Gabbro (basaltic andesite)	Rio Valle Rico	7.615420	-80.351265	Azuero Arc
DB05-059	Granodiorite	Rio Valle Rico	7.615420	-80.351265	Azuero Arc
DB05-064	Granodiorite	La Mesa	7.643992	-80.646398	Azuero Arc
DB05-067	Diorite	La Playa	7.780086	-81.171907	Azuero Arc
DB05-068	Granodiorite	La Playa	7.780086	-81.171907	Azuero Arc
DB05-088	Basaltic trachyandesite	Road Sona-Caledonia	7.982778	-81.367680	Azuero Arc
DB05-092	Andesite	San Rafael	7.838188	-81.450631	Azuero Arc
DB06-052	Basalt	Torio	7.561739	-80.873089	Azuero Arc
DB06-105	Gabbro	Rio Quebro	7.513089	-80.794201	Azuero Arc
DB06-123	Trachyandesite	Coiba	7.364690	-81.607892	Azuero Arc
		Osa Mélange			
DJ01-006	Dacite	North of Rio Claro	8.683113	-83.711062	San Pedrillo Unit
DJ01-028	Monzonite	East of Punta San Jose	8.688539	-83.699250	San Pedrillo Unit
DJ01-112	Dacite	East of Agujitas	8.693966	-83.659267	San Pedrillo Unit
		Osa Igneous Complex			
DB02-107	Basalt	Punta Lista	8.732693	-83.373152	IOIC, plateau-like
DB02-110	Basalt	Golfo Dulce	8.732683	-83.355884	IOIC, plateau-like
DB02-119	Basalt	Punta Esperanza	8.667528	-83.304141	IOIC, OIB-like
DB02-120	Basalt	Golfo Dulce	8.656670	-83.294157	IOIC, plateau-like
DB02-132	Basalt	Golfo Dulce	8.650301	-83.254191	IOIC, plateau-like
DB02-135	Basalt	Golfo Dulce	8.639426	-83.236025	IOIC, plateau-like
DB02-160	Basalt	Playa Chal	8.718276	-83.440406	IOIC, MORB-like
DB02-165	Basalt	Punta Bejuco	8.731813	-83.409500	IOIC, plateau-like
DB02-201	Basalt	Quebrada Sabalo	8.796065	-83.486719	IOIC, MORB-like
DB02-203	Basalt	Quebrada Sabalo	8.794251	-83.484899	IOIC, plateau-like
DB02-204	Basalt	Quebrada Sabalo	8.794251	-83.484899	IOIC, plateau-like
DB02-227	Gabbro	Quebrada Sabalo (Burica)	8.743632	-83.527645	IOIC, plateau-like
DB02-230	Basalt	Punta Isidora	8.722804	-83.458583	IOIC, plateau-like
DB02-232	Trachyandesitic sill	Punta Gruesa	8.720104	-83.472217	IOIC, OIB-like
DB02-246	Basalt	Quebrada Seca	8.759019	-83.554899	IOIC, plateau-like
DB02-266	Basalt	Isla Violin	8.824131	-83.627606	IOIC, plateau-like
DB05-107	Basalt	Dos Brazos	8.531082	-83.403288	IOIC, plateau-like
DB05-108	Basalt	Quebrada Salitre	8.538324	-83.410088	IOIC, plateau-like
DB06-054	Basalt	Río Claro	8.386122	-83.130552	IOIC, plateau-like
DB06-058	Basalt	Rio Claro (Burica)	8.367087	-83.101530	IOIC, plateau-like
DB06-061	Basalt	Pavones-Punta Banco	8.368159	-83.145948	IOIC, plateau-like
DB06-065	Basalt	Punta Banco-El Barco (Burica)	8.332690	-83.111865	IOIC, MORB-like
DB06-066	Basalt	Punta Banco-El Barco (Burica)	8.331911	-83.110635	IOIC, OIB-like
DB06-070	Basalt	Punta Banco-El Barco (Burica)	8.265386	-83.004087	IOIC, plateau-like
DB06-075	Dolerite	Punta Banco (Burica)	8.337365	-83.118388	IOIC, MORB-like
DJ01-022	Basalt	Rio Sierpe	8.765366	-83.647610	IOIC, plateau-like
DJ01-115	Basalt	Isla Violin	8.794295	-83.649423	IOIC, plateau-like
GDM-90303	Basalt	Near mouth of Rio Claro (Burica)	8.400628	-83.132637	IOIC, plateau-like
GDM-91044	Basalt	Rio Claro (Burica)	8.392483	-83.132656	IOIC, plateau-like
DB02-191	Basalt	Rio Aguabuena	8.712889	-83.527656	Güerra
DB02-207	Basalt	Quebrada Banegas	8.702053	-83.549471	Güerra
DB02-198b	Basalt	Fila Ganado	8.721961	-83.615798	Ganado Unit, plateau-like
DB02-260	Basalt	Quebrada Ganado	8.708393	-83.608538	Ganado Unit, plateau-like
DB02-261	Basaltic dyke	Quebrada Ganado	8.708393	-83.608538	Ganado Unit, plateau-like
DB02-262	Gabbro	Quebrada Ganado	8.703874	-83.599443	Ganado Unit, MORB-like
DB05-149	Dolerite	Rio Riyito	8.665884	-83.567652	Ganado Unit, plateau-like
DB05-155	Basalt	Toma de Agua (near Riyito)	8.673127	-83.573559	Ganado Unit, plateau-like
DB05-156	Basalt	Toma de Agua (near Riyito)	8.673120	-83.573286	Ganado Unit, plateau-like
DB05-157	Gabbro	Toma de Agua (near Riyito)	8.673121	-83.573105	Ganado Unit, plateau-like
DB05-158	Gabbro	Road to Drake	8.693473	-83.582180	Ganado Unit, MORB-like
DB05-162	Basalt	Rio Riyito	8.644634	-83.552207	Ganado Unit, plateau-like
DB02-196	Basalt	Quebrada Agua Sucio	8.626993	-83.516784	Riyito Unit
DB02-197	Basalt	Quebrada Agua Sucio	8.627891	-83.517689	Riyito Unit

Table 1. Location of analyzed samples (continued)

Sample	Rock name	Locality	Coordinates (WGS84°) Latitude	Longitude	Unit or Group

Osa Igneous Complex (continued)

Sample	Rock name	Locality	Latitude	Longitude	Unit or Group
DB02-198a	Basalt	Quebrada Agua Sucio	8.627891	-83.517689	Riyito Unit
DB02-216	Basalt	Quebrada Pueblo Viejo	8.735524	-83.606710	Riyito Unit
DB02-239	Basalt	Rio Riyito	8.636944	-83.530408	Riyito Unit
DB05-114	Basalt	Quebrada Vaquedano	8.605960	-83.500891	Riyito Unit
DB05-135	Basalt	Quebrada Agua Sucio	8.623828	-83.528141	Riyito Unit
DB05-152	Gabbro	Rio Riyito	8.661820	-83.572647	Riyito Unit
DJ01-104	Basalt	Punta Ganadito	8.731004	-83.651245	Riyito Unit
DJ01-106	Basalt	Punta Ganadito	8.733712	-83.650338	Riyito Unit
DJ01-107	Basalt	Punta Ganadito	8.736425	-83.644880	Riyito Unit
DB02-242	Basalt	Rio Riyito	8.645992	-83.558573	Vaquedano Unit
DB02-250	Basalt	Quebrada Vaquedano	8.605293	-83.524059	Vaquedano Unit
DB05-113	Basalt	Quebrada Vaquedano	8.602127	-83.514976	Vaquedano Unit
DB05-119	Basalt	Quebrada Vaquedano	8.606649	-83.526783	Vaquedano Unit
DB05-121	Basalt	Quebrada Camarones	8.607101	-83.526786	Vaquedano Unit
DB05-153	Basalt	Rio Riyito	8.667239	-83.564928	Vaquedano Unit
DB05-161	Basalt	Rio Riyito	8.643736	-83.554027	Vaquedano Unit

Azuero Accretionary Complex

Sample	Rock name	Locality	Latitude	Longitude	Unit or Group
DB05-045	Basalt	La Salina	7.432749	-80.204927	Venado
DB07-051	Basalt	Rio El Infiernillo	7.458980	-80.295828	Venado
DB07-052	Dolerite	Rio El Infiernillo	7.458980	-80.295828	Venado
DB05-039	Basalt	road Covachon-Cambutal	7.232562	-80.614145	Punta Blanca
DB05-040	Basalt	road Covachon-Cambutal	7.231504	-80.604109	Punta Blanca
DB05-041	Basalt	road Covachon-Cambutal	7.231504	-80.604109	Punta Blanca
DB06-011	Basalt	Río Horcones	7.243046	-80.563744	Punta Blanca
DB07-029	Basalt	Rio Progreso	7.260826	-80.619981	Punta Blanca
DB07-033	Basalt	Rio Horcones	7.266628	-80.536183	Punta Blanca
DB07-038	Basalt	Rio Horcones	7.280206	-80.545681	Punta Blanca
DB07-040	Basalt	Rio Horcones	7.272510	-80.539347	Punta Blanca
DB05-006	Picrite	road to Japon	7.467147	-80.902726	Hoya
DB05-008	Basalt	Boca del Quebro	7.433554	-80.918040	Hoya
DB05-010	Picrite	Isleta Restin	7.235059	-80.905747	Hoya
DB05-012	Basalt	Isleta Restin	7.235059	-80.905747	Hoya
DB05-014	Basalt	Varadero	7.241699	-80.907938	Hoya
DB06-005	Basalt	Punta Piro	7.212973	-80.749095	Hoya
DB06-006	Basalt	Puerto Escondido	7.213018	-80.852808	Hoya
DB06-007	Hawaiite	Puerto Escondido	7.213018	-80.852808	Hoya
DB06-038	Picrite	El Morillo-Punta Duartes	7.494456	-80.964334	Hoya
DB06-049	Basalt	La Playa	7.433481	-80.918076	Hoya
DB06-076	Basaltic dyke	La Playa-Puerto Naranjo	7.424799	-80.928001	Hoya
DB06-077	Basaltic dyke	La Playa-Puerto Naranjo	7.424799	-80.928001	Hoya
DB06-078	Basalt	La Playa-Puerto Naranjo	7.418558	-80.931898	Hoya
DB06-081	Basalt	La Playa-Puerto Naranjo	7.329360	-80.898208	Hoya
DB06-083	Basalt	La Playa-Puerto Naranjo	7.324522	-80.903871	Hoya
DB06-084	Basalt	La Playa-Puerto Naranjo	7.270884	-80.926938	Hoya
DB06-085	Basalt	La Playa-Puerto Naranjo	7.320635	-80.917961	Hoya
DB06-086	Picrite	La Playa-Puerto Naranjo	7.320635	-80.917961	Hoya
DB06-087	Basalt	Quebrada Los Cativos	7.411927	-80.854782	Hoya
DB06-088	Basalt	Quebrada Los Cativos	7.411756	-80.858769	Hoya
DB06-089	Picrite	Quebrada Los Cativos	7.411756	-80.858769	Hoya
DB06-100	Basalt	Road Guerra-Boca de Quebro	7.461054	-80.852999	Hoya
DB06-101	Basalt	Road Guerra-Boca de Quebro	7.466478	-80.841849	Hoya
DB06-108	Basalt	Río Playita	7.340174	-80.783590	Hoya
DB06-128	Basalt	Río Playita	7.333024	-80.775666	Hoya
DB06-130	Rhyolite	Río Playita	7.329224	-80.774399	Hoya
DB06-134	Basalt	Río Pavo	7.387194	-80.749497	Hoya
DB07-001	Basalt	Rio Varadero	7.299860	-80.858216	Hoya
DB07-004	Basalt	Quebrada Mala	7.404844	-80.752006	Hoya
DB07-006	Basaltic dyke	Quebrada La Barra	7.362682	-80.751277	Hoya
DB07-007	Gabbro	Quebrada La Barra	7.347300	-80.745170	Hoya
DB07-008	Picrite	Quebrada La Barra	7.343681	-80.743133	Hoya

Table 1. Location of analyzed samples (continued)

Sample	Rock name	Locality	Coordinates (WGS84°) Latitude	Longitude	Unit or Group
		Azuero Accretionary Complex (continued)			
DB07-009	Basaltic dyke	Rio Pavo	7.334161	-80.707351	Hoya
DB07-011	Basalt	Rio Pavo	7.352707	-80.710963	Hoya
DB07-012	Basalt	Quebrada La Zumbona	7.432420	-80.778108	Hoya
DB07-013	Basaltic dyke	Quebrada La Zumbona	7.410082	-80.788595	Hoya
DB07-014	Picrite	Quebrada La Zumbona	7.408029	-80.789420	Hoya
DB07-016	Basalt	Rio Varadero	7.302552	-80.801139	Hoya
DB07-017	Basalt	Rio Ventana	7.277677	-80.803415	Hoya
DB07-021	Hawaiite	Rio Colorado	7.237884	-80.824266	Hoya
DB07-024	Picrite	Rio Varadero	7.271053	-80.843087	Hoya
DB07-027	Foid-monzogabbro	Quebrada La Barra	7.376033	-80.735313	Hoya
DB07-028	Basalt	Casacalloso	7.391526	-80.875739	Hoya
DB07-032	Basalt	Rio Porto Velo	7.295651	-80.619499	Hoya
DB05-003	Basalt	Russia	7.460318	-80.907349	Quebro
DB06-036	Basalt	El Morillo	7.480344	-80.957040	Quebro
DB06-037	Basalt	El Morillo	7.480344	-80.957040	Quebro
DB06-040	Basalt	El Morillo-Punta Duartes	7.494818	-80.965739	Quebro
DB06-046	Basalt	El Morillo	7.475367	-80.941587	Quebro
		Azuero Mélange			
DB06-096	Basalt	Higueronoso	7.497354	-80.849887	Higueronoso

Table 2. Major, minor and trace elements (XRF)

Sample	Major and minor elements, wt%												Trace elements, ppm				
	SiO₂	TiO₂	Al₂O₃	Fe₂O₃	MnO	MgO	CaO	Na₂O	K₂O	P₂O₅	LOI	Total	V	Cr	Ni	Sr	Zr

								Golfito Complex									
DB02-042	48.91	0.56	14.08	10.04	0.17	9.26	10.77	3.11	0.23	0.05	2.88	100.06	236	191	109	179	33
DB02-057	52.69	0.86	13.95	12.42	0.20	5.65	7.82	3.45	0.44	0.10	1.71	99.30	293	38	37	157	63
DB02-063	51.20	1.21	14.02	12.06	0.23	5.30	6.63	5.00	0.48	0.22	3.08	99.44	293	6	15	112	69
DB02-073	49.77	0.95	14.28	12.91	0.20	7.03	7.25	4.25	0.31	0.10	2.41	99.46	340	20	35	106	58
DB02-087	49.87	0.77	15.94	10.65	0.19	7.09	9.44	3.42	0.52	0.09	2.23	100.19	250	123	64	198	54
DB02-101	49.35	0.69	14.74	9.64	0.14	7.87	9.63	3.97	0.18	0.08	2.96	99.25	258	131	69	220	46
DB02-138	53.12	0.54	15.03	8.79	0.14	7.17	9.63	2.95	0.47	0.08	1.43	99.35	208	105	61	153	47
DB02-143	49.15	0.86	15.10	11.26	0.17	6.84	8.11	4.42	0.18	0.11	3.06	99.28	296	47	31	221	55
DB02-149	49.10	0.75	14.39	11.49	0.19	8.16	8.24	3.82	0.33	0.08	2.69	99.25	268	105	71	302	55
DB02-151	54.01	1.14	14.51	9.88	0.19	4.12	6.28	6.18	0.46	0.21	2.13	99.12	275	8	23	110	67
DB02-157	49.77	1.19	13.93	14.00	0.22	6.67	9.72	2.71	0.36	0.12	1.28	99.96	339	37	43	124	58
DB02-158	53.77	1.14	14.36	13.25	0.20	4.64	6.99	4.14	0.35	0.11	1.07	100.01	337	2	14	143	93
DB02-174	49.43	0.76	14.62	10.88	0.21	7.75	7.23	4.00	0.85	0.09	3.26	99.09	256	100	68	414	59
DB02-175	55.81	1.06	14.30	10.33	0.18	2.95	5.27	5.17	1.06	0.17	2.91	99.22	344	8	11	789	97
DB02-181	51.35	1.18	14.34	12.11	0.19	5.96	9.00	2.68	0.15	0.21	2.11	99.28	312	23	24	153	73
								Azuero Complex - Azuero Plateau									
DB05-002	47.88	1.12	14.43	12.04	0.22	8.13	12.22	2.39	0.08	0.09	1.38	99.97	318	293	126	152	65
DB05-047	45.98	1.28	13.82	12.63	0.20	7.36	13.42	2.32	0.07	0.11	2.42	99.60	346	213	102	136	73
DB05-072	48.47	1.19	13.73	11.84	0.20	8.16	12.00	2.25	0.42	0.10	1.54	99.90	326	282	122	138	68
DB05-073	49.34	0.99	13.88	11.14	0.18	8.18	11.85	2.57	0.13	0.07	0.15	98.48	344	258	111	106	55
DB05-076	48.43	1.04	14.66	11.69	0.23	8.12	12.66	2.29	0.08	0.09	0.96	100.24	310	318	124	158	61
DB05-080	48.78	1.20	14.11	13.21	0.24	7.02	11.46	2.59	0.10	0.10	0.72	99.53	429	148	72	86	65
DB06-027	48.45	1.28	14.08	12.44	0.22	8.07	11.89	2.42	0.09	0.10	0.74	99.79					
DB06-034	48.87	1.16	14.12	12.10	0.21	8.26	12.29	2.17	0.18	0.09	0.53	99.98					
DB06-093	47.16	1.20	14.06	12.17	0.21	8.36	11.89	2.25	0.30	0.10	2.34	100.04					
DB06-102	47.75	1.27	14.21	12.31	0.20	8.06	11.77	2.51	0.18	0.10	1.71	100.07					
DB06-104	47.92	1.29	14.26	12.30	0.18	7.90	12.03	2.60	0.17	0.11	1.40	100.16					
DB06-117	47.97	1.22	13.96	11.99	0.21	8.35	10.63	3.34	0.11	0.10	2.26	100.14					
DB06-121	47.65	1.34	13.83	12.86	0.22	8.00	10.60	3.07	0.20	0.11	2.22	100.11					
DB06-125	47.70	1.21	14.48	11.84	0.21	8.18	12.41	2.32	0.09	0.10	1.41	99.94					
DB06-126	48.02	1.02	14.52	11.53	0.20	8.39	12.75	2.18	0.04	0.08	1.28	100.01					
DB06-136	47.54	1.55	14.92	12.74	0.22	7.01	11.45	2.45	0.28	0.14	1.33	99.62					
DB06-137	47.04	1.19	14.31	12.11	0.24	8.61	12.17	2.07	0.05	0.10	2.26	100.14					
DB06-138	47.11	1.48	14.28	13.99	0.28	7.41	11.15	2.47	0.12	0.13	1.74	100.15					
DB06-139	47.64	1.24	14.49	12.44	0.20	8.39	10.91	2.77	0.18	0.10	1.83	100.18					
DB06-141	48.30	1.33	14.30	13.04	0.21	7.86	10.77	2.83	0.23	0.11	1.06	100.04					
DB07-043	48.74	1.21	13.28	12.31	0.22	8.05	10.79	3.09	0.28	0.10	2.26	100.34					
DB07-044	48.47	1.19	14.04	12.11	0.19	8.00	11.85	2.52	0.09	0.10	1.44	100.00					
DB07-050	47.51	1.32	14.34	12.86	0.20	7.61	12.54	2.00	0.04	0.11	0.68	99.20					
								Azuero Complex - Azuero Arc									
DB05-030	48.21	1.09	15.88	10.90	0.19	7.33	11.32	2.95	0.22	0.10	1.97	100.16	331	376	154	303	74
DB05-043	48.68	1.62	15.47	12.26	0.21	5.83	9.76	4.00	0.49	0.17	1.74	100.22	343	80	45	170	112
DB05-055	49.59	1.95	14.02	14.44	0.23	5.04	8.66	4.39	0.48	0.24	0.05	99.08	403	48	32	233	136
DB05-057	45.49	1.41	17.76	11.87	0.23	6.94	13.47	1.63	0.35	0.14	0.54	99.83	301	148	60	346	90
DB05-061	48.71	0.86	18.04	11.02	0.19	6.08	12.09	2.13	0.09	0.11	0.45	99.77	338	53	39	270	49
DB05-062	48.08	1.49	16.92	11.42	0.19	5.97	9.98	3.38	0.37	0.12	2.08	99.99	340	63	44	339	70
DB05-069	47.17	1.57	13.75	12.85	0.21	7.46	11.00	3.27	0.30	0.15	2.00	99.73	361	159	97	175	101
DB05-083	46.62	1.59	13.58	12.89	0.19	7.20	10.41	3.62	0.19	0.15	2.48	98.91	375	152	99	111	105
DB05-087	50.07	1.03	16.92	9.01	0.16	6.72	11.38	2.53	0.36	0.13	1.68	99.98	228	244	58	232	78
DB06-035	46.97	1.10	20.89	8.48	0.15	4.20	12.04	3.34	0.18	0.11	2.03	99.48					
DB06-112	51.19	0.76	16.90	8.49	0.16	7.56	10.69	3.25	0.12	0.10	0.37	99.60					
DB06-113	52.44	1.15	17.48	9.62	0.17	3.96	5.96	6.42	0.41	0.16	1.98	99.74					
DB06-120	47.57	1.78	13.69	12.87	0.25	7.93	10.30	2.68	0.90	0.16	1.72	99.85					
DB07-015	49.22	1.83	14.40	13.30	0.22	4.31	8.93	3.00	0.82	0.30	3.01	99.34					
DB07-049	49.86	2.07	14.81	13.16	0.20	4.78	8.58	4.15	0.15	0.30	2.11	100.18					

Table 2. Major, minor and trace elements (XRF) (continued)

Sample	Major and minor elements, wt%												Trace elements, ppm				
	SiO_2	TiO_2	Al_2O_3	Fe_2O_3	MnO	MgO	CaO	Na_2O	K_2O	P_2O_5	LOI	Total	V	Cr	Ni	Sr	Zr
Azuero Complex - Azuero Proto-Arc																	
DB05-024	57.94	0.30	15.34	8.22	0.19	5.90	1.93	4.87	2.04	0.19	2.44	99.36	261	14	6	321	106
DB05-027	53.32	0.47	17.69	9.87	0.19	5.09	4.17	5.93	0.89	0.09	2.02	99.73	433	34	8	389	31
DB05-028	57.07	0.78	17.21	9.03	0.20	3.41	7.46	3.54	1.07	0.17	0.51	100.46	261	14	6	321	106
DB05-048	54.59	1.41	15.70	10.86	0.17	3.40	7.76	3.62	1.16	0.27	0.28	99.22	286	18	9	336	152
DB05-050	52.75	0.61	15.95	8.46	0.18	6.18	10.51	2.76	0.80	0.07	0.61	98.88	256	116	24	288	67
DB05-052	74.82	0.25	12.43	1.16	0.03	0.24	2.12	3.54	2.70	0.02	0.28	97.60	16	4	4	225	197
DB05-053	54.94	0.73	16.05	9.69	0.16	4.50	7.69	3.62	1.31	0.18	0.58	99.45	248	44	25	396	101
DB05-056	66.13	0.64	13.97	6.07	0.10	0.91	2.41	4.78	2.60	0.19	0.58	98.38	16	bdl	3	269	216
DB05-058	53.20	0.55	17.71	8.70	0.16	5.78	9.92	2.72	0.51	0.10	1.09	100.43	232	48	25	331	54
DB05-059	66.61	0.45	15.59	4.44	0.10	1.60	4.52	4.08	1.15	0.10	0.51	99.14	76	8	6	280	105
DB05-064	60.29	0.26	15.60	7.38	0.12	3.55	6.64	3.05	0.88	0.09	1.37	99.22	228	22	10	318	31
DB05-067	61.12	0.55	15.77	6.88	0.12	3.08	6.07	3.24	1.28	0.12	0.79	99.02	192	17	11	252	82
DB05-068	62.32	0.51	15.79	6.13	0.12	2.55	5.93	3.25	1.52	0.11	0.48	98.72	161	17	9	251	79
DB05-088	49.56	0.95	15.81	11.70	0.19	5.31	6.96	3.07	2.44	0.32	2.56	98.88	416	51	23	703	72
DB05-092	61.17	0.33	16.13	6.00	0.12	2.13	8.01	2.77	0.73	0.11	1.87	99.37	260	32	13	327	38
DB06-052	47.96	1.61	15.23	11.56	0.20	6.70	10.68	3.51	0.24	0.29	1.60	99.58					
DB06-105	47.51	1.69	15.67	11.79	0.27	6.05	12.01	2.90	0.25	0.31	1.09	99.54					
DB06-123	55.43	0.73	18.49	6.73	0.25	3.19	8.22	4.51	1.18	0.14	0.55	99.42					
Osa Mélange																	
DJ01-006	69.23	0.52	13.50	5.33	0.12	0.93	1.64	6.70	0.79	0.11	1.08	99.96	19	3	bdl	98	260
DJ01-028	51.50	1.92	14.03	11.73	0.17	3.10	6.81	6.10	0.42	0.61	3.44	99.84	100	bdl	2	113	118
DJ01-112	64.99	0.35	14.16	4.87	0.11	1.80	6.27	3.58	0.47	0.14	3.32	100.05	94	16	8	322	79
Osa Igneous Complex - Inner Osa Igneous Complex																	
DB02-107	47.63	1.08	14.61	11.19	0.34	8.37	12.85	1.81	0.06	0.09	1.90	99.92	284	320	138	107	62
DB02-110	46.92	1.25	14.06	12.56	0.22	7.88	11.71	2.06	0.10	0.10	2.18	99.05					
DB02-119	48.08	1.71	14.18	10.22	0.17	7.16	11.26	3.20	0.29	0.14	2.77	99.18	288	33	95	241	103
DB02-120	48.62	1.12	14.29	12.62	0.20	7.66	11.70	1.89	0.06	0.09	1.48	99.74	304	135	106	116	63
DB02-132	48.94	1.34	14.25	11.49	0.17	7.81	12.42	2.16	0.07	0.11	1.28	100.03	325	236	108	120	78
DB02-135	48.16	1.23	14.55	11.37	0.22	7.55	12.33	2.04	0.09	0.10	1.94	99.57	303	260	131	150	73
DB02-160	46.19	1.10	13.92	13.19	0.18	8.00	11.31	2.36	0.14	0.08	2.66	99.10	318	188	84	106	58
DB02-165	48.70	0.86	14.41	10.69	0.19	8.92	12.45	1.95	0.08	0.07	1.77	100.09	275	390	153	100	48
DB02-201	46.45	0.63	19.25	8.93	0.16	6.12	13.09	2.10	0.09	0.05	3.12	99.99	188	286	68	200	37
DB02-203	48.80	1.64	13.07	15.89	0.25	5.98	6.92	4.37	0.13	0.13	2.85	100.03	417	5	39	50	85
DB02-204	47.11	1.13	14.44	12.45	0.20	6.64	10.17	2.72	0.34	0.09	4.21	99.49	281	96	81	165	64
DB02-227	45.27	0.32	21.38	6.35	0.11	6.41	11.84	2.45	0.28	0.05	4.95	99.41	82	352	103	200	32
DB02-230	48.12	1.28	13.84	12.56	0.35	7.24	12.00	2.09	0.09	0.11	1.43	99.11	330	188	117	111	75
DB02-232	52.57	1.42	14.92	7.54	0.11	6.39	6.79	4.20	1.70	0.59	2.81	99.04	182	370	108	295	297
DB02-246	51.14	1.16	13.46	14.55	0.23	5.17	8.79	2.80	0.13	0.13	1.57	99.12	357	11	24	126	70
DB02-266	48.09	1.32	13.44	13.69	0.22	7.16	9.99	2.73	0.28	0.09	2.19	99.20	339	34	83	136	66
DB05-107	48.50	0.89	14.47	10.63	0.20	8.68	12.82	1.78	0.09	0.07	1.19	99.32					
DB05-108	47.68	0.91	14.61	11.10	0.18	9.13	10.55	2.50	0.23	0.07	2.20	99.16					
DB06-054	48.47	0.90	14.78	10.75	0.16	9.01	12.92	1.78	0.08	0.07	0.68	99.59					
DB06-058	47.53	1.29	14.24	12.75	0.23	7.62	12.10	2.23	0.06	0.11	2.02	100.17					
DB06-061	51.76	2.28	11.57	18.08	0.26	2.65	6.86	3.94	0.07	0.24	1.42	99.12					
DB06-065	46.57	0.96	15.09	11.72	0.23	8.18	12.35	2.22	0.15	0.07	2.04	99.57					
DB06-066	47.33	2.96	13.66	14.24	0.21	6.29	10.58	2.77	0.56	0.29	1.24	100.13					
DB06-070	47.80	1.05	14.27	11.43	0.17	8.28	11.13	3.02	0.07	0.08	2.95	100.25					
DB06-075	48.57	1.48	13.08	15.78	0.24	6.17	9.26	3.68	0.29	0.12	1.67	100.31					
DJ01-022	47.04	0.88	14.73	10.66	0.16	8.33	12.41	2.54	0.12	0.07	2.95	99.89	278	418	161	142	50
DJ01-115	47.67	1.25	13.89	11.92	0.21	7.85	11.06	2.77	0.19	0.11	2.87	99.79	292	269	118	164	74
Inner Osa Igneous Complex - Güerra Unit																	
DB02-191	47.51	1.96	13.50	12.27	0.18	7.06	9.65	3.31	0.19	0.16	3.42	99.22	310	234	107	257	124
DB02-207	44.64	0.70	12.86	12.02	0.16	13.57	8.19	1.71	0.27	0.07	5.22	99.40	171	1407	910	68	39

Table 2. Major, minor and trace elements (XRF) (continued)

Sample	Major and minor elements, wt%												Trace elements, ppm				
	SiO_2	TiO_2	Al_2O_3	Fe_2O_3	MnO	MgO	CaO	Na_2O	K_2O	P_2O_5	LOI	Total	V	Cr	Ni	Sr	Zr
Inner Osa Igneous Complex - Ganado Unit																	
DB02-198b	43.09	1.19	17.76	11.01	0.14	6.96	12.08	2.20	0.32	0.19	3.81	98.75	174	366	220	258	60
DB02-260	49.56	1.49	15.47	11.05	0.18	6.31	9.96	3.09	0.13	0.15	1.69	99.07	289	152	70	175	143
DB02-261	48.50	2.36	13.34	14.50	0.26	6.41	9.34	2.98	0.10	0.23	1.47	99.49	422	86	56	146	165
DB02-262	43.97	6.36	12.77	16.50	0.40	6.40	9.69	2.46	0.09	0.05	1.47	100.16	550	102	106	121	148
DB05-149	47.98	1.05	13.91	11.96	0.18	9.08	11.28	1.78	0.14	0.08	2.08	99.53					
DB05-155	48.83	1.84	13.54	13.20	0.23	6.89	10.38	2.97	0.12	0.17	1.05	99.23					
DB05-156	48.64	2.40	13.17	15.20	0.26	6.03	8.80	3.44	0.17	0.22	1.13	99.44					
DB05-157	53.84	1.40	15.51	8.26	0.09	4.31	8.07	5.76	0.27	0.36	1.25	99.11					
DB05-158	49.79	0.99	14.82	8.98	0.15	7.58	13.04	2.58	0.12	0.07	1.01	99.13					
DB05-162	52.14	0.49	16.98	7.22	0.13	6.61	9.09	2.72	1.35	0.04	2.62	99.38					
Inner Osa Igneous Complex - Riyito Unit																	
DB02-196	47.76	1.00	14.14	11.02	0.18	7.32	10.65	3.48	0.03	0.08	3.64	99.30	294	218	90	32	54
DB02-197	47.65	1.07	15.79	11.61	0.20	6.71	11.11	2.81	0.28	0.08	1.97	99.27	294	182	78	131	60
DB02-198a	48.15	1.02	15.28	11.44	0.20	7.75	9.55	3.10	0.44	0.07	2.41	99.41	285	214	83	149	56
DB02-216	47.03	0.82	16.86	9.83	0.18	6.90	13.66	1.75	0.03	0.06	2.22	99.33	223	290	107	85	47
DB02-239	47.57	1.50	13.11	14.03	0.21	6.36	9.98	3.67	0.03	0.14	2.72	99.32	336	68	57	32	105
DB05-114	49.45	1.35	13.09	15.01	0.22	6.40	10.68	2.58	0.05	0.09	0.55	99.46					
DB05-135	47.77	1.62	14.20	13.97	0.23	6.29	10.57	3.15	0.21	0.14	1.36	99.50					
DB05-152	47.59	0.81	20.44	7.69	0.13	5.45	10.79	2.25	1.91	0.06	2.09	99.21					
DJ01-104	49.73	1.13	14.31	11.20	0.25	6.19	9.67	3.43	0.91	0.10	3.06	99.97	290	141	56	115	66
DJ01-106	49.88	1.00	13.97	10.62	0.18	6.04	11.04	3.71	0.46	0.08	2.95	99.92	291	278	79	116	51
DJ01-107	50.40	1.01	13.92	11.05	0.19	6.51	11.08	3.56	0.38	0.08	1.81	99.99	292	125	58	115	54
Inner Osa Igneous Complex - Vaquedano Unit																	
DB02-242	42.20	1.37	14.05	12.54	0.15	12.35	9.29	1.56	0.18	0.14	5.45	99.29	219	1006	549	151	93
DB02-250	44.23	2.02	16.46	12.99	0.17	7.85	7.31	2.90	0.74	0.20	4.36	99.23	249	138	107	366	156
DB05-113	44.91	2.04	17.19	10.62	0.14	8.07	8.45	2.45	1.76	0.23	3.15	99.02					
DB05-119	43.19	2.18	15.77	13.99	0.22	8.40	6.89	3.32	0.63	0.23	4.30	99.12					
DB05-121	43.99	1.94	16.41	13.27	0.16	7.44	8.04	3.06	0.76	0.18	3.61	98.86					
DB05-153	49.34	1.97	14.70	9.62	0.16	7.03	9.65	3.66	0.40	0.25	2.66	99.43					
DB05-161	44.33	1.73	15.10	10.77	0.14	6.91	12.41	3.25	0.45	0.17	4.15	99.42					
Azuero Accretionary Complex - Venado Unit																	
DB05-045	46.51	2.77	14.65	13.78	0.19	5.68	11.59	2.66	0.29	0.25	0.89	99.25	402	121	82	31	158
DB07-051	48.55	2.80	13.17	13.55	0.19	7.22	5.99	3.78	1.43	0.23	3.02	99.94					
DB07-052	45.19	4.02	13.58	14.43	0.21	5.41	8.76	3.72	0.79	0.23	2.69	99.03					
Azuero Accretionary Complex - Punta Blanca Group																	
DB05-039	47.93	2.99	13.75	14.38	0.19	5.73	11.11	2.51	0.21	0.28	-0.21	98.86	348	96	81	32	39
DB05-040	47.17	2.66	13.65	13.57	0.19	6.49	11.66	2.42	0.19	0.27	-0.05	98.23	392	161	104	33	160
DB05-041	48.14	2.67	13.93	13.76	0.19	7.08	11.25	2.56	0.27	0.23	0.05	100.13	348	137	106	33	143
DB06-011	47.24	2.94	13.67	14.41	0.28	6.61	10.17	3.06	0.59	0.29	0.56	99.82					
DB07-029	49.20	2.65	13.79	12.49	0.19	5.96	11.89	2.63	0.19	0.24	0.73	99.95					
DB07-033	47.65	2.46	15.21	13.04	0.20	6.14	12.20	2.22	0.09	0.22	0.37	99.80					
DB07-038	45.55	2.54	13.36	13.20	0.21	8.30	9.38	3.22	0.26	0.22	3.84	100.09					
DB07-040	48.63	2.78	13.20	13.65	0.24	6.46	8.84	4.08	0.21	0.26	1.71	100.04					
Azuero Accretionary Complex - Hoya Group																	
DB05-006	43.82	1.60	8.06	13.34	0.17	22.58	6.29	1.20	0.21	0.19	1.79	99.23	210	956	1085	78	84
DB05-008	49.02	3.11	13.89	12.74	0.18	6.65	11.19	2.67	0.35	0.32	-0.06	100.07					
DB05-010	39.97	1.08	5.73	12.76	0.17	27.14	5.49	0.54	0.17	0.12	5.05	98.23	149	1772	1147	102	57
DB05-012	46.90	3.81	14.05	12.83	0.23	5.59	9.92	3.56	0.86	0.48	1.37	99.60	368	54	59	35	322
DB05-014	45.06	3.86	13.67	13.94	0.15	5.58	8.41	3.49	1.30	0.47	3.46	99.41	379	71	74	45	293
DB06-005	45.37	3.98	14.12	13.85	0.20	4.19	11.20	3.40	1.19	0.52	1.91	99.93					
DB06-006	45.56	4.10	14.24	13.76	0.21	5.87	9.99	3.11	0.91	0.51	1.34	99.59					
DB06-007	48.00	3.12	17.07	11.35	0.11	2.46	7.60	4.96	1.29	0.93	2.20	99.09					
DB06-038	44.32	1.47	7.30	13.41	0.18	25.22	6.41	1.13	0.10	0.15	0.38	100.07					

Table 2. Major, minor and trace elements (XRF) (continued)

Sample	Major and minor elements, wt%												Trace elements, ppm				
	SiO$_2$	TiO$_2$	Al$_2$O$_3$	Fe$_2$O$_3$	MnO	MgO	CaO	Na$_2$O	K$_2$O	P$_2$O$_5$	LOI	Total	V	Cr	Ni	Sr	Zr
Azuero Accretionary Complex - Hoya Group (continued)																	
DB06-049	47.46	2.81	13.92	12.50	0.18	7.68	12.18	2.18	0.17	0.28	0.49	99.84					
DB06-076	47.28	3.67	14.44	13.15	0.19	5.82	9.89	3.25	1.36	0.43	0.40	99.88					
DB06-077	48.80	2.88	13.92	12.34	0.17	6.57	11.64	2.56	0.29	0.30	0.03	99.51					
DB06-078	47.92	2.95	13.82	12.34	0.18	7.11	10.32	2.97	1.22	0.29	0.85	99.95					
DB06-081	44.65	3.02	14.16	12.17	0.18	7.44	10.20	2.91	0.85	0.32	3.90	99.80					
DB06-083	46.79	3.29	13.88	13.04	0.20	6.60	9.19	3.30	0.96	0.37	1.77	99.39					
DB06-084	46.26	2.94	13.65	12.33	0.18	7.34	10.32	2.65	1.34	0.27	2.37	99.66					
DB06-085	46.98	3.72	14.05	13.91	0.18	5.62	10.19	3.00	0.89	0.44	0.53	99.50					
DB06-086	45.85	2.39	12.93	11.69	0.16	12.31	10.51	2.09	0.60	0.27	1.24	100.04					
DB06-087	46.64	2.72	13.42	11.90	0.18	7.07	10.46	1.58	2.88	0.28	2.01	99.14					
DB06-088	48.09	2.89	13.71	12.30	0.18	7.78	11.06	2.62	0.28	0.29	0.92	100.12					
DB06-089	38.43	0.82	4.05	12.73	0.17	31.24	2.79	0.01	0.01	0.09	9.00	99.34					
DB06-100	46.96	2.80	13.37	11.96	0.17	7.11	10.19	1.71	2.87	0.29	2.27	99.69					
DB06-101	47.07	2.74	13.31	12.18	0.17	7.55	9.05	3.84	0.94	0.25	2.99	100.10					
DB06-108	46.86	3.06	14.00	12.49	0.18	6.25	11.31	2.46	0.89	0.33	1.34	99.16					
DB06-128	46.74	3.50	13.61	13.64	0.17	5.92	8.93	2.94	1.95	0.39	1.70	99.47					
DB06-130	64.23	0.60	14.69	6.52	0.14	0.71	1.89	6.57	1.91	0.10	1.89	99.24					
DB06-134	47.43	2.55	12.98	12.46	0.17	8.89	10.51	2.52	0.52	0.24	1.67	99.93					
DB07-001	46.63	3.85	14.84	13.15	0.21	5.05	10.48	3.05	0.85	0.54	1.24	99.89					
DB07-004	47.84	3.01	13.48	12.38	0.21	7.30	9.75	3.25	0.82	0.30	1.85	100.20					
DB07-006	45.52	3.86	13.30	13.46	0.18	4.99	9.16	3.62	1.46	0.51	3.43	99.51					
DB07-007	43.35	3.74	17.23	12.54	0.12	5.42	12.16	2.21	1.06	0.16	1.50	99.48					
DB07-008	45.14	1.93	11.02	11.69	0.17	15.13	10.71	0.81	0.61	0.20	2.77	100.19					
DB07-009	50.46	3.40	13.34	11.37	0.20	6.24	9.57	2.19	0.25	0.37	2.64	100.04					
DB07-011	45.57	3.60	14.28	12.90	0.22	5.97	12.01	2.54	0.50	0.45	1.81	99.86					
DB07-012	47.95	3.23	14.12	12.85	0.17	6.39	11.32	2.57	0.71	0.35	0.36	100.02					
DB07-013	47.11	2.94	13.24	12.48	0.18	8.07	11.31	2.27	0.67	0.32	1.08	99.67					
DB07-014	44.59	2.29	11.51	11.86	0.18	11.94	9.87	2.12	0.50	0.24	4.76	99.86					
DB07-016	48.71	3.05	14.12	11.95	0.20	5.97	11.42	2.41	0.40	0.32	1.61	100.15					
DB07-017	45.75	4.11	14.19	14.12	0.20	5.50	10.86	2.68	0.22	0.53	1.71	99.86					
DB07-021	48.92	3.08	15.62	11.15	0.20	3.97	7.67	4.60	1.56	1.32	1.31	99.39					
DB07-024	42.94	1.72	8.90	12.61	0.18	20.91	7.95	0.99	0.35	0.19	3.06	99.81					
DB07-027	48.03	3.72	14.30	12.91	0.20	4.11	7.77	4.41	1.79	0.73	1.53	99.49					
DB07-028	47.79	2.79	13.41	12.06	0.18	6.93	9.63	2.69	1.88	0.28	1.81	99.45					
DB07-032	46.13	3.77	14.09	13.88	0.22	6.25	10.21	2.77	0.90	0.47	1.30	99.99					
Azuero Accretionary Complex - Quebro Group																	
DB05-003	46.21	3.25	12.04	14.34	0.21	8.24	10.33	2.25	0.45	0.37	0.61	98.29	406	411	262	56	231
DB06-036	46.76	3.56	13.50	14.14	0.20	6.22	10.58	2.82	0.51	0.41	0.41	99.10					
DB06-037	46.04	2.68	10.69	14.29	0.20	12.37	9.88	1.96	0.39	0.29	0.40	99.20					
DB06-040	47.81	3.26	12.79	14.02	0.20	7.13	9.27	3.71	0.39	0.34	1.20	100.11					
DB06-046	45.67	4.18	12.32	15.28	0.25	5.80	9.13	3.37	0.74	0.50	2.75	99.98					
Azuero Mélange																	
DB06-096	48.46	2.12	17.06	7.62	0.18	6.41	7.92	3.59	1.99	0.42	4.14	99.92					

Table 3. Trace elements (LA-ICP-MS)

Sample	Sc	V	Cr	Ni	Rb	Sr	Y	Zr	Nb	Cs	Ba	La	Ce	Pr	Nd	Sm	Eu	Gd	Tb	Dy	Ho	Er	Tm	Yb	Lu	Hf	Pb	Th	U
Golfito Complex																													
DB02-042	52.72	286	260	97	2.51	184	14.92	25.5	1.14	0.112	71	1.51	3.95	0.65	3.79	1.26	0.56	1.91	0.35	2.54	0.56	1.64	0.25	1.68	0.24	1.01	0.54	bdl	bdl
DB02-057	43.76	324	78	37	9.14	153	26.03	51.8	2.35	0.274	95	2.77	7.35	1.09	5.84	2.09	0.80	2.87	0.55	4.27	1.01	2.99	0.49	3.12	0.48	1.48	0.93	0.28	0.09
DB02-063	49.30	316	41	18	5.55	113	31.87	75.4	3.50	0.072	118	5.23	11.03	1.73	9.34	2.81	1.02	3.87	0.73	5.44	1.14	3.56	0.55	3.69	0.50	1.82	1.89	0.51	0.25
DB02-073	46.55	376	68	47	4.70	105	22.27	49.2	2.27	0.088	116	3.15	7.87	1.26	6.81	2.07	0.75	3.02	0.57	3.88	0.87	2.48	0.36	2.79	0.41	1.48	bdl	0.29	0.09
DB02-087	44.53	288	184	61	13.52	200	19.73	44.2	2.27	1.458	193	2.53	6.63	0.98	5.19	1.70	0.59	2.39	0.45	3.29	0.75	2.12	0.30	2.08	0.33	1.22	1.49	0.22	0.08
DB02-101	48.94	298	176	57	2.65	230	18.12	37.5	2.35	0.122	95	2.74	6.40	0.89	4.22	1.42	0.53	2.10	0.38	2.82	0.66	1.95	0.34	2.38	0.39	1.05	0.70	0.27	0.09
DB02-138	40.51	231	196	55	8.80	151	15.59	37.1	2.52	0.099	82	3.30	7.53	0.99	5.14	1.49	0.56	1.93	0.37	2.62	0.60	1.71	0.28	1.84	0.30	1.17	1.00	0.36	0.12
DB02-143	53.76	329	87	29	2.06	227	25.47	51.3	2.79	0.122	186	3.35	7.64	1.13	6.41	2.20	0.87	3.34	0.62	4.22	1.00	3.04	0.48	2.75	0.44	1.32	0.79	0.42	0.12
DB02-149	50.56	300	138	71	5.39	302	22.00	46.9	2.16	0.238	270	2.58	5.82	1.00	4.79	1.51	0.66	2.52	0.49	3.98	0.88	2.51	0.39	3.02	0.37	1.28	1.31	0.26	0.10
DB02-157	51.55	382	79	45	5.30	123	22.94	48.5	3.25	0.281	177	3.23	8.06	1.14	6.34	2.09	0.78	3.01	0.54	3.96	0.87	2.57	0.41	2.70	0.39	1.35	1.05	0.27	0.11
DB02-174	46.95	294	136	67	6.38	424	19.78	42.9	2.37	0.221	1570	3.44	8.09	1.22	6.37	1.93	0.72	2.69	0.47	3.44	0.76	2.20	0.33	2.25	0.34	1.29	1.32	0.35	0.09
DB02-175	36.46	374	42	12	16.59	799	24.50	69.5	3.77	0.097	2222	6.02	11.89	1.84	9.27	2.47	0.91	3.07	0.54	3.93	0.81	2.44	0.35	2.58	0.43	1.72	0.83	0.76	0.15
DB02-181	44.17	324	78	24	1.94	153	25.32	59.1	3.23	0.073	58	4.47	11.15	1.68	8.36	2.43	0.91	3.30	0.61	4.42	0.95	2.89	0.41	2.87	0.43	1.65	1.72	0.42	0.13
Azuero Complex - Azuero Plateau																													
DB05-002	52.34	341	407	117	0.95	152	20.85	53.6	3.45	bdl	14	2.87	8.28	1.33	6.98	2.06	0.86	3.10	0.51	3.73	0.76	2.23	0.36	2.01	0.33	1.43	0.58	0.20	0.09
DB05-047	51.70	353	252	92	0.79	135	23.74	61.5	3.65	0.013	11	3.45	8.86	1.47	7.54	2.46	0.99	3.36	0.65	4.22	0.89	2.66	0.36	2.64	0.38	1.70	0.60	0.26	0.09
DB05-072	49.14	340	357	115	2.78	135	20.90	55.2	3.47	0.021	80	2.89	7.91	1.34	7.38	2.22	0.86	3.11	0.59	3.82	0.78	2.24	0.41	2.20	0.32	1.81	0.48	0.24	0.07
DB05-073	52.38	354	380	110	1.25	105	19.03	43.9	3.02	0.073	42	2.48	6.88	1.00	5.89	1.98	0.72	2.65	0.49	3.31	0.72	2.13	0.33	2.29	0.32	1.26	0.36	0.20	0.12
DB05-076	48.72	309	364	111	0.68	152	19.10	46.0	2.64	0.007	27	2.33	6.92	1.33	5.94	2.12	0.70	2.77	0.50	3.34	0.73	1.95	0.31	1.92	0.33	1.31	0.47	0.19	0.08
DB05-080	52.87	393	180	64	0.62	81	27.19	53.4	3.17	0.007	19	2.82	7.41	1.16	6.67	2.29	0.90	3.44	0.56	4.57	1.05	3.17	0.42	3.21	0.47	1.55	0.48	0.21	0.09
DB06-027	51.24	378	828	106	0.84	114	23.89	65.2	3.74	0.059	15	3.41	9.03	1.42	7.31	2.50	0.96	3.43	0.57	3.88	0.85	2.35	0.37	2.35	0.36	1.86	0.63	0.28	0.15
DB06-034	49.64	333	880	116	1.62	122	22.94	52.0	3.27	0.024	20	2.74	7.62	1.18	6.87	2.25	0.92	2.73	0.52	3.54	0.76	2.20	0.33	2.28	0.35	1.53	0.45	0.21	0.07
DB06-093	50.26	351	373	117	5.47	260	21.82	56.0	3.38	0.019	324	2.97	8.61	1.31	7.12	2.33	0.82	3.11	0.57	3.92	0.79	2.30	0.38	2.27	0.35	1.61	0.39	0.24	0.08
DB06-102	53.55	369	852	134	3.20	195	25.40	67.3	4.02	0.044	43	3.34	9.84	1.52	7.85	2.43	0.89	3.83	0.63	4.22	0.87	2.54	0.41	2.55	0.37	1.64	0.61	0.26	0.12
DB06-104	55.75	375	490	123	1.72	161	24.70	65.5	3.87	0.018	28	3.33	9.32	1.48	8.07	2.65	1.01	3.61	0.60	4.38	0.87	2.61	0.39	2.59	0.39	1.80	0.26	0.23	0.09
DB06-117	49.08	353	660	131	1.74	101	22.79	59.8	3.44	0.260	22	3.03	8.44	1.31	6.93	2.26	0.91	3.21	0.57	3.86	0.83	2.32	0.35	2.21	0.33	1.55	0.77	0.25	0.10
DB06-121	52.66	373	219	105	1.94	150	24.68	64.3	3.79	0.030	47	3.57	9.26	1.54	8.23	2.65	1.07	3.71	0.69	4.61	0.95	2.82	0.44	2.69	0.44	1.94	0.24	0.28	0.11
DB06-125	51.41	341	368	114	0.89	130	22.11	58.5	3.41	0.042	18	3.15	8.36	1.39	7.33	2.39	0.95	3.31	0.56	3.98	0.90	2.41	0.37	2.40	0.34	1.54	0.41	0.23	0.08
DB06-126	52.90	336	632	137	0.49	113	19.53	49.0	2.81	0.060	12	2.35	7.11	1.20	5.78	1.96	0.76	2.64	0.45	3.27	0.67	1.93	0.31	1.99	0.31	1.34	0.71	0.19	0.08
DB06-136	48.99	382	225	78	3.96	150	28.90	83.7	5.01	0.056	75	5.05	12.83	1.94	10.58	3.47	1.12	4.27	0.79	5.19	1.07	3.17	0.48	3.15	0.46	2.43	0.69	0.45	0.13
DB06-137	51.91	335	3152	103	0.39	103	21.74	53.5	3.17	bdl	33	3.11	8.45	1.28	7.17	2.41	0.90	3.33	0.56	3.94	0.84	2.41	0.38	2.37	0.35	1.72	0.35	0.21	0.07
DB06-138	51.37	388	128	71	1.26	238	27.17	72.4	4.91	0.022	277	4.24	11.55	1.89	9.59	2.97	1.12	4.02	0.66	4.84	1.04	2.99	0.43	2.77	0.43	2.10	0.40	0.33	0.13
DB06-139	50.70	334	328	99	2.08	161	22.04	57.6	3.38	0.019	28	3.24	8.93	1.41	7.46	2.60	0.90	3.37	0.55	4.02	0.87	2.32	0.32	2.46	0.34	1.67	0.82	0.26	0.10
DB06-141	51.12	353	282	102	3.31	155	23.79	61.1	3.55	0.028	29	3.32	9.21	1.40	7.76	2.52	1.08	3.55	0.61	4.31	0.95	2.53	0.41	2.63	0.38	1.65	0.39	0.26	0.09
DB07-043	55.36	349	162	75	2.90	200	21.73	52.7	3.13	0.122	35	2.85	7.69	1.26	6.37	2.29	0.85	2.89	0.52	3.88	0.84	2.55	0.39	2.43	0.37	1.51	0.37	0.20	0.08
DB07-044	50.17	325	317	93	0.89	130	21.41	55.8	3.33	0.032	9	3.02	8.31	1.29	7.10	2.27	0.81	3.10	0.55	3.88	0.80	2.37	0.31	2.36	0.32	1.60	0.39	0.23	0.08
DB07-050	50.64	359	260	105	0.24	110	26.62	62.1	3.70	0.031	12	3.46	9.60	1.55	8.36	2.67	1.03	3.41	0.62	4.40	0.94	2.64	0.43	2.59	0.41	1.89	0.85	0.24	0.10

Table 3. Trace elements (LA-ICP-MS) (continued)

Sample	Sc	V	Cr	Ni	Rb	Sr	Y	Zr	Nb	Cs	Ba	La	Ce	Pr	Nd	Sm	Eu	Gd	Tb	Dy	Ho	Er	Tm	Yb	Lu	Hf	Pb	Th	U
Azuero Complex - Azuero Arc																													
DB05-030	49.31	353	530	142	2.86	302	25.13	56.9	3.01	0.271	82	3.24	8.48	1.24	6.97	2.45	0.92	3.26	0.64	4.04	0.88	2.78	0.35	2.85	0.43	1.74	1.10	0.28	0.11
DB05-043	47.25	355	530	142	6.25	169	34.63	109.0	2.83	0.747	180	5.47	14.15	2.29	12.18	3.98	1.42	5.37	0.93	5.58	1.31	3.78	0.61	3.86	0.55	2.82	1.29	0.40	0.14
DB05-055	42.57	462	113	32	6.31	230	43.23	118.8	2.85	bdl	102	5.96	16.79	2.89	15.12	4.82	1.73	6.53	1.17	7.79	1.66	4.97	0.66	4.36	0.63	2.89	0.82	0.44	0.12
DB05-057	58.78	347	240	59	6.25	330	26.18	74.5	2.77	0.428	131	3.19	9.28	1.50	8.69	3.17	0.73	3.82	0.71	4.87	0.97	2.74	0.40	2.78	0.36	1.99	2.39	0.21	0.07
DB05-061	44.60	355	89	34	0.63	271	16.61	37.4	1.33	0.027	51	3.90	9.00	1.25	6.30	1.87	0.67	2.45	0.42	2.85	0.64	1.91	0.28	1.82	0.26	1.09	1.57	0.61	0.22
DB05-062	37.53	372	126	44	6.09	332	19.25	60.5	4.42	0.318	150	4.36	11.97	1.85	9.83	2.92	1.09	3.32	0.55	3.73	0.80	2.11	0.32	2.02	0.29	1.95	1.12	0.35	0.14
DB05-069	65.50	473	260	107	2.72	234	48.35	133.3	10.28	bdl	543	8.96	20.68	3.03	16.20	5.60	1.85	7.60	1.33	9.36	1.80	5.61	0.74	4.84	0.86	4.12	1.15	0.89	0.49
DB05-083	52.55	379	206	90	2.09	108	31.80	90.0	6.49	0.086	37	6.12	15.29	2.25	11.52	3.52	1.24	4.83	0.85	5.76	1.25	3.38	0.50	3.27	0.53	2.46	0.40	0.51	0.16
DB05-087	43.69	270	355	57	4.21	234	19.76	71.5	2.00	0.058	87	3.56	10.21	1.61	8.27	2.62	1.03	2.97	0.50	3.41	0.72	2.18	0.32	2.07	0.34	1.80	1.50	0.21	0.07
DB06-035	30.99	243	240	41	1.94	223	24.11	73.2	1.76	0.030	41	2.77	8.48	1.47	7.60	2.35	0.94	3.38	0.59	4.05	0.84	2.46	0.37	2.57	0.41	1.82	2.42	0.18	0.09
DB06-112	36.40	238	889	90	1.16	168	20.42	57.4	2.47	0.042	98	3.47	7.56	1.21	5.97	2.00	0.76	2.56	0.47	3.48	0.75	2.25	0.32	2.20	0.33	1.64	1.67	0.38	0.12
DB06-113	31.45	272	357	23	6.74	175	29.40	96.6	4.62	0.656	259	6.35	14.22	2.04	10.62	3.04	1.04	3.97	0.67	4.83	1.04	3.02	0.46	3.34	0.51	2.40	1.40	0.69	0.33
DB06-120	50.99	382	1858	70	3.33	155	29.11	93.1	7.76	0.023	108	6.63	16.50	2.30	12.08	3.77	1.40	4.64	0.82	5.28	1.07	3.29	0.40	3.31	0.46	2.70	0.56	0.59	0.21
DB07-015	42.35	485	377	17	15.54	507	35.02	92.5	3.46	0.288	323	8.73	20.71	3.06	16.05	4.51	1.55	5.46	0.86	6.42	1.27	3.66	0.55	3.64	0.54	2.58	1.31	0.74	0.27
DB07-049	42.07	383	75	17	1.34	243	37.43	109.1	4.06	0.023	56	7.19	18.74	3.05	16.31	4.75	1.80	5.92	1.03	6.78	1.42	3.95	0.57	3.70	0.54	2.98	0.62	0.52	0.21
Azuero Complex - Azuero Proto-Arc																													
DB05-027	38.09	357	63	10	17.48	385	12.32	29.3	0.92	0.417	384	3.57	8.07	1.19	5.87	1.64	0.57	1.92	0.33	2.04	0.44	1.38	0.22	1.45	0.22	0.87	1.20	0.48	0.19
DB05-028	29.28	266	44	7	20.66	315	28.36	94.5	2.84	0.153	545	14.04	29.11	3.98	17.20	4.52	1.33	4.16	0.65	4.81	1.04	3.09	0.49	3.26	0.48	2.69	2.34	2.25	0.67
DB05-048	30.58	294	54	12	18.54	323	30.70	135.7	4.38	0.329	278	13.66	31.21	4.30	19.44	4.75	1.65	5.20	0.87	5.32	1.15	3.31	0.50	3.21	0.48	3.23	2.75	1.86	0.61
DB05-050	47.02	275	173	26	16.75	277	14.46	55.9	1.68	0.364	209	5.84	12.29	1.76	7.40	1.98	0.65	1.98	0.34	2.33	0.55	1.55	0.24	1.52	0.23	1.53	1.51	1.22	0.40
DB05-053	31.49	236	90	23	17.76	358	21.53	87.4	3.00	0.396	381	16.54	33.03	4.27	18.45	4.32	1.13	3.79	0.58	3.85	0.76	2.18	0.31	2.23	0.34	2.16	3.11	2.82	0.76
DB05-056	22.35	36	67	6	40.65	236	50.00	221.3	5.98	1.015	771	19.20	40.33	5.26	23.88	6.29	1.52	7.39	1.31	8.32	1.99	4.89	0.92	5.26	0.74	5.89	3.56	4.78	1.41
DB05-058	37.50	254	100	28	10.34	322	14.99	48.0	1.70	0.663	219	5.32	11.23	1.56	6.98	1.99	0.68	2.25	0.39	2.50	0.56	1.55	0.26	1.55	0.23	1.28	2.29	0.93	0.33
DB05-059	5.59	33	17	3	6.99	88	6.60	38.3	1.19	0.131	169	3.15	6.48	0.83	3.71	0.78	0.29	0.97	0.15	1.11	0.22	0.72	0.10	0.71	0.11	1.08	0.91	0.57	0.19
DB05-064	20.00	129	55	6	9.52	155	5.56	17.1	0.84	0.234	112	2.29	4.60	0.59	3.04	0.66	0.20	1.00	0.14	0.82	0.20	0.68	0.13	0.95	0.16	0.68	1.22	0.42	0.11
DB05-067	30.63	210	bdl	13	23.60	240	25.35	91.1	2.68	0.500	397	10.88	21.25	2.69	12.48	3.37	0.79	4.39	0.60	3.88	0.79	2.51	0.44	2.78	0.50	3.51	3.94	2.38	0.80
DB05-088	36.16	374	72	22	38.18	707	20.75	61.0	3.39	1.168	1238	8.70	18.65	2.85	12.63	3.29	1.13	3.70	0.59	3.85	0.79	2.20	0.35	2.36	0.35	1.78	3.03	0.80	0.39
DB06-052	50.84	338	358	59	3.11	235	33.04	143.9	8.53	0.109	105	15.41	34.68	4.41	20.30	4.68	1.74	5.35	0.85	5.81	1.18	3.53	0.50	3.21	0.50	3.44	0.74	1.06	0.34
DB06-105	53.85	362	341	58	2.40	192	35.54	149.4	9.11	0.054	83	14.74	34.96	4.65	20.14	4.91	1.63	5.42	0.93	6.13	1.33	3.87	0.59	3.74	0.54	3.69	2.58	1.01	0.37
DB06-123	30.56	265	360	51	11.99	304	17.66	88.8	2.92	0.129	507	7.91	15.12	2.15	9.70	2.44	0.83	2.70	0.41	2.86	0.59	1.74	0.27	1.86	0.27	2.12	3.01	1.51	0.44
Azuero Mélange																													
DJ01-006	14.76	38	bdl	4	10.61	93	68.04	272.4	7.83	0.058	233	13.40	29.56	4.10	22.36	7.76	1.97	10.07	1.62	11.93	2.38	7.61	1.16	8.63	1.27	7.11	3.66	2.24	0.76
DJ01-028	28.85	133	38	9	4.20	110	56.50	125.8	2.02	0.092	57	4.61	12.53	2.28	14.73	5.98	1.81	7.90	1.43	10.69	2.22	6.02	0.76	6.08	0.79	3.77	2.04	0.26	0.10
DJ01-112	13.59	115	50	10	3.33	322	10.98	71.9	2.77	0.073	387	9.58	16.51	2.15	8.33	2.28	0.84	1.92	0.31	1.67	0.34	1.17	0.13	1.47	0.24	2.11	3.54	2.18	0.34

Trace elements, ppm

Table 3. Trace elements (LA-ICP-MS) (continued)

Trace elements, ppm

Sample	Sc	V	Cr	Ni	Rb	Sr	Y	Zr	Nb	Cs	Ba	La	Ce	Pr	Nd	Sm	Eu	Gd	Tb	Dy	Ho	Er	Tm	Yb	Lu	Hf	Pb	Th	U
Osa Igneous Complex - Inner Osa Igneous Complex																													
DB02-107	50.83	314	404	114	0.86	103	20	49.4	3.00	0.042	28	2.71	7.15	1.10	5.92	2.08	0.79	2.98	0.54	3.52	0.82	2.27	0.33	2.06	0.34	1.34	0.70	0.21	0.08
DB02-110	48.80	331	245	101	1.08	129	21.50	57.6	3.60	0.036	17	3.12	8.50	1.41	7.56	2.45	0.87	3.08	0.54	3.98	0.84	2.38	0.34	2.35	0.32	1.55	1.08	0.25	0.09
DB02-119	46.50	340	55	85	4.09	231	21.04	85.2	6.62	0.027	54	6.38	16.34	2.33	12.56	4.00	1.21	4.35	0.59	4.43	0.85	2.07	0.30	1.80	0.28	2.37	0.60	0.45	0.13
DB02-120	52.47	355	202	94	0.68	112	21.30	52.7	3.64	0.047	20	3.03	8.21	1.37	6.41	2.50	1.10	3.11	0.50	3.86	0.85	2.26	0.34	2.63	0.34	1.59	0.99	0.23	0.11
DB02-132	51.66	357	284	93	0.86	116	23.30	62.8	3.82	0.014	34	3.33	9.35	1.48	8.16	2.65	1.03	3.62	0.59	4.23	0.85	2.48	0.37	2.47	0.37	1.89	0.74	0.27	0.09
DB02-135	50.03	341	306	109	0.94	143	22.05	57.6	3.54	0.031	40	3.13	8.54	1.42	7.15	2.66	0.96	2.99	0.57	4.00	0.93	2.28	0.32	2.49	0.38	1.59	0.91	0.25	0.09
DB02-160	54.32	350	248	73	2.04	101	23.61	47.0	1.96	0.031	118	2.01	5.57	0.90	5.33	1.96	0.77	2.92	0.53	4.18	0.90	2.79	0.37	2.66	0.41	1.33	0.82	0.14	0.05
DB02-165	49.40	302	439	128	1.02	97	16.91	36.5	2.60	0.037	15	2.06	5.67	0.89	4.79	1.64	0.61	2.16	0.38	2.85	0.63	1.75	0.26	1.92	0.25	1.11	1.11	0.16	0.06
DB02-201	39.68	233	363	68	1.75	195	15.39	26.2	1.05	0.026	20	1.08	2.99	0.53	3.37	1.31	0.48	1.68	0.33	2.70	0.61	1.73	0.23	1.59	0.26	0.77	0.81	0.09	0.04
DB02-203	52.77	459	30	38	1.94	47	30.90	76.4	4.68	0.030	6	5.01	12.47	1.87	10.89	3.57	1.24	4.57	0.76	5.46	1.19	3.18	0.47	3.41	0.47	2.27	1.29	0.31	0.10
DB02-204	48.64	348	128	76	4.62	165	21.52	53.9	3.23	0.093	47	3.54	8.82	1.40	6.73	2.62	0.93	3.21	0.53	3.73	0.84	2.30	0.32	2.19	0.35	1.65	0.93	0.23	0.08
DB02-227	29.34	112	452	94	6.91	201	11.84	22.7	0.93	0.434	76	1.20	3.18	0.48	2.83	0.99	0.47	1.59	0.31	2.14	0.40	1.21	0.16	1.30	0.18	0.69	0.74	0.12	0.07
DB02-230	49.88	352	236	98	0.98	107	23.73	61.6	3.86	0.021	16	3.08	9.10	1.40	7.48	2.45	1.04	3.38	0.65	4.18	0.90	2.75	0.35	2.60	0.37	1.80	0.99	0.24	0.09
DB02-232	20.65	213	466	bdl	21.61	297	17.68	264.4	24.47	0.063	401	36.18	73.89	8.41	34.55	6.20	1.81	4.60	0.62	3.83	0.63	1.58	0.24	1.38	0.27	5.64	4.7	3.36	1.05
DB02-246	46.29	410	34	22	1.98	123	28.02	57.6	2.81	0.024	58	3.57	8.80	1.29	7.63	2.67	0.98	3.58	0.63	4.69	0.99	3.25	0.50	3.21	0.52	1.77	1.00	0.32	0.10
DB02-266	50.74	406	49	72	4.51	130	22.59	55.7	4.05	0.105	22	3.35	8.86	1.39	7.26	2.17	0.97	3.00	0.54	3.70	0.81	2.46	0.36	2.30	0.37	1.47	0.91	0.26	0.09
DB05-107	49.84	314	492	147	1.10	130	18.78	44.2	3.14	bdl	16	2.62	7.03	1.11	5.84	1.95	0.70	2.55	0.41	3.10	0.70	1.97	0.32	2.12	0.30	1.25	0.32	0.21	0.07
DB05-108	50.13	330	493	127	3.08	128	19.68	44.8	3.04	bdl	24	2.68	7.12	0.99	5.66	1.70	0.76	2.27	0.42	3.08	0.63	1.98	0.27	2.01	0.29	1.24	0.22	0.20	0.05
DB06-054	49.49	305	475	128	1.40	135	15.73	35.4	2.41	bdl	23	2.12	5.69	0.88	5.10	1.73	0.60	2.31	0.40	2.84	0.64	1.82	0.28	1.88	0.31	1.15	0.49	0.16	0.09
DB06-058	51.30	357	243	107	0.64	202	24.08	59.3	3.44	bdl	115	2.95	8.37	1.28	7.42	2.69	0.95	3.23	0.64	4.23	0.89	2.67	0.36	2.65	0.40	1.71	0.58	0.25	0.09
DB06-061	44.56	321	21	8	0.85	53	53.16	147.8	10.4	bdl	18	8.4	22.5	3.42	17.8	5.51	2.13	7.70	1.35	9.42	1.94	5.91	0.91	5.82	0.86	4.22	0.50	0.72	0.22
DB06-065	52.32	311	326	106	1.41	123	21.97	39.1	1.47	bdl	742	1.60	4.45	0.85	4.64	1.88	0.77	2.57	0.50	3.65	0.83	2.33	0.30	2.60	0.36	1.31	0.31	0.10	0.04
DB06-066	38.73	399	341	87	6.50	291	33.09	162.8	16.53	bdl	384	13.90	34.37	4.89	23.42	6.30	1.95	6.89	1.07	6.40	1.11	3.23	0.46	2.86	0.41	4.33	0.82	1.22	0.40
DB06-070	52.78	356	272	108	0.92	230	21.47	44.2	3.12	bdl	31	2.93	6.94	1.16	6.00	1.87	0.81	2.75	0.52	3.56	0.74	2.16	0.32	2.24	0.34	1.45	0.35	0.20	0.08
DB06-075	50.09	414	41	43	4.48	141	34.23	70.2	2.96	bdl	69	2.97	8.25	1.42	7.74	3.07	1.04	4.57	0.82	5.87	1.27	3.74	0.60	3.82	0.56	2.02	0.34	0.22	0.08
DJ01-022	49.34	311	442	136	2.10	140	17.46	40.8	2.56	0.072	32	2.31	6.17	0.91	4.79	1.81	0.70	2.27	0.44	3.05	0.65	1.98	0.26	2.02	0.27	1.12	2.20	0.21	0.06
DJ01-115	48.24	330	323	103	2.58	157	21.74	58.1	3.42	0.095	116	2.93	8.28	1.38	7.16	2.58	0.90	3.21	0.58	3.87	0.83	2.36	0.38	2.22	0.35	1.65	2.79	0.25	0.12
GDM-90303	51.99	338	431	114	15.01	152	16.95	38.1	2.93	0.334	209	2.52	6.69	1.09	5.42	2.04	0.72	2.64	0.47	3.38	0.81	2.04	0.32	2.22	0.35	1.34	1.78	0.22	0.08
GDM-91044	48.16	304	472	132	3.04	250	19.26	42.7	2.51	0.213	80	2.33	6.10	0.96	5.01	1.61	0.59	2.31	0.40	3.12	0.59	2.01	0.24	1.68	0.28	1.13	2.08	0.17	0.09
Osa Igneous Complex - Güerra Unit																													
DB02-191	43.64	368	274	85	2.67	251	26.15	103.4	8.07	0.188	95	6.91	17.54	2.50	12.67	3.66	1.38	4.80	0.74	5.07	0.99	2.58	0.38	2.32	0.37	2.88	1.14	0.58	0.19
DB02-207	44.43	228	1482	bdl	6.86	69	19.43	33.7	0.75	0.207	10	0.82	2.51	0.53	2.88	1.46	0.59	2.32	0.46	3.29	0.74	2.18	0.32	2.25	0.28	0.87	0.84	0.06	0.05
Osa Igneous Complex - Ganado Unit																													
DB02-198b	38.96	249	426	bdl	5.72	244	23.83	68.5	5.66	0.131	144	4.14	9.55	1.42	7.73	2.65	1.06	3.51	0.69	4.28	0.91	2.69	0.36	2.59	0.43	1.75	3.14	0.31	0.00
DB02-260	40.98	323	245	bdl	1.34	171	39.34	127.0	5.24	0.000	25	5.92	16.25	2.39	12.82	4.14	1.42	5.53	0.92	6.71	1.42	4.27	0.68	4.18	0.65	3.32	0.64	0.42	0.13
DB02-261	48.69	460	113	49	1.44	144	49.97	145.9	5.11	0.031	21	6.15	17.78	2.96	16.53	5.09	1.73	7.14	1.25	8.88	1.88	5.39	0.79	5.31	0.79	4.06	28.84	0.35	0.13
DB02-262	54.83	639	206	88	1.16	118	32.86	145.6	13.35	0.041	19	3.08	8.97	1.49	8.69	3.03	1.19	4.61	0.81	6.22	1.22	3.61	0.57	4.11	0.58	4.03	1.02	0.22	0.10

Table 3. Trace elements (LA-ICP-MS) (continued)

Trace elements, ppm

Sample	Sc	V	Cr	Ni	Rb	Sr	Y	Zr	Nb	Cs	Ba	La	Ce	Pr	Nd	Sm	Eu	Gd	Tb	Dy	Ho	Er	Tm	Yb	Lu	Hf	Pb	Th	U
Osa Igneous Complex - Ganado Unit (continued)																													
DB05-149	58.97	392	762	153	1.80	95	20.85	47.6	3.31	bdl	62	2.68	7.03	1.11	6.09	1.80	0.88	2.88	0.51	3.47	0.75	2.17	0.32	2.35	0.36	1.44	0.28	0.21	0.08
DB05-155	49.20	412	145	65	1.19	150	42.12	112.7	4.06	bdl	32	5.04	14.40	2.26	12.77	4.14	1.52	6.10	1.00	7.25	1.47	4.69	0.64	4.25	0.64	3.26	0.71	0.32	0.09
DB05-156	52.33	515	72	48	1.68	177	52.05	155.9	5.75	bdl	34	6.58	19.38	2.96	17.55	5.45	1.77	7.96	1.22	9.22	1.94	5.49	0.83	5.41	0.82	4.18	0.64	0.46	0.16
DB05-157	27.16	183	74	46	2.72	196	83.74	257.0	11.29	bdl	45	12.39	40.66	6.58	32.73	9.10	2.47	12.62	2.26	14.57	2.92	8.70	1.21	8.55	1.36	6.39	0.26	1.25	0.21
DB05-158	53.86	333	1336	127	0.80	112	22.74	43.1	1.48	bdl	12	1.93	5.48	1.01	4.95	1.97	0.94	3.07	0.50	3.88	0.78	2.43	0.33	2.36	0.31	1.15	0.26	0.10	0.03
DB05-162	33.15	192	262	71	16.88	181	25.01	61.7	1.77	bdl	442	2.68	5.77	0.95	4.12	1.87	0.50	2.52	0.53	3.65	0.89	2.56	0.37	2.54	0.40	2.24	0.51	0.25	0.10
Osa Igneous Complex - Riyito Unit																													
DB02-196	46.76	350	235	78	0.66	29	26.34	45.3	0.55	0.050	5	1.07	3.93	0.90	4.92	2.20	0.90	3.40	0.55	4.36	1.02	2.85	0.46	2.88	0.43	1.60	1.66	0.05	0.08
DB02-197	49.71	330	280	68	4.63	128	28.00	49.7	0.65	0.590	51	1.13	4.52	0.81	5.51	2.02	0.86	3.74	0.66	4.77	1.08	2.88	0.48	3.14	0.39	1.51	1.47	0.05	0.00
DB02-198a	48.91	320	264	67	6.45	143	25.72	44.6	0.53	0.383	48	1.04	3.79	0.73	4.82	2.12	0.84	3.12	0.59	4.55	1.02	2.85	0.45	3.06	0.48	1.33	1.23	0.04	0.05
DB02-216	49.12	282	389	96	0.90	83	21.86	40.0	0.42	bdl	1	0.76	3.31	0.65	4.10	1.76	0.79	2.73	0.50	3.71	0.82	2.36	0.33	2.46	0.39	1.16	0.89	0.02	0.03
DB02-239	51.56	392	174	bdl	0.53	29	43.11	97.3	1.22	0.000	6	2.39	8.36	1.59	9.47	3.79	1.29	5.47	0.98	7.47	1.63	4.92	0.76	4.88	0.72	2.64	0.81	0.14	0.09
DB05-114	54.25	474	133	54	0.54	66	40.90	64.6	0.85	bdl	13	1.48	5.24	1.12	6.75	2.96	1.11	4.56	0.82	6.55	1.36	4.65	0.64	4.28	0.65	1.86	0.24	0.07	0.03
DB05-135	55.67	435	97	50	2.89	130	44.96	102.7	1.24	bdl	26	2.41	8.30	1.70	9.98	4.05	1.60	5.86	1.05	7.37	1.74	5.02	0.76	5.08	0.78	2.85	0.25	0.10	0.06
DB05-152	39.09	254	273	66	29.27	194	20.36	44.1	0.62	bdl	1181	1.16	3.63	0.68	4.23	1.71	0.71	2.73	0.45	3.37	0.69	1.96	0.31	2.11	0.28	1.26	0.51	0.08	0.04
DJ01-104	43.31	313	158	47	20.36	108	27.77	51.7	0.75	0.220	58	1.41	4.68	0.91	5.60	2.39	0.92	3.60	0.62	4.74	1.03	3.24	0.44	3.13	0.45	1.66	1.72	0.08	0.12
DJ01-106	44.04	304	288	66	7.53	107	23.64	38.0	0.50	0.150	11	1.02	3.53	0.68	4.18	1.86	0.75	2.87	0.56	3.93	0.84	2.64	0.45	2.72	0.42	1.18	1.08	0.04	0.03
DJ01-107	45.83	320	134	53	7.88	111	24.81	41.6	0.65	0.142	30	1.09	3.75	0.69	4.85	1.88	0.79	3.23	0.56	4.21	1.04	2.71	0.37	2.69	0.41	1.25	1.44	0.06	0.08
Osa Igneous Complex - Vaquedano Unit																													
DB02-242	40.18	276	1108	bdl	3.72	154	22.65	85.3	14.21	0.315	48	10.72	24.14	3.14	13.32	3.46	1.14	3.95	0.65	4.28	0.93	2.62	0.33	2.09	0.31	2.40	1.45	0.98	0.27
DB02-250	35.14	268	154	89	13.52	362	30.93	129.4	7.93	1.957	108	6.98	18.66	2.91	15.99	4.15	1.62	5.48	0.85	5.82	1.26	3.39	0.51	2.88	0.44	3.53	1.05	0.59	0.19
DB05-113	32.00	278	496	147	18.86	606	23.75	141.6	12.91	bdl	362	11.38	27.17	3.76	18.72	5.34	1.80	5.26	0.75	4.87	0.91	2.28	0.30	2.08	0.28	3.61	0.84	0.90	0.27
DB05-119	37.81	290	235	137	15.07	623	35.46	161.1	9.42	bdl	158	8.56	22.53	3.38	17.60	5.88	1.78	5.77	0.98	6.63	1.28	3.79	0.57	3.63	0.51	4.13	0.71	0.75	0.21
DB05-121	37.24	277	155	92	16.45	437	31.36	122.8	7.54	bdl	117	7.39	18.61	2.78	13.45	3.66	1.57	5.21	0.77	6.35	1.18	3.07	0.50	2.89	0.49	3.11	0.89	0.53	0.27
DB05-153	45.24	365	329	70	4.45	240	37.95	158.2	13.81	bdl	60	11.45	27.94	3.77	17.42	4.94	1.59	5.60	0.96	6.67	1.36	3.92	0.52	3.58	0.55	3.57	0.43	0.95	0.31
DB05-161	46.72	339	236	122	12.59	203	27.63	101.9	13.25	bdl	65	9.73	24.39	3.46	13.33	3.89	1.70	4.75	0.75	5.13	1.03	2.83	0.42	2.70	0.40	2.93	0.42	0.89	0.84
Azuero Accretionary Complex - Venado Unit																													
DB05-045	41.75	411	169	71	3.14	234	35.30	178.6	16.07	bdl	53	12.05	29.98	4.22	22.05	6.23	2.12	7.04	1.04	7.12	1.32	3.69	0.49	3.08	0.45	4.87	1.46	1.02	0.26
DB07-051	40.10	445	437	89	19.68	128	32.99	140.5	12.46	0.122	355	9.74	24.84	3.62	17.81	5.12	1.79	5.85	0.92	6.04	1.08	3.21	0.43	2.89	0.40	3.93	0.81	0.82	0.30
DB07-052	37.41	605	70	41	9.19	96	30.81	140.9	13.48	0.054	139	8.02	22.29	3.39	17.10	5.43	1.82	6.02	0.92	6.12	1.18	3.24	0.43	2.94	0.40	3.79	0.48	0.84	0.27
Azuero Accretionary Complex - Punta Blanca Group																													
DB05-041	43.78	390	235	93	2.33	242	34.08	165.5	14.10	bdl	58	11.30	27.38	4.02	20.20	5.58	1.85	6.55	1.08	6.70	1.27	3.36	0.46	2.64	0.44	4.58	1.18	1.01	0.27
DB06-011	39.12	422	60	66	6.36	244	33.89	171.2	15.62	0.090	105	13.02	33.32	4.80	23.40	6.20	2.16	6.90	1.04	6.84	1.25	3.42	0.44	3.06	0.46	4.87	0.98	1.15	0.48
DB07-029	37.87	376	199	95	1.64	259	28.57	137.7	13.04	0.035	54	10.30	26.81	3.93	18.32	5.20	1.71	5.75	0.86	5.53	1.20	2.91	0.37	2.71	0.33	3.61	0.75	0.79	0.33

Table 3. Trace elements (LA-ICP-MS) (continued)

Trace elements, ppm

Sample	Sc	V	Cr	Ni	Rb	Sr	Y	Zr	Nb	Cs	Ba	La	Ce	Pr	Nd	Sm	Eu	Gd	Tb	Dy	Ho	Er	Tm	Yb	Lu	Hf	Pb	Th	U
Azuero Accretionary Complex - Punta Blanca Group (continued)																													
DB07-033	37.34	357	199	85	0.37	261	26.51	127.5	12.08	bdl	31	9.87	25.37	3.57	18.23	4.93	1.86	4.94	0.79	5.36	1.12	2.80	0.41	2.40	0.34	3.62	0.72	0.81	0.26
DB07-038	39.30	356	353	99	2.91	323	27.09	130.5	12.48	0.050	103	9.92	25.36	3.50	17.39	4.86	1.68	5.58	0.81	5.43	0.98	2.67	0.37	2.43	0.33	3.52	1.43	0.73	0.28
DB07-040	37.86	409	86	66	1.82	317	30.37	152.4	14.31	0.436	121	11.78	29.97	4.20	21.49	5.77	2.05	6.32	0.95	6.20	1.21	3.04	0.40	2.53	0.41	4.00	0.81	0.98	0.56
Azuero Accretionary Complex - Hoya Group																													
DB05-006	22.05	213	1368	1087	7.00	163	14.25	91.1	11.67	0.220	57	9.41	22.15	2.88	14.13	3.39	1.13	3.04	0.50	2.88	0.51	1.34	0.17	1.20	0.15	2.46	0.90	0.74	0.26
DB05-008	32.66	353	184	92	9.14	357	29.12	192.4	26.00	0.077	95	19.81	47.10	6.05	28.30	6.61	2.18	7.03	1.04	6.18	1.22	3.03	0.42	2.64	0.34	5.01	1.18	1.84	0.52
DB05-012	34.90	379	101	54	10.60	426	41.73	337.0	41.60	0.098	183	32.75	71.23	9.35	43.63	10.09	2.93	9.63	1.48	9.15	1.56	3.75	0.57	2.87	0.45	8.17	1.75	3.16	0.84
DB06-005	30.28	382	52	57	24.60	468	38.71	291.3	40.76	0.378	231	30.62	70.32	9.26	39.03	9.23	2.99	9.48	1.25	8.03	1.49	3.77	0.49	3.13	0.43	7.14	1.62	2.90	0.80
DB06-006	31.99	388	351	54	15.13	466	38.84	316.0	43.65	0.131	364	32.57	73.42	9.84	43.65	9.48	3.17	9.24	1.41	7.91	1.45	3.77	0.52	3.27	0.45	7.13	2.16	2.93	0.88
DB06-007	20.69	334	131	48	30.19	695	48.96	436.3	59.73	0.874	334	54.09	124.68	15.33	67.22	14.38	4.78	13.23	1.85	10.49	1.88	4.65	0.59	3.83	0.51	9.50	5.96	4.83	1.50
DB06-038	20.56	177	1195	1231	2.01	170	13.10	82.9	10.57	0.066	34	8.18	19.29	2.51	11.92	2.94	0.97	2.99	0.40	2.79	0.51	1.32	0.15	1.09	0.15	2.04	0.53	0.72	0.21
DB06-049	35.29	330	367	136	1.61	331	25.73	166.4	21.95	0.013	44	16.64	39.90	5.33	23.47	6.07	2.05	6.14	0.87	5.35	1.01	2.65	0.33	2.18	0.29	4.24	1.12	1.48	0.46
DB06-076	30.65	348	56	51	19.53	424	33.22	254.2	35.30	0.030	185	26.60	62.39	7.88	36.01	8.37	2.62	8.12	1.14	7.23	1.24	3.18	0.47	2.71	0.36	6.31	2.07	2.47	0.70
DB06-077	34.61	342	260	102	9.39	347	27.07	182.2	24.19	0.049	86	19.64	45.66	6.13	28.37	6.23	2.12	6.54	0.95	5.73	1.11	2.74	0.38	2.34	0.33	4.64	1.57	1.74	0.50
DB06-078	34.37	337	184	105	14.90	345	27.93	177.9	24.91	0.025	183	18.66	42.68	5.77	26.17	6.20	2.19	6.38	0.95	5.70	1.08	2.95	0.39	2.48	0.32	4.82	1.58	1.63	0.51
DB06-081	34.78	349	212	132	9.36	604	29.22	201.0	29.37	0.149	178	20.75	48.38	6.21	27.94	6.83	2.19	6.96	1.02	5.94	1.10	2.92	0.37	2.19	0.34	4.95	1.33	1.81	0.37
DB06-083	33.58	350	136	87	17.83	352	32.39	225.7	31.78	0.192	316	23.03	52.65	6.73	31.68	7.75	2.33	7.79	1.00	6.79	1.19	3.02	0.40	2.43	0.33	5.63	1.54	2.12	0.62
DB06-084	35.49	344	275	101	16.59	537	25.51	165.2	23.04	0.149	224	16.87	39.47	5.20	24.11	6.02	1.87	6.22	0.86	5.47	1.01	2.61	0.34	2.11	0.30	4.32	1.06	1.51	0.46
DB06-085	31.84	362	37	56	13.04	417	34.73	249.4	35.31	0.041	180	25.83	59.81	7.70	34.68	7.97	2.60	8.31	1.17	7.32	1.33	3.45	0.48	2.85	0.41	6.01	1.29	2.39	0.69
DB06-086	32.42	251	758	335	11.01	346	22.06	151.5	22.10	0.093	120	16.20	38.38	5.02	22.40	5.58	1.73	5.37	0.74	4.73	0.91	2.14	0.31	1.83	0.24	3.86	0.94	1.46	0.45
DB06-087	34.36	342	235	106	21.10	1831	25.18	165.6	24.35	0.065	1008	18.09	43.98	5.55	25.09	6.00	1.93	6.20	0.92	5.34	0.96	2.55	0.31	2.36	0.32	4.37	1.50	1.64	0.51
DB06-088	35.79	340	253	112	2.12	405	27.26	172.0	22.21	0.021	96	17.24	40.30	5.47	24.62	6.05	2.09	6.02	0.86	5.50	1.06	2.74	0.34	2.32	0.32	4.52	1.50	1.58	0.40
DB06-089	15.36	115	1672	1711	1.19	14	8.19	52.8	6.90	0.106	3	5.35	12.37	1.69	7.82	1.76	0.60	2.19	0.28	1.65	0.30	0.74	0.10	0.69	0.09	1.25	0.38	0.50	0.15
DB06-100	33.41	329	249	94	17.69	2534	28.54	177.6	23.22	0.047	763	18.33	43.09	5.53	26.59	6.20	2.04	6.19	0.93	5.83	1.01	2.69	0.37	2.25	0.33	4.59	1.19	1.60	0.50
DB06-101	34.32	340	357	137	13.26	323	23.76	150.7	20.98	0.062	144	16.13	37.49	4.86	22.89	5.12	1.88	5.50	0.79	4.99	0.92	2.29	0.32	2.02	0.28	3.91	0.68	1.39	0.42
DB06-108	33.50	338	192	93	15.85	384	28.58	194.2	28.59	0.111	157	20.94	48.39	6.25	27.59	6.50	2.07	6.81	0.93	5.83	1.07	2.88	0.36	2.31	0.32	4.88	1.22	1.87	0.55
DB06-128	31.97	359	44	66	42.89	349	33.25	225.9	33.20	0.367	229	24.33	55.33	6.91	33.13	7.45	2.55	7.95	1.13	6.94	1.24	3.24	0.41	2.56	0.38	5.69	1.45	2.19	0.63
DB06-130	7.07	10	9	5	27.07	24	71.45	973.8	123.13	0.036	458	90.86	190.34	21.30	84.61	17.36	4.05	14.70	2.19	14.01	2.69	7.03	0.96	6.72	0.98	21.49	3.76	11.55	3.39
DB06-134	35.64	315	401	164	4.86	389	22.93	139.3	19.58	0.015	151	15.20	34.73	4.61	21.44	4.93	1.76	5.41	0.77	4.63	0.87	2.27	0.28	1.86	0.27	3.86	1.03	1.39	0.40
DB07-001	25.96	332	144	66	15.85	540	36.79	323.5	48.43	0.085	265	36.11	80.93	10.21	46.33	9.95	3.32	9.53	1.32	7.95	1.42	3.49	0.47	2.91	0.40	8.06	2.02	3.44	0.79
DB07-004	35.99	355	279	100	11.06	551	26.89	172.2	22.32	0.038	233	18.17	43.67	5.62	25.73	6.07	2.11	6.31	0.85	5.48	1.04	2.66	0.35	2.19	0.35	4.39	0.96	1.65	0.55
DB07-006	26.58	343	53	49	20.93	445	34.10	288.0	41.59	0.273	316	30.89	69.65	8.87	39.50	9.04	2.95	8.57	1.16	7.43	1.26	3.26	0.46	2.61	0.37	7.08	1.60	2.87	0.86
DB07-007	33.70	479	107	115	26.65	565	14.76	94.1	13.71	0.626	133	9.56	22.22	2.92	14.35	3.48	1.43	3.74	0.54	3.24	0.58	1.44	0.19	1.16	0.15	2.46	1.00	0.73	0.21
DB07-008	34.49	228	1753	525	18.88	251	21.00	143.7	18.89	0.850	83	14.45	33.99	4.29	20.68	4.96	1.45	4.87	0.72	4.25	0.83	1.95	0.27	1.61	0.24	3.72	0.75	1.35	0.41
DB07-009	30.31	338	102	71	1.82	374	27.14	208.0	30.26	0.033	120	19.91	48.41	6.38	28.38	6.82	2.14	7.09	1.02	6.11	1.05	2.79	0.39	2.40	0.35	5.41	1.11	2.02	0.62
DB07-011	32.08	356	bdl	72	6.13	424	35.59	268.5	37.74	0.027	191	28.48	65.43	8.49	37.21	9.19	2.73	8.34	1.22	7.37	1.37	3.48	0.47	2.97	0.42	6.70	1.42	2.60	0.77
DB07-012	34.07	359	229	120	12.56	389	30.06	203.2	30.03	0.043	144	22.32	51.07	6.81	31.70	7.30	2.25	6.95	1.00	6.26	1.11	3.03	0.40	2.50	0.34	5.23	1.59	2.01	0.56
DB07-013	34.68	344	380	132	8.38	346	27.52	183.0	26.33	0.042	115	20.62	47.87	6.41	28.63	6.66	2.20	6.42	0.91	5.75	1.00	2.70	0.37	2.40	0.34	4.77	0.98	1.75	0.54

Table 3. Trace elements (LA-ICP-MS) (continued)

Trace elements, ppm

Sample	Sc	V	Cr	Ni	Rb	Sr	Y	Zr	Nb	Cs	Ba	La	Ce	Pr	Nd	Sm	Eu	Gd	Tb	Dy	Ho	Er	Tm	Yb	Lu	Hf	Pb	Th	U
Azuero Accretionary Complex - Hoya Group (continued)																													
DB07-014	31.16	288	682	434	10.31	215	24.31	136.9	18.92	0.226	123	15.16	35.09	4.81	20.44	5.16	1.59	5.14	0.70	4.44	0.88	2.08	0.27	1.88	0.25	3.56	0.92	1.28	0.45
DB07-016	32.29	325	227	90	3.13	430	27.22	187.4	26.46	0.037	167	19.81	44.86	5.80	26.38	6.72	2.25	7.09	0.94	5.92	1.08	2.87	0.34	2.21	0.31	4.64	1.31	1.77	0.51
DB07-017	29.63	376	75	48	1.61	474	37.30	301.9	41.71	0.037	145	32.27	74.51	9.46	42.43	9.81	3.09	9.72	1.36	8.07	1.51	3.85	0.53	3.10	0.45	7.40	1.57	2.99	0.83
DB07-021	17.93	163	153	10	25.54	785	55.25	452.3	68.98	0.113	443	70.31	156.26	19.49	84.31	17.41	5.80	15.87	2.05	12.09	2.23	5.04	0.67	3.94	0.56	10.55	4.01	5.70	1.69
DB07-024	29.01	192	1568	728	7.08	197	16.94	114.1	15.54	0.215	71	11.49	27.54	3.72	16.22	3.88	1.15	3.62	0.54	3.29	0.60	1.61	0.18	1.21	0.17	2.94	0.67	1.05	0.32
DB07-027	21.70	277	63	9	37.84	463	45.34	410.2	59.98	0.165	384	46.99	106.46	13.30	58.51	13.02	3.82	12.21	1.60	10.24	1.90	4.49	0.66	3.99	0.53	10.03	2.16	4.65	1.40
DB07-028	32.91	325	260	91	15.11	530	25.84	165.1	23.12	0.275	535	18.60	41.95	5.57	24.26	6.33	2.06	5.98	0.86	5.50	1.04	2.59	0.33	2.20	0.30	4.21	1.28	1.68	0.47
DB07-032	31.27	358	65	51	17.12	425	36.18	267.9	37.69	0.121	180	28.54	65.84	8.31	38.70	8.84	2.86	8.56	1.28	7.67	1.34	3.44	0.41	2.80	0.42	6.39	1.14	2.63	0.73
Azuero Accretionary Complex - Quebro Group																													
DB05-003	39.68	404	536	228	8.54	244	36.93	209.5	19.63	bdl	82	16.88	41.73	5.78	27.00	7.97	2.42	7.52	1.22	7.63	1.31	3.67	0.52	3.35	0.44	5.30	1.85	1.34	0.59
DB06-036	37.14	424	288	98	6.30	270	40.22	229.3	22.02	0.032	84	17.42	44.03	6.04	28.75	8.07	2.54	9.05	1.25	8.20	1.57	3.98	0.56	3.44	0.49	5.92	1.98	1.53	0.47
DB06-037	35.57	342	690	356	6.84	211	30.23	165.0	15.31	0.078	69	12.53	32.13	4.48	21.57	6.04	1.88	6.30	1.02	5.82	1.14	3.04	0.42	2.73	0.37	4.08	1.50	1.11	0.33
DB06-040	38.17	415	237	109	6.42	302	34.53	192.7	18.59	0.070	262	14.69	37.01	5.10	25.13	6.96	2.21	7.40	1.13	7.12	1.25	3.34	0.44	3.15	0.40	4.68	0.90	1.25	0.42
DB06-046	38.14	472	93	69	10.42	312	46.62	286.1	27.76	0.043	357	22.75	54.89	7.55	36.43	9.58	3.04	10.17	1.44	9.77	1.76	4.94	0.63	4.08	0.55	7.24	1.59	1.96	0.61
Azuero Mélange																													
DB06-096	34.24	318	289	76	15.74	301	32.19	224.8	38.25	0.133	370	28.72	60.12	7.33	30.39	6.32	2.13	6.58	0.96	6.22	1.11	3.20	0.48	2.93	0.44	5.08	2.14	3.56	1.27

Table 4. Microbrobe Analyses from the Cpxs of the Golfito Complex (Costa Rica)

Samples			SiO_2	Al_2O_3	TiO_2	Fe_2O_3	MnO	MgO	Cr_2O_3	CaO	Na_2O	Total
DB02-042	Cpx1		52.64	2.16	0.24	6.46	0.19	17.43	0.27	19.34	0.18	98.90
		±2σ (n=3)	1.06	1.24	0.05	0.40	0.15	0.46	0.28	0.45	0.06	0.27
DB02-042	Cpx2		52.64	1.86	0.26	6.93	0.21	17.48	0.14	19.23	0.18	98.94
		±2σ (n=3)	0.44	0.26	0.06	0.24	0.06	0.22	0.05	0.40	0.05	0.53
DB02-101	Cpx1		53.11	1.72	0.22	6.19	0.20	17.56	0.26	19.67	0.19	99.11
		±2σ (n=3)	0.25	0.18	0.01	0.69	0.04	0.37	0.16	1.01	0.02	0.77
DB02-101	Cpx2		55.93	1.79	0.20	4.06	0.17	19.50	0.16	17.97	0.21	100*
		±2σ (n=3)	0.22	0.29	0.02	0.37	0.02	0.63	0.07	0.48	0.01	0.00
DB02-175	Cpx2		52.14	2.89	0.54	9.33	0.22	15.57	0.08	19.43	0.24	100.44
		±2σ (n=3)	0.99	0.73	0.19	0.86	0.02	0.39	0.01	0.77	0.02	0.27
DB02-175	Cpx3		51.45	3.15	0.62	10.82	0.25	15.48	0.04	18.04	0.25	100.10
		±2σ (n=3)	0.87	0.60	0.12	1.61	0.06	1.35	0.06	2.88	0.07	0.37
DB02-175	Cpx4		50.52	3.19	0.58	10.76	0.28	15.40	0.01	16.93	0.26	97.93
		±2σ (n=2)	0.14	0.12	0.01	0.06	0.04	0.28	0.03	0.52	0.01	1.20
DB02-175	Cpx5		51.28	2.98	0.59	10.67	0.28	15.60	0.04	17.68	0.28	99.39
		±2σ (n=2)	0.70	0.25	0.00	3.24	0.10	2.03	0.03	5.55	0.14	12.05
DB02-175	Cpx6		50.69	3.62	0.61	10.88	0.29	15.06	0.04	17.92	0.31	99.42
		±2σ (n=2)	1.51	0.95	0.16	1.69	0.01	1.32	0.04	0.03	0.08	5.80
DB02-175	Cpx7		51.08	3.40	0.62	10.24	0.22	15.10	0.05	18.77	0.29	99.76
		±2σ (n=3)	0.81	0.38	0.12	2.50	0.07	0.72	0.02	3.74	0.03	0.71
DB02-175	Cpx9		51.07	3.25	0.63	10.32	0.22	15.23	0.04	18.72	0.29	99.78
		±2σ (n=2)	0.85	0.77	0.20	1.83	0.03	0.50	0.05	1.47	0.10	0.06
DB02-175	Cpx10		51.51	3.05	0.58	10.35	0.26	15.44	0.04	18.57	0.26	100.05
		±2σ (n=3)	0.54	0.25	0.12	0.41	0.03	0.75	0.06	1.30	0.03	0.35
DB02-175	Cpx11		52.16	2.82	0.50	10.56	0.27	16.05	0.05	17.93	0.26	100.61
		±2σ (n=3)	1.56	1.33	0.19	1.78	0.05	2.14	0.05	3.62	0.06	0.48
DB02-175	Cpx12		51.67	3.06	0.59	10.80	0.27	15.60	0.04	17.85	0.27	100.15
		±2σ (n=4)	1.76	1.49	0.34	1.12	0.09	2.54	0.03	3.48	0.09	0.46
DB02-175	Cpx13		51.59	3.10	0.61	10.99	0.27	15.12	0.05	18.27	0.27	100.27
		±2σ (n=3)	1.81	1.06	0.25	1.66	0.08	1.40	0.14	1.66	0.02	0.53
DB02-175	Cpx14		51.49	2.88	0.58	11.17	0.27	15.23	0.01	18.06	0.28	99.98
		±2σ (n=3)	0.80	0.87	0.23	1.16	0.03	1.03	0.03	1.18	0.08	0.55
DB02-175	Cpx15		51.38	3.28	0.59	10.60	0.26	15.78	0.07	17.64	0.27	99.87
		±2σ (n=3)	1.31	0.88	0.21	2.00	0.09	2.44	0.03	4.32	0.10	0.49
DB02-175	Cpx16		51.89	2.88	0.53	10.73	0.27	16.35	0.06	16.64	0.24	99.59
		±2σ (n=2)	0.03	0.18	0.00	0.36	0.00	0.08	0.03	0.06	0.03	0.13
DB02-175	Cpx17		50.76	3.42	0.74	11.02	0.26	14.92	0.02	18.32	0.27	99.75
		±2σ (n=3)	1.35	1.17	0.43	1.28	0.06	1.13	0.01	0.89	0.04	0.35
DB02-175	Cpx18		51.16	3.02	0.58	10.58	0.26	15.02	0.03	18.32	0.27	99.24
		±2σ (n=3)	1.74	1.49	0.26	0.43	0.07	2.19	0.04	2.08	0.07	0.67
DB02-175	Cpx19		50.63	3.50	0.60	10.69	0.26	15.18	0.02	17.58	0.25	98.71
		±2σ (n=3)	0.30	0.69	0.06	0.07	0.04	0.69	0.02	0.61	0.02	0.49
DB02-175	Cpx20		51.60	3.05	0.60	11.32	0.31	16.36	0.06	16.46	0.24	99.99
		±2σ (n=2)	0.29	0.36	0.07	1.40	0.07	0.12	0.06	1.59	0.02	0.18
DB02-175	Cpx21		50.92	3.15	0.65	10.38	0.25	15.66	0.05	17.73	0.24	99.03
		±2σ (n=3)	0.60	0.32	0.07	1.00	0.08	1.19	0.05	2.40	0.03	0.08

Table 5. Trace Elements Data from the Clinopyroxenes of the Golfito Complex (Costa Rica)

Samples	Cpx	Sc	V	Cr	Co	Ni	Cu	Zn	Ga	Rb	Sr	Y	Zr	Nb	Ba	La	Ce	Pr	Nd	Sm	Eu	Gd	Tb	Dy	Ho	Er	Tm	Yb	Lu	Hf	Pb	Th	U
DB02-042	Cpx1	112	274	801	47	142	1.44	30.39	2.99	0.05	4.87	8.95	2.42	0.02	0.15	0.12	0.48	0.12	0.90	0.59	0.17	1.01	0.20	1.58	0.37	1.02	0.15	1.08	0.15	0.12	0.09	bdl	bdl
	±2σ (n=2)	2	13	84	4	5	0.70	1.31	0.55	0.07	0.41	0.49	0.20	0.02	0.11	0.05	0.07	0.04	0.16	0.21	0.04	0.05	0.03	0.20	0.00	0.04	0.03	0.06	0.00	0.03	0.04		
DB02-042	Cpx2	100	286	845	48	152	0.86	32.03	3.08	bdl	4.99	8.07	2.47	0.13	0.23	0.12	0.52	0.12	0.90	0.49	0.16	0.87	0.18	1.39	0.34	0.99	0.15	1.02	0.15	0.14	0.08	bdl	bdl
	±2σ (n=3)	16	32	45	3	7	0.01	3.58	0.53		0.37	2.02	0.70	0.20	0.31	0.08	0.25	0.07	0.32	0.28	0.03	0.24	0.02	0.31	0.12	0.33	0.05	0.22	0.04	0.09	0.08		
DB02-101	Cpx1	97	240	1553	46	154	5.06	29.92	3.77	0.12	10.22	8.00	2.84	0.05	2.52	0.50	1.19	0.22	1.50	0.52	0.16	1.01	0.19	1.48	0.31	0.91	0.15	0.93	0.12	0.12	0.15	bdl	bdl
	±2σ (n=2)	3	9	397	3	2		7.20	1.69	0.21	6.05	1.30	1.57	0.09	4.53	0.54	1.30	0.15	0.36	0.20	0.07	0.21	0.04	0.14	0.04	0.22	0.02	0.30	0.06	0.07	0.09		
DB02-101	Cpx2	96	253	1316	45	149	6.47	29.99	3.43	0.45	8.73	9.43	3.92	0.13	2.61	0.41	1.38	0.26	1.61	0.73	0.22	1.01	0.21	1.84	0.37	1.08	0.15	1.07	0.19	0.17	0.22	bdl	bdl
	±2σ (n=2)	4	0	1060	0	24	8.04	3.38	1.22	0.56	3.50	4.08	3.38	n=1	3.84	0.41	1.19	0.15	1.30	0.24	0.03	0.32	0.11	0.79	0.19	0.39	0.09	0.54	0.04	0.09	0.07		
DB02-175	Cpx2 n=1	148	434	436	53	104	3.25	40.11	5.09	0.02	10.66	13.56	8.67	0.01	0.36	0.41	1.47	0.36	2.42	1.27	0.42	1.61	0.34	2.47	0.56	1.51	0.20	1.44	0.16	0.46	0.04	0.01	bdl
DB02-175	Cpx5 n=1	159	509	300	61	108	3.35	47.10	6.55	0.30	9.25	16.71	13.52	0.03	1.05	0.42	1.79	0.44	3.30	1.50	0.56	2.19	0.44	3.23	0.66	1.98	0.28	1.65	0.24	0.66	0.05	bdl	bdl
DB02-175	Cpx6 n=1	151	494	385	62	115	4.14	53.94	6.09	0.67	9.13	15.83	12.42	0.05	1.41	0.35	1.55	0.36	2.38	1.23	0.52	2.13	0.38	2.97	0.66	1.99	0.28	1.81	0.28	0.65	bdl	0.01	0.01
DB02-175	Cpx10 n=1	186	528	269	64	121	3.71	58.80	7.53	0.05	9.30	22.57	16.97	0.06	1.37	0.49	2.07	0.47	3.19	1.76	0.64	3.12	0.54	4.15	0.98	2.76	0.40	2.57	0.35	0.90	0.06	0.02	bdl
DB02-175	Cpx12 n=1	154	459	306	67	122	11.88	58.11	6.48	0.93	12.96	17.68	17.56	0.22	5.77	0.59	1.99	0.42	2.82	1.13	0.44	2.19	0.46	3.08	0.64	2.12	0.26	2.06	0.30	0.61	0.06	0.03	0.01
DB02-175	Cpx13 n=1	153	516	199	63	99	5.53	59.19	9.97	1.10	25.41	19.21	18.68	0.29	35.33	1.01	3.15	0.59	3.97	1.73	0.54	2.61	0.47	3.40	0.87	2.22	0.34	2.45	0.37	0.83	0.07	0.06	0.03
DB02-175	Cpx14	160	527	169	56	92	7.40	50.23	6.92	0.46	11.08	18.73	17.37	0.03	2.64	0.49	2.18	0.47	3.53	1.76	0.57	2.72	0.45	3.41	0.70	2.17	0.32	1.95	0.32	0.84	0.04	0.02	0.01
	±2σ (n=2)	10	10	67	6	10	6.80	6.84	0.56	0.82	4.21	0.57	10.58	0.03	4.38	0.22	0.29	0.05	0.71	0.13	0.16	0.36	0.05	0.20	0.02	0.13	0.03	0.11	0.02	0.28	0.02	0.02	0.00

Table 6. Isotope analyses (test run)

Sample	Unit	$^{87}Sr/^{86}Sr_m$	2σ	$^{143}Nd/^{144}Nd_m$	2σ	$^{206}Pb/^{204}Pb_m$	2σ	$^{207}Pb/^{204}Pb_m$	2σ	$^{208}Pb/^{204}Pb_m$	2σ
DB02-132 L	Inner Osa Igneous Complex (plateau-like)	0.703404	0.000009	0.513000	0.000017	18.922	0.004	15.552	0.004	38.562	0.009
DB02-132 R	Inner Osa Igneous Complex (plateau-like)	0.703196	0.000009	0.513073	0.000035	19.990	0.013	15.613	0.011	39.076	0.027
DB02-160 L	Inner Osa Igneous Complex (MORB-like)	0.703935	0.000007	0.513045	0.000012	18.765	0.021	15.542	0.017	38.376	0.043
DB02-160 R	Inner Osa Igneous Complex (MORB-like)	0.703352	0.000007	0.513128	0.000009	20.128	0.031	15.618	0.026	39.339	0.063
DB02-165 L	Inner Osa Igneous Complex (plateau-like)	0.703334	0.000007	0.513001	0.000073	18.730	0.003	15.573	0.002	38.444	0.005
DB02-165 R	Inner Osa Igneous Complex (plateau-like)					19.049	0.004	15.614	0.004	38.857	0.009
DB02-197 L	Riyito Unit	0.703521	0.000008	0.513165	0.000018	18.419	0.004	15.540	0.003	38.024	0.008
DB02-197 R	Riyito Unit	0.703716	0.000007	0.513163	0.000008	18.556	0.014	15.546	0.011	38.108	0.028
DB02-216 L	Riyito Unit	0.702669	0.000009	0.513188	0.000013	18.240	0.005	15.482	0.004	37.741	0.010
DB02-216 R	Riyito Unit	0.702574	0.000010			18.322	0.005	15.494	0.004	37.815	0.010
DB02-239 L	Riyito Unit	0.704083	0.000011	0.513069	0.000015	18.514	0.010	15.523	0.009	38.003	0.022
DB02-239 R	Riyito Unit	0.704133	0.000007			18.499	0.008	15.483	0.007	38.010	0.017

L=Leachate, R=Residue

Table 7. DB02-216 plagioclases and melt inclusions, XRF analyses

Plagioclase xenocryst 1 - profile 1

Label	Profile (µm)	Material	SiO2	TiO2	Al2O3	FeO	MnO	MgO	CaO	Na2O	K2O	BaO	Total	An	Ab	Or
DB02-216_pl1_1_1	0	Plagioclase	45.66	0.07	33.85	0.47	0.07	0.20	17.86	1.32	0.00	0.19	99.69	88.23	11.77	0.00
DB02-216_pl1_1_2	20	Plagioclase	45.65	0.04	33.58	0.34	0.02	0.18	17.84	1.24	0.00	0.17	99.06	88.85	11.13	0.02
DB02-216_pl1_1_3	40	Plagioclase	45.60	0.03	33.66	0.39	0.05	0.20	17.87	1.25	0.00	0.08	99.13	88.74	11.24	0.02
DB02-216_pl1_1_4	60	Plagioclase	45.63	0.06	33.53	0.36	0.11	0.17	17.81	1.31	0.01	0.00	98.99	88.20	11.77	0.04
DB02-216_pl1_1_5	80	Plagioclase	45.32	0.03	33.65	0.39	0.03	0.17	17.66	1.25	0.00	0.01	98.51	88.64	11.36	0.01
DB02-216_pl1_1_6	100	Plagioclase	45.52	0.00	33.74	0.47	0.04	0.20	17.90	1.20	0.01	0.08	99.16	89.10	10.83	0.06
DB02-216_pl1_1_7	120	Plagioclase	45.91	0.03	33.88	0.35	0.10	0.19	17.88	1.16	0.00	0.00	99.50	89.51	10.48	0.01
DB02-216_pl1_1_8	140	Plagioclase	45.74	0.02	33.63	0.52	0.00	0.19	17.79	1.24	0.00	0.08	99.20	88.82	11.18	0.00
DB02-216_pl1_1_9	160	Plagioclase	45.92	0.01	33.72	0.37	0.02	0.20	17.65	1.36	0.00	0.00	99.25	87.78	12.22	0.00
DB02-216_pl1_1_10	180	Inclusion	46.21	0.00	32.12	0.96	0.03	1.17	16.83	1.50	0.01	0.03	98.86			
DB02-216_pl1_1_11	200	Plagioclase	46.06	0.01	33.60	0.45	0.01	0.21	17.59	1.40	0.00	0.06	99.39	87.41	12.57	0.02
DB02-216_pl1_1_12	220	Plagioclase	46.17	0.03	33.67	0.33	0.00	0.21	17.78	1.33	0.01	0.06	99.59	88.04	11.90	0.07
DB02-216_pl1_1_13	240	Plagioclase	45.89	0.03	33.60	0.40	0.06	0.19	17.76	1.29	0.00	0.05	99.27	88.33	11.65	0.01
DB02-216_pl1_1_14	260	Plagioclase	45.84	0.07	33.57	0.42	0.02	0.22	17.81	1.31	0.01	0.12	99.39	88.22	11.73	0.05
DB02-216_pl1_1_15	280	Plagioclase	46.03	0.02	33.49	0.40	0.02	0.17	17.72	1.32	0.01	0.05	99.24	88.04	11.88	0.08
DB02-216_pl1_1_16	300	Plagioclase	46.00	0.00	33.45	0.35	0.05	0.20	17.76	1.26	0.02	0.00	99.09	88.55	11.36	0.09
DB02-216_pl1_1_17	320	Plagioclase	46.34	0.07	33.07	0.54	0.00	0.22	17.52	1.40	0.00	0.00	99.16	87.37	12.63	0.00
DB02-216_pl1_1_18	340	Plagioclase	46.05	0.02	33.72	0.63	0.04	0.22	17.69	1.45	0.02	0.22	100.05	86.98	12.90	0.11
DB02-216_pl1_1_19	360	Rim	44.01	0.52	4.97	18.37	0.31	14.74	8.82	0.17	0.02	0.13	92.07	96.35	3.40	0.25
DB02-216_pl1_1_20	380	Inclusion	50.91	0.77	8.37	12.92	0.29	11.72	11.28	1.84	0.05	0.00	98.15			
DB02-216_pl1_1_21	400	Inclusion	48.23	1.06	5.04	15.25	0.31	15.81	11.74	0.44	0.03	0.00	97.92			
DB02-216_pl1_1_22	420	Inclusion	49.41	0.83	3.09	16.62	0.39	13.97	13.83	0.28	0.00	0.07	98.50			
DB02-216_pl1_1_23	440	Inclusion	46.91	0.82	4.83	16.81	0.32	14.48	11.03	0.23	0.02	0.17	95.64			
DB02-216_pl1_1_24	460	Inclusion	47.97	1.12	4.43	16.33	0.34	14.58	12.57	0.37	0.04	0.01	97.77			
DB02-216_pl1_1_25	480	Inclusion	45.61	0.01	33.43	0.45	0.00	0.20	17.68	1.38	0.00	0.13	98.88			
DB02-216_pl1_1_26	500	Inclusion	45.10	0.01	33.91	0.49	0.02	0.19	18.02	1.09	0.01	0.10	98.94			
DB02-216_pl1_1_27	520	Inclusion	45.09	0.00	34.00	0.45	0.06	0.15	18.08	1.08	0.00	0.04	98.96			
DB02-216_pl1_1_28	540	Rim	38.67	0.03	10.84	20.56	0.10	15.70	2.41	0.03	0.04	0.00	88.38	96.29	1.97	1.74
DB02-216_pl1_1_29	560	Plagioclase	46.12	0.04	33.41	0.40	0.07	0.23	17.72	1.32	0.00	0.00	99.30	88.07	11.91	0.02
DB02-216_pl1_1_30	580	Plagioclase	46.06	0.00	33.70	0.44	0.00	0.18	17.52	1.47	0.00	0.09	99.47	86.82	13.16	0.02
DB02-216_pl1_1_31	600	Plagioclase	46.11	0.03	33.45	0.47	0.00	0.19	17.49	1.37	0.01	0.23	99.35	87.49	12.44	0.07
DB02-216_pl1_1_32	620	Plagioclase	45.55	0.02	33.88	0.40	0.00	0.16	18.01	1.21	0.01	0.09	99.32	89.12	10.80	0.07
DB02-216_pl1_1_33	640	Plagioclase	45.32	0.05	33.84	0.42	0.00	0.16	18.03	1.10	0.00	0.00	98.91	90.09	9.91	0.00
DB02-216_pl1_1_34	660	Plagioclase	45.77	0.05	33.50	0.40	0.05	0.18	17.60	1.26	0.00	0.00	98.82	88.54	11.46	0.00
DB02-216_pl1_1_35	680	Plagioclase	45.70	0.03	33.79	0.45	0.11	0.20	17.69	1.41	0.00	0.00	99.39	87.41	12.59	0.00
DB02-216_pl1_1_36	700	Plagioclase	46.14	0.01	33.37	0.46	0.05	0.22	17.32	1.41	0.01	0.00	98.98	87.12	12.80	0.08
DB02-216_pl1_1_37	720	Plagioclase	47.49	0.05	32.53	0.46	0.02	0.29	16.61	2.08	0.01	0.18	99.72	81.48	18.45	0.07
DB02-216_pl1_1_38	740	Plagioclase	47.59	0.04	32.22	0.52	0.04	0.25	16.30	2.14	0.00	0.00	99.10	80.81	19.16	0.03
DB02-216_pl1_1_39	760	Plagioclase	48.80	0.03	30.97	0.59	0.00	0.26	15.34	2.66	0.00	0.13	98.79	76.08	23.89	0.03
DB02-216_pl1_1_40	780	Plagioclase	49.84	0.04	30.32	0.58	0.00	0.34	14.70	2.92	0.00	0.00	98.75	73.51	26.46	0.02

Table 7. DB02-216 plagioclases and melt inclusions, XRF analyses (continued)

Label	Profile (µm)	Material	SiO2	TiO2	Al2O3	FeO	MnO	MgO	CaO	Na2O	K2O	BaO	Total	An	Ab	Or
		Plagioclase xenocryst 1 - profile 4															
DB02-216_pl1_4_1	4	Plagioclase	45.91	0.04	33.57	0.44	0.02	0.18	17.79	1.33	0.00	0.01	99.29	88.08	11.92	0.00
DB02-216_pl1_4_2	8	Plagioclase	46.11	0.04	33.54	0.39	0.00	0.23	17.75	1.34	0.00	0.03	99.42	87.98	12.02	0.00
DB02-216_pl1_4_3	12	Plagioclase	46.34	0.00	33.58	0.36	0.00	0.19	17.66	1.30	0.00	0.03	99.45	88.23	11.77	0.00
DB02-216_pl1_4_4	16	Plagioclase	46.09	0.00	33.57	0.46	0.11	0.22	17.80	1.30	0.00	0.00	99.56	88.31	11.69	0.00
DB02-216_pl1_4_5	20	Plagioclase	46.32	0.00	33.45	0.43	0.00	0.18	17.67	1.36	0.01	0.29	99.71	87.69	12.25	0.05
DB02-216_pl1_4_6	24	Plagioclase	46.11	0.05	33.67	0.47	0.01	0.21	17.67	1.30	0.00	0.09	99.58	88.25	11.75	0.00
DB02-216_pl1_4_7	28	Plagioclase	46.31	0.01	33.63	0.50	0.03	0.21	17.80	1.36	0.00	0.00	99.84	87.85	12.15	0.00
DB02-216_pl1_4_8	32	Plagioclase	46.25	0.06	33.58	0.53	0.02	0.19	17.77	1.41	0.01	0.00	99.82	87.42	12.54	0.04
DB02-216_pl1_4_9	36	Plagioclase	45.95	0.04	33.36	0.44	0.07	0.18	17.89	1.26	0.01	0.00	99.20	88.68	11.26	0.06
DB02-216_pl1_4_10	40	Plagioclase	46.22	0.03	33.71	0.41	0.00	0.23	17.80	1.30	0.01	0.00	99.70	88.34	11.66	0.00
DB02-216_pl1_4_11	44	Plagioclase	45.97	0.00	33.90	0.42	0.03	0.17	17.81	1.29	0.01	0.00	99.61	88.39	11.57	0.04
DB02-216_pl1_4_12	48	Plagioclase	46.35	0.03	34.01	0.50	0.00	0.23	17.85	1.31	0.00	0.00	100.28	88.31	11.69	0.00
DB02-216_pl1_4_13	52	Plagioclase	46.21	0.00	34.01	0.35	0.00	0.21	17.94	1.24	0.00	0.00	99.97	88.86	11.12	0.03
DB02-216_pl1_4_14	56	Plagioclase	46.18	0.10	33.60	0.46	0.04	0.19	17.93	1.30	0.01	0.00	99.80	88.35	11.59	0.06
DB02-216_pl1_4_15	60	Plagioclase	46.30	0.03	33.98	0.59	0.01	0.21	17.87	1.29	0.00	0.12	100.39	88.47	11.53	0.01
DB02-216_pl1_4_16	64	Plagioclase	46.46	0.02	33.65	0.46	0.03	0.25	17.82	1.27	0.00	0.12	100.09	88.57	11.42	0.01
DB02-216_pl1_4_17	68	Plagioclase	46.24	0.01	33.92	0.67	0.03	0.20	18.02	1.28	0.00	0.00	100.38	88.62	11.35	0.03
DB02-216_pl1_4_18	72	Rim	46.16	0.07	33.65	0.58	0.00	0.20	17.77	1.33	0.00	0.03	99.80	88.09	11.91	0.00
DB02-216_pl1_4_19	76	Rim	49.13	0.00	31.31	0.69	0.00	0.35	15.70	2.62	0.00	0.00	99.81	76.78	23.20	0.02
DB02-216_pl1_4_20	80	Rim	52.61	0.04	28.88	0.86	0.00	0.50	13.29	4.05	0.01	0.17	100.41	64.40	35.51	0.08
DB02-216_pl1_4_21	84	Inclusion	50.85	0.75	13.48	11.14	0.26	9.84	11.99	2.10	0.03	0.04	100.48			
DB02-216_pl1_4_22	88	Inclusion	48.90	1.04	5.25	15.15	0.35	14.79	12.43	0.50	0.02	0.00	98.43			
DB02-216_pl1_4_23	92	Inclusion	49.61	1.07	5.37	15.54	0.29	15.24	12.02	0.53	0.02	0.00	99.69			
DB02-216_pl1_4_24	96	Inclusion	47.39	1.58	6.95	16.49	0.30	13.21	11.55	1.48	0.07	0.04	99.05			
DB02-216_pl1_4_25	100	Inclusion	46.75	1.39	5.02	17.62	0.36	13.92	12.60	0.48	0.01	0.05	98.20			
DB02-216_pl1_4_26	104	Inclusion	50.64	0.82	9.21	12.66	0.28	11.03	11.04	2.22	0.04	0.00	97.93			
DB02-216_pl1_4_27	108	Inclusion	48.16	0.80	5.60	16.75	0.29	13.28	10.48	0.64	0.05	0.22	96.28			
DB02-216_pl1_4_28	112	Inclusion	44.32	0.75	6.17	17.68	0.20	13.29	9.10	0.45	0.08	0.00	92.05			
DB02-216_pl1_4_29	116	Inclusion	39.74	2.72	4.64	25.86	0.56	13.14	8.05	0.36	0.05	0.00	95.11			
DB02-216_pl1_4_30	120	Inclusion	44.05	0.87	6.35	18.80	0.16	14.89	5.32	0.23	0.14	0.12	90.94			
DB02-216_pl1_4_31	124	Olivine pseudomorph	44.81	0.12	8.59	20.09	0.19	15.23	2.69	0.20	0.19	0.00	92.10			
DB02-216_pl1_4_32	128	Olivine pseudomorph	41.15	0.13	8.06	18.08	0.02	13.89	2.58	0.16	0.16	0.01	84.24			
DB02-216_pl1_4_33	132	Olivine pseudomorph	41.67	0.15	8.20	18.36	0.15	14.44	2.68	0.19	0.18	0.18	86.20			
DB02-216_pl1_4_34	136	Olivine pseudomorph	40.85	0.17	8.32	18.73	0.10	13.22	2.82	0.16	0.15	0.16	84.68			
DB02-216_pl1_4_35	140	Inclusion	47.08	0.46	5.70	21.10	0.23	13.02	6.43	0.54	0.17	0.01	94.75			
DB02-216_pl1_4_36	144	Inclusion	50.57	0.72	4.29	19.42	0.38	13.39	8.84	1.08	0.24	0.06	98.97			
DB02-216_pl1_4_37	148	Inclusion	45.58	0.36	7.15	19.97	0.20	15.07	4.24	0.25	0.15	0.20	93.15			
DB02-216_pl1_4_38	152	Inclusion	50.07	0.94	5.53	16.08	0.35	14.28	11.31	0.80	0.05	0.00	99.40			
DB02-216_pl1_4_39	156	Inclusion	49.93	1.18	6.03	14.21	0.35	14.06	13.00	1.03	0.01	0.06	99.86			
DB02-216_pl1_4_40	160	Inclusion	49.56	0.96	6.22	15.38	0.33	14.30	11.38	0.89	0.04	0.16	99.07			
DB02-216_pl1_4_41	164	Inclusion	43.29	0.45	7.41	19.20	0.20	16.15	4.36	0.19	0.22	0.00	91.47			
DB02-216_pl1_4_42	168	Inclusion	46.26	0.11	9.09	17.81	0.12	13.36	3.56	0.53	0.10	0.14	91.07			
DB02-216_pl1_4_43	172	Inclusion	49.49	1.15	5.54	13.95	0.34	14.88	12.50	0.72	0.01	0.13	98.68			
DB02-216_pl1_4_44	176	Rim	54.24	0.58	13.75	9.10	0.14	7.40	10.53	3.88	0.03	0.00	99.64	59.88	39.92	0.20

Table 7. DB02-216 plagioclases and melt inclusions, XRF analyses (continued)

Plagioclase xenocryst 1 - profile 4 (continued)

Label	Profile (µm)	Material	SiO2	TiO2	Al2O3	FeO	MnO	MgO	CaO	Na2O	K2O	BaO	Total	An	Ab	Or
DB02-216_pl1_4_45	180	Rim	53.30	0.29	19.97	5.92	0.19	4.77	11.11	4.15	0.04	0.00	99.73	59.53	40.21	0.26
DB02-216_pl1_4_46	184	Rim	53.01	0.04	27.98	0.95	0.07	0.63	13.04	4.04	0.02	0.03	99.79	63.99	35.90	0.11
DB02-216_pl1_4_47	188	Rim	50.71	0.02	30.08	0.90	0.00	0.51	14.71	2.98	0.00	0.06	99.97	73.20	26.80	0.00
DB02-216_pl1_4_48	192	Plagioclase	46.62	0.00	33.53	0.60	0.04	0.23	17.69	1.31	0.00	0.29	100.30	88.16	11.84	0.00
DB02-216_pl1_4_49	196	Plagioclase	45.51	0.09	33.99	0.59	0.06	0.18	18.02	1.17	0.01	0.05	99.67	89.41	10.55	0.04
DB02-216_pl1_4_50	200	Plagioclase	45.47	0.01	34.18	0.53	0.07	0.15	18.18	1.09	0.01	0.04	99.73	90.13	9.82	0.05
DB02-216_pl1_4_51	204	Plagioclase	45.18	0.04	34.21	0.50	0.07	0.18	18.25	1.02	0.01	0.16	99.61	90.73	9.22	0.06
DB02-216_pl1_4_52	208	Plagioclase	45.26	0.00	34.23	0.46	0.08	0.18	18.13	1.09	0.00	0.00	99.42	90.15	9.85	0.01
DB02-216_pl1_4_53	212	Plagioclase	45.62	0.05	33.90	0.47	0.08	0.17	18.16	1.05	0.00	0.00	99.50	90.52	9.46	0.01
DB02-216_pl1_4_54	216	Inclusion	45.49	0.01	32.81	1.28	0.00	0.87	17.15	1.17	0.00	0.10	98.89			
DB02-216_pl1_4_55	220	Plagioclase	46.01	0.00	33.97	0.54	0.05	0.22	18.01	1.13	0.01	0.17	100.10	89.74	10.21	0.05
DB02-216_pl1_4_56	224	Plagioclase	45.89	0.10	33.75	0.51	0.06	0.16	18.04	1.19	0.01	0.00	99.71	89.30	10.63	0.06
DB02-216_pl1_4_57	228	Plagioclase	45.52	0.04	33.55	0.46	0.00	0.17	18.01	1.19	0.00	0.08	99.01	89.32	10.68	0.00
DB02-216_pl1_4_58	232	Inclusion	45.52	0.00	32.67	1.33	0.05	1.24	17.27	0.99	0.03	0.07	99.16			
DB02-216_pl1_4_59	236	Inclusion	43.91	0.01	29.91	3.79	0.09	3.36	15.41	0.91	0.03	0.00	97.42			
DB02-216_pl1_4_60	240	Plagioclase	45.61	0.00	33.98	0.45	0.05	0.16	18.17	1.07	0.00	0.00	99.49	90.33	9.67	0.00
DB02-216_pl1_4_61	244	Plagioclase	45.68	0.03	34.23	0.48	0.06	0.18	17.94	1.23	0.00	0.12	99.94	88.95	11.05	0.00
DB02-216_pl1_4_62	248	Plagioclase	45.92	0.01	33.74	0.54	0.05	0.20	17.81	1.33	0.00	0.19	99.80	88.09	11.91	0.00
DB02-216_pl1_4_63	252	Plagioclase	46.08	0.01	33.33	0.46	0.06	0.20	17.64	1.43	0.00	0.04	99.25	87.19	12.81	0.00
DB02-216_pl1_4_64	256	Plagioclase	46.28	0.05	33.60	0.54	0.09	0.22	17.77	1.39	0.00	0.00	99.93	87.61	12.39	0.00
DB02-216_pl1_4_65	260	Plagioclase	45.92	0.03	33.66	0.52	0.09	0.20	17.70	1.43	0.01	0.00	99.55	87.18	12.74	0.08
DB02-216_pl1_4_66	264	Inclusion	43.71	0.06	28.39	4.01	0.09	3.52	14.80	1.10	0.04	0.08	95.80			
DB02-216_pl1_4_67	268	Inclusion	36.78	0.08	11.89	20.43	0.09	12.83	2.66	0.20	0.18	0.00	85.15			
DB02-216_pl1_4_68	272	Plagioclase	46.33	0.05	33.21	0.65	0.00	0.38	17.58	1.42	0.01	0.00	99.64	87.14	12.77	0.08
DB02-216_pl1_4_69	276	Plagioclase	46.26	0.03	33.56	0.37	0.04	0.23	17.85	1.42	0.00	0.03	99.79	87.38	12.62	0.00
DB02-216_pl1_4_70	280	Plagioclase	46.07	0.04	33.62	0.47	0.00	0.21	17.74	1.29	0.00	0.07	99.50	88.35	11.62	0.03
DB02-216_pl1_4_71	284	Plagioclase	46.14	0.02	33.81	0.51	0.06	0.20	17.82	1.41	0.00	0.00	99.97	87.47	12.53	0.01

Plagioclase xenocryst 1 - profile 5

Label	Profile (µm)	Material	SiO2	TiO2	Al2O3	FeO	MnO	MgO	CaO	Na2O	K2O	BaO	Total	An	Ab	Or
DB02-216_Pl1_5_1	0	Inclusion	46.89	1.51	5.73	15.38	0.32	14.32	12.41	1.03	0.02	0.20	97.81			
DB02-216_Pl1_5_2	2	Inclusion	48.26	1.12	5.33	15.49	0.33	14.09	12.71	0.80	0.04	0.16	98.33			
DB02-216_Pl1_5_3	4	Inclusion	50.24	0.92	7.47	13.29	0.28	11.50	11.54	1.61	0.05	0.00	96.90			
DB02-216_Pl1_5_4	6	Inclusion	43.38	2.84	5.30	23.70	0.66	13.15	10.72	0.49	0.02	0.00	100.26			
DB02-216_Pl1_5_5	8	Inclusion	47.11	1.68	7.43	18.88	0.28	12.02	10.11	1.76	0.08	0.09	99.44			
DB02-216_Pl1_5_6	10	Inclusion	42.97	2.28	5.33	22.30	0.33	12.79	11.35	0.77	0.02	0.04	98.17			
DB02-216_Pl1_5_7	12	Inclusion	46.87	1.53	5.81	16.83	0.33	14.35	12.03	0.93	0.03	0.22	98.94			
DB02-216_Pl1_5_8	14	Inclusion	46.13	1.35	6.21	15.79	0.32	14.05	11.22	1.15	0.06	0.00	96.28			
DB02-216_Pl1_5_9	16	Inclusion	43.44	2.20	4.37	21.52	0.51	13.14	11.28	0.40	0.02	0.02	96.90			
DB02-216_Pl1_5_10	18	Inclusion	36.37	4.91	4.50	32.65	0.97	11.49	9.36	0.31	0.00	0.13	100.70			
DB02-216_Pl1_5_11	20	Inclusion	49.38	1.01	5.67	14.46	0.23	13.88	12.58	0.75	0.02	0.00	97.99			
DB02-216_Pl1_5_12	22	Inclusion	48.67	1.06	4.97	14.95	0.30	14.62	12.62	0.49	0.00	0.09	97.76			
DB02-216_Pl1_5_13	24	Inclusion	49.72	0.99	6.10	13.86	0.34	13.70	12.08	0.96	0.02	0.10	97.88			
DB02-216_Pl1_5_14	26	Inclusion	49.90	1.10	6.62	14.03	0.25	13.17	12.03	1.29	0.02	0.00	98.42			

Table 7. DB02-216 plagioclases and melt inclusions, XRF analyses (continued)

Plagioclase xenocryst 1 - profile 5 (continued)

Label	Profile (µm)	Material	SiO2	TiO2	Al2O3	FeO	MnO	MgO	CaO	Na2O	K2O	BaO	Total	An	Ab	Or
DB02-216_Pl1_5_15	28	Inclusion	49.67	1.14	7.00	14.18	0.24	13.27	11.50	1.50	0.03	0.04	98.56			
DB02-216_Pl1_5_16	30	Inclusion	48.47	1.38	4.88	14.77	0.37	15.40	12.67	0.57	0.00	0.00	98.51			
DB02-216_Pl1_5_17	32	Inclusion	48.82	1.32	4.38	14.76	0.31	14.80	13.36	0.44	0.01	0.00	98.19			
DB02-216_Pl1_5_18	34	Inclusion	48.35	1.27	4.91	15.54	0.34	14.66	12.59	0.51	0.01	0.05	98.24			
DB02-216_Pl1_5_19	36	Inclusion	49.08	0.97	4.63	14.67	0.29	14.47	13.06	0.54	0.02	0.00	97.73			
DB02-216_Pl1_5_20	38	Rim	51.26	0.87	8.85	12.83	0.27	12.30	11.68	2.06	0.02	0.01	100.15	75.70	24.14	0.16
DB02-216_Pl1_5_21	40	Rim	53.87	0.38	20.49	4.61	0.11	3.93	11.06	4.30	0.04	0.06	98.85	58.54	41.19	0.26
DB02-216_Pl1_5_22	42	Rim	53.53	0.04	26.77	1.31	0.04	0.82	12.05	4.46	0.02	0.00	99.05	59.80	40.09	0.11
DB02-216_Pl1_5_23	44	Rim	53.18	0.05	27.15	1.17	0.04	0.76	11.87	4.42	0.03	0.03	98.69	59.67	40.17	0.16
DB02-216_Pl1_5_24	46	Rim	47.58	0.00	32.46	0.70	0.06	0.20	16.58	1.91	0.01	0.03	99.54	82.70	17.22	0.08
DB02-216_Pl1_5_25	48	Rim	46.18	0.08	33.33	0.61	0.08	0.17	17.46	1.52	0.00	0.00	99.43	86.42	13.58	0.00
DB02-216_Pl1_5_26	50	Plagioclase	46.31	0.02	33.22	0.58	0.00	0.15	17.40	1.42	0.00	0.00	99.10	87.11	12.89	0.00
DB02-216_Pl1_5_27	52	Plagioclase	45.69	0.02	33.40	0.57	0.10	0.23	17.45	1.40	0.00	0.00	98.86	87.30	12.69	0.02
DB02-216_Pl1_5_28	54	Plagioclase	46.25	0.01	33.59	0.54	0.04	0.25	17.41	1.47	0.00	0.08	99.65	86.73	13.27	0.00
DB02-216_Pl1_5_29	56	Plagioclase	46.25	0.05	33.27	0.56	0.04	0.18	17.44	1.37	0.00	0.00	99.16	87.52	12.46	0.01
DB02-216_Pl1_5_30	58	Plagioclase	45.82	0.02	33.43	0.45	0.01	0.22	17.38	1.42	0.01	0.05	98.80	87.07	12.89	0.04
DB02-216_Pl1_5_31	60	Plagioclase	45.92	0.10	33.34	0.50	0.00	0.18	17.39	1.44	0.00	0.00	98.88	86.94	13.06	0.00
DB02-216_Pl1_5_32	62	Plagioclase	46.40	0.06	33.45	0.52	0.01	0.18	17.40	1.50	0.01	0.00	99.53	86.45	13.52	0.03
DB02-216_Pl1_5_33	64	Plagioclase	46.00	0.00	33.38	0.39	0.00	0.19	17.48	1.47	0.00	0.00	98.90	86.81	13.17	0.02
DB02-216_Pl1_5_34	66	Plagioclase	46.40	0.04	33.23	0.38	0.00	0.17	17.54	1.42	0.00	0.03	99.20	87.22	12.77	0.01
DB02-216_Pl1_5_35	68	Plagioclase	46.48	0.02	33.05	0.46	0.08	0.19	17.41	1.45	0.00	0.01	99.14	86.92	13.08	0.00
DB02-216_Pl1_5_36	70	Plagioclase	46.27	0.03	33.42	0.44	0.09	0.21	17.42	1.49	0.01	0.00	99.36	86.58	13.38	0.04
DB02-216_Pl1_5_37	72	Plagioclase	46.04	0.06	33.28	0.55	0.03	0.18	17.32	1.38	0.01	0.00	98.86	87.32	12.59	0.09
DB02-216_Pl1_5_38	74	Plagioclase	46.37	0.02	33.28	0.32	0.08	0.19	17.43	1.48	0.02	0.10	99.29	86.60	13.30	0.10
DB02-216_Pl1_5_39	76	Plagioclase	46.23	0.03	33.41	0.42	0.08	0.20	17.52	1.49	0.01	0.01	99.40	86.65	13.32	0.03
DB02-216_Pl1_5_40	78	Plagioclase	45.97	0.06	33.01	0.50	0.03	0.20	17.47	1.47	0.00	0.01	98.71	86.81	13.19	0.00
DB02-216_Pl1_5_41	80	Plagioclase	46.10	0.06	33.14	0.42	0.03	0.18	17.52	1.45	0.02	0.00	98.91	86.89	13.02	0.09
DB02-216_Pl1_5_42	82	Plagioclase	46.19	0.05	33.39	0.41	0.01	0.19	17.60	1.40	0.00	0.00	99.24	87.44	12.56	0.01
DB02-216_Pl1_5_43	84	Plagioclase	45.97	0.06	33.37	0.40	0.04	0.22	17.55	1.39	0.00	0.00	99.00	87.49	12.50	0.01
DB02-216_Pl1_5_44	86	Plagioclase	46.12	0.05	33.51	0.45	0.00	0.21	17.59	1.40	0.00	0.00	99.33	87.44	12.56	0.00
DB02-216_Pl1_5_45	88	Plagioclase	45.69	0.05	33.34	0.41	0.05	0.22	17.60	1.30	0.00	0.19	98.67	88.18	11.79	0.03
DB02-216_Pl1_5_46	90	Plagioclase	45.92	0.02	33.71	0.42	0.03	0.18	17.64	1.35	0.00	0.09	99.47	87.85	12.14	0.01
DB02-216_Pl1_5_47	92	Plagioclase	46.02	0.00	33.48	0.36	0.02	0.19	17.64	1.32	0.00	0.18	99.13	88.06	11.92	0.02
DB02-216_Pl1_5_48	94	Plagioclase	46.18	0.03	33.51	0.37	0.00	0.16	17.62	1.31	0.00	0.00	99.37	88.10	11.89	0.01
DB02-216_Pl1_5_49	96	Plagioclase	45.79	0.04	33.54	0.45	0.05	0.20	17.79	1.36	0.00	0.10	99.22	87.82	12.18	0.00
DB02-216_Pl1_5_50	98	Plagioclase	45.75	0.01	33.51	0.43	0.00	0.19	17.64	1.24	0.01	0.03	98.87	88.69	11.30	0.00
DB02-216_Pl1_5_51	100	Plagioclase	45.69	0.01	33.34	0.38	0.08	0.20	17.63	1.31	0.01	0.00	98.67	88.12	11.81	0.07
DB02-216_Pl1_5_52	102	Plagioclase	45.27	0.05	33.25	0.37	0.04	0.26	17.81	1.36	0.03	0.01	98.44	87.67	12.14	0.19
DB02-216_Pl1_5_53	104	Plagioclase	45.69	0.05	33.33	0.39	0.03	0.17	17.70	1.36	0.01	0.00	98.75	87.77	12.17	0.06
DB02-216_Pl1_5_54	106	Plagioclase	45.83	0.00	33.54	0.43	0.05	0.16	17.44	1.34	0.01	0.01	98.81	87.72	12.22	0.06
DB02-216_Pl1_5_55	108	Plagioclase	45.53	0.04	33.47	0.38	0.00	0.19	17.65	1.30	0.01	0.08	98.65	88.19	11.74	0.07
DB02-216_Pl1_5_56	110	Plagioclase	45.60	0.00	33.42	0.39	0.01	0.21	17.73	1.27	0.01	0.00	98.64	88.45	11.51	0.05
DB02-216_Pl1_5_57	112	Plagioclase	46.03	0.01	33.14	0.44	0.08	0.18	17.69	1.25	0.01	0.00	98.82	88.62	11.31	0.07
DB02-216_Pl1_5_58	114	Plagioclase	45.82	0.00	33.33	0.29	0.06	0.18	17.61	1.33	0.02	0.00	98.64	87.87	12.01	0.11

Table 7. DB02-216 plagioclases and melt inclusions, XRF analyses (continued)

Label	Profile (µm)	Material	SiO2	TiO2	Al2O3	FeO	MnO	MgO	CaO	Na2O	K2O	BaO	Total	An	Ab	Or
		Plagioclase xenocryst 1 - profile 5 (continued)														
DB02-216_Pl1_5_59	116	Plagioclase	45.85	0.03	33.51	0.40	0.00	0.19	17.70	1.31	0.00	0.00	98.99	88.13	11.85	0.02
DB02-216_Pl1_5_60	118	Plagioclase	45.51	0.04	33.36	0.37	0.00	0.18	17.65	1.32	0.00	0.00	98.44	88.04	11.94	0.01
DB02-216_Pl1_5_61	120	Plagioclase	45.86	0.04	33.65	0.44	0.00	0.18	17.64	1.33	0.00	0.10	99.24	87.97	12.01	0.03
DB02-216_Pl1_5_62	122	Plagioclase	45.63	0.02	33.14	0.31	0.01	0.17	17.56	1.35	0.00	0.00	98.19	87.82	12.18	0.00
DB02-216_Pl1_5_63	124	Plagioclase	45.78	0.04	33.46	0.40	0.05	0.23	17.57	1.26	0.01	0.00	98.80	88.49	11.46	0.05
DB02-216_Pl1_5_64	126	Plagioclase	45.95	0.02	33.72	0.36	0.06	0.22	17.62	1.33	0.01	0.15	99.46	87.90	12.04	0.06
DB02-216_Pl1_5_65	128	Plagioclase	45.95	0.01	33.63	0.48	0.08	0.21	17.74	1.38	0.01	0.15	99.64	87.61	12.33	0.05
DB02-216_Pl1_5_66	130	Plagioclase	46.05	0.00	33.31	0.37	0.08	0.19	17.66	1.23	0.00	0.00	98.89	88.79	11.21	0.00
DB02-216_Pl1_5_67	132	Plagioclase	45.93	0.06	33.55	0.43	0.12	0.21	17.81	1.30	0.01	0.06	99.48	88.27	11.69	0.04
DB02-216_Pl1_5_68	134	Plagioclase	45.92	0.00	33.53	0.50	0.06	0.18	17.68	1.26	0.00	0.00	99.13	88.54	11.45	0.00
DB02-216_Pl1_5_69	136	Plagioclase	45.68	0.00	33.49	0.38	0.03	0.16	17.69	1.32	0.00	0.10	98.86	88.08	11.91	0.00
DB02-216_Pl1_5_70	138	Plagioclase	45.77	0.00	33.65	0.35	0.03	0.15	17.90	1.26	0.01	0.00	99.11	88.69	11.26	0.04
DB02-216_Pl1_5_71	140	Plagioclase	45.90	0.02	33.61	0.40	0.03	0.16	17.75	1.24	0.01	0.01	99.14	88.77	11.19	0.04
DB02-216_Pl1_5_72	142	Plagioclase	46.23	0.00	33.74	0.43	0.00	0.15	17.70	1.30	0.00	0.11	99.67	88.26	11.73	0.01
DB02-216_Pl1_5_73	144	Plagioclase	45.88	0.04	33.91	0.36	0.09	0.17	17.66	1.31	0.00	0.09	99.51	88.18	11.81	0.02
DB02-216_Pl1_5_74	146	Plagioclase	46.08	0.03	33.48	0.41	0.06	0.18	17.78	1.26	0.01	0.09	99.38	88.59	11.37	0.04
DB02-216_Pl1_5_75	148	Plagioclase	45.95	0.05	33.70	0.38	0.08	0.22	17.74	1.25	0.01	0.08	99.45	88.67	11.29	0.03
		Plagioclase xenocryst 2 - profile 1														
DB02-216_Pl2_1_1	0	Inclusion	51.52	0.65	7.40	14.91	0.30	12.02	10.10	1.78	0.04	0.00	98.71	83.57	16.33	0.10
DB02-216_Pl2_1_2	4	Inclusion	45.87	1.96	7.31	16.14	0.28	13.74	11.23	1.45	0.04	0.07	98.08	56.83	42.92	0.25
DB02-216_Pl2_1_3	8	Inclusion	48.18	1.14	4.82	15.93	0.41	14.19	12.43	0.63	0.03	0.15	97.90	65.41	34.46	0.13
DB02-216_Pl2_1_4	12	Inclusion	47.12	1.39	5.83	15.96	0.33	14.69	11.91	0.93	0.01	0.00	98.17	72.67	27.25	0.07
DB02-216_Pl2_1_5	16	Inclusion	49.21	0.98	4.40	14.73	0.29	15.04	12.98	0.37	0.00	0.01	98.01	87.12	12.86	0.01
DB02-216_Pl2_1_6	20	Inclusion	49.28	0.94	5.94	14.94	0.29	13.45	12.29	0.85	0.01	0.00	97.98	86.86	13.11	0.03
DB02-216_Pl2_1_7	24	Inclusion	49.45	1.09	4.28	15.91	0.30	15.42	12.65	0.46	0.01	0.11	99.68	86.74	13.20	0.06
DB02-216_Pl2_1_8	28	Inclusion	49.11	1.05	4.27	15.61	0.34	14.85	13.49	0.36	0.01	0.12	99.21	86.82	13.17	0.01
DB02-216_Pl2_1_9	32	Inclusion	52.14	0.69	10.44	13.68	0.31	11.11	9.76	2.09	0.03	0.01	100.27			
DB02-216_Pl2_1_10	36	Rim	50.61	1.04	6.60	15.08	0.38	13.79	11.64	1.26	0.01	0.00	100.40			
DB02-216_Pl2_1_11	40	Rim	54.30	0.06	26.39	1.44	0.01	0.86	11.14	4.65	0.04	0.00	98.89			
DB02-216_Pl2_1_12	44	Rim	52.32	0.04	28.55	0.85	0.00	0.50	13.22	3.85	0.02	0.00	99.34			
DB02-216_Pl2_1_13	48	Rim	50.04	0.01	30.26	0.84	0.00	0.51	14.64	3.03	0.01	0.00	99.33			
DB02-216_Pl2_1_14	52	Plagioclase	46.11	0.07	33.70	0.63	0.00	0.18	17.44	1.42	0.00	0.00	99.56	87.12	12.86	0.01
DB02-216_Pl2_1_15	56	Plagioclase	46.14	0.06	33.63	0.46	0.00	0.16	17.46	1.46	0.01	0.00	99.36	86.86	13.11	0.03
DB02-216_Pl2_1_16	60	Plagioclase	46.58	0.06	33.45	0.54	0.00	0.20	17.32	1.46	0.01	0.00	99.63	86.74	13.20	0.06
DB02-216_Pl2_1_17	64	Plagioclase	46.43	0.03	33.23	0.46	0.08	0.17	17.40	1.46	0.00	0.00	99.27	86.82	13.17	0.01
DB02-216_Pl2_1_18	68	Plagioclase	46.42	0.02	33.44	0.52	0.06	0.19	17.39	1.41	0.01	0.04	99.50	87.14	12.82	0.04
DB02-216_Pl2_1_19	72	Plagioclase	46.44	0.00	33.67	0.43	0.00	0.19	17.71	1.39	0.01	0.11	99.95	87.48	12.47	0.05
DB02-216_Pl2_1_20	76	Plagioclase	46.33	0.02	33.37	0.39	0.02	0.19	17.70	1.37	0.01	0.11	99.52	87.65	12.29	0.06
DB02-216_Pl2_1_21	80	Plagioclase	46.28	0.00	33.80	0.52	0.00	0.19	17.77	1.27	0.01	0.00	99.84	88.48	11.47	0.05
DB02-216_Pl2_1_22	84	Plagioclase	46.06	0.01	33.68	0.55	0.12	0.17	17.80	1.37	0.00	0.14	99.76	87.76	12.23	0.01
DB02-216_Pl2_1_23	88	Plagioclase	46.53	0.05	33.75	0.43	0.00	0.14	17.72	1.32	0.01	0.11	100.08	88.07	11.85	0.08
DB02-216_Pl2_1_24	92	Plagioclase	46.29	0.00	33.84	0.43	0.09	0.19	17.72	1.33	0.02	0.08	99.97	87.97	11.92	0.11
DB02-216_Pl2_1_25	96	Plagioclase	46.08	0.04	33.59	0.51	0.01	0.20	17.83	1.36	0.01	0.00	99.63	87.81	12.14	0.06

Table 7. DB02-216 plagioclases and melt inclusions, XRF analyses (continued)

Label	Profile (µm)	Material	SiO2	TiO2	Al2O3	FeO	MnO	MgO	CaO	Na2O	K2O	BaO	Total	An	Ab	Or
Plagioclase xenocryst 2 - profile 1 (continued)																
DB02-216_Pl2_1_26	100	Plagioclase	46.49	0.06	33.71	0.37	0.05	0.19	17.73	1.31	0.00	0.14	100.05	88.21	11.78	0.01
DB02-216_Pl2_1_27	104	Plagioclase	46.61	0.03	33.87	0.49	0.03	0.21	17.59	1.32	0.01	0.00	100.14	87.99	11.96	0.05
DB02-216_Pl2_1_28	108	Plagioclase	46.32	0.04	33.61	0.47	0.07	0.16	17.68	1.36	0.01	0.05	99.76	87.69	12.24	0.06
DB02-216_Pl2_1_29	112	Plagioclase	46.22	0.06	33.76	0.37	0.07	0.21	17.70	1.35	0.01	0.00	99.76	87.79	12.16	0.05
DB02-216_Pl2_1_30	116	Plagioclase	46.26	0.04	33.80	0.32	0.00	0.21	17.91	1.28	0.01	0.00	99.84	88.48	11.46	0.06
DB02-216_Pl2_1_31	120	Plagioclase	46.19	0.09	33.69	0.40	0.00	0.20	17.77	1.33	0.00	0.20	99.87	88.07	11.93	0.01
DB02-216_Pl2_1_32	124	Plagioclase	46.26	0.03	33.72	0.41	0.00	0.18	17.68	1.28	0.00	0.03	99.60	88.40	11.59	0.01
DB02-216_Pl2_1_33	128	Plagioclase	46.21	0.04	33.68	0.28	0.00	0.18	17.69	1.34	0.00	0.11	99.55	87.95	12.02	0.03
DB02-216_Pl2_1_34	132	Plagioclase	46.14	0.03	33.63	0.38	0.00	0.17	17.85	1.37	0.01	0.06	99.64	87.77	12.15	0.08
DB02-216_Pl2_1_35	136	Plagioclase	46.20	0.04	33.80	0.43	0.04	0.16	17.72	1.26	0.00	0.01	99.65	88.60	11.38	0.02
DB02-216_Pl2_1_36	140	Plagioclase	46.38	0.00	33.79	0.41	0.01	0.19	17.77	1.32	0.00	0.00	99.87	88.17	11.83	0.00
DB02-216_Pl2_1_37	144	Plagioclase	46.21	0.04	33.63	0.33	0.03	0.17	17.89	1.35	0.01	0.00	99.62	87.96	12.00	0.04
DB02-216_Pl2_1_38	148	Plagioclase	46.12	0.00	33.41	0.40	0.03	0.21	17.84	1.24	0.01	0.01	99.28	88.76	11.20	0.04
Plagioclase xenocryst 2 - profile 2																
DB02-216_Pl2_2_1	0	Plagioclase	47.32	0.02	33.06	0.45	0.11	0.23	17.01	1.82	0.01	0.00	100.02	83.75	16.19	0.05
DB02-216_Pl2_2_2	2	Plagioclase	47.37	0.00	32.84	0.41	0.04	0.25	16.92	1.70	0.00	0.01	99.53	84.61	15.39	0.00
DB02-216_Pl2_2_3	4	Plagioclase	47.18	0.00	32.74	0.40	0.00	0.26	16.95	1.72	0.01	0.00	99.26	84.45	15.50	0.05
DB02-216_Pl2_2_4	6	Plagioclase	47.45	0.04	33.00	0.43	0.00	0.22	16.87	1.71	0.00	0.10	99.83	84.49	15.49	0.02
DB02-216_Pl2_2_5	8	Plagioclase	47.25	0.09	32.86	0.60	0.04	0.27	16.97	1.76	0.01	0.08	99.92	84.21	15.79	0.00
DB02-216_Pl2_2_6	10	Plagioclase	47.21	0.05	32.78	0.56	0.00	0.25	16.97	1.71	0.01	0.05	99.61	84.50	15.41	0.09
DB02-216_Pl2_2_7	12	Plagioclase	47.21	0.03	32.76	0.43	0.00	0.25	16.97	1.83	0.02	0.00	99.50	83.61	16.30	0.09
DB02-216_Pl2_2_8	14	Plagioclase	47.50	0.04	32.72	0.43	0.02	0.23	16.92	1.79	0.01	0.00	99.66	83.91	16.06	0.03
DB02-216_Pl2_2_9	16	Plagioclase	47.34	0.00	31.96	0.58	0.05	0.31	16.74	1.76	0.01	0.00	98.75	84.00	15.97	0.03
DB02-216_Pl2_2_10	18	Plagioclase	47.19	0.03	32.26	1.03	0.06	0.46	16.41	1.72	0.00	0.09	99.26	84.07	15.90	0.03
DB02-216_Pl2_2_11	20	Plagioclase	47.35	0.04	32.85	0.46	0.00	0.22	16.93	1.76	0.00	0.04	99.64	84.20	15.80	0.00
DB02-216_Pl2_2_12	22	Plagioclase	47.35	0.04	32.72	0.47	0.00	0.22	16.88	1.73	0.01	0.00	99.41	84.32	15.65	0.03
DB02-216_Pl2_2_13	24	Plagioclase	47.13	0.05	33.04	0.53	0.08	0.22	16.88	1.85	0.01	0.00	99.78	83.44	16.56	0.00
DB02-216_Pl2_2_14	26	Plagioclase	47.24	0.04	32.80	0.51	0.05	0.27	16.76	1.79	0.01	0.01	99.48	83.77	16.16	0.07
DB02-216_Pl2_2_15	28	Plagioclase	47.41	0.03	32.70	0.53	0.00	0.20	16.76	1.75	0.01	0.00	99.39	84.11	15.85	0.04
DB02-216_Pl2_2_16	30	Plagioclase	47.47	0.04	32.82	0.48	0.03	0.25	17.01	1.81	0.01	0.00	99.91	83.81	16.14	0.04
DB02-216_Pl2_2_17	32	Plagioclase	47.45	0.01	32.96	0.48	0.05	0.25	16.91	1.76	0.00	0.11	99.98	84.12	15.87	0.01
DB02-216_Pl2_2_18	34	Plagioclase	47.26	0.00	32.98	0.50	0.01	0.22	16.88	1.78	0.01	0.00	99.64	83.94	15.99	0.08
DB02-216_Pl2_2_19	36	Plagioclase	47.34	0.01	32.90	0.50	0.03	0.26	16.97	1.76	0.01	0.00	99.77	84.19	15.77	0.04
DB02-216_Pl2_2_20	38	Plagioclase	47.23	0.02	32.70	0.48	0.02	0.24	16.90	1.81	0.00	0.00	99.40	83.74	16.26	0.00
DB02-216_Pl2_2_21	40	Plagioclase	47.20	0.03	32.88	0.43	0.05	0.27	16.99	1.71	0.01	0.00	99.57	84.59	15.38	0.03
DB02-216_Pl2_2_22	42	Plagioclase	47.59	0.00	32.91	0.41	0.02	0.21	16.97	1.80	0.01	0.13	100.05	83.89	16.06	0.05
DB02-216_Pl2_2_23	44	Plagioclase	47.35	0.04	32.80	0.44	0.04	0.23	17.01	1.72	0.01	0.08	99.72	84.47	15.48	0.05
DB02-216_Pl2_2_24	46	Plagioclase	47.45	0.00	32.78	0.38	0.05	0.23	16.89	1.76	0.00	0.13	99.67	84.11	15.89	0.00
DB02-216_Pl2_2_25	48	Plagioclase	47.26	0.05	33.01	0.44	0.11	0.23	17.10	1.68	0.01	0.00	99.87	84.87	15.13	0.00
DB02-216_Pl2_2_26	50	Plagioclase	46.82	0.02	33.04	0.48	0.03	0.25	17.23	1.63	0.01	0.00	99.51	85.29	14.64	0.07
DB02-216_Pl2_2_27	52	Plagioclase	46.84	0.02	33.25	0.42	0.00	0.23	17.05	1.62	0.00	0.15	99.59	85.36	14.64	0.00
DB02-216_Pl2_2_28	54	Rim	49.11	0.05	29.92	1.19	0.06	0.71	14.39	2.68	0.00	0.00	98.10	74.77	25.20	0.02
DB02-216_Pl2_2_29	56	Rim	51.55	0.02	29.07	0.93	0.09	0.56	13.73	3.48	0.02	0.06	99.50	68.51	31.39	0.10

Table 7. DB02-216 plagioclases and melt inclusions, XRF analyses (continued)

Plagioclase xenocryst 2 - profile 2 (continued)

Label	Profile (μm)	Material	SiO2	TiO2	Al2O3	FeO	MnO	MgO	CaO	Na2O	K2O	BaO	Total	An	Ab	Or
DB02-216_Pl2_2_30	58	Rim	52.51	0.04	28.61	1.02	0.05	0.54	13.17	3.94	0.01	0.00	99.90	64.82	35.13	0.05
DB02-216_Pl2_2_31	60	Rim	52.56	0.08	25.92	1.73	0.07	1.45	12.50	3.84	0.01	0.05	98.21	64.23	35.69	0.09
DB02-216_Pl2_2_32	62	Rim	49.86	1.33	7.53	13.26	0.27	12.96	12.43	1.23	0.03	0.00	98.91	84.57	15.20	0.23
DB02-216_Pl2_2_33	64	Inclusion	50.40	1.17	7.12	13.76	0.27	13.18	11.95	1.34	0.02	0.06	99.27			
DB02-216_Pl2_2_34	66	Inclusion	49.50	1.17	4.54	15.60	0.52	15.14	12.39	0.45	0.01	0.11	99.43			
DB02-216_Pl2_2_35	68	Inclusion	50.34	1.07	6.50	13.56	0.28	13.38	11.77	1.14	0.02	0.02	98.09			
DB02-216_Pl2_2_36	70	Inclusion	50.02	1.21	5.07	15.37	0.39	14.92	11.75	0.77	0.03	0.00	99.52			
DB02-216_Pl2_2_37	72	Inclusion	51.81	0.96	7.50	12.51	0.33	12.57	12.02	1.64	0.04	0.00	99.40			
DB02-216_Pl2_2_38	74	Inclusion	53.22	0.71	10.26	10.97	0.24	10.76	10.51	2.56	0.06	0.06	99.36			
DB02-216_Pl2_2_39	76	Inclusion	51.18	1.01	6.66	13.30	0.24	12.98	12.33	1.26	0.03	0.00	98.99			
DB02-216_Pl2_2_40	78	Inclusion	44.45	3.54	4.08	21.82	0.68	13.58	12.20	0.40	0.00	0.00	100.75			
DB02-216_Pl2_2_41	80	Inclusion	49.83	1.26	5.53	14.04	0.35	13.67	13.16	0.90	0.02	0.00	98.76			
DB02-216_Pl2_2_42	82	Inclusion	50.00	1.18	5.95	13.42	0.21	12.44	12.73	0.90	0.06	0.00	96.90			
DB02-216_Pl2_2_43	84	Inclusion	49.66	1.20	5.13	14.47	0.29	13.78	13.55	0.79	0.04	0.00	98.90			
DB02-216_Pl2_2_44	86	Inclusion	49.15	1.69	4.27	16.86	0.41	14.16	12.24	0.57	0.02	0.04	99.42			
DB02-216_Pl2_2_45	88	Inclusion	49.35	1.22	4.87	14.81	0.37	13.82	13.50	0.69	0.04	0.15	98.83			
DB02-216_Pl2_2_46	90	Olivine pseudomorph	41.75	0.39	6.44	20.71	0.28	13.71	4.51	0.28	0.04	0.00	88.12			
DB02-216_Pl2_2_47	92	Olivine pseudomorph	41.71	0.18	9.18	18.93	0.16	13.61	3.27	0.07	0.05	0.01	87.18			
DB02-216_Pl2_2_48	94	Olivine pseudomorph	45.18	0.20	9.44	17.64	0.13	14.25	3.73	0.10	0.06	0.00	90.71			
DB02-216_Pl2_2_49	96	Olivine pseudomorph	47.34	0.14	12.03	12.84	0.09	9.59	5.63	0.93	0.08	0.00	88.67			
DB02-216_Pl2_2_50	98	Rim	50.59	0.02	30.42	0.77	0.01	0.45	15.99	2.10	0.01	0.06	100.43	80.73	19.20	0.07
DB02-216_Pl2_2_51	100	Plagioclase	46.62	0.00	33.51	0.53	0.05	0.21	17.48	1.46	0.00	0.00	99.86	86.91	13.09	0.00
DB02-216_Pl2_2_52	102	Plagioclase	46.78	0.08	33.47	0.53	0.04	0.22	17.38	1.41	0.01	0.00	99.92	87.15	12.81	0.04
DB02-216_Pl2_2_53	104	Plagioclase	46.59	0.01	33.62	0.48	0.06	0.20	17.49	1.44	0.01	0.00	99.89	87.01	12.96	0.03
DB02-216_Pl2_2_54	106	Plagioclase	46.49	0.04	33.49	0.54	0.00	0.20	17.62	1.38	0.00	0.00	99.76	87.59	12.38	0.03
DB02-216_Pl2_2_55	108	Plagioclase	46.19	0.10	33.66	0.46	0.04	0.15	17.59	1.33	0.01	0.00	99.52	87.92	12.03	0.05
DB02-216_Pl2_2_56	110	Plagioclase	46.28	0.04	33.80	0.43	0.06	0.16	17.51	1.38	0.00	0.22	99.87	87.51	12.48	0.00
DB02-216_Pl2_2_57	112	Plagioclase	46.25	0.11	33.51	0.45	0.04	0.15	17.56	1.37	0.00	0.00	99.44	87.63	12.37	0.00
DB02-216_Pl2_2_58	114	Plagioclase	46.33	0.00	33.67	0.44	0.05	0.17	17.66	1.34	0.00	0.00	99.67	87.94	12.03	0.02
DB02-216_Pl2_2_59	116	Plagioclase	46.41	0.03	33.70	0.48	0.03	0.19	17.49	1.42	0.00	0.00	99.75	87.18	12.82	0.00
DB02-216_Pl2_2_60	118	Plagioclase	46.49	0.04	33.57	0.50	0.00	0.18	17.53	1.29	0.00	0.00	99.60	88.22	11.78	0.00
DB02-216_Pl2_2_61	120	Plagioclase	46.52	0.01	33.60	0.42	0.00	0.16	17.61	1.38	0.00	0.08	99.77	87.56	12.44	0.00
DB02-216_Pl2_2_62	122	Plagioclase	46.22	0.00	33.71	0.48	0.08	0.19	17.57	1.33	0.02	0.00	99.59	87.87	12.02	0.11
DB02-216_Pl2_2_63	124	Plagioclase	46.43	0.03	33.51	0.41	0.01	0.20	17.68	1.39	0.00	0.00	99.66	87.53	12.44	0.03
DB02-216_Pl2_2_64	126	Plagioclase	46.04	0.08	33.49	0.61	0.06	0.25	17.43	1.43	0.00	0.08	99.47	87.08	12.90	0.02
DB02-216_Pl2_2_65	128	Plagioclase	46.26	0.02	33.52	0.37	0.00	0.20	17.50	1.42	0.00	0.28	99.58	87.17	12.82	0.00
DB02-216_Pl2_2_66	130	Plagioclase	46.53	0.01	33.59	0.50	0.03	0.21	17.58	1.40	0.00	0.10	99.94	87.41	12.56	0.02
DB02-216_Pl2_2_67	132	Plagioclase	46.32	0.04	33.54	0.41	0.00	0.21	17.60	1.48	0.01	0.03	99.60	86.76	13.22	0.02
DB02-216_Pl2_2_68	134	Plagioclase	46.80	0.02	33.32	0.41	0.02	0.19	17.43	1.47	0.00	0.00	99.69	86.71	13.24	0.06
DB02-216_Pl2_2_69	136	Plagioclase	46.89	0.00	33.19	0.37	0.03	0.22	17.41	1.57	0.01	0.00	99.69	85.96	14.03	0.02
DB02-216_Pl2_2_70	138	Plagioclase	46.60	0.03	32.91	0.50	0.02	0.23	17.37	1.47	0.00	0.00	99.12	86.72	13.27	0.00
DB02-216_Pl2_2_71	140	Plagioclase	46.83	0.06	33.28	0.46	0.03	0.25	17.22	1.55	0.00	0.18	99.87	86.01	13.99	0.00
DB02-216_Pl2_2_72	142	Plagioclase	46.79	0.02	33.28	0.42	0.00	0.19	17.28	1.52	0.00	0.13	99.64	86.23	13.77	0.00
DB02-216_Pl2_2_73	144	Plagioclase	46.87	0.01	33.18	0.38	0.11	0.19	17.34	1.52	0.00	0.00	99.60	86.34	13.66	0.00

Table 7. DB02-216 plagioclases and melt inclusions, XRF analyses (continued)

Label	Profile (µm)	Material	SiO2	TiO2	Al2O3	FeO	MnO	MgO	CaO	Na2O	K2O	BaO	Total	An	Ab	Or
—*Plagioclase xenocryst 2 - profile 2 (continued)*																
DB02-216_PI2_2_74	146	Plagioclase	47.08	0.04	33.31	0.49	0.00	0.24	17.27	1.59	0.01	0.00	100.02	85.69	14.28	0.03
DB02-216_PI2_2_75	148	Plagioclase	46.70	0.00	33.38	0.38	0.11	0.18	17.28	1.55	0.01	0.00	99.59	86.00	13.94	0.06
DB02-216_PI2_2_76	150	Plagioclase	46.63	0.01	33.16	0.44	0.00	0.22	17.22	1.61	0.00	0.04	99.34	85.53	14.47	0.00
DB02-216_PI2_2_77	152	Plagioclase	47.12	0.05	33.27	0.41	0.09	0.22	17.25	1.66	0.01	0.10	100.19	85.13	14.82	0.05
DB02-216_PI2_2_78	154	Plagioclase	47.03	0.00	33.30	0.48	0.08	0.24	17.33	1.55	0.00	0.00	100.00	86.05	13.95	0.00
Plagioclase xenocryst 3 - profile 1																
DB02-216_PI3_1_1	0	Inclusion	46.22	0.88	7.38	16.40	0.38	13.59	10.22	1.66	0.05	0.17	96.95			
DB02-216_PI3_1_2	4	Inclusion	47.28	0.98	6.58	15.01	0.34	14.51	12.36	1.18	0.02	0.12	98.39			
DB02-216_PI3_1_3	8	Inclusion	48.50	0.74	6.93	14.51	0.25	13.54	11.87	1.14	0.02	0.04	97.54			
DB02-216_PI3_1_4	12	Inclusion	47.95	1.39	6.45	15.49	0.36	12.96	12.52	0.94	0.02	0.05	98.12			
DB02-216_PI3_1_5	16	Inclusion	48.90	0.98	4.88	14.07	0.32	14.94	14.06	0.44	0.02	0.04	98.64			
DB02-216_PI3_1_6	20	Inclusion	49.05	0.86	4.89	13.59	0.22	15.12	13.83	0.69	0.01	0.00	98.26			
DB02-216_PI3_1_7	24	Inclusion	48.77	1.09	5.66	14.38	0.38	15.94	12.57	0.66	0.02	0.00	99.47			
DB02-216_PI3_1_8	28	Inclusion	48.28	0.93	5.51	15.15	0.30	15.52	12.27	0.48	0.01	0.00	98.44			
DB02-216_PI3_1_9	32	Inclusion	50.70	0.62	9.84	11.59	0.27	10.88	12.21	2.18	0.03	0.00	98.33			
DB02-216_PI3_1_10	36	Inclusion	47.75	0.88	6.25	14.18	0.24	14.77	12.03	1.08	0.03	0.21	97.42			
DB02-216_PI3_1_11	40	Inclusion	50.43	0.68	9.26	12.60	0.32	13.44	10.71	1.70	0.03	0.16	99.34			
DB02-216_PI3_1_12	44	Inclusion	50.60	0.92	6.01	13.78	0.35	14.69	12.78	0.92	0.00	0.00	100.06			
DB02-216_PI3_1_13	48	Inclusion	51.92	0.63	10.28	10.36	0.25	10.41	11.19	2.53	0.02	0.00	97.58			
DB02-216_PI3_1_14	52	Inclusion	46.44	0.71	4.60	24.22	0.24	13.45	6.74	0.45	0.02	0.10	96.96			
DB02-216_PI3_1_15	56	Inclusion	49.29	0.89	5.13	15.28	0.36	14.53	12.53	0.81	0.02	0.02	98.88			
DB02-216_PI3_1_16	60	Inclusion	47.88	0.95	5.19	16.23	0.35	15.04	12.20	0.32	0.01	0.02	98.19			
DB02-216_PI3_1_17	64	Olivine pseudomorph	43.98	0.27	7.91	18.14	0.16	14.93	5.13	0.09	0.03	0.00	90.64			
DB02-216_PI3_1_18	68	Olivine pseudomorph	43.92	0.11	9.31	17.74	0.08	15.11	3.24	0.01	0.04	0.04	89.60			
DB02-216_PI3_1_19	72	Olivine pseudomorph	41.17	0.16	7.93	17.28	0.06	13.74	3.17	0.03	0.06	0.01	83.62			
DB02-216_PI3_1_20	76	Olivine pseudomorph	42.32	0.10	9.31	17.02	0.12	14.11	3.14	0.01	0.05	0.11	86.29			
DB02-216_PI3_1_21	80	Rim	46.02	0.11	13.12	12.44	0.15	8.06	3.78	1.96	0.07	0.09	85.81	51.06	47.82	1.12
DB02-216_PI3_1_22	84	Rim	50.69	0.02	26.30	2.18	0.10	1.26	10.31	4.37	0.02	0.03	95.29	56.50	43.35	0.15
DB02-216_PI3_1_23	88	Rim	49.23	0.03	30.86	0.77	0.03	0.36	15.16	2.81	0.01	0.08	99.34	74.83	25.13	0.04
DB02-216_PI3_1_24	92	Rim	47.85	0.02	32.37	0.64	0.06	0.29	16.35	2.07	0.01	0.00	99.67	81.26	18.65	0.09
DB02-216_PI3_1_25	96	Rim	45.49	0.00	34.14	0.42	0.10	0.18	18.26	1.06	0.00	0.01	99.66	90.47	9.53	0.00
DB02-216_PI3_1_26	100	Plagioclase	45.35	0.02	34.24	0.46	0.06	0.15	18.29	0.94	0.00	0.40	99.91	91.49	8.49	0.02
DB02-216_PI3_1_27	104	Plagioclase	45.32	0.03	34.28	0.42	0.00	0.17	18.29	0.99	0.01	0.04	99.56	90.99	8.96	0.05
DB02-216_PI3_1_28	108	Plagioclase	45.25	0.04	34.31	0.46	0.02	0.19	18.18	1.05	0.02	0.10	99.64	90.42	9.45	0.12
DB02-216_PI3_1_29	112	Plagioclase	45.17	0.03	34.19	0.52	0.04	0.13	18.36	0.98	0.00	0.00	99.44	91.14	8.84	0.02
DB02-216_PI3_1_30	116	Plagioclase	45.12	0.00	34.08	0.54	0.08	0.15	18.36	0.98	0.02	0.00	99.33	91.09	8.81	0.10
DB02-216_PI3_1_31	120	Plagioclase	45.40	0.02	34.13	0.45	0.00	0.15	18.35	1.04	0.01	0.00	99.55	90.64	9.32	0.04
DB02-216_PI3_1_32	124	Plagioclase	45.18	0.02	34.28	0.43	0.00	0.16	18.25	0.97	0.00	0.15	99.45	91.23	8.75	0.03
DB02-216_PI3_1_33	128	Plagioclase	45.37	0.06	34.58	0.47	0.06	0.18	18.34	1.01	0.00	0.09	100.16	90.88	9.08	0.04
DB02-216_PI3_1_34	132	Plagioclase	45.34	0.03	34.18	0.36	0.04	0.17	18.24	1.04	0.00	0.09	99.48	90.68	9.32	0.00
DB02-216_PI3_1_35	136	Plagioclase	45.32	0.04	34.18	0.31	0.09	0.17	18.24	1.06	0.00	0.08	99.49	90.53	9.47	0.00
DB02-216_PI3_1_36	140	Plagioclase	45.06	0.02	34.09	0.39	0.11	0.16	18.19	1.02	0.00	0.08	99.11	90.80	9.18	0.01
DB02-216_PI3_1_37	144	Plagioclase	45.55	0.06	34.31	0.46	0.00	0.18	18.08	0.94	0.01	0.09	99.68	91.35	8.61	0.04

Table 7. DB02-216 plagioclases and melt inclusions, XRF analyses (continued)

Label	Profile (µm)	Material	SiO2	TiO2	Al2O3	FeO	MnO	MgO	CaO	Na2O	K2O	BaO	Total	An	Ab	Or
Plagioclase xenocryst 3 - profile 1 (continued)																
DB02-216_PI3_1_38	148	Plagioclase	45.26	0.07	34.00	0.39	0.00	0.16	18.13	1.03	0.00	0.04	99.09	90.64	9.36	0.00
DB02-216_PI3_1_39	152	Plagioclase	44.93	0.05	34.06	0.34	0.02	0.14	18.14	1.06	0.00	0.10	98.85	90.42	9.55	0.02
DB02-216_PI3_1_40	156	Plagioclase	45.15	0.00	34.24	0.42	0.04	0.14	18.27	1.03	0.01	0.00	99.29	90.74	9.23	0.04
DB02-216_PI3_1_41	160	Plagioclase	45.53	0.01	34.38	0.39	0.00	0.17	18.20	1.07	0.00	0.01	99.77	90.37	9.63	0.00
DB02-216_PI3_1_42	164	Plagioclase	45.08	0.04	34.07	0.42	0.00	0.19	18.14	1.06	0.01	0.00	99.01	90.43	9.53	0.05
DB02-216_PI3_1_43	168	Plagioclase	45.50	0.07	34.18	0.46	0.10	0.16	18.21	1.06	0.00	0.23	99.97	90.45	9.55	0.01
DB02-216_PI3_1_44	172	Plagioclase	45.39	0.01	34.20	0.33	0.01	0.17	18.09	1.01	0.00	0.01	99.23	90.84	9.16	0.00
DB02-216_PI3_1_45	176	Plagioclase	45.42	0.02	34.21	0.44	0.00	0.14	18.29	1.06	0.00	0.13	99.72	90.46	9.53	0.01
DB02-216_PI3_1_46	180	Plagioclase	45.23	0.03	33.93	0.41	0.04	0.18	18.06	1.07	0.01	0.00	98.96	90.27	9.68	0.05
DB02-216_PI3_1_47	184	Plagioclase	45.54	0.01	34.23	0.43	0.04	0.18	18.28	1.16	0.00	0.05	99.91	89.69	10.31	0.00
Plagioclase xenocryst 3 - profile 2																
DB02-216_PI3_2_1	0	Inclusion	48.99	0.98	5.61	13.68	0.32	14.68	14.02	0.89	0.02	0.00	99.19			
DB02-216_PI3_2_2	4	Inclusion	48.34	1.02	6.54	13.95	0.23	13.97	12.83	1.48	0.04	0.01	98.40			
DB02-216_PI3_2_3	8	Inclusion	48.95	0.95	5.68	15.01	0.38	13.86	12.86	0.77	0.02	0.01	98.49			
DB02-216_PI3_2_4	12	Inclusion	51.71	0.73	7.24	11.93	0.33	13.21	12.13	1.86	0.03	0.06	99.24			
DB02-216_PI3_2_5	16	Inclusion	49.82	0.81	5.52	14.18	0.31	15.08	12.35	0.96	0.01	0.00	99.05			
DB02-216_PI3_2_6	20	Inclusion	45.38	1.30	8.82	14.36	0.29	13.87	10.91	2.56	0.04	0.09	97.61			
DB02-216_PI3_2_7	24	Inclusion	50.10	0.91	5.80	14.89	0.34	14.03	13.09	0.85	0.03	0.12	100.16			
DB02-216_PI3_2_8	28	Inclusion	52.65	0.61	13.43	8.57	0.17	6.94	9.16	3.98	0.04	0.00	95.56			
DB02-216_PI3_2_9	32	Inclusion	50.37	0.81	6.50	13.75	0.27	13.82	11.55	1.39	0.03	0.00	98.50			
DB02-216_PI3_2_10	36	Inclusion	48.96	0.94	6.03	14.20	0.27	14.16	11.92	0.81	0.02	0.00	97.31			
DB02-216_PI3_2_11	40	Inclusion	48.90	0.92	4.82	14.53	0.35	15.72	11.92	0.32	0.00	0.00	97.47			
DB02-216_PI3_2_12	44	Inclusion	47.54	1.17	2.74	23.16	0.48	17.52	5.30	0.16	0.02	0.00	98.09			
DB02-216_PI3_2_13	48	Inclusion	50.02	0.93	6.68	14.35	0.37	14.15	11.67	1.25	0.02	0.00	99.45			
DB02-216_PI3_2_14	52	Inclusion	49.40	1.06	5.47	14.26	0.41	14.29	12.74	0.66	0.01	0.00	98.31			
DB02-216_PI3_2_15	56	Inclusion	49.44	0.83	3.96	14.91	0.36	14.45	13.90	0.41	0.02	0.00	98.28			
DB02-216_PI3_2_16	60	Inclusion	48.33	0.93	5.41	14.59	0.37	15.10	12.43	0.71	0.01	0.00	97.89			
DB02-216_PI3_2_17	64	Inclusion	51.07	0.73	10.53	10.34	0.24	12.05	11.40	2.22	0.02	0.00	98.58			
DB02-216_PI3_2_18	68	Inclusion	47.36	1.11	5.20	15.20	0.30	15.72	11.51	0.33	0.02	0.00	96.74			
DB02-216_PI3_2_19	72	Inclusion	48.83	1.14	5.26	13.25	0.38	16.86	12.20	0.26	0.01	0.05	98.25			
DB02-216_PI3_2_20	76	Inclusion	49.42	0.94	7.34	12.63	0.27	14.81	12.44	0.81	0.00	0.16	98.83			
DB02-216_PI3_2_21	80	Rim	51.47	0.06	28.11	1.88	0.07	1.28	12.81	3.63	0.00	0.04	99.35	66.10	33.88	0.03
DB02-216_PI3_2_22	84	Rim	48.23	0.00	31.79	0.75	0.07	0.27	16.25	2.30	0.01	0.00	99.67	79.56	20.41	0.03
DB02-216_PI3_2_23	88	Plagioclase	45.66	0.05	33.59	0.48	0.07	0.19	17.73	1.35	0.02	0.05	99.19	87.78	12.10	0.12
DB02-216_PI3_2_24	92	Plagioclase	46.04	0.00	33.81	0.56	0.07	0.20	17.87	1.25	0.01	0.00	99.81	88.69	11.25	0.06
DB02-216_PI3_2_25	96	Plagioclase	45.91	0.01	33.93	0.43	0.01	0.20	17.97	1.18	0.01	0.05	99.71	89.32	10.62	0.06
DB02-216_PI3_2_26	100	Plagioclase	45.91	0.00	33.98	0.53	0.01	0.18	18.02	1.17	0.00	0.03	99.82	89.46	10.54	0.00
DB02-216_PI3_2_27	104	Plagioclase	45.69	0.00	34.04	0.41	0.01	0.17	18.05	1.13	0.00	0.00	99.49	89.82	10.18	0.00
DB02-216_PI3_2_28	108	Plagioclase	45.66	0.04	34.28	0.50	0.02	0.18	18.15	1.05	0.00	0.20	100.09	90.51	9.49	0.00
DB02-216_PI3_2_29	112	Plagioclase	45.53	0.02	34.38	0.32	0.05	0.16	18.14	1.05	0.01	0.14	99.79	90.50	9.46	0.05
DB02-216_PI3_2_30	116	Plagioclase	45.56	0.01	33.84	0.42	0.06	0.21	18.13	1.15	0.01	0.00	99.40	89.62	10.31	0.07
DB02-216_PI3_2_31	120	Plagioclase	45.58	0.07	34.29	0.48	0.09	0.20	18.02	1.15	0.00	0.09	99.97	89.62	10.38	0.00
DB02-216_PI3_2_32	124	Plagioclase	45.61	0.02	33.71	0.43	0.06	0.19	18.12	1.16	0.00	0.00	99.30	89.62	10.38	0.00

Table 7. DB02-216 plagioclases and melt inclusions, XRF analyses (continued)

Label	Profile (µm)	Material	SiO2	TiO2	Al2O3	FeO	MnO	MgO	CaO	Na2O	K2O	BaO	Total	An	Ab	Or
Plagioclase xenocryst 3 - profile 2 (continued)																	
DB02-216_PI3_2_33	128	Plagioclase	46.10	0.00	34.05	0.35	0.07	0.15	17.89	1.13	0.00	0.00	99.74	89.76	10.23	0.01
DB02-216_PI3_2_34	132	Plagioclase	46.08	0.04	33.83	0.51	0.01	0.19	17.76	1.28	0.00	0.12	99.83	88.47	11.50	0.03
DB02-216_PI3_2_35	136	Plagioclase	46.06	0.00	33.85	0.42	0.07	0.19	17.82	1.31	0.00	0.18	99.90	88.25	11.73	0.02
DB02-216_PI3_2_36	140	Plagioclase	46.28	0.00	33.82	0.38	0.00	0.20	17.63	1.35	0.00	0.00	99.66	87.81	12.16	0.03
DB02-216_PI3_2_37	144	Plagioclase	45.97	0.06	33.84	0.42	0.06	0.20	17.70	1.36	0.00	0.15	99.76	87.76	12.24	0.00
DB02-216_PI3_2_38	148	Plagioclase	46.16	0.02	33.78	0.46	0.07	0.20	17.70	1.36	0.00	0.00	99.74	87.82	12.18	0.00
DB02-216_PI3_2_39	152	Plagioclase	46.37	0.00	33.60	0.48	0.07	0.22	17.62	1.34	0.01	0.09	99.79	87.85	12.09	0.06
DB02-216_PI3_2_40	156	Plagioclase	46.45	0.04	33.61	0.40	0.06	0.24	17.66	1.37	0.01	0.00	99.83	87.66	12.30	0.04
DB02-216_PI3_2_41	160	Plagioclase	46.26	0.00	33.64	0.38	0.05	0.22	17.61	1.42	0.01	0.10	99.70	87.17	12.76	0.07
DB02-216_PI3_2_42	164	Plagioclase	46.24	0.00	33.44	0.41	0.07	0.12	17.79	1.29	0.01	0.15	99.52	88.35	11.61	0.03
DB02-216_PI3_2_43	168	Plagioclase	45.81	0.00	33.59	0.40	0.01	0.20	17.88	1.30	0.01	0.09	99.29	88.38	11.58	0.04
DB02-216_PI3_2_44	172	Plagioclase	45.80	0.01	33.60	0.38	0.04	0.20	17.77	1.33	0.02	0.00	99.14	88.00	11.91	0.09
DB02-216_PI3_2_45	176	Plagioclase	46.13	0.00	33.65	0.36	0.04	0.19	17.69	1.42	0.01	0.00	99.50	87.28	12.67	0.06
DB02-216_PI3_2_46	180	Plagioclase	46.06	0.02	33.39	0.47	0.01	0.23	17.71	1.40	0.01	0.00	99.31	87.44	12.53	0.03
DB02-216_PI3_2_47	184	Plagioclase	46.68	0.05	33.63	0.38	0.04	0.20	17.71	1.41	0.01	0.00	100.10	87.40	12.57	0.03
Plagioclase xenocryst 3 - profile 3																	
DB02-216_PI3_3_1	0	Inclusion	49.26	1.23	6.14	14.91	0.24	14.31	12.32	1.13	0.02	0.04	99.61			
DB02-216_PI3_3_2	3	Inclusion	49.19	1.13	4.95	14.16	0.31	16.39	12.46	0.53	0.01	0.10	99.24			
DB02-216_PI3_3_3	6	Inclusion	47.01	1.07	5.64	16.33	0.34	14.34	12.27	0.89	0.02	0.07	97.97			
DB02-216_PI3_3_4	9	Inclusion	47.52	1.74	6.55	16.23	0.35	13.43	12.37	1.39	0.03	0.00	99.61			
DB02-216_PI3_3_5	12	Inclusion	50.24	0.92	5.29	14.69	0.28	15.09	12.26	0.64	0.03	0.05	99.49			
DB02-216_PI3_3_6	15	Inclusion	50.13	0.98	5.32	15.13	0.35	14.29	12.47	0.82	0.02	0.05	99.57			
DB02-216_PI3_3_7	18	Inclusion	48.09	0.58	4.76	17.18	0.28	17.31	8.27	0.14	0.03	0.00	96.63			
DB02-216_PI3_3_8	21	Olivine pseudomorph	40.42	0.05	8.83	17.07	0.15	16.93	2.12	0.06	0.08	0.00	85.70			
DB02-216_PI3_3_9	24	Olivine pseudomorph	40.50	0.03	8.72	16.84	0.08	17.35	1.87	0.07	0.09	0.00	85.56			
DB02-216_PI3_3_10	27	Olivine pseudomorph	41.27	0.03	9.30	17.10	0.11	17.55	1.94	0.05	0.08	0.00	87.44			
DB02-216_PI3_3_11	30	Olivine pseudomorph	42.04	0.08	8.94	17.36	0.11	18.22	1.95	0.06	0.09	0.00	88.86			
DB02-216_PI3_3_12	33	Inclusion	44.87	0.24	13.54	11.58	0.12	8.58	5.47	3.55	0.07	0.11	88.14			
DB02-216_PI3_3_13	36	Inclusion	44.57	1.82	5.21	23.70	0.35	13.41	10.21	0.72	0.00	0.19	100.20			
DB02-216_PI3_3_14	39	Inclusion	49.01	1.08	5.13	15.67	0.34	14.88	12.26	0.68	0.02	0.00	99.08			
DB02-216_PI3_3_15	42	Inclusion	49.36	1.17	5.10	14.49	0.31	15.20	12.93	0.67	0.02	0.00	99.23			
DB02-216_PI3_3_16	45	Inclusion	49.53	0.99	5.15	14.92	0.37	15.07	12.62	0.54	0.01	0.00	99.20			
DB02-216_PI3_3_17	48	Inclusion	49.02	1.10	5.83	15.58	0.32	14.12	12.32	1.15	0.01	0.05	99.51			
DB02-216_PI3_3_18	51	Inclusion	49.13	1.11	4.96	15.34	0.35	15.48	12.40	0.64	0.02	0.00	99.41			
DB02-216_PI3_3_19	54	Rim	53.36	0.06	27.17	1.08	0.07	0.79	12.60	4.18	0.02	0.00	99.33	62.40	37.47	0.14
DB02-216_PI3_3_20	57	Rim	50.72	0.04	30.49	0.67	0.04	0.37	14.52	3.16	0.01	0.00	100.02	71.69	28.25	0.06
DB02-216_PI3_3_21	60	Rim	46.96	0.03	33.40	0.51	0.00	0.24	17.39	1.64	0.01	0.00	100.17	85.38	14.57	0.05
DB02-216_PI3_3_22	63	Plagioclase	46.41	0.08	33.87	0.42	0.06	0.16	17.84	1.18	0.00	0.00	100.02	89.32	10.66	0.02
DB02-216_PI3_3_23	66	Plagioclase	46.41	0.00	33.42	0.34	0.00	0.16	17.88	1.23	0.01	0.06	99.52	88.85	11.11	0.04
DB02-216_PI3_3_24	69	Plagioclase	46.04	0.04	33.97	0.46	0.03	0.19	17.80	1.18	0.00	0.00	99.72	89.27	10.73	0.00
DB02-216_PI3_3_25	72	Plagioclase	46.12	0.05	33.94	0.46	0.04	0.18	17.87	1.17	0.00	0.15	99.98	89.44	10.56	0.00
DB02-216_PI3_3_26	75	Plagioclase	46.08	0.01	33.96	0.50	0.00	0.20	17.97	1.29	0.02	0.00	100.03	88.42	11.46	0.12
DB02-216_PI3_3_27	78	Plagioclase	45.94	0.00	34.05	0.44	0.03	0.20	17.88	1.20	0.00	0.00	99.75	89.12	10.86	0.02

Table 7. DB02-216 plagioclases and melt inclusions, XRF analyses (continued)

Label	Profile (µm)	Material	SiO2	TiO2	Al2O3	FeO	MnO	MgO	CaO	Na2O	K2O	BaO	Total	An	Ab	Or
Plagioclase xenocryst 3 - profile 3 (continued)																	
DB02-216_Pl3_3_28	81	Plagioclase	46.46	0.02	33.84	0.54	0.06	0.15	17.93	1.20	0.01	0.14	100.36	89.14	10.79	0.07
DB02-216_Pl3_3_29	84	Plagioclase	46.17	0.00	33.85	0.41	0.06	0.18	18.02	1.18	0.00	0.04	99.91	89.37	10.63	0.00
DB02-216_Pl3_3_30	87	Plagioclase	46.17	0.01	33.97	0.46	0.00	0.20	18.03	1.19	0.01	0.00	100.04	89.30	10.70	0.01
DB02-216_Pl3_3_31	90	Plagioclase	46.23	0.00	34.11	0.47	0.03	0.20	17.90	1.18	0.01	0.04	100.16	89.33	10.64	0.03
DB02-216_Pl3_3_32	93	Plagioclase	45.83	0.02	33.97	0.49	0.04	0.22	17.95	1.19	0.01	0.00	99.73	89.27	10.68	0.05
DB02-216_Pl3_3_33	96	Plagioclase	46.41	0.00	33.79	0.44	0.04	0.18	18.03	1.24	0.01	0.32	100.13	88.92	11.03	0.05
DB02-216_Pl3_3_34	99	Plagioclase	45.88	0.04	33.93	0.41	0.07	0.16	18.08	1.21	0.01	0.00	100.10	89.15	10.82	0.03
DB02-216_Pl3_3_35	102	Plagioclase	45.89	0.00	33.79	0.40	0.05	0.19	17.95	1.14	0.00	0.00	99.41	89.64	10.34	0.02
DB02-216_Pl3_3_36	105	Plagioclase	45.91	0.00	34.09	0.38	0.08	0.13	18.32	1.08	0.01	0.00	99.98	90.37	9.63	0.00
DB02-216_Pl3_3_37	108	Plagioclase	45.95	0.05	34.40	0.39	0.09	0.18	18.27	1.07	0.01	0.04	100.45	90.38	9.55	0.07
DB02-216_Pl3_3_38	111	Plagioclase	46.21	0.02	34.33	0.42	0.08	0.21	18.16	1.06	0.00	0.08	100.58	90.42	9.58	0.00
DB02-216_Pl3_3_39	114	Plagioclase	45.78	0.02	34.05	0.42	0.03	0.19	18.24	1.03	0.00	0.00	99.77	90.74	9.25	0.01
DB02-216_Pl3_3_40	117	Plagioclase	45.91	0.07	34.36	0.47	0.00	0.14	18.39	1.07	0.00	0.00	100.41	90.44	9.56	0.00
DB02-216_Pl3_3_41	120	Plagioclase	45.69	0.09	34.28	0.36	0.03	0.18	18.36	0.98	0.01	0.00	99.97	91.18	8.78	0.05
DB02-216_Pl3_3_42	123	Plagioclase	45.96	0.04	34.14	0.40	0.07	0.16	18.27	1.08	0.01	0.18	100.31	90.32	9.64	0.05
DB02-216_Pl3_3_43	126	Plagioclase	46.03	0.00	34.27	0.51	0.00	0.17	18.19	1.01	0.00	0.01	100.20	90.86	9.13	0.01
DB02-216_Pl3_3_44	129	Plagioclase	45.98	0.00	34.04	0.46	0.08	0.17	18.21	1.02	0.01	0.00	99.97	90.72	9.22	0.06
DB02-216_Pl3_3_45	132	Plagioclase	46.18	0.02	34.42	0.50	0.01	0.15	18.13	1.04	0.00	0.00	100.46	90.58	9.42	0.00
DB02-216_Pl3_3_46	135	Plagioclase	45.64	0.05	34.44	0.46	0.00	0.16	18.19	1.10	0.00	0.00	100.04	90.16	9.84	0.00
DB02-216_Pl3_3_47	138	Plagioclase	45.77	0.00	34.23	0.56	0.00	0.19	18.27	0.98	0.00	0.04	100.04	91.19	8.81	0.00
Plagioclase xenocryst 7 - profile 1																	
DB02-216_Pl7_1_1	0	Inclusion	48.24	1.54	4.76	21.08	0.46	4.30	17.61	1.25	0.04	0.01	99.29			
DB02-216_Pl7_1_2	3	Inclusion	51.90	1.17	9.16	14.69	0.37	3.09	14.45	3.24	0.07	0.00	98.15			
DB02-216_Pl7_1_3	6	Inclusion	48.45	1.54	4.06	21.38	0.47	4.17	18.46	0.96	0.02	0.02	99.54			
DB02-216_Pl7_1_4	9	Inclusion	40.35	0.39	7.16	23.79	0.22	12.65	5.92	0.25	0.01	0.00	90.73			
DB02-216_Pl7_1_5	12	Inclusion	42.07	12.32	6.92	12.08	0.10	4.33	16.67	1.92	0.07	0.00	96.48			
DB02-216_Pl7_1_6	15	Inclusion	47.93	2.27	5.45	19.71	0.44	5.38	17.39	1.14	0.04	0.00	99.74			
DB02-216_Pl7_1_7	18	Inclusion	47.35	1.46	5.28	19.66	0.30	6.77	15.33	0.90	0.05	0.17	97.27			
DB02-216_Pl7_1_8	21	Inclusion	49.18	2.11	5.47	20.12	0.43	4.70	17.75	1.28	0.04	0.00	101.08			
DB02-216_Pl7_1_9	24	Inclusion	45.24	1.43	7.70	19.62	0.33	7.07	12.09	1.48	0.06	0.05	95.06			
DB02-216_Pl7_1_10	27	Inclusion	46.53	2.33	3.07	20.88	0.42	4.62	20.91	0.29	0.06	0.10	99.15			
DB02-216_Pl7_1_11	30	Inclusion	54.24	8.14	14.32	3.63	0.20	1.20	10.87	5.27	0.04	0.00	97.92			
DB02-216_Pl7_1_12	33	Inclusion	44.81	0.92	5.89	19.91	0.35	6.20	14.20	0.73	0.02	0.09	93.10			
DB02-216_Pl7_1_13	36	Inclusion	46.51	2.33	3.38	20.34	0.34	4.90	20.80	0.27	0.00	0.00	98.88			
DB02-216_Pl7_1_14	39	Inclusion	47.72	1.34	6.46	20.12	0.46	5.68	16.03	1.50	0.04	0.20	99.54			
DB02-216_Pl7_1_15	42	Inclusion	43.08	0.89	9.00	21.62	0.27	11.42	7.57	1.22	0.06	0.02	95.14			
DB02-216_Pl7_1_16	45	Inclusion	50.60	1.21	8.32	16.19	0.23	4.09	14.41	3.06	0.09	0.06	98.26			
DB02-216_Pl7_1_17	48	Inclusion	51.87	0.97	13.51	12.13	0.28	3.40	11.94	3.64	0.02	0.09	97.85			
DB02-216_Pl7_1_18	51	Inclusion	47.53	2.16	6.29	19.16	0.40	5.31	16.50	1.28	0.02	0.00	98.65			
DB02-216_Pl7_1_19	54	Inclusion	46.81	1.86	5.68	19.63	0.36	6.59	16.12	1.02	0.03	0.26	98.36			
DB02-216_Pl7_1_20	57	Inclusion	47.42	1.57	7.89	18.34	0.35	6.51	13.53	1.76	0.06	0.04	97.45			
DB02-216_Pl7_1_21	60	Inclusion	46.30	1.63	6.21	18.38	0.30	6.35	14.25	0.94	0.05	0.00	94.43			
DB02-216_Pl7_1_22	63	Inclusion	45.00	1.53	6.14	20.40	0.31	9.05	11.89	0.66	0.03	0.00	95.01			

Table 7. DB02-216 plagioclases and melt inclusions, XRF analyses (continued)

Label	Profile (µm)	Material	SiO2	TiO2	Al2O3	FeO	MnO	MgO	CaO	Na2O	K2O	BaO	Total	An	Ab	Or
Plagioclase xenocryst 7 - profile 1 (continued)																
DB02-216_PI7_1_23	66	Inclusion	48.58	0.91	7.73	15.91	0.36	4.14	14.99	2.19	0.06	0.00	94.87			
DB02-216_PI7_1_24	69	Inclusion	49.78	1.93	7.88	15.30	0.41	3.72	17.85	2.02	0.02	0.00	98.93			
DB02-216_PI7_1_25	72	Rim	54.10	0.59	21.79	4.01	0.15	0.89	12.48	4.64	0.01	0.16	98.83	59.72	40.20	0.08
DB02-216_PI7_1_26	75	Rim	52.46	0.05	28.91	1.00	0.00	0.34	13.57	3.71	0.00	0.00	100.04	66.91	33.07	0.03
DB02-216_PI7_1_27	78	Rim	49.28	0.05	30.79	1.06	0.03	0.49	15.34	2.55	0.01	0.00	99.59	76.85	23.09	0.06
DB02-216_PI7_1_28	81	Rim	46.83	0.09	31.90	1.31	0.08	0.66	16.53	1.72	0.01	0.00	99.13	84.10	15.86	0.04
DB02-216_PI7_1_29	84	Rim	47.31	0.00	33.21	0.37	0.11	0.20	17.10	1.66	0.01	0.23	100.21	85.00	14.96	0.05
DB02-216_PI7_1_30	87	Rim	46.61	0.09	33.36	0.45	0.00	0.22	17.47	1.34	0.01	0.00	99.56	87.74	12.21	0.05
DB02-216_PI7_1_31	90	Rim	46.13	0.00	33.83	0.46	0.05	0.19	17.83	1.37	0.00	0.19	100.06	87.79	12.20	0.01
DB02-216_PI7_1_32	93	Rim	47.05	0.12	33.71	0.50	0.11	0.21	17.46	1.45	0.00	0.05	100.65	86.88	13.09	0.02
DB02-216_PI7_1_33	96	Rim	47.79	0.01	32.75	0.53	0.02	0.20	16.93	1.73	0.02	0.00	99.98	84.28	15.59	0.12
DB02-216_PI7_1_34	99	Plagioclase	47.75	0.00	32.75	0.59	0.00	0.24	17.02	1.80	0.01	0.03	100.18	83.93	16.04	0.03
DB02-216_PI7_1_35	102	Plagioclase	47.74	0.00	32.84	0.41	0.05	0.26	16.88	1.77	0.00	0.03	99.98	84.01	15.98	0.01
DB02-216_PI7_1_36	105	Plagioclase	47.80	0.07	32.72	0.46	0.01	0.27	16.93	1.79	0.00	0.00	100.05	83.92	16.08	0.00
DB02-216_PI7_1_37	108	Plagioclase	47.91	0.00	32.45	0.60	0.08	0.26	16.80	1.81	0.02	0.00	99.92	83.59	16.30	0.11
DB02-216_PI7_1_38	111	Plagioclase	47.38	0.05	32.44	0.47	0.05	0.23	17.03	1.77	0.00	0.00	99.43	84.14	15.84	0.02
DB02-216_PI7_1_39	114	Plagioclase	47.47	0.04	32.53	0.51	0.07	0.29	17.01	1.80	0.02	0.00	99.73	83.89	16.10	0.01
DB02-216_PI7_1_40	117	Plagioclase	47.80	0.02	32.72	0.46	0.06	0.28	17.08	1.79	0.00	0.00	100.23	84.01	15.90	0.09
DB02-216_PI7_1_41	120	Plagioclase	47.52	0.01	32.87	0.46	0.03	0.31	16.94	1.84	0.01	0.24	100.22	83.59	16.39	0.02
DB02-216_PI7_1_42	123	Plagioclase	47.61	0.06	32.92	0.47	0.01	0.26	17.05	1.80	0.01	0.15	100.33	83.95	16.00	0.05
DB02-216_PI7_1_43	126	Plagioclase	48.00	0.01	33.13	0.53	0.06	0.25	17.07	1.72	0.01	0.00	100.78	84.54	15.40	0.06
DB02-216_PI7_1_44	129	Plagioclase	47.97	0.05	33.01	0.55	0.00	0.27	17.15	1.77	0.01	0.14	100.93	84.18	15.75	0.07
DB02-216_PI7_1_45	132	Plagioclase	47.69	0.00	32.68	0.53	0.00	0.23	17.17	1.75	0.00	0.00	100.07	84.41	15.56	0.02
DB02-216_PI7_1_46	135	Plagioclase	47.50	0.03	33.06	0.46	0.14	0.23	17.13	1.68	0.01	0.20	100.46	84.87	15.10	0.03
Plagioclase xenocryst 7 - profile 2																
DB02-216_PI7_2_1	0	Inclusion	44.70	0.10	10.73	11.49	0.10	10.97	3.66	1.91	0.09	0.00	83.75			
DB02-216_PI7_2_2	2	Inclusion	42.30	0.13	9.10	15.96	0.07	13.80	3.41	0.07	0.08	0.00	84.92			
DB02-216_PI7_2_3	4	Inclusion	42.26	0.15	9.21	16.00	0.04	13.52	3.54	0.06	0.05	0.00	84.84			
DB02-216_PI7_2_4	6	Inclusion	40.24	0.27	8.02	19.64	0.25	13.26	5.76	0.17	0.05	0.00	87.66			
DB02-216_PI7_2_5	8	Inclusion	48.86	1.21	3.82	16.62	0.39	14.85	12.28	0.55	0.02	0.27	98.86			
DB02-216_PI7_2_6	10	Inclusion	44.11	1.06	6.48	19.66	0.31	14.59	7.62	0.49	0.07	0.15	94.54			
DB02-216_PI7_2_7	12	Inclusion	43.49	0.87	7.09	20.14	0.31	14.28	5.79	0.74	0.10	0.00	92.80			
DB02-216_PI7_2_8	14	Inclusion	37.98	0.21	7.50	20.73	0.18	13.36	2.72	0.12	0.08	0.19	83.05			
DB02-216_PI7_2_9	16	Inclusion	42.08	0.12	9.40	19.59	0.17	14.61	2.98	0.15	0.09	0.00	89.18			
DB02-216_PI7_2_10	18	Inclusion	42.65	0.19	10.39	17.79	0.18	11.33	3.99	1.08	0.05	0.00	87.66			
DB02-216_PI7_2_11	20	Inclusion	49.89	1.06	7.91	15.24	0.28	12.05	11.72	1.47	0.03	0.04	99.69			
DB02-216_PI7_2_12	22	Inclusion	50.67	1.18	7.36	13.93	0.33	12.50	11.68	1.57	0.01	0.00	99.23			
DB02-216_PI7_2_13	24	Inclusion	49.57	1.43	5.05	16.32	0.37	14.05	12.03	0.75	0.02	0.00	99.59			
DB02-216_PI7_2_14	26	Inclusion	50.20	1.22	5.38	15.40	0.31	13.96	12.44	0.89	0.01	0.12	99.93			
DB02-216_PI7_2_15	28	Inclusion	50.03	1.35	5.57	14.75	0.39	14.22	12.61	0.81	0.01	0.16	99.91			
DB02-216_PI7_2_16	30	Inclusion	49.76	1.38	5.55	15.33	0.34	14.36	12.33	0.78	0.01	0.00	99.83			
DB02-216_PI7_2_17	32	Inclusion	47.88	1.10	7.39	14.90	0.33	12.31	10.18	1.00	0.02	0.00	95.09			
DB02-216_PI7_2_18	34	Olivine pseudomorph	42.79	0.32	8.01	17.73	0.12	12.51	4.71	0.17	0.05	0.01	86.42			

Table 7. DB02-216 plagioclases and melt inclusions, XRF analyses (continued)

Plagioclase xenocryst 7 - profile 2 (continued)

Label	Profile (µm)	Material	SiO2	TiO2	Al2O3	FeO	MnO	MgO	CaO	Na2O	K2O	BaO	Total	An	Ab	Or
DB02-216_PI7_2_19	36	Olivine pseudomorph	45.13	0.14	9.50	17.99	0.11	15.02	3.32	0.10	0.11	0.02	91.45			
DB02-216_PI7_2_20	38	Olivine pseudomorph	45.30	0.13	9.67	17.82	0.12	15.21	3.27	0.12	0.11	0.02	91.78			
DB02-216_PI7_2_21	40	Olivine pseudomorph	45.13	0.07	9.24	17.99	0.08	15.41	3.25	0.11	0.08	0.02	91.38			
DB02-216_PI7_2_22	42	Olivine pseudomorph	42.46	0.11	8.60	17.94	0.08	14.59	3.16	0.06	0.09	0.01	87.10			
DB02-216_PI7_2_23	44	Olivine pseudomorph	44.50	0.21	9.52	18.22	0.12	15.35	3.38	0.09	0.08	0.00	91.48			
DB02-216_PI7_2_24	46	Olivine pseudomorph	44.69	0.15	8.85	18.91	0.20	14.60	3.65	0.12	0.07	0.00	91.24			
DB02-216_PI7_2_25	48	Olivine pseudomorph	42.50	0.14	8.09	19.99	0.19	14.42	3.54	0.07	0.04	0.00	88.99			
DB02-216_PI7_2_26	50	Inclusion	44.21	0.97	6.87	13.93	0.30	10.41	11.59	0.95	0.03	0.07	89.33			
DB02-216_PI7_2_27	52	Inclusion	49.14	1.16	6.47	13.62	0.26	12.79	11.84	1.39	0.05	0.01	96.73			
DB02-216_PI7_2_28	54	Inclusion	50.31	1.28	5.58	14.22	0.27	13.70	12.66	0.56	0.05	0.00	98.63			
DB02-216_PI7_2_29	56	Inclusion	49.69	1.19	4.52	15.94	0.39	14.89	12.16	0.41	0.00	0.06	99.26			
DB02-216_PI7_2_30	58	Inclusion	47.89	1.20	5.21	16.78	0.33	15.28	11.52	0.20	0.02	0.00	98.42			
DB02-216_PI7_2_31	60	Inclusion	50.03	1.37	4.73	15.85	0.43	14.82	12.57	0.56	0.02	0.00	100.37			
DB02-216_PI7_2_32	62	Inclusion	51.81	1.28	4.94	16.16	0.33	14.73	11.24	0.54	0.03	0.00	101.07			
DB02-216_PI7_2_33	64	Olivine pseudomorph	46.38	0.21	9.11	17.89	0.19	15.55	3.66	0.12	0.09	0.00	93.22			
DB02-216_PI7_2_34	66	Olivine pseudomorph	38.13	0.10	8.42	17.83	0.10	11.63	3.46	0.08	0.05	0.00	79.82			
DB02-216_PI7_2_35	68	Olivine pseudomorph	41.64	0.13	9.69	17.04	0.15	14.09	3.62	0.06	0.07	0.00	86.49			
DB02-216_PI7_2_36	70	Olivine pseudomorph	40.55	0.67	9.76	18.07	0.08	13.38	3.73	0.14	0.06	0.07	86.52			
DB02-216_PI7_2_37	72	Rim	48.91	0.22	18.22	9.35	0.12	6.77	8.83	3.15	0.04	0.03	95.64	60.58	39.11	0.32
DB02-216_PI7_2_38	74	Rim	49.50	0.05	31.42	0.66	0.00	0.30	15.72	2.58	0.02	0.09	100.34	77.00	22.89	0.11
DB02-216_PI7_2_39	76	Rim	48.32	0.08	32.17	0.71	0.09	0.27	16.37	2.24	0.01	0.18	100.44	80.10	19.84	0.06
DB02-216_PI7_2_40	78	Rim	46.72	0.01	33.57	0.57	0.04	0.18	17.50	1.47	0.01	0.00	100.08	86.77	13.15	0.08
DB02-216_PI7_2_41	80	Plagioclase	46.55	0.00	34.00	0.62	0.04	0.12	17.86	1.28	0.02	0.08	100.57	88.45	11.45	0.10
DB02-216_PI7_2_42	82	Plagioclase	46.76	0.06	33.82	0.54	0.05	0.17	17.76	1.26	0.00	0.00	100.43	88.57	11.40	0.02
DB02-216_PI7_2_43	84	Plagioclase	46.70	0.00	33.51	0.46	0.10	0.19	17.75	1.44	0.01	0.00	100.16	87.17	12.79	0.05
DB02-216_PI7_2_44	86	Plagioclase	46.47	0.01	34.12	0.44	0.00	0.21	17.57	1.36	0.01	0.00	100.19	87.71	12.26	0.03
DB02-216_PI7_2_45	88	Plagioclase	46.65	0.00	33.84	0.45	0.03	0.16	17.73	1.37	0.00	0.23	100.47	87.76	12.24	0.00
DB02-216_PI7_2_46	90	Plagioclase	46.60	0.07	33.75	0.57	0.06	0.21	17.71	1.29	0.01	0.00	100.27	88.31	11.62	0.07
DB02-216_PI7_2_47	92	Plagioclase	46.59	0.02	33.55	0.57	0.13	0.19	17.77	1.33	0.01	0.10	100.25	88.01	11.92	0.07
DB02-216_PI7_2_48	94	Plagioclase	46.58	0.01	33.83	0.50	0.01	0.21	17.62	1.33	0.01	0.06	100.15	87.98	11.99	0.04
DB02-216_PI7_2_49	96	Plagioclase	46.93	0.00	33.63	0.36	0.00	0.16	17.63	1.41	0.00	0.00	100.13	87.32	12.68	0.00
DB02-216_PI7_2_50	98	Plagioclase	46.55	0.03	33.76	0.50	0.05	0.21	17.73	1.33	0.01	0.03	100.20	88.02	11.90	0.08
DB02-216_PI7_2_51	100	Plagioclase	46.86	0.03	33.85	0.45	0.11	0.22	17.69	1.29	0.01	0.08	100.58	88.27	11.66	0.06
DB02-216_PI7_2_52	102	Plagioclase	46.59	0.01	33.72	0.45	0.01	0.20	17.60	1.39	0.01	0.20	100.18	87.48	12.48	0.05
DB02-216_PI7_2_53	104	Plagioclase	46.66	0.08	33.71	0.49	0.10	0.17	17.80	1.40	0.00	0.00	100.42	87.51	12.49	0.00
DB02-216_PI7_2_54	106	Plagioclase	46.94	0.02	33.54	0.53	0.00	0.19	17.72	1.44	0.00	0.17	100.55	87.18	12.82	0.00
DB02-216_PI7_2_55	108	Plagioclase	47.45	0.02	33.37	0.46	0.01	0.20	17.20	1.57	0.02	0.14	100.45	85.74	14.16	0.11
DB02-216_PI7_2_56	110	Plagioclase	48.18	0.00	32.73	0.54	0.04	0.25	16.83	1.91	0.01	0.00	100.49	82.95	17.00	0.06
DB02-216_PI7_2_57	112	Plagioclase	48.05	0.04	32.89	0.51	0.02	0.23	16.79	1.81	0.00	0.00	100.34	83.65	16.35	0.00
DB02-216_PI7_2_58	114	Plagioclase	47.56	0.02	32.72	0.47	0.06	0.24	16.93	1.80	0.00	0.01	99.80	83.89	16.11	0.00

Table 7. DB02-216 plagioclases and melt inclusions, XRF analyses (continued)

Label	Profile (µm)	Material	SiO2	TiO2	Al2O3	FeO	MnO	MgO	CaO	Na2O	K2O	BaO	Total	An	Ab	Or
		Plagioclase xenocryst 7 - profile 3															
DB02-216_PI7_3_1	0	Plagioclase	46.31	0.00	33.87	0.55	0.10	0.23	17.85	1.26	0.00	0.00	100.17	88.64	11.35	0.00
DB02-216_PI7_3_2	2	Plagioclase	46.35	0.05	33.87	0.50	0.08	0.21	17.81	1.25	0.00	0.00	100.12	88.72	11.28	0.00
DB02-216_PI7_3_3	4	Plagioclase	46.06	0.01	33.61	0.58	0.03	0.23	17.89	1.23	0.01	0.21	99.85	88.93	11.02	0.04
DB02-216_PI7_3_4	6	Plagioclase	46.12	0.11	33.85	0.49	0.02	0.21	17.89	1.23	0.00	0.12	100.02	88.96	11.04	0.00
DB02-216_PI7_3_5	8	Plagioclase	46.09	0.05	33.75	0.39	0.01	0.17	17.70	1.31	0.00	0.10	99.57	88.20	11.77	0.02
DB02-216_PI7_3_6	10	Plagioclase	46.28	0.05	33.81	0.49	0.03	0.22	17.77	1.24	0.00	0.00	99.89	88.78	11.20	0.02
DB02-216_PI7_3_7	12	Plagioclase	46.28	0.07	33.45	0.55	0.03	0.19	17.74	1.19	0.00	0.05	99.56	89.19	10.79	0.02
DB02-216_PI7_3_8	14	Plagioclase	46.61	0.03	33.59	0.57	0.02	0.19	17.91	1.28	0.00	0.01	100.20	88.55	11.45	0.00
DB02-216_PI7_3_9	16	Plagioclase	46.14	0.00	33.67	0.42	0.07	0.21	17.82	1.21	0.00	0.00	99.54	89.09	10.90	0.01
DB02-216_PI7_3_10	18	Plagioclase	46.45	0.00	33.85	0.49	0.02	0.23	17.67	1.24	0.01	0.05	100.01	88.66	11.29	0.05
DB02-216_PI7_3_11	20	Plagioclase	46.08	0.00	33.58	0.36	0.09	0.21	17.70	1.28	0.00	0.10	99.41	88.39	11.60	0.01
DB02-216_PI7_3_12	22	Plagioclase	46.72	0.02	33.73	0.58	0.00	0.18	17.94	1.41	0.00	0.00	100.58	87.55	12.45	0.00
DB02-216_PI7_3_13	24	Plagioclase	46.64	0.00	33.68	0.54	0.01	0.19	17.76	1.24	0.00	0.01	100.08	88.77	11.21	0.02
DB02-216_PI7_3_14	26	Plagioclase	46.77	0.05	33.78	0.60	0.04	0.19	17.67	1.29	0.00	0.01	100.38	88.32	11.66	0.01
DB02-216_PI7_3_15	28	Plagioclase	46.34	0.01	33.55	0.68	0.02	0.23	17.67	1.31	0.00	0.00	99.80	88.15	11.85	0.00
DB02-216_PI7_3_16	30	Plagioclase	46.76	0.05	33.46	0.58	0.00	0.22	17.54	1.35	0.00	0.00	99.97	87.74	12.24	0.02
DB02-216_PI7_3_17	32	Plagioclase	46.43	0.00	33.47	0.65	0.02	0.21	17.62	1.28	0.01	0.00	99.68	88.36	11.59	0.06
DB02-216_PI7_3_18	34	Plagioclase	46.49	0.01	33.58	0.60	0.03	0.18	17.62	1.35	0.01	0.33	100.21	87.78	12.14	0.08
DB02-216_PI7_3_19	36	Rim	47.13	0.01	33.12	0.63	0.05	0.23	17.52	1.27	0.01	0.03	100.00	88.39	11.57	0.04
DB02-216_PI7_3_20	38	Rim	44.23	0.02	25.73	9.16	0.00	4.97	11.12	0.89	0.03	0.00	96.16	87.08	12.64	0.28
DB02-216_PI7_3_21	40	Olivine pseudomorph	33.61	0.03	13.85	23.04	0.12	11.14	2.59	0.18	0.09	0.00	84.65			
DB02-216_PI7_3_22	42	Olivine pseudomorph	32.34	0.01	14.42	24.33	0.15	11.92	2.08	0.08	0.08	0.04	85.44			
DB02-216_PI7_3_23	44	Olivine pseudomorph	32.84	0.09	14.91	24.42	0.24	12.06	2.09	0.06	0.07	0.00	86.78			
DB02-216_PI7_3_24	46	Olivine pseudomorph	33.26	0.04	14.22	24.61	0.26	12.55	2.13	0.05	0.07	0.07	87.25			
DB02-216_PI7_3_25	48	Olivine pseudomorph	31.13	0.08	13.99	23.74	0.20	10.96	2.34	0.12	0.05	0.13	82.75			
DB02-216_PI7_3_26	50	Plagioclase	42.71	0.08	27.11	7.38	0.10	3.26	11.67	1.82	0.03	0.00	94.15	77.83	21.93	0.24
DB02-216_PI7_3_27	52	Plagioclase	51.53	0.00	29.98	0.96	0.04	0.42	14.04	3.22	0.02	0.00	100.20	70.61	29.27	0.13
DB02-216_PI7_3_28	54	Plagioclase	52.50	0.04	28.93	0.92	0.03	0.40	13.30	3.71	0.02	0.10	99.95	66.41	33.49	0.10
DB02-216_PI7_3_29	56	Plagioclase	52.47	0.13	25.19	2.50	0.13	1.99	12.74	3.95	0.02	0.00	99.14	63.96	35.90	0.14
DB02-216_PI7_3_30	58	Inclusion	49.25	1.21	5.13	14.85	0.36	14.62	12.71	0.61	0.02	0.02	98.78			
DB02-216_PI7_3_31	60	Inclusion	49.07	1.35	4.51	15.26	0.30	14.87	12.50	0.68	0.01	0.00	98.57			
DB02-216_PI7_3_32	62	Inclusion	48.68	1.47	4.88	15.17	0.35	14.93	12.24	0.82	0.01	0.00	98.55			
DB02-216_PI7_3_33	64	Inclusion	47.19	1.66	5.69	15.63	0.22	14.16	11.81	1.11	0.04	0.06	97.58			
DB02-216_PI7_3_34	66	Inclusion	48.88	1.30	4.18	15.66	0.36	14.26	13.10	0.61	0.02	0.00	98.38			
DB02-216_PI7_3_35	68	Inclusion	48.32	1.61	5.09	16.04	0.32	15.16	11.37	1.07	0.03	0.00	99.01			
DB02-216_PI7_3_36	70	Inclusion	45.63	2.66	8.19	16.14	0.27	13.49	10.15	1.97	0.04	0.17	98.71			
DB02-216_PI7_3_37	72	Inclusion	49.50	1.21	6.21	15.16	0.38	14.00	11.46	0.98	0.02	0.00	98.92			
DB02-216_PI7_3_38	74	Rim	51.62	0.37	21.97	3.29	0.08	4.17	13.39	2.71	0.00	0.15	97.76	73.17	26.82	0.00
DB02-216_PI7_3_39	76	Rim	47.31	0.04	32.52	0.65	0.00	0.27	17.11	1.70	0.00	0.01	99.62	84.75	15.23	0.02
DB02-216_PI7_3_40	78	Rim	46.32	0.00	33.59	0.60	0.04	0.18	17.75	1.37	0.00	0.09	99.95	87.72	12.28	0.00
DB02-216_PI7_3_41	80	Plagioclase	46.75	0.05	33.76	0.60	0.00	0.16	17.83	1.24	0.01	0.05	100.46	88.81	11.14	0.05
DB02-216_PI7_3_42	82	Plagioclase	46.50	0.01	33.77	0.47	0.00	0.15	17.83	1.21	0.00	0.06	100.01	89.06	10.92	0.02
DB02-216_PI7_3_43	84	Plagioclase	46.62	0.01	33.94	0.47	0.01	0.23	17.77	1.17	0.01	0.00	100.23	89.32	10.64	0.04
DB02-216_PI7_3_44	86	Plagioclase	46.43	0.02	33.91	0.50	0.00	0.22	17.84	1.23	0.01	0.17	100.33	88.84	11.12	0.04

Table 7. DB02-216 plagioclases and melt inclusions, XRF analyses (continued)

Label	Profile (µm)	Material	SiO2	TiO2	Al2O3	FeO	MnO	MgO	CaO	Na2O	K2O	BaO	Total	An	Ab	Or
						Plagioclase xenocryst 7 - profile 3 (continued)										
DB02-216_PI7_3_45	88	Plagioclase	46.33	0.01	33.60	0.52	0.06	0.21	17.73	1.24	0.00	0.00	99.71	88.74	11.26	0.00
DB02-216_PI7_3_46	90	Plagioclase	46.17	0.02	33.82	0.49	0.07	0.23	17.82	1.24	0.00	0.00	99.86	88.82	11.16	0.02
DB02-216_PI7_3_47	92	Plagioclase	46.28	0.06	30.68	3.54	0.08	2.60	14.96	1.05	0.01	0.08	99.33	88.65	11.29	0.06
DB02-216_PI7_3_48	94	Plagioclase	44.50	0.02	30.84	2.90	0.02	2.35	15.82	1.12	0.00	0.01	97.57	88.68	11.32	0.00
DB02-216_PI7_3_49	96	Plagioclase	46.80	0.02	33.79	0.41	0.03	0.20	17.82	1.26	0.01	0.00	100.34	88.60	11.37	0.03
DB02-216_PI7_3_50	98	Plagioclase	46.55	0.01	33.79	0.54	0.04	0.22	17.86	1.18	0.01	0.00	100.20	89.27	10.66	0.08
DB02-216_PI7_3_51	100	Plagioclase	46.56	0.00	33.57	0.38	0.08	0.21	17.75	1.22	0.01	0.00	99.78	88.90	11.02	0.08
DB02-216_PI7_3_52	102	Plagioclase	46.23	0.03	33.78	0.48	0.05	0.19	17.86	1.25	0.01	0.19	100.08	88.70	11.25	0.05
DB02-216_PI7_3_53	104	Plagioclase	46.25	0.01	33.89	0.54	0.02	0.21	17.85	1.21	0.01	0.01	100.00	89.08	10.89	0.03
DB02-216_PI7_3_54	106	Plagioclase	46.46	0.09	33.66	0.43	0.04	0.22	17.82	1.18	0.00	0.00	99.91	89.30	10.70	0.00
DB02-216_PI7_3_55	108	Plagioclase	46.44	0.06	33.89	0.46	0.02	0.21	17.76	1.21	0.00	0.01	100.07	88.97	11.01	0.02
DB02-216_PI7_3_56	110	Plagioclase	46.05	0.00	33.58	0.43	0.02	0.20	17.72	1.13	0.00	0.00	99.14	89.67	10.32	0.02
DB02-216_PI7_3_57	112	Plagioclase	46.24	0.04	33.69	0.43	0.00	0.22	17.80	1.25	0.01	0.08	99.76	88.67	11.25	0.09
DB02-216_PI7_3_58	114	Plagioclase	46.50	0.01	33.70	0.42	0.01	0.23	17.77	1.29	0.00	0.19	100.13	88.37	11.61	0.02
DB02-216_PI7_3_59	116	Plagioclase	46.11	0.05	33.42	0.49	0.03	0.20	17.71	1.14	0.00	0.05	99.21	89.55	10.45	0.00
DB02-216_PI7_3_60	118	Plagioclase	46.68	0.05	33.42	0.40	0.05	0.21	17.81	1.21	0.01	0.00	99.83	89.04	10.91	0.05
DB02-216_PI7_3_61	120	Plagioclase	46.15	0.09	33.72	0.41	0.04	0.21	17.89	1.23	0.01	0.03	99.78	88.87	11.10	0.03
						Plagioclase xenocryst 8 - profile 1										
DB02-216_PI8_1_1	0	Plagioclase	47.05	0.03	33.58	0.52	0.03	0.18	17.47	1.47	0.00	0.21	100.53	86.79	13.21	0.00
DB02-216_PI8_1_2	4	Rim	51.47	0.03	29.36	0.85	0.02	0.53	14.07	3.40	0.03	0.03	99.79	69.46	30.35	0.19
DB02-216_PI8_1_3	8	Rim	53.55	0.64	11.43	10.26	0.23	9.66	12.29	3.11	0.05	0.00	101.23	68.36	31.33	0.31
DB02-216_PI8_1_4	12	Inclusion	51.13	0.78	6.27	13.21	0.24	13.32	12.13	1.24	0.03	0.05	98.41			
DB02-216_PI8_1_5	16	Inclusion	50.84	0.76	5.46	15.05	0.39	13.64	11.84	1.05	0.09	0.10	99.22			
DB02-216_PI8_1_6	20	Inclusion	50.23	0.67	4.06	16.82	0.39	15.00	11.82	0.34	0.03	0.04	99.39			
DB02-216_PI8_1_7	24	Inclusion	42.94	0.13	8.20	16.34	0.19	14.35	3.13	0.06	0.06	0.02	85.43			
DB02-216_PI8_1_8	28	Inclusion	41.37	0.56	5.77	17.05	0.26	13.11	7.86	0.26	0.02	0.02	86.29			
DB02-216_PI8_1_9	32	Inclusion	50.48	0.95	5.40	15.44	0.28	14.36	11.98	0.84	0.03	0.10	99.88			
DB02-216_PI8_1_10	36	Inclusion	52.06	0.80	5.83	14.42	0.31	13.66	11.63	0.75	0.07	0.00	99.51			
DB02-216_PI8_1_11	40	Inclusion	52.42	0.72	5.95	14.69	0.34	13.94	12.07	1.15	0.02	0.00	101.28			
DB02-216_PI8_1_12	44	Inclusion	43.97	0.21	9.40	0.00	0.07	14.00	3.39	0.08	0.06	0.00	71.18			
DB02-216_PI8_1_13	48	Inclusion	41.04	0.16	9.09	0.00	0.19	13.01	3.00	0.06	0.05	0.00	66.59			
DB02-216_PI8_1_14	52	Inclusion	48.66	0.88	4.83	0.00	0.19	13.93	11.77	0.54	0.02	0.00	80.83			
DB02-216_PI8_1_15	56	Inclusion	47.13	0.97	5.13	0.00	0.39	14.24	10.89	0.37	0.05	0.00	79.18			
DB02-216_PI8_1_16	60	Inclusion	50.53	0.81	5.37	14.78	0.31	13.85	12.44	0.95	0.05	0.00	99.10			
DB02-216_PI8_1_17	64	Inclusion	50.03	0.80	4.73	15.80	0.32	15.27	11.91	0.36	0.00	0.06	99.28			
DB02-216_PI8_1_18	68	Inclusion	50.17	0.92	5.67	15.93	0.31	13.39	11.91	1.14	0.01	0.20	99.66			
DB02-216_PI8_1_19	72	Inclusion	50.72	0.80	5.56	14.40	0.36	13.77	12.46	0.92	0.03	0.02	99.05			
DB02-216_PI8_1_20	76	Rim	52.32	0.56	12.50	12.56	0.20	9.15	12.40	2.03	0.01	0.11	101.84	77.07	22.87	0.06
DB02-216_PI8_1_21	80	Rim	48.81	0.09	32.15	0.62	0.04	0.28	16.16	2.29	0.01	0.15	100.62	79.53	20.38	0.08
DB02-216_PI8_1_22	84	Plagioclase	46.94	0.06	33.38	0.70	0.01	0.18	17.40	1.49	0.01	0.00	100.17	86.56	13.40	0.04
DB02-216_PI8_1_23	88	Plagioclase	46.90	0.01	33.47	0.00	0.09	0.21	17.51	1.46	0.01	0.00	99.65	86.87	13.09	0.03
DB02-216_PI8_1_24	92	Rim	48.65	0.07	30.24	0.00	0.02	1.15	15.84	2.12	0.02	0.00	98.12	80.39	19.50	0.11
DB02-216_PI8_1_25	96	Inclusion	50.29	0.90	5.75	0.00	0.36	14.71	13.32	0.44	0.00	0.00	85.77			

Table 7. DB02-216 plagioclases and melt inclusions, XRF analyses (continued)

Label	Profile (µm)	Material	SiO2	TiO2	Al2O3	FeO	MnO	MgO	CaO	Na2O	K2O	BaO	Total	An	Ab	Or
		Plagioclase xenocryst 8 - profile 1 (continued)														
DB02-216_PI8_1_26	100	Inclusion	51.10	0.78	8.00	11.85	0.20	12.92	14.08	1.21	0.00	0.00	100.14			
DB02-216_PI8_1_27	104	Inclusion	51.26	0.83	8.25	13.12	0.30	11.27	13.40	1.65	0.03	0.17	100.29			
DB02-216_PI8_1_28	108	Inclusion	50.59	0.87	6.59	13.40	0.34	16.32	11.76	0.66	0.02	0.01	100.57			
DB02-216_PI8_1_29	112	Inclusion	52.92	0.49	15.30	7.96	0.21	7.24	12.18	3.36	0.05	0.00	99.72			
DB02-216_PI8_1_30	116	Inclusion	51.45	0.27	15.87	9.85	0.23	7.70	8.73	2.83	0.07	0.00	96.99			
DB02-216_PI8_1_31	120	Inclusion	50.94	0.76	10.18	10.60	0.23	11.97	13.93	1.42	0.02	0.00	100.06			
DB02-216_PI8_1_32	124	Inclusion	50.62	0.43	14.74	9.66	0.22	6.50	9.99	2.38	0.07	0.03	94.63			
DB02-216_PI8_1_33	128	Inclusion	51.21	0.66	7.41	14.22	0.46	14.64	11.87	1.06	0.02	0.00	101.53			
DB02-216_PI8_1_34	132	Inclusion	49.03	0.55	5.38	17.55	0.39	13.94	10.92	0.76	0.02	0.00	98.54			
DB02-216_PI8_1_35	136	Inclusion	41.57	0.34	7.69	19.78	0.23	14.93	6.34	0.32	0.02	0.27	91.49			
DB02-216_PI8_1_36	140	Inclusion	50.85	0.72	8.22	11.90	0.39	14.44	11.34	1.14	0.03	0.00	99.02			
DB02-216_PI8_1_37	144	Rim	52.62	0.43	16.31	8.34	0.10	6.42	12.59	2.52	0.06	0.00	99.40	73.14	26.46	0.40
DB02-216_PI8_1_38	148	Rim	46.72	0.02	31.65	2.44	0.01	1.18	15.85	1.54	0.02	0.00	99.42	84.93	14.97	0.10
DB02-216_PI8_1_39	152	Rim	46.83	0.02	33.23	0.59	0.00	0.19	17.31	1.56	0.01	0.00	99.73	85.94	14.03	0.03
DB02-216_PI8_1_40	156	Rim	45.83	0.02	30.98	2.41	0.04	2.12	15.93	1.41	0.00	0.05	98.79	86.16	13.84	0.00
DB02-216_PI8_1_41	160	Plagioclase	46.75	0.00	33.46	0.46	0.06	0.22	17.53	1.53	0.01	0.33	100.35	86.34	13.60	0.06
DB02-216_PI8_1_42	164	Plagioclase	46.90	0.00	33.44	0.55	0.01	0.19	17.45	1.50	0.01	0.00	100.07	86.43	13.49	0.08
DB02-216_PI8_1_43	168	Plagioclase	46.99	0.07	33.65	0.48	0.00	0.23	17.53	1.51	0.00	0.00	100.46	86.47	13.52	0.00
DB02-216_PI8_1_44	172	Plagioclase	46.75	0.00	33.58	0.39	0.02	0.23	17.43	1.50	0.00	0.00	99.89	86.54	13.46	0.05
DB02-216_PI8_1_45	176	Plagioclase	47.23	0.05	33.36	0.50	0.00	0.19	17.52	1.50	0.01	0.00	100.37	86.53	13.42	0.06
DB02-216_PI8_1_46	180	Plagioclase	46.80	0.02	33.50	0.44	0.00	0.22	17.68	1.39	0.01	0.01	100.07	87.45	12.49	0.00
DB02-216_PI8_1_47	184	Plagioclase	46.77	0.05	33.68	0.48	0.03	0.23	17.56	1.42	0.00	0.10	100.32	87.24	12.76	0.02
DB02-216_PI8_1_48	188	Rim	46.46	0.04	32.69	0.71	0.00	0.76	17.20	1.33	0.00	0.08	99.27	87.70	12.28	0.00
DB02-216_PI8_1_49	192	Rim	46.28	0.02	32.23	1.99	0.04	1.12	16.56	1.35	0.00	0.00	99.59	87.18	12.82	0.13
DB02-216_PI8_1_50	196	Rim	46.58	0.01	29.33	4.94	0.10	3.44	14.16	1.20	0.02	0.03	99.79	86.64	13.23	0.03
DB02-216_PI8_1_51	200	Rim	49.66	0.00	31.22	0.93	0.16	0.57	15.36	2.56	0.01	0.00	100.46	76.83	23.14	0.03
DB02-216_PI8_1_52	204	Rim	52.30	0.01	28.88	0.99	0.03	0.63	13.69	3.56	0.01	0.00	100.09	67.95	31.99	0.05
DB02-216_PI8_1_53	208	Rim	54.57	0.02	25.22	1.99	0.05	1.90	11.29	4.55	0.04	0.01	99.65	57.68	42.10	0.22
DB02-216_PI8_1_54	212	Inclusion	49.64	0.95	4.39	15.41	0.32	14.29	12.56	0.60	0.04	0.00	98.20			
DB02-216_PI8_1_55	216	Inclusion	51.06	0.80	5.20	14.93	0.35	13.80	12.57	0.91	0.06	0.00	99.68			
DB02-216_PI8_1_56	220	Inclusion	49.85	0.86	4.46	15.55	0.44	14.73	12.79	0.58	0.02	0.00	99.29			
DB02-216_PI8_1_57	224	Inclusion	49.94	1.03	4.02	16.04	0.35	14.75	13.25	0.51	0.01	0.15	100.05			
DB02-216_PI8_1_58	228	Inclusion	51.25	0.86	5.80	15.12	0.36	13.77	12.05	1.03	0.02	0.00	100.25			
DB02-216_PI8_1_59	232	Inclusion	49.90	0.80	4.15	16.18	0.30	15.39	11.78	0.39	0.03	0.09	99.01			
DB02-216_PI8_1_60	236	Inclusion	48.04	0.64	4.95	17.94	0.35	15.15	9.95	0.32	0.02	0.00	97.36			
DB02-216_PI8_1_61	240	Inclusion	45.81	0.36	6.14	16.11	0.21	15.52	5.86	0.17	0.05	0.00	90.22			
DB02-216_PI8_1_62	244	Inclusion	51.39	0.72	7.18	14.36	0.23	11.37	10.83	1.67	0.04	0.00	97.78			
DB02-216_PI8_1_63	248	Inclusion	50.25	0.77	6.05	15.33	0.29	12.63	11.95	1.17	0.03	0.04	98.50			
DB02-216_PI8_1_64	252	Rim	51.41	0.87	8.15	13.36	0.25	12.81	12.24	1.16	0.02	0.17	100.45	85.25	14.59	0.16
DB02-216_PI8_1_65	256	Rim	53.86	0.00	27.94	0.72	0.00	0.59	12.69	4.48	0.01	0.00	100.29	60.96	38.98	0.05
DB02-216_PI8_1_66	260	Rim	50.44	0.04	30.77	0.76	0.07	0.51	15.12	2.83	0.01	0.17	100.71	74.68	25.28	0.04
DB02-216_PI8_1_67	264	Rim	46.57	0.00	32.06	1.12	0.02	1.06	16.82	1.43	0.01	0.00	99.10	86.58	13.35	0.07
DB02-216_PI8_1_68	268	Rim	45.97	0.00	30.57	3.60	0.07	2.50	15.08	1.34	0.01	0.00	99.13	86.11	13.82	0.06

Table 7. DB02-216 plagioclases and melt inclusions, XRF analyses (continued)

Label	Profile (µm)	Material	SiO2	TiO2	Al2O3	FeO	MnO	MgO	CaO	Na2O	K2O	BaO	Total	An	Ab	Or
Plagioclase xenocryst 8 - profile 1 (continued)
DB02-216_Pl8_1_69	272	Rim	46.57	0.01	32.68	0.83	0.00	0.60	16.93	1.48	0.01	0.00	99.12	86.28	13.67	0.05
DB02-216_Pl8_1_70	276	Plagioclase	47.05	0.04	33.27	0.60	0.09	0.22	17.31	1.56	0.00	0.04	100.19	85.93	14.05	0.01
DB02-216_Pl8_1_71	280	Plagioclase	47.46	0.01	33.50	0.29	0.07	0.24	17.35	1.59	0.00	0.03	100.55	85.76	14.23	0.00
DB02-216_Pl8_1_72	284	Plagioclase	47.06	0.00	33.19	0.49	0.03	0.20	17.35	1.53	0.01	0.00	99.87	86.19	13.76	0.04
DB02-216_Pl8_1_73	288	Plagioclase	47.15	0.03	33.38	0.46	0.02	0.24	17.38	1.63	0.00	0.06	100.36	85.51	14.47	0.02
DB02-216_Pl8_1_74	292	Plagioclase	47.25	0.00	33.08	0.57	0.05	0.27	17.39	1.63	0.01	0.00	100.25	85.47	14.47	0.06
DB02-216_Pl8_1_75	296	Plagioclase	47.29	0.06	33.47	0.50	0.09	0.20	17.35	1.50	0.00	0.13	100.58	86.46	13.53	0.01
DB02-216_Pl8_1_76	300	Plagioclase	47.37	0.00	33.24	0.43	0.00	0.21	17.28	1.58	0.01	0.00	100.14	85.75	14.20	0.05
DB02-216_Pl8_1_77	304	Plagioclase	47.20	0.02	33.06	0.57	0.03	0.32	17.33	1.55	0.00	0.09	100.17	86.05	13.95	0.00
Plagioclase xenocryst 8 - profile 2
DB02-216_Pl8_2_1	0	Inclusion	50.38	0.97	4.64	15.42	0.35	13.74	13.20	0.73	0.03	0.00	99.47			
DB02-216_Pl8_2_2	3	Inclusion	50.13	1.08	5.21	14.89	0.40	14.47	12.70	0.78	0.01	0.00	99.68			
DB02-216_Pl8_2_3	6	Inclusion	49.23	0.88	6.66	14.83	0.38	12.98	11.38	1.13	0.03	0.01	97.51			
DB02-216_Pl8_2_4	9	Inclusion	46.95	0.87	5.36	16.81	0.31	14.49	11.57	0.52	0.12	0.00	97.00			
DB02-216_Pl8_2_5	12	Inclusion	47.53	0.80	5.30	16.18	0.37	14.14	11.56	0.36	0.04	0.11	96.38			
DB02-216_Pl8_2_6	15	Inclusion	49.98	0.99	6.48	14.74	0.28	12.92	12.57	1.20	0.02	0.00	99.17			
DB02-216_Pl8_2_7	18	Inclusion	42.04	0.39	8.09	19.40	0.21	14.91	5.74	0.11	0.16	0.00	91.05			
DB02-216_Pl8_2_8	21	Inclusion	41.59	0.14	7.91	18.16	0.10	14.67	3.11	0.10	0.07	0.00	85.85			
DB02-216_Pl8_2_9	24	Inclusion	48.71	0.59	6.11	17.01	0.32	16.27	8.00	0.44	0.08	0.00	97.52			
DB02-216_Pl8_2_10	27	Inclusion	51.02	0.82	7.08	14.53	0.28	12.02	12.25	1.55	0.03	0.10	99.67			
DB02-216_Pl8_2_11	30	Inclusion	50.08	1.15	6.37	15.43	0.29	12.82	11.86	1.29	0.01	0.01	99.31			
DB02-216_Pl8_2_12	33	Inclusion	48.89	0.87	4.93	16.49	0.29	14.57	11.15	0.57	0.01	0.02	97.79			
DB02-216_Pl8_2_13	36	Inclusion	50.13	0.99	6.48	14.75	0.29	13.98	12.66	0.68	0.01	0.21	100.18			
DB02-216_Pl8_2_14	39	Rim	51.01	0.02	30.66	0.59	0.08	0.41	14.71	3.10	0.00	0.13	100.70	72.41	27.58	0.01
DB02-216_Pl8_2_15	42	Rim	49.06	0.01	31.93	0.60	0.07	0.28	16.07	2.31	0.01	0.04	100.38	79.33	20.60	0.07
DB02-216_Pl8_2_16	45	Plagioclase	46.57	0.01	33.96	0.51	0.05	0.21	17.82	1.46	0.00	0.00	100.59	87.11	12.89	0.00
DB02-216_Pl8_2_17	48	Plagioclase	46.69	0.00	33.43	0.57	0.08	0.17	17.74	1.35	0.00	0.00	100.03	87.94	12.06	0.00
DB02-216_Pl8_2_18	51	Plagioclase	46.56	0.00	33.68	0.45	0.00	0.14	17.76	1.33	0.01	0.17	100.09	88.04	11.89	0.07
DB02-216_Pl8_2_19	54	Plagioclase	46.79	0.01	33.85	0.50	0.09	0.20	17.69	1.28	0.01	0.03	100.42	88.42	11.55	0.03
DB02-216_Pl8_2_20	57	Plagioclase	46.24	0.06	33.87	0.55	0.08	0.19	17.86	1.21	0.00	0.00	100.07	89.06	10.94	0.00
DB02-216_Pl8_2_21	60	Plagioclase	46.58	0.02	33.80	0.44	0.01	0.20	17.66	1.33	0.01	0.00	100.06	87.97	12.00	0.03
DB02-216_Pl8_2_22	63	Plagioclase	46.37	0.03	33.90	0.41	0.06	0.18	17.74	1.29	0.01	0.03	100.01	88.34	11.61	0.05
DB02-216_Pl8_2_23	66	Plagioclase	46.25	0.05	33.85	0.46	0.02	0.19	17.73	1.32	0.00	0.00	99.86	88.13	11.87	0.00
DB02-216_Pl8_2_24	69	Plagioclase	46.44	0.02	33.79	0.44	0.00	0.17	17.65	1.29	0.01	0.00	99.81	88.23	11.71	0.05

Table 7. DB02-216 plagioclases and melt inclusions, XRF analyses (continued)

Label	Profile (µm)	Material	SiO2	TiO2	Al2O3	FeO	MnO	MgO	CaO	Na2O	K2O	BaO	Total	An	Ab	Or
				Plagioclase xenocryst 8 - profile 2 (continued)												
DB02-216_Pl8_2_25	72	Plagioclase	46.42	0.08	33.66	0.45	0.05	0.18	17.64	1.29	0.01	0.03	99.79	88.28	11.68	0.03
				Plagioclase xenocryst 8 - profile 3												
DB02-216_Pl8_3_1		Plagioclase	32.71	0.10	16.58	22.28	0.15	13.12	2.70	0.05	0.03	0.00	87.72	95.59	3.16	1.25
DB02-216_Pl8_3_2		Plagioclase	32.53	0.11	15.18	21.23	0.16	12.15	3.01	0.06	0.05	0.00	84.48	94.78	3.45	1.77
DB02-216_Pl8_3_3		Plagioclase	35.19	0.11	14.71	20.81	0.14	13.14	2.81	0.19	0.02	0.00	87.10	88.27	10.96	0.77
DB02-216_Pl8_4_1		Plagioclase	33.76	0.08	15.97	21.54	0.11	12.85	2.96	0.08	0.07	0.00	87.44	92.67	4.73	2.60
DB02-216_Pl8_4_2		Plagioclase	33.78	0.03	15.86	21.84	0.17	13.22	3.06	0.07	0.04	0.05	88.12	94.70	3.99	1.31
DB02-216_Pl8_4_3		Plagioclase	32.13	0.08	16.37	22.65	0.29	12.72	2.62	0.04	0.02	0.01	86.93	96.40	2.66	0.94
DB02-216_Pl8_5_1		Plagioclase	46.75	0.06	33.67	0.48	0.02	0.23	17.71	1.31	0.02	0.05	100.29	88.15	11.75	0.10
DB02-216_Pl8_5_2		Plagioclase	46.44	0.00	33.69	0.33	0.10	0.22	17.67	1.31	0.01	0.06	99.83	88.11	11.83	0.06
				Matrix plagioclases												
DB02-216_Pl9_1		Plagioclase	55.80	0.07	26.82	1.11	0.06	0.10	10.62	5.47	0.01	0.00	100.08	51.73	48.21	0.06
DB02-216_Pl9_2		Plagioclase	54.38	0.11	27.98	0.96	0.02	0.16	11.63	5.14	0.02	0.10	100.50	55.53	44.38	0.09
DB02-216_Pl10_1		Plagioclase	53.11	0.09	28.95	0.95	0.12	0.20	12.64	4.20	0.02	0.00	100.27	62.42	37.49	0.09
DB02-216_Pl10_2		Plagioclase	54.57	0.12	28.01	1.01	0.00	0.18	11.59	4.77	0.02	0.00	100.26	57.25	42.61	0.14
DB02-216_Pl11_1		Plagioclase	53.51	0.03	28.91	1.00	0.00	0.18	12.60	4.33	0.01	0.09	100.67	61.60	38.31	0.09
DB02-216_Pl12_1		Plagioclase	49.74	0.05	31.72	0.64	0.08	0.25	15.56	2.54	0.00	0.00	100.58	77.23	22.77	0.00

Table 8. LA-ICP-MS analyses of plagioclase xenocrysts and melt inclusions (sample DB02-216)

Label	CaO*	Sc	Ti	V	Cr	Ni	Rb	Sr	Y	Zr	Nb	Ba	La	Ce	Pr	Nd	Sm	Eu	Gd	Tb	Dy	Ho	Er	Tm	Yb	Lu	Hf	Pb	Th	U
	wt%	ppm	ppm	ppm	ppm	ppm	ppm	ppm	ppm	ppm	ppm	ppm	ppm	ppm	ppm	ppm	ppm	ppm	ppm	ppm	ppm	ppm	ppm	ppm	ppm	ppm	ppm	ppm	ppm	ppm
Plagioclase xenocrysts																														
PI1-1	17.80	1.44	132	3.47	7.41	1.44	bdl	118.8	0.14	0.01	bdl	0.30	0.05	0.11	0.01	0.08	bdl	0.13	0.09	bdl	0.01	0.01	bdl	bdl	bdl	bdl	bdl	0.04	bdl	bdl
PI1-2	17.80	1.49	132	3.06	6.08	0.70	bdl	117.5	0.13	0.00	bdl	0.27	0.05	0.11	0.03	0.06	bdl	0.12	0.06	bdl	0.02	bdl	0.01	0.01	bdl	bdl	bdl	0.07	bdl	bdl
PI1-3	17.80	1.49	132	2.95	5.31	1.21	0.03	119.9	0.11	bdl	bdl	0.24	0.04	0.07	0.03	0.10	0.07	0.18	bdl	0.01	0.02	0.01	0.02	bdl	bdl	bdl	0.01	0.04	bdl	0
PI2-1	17.41	1.26	138	3.97	7.25	0.76	bdl	118.4	0.17	bdl	bdl	0.25	0.05	0.11	0.03	bdl	bdl	0.15	bdl	0.01	0.04	bdl	0.02	bdl	bdl	bdl	bdl	0.04	bdl	bdl
PI2-2	17.41	1.48	126	3.01	4.32	1.20	0.03	117.9	0.08	bdl	bdl	0.24	0.06	0.14	0.03	0.12	0.07	0.14	0.12	0.01	bdl	bdl	0.01	bdl	0.03	bdl	bdl	0.05	bdl	0
PI2-3	17.41	1.34	138	3.55	bdl	1.74	0.03	120.6	0.12	bdl	bdl	0.33	0.05	0.13	0.02	0.20	bdl	0.14	0.04	0.01	bdl	bdl	0.01	0.00	bdl	bdl	bdl	bdl	bdl	bdl
PI2-4	17.41	1.36	132	3.28	3.57	1.43	bdl	117.4	0.13	bdl	bdl	0.38	0.03	0.16	0.03	0.14	bdl	0.15	0.06	0.01	bdl	0.01	0.01	bdl	bdl	bdl	bdl	0.02	0.002	0.01
PI7-1	16.99	1.44	162	6.08	8.09	1.33	0.12	113.6	0.17	0.10	bdl	0.40	0.03	0.14	0.02	0.06	bdl	0.16	0.04	bdl	0.02	0.01	0.03	bdl	bdl	bdl	bdl	0.05	bdl	0.01
PI7-2	17.69	1.23	138	3.67	6.63	1.41	bdl	116.5	0.12	0.07	bdl	0.10	0.03	0.13	bdl	0.09	bdl	0.13	0.07	0.01	bdl	0.01	bdl	bdl	bdl	bdl	bdl	0.03	bdl	bdl
PI7-3	17.69	1.39	150	5.05	6.66	2.53	0.03	114.6	0.16	0.06	bdl	0.35	0.03	0.12	0.03	0.05	bdl	0.18	0.07	0.01	0.03	bdl	0.02	0.01	bdl	bdl	bdl	0.03	bdl	bdl
PI7-4	17.69	1.50	138	3.21	4.69	0.61	0.03	119.0	0.15	bdl	bdl	0.29	0.04	0.09	0.01	0.08	0.06	0.15	bdl	bdl	0.03	bdl	bdl	bdl	bdl	bdl	bdl	0.04	0.002	0
PI8-1	17.51	0.93	138	3.38	bdl	bdl	0.03	116.4	0.13	0.38	0.02	0.31	0.03	0.10	0.02	0.08	bdl	0.10	bdl	bdl	0.03	0.01	0.01	bdl	bdl	bdl	bdl	0.04	0.007	0.02
PI8-2	17.51	1.28	216	4.96	8.58	4.26	0.04	121.7	0.14	0.18	bdl	0.48	0.03	0.14	0.03	0.11	bdl	0.14	bdl	bdl	0.03	0.01	0.01	bdl	bdl	bdl	bdl	0.08	bdl	bdl
PI8-3	17.51	1.31	162	4.77	14.69	3.47	bdl	111.6	0.25	0.02	bdl	0.09	0.02	bdl	0.03	0.09	0.10	0.16	bdl	bdl	0.06	0.01	0.02	bdl	0.03	bdl	bdl	0.03	0.002	bdl
PI8-4	17.51	1.86	174	5.83	14.17	2.53	0.03	114.2	0.31	0.07	bdl	0.26	0.03	0.12	0.01	0.16	bdl	0.14	0.08	0.02	0.06	0.01	0.04	0.01	0.05	bdl	bdl	0.07	bdl	bdl
PI8-5	17.51	0.97	144	3.48	5.97	2.36	bdl	113.0	0.08	0.02	bdl	0.37	0.03	0.10	0.03	0.13	bdl	0.14	bdl	bdl	bdl	0.00	0.01	bdl	bdl	bdl	bdl	0.04	bdl	bdl
PI8-6	17.51	1.20	138	2.96	8.35	2.79	bdl	111.4	0.09	0.02	bdl	0.45	0.04	0.13	0.02	0.11	0.05	0.14	bdl	bdl	bdl	bdl	bdl	bdl	bdl	bdl	bdl	0.04	bdl	bdl
PI8-7	17.51	1.24	138	3.92	4.86	2.95	0.02	113.4	0.14	0.06	bdl	0.25	0.03	0.13	0.02	0.04	0.05	0.14	0.09	bdl	0.03	bdl	bdl	bdl	bdl	bdl	bdl	0.03	bdl	bdl
Melt Inclusions																														
PI1-incl1-1	12.33	70.7	8720	361	617	77	0.52	41.6	30.9	51.3	0.28	1.39	1.13	4.80	1.05	6.41	2.20	1.07	3.82	0.71	5.28	1.25	3.71	0.53	4.22	0.62	1.67	0.25	0.015	bdl
PI1-incl1-2	12.33	67.6	7845	351	569	142	1.60	55.6	30.2	48.4	0.25	1.68	1.25	4.53	1.02	6.01	3.09	1.10	3.79	0.72	5.19	1.17	3.92	0.61	4.75	0.70	1.40	0.33	0.014	0.013
PI2-incl1-1	12.53	69.7	10045	422	487	96	0.48	60.7	35.4	61.6	0.36	3.00	1.49	5.76	1.02	7.37	2.63	0.93	4.10	0.84	6.65	1.28	4.31	0.56	4.16	0.69	1.95	0.23	0.030	0.031
PI2-incl1-2	12.53	69.2	9937	403	495	94	0.34	53.5	33.8	59.9	0.37	2.66	1.39	5.40	1.06	6.81	3.19	1.30	4.69	0.68	5.77	1.31	3.78	0.62	4.18	0.72	1.58	0.26	0.015	0.024
PI7-incl1-1	12.21	67.5	8001	385	474	138	0.70	81.7	29.4	57.8	0.44	3.47	1.36	4.38	0.77	3.92	4.48	0.98	5.46	0.71	5.10	0.93	3.08	0.36	4.73	0.71	1.39	1.19	bdl	bdl
PI7-incl2-1	12.20	66.3	7851	362	525	95	0.51	62.0	33.1	54.6	0.46	2.05	1.29	4.17	0.97	7.36	2.18	0.69	4.11	0.78	5.18	1.16	2.97	0.61	4.21	0.72	1.42	0.36	bdl	bdl
PI7-incl3-1	16.33	128.7	17363	715	505	89	0.62	73.2	63.1	100.3	0.95	3.31	2.96	11.64	2.58	16.37	6.46	2.97	8.54	1.70	11.18	2.46	7.17	1.12	7.54	1.30	2.90	0.42	0.047	0.011
PI7-incl4-1	12.50	62.3	6347	309	552	340	0.77	70.1	24.6	39.3	0.30	1.71	1.02	3.76	0.59	4.59	2.09	0.90	2.56	0.59	4.10	0.85	3.13	0.50	3.25	0.46	0.98	0.15	0.051	bdl
PI7-incl5-1	12.20	55.1	5616	273	437	30	0.83	57.7	19.6	31.9	0.09	0.75	0.85	3.43	0.45	2.73	1.53	0.82	2.36	0.52	3.59	0.65	2.04	0.44	1.63	0.19	1.14	0.13	bdl	bdl
PI8-incl1-1	12.39	54.7	4855	252	526	106	0.62	57.2	20.9	27.6	0.10	3.21	1.05	3.29	0.53	3.94	2.19	0.72	2.00	0.41	2.91	0.73	2.09	0.40	3.30	0.39	0.83	0.45	0.028	bdl
PI8-incl2-1	12.32	47.7	4945	251	453	120	0.25	71.9	24.3	36.2	0.17	3.03	1.08	4.08	0.67	4.09	2.28	0.92	2.82	0.46	3.70	0.84	3.23	0.36	3.44	0.56	1.37	0.17	0.030	0.140
PI8-incl3-1	12.21	37.4	5376	234	450	85	0.56	61.0	18.2	25.9	0.23	3.63	0.95	3.53	0.68	4.06	1.37	0.88	3.25	0.33	3.04	0.71	2.34	0.55	3.11	0.29	0.93	0.26	bdl	bdl
PI8-incl4-1	12.33	68.7	6910	336	547	99	0.76	55.4	24.7	41.1	0.24	2.30	1.06	4.22	0.89	4.57	2.24	1.08	3.57	0.51	4.34	0.88	2.92	0.52	3.07	0.54	1.29	0.30	0.023	bdl
PI8-incl5-1	12.30	64.1	7570	332	523	102	0.39	52.6	27.2	40.2	0.31	3.14	0.97	4.44	0.79	5.71	2.63	1.14	2.12	0.50	5.28	1.12	3.62	0.58	4.07	0.68	1.08	0.32	bdl	bdl
PI8-incl5-2	12.30	48.8	5808	262	367	93	0.73	69.0	20.7	29.4	0.18	3.40	0.93	3.65	0.59	3.57	1.11	0.84	2.47	0.46	3.57	0.73	2.28	0.44	2.70	0.41	0.80	0.65	0.009	bdl

* CaO content is based on XRF averaged measures (Table 7.)